Profiles of
Drug Substances, Excipients, and Related Methodology
Volume 34

Profiles of
DRUG SUBSTANCES, EXCIPIENTS, AND RELATED METHODOLOGY

VOLUME **34**

CONTRIBUTING EDITORS

ABDULLAH A. AL-BADR

ALEKHA K. DASH

FOUNDING EDITOR

KLAUS FLOREY

Profiles of

DRUG SUBSTANCES, EXCIPIENTS, AND RELATED METHODOLOGY

VOLUME **34**

Edited by

HARRY G. BRITTAIN
Center for Pharmaceutical Physics,
Milford, New Jersey 08848

Notice
No responsibility is assumed by the publisher for any injury and/or
damage to persons or property as a matter of products liability, negli-
gence or otherwise, or from any use or operation of any methods, pro-
ducts, instructions or ideas contained in the material herein. Because of
rapid advances in the medical sciences, in particular, independent
verification of diagnoses and drug dosages should be made

For information on all Academic Press publications
visit our website at elsevierdirect.com

Printed and Bound in USA
09   10   11   12   10 9 8 7 6 5 4 3 2 1

Working together to grow
libraries in developing countries
www.elsevier.com | www.bookaid.org | www.sabre.org

ELSEVIER   BOOK AID   Sabre Foundation
            International

CONTENTS

This page intentionally left blank

The comprehensive profiling of drug substances and pharmaceutical excipients as to their physical and analytical characteristics remains at the core of pharmaceutical development. As a result, the compilation and publication of comprehensive summaries of physical and chemical data, analytical methods, routes of compound preparation, degradation pathways, uses and applications, *etc.*, have always been a vital function to both academia and industry.

As the science of pharmaceutics grows and matures, the need for information similarly expands along new fronts and causes equivalent growth in the vehicles where investigators find the information they need. The content of the *Profiles* series has expanded to meet this need, with chapters falling into one or more of the following main categories:

1. Comprehensive profiles of a drug substance or excipient
2. Physical characterization of a drug substance or excipient
3. Analytical methods for a drug substance or excipient
4. Detailed discussions of the clinical uses, pharmacology, pharmaco-kinetics, safety, or toxicity of a drug substance or excipient
5. Reviews of methodology useful for the characterization of drug substances or excipients
6. Annual reviews of areas of importance to pharmaceutical scientists

As it turns out, all of the chapters in the current volume are comprehensive in nature, and provide detailed profiles of the drug substances involved. Volumes in the recent past have contained reviews of methodology, and it is anticipated that future volumes in the of the *Profiles* series will contain similar reviews, as well as other types of review articles that summarize the current state in a particular field of pharmaceutics. As always, I welcome communications from anyone in the pharmaceutical community who might want to provide an opinion or a contribution.

Harry G. Brittain

Editor, Profiles of Drug Substances, Excipients, and Related Methodology

hbrittain@centerpharmphysics.com

This page intentionally left blank

Creatine Monohydrate

Somnath Singh and **Alekha K. Dash**

Department of Pharmacy Sciences, School of Pharmacy and Health Professions, Creighton University, Omaha, NE 68178, USA

1. HISTORY AND THERAPEUTIC ASPECTS

Creatine was discovered in 1832 by a French scientist, Michel Eugene Chevreul, who extracted a new organic constituent from meat and named it creatine after the Greek word for flesh, *Kreas*. Justus von Liebig, in 1847, confirmed that creatine was a regular constituent of animal flesh. In the mid-1880s, creatinine was discovered in the urine, and later researchers speculated that creatinine was derived from creatine and was related to total muscle mass. In the late 1920s, scientists found that the intramuscular stores of creatine can be increased by ingesting creatine in higher than normal amounts. Phosphocreatine (PCr), the phosphorylated form of creatine, was discovered in 1927 and found to be involved in exercise energy expenditure. Creatine kinase, the enzyme which catalyzes PCr, was discovered in 1934 [1].

Although creatine's influence on physical performance has been well documented since the early twentieth century, it came into public view following the 1992 Olympics in Barcelona, when several newspapers reported about the use of creatine by several gold medalists. Creatine supplements designed for strength enhancement were not commercially available until 1993 when a company called EAS (Experimental and Applied Sciences) introduced the compound to the sports nutrition market under the name Phosphagen. Since that time, numerous creatine supplements have been introduced, with the most notable advancements coming in 1998, with the launch of the first creatine–carbohydrate–alpha lipoic acid supplement, Cell-Tech, by MuscleTech Research and Development, and in 2003 with the introduction of the first creatine ethyl ester supplements. To date, the most extensively researched and proven brand-name creatine supplement is Cell-Tech [2], which remains one of the most-used creatine supplements in the world.

Creatine ethyl ester is also becoming a widely used form of creatine, with many companies now carrying both creatine monohydrate-based supplements and creatine ethyl ester supplements. Creatine monohydrate ($400 million in annual sales in the United States alone) still easily outsells all other forms of creatine [3].

Creatine in its free or phosphorylated form plays an important role in the regulation and homeostasis of muscle energy metabolism [4]. Its popular role in sports performance enhancement is well documented [5–7]. Recently, creatine has been shown to occur throughout the brain, affecting energy metabolism by working as a neuromodulator [8]. Nervous tissue and the role of creatine supplementation are rapidly garnering more attention [9, 10]. Creatine is being looked at for its neuroprotective effects [11] because high energy phosphate metabolism plays a critical role in progression of neurodegenerative diseases. Huntington's disease [12, 13], Parkinson's disease, and amylotrophic lateral sclerosis [14–17] have all been investigated and appear to be beneficially affected by the consumption of creatine. While creatine may directly improve bioenergetic defects, it may also benefit other pathophysiological mechanisms associated with Huntington's disease. The major source of energy in the brain is ATP, which is tightly coupled to creatine and PCr levels within the cell. Creatine is shuttled across membranes via a sodium-dependent creatine transporter protein (CreaT) [18], which regulates tissue levels in response to low dietary intake or high endogenous creatine levels. Creatine kinase catalyzes the reversible transfer of a phosphoryl group from PCr to ADP, forming ATP. Thus, creatine offsets energy depletion by forming PCr, which provides a spatial energy buffer to rephosphorylate ADP to ATP at cellular sites of needed energy consumption and in the reversible reaction forming PCr and ADP from creatine and ATP [19]. Thereby, augmenting creatine levels in HD may therefore help to prevent reduced energy stores

and improve neuronal function. Another potential neuroprotective mechanism of creatine supplementation is the ability of PCr to stimulate synaptic glutamate uptake and thereby reduce extracellular glutamate [20]. In addition, creatine has also been reported to act as an antioxidant, scavenging reactive oxygen species [21].

Moreover, there are a number of researches using creatine in the treatment of various clinically relevant diseases such as arthritis [22], congestive heart failure [23], gyrate atrophy [24], disuse atrophy [25], McArdles disease [26], mitochondrial diseases [27, 28], and muscular dystrophy [29]. The aging process is associated with a reduction in total skeletal muscle mass and strength. The increase in total muscle creatine and PCr in response to dietary creatine monohydrate supplementation is higher in those with lower muscle concentration [30].

2. DESCRIPTION

2.1. Nomenclature

2.1.1. Chemical name
N-(Aminoiminomethyl)-*N*-methylglycine; *N*-amidinosarcosine; (α-methylguanido) acetic acid; *N*-methyl-*N*-guanylglycine; methylglycocyamine

2.1.2. Generic name
Creatine

2.2. Formulae

2.2.1. Empirical formula, molecular weight, CAS number
$C_4H_9N_3O_2$, 131.133 g/mol, CAS 57-00-1

2.2.2. Structural formula
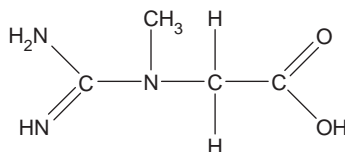
2.3. Elemental composition[31]

The calculated elemental composition of creatine is as follows:

Carbon   36.64%
Hydrogen   6.92%

Nitrogen   32.04%
Oxygen   24.40%

2.4. Appearance, color and odor

Creatine is a white, crystalline, and odorless powder, which forms clear and colorless solution in water.

2.5. Pharmaceutical dosage forms

Table 1.1 shows the various dosage forms of creatine manufactured by various companies under different brand names:

3. SYNTHESIS

Creatine is synthesized in the liver and kidneys and released into the blood stream to be taken up into muscle cells via a protein-based transport system. The liver produces creatine in a two step process: (1) Glycine and arginine are reacted to form guanidinoacetate and ornithine, and then (2) guanidinoacetate is methylated to creatine and released into the blood. The transport protein on the cell membrane has a high affinity for creatine and easily transports it into the cell.

Early researchers used creatine extracted from animal flesh, which was an expensive process. Today, commercial creatine is produced through chemical synthesis, which uses various muscle-related compounds as the principal starting materials as shown below [32]:

i. Glycine + Urea $\longrightarrow$ Hydantoic acid $\longrightarrow$ Glycocyamine $\longrightarrow$ Creatine

ii. Sarcosine + Urea ⟶ Creatine and creatinine

Sarcosine   Urea   Creatine

iii. Arginine ⟶ Guanidine Butyricacid ⟶ Glycocyamine ⟶ Creatine

Arginine   Guanidino butyric acid   Glycocyamine   Creatine

iv. Creatinine + Water ⟶ Creatine

Creatinine   Creatine
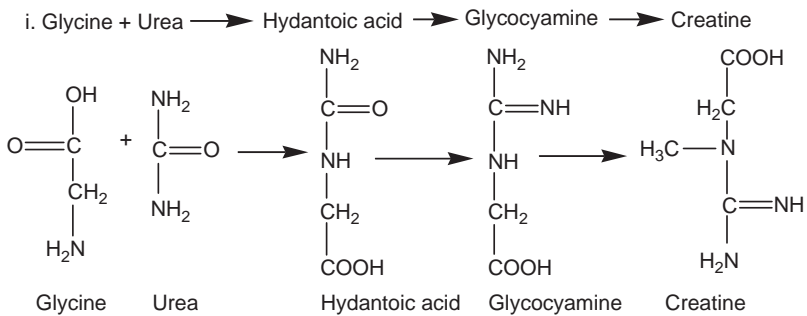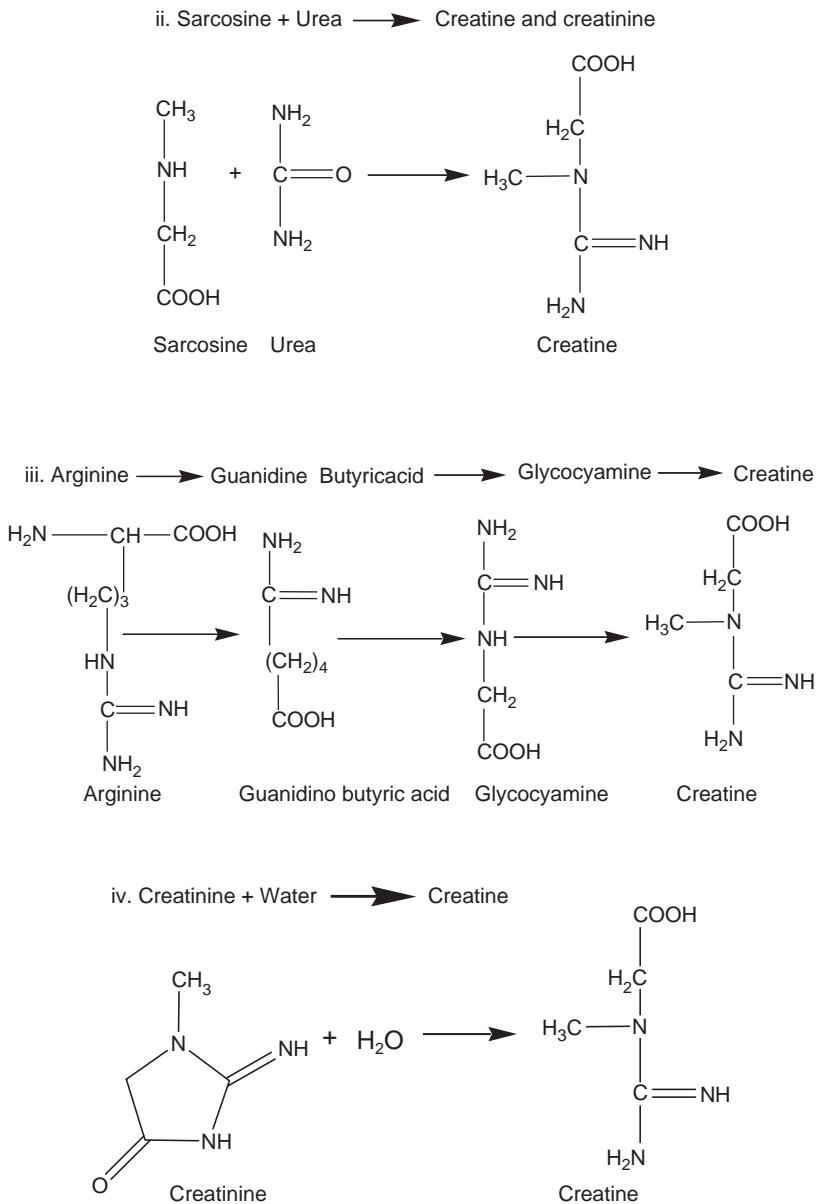
Figure 1.1 shows the biosynthesis of creatine using three amino acids as starting materials [33]. L-Arginineglycine amidinotransferase (AGAT) catalyzes reaction 1, which is the rate-limiting step in the creatine biosynthesis. AGAT expression is also reduced by the presence of creatine,

TABLE 1.1 List of different dosage forms of creatine available under various brand names

Chemical form	Brand name	Dosage form	Company
Micronized Creatine	AST Micronized Creatine	Powder	AST Sports Science
Creatine Monohydrate	Creatine Monohydrate Powder	Powder	ProLab
Creatine Monohydrate	American Creatine Powder	Powder	American Sports Nutrition
Creatine Monohydrate	Pure Creatine Monohydrate	Powder	Inter-Sport Technology
Creatine Monohydrate	IST Pure Creatine	Powder	Optimum Nutrition
Creatine Monohydrate	Mega Creatine Fuel	Capsule	Twin Lab
Creatine	Cell Pro	Powder	Universal Nutrition
Creatine Monohydrate	Cell-Tech	Powder	Muscle Tech
Creatine Monohydrate	ATP Advantage Creatine Serum	Liquid (sublingual)	Muscle Marketing USA
Micronized Creatine	Creatine Effervescent	Effervescent powder	ISS Research Monohydrate
Creatine Monohydrate	Creatine Edge powder	Effervescent	FSI Nutrition
Di-Creatine Citrate	Creatine Clear	Effervescent powder	FSI Nutrition
Creatine Monohydrate	Betagen	Powder	EAS
Creatine	Creatine Gum	Chewing Gum	NuCare

which raises concerns that prolonged creatine supplementation might inhibit endogenous creatine synthesis for an indefinite period of time. This synthetic scheme shows that at last, glycine is completely incorporated into the creatine backbone while arginine and methionine only contribute side groups.
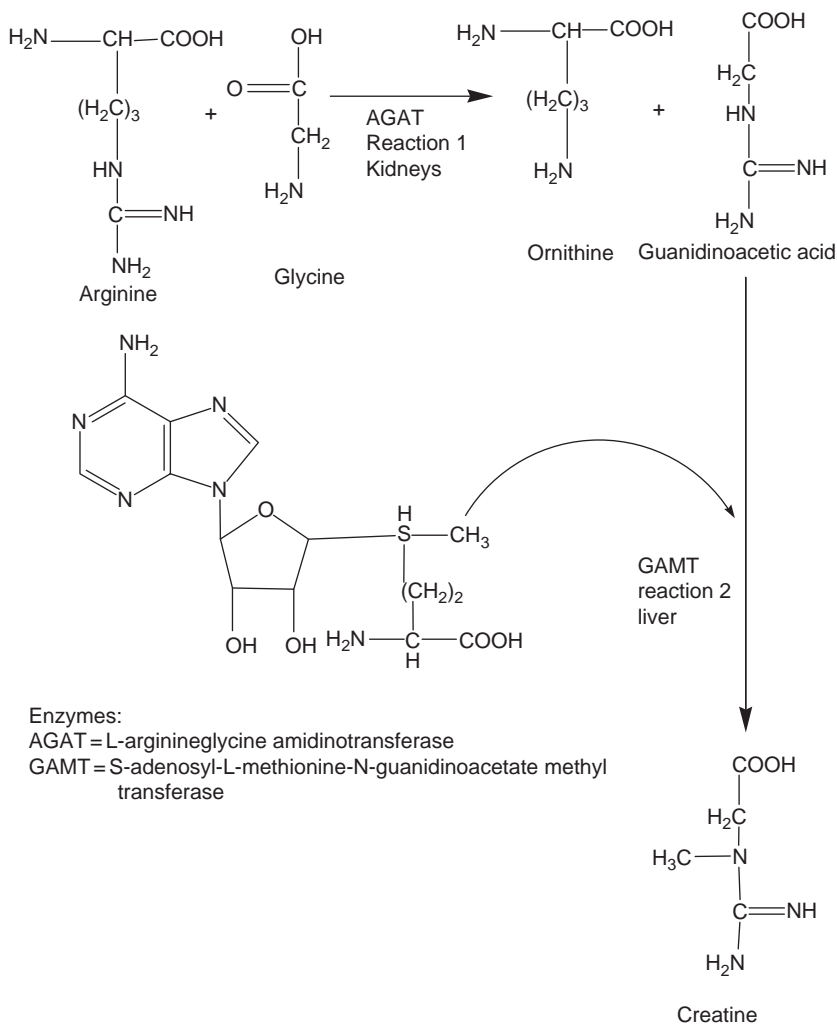
FIGURE 1.1   Synthesis of creatine from amino acids.

4. PHYSICAL PROPERTIES

4.1. Infrared spectrum

Figure 1.2 shows the infrared absorption spectrum [34] of creatine measured on dispersive instruments in carefully selected solvents, and hence may differ in detail from measurements on a FTIR instrument or in other chemical environments [35]. No band appears at 3520 cm^{-1}, which could be due to dimerization of carboxylic acid groups caused by strong hydrogen bonds between OH group of one carboxylic acid and C=O
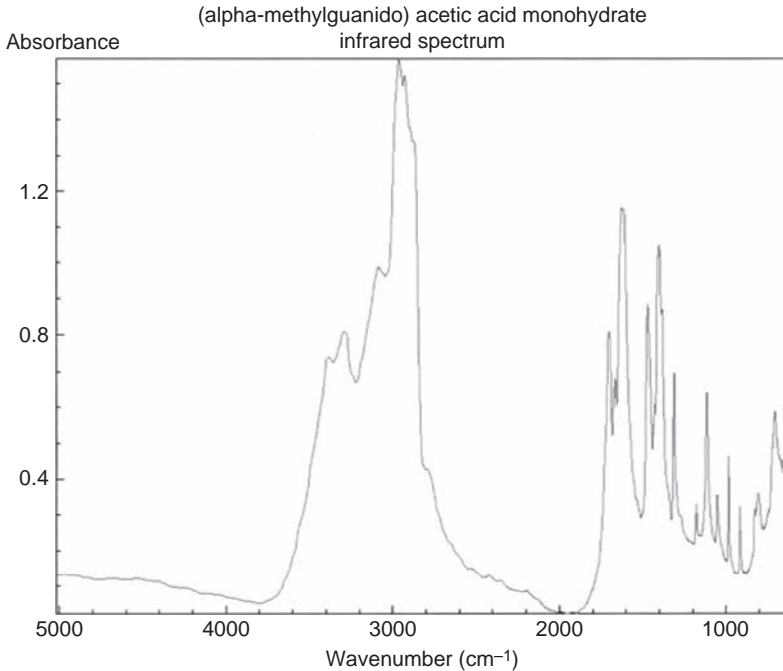
FIGURE 1.2 Infrared absorption spectrum of creatine.

group of another. The weaker C–H stretching bands are seen superimposed upon the broad O–H band. Vibration because of N–H stretching mode of primary amine group (NH_2) is overlapped with that of O–H group of carboxylic acid. The N–H bending band is seldom detectable in the spectra of aliphatic secondary amines, and was not observed. Major peaks were assigned to different functional groups as shown in Table 1.2.

4.2. ^{1}H-Nuclear magnetic resonance (NMR) spectrum

The 400 MHz proton nuclear magnetic resonance spectrum of creatine was obtained at room temperature using a Varian XL-400 NMR spectrophotometer and water as the solvent. The resulting NMR spectrum is shown in Fig. 1.3 in which the alcohol group is deprotonated and held by an imino group, and Table 1.3 shows the peak assignments.

4.3. ^{13}C-Nuclear magnetic resonance spectrum

The 400 MHz ^{13}C nuclear magnetic resonance spectrum of creatine was obtained at room temperature using a Varian XL-400 NMR spectrophotometer and water as solvent. The resulting NMR spectrum is shown in Fig. 1.4, and Table 1.4 shows the peak assignments.

TABLE 1.2 Assignments for the major infrared absorption transitions of creatine monohydrate

Wavenumber	Assignment
1672	$C=O$ stretching mode of carboxyl group
910	Out-of-plane bending of O–H of carboxylic acid group
3300–2500	Broad O–H stretching absorption
3270, 3060	Intense O–H stretching mode
2885	Overtone of O–H stretching mode
1510	A very weak intensity C–H bending vibration of methyl group
1585	N-H bending vibration of primary amine group (NH_2)
1250–1020	Medium-to-weak C–N stretching vibrations due to C–N linkages in primary, secondary, and tertiary amines

Index	Frequency	PPM	Height
1	2391.113	4.786	299.6
2	1964.355	3.932	124.3
3	1519.043	3.041	175.1
4	0.000	0.000	23.9
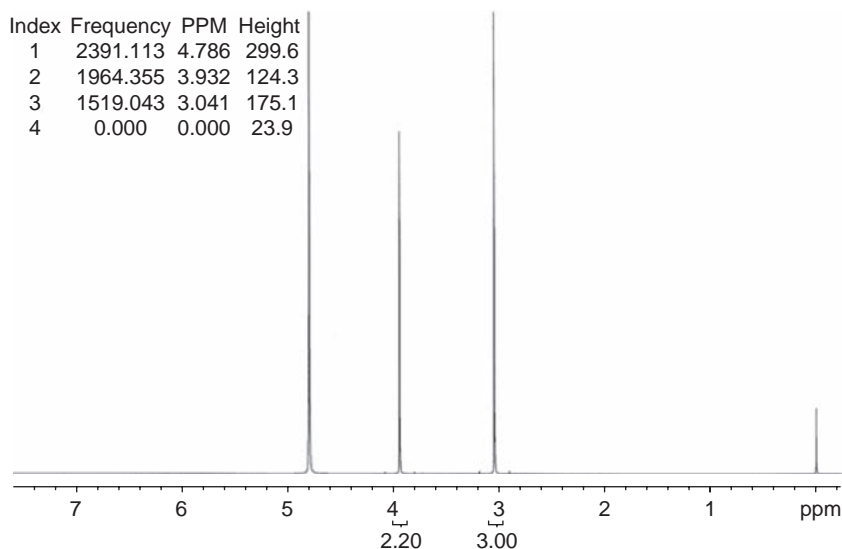
FIGURE 1.3 ^{1}H nuclear magnetic resonance spectrum of creatine.

4.4. UV–Vis spectroscopy

The UV absorption spectrum of creatine was recorded on a UV–Vis spectrophotometer (Shimadzu, model UV-1601 PC) over the spectral range of 190–400 nm at a concentration of 100 µg/ml. The absorption spectra obtained both in water and methanol are shown in Fig. 1.5A and B, respectively. The absorption maxima of creatine in methanol and water were found to be 204 and 205 nm, respectively.

TABLE 1.3   Assignments for the resonance bands in the ^1H NMR spectra of creatine
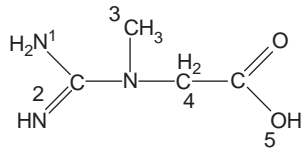
Chemical shift (ppm)	Number of protons	Assignments
3.04	3	Protons at positions 3
3.93	2	Protons at positions 4
4.79	4	Proton at position 1 and 2

Index	Frequency	ppm	Height
1	21953.912	174.760	25.4
2	6785.587	54.016	104.4
3	4657.487	37.075	49.6
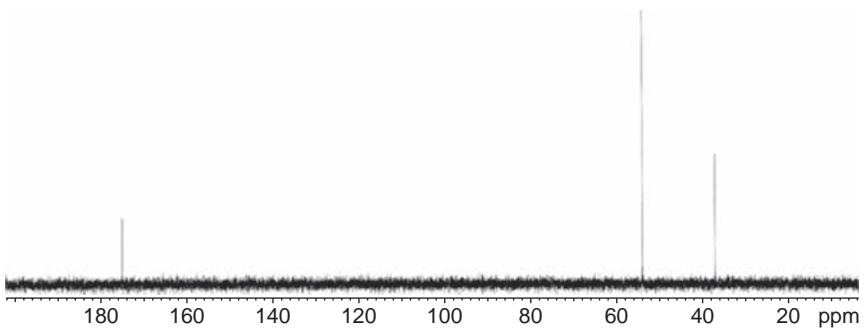
FIGURE 1.4 ^{13}C nuclear magnetic resonance spectrum of creatine.

TABLE 1.4   Assignments for the resonance bands in the ^{13}C NMR spectra of creatine
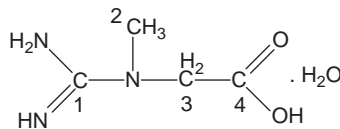
Chemical shift (ppm)	Assignments
37.07	Methyl carbon at position 2
54.01	Methylene carbon at position 3
157.27	Carbon at position 1
174.75	Carboxylic acid carbon at position 4
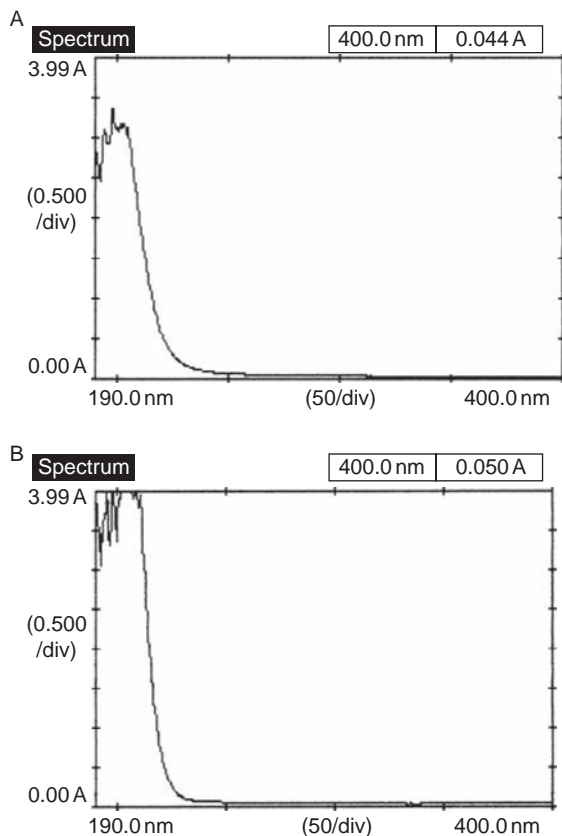
FIGURE 1.5 Ultraviolet absorption spectrum of creatine dissolved at a concentration of 100 μg/ml in (A) methanol and (B) water.

4.5. Mass spectrum

Figure 1.6 [36] shows the mass spectrum of creatine in which no molecular ion peak was observed because creatine, being a glycine derivative, easily loses its carboxyl group. This results in the appearance of fragmentations at m/z 45 (–COOH) and 86 because of fragment M-45 (mol. wt. of creatine = 131.31). The peak of highest intensity is due to the formation of cyanamide from the fragment bearing m/z 43. Fragment $NCH_3CH_2COOH^+$ can become converted into either 2-oxazolidine or pyruvate aldehyde 1-oxime. The mass spectrum of 2-oxazolidone shows a peak of 100% intensity at m/z 87, and weak peaks at m/z 88 and 89, which are not discernible in the spectrum of creatine. Therefore, we rule out the possibility of conversion of $NCH_3CH_2COOH^+$ to 2-oxazolidone and hypothesize the possible formation of pyruvate aldehyde 1-oxime, which can produce peaks at m/z 86,
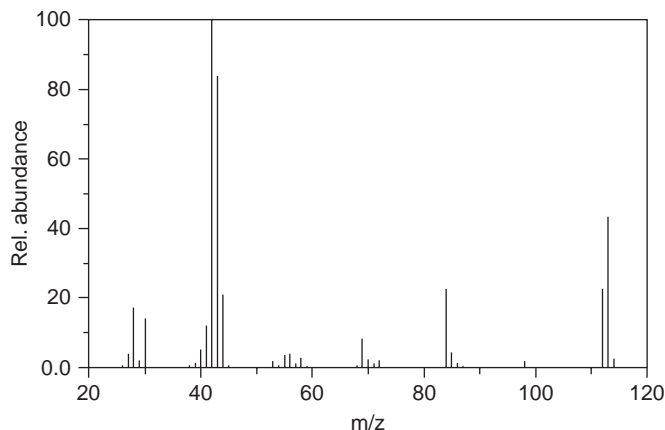
FIGURE 1.6 Mass spectrum of creatine (Adapted from NIST Chemistry WebBook available at http://webbok.nist.gov/chemistry).

85, and 84 (Fig. 1.7). The fragmentation ions of creatine and their relative intensity are presented in Table 1.5.

During the solid-state characterization of creatine monohydrate [37], mass spectra were obtained on a Waters/Micromass ZMD, Quadropole instrument (Milford, MA, USA) using the electrospray ionization (ESI) mode. The evaporation temperature was 350°C, with 3–4 V applied voltage, and the sheath gas (N_2) flow was set at 400 l/h. All data were collected in the full scan mode (100–1000 m/z). The mass spectra of creatine monohydrate heated to 260°C, and creatinine heated to the same temperature, are shown in Fig. 1.8. Both mass spectra were identical. Interestingly, both samples showed a peak around m/z of 227. The appearance of this peak in the mass spectrum can be explained to be due to the formation of dimers as shown in Fig. 1.9.

4.6. Thermal behavior

4.6.1. Melting point

Creatine monohydrate dehydrates to anhydrous creatine at 100°C and finally melts at 300°C with decomposition [31].

4.6.2. Differential scanning calorimetric data

The DSC thermogram of creatine monohydrate is composed of four endothermic events with peaks at 102, 255, 270, and 293°C, and is shown in Fig. 1.10A [37]. Reversibility studies of the three initial endothermic peaks were carried out in DSC by heating creatine monohydrate from 30 to 320°C (Fig. 1.11A) and from 30 to 270°C (Fig. 1.11B) which was cooled to room temperature, and reheated to 30–320°C (Fig. 1.11C). The
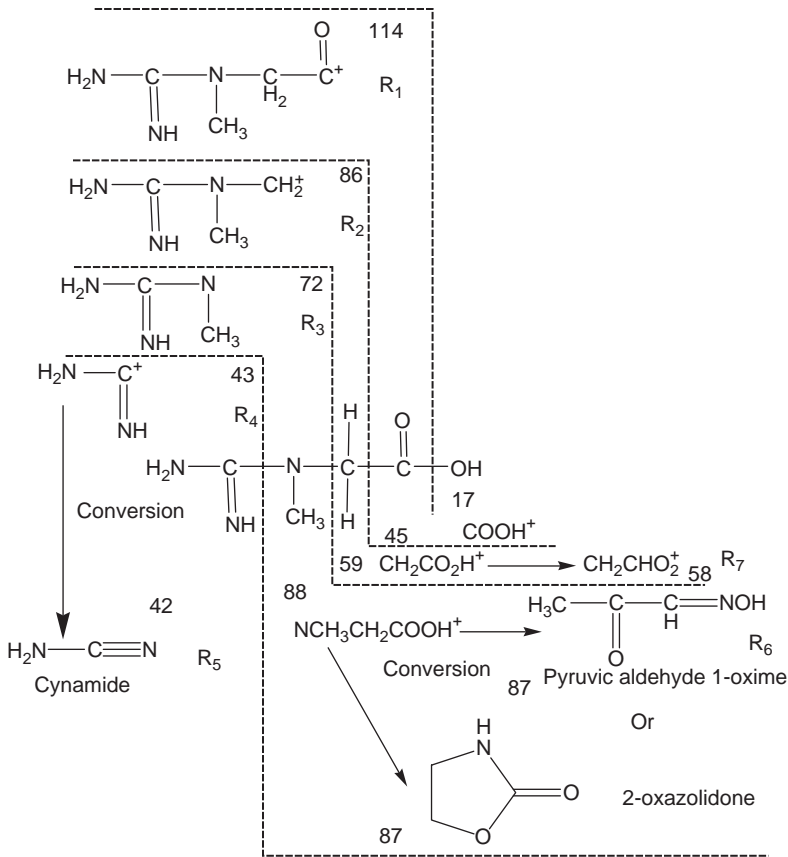
FIGURE 1.7   Fragmentation scheme of creatine.

first, second, and third endothermic peaks were absent in the DSC thermogram obtained with creatine monohydrate reheated from 30 through 270°C (Fig. 1.11C), which indicates that none of these events is reversible.

The second endothermic peak occurred between 230 and 260°C which appeared as a shoulder (Fig. 1.11A) and was thought to be due to a possible solid–solid polymorphic transition of anhydrous creatine. However, solid–solid polymorphic transitions are usually weak, that is, the enthalpy of transition is small. The second endotherm is not really small (Fig. 1.10A), which ruled out the probability of solid–solid polymorphic transition after dehydration of creatine monohydrate to form the anhydrous creatine. The overlapping second and third endotherms can be explained to be due to the intramolecular cyclization of creatine with a loss of 1 mole of water to form creatinine (Fig. 1.12). This cyclization event is expected to be highly energetic and endothermic. The last and final endotherm can be attributed to the melt decomposition of creatinine [37].

TABLE 1.5   Mass spectra fragmentation ions of creatine

m/z	Relative intensity (% I)	Fragments
114	2	M*-17 (OH^+)
113	43	R_1–H
112	23	R_1–H
98	2	R_1–NH_2
86	1	R_2 and R_6–H
85	4	R_2–H and R_6–H
84	23	R_2–H and R_6–2H
72	2	R_3
71	1	R_3–H
70	2	R_6–OH^+ = R_8
69	8	R_8–H
58	2	R_7
57	1	R_7–H
56	3	R_3–NH_2
45	1	COOH
44	21	COOH–H^+
43	83	R_4
42	100	R_5
41	14	R_5–H
40	6	R_7–OH

* M = Creatine

4.6.3. Thermogravimetric analysis

Thermogravimetric data were obtained using a thermogravimetric ana-
lyzer (TGA) (model TGA-50, Shimadzu, Kyoto, Japan) connected to a
thermal analysis operating system (TA-50WS, Shimadzu, Kyoto, Japan).
The TGA curve of creatine monohydrate (Fig. 1.10B) showed a two-step
weight loss within the same temperature range (30–320°C) used for the
DSC study. When samples were heated in a TGA a weight loss of 11.9%
occurred between 55 and 125°C. Stoichiometric calculation from the
molecular formula of creatine monohydrate indicates that it should con-
tain 12.07% (w/w) water. Therefore, the first endothermic event at 102°C
(Fig. 1.10B) was attributed to the dehydration of creatine monohydrate.

The second weight loss begins at 230°C, exactly at the temperature
where loss of one molecule of water occurs during the intramolecular
cyclization of creatine. If it were a polymorphic transition instead of
intramolecular cyclization, weight loss should not have been during this
transition. This confirms the validity of Pathway II over that of Pathway I.
Because these two events are occurring simultaneously, one should
expect overlaps of these two endothermic events [37].

A

SE1001-SS2-CRNINE-26 17 (0.337) Cm (11:36–8)

16:29:13
1: Scan ES+
3.17e5

227.2

100

%

136.0

249.1

177.1   250.2   307.0   362.2 385.1 420.1   498.1 521.1   579.0 634.1 657.1 692.0   770.1   828.3 885.8 906.1   963.6   995.0

0

B

SE1001-SS2-CRNE-26 18 (0.355) Cm (13:31–8)

1: Scan ES+
4.90e5

227.2

100

%

136.0

249.1

177.1 226.5   250.2 285.1   362.2 385.1   416.2 498.1   516.1 552.0   634.1   652.2 699.3 740.6   801.4   867.3 882.5   993.5

0

150   200   250   300   350   400   450   500   550   600   650   700   750   800   850   900   950   m/z

FIGURE 1.8   Mass Spectra of (A) creatine monohydrate heated to 260 °C and (B) creatinine heated to 260 °C.

4.6.4. Thermomicroscopy

A thermomicroscopic study was undertaken to confirm the weight loss observed during the TGA study, which was performed by placing about 0.1 mg of the sample with or without silicone oil on a glass slide covered by a glass cover slip. Samples were heated from 30 to 320°C at a programmed rate (10°C/min) on a hot stage (model FP900 Thermosystem, Mettler-Toledo AG, Greifensee, Switzerland). Physical changes (e.g., dehydration, phase transition, and melting) and chemical changes (e.g., degradation) were confirmed visually. A Pt-90 central processor and Pt-100 temperature sensor were used and a Nikonopitphot microscope (Nippon Kogaku, Garden City, NY) was attached to the hot stage. The hot stage microscope was calibrated by measuring the melting temperature of stearic acid (69–70°C). The observed melting temperature of stearic acid was 68–70°C, which was in agreement with the reported melting temperature of stearic acid (69–70°C) [37].

Figures 1.13A and B depict the thermomicrographs of creatine monohydrate in silicon oil immersion heated to 97 and 215°C, respectively. The liberation of bubbles through the silicone oil provided direct visual evidence of water loss from the sample within this temperature range. During the
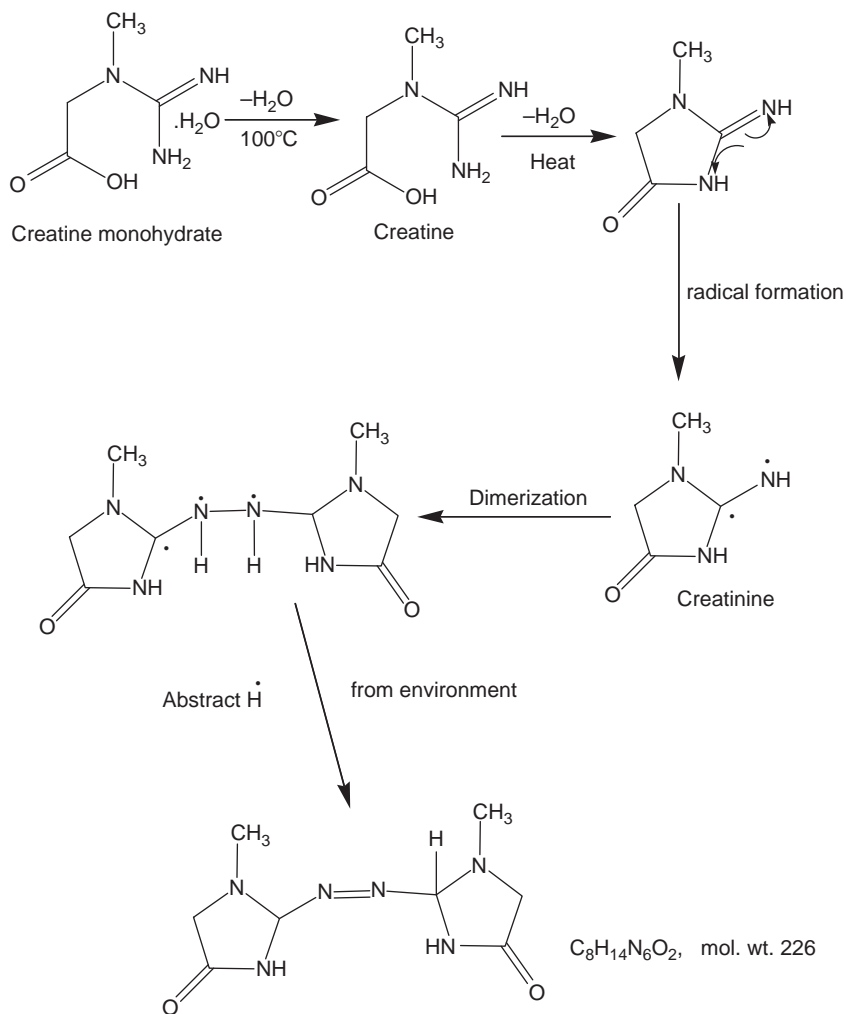
FIGURE 1.9 Possible pathways of dimerization of creatinine during the thermal transformation of creatine to creatinine.

thermomicroscopic studies without silicone oil immersion (Figs. 1.13C–F), it was observed that fine needle-like crystals appeared exactly at the same temperature range (230–260°C) corresponding to the second endothermic peak in DSC study (Fig. 1.10A), which has been hypothesized to be due to the formation creatinine by intramolecular cyclization of creatine monohydrate. The creatinine formed undergoes melt decomposition at around 280–320°C. Therefore, the last endothermic peak corresponds to the melting with decomposition of creatinine. Thermomicroscopic photographs of creatine monohydrate heated to 255 and 320°C are shown in Figs. 1.13E and F,
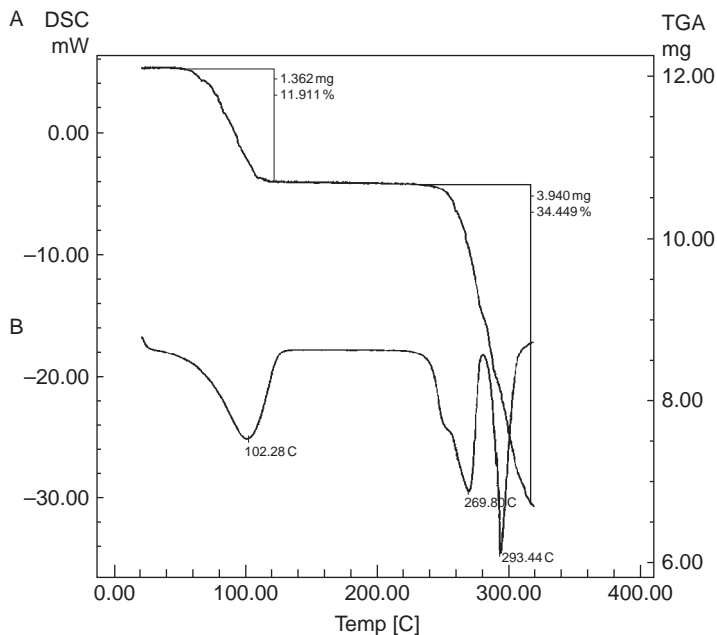
FIGURE 1.10 Differential scanning calorimetry (A) and thermogravimetric analysis (B) thermograms of creatine monohydrate.

respectively. Based on the direct visual evidence provided by thermomicroscopy, the final endotherm was further confirmed to be due to the decomposition of creatinine around 280–320°C as depicted in Fig. 1.13F [37].

4.7. Karl Fischer titrimetry

The total water content of creatine monohydrate was determined using a Karl Fischer titrimeter (Model CA-05 Moisture Meter, Mitsubishi, Japan). Sample sizes for this study ranged from 5 to 10 mg. The total water content of creatine monohydrate was found to be $11.53 \pm 0.19\%$ (w/w) (mean $\pm$ SD; $n = 3$). The result of the KFT study was in good agreement with the TGA results (4.6.3), which showed weight loss of 11.9% when creatine monohydrate was heated from 55 to 125°C (Fig. 1.10B) [37].

4.8. Solubility

Creatine monohydrate is only slightly soluble in water (i.e., 1 g in 75 ml at room temperature). The di-creatine salt has a higher aqueous solubility as compared with creatine monohydrate [38]. The solubility of creatine monohydrate at room temperature, creatine monohydrate samples heated to
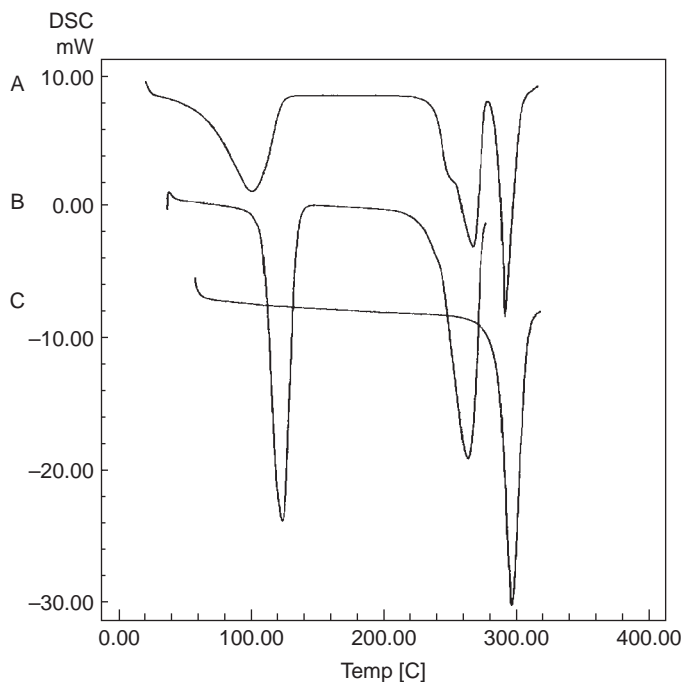
FIGURE 1.11   Differential scanning calorimetry curves of (A) creatine monohydrate heated from 30 to 320 °C, (B) creatine monohydrate heated from 30 to 270 °C, and (C) sample from (B) cooled to room temperature and reheated from 30 to 320 °C.

140°C (anhydrous creatine), and creatine monohydrate samples heated to 260°C (after the solid-state thermal transformation) were 27.97 ± 5.12, 69.67 ± 5.10, and, 79.46 ± 4.60 mg/ml (mean $\pm$ SD; $n = 3$), respectively [37]. Since the anhydrous form has a higher solubility relative to the monohydrate, one should expect a higher solubility for creatine monohydrate heated to 140°C (anhydrous form) as compared with the parent creatine monohydrate [39]. Since we have already confirmed that creatine is converted to creatinine around 230–260°C, one should also expect a higher solubility for creatine monohydrate sample heated to 260°C (which is virtually creatinine) as compared with creatine monohydrate. Creatinine is known to be more water-soluble than creatine monohydrate [38].

4.9. X-ray diffraction

Mendel and Hodgkin [40] elucidated the crystal structure of creatine monohydrate, using three-dimensional X-ray data that was analyzed using least-square calculations. Jensen [41] reported the crystal structure of creatine monohydrate using a two-dimensional model. Kato and
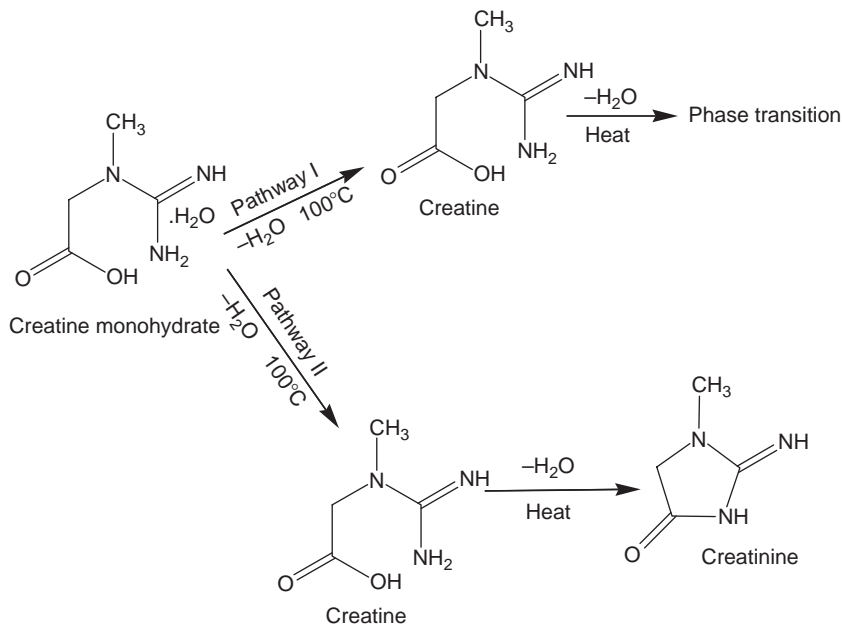
FIGURE 1.12 Two possible pathways of solid-state transformation of creatine monohydrate.

coworkers also described a refinement of the crystal structure of creatine monohydrate [42]. The latter study determined positions of the hydrogen molecules and confirmed the existence of a zwitterion in the solid-state of creatine monohydrate.

The powder patterns of commercially available creatine monohydrate were obtained in a wide angle powder X-ray diffractometer (Model XDS 2000, Scintag; CuKα radiation; 45 kV × 40 mA). The Bragg–Brentano focusing geometry was used, with a 1 mm incident slit, a 0.3 mm detector slit, and a solid-state germanium detector. Using a temperature controller attachment (Model 828D, Micristar, R.G. Hansen and Associates) mounted on the diffractometer, the sample could be subjected to a controlled temperature program ranging from −190 to +300°C. The samples were heated at 5 or 10°C/min from room temperature up to 270°C. This permitted XRD patterns to be obtained at the desired temperatures. However, during the XRD runs, the samples (150 mg) were maintained under isothermal conditions for 10 min at the selected temperatures. The angular range was 5–40° 2θ and data was collected in a continuous mode at chopper increments of 0.03° 2θ. When the scanning rate was 5° 2θ/min, the entire scan took about 11 min [37].

The variable temperature diffraction (VTXRD) patterns of creatine monohydrate sample heated to various temperatures are shown in
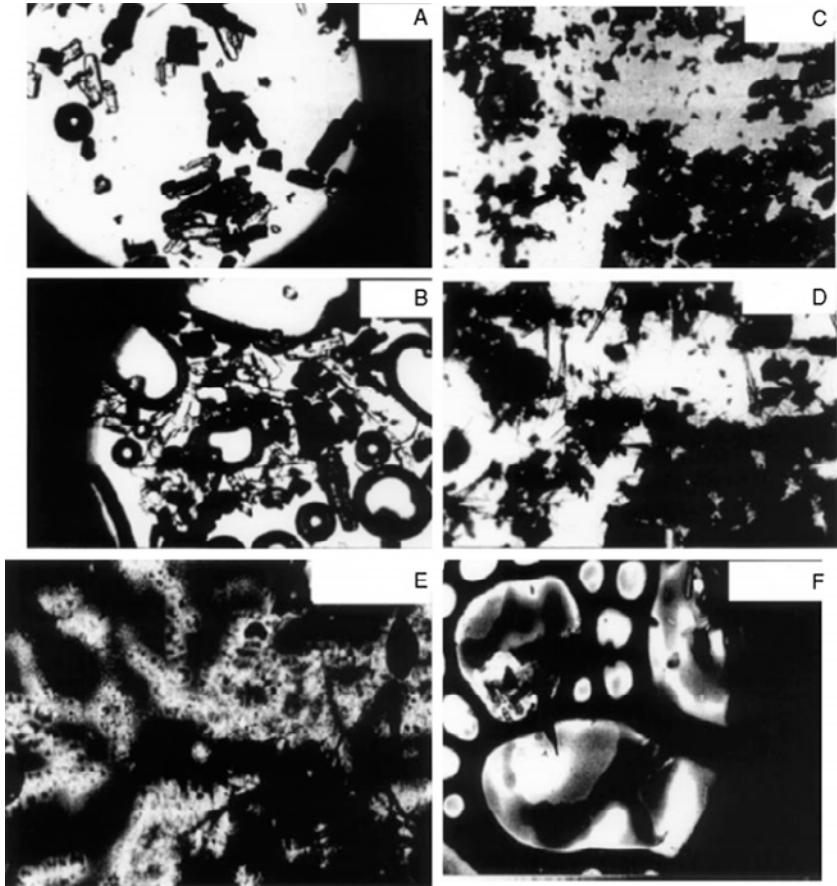
FIGURE 1.13 Thermomicroscopic photographs of creatine monohydrate subjected to
(A) 97 °C in a silicone oil immersion, (B) 215 °C in a silicone oil immersion, (C) room
temperature (before heating) without silicone oil, (D) 230 °C without silicone oil,
(E) 255 °C without silicone oil, and (F) 320 °C without silicone oil.

Fig. 1.14. The powder pattern of creatine monohydrate as depicted in
Fig. 1.14A was different from that of the sample heated to 140°C, that is,
after dehydration (Fig. 1.14B). The difference in the diffraction patterns
suggests the appearance of a phase change after dehydration.

VTXRD patterns, between 230 and 260°C as shown in Fig. 1.14D
provided supporting evidence for possible solid–solid transition of anhy-
drous creatine at region 230–260°C of DSC thermogram (Fig. 1.10A). The
X-ray diffraction patterns of creatine monohydrate samples heated to 140°C,
that is, after dehydration and prior to the second endothermic peak at 225°C
in the DSC curve, were identical as shown in Fig. 1.14A and B. However,
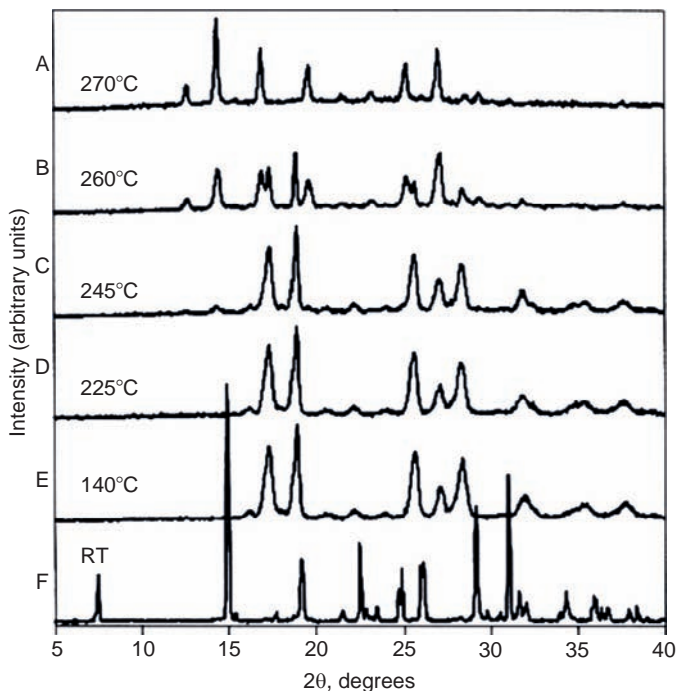
FIGURE 1.14   Variable temperature X-ray diffraction powder patterns of creatine monohydrate at (A) room temperature, (B) at 140 °C, (C) at 225 °C, (D) at 245 °C, (E) at 260 °C and (F) at 270 °C.

when the samples were heated to 245 and 260°C and subjected to powder X-ray analysis, appearance of some new peaks and decrease in the intensities of some existing peaks were clearly evidenced [37].

   To confirm the solid-state transformation of creatine to creatinine (as shown in pathway II of Fig. 1.12), creatinine (Acros Organics, NJ) was subjected to VTXRD, and the powder patterns are shown in Fig. 1.15. No differences in the powder patterns were noticed at different temperatures. The powder patterns of creatine monohydrate heated to 260°C and creatinine samples heated to the same temperature were then compared and presented in Fig. 1.16. Both the powder patterns were found to be identical, which confirms the solid-state transformation of creatine to creatinine around 230–260°C [37].

4.10. Partition behavior

The solubility of creatine in water has been reported to be ~13 mg/ml, with a calculated octanol/water partition coefficient of 2.7 [43].
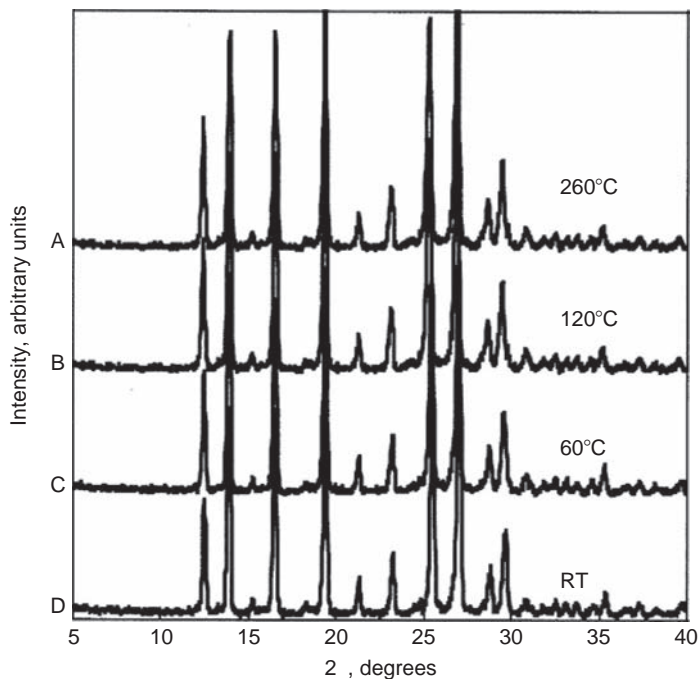
FIGURE 1.15 Variable temperature X-ray diffraction powder patterns of creatinine at (A) room temperature, (B) at 60 °C, (C) at 120 °C, and (D) at 260 °C.

4.11. Ionization constant

Creatine is characterized by an ionization constant of ~3, and is converted to creatinine in acidic conditions [44, 45].

5. METHODS OF ANALYSIS

5.1. Chromatographic methods of analysis

The percentage adsorption of creatine by different hydrous oxides and Fuller's earth has been reported [46]. Various chromatographic techniques have been used for the analysis of creatine.

5.1.1. Thin layer chromatography

Separation and quantification of creatine from creatine phosphate and other naturally occurring phosphorous compounds has been reported by Breccia *et al.* [47]. This method describes the use of a cellulose thin layer chromatographic (TLC) method using various solvent systems. Creatine can be separated and quantified from creatine phosphate, dextrose,
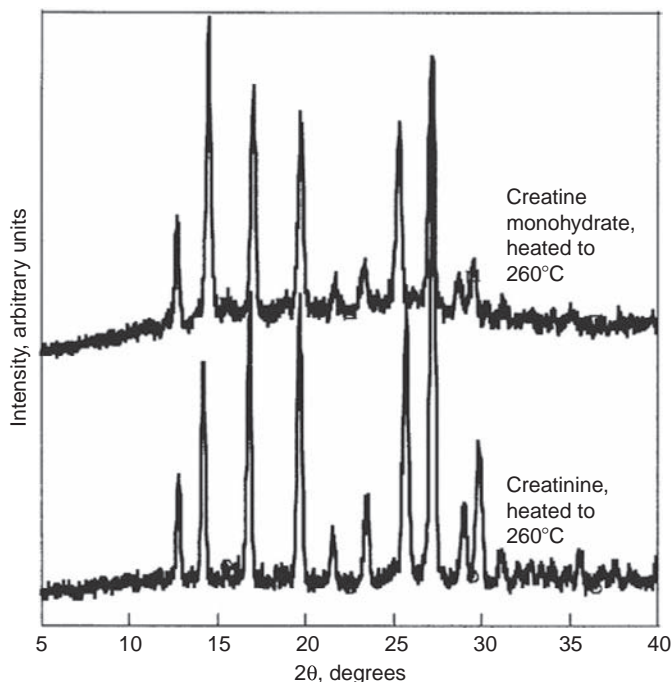
FIGURE 1.16   Comparison of the X-ray diffraction patterns of creatine monohydrate heated to 260 °C versus creatinine heated to 260 °C.

glycerol, choline, and other naturally occurring phosphorylated compounds. Another TLC method has been reported for quantifying creatine in nutritional supplement [48]. This method uses silica gel HPTLC plates with fluorescent indicator and automated UV absorption densitometry.

A simple, rapid, and economic TLC method for the simultaneous screening and quantitation of creatine along with creatinine and uric acid in biological samples such as urine or serum has been reported [49]. This method consisted of separation on an amino-modified HPTLC precoated plate and detection is performed by simply heating the chromatogram to yield stable fluorescent derivatives.

5.1.2. High pressure liquid chromatography

Various HPLC methods have been reported for the analysis of creatine [50, 51]. A simple HPLC method with UV detection was reported [52] for creatine and creatinine, which is also applicable in several creatine formulations. The chromatographic system was comprised of a LC-600 pump, SCL-6B system controller, and SPD-6AV detector (Shimadzu, Japan). The mobile phase consisted of 0.045 M ammonium sulfate in water. The chromatographic separation was achieved at ambient temperature on a

Betabasic C-18 column (250 × 4.6 mm, Keystone Sci.). The flow rate was maintained at 0.75 ml/min and effluents are monitored at 205 nm. 4-(2-Aminoethyl) benzene sulfonamide was used as an internal standard. This method required less than 7 min of chromatographic time. The standard curves were linear over the concentration range of 1–100 μg/ml for creatine and 2–100 μg/ml for creatinine, respectively. This method was used to determine: (i) the creatine concentration in various marketed products; (ii) saturated solubility of various creatine salts; and (iii) stability of creatine in aqueous solution. Di-creatine citrate salt showed a higher aqueous solubility (at 25°C) as compared with creatine and creatine monohydrate. Some of the over-the-counter (OTC) products tested contained a very low level of creatine in contrast to their label claim. Substantial conversion of creatine into creatinine was noticed in liquid formulation.

An HPLC method has been reported for the determination of creatine in aqueous solutions as well as in rat plasma using electrochemical detection [53]. Electrochemical detection also offers some potential advantages for future work in situations such as: (i) when direct analysis of samples with minimal sample volume is needed, and (ii) when online detection is essential to determine the tissue distribution of this analyte (e.g., microdialysis sampling techniques). The chromatographic system consisted of a GP50 gradient pump, an ED40 pulsed electrochemical detector, and an AI-450 chromatography automation system (Dionex). The mobile phase consisted of a mixture of water, acetonitrile, 0.01 M sodium acetate, and 1.0 M sodium hydroxide (2.5 : 2.5 : 90 : 5, v/v/v/v) at a flow rate of 1.0 ml/min. The chromatographic separation was achieved at 45 °C on a column with a polyhydroxylated glucose and sulfonated stationary phase. The retention times of creatine and creatinine was 3.50 and 4.73 min, respectively, with creatine fully resolved from its major degradation product, creatinine. The standard curves were linear over the concentration range of 0–20 μg/ml. Within-day and day-to-day relative standard deviations (RSD) were less than 10%. This method was used to study dissolution characteristics of various creatine salts in water [52, 53].

5.1.3. Gas chromatography

A gas chromatography–mass spectrometric (GC–MS) analysis method for creatine was reported recently [54], which is applicable to biological samples as well. Creatine must be derivatized to allow passage through the GC, but in most cases it forms the same derivative as creatinine, necessitating separation of creatine before pursuing its derivatization [55]. Creatine was selectively derivatized by adding 500 μl of its sample (1 mM creatine) to equal amount of 0.4 M acetate buffer (pH 4.2), followed by the addition of 250 μl of 8 mM of 1-pyrenyldiazomethane (PDAM) in

acetone. Samples were vortexed for 30 s at room temperature to ensure that the reaction was complete.

Samples were extracted by immersing an 85 mm polyacrylate SPME fiber in NaCl saturated solutions of PDAM–creatine. The fiber was desorbed for each sample for 30 s at 230 °C. The initial oven temperature was 40°C for 5 min, followed by ramping at 10°C/min until reaching a final temperature of 300 °C. Chromatographic separation was achieved using a 30 m × 0.24 mm × 0.2 mm dimethylsiloxane column at a flow rate of 1.0 ml/min.

A GC analysis of creatine is difficult owing to its polar nature. Following derivatization with PDAM, the thermal stability of creatine increased significantly. As a result, it was more effectively introduced into the gas phase for subsequent MS analysis. Unstabilized creatine has difficulty entering the gas phase, with the resultant mass spectrum displaying poor relative abundance and fragment stability. In contrast, the PDAM-stabilized creatine is carried much more readily into the gas phase as evidenced by more intense fragment peaks and a more stable fragment pattern.

5.1.4. Cation exchange chromatography

A simple and versatile cation-exchange chromatography technique for the determination of creatine in urine has been reported [56], which uses a novel low-capacity cation-exchange column packed with sulfoacylated hypercross-linked macroreticular polystyrene–divinylbenzene resin and a binary dual-mode gradient eluting system. Chromatographic conditions consisted of mobile phase composed of: (A) 25 mM phosphoric acid–methanol (30:70, v/v) and (B) 25 mM disodium hydrogen phosphate–methanol (30:70, v/v) which were used by mixing in a stepwise manner by a time-programming B% from the delivery control pump for solvent (A). Other chromatographic conditions were column temperature, 40°C; detection, UV at 210 nm; and sample size 50 μl. The minimum concentration of creatine detected was 0.02 μM.

5.1.5. Liquid chromatography coupled mass spectrometry

Separation and identification of creatine along with 19 amino acids and related compounds was achieved in less than 3 min using a liquid chromatographic equipment coupled with a time-of-flight mass spectrometer [57]. The mass spectrometric experimental conditions used were: Unique® LC-TOFMS with high flow ESI source (Leco Corporation), 65 V nozzle voltage, 250°C desolvation temperature, 3000 V electrospray voltage, 7.5 l/min desolvation flow of nitrogen, 100°C interface temperature, 425 kPa nebulization pressure (N_2), and 0.2 ml/min to source; 1.8 ml to waste split flow. Tetramethylammonium chloride was used as external mass calibrant. Liquid chromatographic conditions used were: 1100 series

Creatine + H$_2$O $\xrightarrow{\text{Creatine amidinohydrolase}}$ Urea + Sarcosine

Sarcosine + H$_2$O + O$_2$ $\xrightarrow{\text{Sarcosine oxidase}}$ Glycine + Formaldehyde + H$_2$O$_2$

H$_2$O$_2$ + 3,5-dichloro-2-hydroxybenzenesulfonic acid + 4-aminiophenazone

K$_4$Fe(CN)$_6$

↓

K$_3$Fe(CN)$_6$

Horseradish peroxidase

Quinone-monoimine dye + 2H$_2$O + HCl
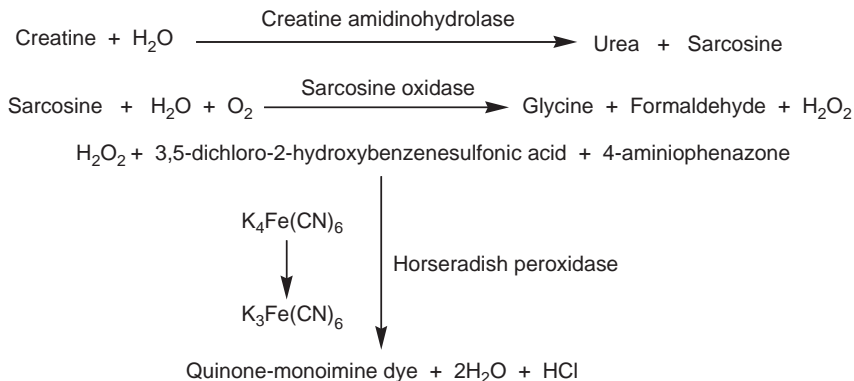
FIGURE 1.17 Reactions involved in the enzymatic assay of creatine.

LC (Agilent Technologies, Wilmington, Delaware), 2.0 ml/min flow rate, 1 mM aqueous perfluoroheptanoic acid as mobile phase A, acetonitrile as mobile phase B, gradient flow pattern (100% A to 80% A in 30 s to 60% A in 2 min; 100% A at 2:05 min), 1 μl injection volume, and a reverse phase column (Chromolith Performance RP-18e 100 × 4.6 mm; Merck KGaA, Darmstadt, Germany). Test solutions used were amino acids standard 0.05 mmol/ml (Pierce H), hydroxyproline, and creatine 0.01 μmol/ml.

5.2. Biological

A colorimetric enzyme-based assay has been reported which can be used for measuring creatine even in serum or urine [58, 59]. Creatine is sequentially assayed in reactions catalyzed by creatine amidinohydrolase and sarcosine oxidase that result in the production of hydrogen peroxide. This product is measured spectrophotometrically at 510 nm in a reaction catalyzed by horseradish peroxidase with 3,5-dichloro-2-hydroxybenzene-sulfonic acid/4-aminophenazone as the chromogen (Fig. 1.17).

6. STABILITY AND DEGRADATION

Creatine is stable under ordinary conditions of use and storage. Solid creatine monohydrate dehydrates to anhydrous creatine after the evolution of 1 mol of water by heating at 97–125°C. Anhydrous creatine undergoes an intramolecular cyclization accompanied by a loss of 1 molecule of water (Fig. 1.12) to form creatinine which undergoes melting with decomposition around 280–310°C [60].

The stability of creatine in solution, prepared from di-creatine citrate, has been reported, where it changes to creatine under acidic conditions [44, 61]. In presence of water, creatine forms creatine monohydrate, which crystallizes out from solution on long term storage because of its poor solubility relative to that of soluble di-creatine citrate. This was confirmed by the DSC thermograms and XRD patterns of the crystallized samples obtained after filtering the di-creatine citrate solution. DSC thermograms and XRD patterns of the sample were similar to those of creatine monohydrate but were different from those of di-creatine citrate.

7. PHARMACOKINETICS, METABOLISM, AND TOXICITY

7.1. Pharmacokinetics

Creatine supplementation has been investigated as a possible therapeutic approach for the treatment of muscular, neurological, and neuromuscular diseases. The success of creatine in the treatment of various diseases is dependent on the understanding of its pharmacokinetic (i.e., volume of distribution, clearance, bioavailability, mean residence time, absorption rate, and half-life) behavior which are discussed below.

7.1.1. Absorption and plasma concentration

The bioavailability of various creatine dosage forms such as solutions, suspensions, and lozenges was compared, and maximal peak plasma concentrations (C_{max}) were found for the solution formulation relative to the suspension and lozenge formulations [62]. The area under the concentration–time curve (AUC) for the solution formulation was determined to be greater than that with lozenge or suspension formulations [63].

The mechanism of creatine absorption in the gastrointestinal tract is poorly understood. An mRNA involved in creatine transport has been identified which suggest the possibility of active transport mechanism [64]. Moreover, creatine is structurally similar to basic amino acids (e.g., arginine and lysine) and may enter the systemic circulation through the amino acid transporter or peptide transporters located in the small intestine. Creatine is a hydrophilic and polar molecule containing carboxyl and guanidine functional groups possessing negative and positive charges, respectively which would hinder its passive diffusion through membranes. Active transport mechanism is further supported by poor apical-to-basolateral transport of creatine through caco-2 cell layers [60].

Although creatine is not subjected to first-pass metabolism, the bioavailability is less than 100% after oral administration. The rate of formation of its degradation product, creatinine, is increased in presence of acid and therefore accelerated degradation is possible in the lower pH of the

stomach. The degradation half-lives for the conversion of creatine to creatinine at pH values 1.4, 3.7, and 6.8 are 55, 7.5, and 40.5 days, respectively [63]. At these rates, less than 0.1 g of a 5 g dose would be lost in 1 h. Therefore, conversion of creatine to creatinine is of minimum concern, regardless of its transit time in gastrointestinal tract. Furthermore, there is evidence that fecal excretion of creatine is increased with a higher creatine intake and gut flora have ability to metabolize creatine into creatinine [65,66]. Creatine t_{max} in humans can be <2 h for oral doses of less than 10 g [67,68]. At doses above 10 g, t_{max} increases to >3 h. A steady-state like plateau is observed when the dose is increased to 20 mg, which suggest zero-order absorption as a function of saturation of gastrointestinal transporters. t_{max} is also found to increase with coadministration of carbohydrates [63].

7.1.2. Volume of distribution and protein binding

Creatine is distributed to blood cells, brain and nervous tissue, cardiac muscle, spermatozoa, and the retina. However, the main depository is skeletal muscle [33]. If diffusion is the only mechanism controlling its distribution, the apparent volume of distribution probably should not exceed extracellular water because of the polar nature of creatine. Plasma protein binding is also expected to be negligible because of the hydrophilicity of the creatine molecule, which results in high free levels of creatine available as substrate for the creatine transporter. The presence of creatine transporter suggests a volume of distribution greater than the predicted extracellular water, approaching that of total body water [68]. Moreover, skeletal muscle has a finite storage capacity which results in decrease in volume of distribution with repeated administration of creatine because of the saturation of storage capacity. Furthermore, the accumulation and subsequent saturation may be a result of possible downregulation of creatine transporter number or function.

7.1.3. Fluid and tissue penetration

Sodium- and chloride-dependent transporters that are similar in structure to the transporters for dopamine, γ-aminobutyric acid (GABA), and taurine, have been involved in creatine transport into tissues against a large concentration gradient [18]. The creatine transporter gene, Crea T1, is located in a variety of tissues including kidney, heart, skeletal muscle, brain, testes, colon, and intestine while Crea T2 is limited to testes. Activation of creatine transporters and their increased translocation in the muscle membrane, rather than increased blood flow, are hypothesized for the increase in creatine uptake with exercise [69]. Creatine is distributed throughout the body, with more than 95% of total creatine being found in skeletal muscle and the remaining located in the brain, eye, kidney, and testes.

7.1.4. Half-life

There is a lack of data regarding disposition of creatine in blood after intravenous administration. A half-life in plasma of 20–70 min was reported when about 3 mg of radiolabeled creatine was injected into five patients with various muscular disorders [70]. Three patients showed mono-exponential decline of creatine but two patients, who were older and heavier, showed bi-exponential decline. The wide variation in half-life might be due to age because older age is associated with reduction in the creatine transporter [63]. The above half-life value is not significant in actual practice, where a loading dose of 20 g/day followed by maintenance dose of 2 g/day is used. Creatine levels in humans are reported to remain elevated up to 1 month post-supplementation, in part due to lack of passive movement of creatine out of the cell and the slow turn over of creatine to creatinine [71].

7.1.5. Influence of age on pharmacokinetic parameters

In one study, blood levels of creatine were compared after a 5 g dose in young and elderly (>60 years) healthy men [68]. No statistically significant difference in terminal half-life, AUC, C_{max}, or t_{max} was found between these two groups, but in elderly men the intramuscular PCr level did not increase and clearance was lower. Since both the groups had similar renal excretion rates, the difference in clearance may be due to skeletal muscle differences [63].

7.1.6. Influence of diet on pharmacokinetic parameters

Various studies have investigated the effect of insulin and carbohydrate on the AUC after oral administration of creatine. In one study [72], creatine was infused (100 mmol/l at 2.5 ml/min) along with an insulin infusion of 5 mU/m^2/min. The results suggested an apparent clearance of 15–20 l/h depending on the infusion rate, with the slower insulin rate eliciting a smaller clearance. On the contrary, a threefold reduction in plasma creatine AUC was found when 5 g of creatine was ingested with a simple sugar solution [73]. Other have reported that the ingestion of carbohydrate and/or protein increases whole body creatine retention by decreasing plasma AUC and decreasing urine output [67].

7.1.7. Influence of disease on the pharmacokinetic parameters

Patients with muscular dystrophy can have hypercreatinaemia and creatinuria, along with lower muscle levels of creatine and PCr [74]. Patients with failing hearts [75] and populations with myopathies [2] have shown lower CreaT1 content and lower creatine and PCr levels. Inborn errors in creatine metabolism have been reported in case of gyrate atrophy [76].

An intravenous bolus of creatine was administered in five patients, three of whom had primary muscle disease and two did not [70]. Patients with primary muscle disease demonstrated an average half-life of 50 min, and 24 min in case of without primary muscle disease. This difference in the half-life was hypothesized due to differences in creatine uptake by skeletal muscle and decreases in creatine trapping by skeletal muscle in specific patient populations [74].

7.2. Metabolism

Creatine and phosphocreatinine are nonenzymatically degraded to creatinine at a rate of 2 g/day, which is based on assumption of total body weight of 70 kg, total creatine pool of 120 g, and a rate constant (k_{cm}) of 0.0017 per day [77]. Creatine and creatinine are both eliminated from the body via the kidney. Supplementation with exogenous creatine has been found to reduce the endogenous production; however, normal level returns upon termination of supplementation.

7.2.1. Clearance

Creatine can be removed from the body by both the skeletal muscle as well as by the kidney. The relative contribution of skeletal muscle and kidney in the total creatine clearance depends on the dose and frequency of creatine supplementation. For example, with the first dose, creatine clearance can rely on both muscle and kidney, but after a number of doses, when muscle creatine stores are saturated, clearance may occur only via the kidney [63].

Creatine uptake in muscle is a pseudo-irreversible process and its subsequent conversion to PCr and creatinine is responsible for its clearance from skeletal muscle. It has been found that creatine clearance in nonmuscle compartment occurs at a faster rate than in the muscle compartment [74].

Some researchers have reported the rate of renal excretion close to glomerular filtration rate (GFR) [78], although others have reported that creatine is reabsorbed in the kidney [79]. This is supported by the low creatine concentration in urine in unsupplemented conditions and the location of the creatine transporters in the kidney. With supplementation, renal creatine clearance (CL_R) was found to increase to 9–22 l/h which is close to GFR (7.5 l/h) to well above GFR suggesting active secretion [80].

7.3. Toxicity

There is no strong scientific evidence to support any toxicity or adverse effects from creatine supplementation. Most of the reports have been minor in nature and purely anecdotal; however, caution should still be

used while taking creatine for long time because studies investigating its long-term effect in humans are lacking [81].

There are reports that creatine can cause gastrointestinal pain, nausea, and diarrhea [82] muscle cramping. However, a double-blinded study involving a placebo indicated no such effects [83]. In one study it was demonstrated that the renal excretion of creatinine increased in response to an acute creatine monohydrate dose, which suggests that the kidneys can respond to an increase in creatine level by excreting extra creatinine [84]. Creatine typically causes a weight gain that increases with its continued use [85], which is most likely due to water retention and hence has been thought to increase the risk for high blood pressure. However, a recent study showed no effect of 20 g daily of creatine for 5 days on blood pressure [86].

There are some reports that suggest combining caffeine, ephedra, and creatine might increase the risk of serious adverse effects. An athlete suffered a serious ischemic stroke after consuming creatine monohydrate 6 g, caffeine 400–600 mg, and ephedra 40–60 mg for 6 weeks [87]. Caffeine might also decrease the beneficial effects of creatine on athletic performance possibly by inhibiting PCr resynthesis [88]. High doses of creatine might adversely affect renal function, combining it with potentially nephrotoxic drugs (cyclosporine, aminoglycosides, nonsteroidal antiinflammatory drugs, etc.) might have additive harmful effect on kidney function [82].

ACKNOWLEDGMENTS

REFERENCES

[1] M. H. Williams, R. B. Kreider and J. D. Branch, *Creatine: The Power supplement*, Human Kinetics, Champaign, IL, 1999, pp. 6.
[2] M. A. Tarnopolsky, G. Parise, N. J. Yardley, C. S. Ballantyne, S. Olatinji and S. M. Phillips, *Med. Sci. Sports Exerc.*, 2001, **33**, 2044–2052.
[3] Wikipedia contributors, Creatine, *Wikipedia, The Free Encyclopedia*, Retrieved 19:17, January 5, 2006 from, 2006 http://en.wikipedia.org/w/index.php?title=Creatine&oldid=33934016.
[4] J. Volek and W. Kraemer, *J. Strength Cond. Res.*, 1996, **10**, 200–210.
[5] S. B. Racette and J. Orthop, *Sports Phys. Ther.*, 2003, **33**, 615–621.
[6] M. G. Bemben and H. S. Lamont, *Sports Med.*, 2005, **35**, 107–125.
[7] P. Hespel, R. J. Maughan and P. L. Greenhaff, *J. Sports Sci.*, 2006, **24**, 749–761.
[8] L. S. Almeida, G. S. Salomons, F. Hogenboom, C. Jakobs and A. N. Schoffelmeer, *Synapse*, 2006, **60**, 118–123.
[9] M. Balestrino, R. Rebaudo and G. Lunardi, *Brain Res.*, 1999, **816**, 124–130.
[10] M. A. Brudnak, *Toxicol. Lett.*, 2004, **150**, 123–130.

[11] L. B. Menalled and M. F. Chesselet, *Trends Pharmacol. Sci.*, 2002, **23**, 32–39.

[12] R. J. Ferrante, O. A. Andreassen, B. G. Jenkins, A. Dedeoglu, S. Kuemmerle, J. K. Kubilus, R. K. Daouk, S. M. Hersch and M. F. Beal, *J. Neurosci.*, 2000, **20**, 4389–4397.

[13] O. A. Andreassen, A. Dedeoglu, R. J. Ferrante, B. G. Jenkins, K. L. Ferrante, M. Thomas, A. Friedlich[e], S. E. Browne[e], G. Schilling[g], D. R. Borchelt[g], S. M. Hersch[h], C. A. Ross[i], *et al*. *Neurobiol. Dis.*, 2001, **8**, 479–491.

[14] A. Bender, D. P. Auer, T. Merl, R. Reilmann, P. Saemann, A. Yassouridis, J. Bender, A. Weindl, M. Dose, T. Gasser and T. Klopstock, *J. Neurol.*, 2005, **252**, 36–41.

[15] A. C. Ellis and J. Rosenfeld, *CNS Drugs*, 2004, **18**, 967–980.

[16] L. Mazzini, C. Balzarini, R. Colombo, G. Mora, I. Pastore, R. De Ambrogio and M. Caligari, *J. Neurol. Sci.*, 2001, **191**, 139–144.

[17] M. A. Tarnopolsky, *Curr. Opin. Clin. Nutr. Metab. Care*, 2000, **3**, 497–502.

[18] R. J. Snow and R. M. Murphy, *Mol. Cell. Biochem.*, 2001, **224**, 169–181.

[19] R. M. Tombes and B. M. Shapiro, *Cell*, 1985, **41**, 325–334.

[20] C. J. Xu, W. E. Klunk, J. N. Kanfer, Q. Xiong, G. Miller and J. W. Pettegrew, *J. Bio. Chem.*, 1996, **27**, 13435–13440.

[21] J. M. Lawler, W. S. Barnes, G. Wu, W. Song and S. Demaree, *Biochem. Biophys. Res. Commun.*, 2002, **290**, 47–52.

[22] B. Willer, G. Stucki, H. Hoppeler, P. Brühlmann and S. Krähenbühl, *Rheumatology*, 2000, **39**, 293–298.

[23] M. T. Hove, S. Chan, C. Lygate, M. Monfared, E. Boehm, K. Hulbert, H. Watkins, K. Clarke and S. Neubauer, *J. Mol. Cell. Cardiol.*, 2005, **38**, 309–313.

[24] K. Heinanen, K. Nanto-Salonen, M. Komu, M. Erkintalo, A. Alanen, O. J. Heinonen, K. Pulkki, E. Nikoskelainen, I. Sipila and O. Simell, *Eur. J. Clin. Invest.*, 1999, **29**, 1060–1065.

[25] P. Hespel, B. Op't Eijnde, M. V. Leemputte, B. Ursø, P. L. Greenhaff, V. Labarque, S. Dymarkowski, P. V. Hecke and E. A. Richter, *J. Physiol.*, 2001, **536**, 625–633.

[26] M. Vorgerd, J. Zange, R. Kley, T. Grehl, A. Hüsing, M. Jäger, K. Müller, R. Schröder, W. Mortier, K. Fabian, J. P. Malin and A. Luttmann, *Arch. Neurol.*, 2002, **59**, 97–101.

[27] D. J. Mahoney, G. Parise and M. A. Tarnopolsky, *Curr. Opin. Clin. Nutr. Meta. Care*, 2002, **5**, 619–629.

[28] M. A. Tarnopolsky, A. Parshad, B. Walzel, U. Schlattner and T. Wallimann, *Muscle Nerve*, 2001, **24**, 682–688.

[29] M. C. Walter, H. Lochmüller, P. Reilich, T. Klopstock, R. Huber, M. Hartard, M. Hennig, D. Pongratz and W. Müller–Felber, *Neurology*, 2000, **54**, 1848–1850.

[30] R. C. Harris, K. Soderlund and E. Hultman, *Clin. Sci.*, 1992, **83**, 367–374.

[31] *The Merck Index*, 13th edn., Merck and Co., Inc., Whitehouse Station, N.J., U.S.A, 2001, p. 450.

[32] H. H. Beard, Origin of creatine, *Creatine and Creatinine Metabolism*, Chemical Publishing Co., Inc, Brooklyn, New York, 1943, p. 49.

[33] M. Wyss and R. Kaddurah-Daouk, *Physiol. Rev.*, 2000, **80**, 1107–1213.

[34] Coblentz Society, Inc., ''Evaluated Infrared Reference Spectra'' in NIST Chemistry WebBook, NIST Standard Reference Database Number 69, Eds. P. J. Linstrom and W. G. Mallard, June 2005, National Institute of Standards and Technology, Gaithersburg MD, p. 20899 (Http://webbook.nist.gov).

[35] A. L. Smith, The coblentz society desk book of infrared spectra, in *The Coblentz Society Desk Book of Infrared Spectra* (ed. C. D. Carvered.), 3rd edn., The Coblentz Society, Kirkwood, MO, 1982, pp. 1–24.

[36] NIST Mass Spec Data Center, S.E. Stein, director, ''Mass Spectra'' in NIST Chemistry WebBook, NIST Standard Reference Database Number 69, Eds. Linstrom and W. G. Mallard June 2005, National Institute of Standards and Technology, Gaithersburg MD, p. 20899 (Http://webbook.nist.gov).

[37] A. K. Dash, Y. Mo and A. Pyne, *J. Pharm. Sci.*, 2002, **91**, 708–718.

[38] S. Budavari, *The Merck Index*, 11th edn., Merck and Co. Inc., Rahway, NJ, 1989, p. 2577.

[39] D. Grant and H. Brittain, Solubility of pharmaceutical solids, in *Physical Characterization of Pharmaceutical Solids,* (ed. H.G Brittained.), 1st edn., Marcel Dekker, New York, 1995, pp. 321–386.

[40] H. Mendel and D. C. Hodgkin, *Acta Crystallogr.*, 1954, **7**, 443–446.

[41] L. H. Jensen, *Acta Crystallogr.*, 1955, **8**, 237–240.

[42] Y. Kato, Y. Haimoto and K. Sakurai, *Bull. Chem. Soc. Jpn.*, 1979, **52**, 233–234.

[43] A. Persky and G. Brazeau, *Pharmacol. Rev.*, 2001, **53**, 161–176.

[44] G. Edgar and H. Shiver, *J. Am. Chem. Soc.*, 1925, **47**, 1170–1188.

[45] R. Cannan and A. Shore, *Biochem. J.*, 1928, **22**, 921–929.

[46] D. P. Grettie and R. J. Williams, *J. Am. Chem. Soc.*, 1928, **50**, 668–672.

[47] A. Breccia, A. Fini, S. Girotti and E. Salatelli, *Boll. Chim. Farm.*, 1983, **122**, 556–559.

[48] S. D. Wagner, S. W. Kaufer and J. Sherma, *J. Liq. Chrom. Rel. Tech.*, 2001, **24**, 2525–2530.

[49] R. Klaus, W. Fischer and H. E. Hauck, *Chromatographia*, 1991, **32**, 307–316.

[50] E. Harmsen, P. P. De Tombe and J. W. De Jong, *J. Chromatogr.*, 1982, **230**, 131–136.

[51] M. Tranberg, M. H. Stridh, B. Jilderos, S. G. Weber and M. Sandberg, *Anal. Biochem.*, 2005, **343**, 179–182.

[52] A. K. Dash and A. Sawhney, *J. Pharm. Biomed. Anal.*, 2002, **29**, 939–945.

[53] Y. Mo, D. Dobberpuhl and A. K. Dash, *J. Pharm. Biomed. Anal.*, 2003, **24**, 125–132.

[54] L. MacNeil, L. Hill, D. MacDonald, L. Keefe, J. F. Cormier, D. G. Burke and T. Smith-Palmer, *J. Chromatogr. B Analyt. Technol. Biomed. Life Sci.*, 2005, **827**, 210–215.

[55] L. Seikmann, *J. Clin. Chem. Biochem.*, 1985, **23**, 371–376.

[56] Y. Yokoyama, S. Tsuji and H. Sato, *J. Chromatogr. A*, 2005, **1085**, 110–116.

[57] P. Kennedy, *Biol. Advertising Suppl. The Application Note book, Leco Corporation,* 2006, **24**.

[58] P. Fossati, L. Prenclpe and G. Bert, *Clin. Chem.*, 1963, **29**, 1494–1496.

[59] J. A. Weber and A. P. van Zanten, *Clin. Chem.*, 1991, **37**, 695–700.

[60] A. K. Dash, D. W. Miller, H. Y. Han, J. Carnazzo and J. R. Stout, *J. Pharm. Sci.*, 2001, **90**, 1593–1598.

[61] S. Ganguly, S. Jayappa and A. K. Dash, *AAPS Pharm. Sci. Tech.*, **4**, Article 26. ***

[62] R. C. Harris, M. Nevill, D. B. Harris, J. L. Fallowfield, G. C. Bogdanis and J. A. Wise, *J. Sports Sci.*, 2002, **20**, 147–151.

[63] A. M. Persky, G. A. Braze and G. Hochhaus, *Clin. Pharmacokinet.*, 2003, **42**, 557–574.

[64] S. R. Nash, B. Giros, S. F. Kingsmore, J. M. Rochelle, S. T. Suter, P. Gregor, M. F. Seldin and M. G. Caron, *Recept. Channels*, 1994, **2**, 165–174.

[65] R. L. Wixom, G. E. Davis, M. A. Flynn, R. T. Tsutakawa and D. J. Hentges, *Proc. Soc. Exp. Biol. Med.*, 1979, **161**, 452–457.

[66] F. Twort and E. Mellanby, *J. Physiol.*, 1912, **44**, 43–49.

[67] G. R. Steenge, E. J. Simpson and P. L. Greenhalff, *J. Appl. Physiol.*, 2000, **89**, 1165–1171.

[68] E. S. Rawson, P. M. Clarkson, T. B. Price and M. P. Miles, *Acta Physiol. Scand.*, 2002, **174**, 57–65.

[69] T. M. Robinson, D. A. Sewell, E. Hultman and P. L. Greenhaff, *J. Appl. Physiol.*, 1999, **87**, 598–604.

[70] C. D. Fitch and D. Sinton, *J. Clin. Invest.*, 1964, **43**, 444–452.

[71] E. Hultman, K. Soderlund, J. A. Timmons, G. Cederblad and P. L. Greenhaff, *J. Appl. Physiol.*, 1996, **81**, 232–237.

[72] G. R. Steenge, J. Lambourne, A. Casey, I. A. Macdonald and P. L. Greenhaff, *Am. J. Physiol.*, 1998, **275**, E974–E979.

[73] A. L. Green, E. Hultman, I. A. Macdonald, D. A. Sewell and P. L. Greenhaff, *Am. J. Physiol.*, 1996, **271**, E821–E826.

[74] C. D. Fitch, R. P. Shields, W. F. Payne and J. M. Dacus, *J. Biol. Chem.*, 1968, **243**, 2024–2027.

[75] S. Neubauer, H. Remkes, M. Spindler, M. Horn, F. Wiesmann, J. Prestle, B. Walzel, G. Ertl, G. Hasenfuss and T. Wallimann, *Circulation*, 1999, **100**, 1847–1850.

[76] K. Vannas-Sulonen, I. Sipila, A. Vannas, O. Simell and J. Rapola, *Ophthalmology*, 1985, **12**, 1719–1727.

[77] J. Walker, *Adv. Enzymol. Relat. Areas Mol. Biol.*, 1979, **50**, 117–242.

[78] R. F. Pitts, *Am. J. Physiol.*, 1934, **109**, 532–541.

[79] E. Sims and D. Seldin, *Am. J. Physiol.*, 1949, **157**, 14–20.

[80] J. R. Poortmans and M. Francaux, *Mol. Sci. Sports Exerc.*, 1999, **31**, 1108–1110.

[81] M. G. Bemben and H. S. Lamont, *Sports Med.*, 2005, **35**, 107–125.

[82] R. L. Terjung, P. Clarkson, E. R. Eichner, P. L. Greenhaff, P. J. Hespel, R. G. Israel, W. J. Kraemer, R. A. Meyer, L. L. Spriet, M. A. Tarnopolsky, A. J. Wagenmakers and M. H. Williams, *Med. Sci. Sports Exerc.*, 2000, **32**, 706–717.

[83] L. M. Romer, J. P. Barrington and A. F. Jeukendrup, *Int. J. Sports Med.*, 2001, **22**, 546–552.

[84] S. Bermon, P. Venembre, C. Sachet, S. Valour and C. Dolisi, *Acta Physiol. Scand.*, 1998, **164**, 147–155.

[85] M. S. Juhn and M. Tarnopolsky, *Clin. J. Sport Med.*, 1998, **8**, 298–304.

[86] S. Mihic, J. R. MacDonald, S. McKenzie and M. A. Tarnopolsky, *Med. Sci. Sports Exerc.*, 2000, **32**, 291–296.

[87] K. Vahedi, V. Domingo, P. Amarenco and M. G. Bousser, *J. Neurol. Neurosurg. Psychiatr.*, 2000, **68**, 112–113.

[88] M. H. Williams and J. D. Branch, *J. Am. Coll. Nutr.*, 1998, **17**, 216–234.

This page intentionally left blank

Cytarabine

Hussein I. El-Subbagh and **Abdullah A. Al-Badr**

Department of Pharmaceutical Chemistry, College of Pharmacy, King Saud University, Riyadh 11451,
Kingdom of Saudi Arabia

1. DESCRIPTION

1.1. Nomenclature

1.1.1. Systematic chemical names

1-β-D-Arabinofuranosyl cytosine.
Arabinofuranosyl cytosine
1-β-D-(Arabinofuranosyl) cytosine.
1-Arabinofuranosyl cytosine.
1-β-Arabinofuranosyl cytosine.
1-β-Arabinosylcytosine.
1-β-D-Arabinofuranosyl4-amino-2-($1 H$)pyrimidinone.
1-β-D-Arabinosyl-4-amino-2($1 H$)pyrimidinone.
4-Amino-1-arabinofuranosyl-2-oxo-1,2-dihydropyrimidine.
4-Amino-1-β-D-arabinofuranosylpyrimidin-2($1 H$)-one.
4-Amino-1-[3,4-dihydroxy-5-(hydroxymethyl)oxolan-2-yl]pyrimidin-
   2-one.
4-Amino-1-β-D-arabinofuranosyl-2($1 H$)-pyrimidinone.

Cytosine, 1,*β*-D-arabinofuronsyl.
Cytosine, 1-*β*-D-arabinosyl.
2(*1 H*)-Pyrimidinone, 4-amino-1-*β*-D-arabinofuranosyl.
2(*1 H*)-Pyrimidinone, 4-amino-1-arabinofuranosyl.
(*1 H*)-Pyrimidin-2-one, 4-amino-1-*β*-D-arabinofuranosyl. [1–7]

1.1.2. Nonproprietary names
Cytarabine, cytarabinum, Cytarabina, Cytarabin. [3]

1.1.3. Proprietary names
1.1.3.1. Cytarabine Alexan®, Arabine®, Arabitin®, Ara-C®, Ara-Cell®, Aracytin®, Aracytin®, Aracytine®, Arafcyt®, Citagenin®, Citarabina Filaxis®, Citarabina Martian®, Citarabina®, Cyclocide®, Cycloside®, Cytarabel®, Cytarabin®, Cytarabina®, Cytarabine Injection®, Cytarabine®, Cytarabinum Delta West®, Cytonal®, Cytosar®, Cytosar-U®, Cytovis®, Cytozar®, Depocyt®, Erpalfa®, Iretin®, Laracit®, Tarabine PFS®.Tarabine®, Udicil®. [1–7]

1.1.3.2. Cytarabine hydrochloride Alcysten®, Alexan®, Arabitin®, Cylocide®, Cytarabina®, Cytosar®.

1.1.3.3. Cytarabine ocphosphate Starasid®

1.1.3.4. Synonym Ara C; Arabinosylcytosine; Aracytidine cytosine arabinoside; Cytarabinoside; Spongocytidine; Cytosine arabinosine; *β*-Cytosine arabinoside; Arabinocytidine; *β*-D-Arabinosyl cytosine; Cytosine arabinofuranoside: Cytosine arabinose; Cytosine-*β*-D-arabinofuranoside; Cytosine-*β*-D-arabinoside. AC 1075, CHX-3311; U 19920 A; NSC 63878; NCI-CO4728; U-19920; WR-28453. [1–5]

1.2. Formulae

1.2.1. Empirical formula, molecular weight, CAS number

Cytarabine	$C_9H_{13}N_3O_5$	243.22	147-94-4
Cytarabine hydrochloride	$C_9H_{14}N_3O_5Cl$	279.70	69-74-9 [3]

1.2.2. Structural formula
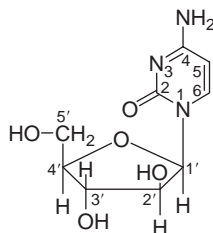
1.3. Elemental analysis

Cytarabine   C, 44.45% H, 5.39% N, 17.28% O, 32.88%
Cytarabine   C, 38.65% H, 5.05% N, 15.02% O, 28.60% Cl, 12.68% [3]
  hydrochloride

1.4. Appearance

Cytarabine: prisms from 50% ethanol.
Cytarabine hydrochloride: a white crystalline powder. [1]

1.5. Uses and applications

Cytarabine, a pyrimidine nucleoside analog, is an antimetabolite, antineo-
plastic which inhibits the synthesis of deoxyribonucleic acid. Its actions
are specific for the S-shape of the cell cycle. It also has antiviral and
immunosuppressant properties. Cytarabine is mainly used in the treat-
ment of acute leukemia, especially acute nonlymphoblastic leukemia
when it is often given in association with thioguanine and an anthracy-
cline such as doxorubicin or daunorubicin. It has also been given in the
blast crisis of chronic myeloid leukemia and in the treatment of lym-
phoma, and has been tried in the management of myelodesplasia [2].
    Cytarabine is given by the intravenous route. Higher doses can be
tolerated when given by rapid injection rather than the slow infusion,
because of the rapid clearance of cytarabine, but there is a little incidence
of clinical advantage for either route. For the induction of remission in
adults and children with acute leukemia a wide variety of dosage regimen
have been used: 100 mg/m^2 body-surface twice daily by rapid intrave-
nous injection, or 100 mg/m^2 daily by continuous intravenous infusion,
have been employed. These doses are generally given for 5–10 days,
depending on therapeutic response and toxicity. Children reportedly
tolerate high doses better than adults. For maintenance, 75–100 mg/m^2
or 1–1.5 mg/kg or more may be given intramuscularly, or subcutaneously
once or twice weekly; other regimens have been used [2].
    In the treatment of refractory disease high-dose regimens have been
employed, with cytarabine given in doses of up to 3 g/m^2 every 12 h for
up to 6 days. These doses should be given by intravenous infusion over at
least 1 h. In leukemia meningitis cytarabine has been given intrathecally,
often in a dose of 10–30 mg/m^2 body surface every 2–4 days, it has also been
used prophylactically. A depot formulation of cytarabine has also been
investigated in meningeal metastasis. While all and platelet counts should
be determined regularly during treatment with cytarabine and therapy
should be stopped immediately if the count falls rapidly or to low values [2].

2. METHODS OF PREPARATION

1. Hunter [8] synthesized cytarabine from uracil arabinoside as follows: Uracil-1-nucleoside **1** was fully acetylated **2** and then treated with phosphorous pentasulfide to give the fully acetylated-4-thiouracil-1-nucleoside **3** which was then treated with ammonia and deacetylated to give cytarabine **4**.
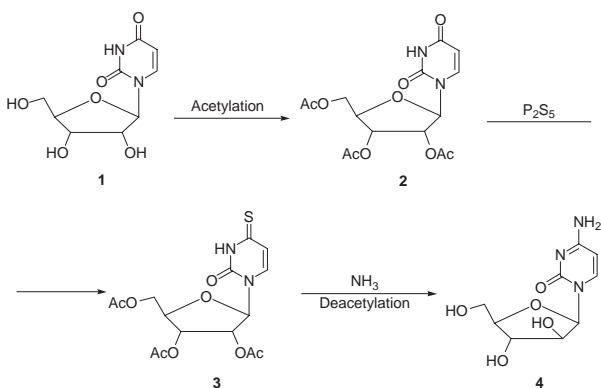
2. Shen *et al.* [9] reported the following method for the synthesis of cytarabine:

   2′,3′,5′-tri-*O*-benzyl-D-arabinofuranosyl chloride **1** was reacted with 2,4-dimethoxy pyrimidine **2** with methylene chloride as the solvent. The reaction was carried out at room temperature. After 3 days, reaction mixture was evaporated *in vacuo* to give sirupy product of 1-(2′,3′,5′-tri-*O*-benzyl-β-D-arabinofuranosyl)-4-methoxy-2-(*1 H*)-pyrimidinone **3**. Treatment of compound **3** with ammonia gives compound **4**. The benzyl groups in compound **4** were smoothly removed by hydrogenolysis in methanol in the presence of prereduced palladium chloride as catalyst to give cytarabine **5**.
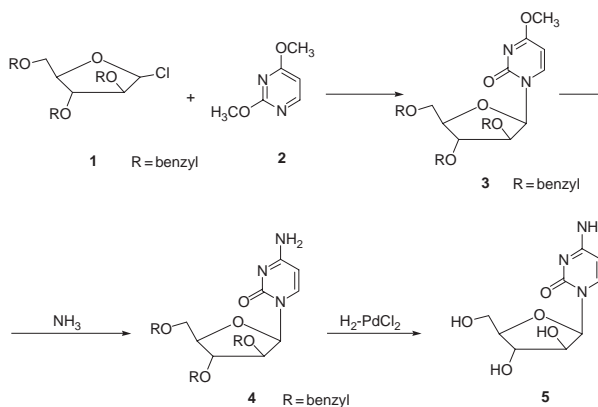
3. Fromogeot and Reese [10] prepared cytarabine as follows:
   An equilibrium mixture of $N^4,O^{3'},O^{5'}$-triacetylcytidine **2**, and its N^4, $O^{2'}$, $O^{5'}$-isomer (1.5:1) was readily prepared from cytidine **1**. This material **2** was allowed to react with a slight excess of toluene-*p*-sulfonyl chloride, in anhydrous pyridine solution, until no starting material remained. The products **3** were then concentrated to small volume, dissolved in dichloromethane (1 volume) and extracted with water (6 × 1 volume) within a period of 10 min. When the combined aqueous extracts were allowed to stand at room temperature, a precipitate of colorless needles of $N^4,O^{3'},O^{5'}$-triacetyl-*β*-D-arabinofuranosyl cytosine probably through the formation of the 2,2′-anhydro product **4**. When the letter product **4** was treated with methanolic ammonia for 24 h at 20 °C, cytarabine **5** was obtained.
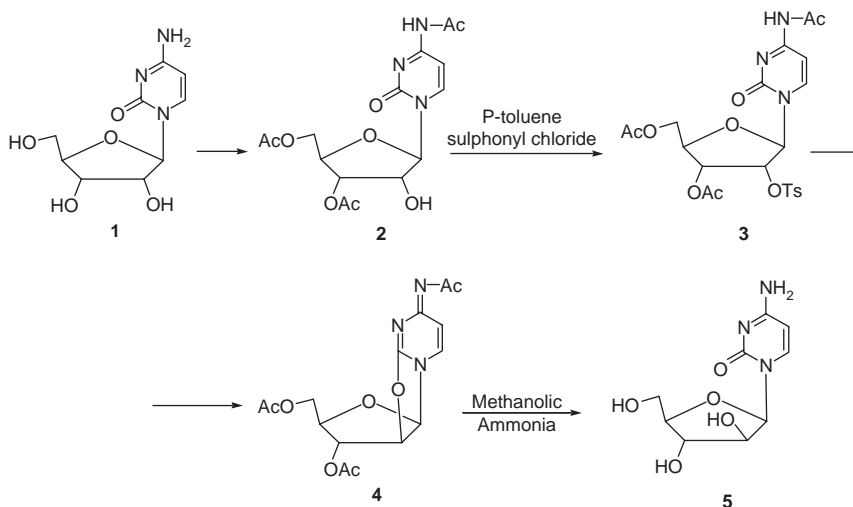
4. Roberts and Dekker [11] described a convenient method for the synthesis of cytarabine. Cytidine **1** was treated with polyphosphoric acid gave the 3′,5′-*O*-phosphorylated 2,2′-anhydrocytidine **2** which was hydrolyzed at pH 9 with lithium hydroxide to cytarabine-3′,5′-diphosphate **3**. Cytarabine **4** was then obtained by hydrolysis of the diphosphate **3** using alkaline phosphatase.
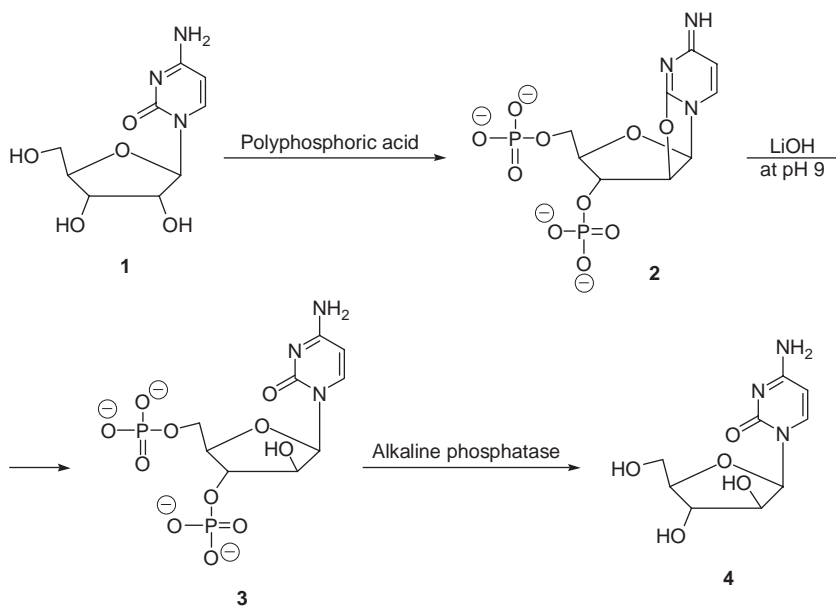
5. Nagyvary and Tapiero [12] used the following method for synthesis of cytarabine.

One millimole of 5′-O,N⁴-diacetylcytidine-2′,3′-cyclic phosphate tri-*n*-butylammonium salt **1**, was dissolved in a mixture of 20 ml of anhydrous dioxane and 2 ml of tri-*n*-butylamine, 1.2–1.6 equivalents of an activating agent were added under cooling. As activating agents, diphenyl phosphorochloridate, methanesulfonyl chloride and *p*-toluenesulfonyl chloride were employed, of which the sulfonyl chlorides were found to preferable. The rearrangement from compound **2** to compound **3** took about 15 h at 20 °C or 2 h at 50 °C. The hydrolysis of the unstable intermediate **3** (O^2, 2′-cyclocytidine) was affected by the addition of 5 ml 1 *M* triethylammonium bicarbonate directly to the reaction mixture gave **5**. In water alone, the initial hydrolysis product **4** reverted to the starting material. The separation of the starting material **1** from 5′-O,N⁴-diacetylaracytidine-3′-phosphate **5** was achieved on a diethylaminoethyl (bicarbonate) columns. The acetyl groups in **5** were hydrolyzed with methanolic ammonia, and the resulting aracytidine-3′-phosphate **6** was further purified by absorption on a Dowex 1-X2 (formate) column and elution with dilute formic acid. Treatment of compound **6** with alkaline phosphatase produced cytarabine **7**.
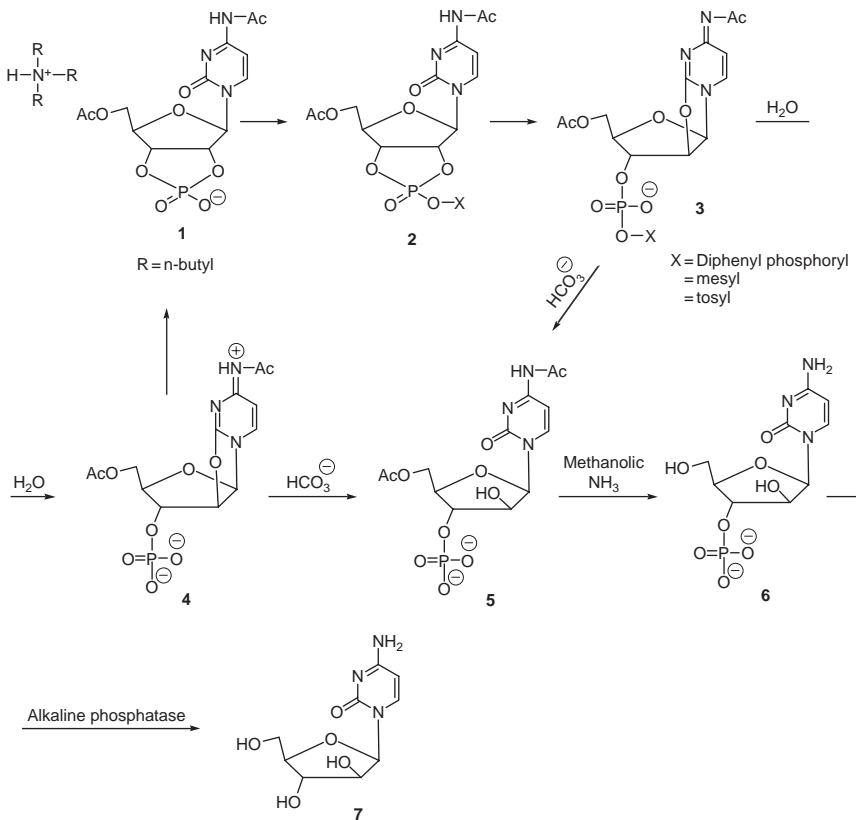
6. Shannahoff and Sanchez [13] described the following scheme for the synthesis of cytarabine. The reaction of D-arabinose **1** with cyanamide **2** to form 2-amino-β-D-arabinofurano[1′,2′-4,5]-2-oxazoline **3** is followed by reaction of compound **3** with propiolonitrile **4** to yield a cyanovinyl as the *trans* adduct **5**. Treatment of compound **5** with aqueous ammonia gave a high yield of cytarabine **7**, via 2,2′-anhydro-1-β-D-arabinofuranosylcytosine **6**.
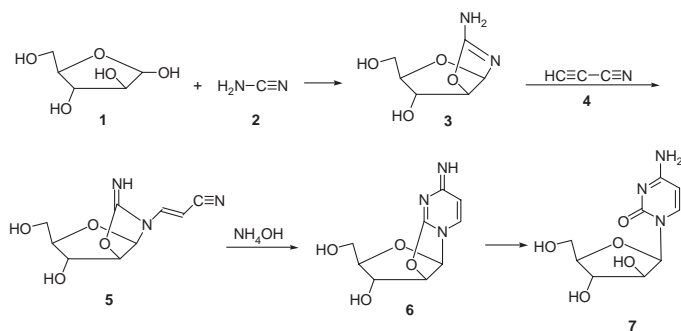
7. Hessler [14] used the following method for the synthesis of cytarabine: *Cis-β*-trimethylammoniumacrylonitrile tosylate **1** which is a stable, white crystalline solid was used as a substitute for propiolonitrile in the previous synthesis [13]. Reaction of compound **1** with 2-amino-β-D-arabinofurano[1′,2′-4,5]-2-oxazoline **2** was carried out in dimethyl formamide at 50°C gives the cyanovinyl adduct **3**. Use of protic solvents such as water, methanol or propanol for the reaction gave only poor yields of cytarabine. However, dipolar aprotic solvents were effective, with dimethyl formamide giving the highest yield. Addition of acetonitrile at the end of the reaction caused crystallization of a white solid isolated in 70-74% yield, which is assigned as the acetonitrile solvate of 2,2′-anhydrocytarabine tosylate salt **4** (**4** TsOH.CH₃CN) by NMR comparison with authentic 2,2′-anhydrocytarabine hydrochloride. Hydrolysis of compound **4** (**4** TsOH.CH₃CN) to cytarabine **5** occurs readily in dilute aqueous ammonia which was purified by adsorption, then elution from a sulfonic acid ion-exchange resin.
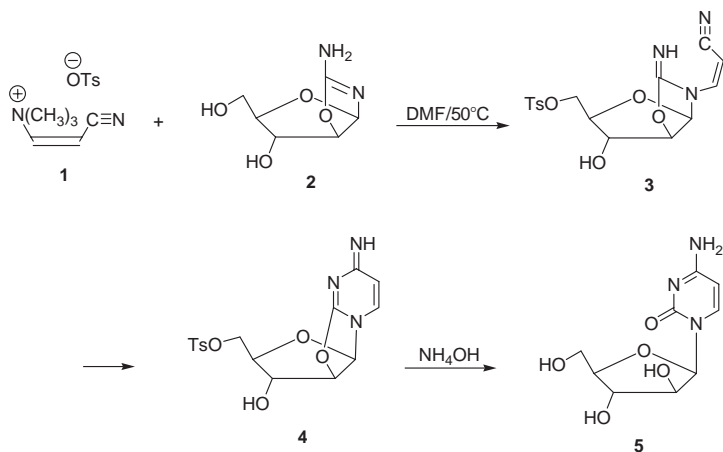
8. Kanai *et al.* [15] used the following method for the synthesis of cytarabine:

   Cytidine **1** was nitrated with fuming nitric acid to give 2′-3′-5′-tri-*O*-nitrocytidine **2** and/or 2′-5′-di-*O*-nitrocytidine which was boiled in an alcohol containing 1–3 moles of dilute alkali hydroxide or with organic amines to give the 2′-hydroxy inverted product **3**. This product was reduced to remove the nitro radical and gave cytarabine **4**.
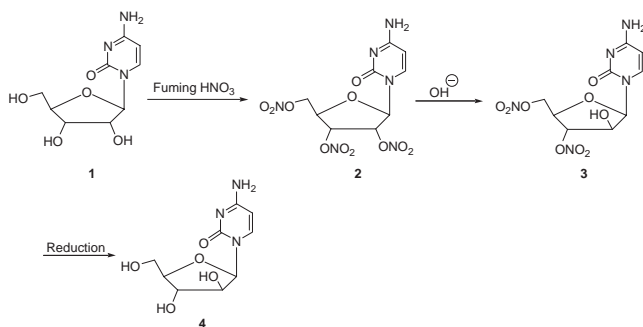
9. Jin *et al.* [16] described a method for the preparation of cytarabine:

   The reaction of 1-β-ᴅ-arabinofuranosyluracil **1** with acetic acid anhydride or acetyl chloride or acetyl bromide in pyridine to obtain 1-β-ᴅ-arabinofuranosyluracil triacetate **2**. Reacting 1-β-ᴅ-arabinofuranosyluracil triacetate **2** with a triazole compound in the presence of phosphorous oxychloride and inert organic solvent to obtain 1,2,4-triazole substituted 1-β-ᴅ-arabinofuranosyl uracil triacetate, and subjecting to ammonolysis to obtain cytarabine. Additionally, strongly acidic cation-exchange resin is adopted for the separation and purification of the crude product of cytarabine **3**.
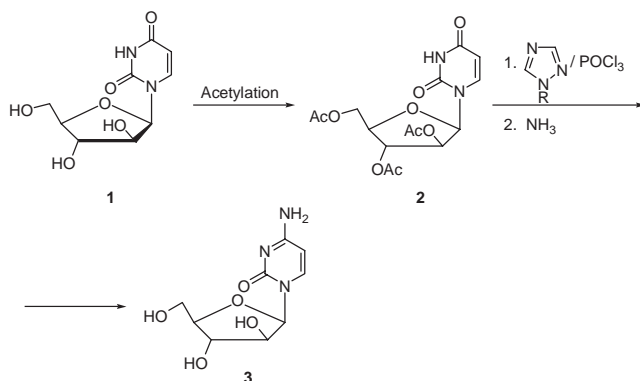
3. PHYSICAL CHARACTERISTICS

3.1. Ionization constant

pK_a 4.3 [1]

3.2. Solubility characteristics

Cytarabine: Soluble 1 in 10 of water, 1 in 1000 of ethanol and 1 in 1000 of chloroform.

Cytarabine hydrochloride: Soluble 1 in 1 water; less soluble inorganic solvents. [1]

3.3. Optical activity

+154 to +160. [1]

3.4. X-ray powder diffraction pattern

The X-ray powder diffraction pattern of cytarabine was performed using a Simmons XRD-5000 diffractometer. Fig. 2.1 shows the X-ray powder diffraction pattern of cytarabine, which was obtained on a pure sample of the drug substance. Table 2.1 shows the values for the scattering angles
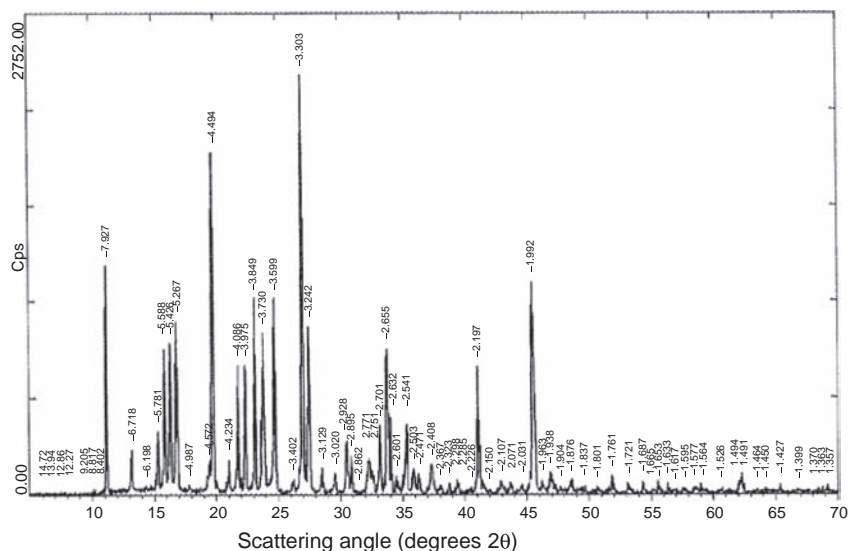
FIGURE 2.1   The X-ray powder diffraction pattern of cytarabine.

TABLE 2.1 The X-ray powder diffraction pattern of cytarabine

Scattering angle (degree 2θ)	d-spacing (Å)	Relative intensity (%)	Scattering angle (degree 2θ)	d-spacing (Å)	Relative intensity (%)
6.000	14.7180	8.30	36.317	2.4716	4.07
6.335	13.9411	0.48	37.308	2.4083	5.98
6.870	12.8552	0.29	37.984	2.3669	1.68
7.199	12.2700	0.17	38.726	2.3233	2.17
9.600	9.2054	0.43	39.160	2.2985	1.25
10.024	8.8167	1.21	39.398	2.2852	2.80
10.520	8.4023	0.55	40.498	2.2256	1.15
11.152	7.9274	47.87	41.056	2.1966	26.85
13.168	6.7180	9.26	41.979	2.1504	0.85
14.278	6.1981	1.61	42.889	2.1069	2.59
15.313	5.7814	13.10	43.661	2.0714	2.32
15.845	5.5884	30.37	44.580	2.0308	1.60
16.323	5.4257	31.52	45.491	1.9922	44.40
16.819	5.2671	35.98	46.219	1.9626	2.50
17.771	4.9870	1.91	46.844	1.9378	4.54
19.400	4.5717	6.13	47.716	1.9044	1.52
19.741	4.4936	71.97	48.478	1.8762	2.47
20.963	4.2342	7.16	49.584	1.8369	1.55
21.730	4.0864	27.04	50.639	1.8011	1.27
22.345	3.9754	26.83	51.886	1.7607	3.57
23.087	3.8493	40.79	53.161	1.7215	2.07
23.839	3.7296	33.88	54.334	1.6870	2.29
24.720	3.5986	40.80	55.120	1.6648	0.57
26.176	3.4016	2.96	55.550	1.6530	0.94
26.969	3.3034	100.00	56.303	1.6326	2.01
27.493	3.2416	35.13	56.909	1.6167	0.80
28.503	3.1289	5.36	57.760	1.5949	1.03
29.550	3.0205	4.35	58.489	1.5767	1.30
30.500	2.9284	11.07	59.009	1.5640	2.08
30.862	2.8949	7.82	60.643	1.5258	0.86
31.223	2.8623	0.53	62.080	1.4938	2.59
32.274	2.7715	7.44	62.225	1.4907	4.18
32.519	2.7512	4.86	63.506	1.4637	0.67
33.139	2.7011	14.20	64.191	1.4497	1.11
33.731	2.6550	30.39	65.331	1.4271	1.86
34.040	2.6316	16.18	66.837	1.3986	0.60
34.449	2.6012	3.37	68.437	1.3698	0.99

(continued)

TABLE 2.1   (*continued*)

Scattering angle (degree 2θ)	d-spacing (Å)	Relative intensity (%)	Scattering angle (degree 2θ)	d-spacing (Å)	Relative intensity (%)
35.295	2.5408	14.30	68.803	1.3634	1.15
35.849	2.5028	5.13	69.140	1.3575	1.75

(deg, 2θ), the interplanar *d*-spacing (Å), and the relative intensities (%) observed for the major diffraction peaks of cytarabine.

3.5. Thermal method of analysis

3.5.1. Melting behavior

Cytarabine melts at 212–213 °C.
Cytarabine hydrochloride melts at 180–182 °C. [1]

3.5.2. Differential scanning calorimetry

The differential scanning calorimetry thermogram of cytarabine was obtained using a DuPont 2100 thermal analyzer system. The thermogram shown in Fig. 2.2 was obtained at a heating rate of 10 °C/min and was run over the range 25–400 °C. Cytarabine was found to melt at 226 °C.

3.6. Spectroscopy

3.6.1. Ultraviolet spectroscopy

The UV absorption spectrum of cytarabine in 0.1 N hydrochloric acid shown in Fig. 2.3 was recorded using a Shimadzu UV-vis Spectrophotometer 1601 PC. The compound exhibited a maximum at 281 nm (A 1%, 1 cm = 596.97). Clarke reported the following: Aqueous acid—280 nm (A 1%, 1 cm = 555); aqueous alkali—274 nm [1].

3.6.2. Vibrational spectroscopy

The infrared absorption spectrum of cytarabine was obtained in a KBr pellet using a Perkin-Elmer infrared spectrophotometer. The infrared spectrum is shown in Fig. 2.4, where the principal peaks are observed at 3477, 3441, 3357, 3264, 2938, 2656, 1656, 1581, 1529, 1480, 1280, 1111, 1071, 798 cm^{-1}. Assignment for the major infrared absorption bands are show in Table 2.2.

   Clarke reported principal peaks at wavenumbers 1075, 1027, 1145, 1109, 1178, 1002 cm^{-1} (KBr disc) [1].
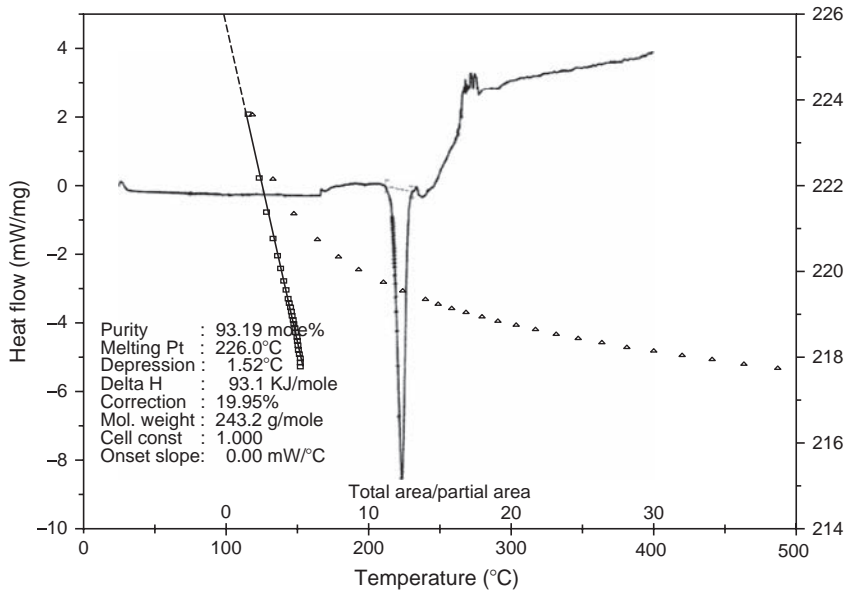
FIGURE 2.2 The differential scanning calorimetry thermogram of cytarabine.
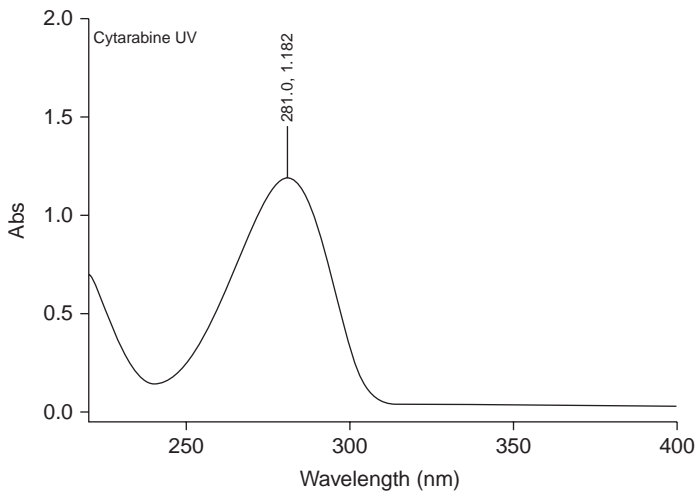
FIGURE 2.3 The UV absorption spectrum of cytarabine.

3.6.3. Nuclear magnetic resonance spectrometry

3.6.3.1. ^{1}H NMR spectra The proton nuclear resonance (^{1}H NMR) spectra of cytarabine were obtained using a Bruker instrument operating at 500 MHz. Standard Bruker software was used to execute the recording
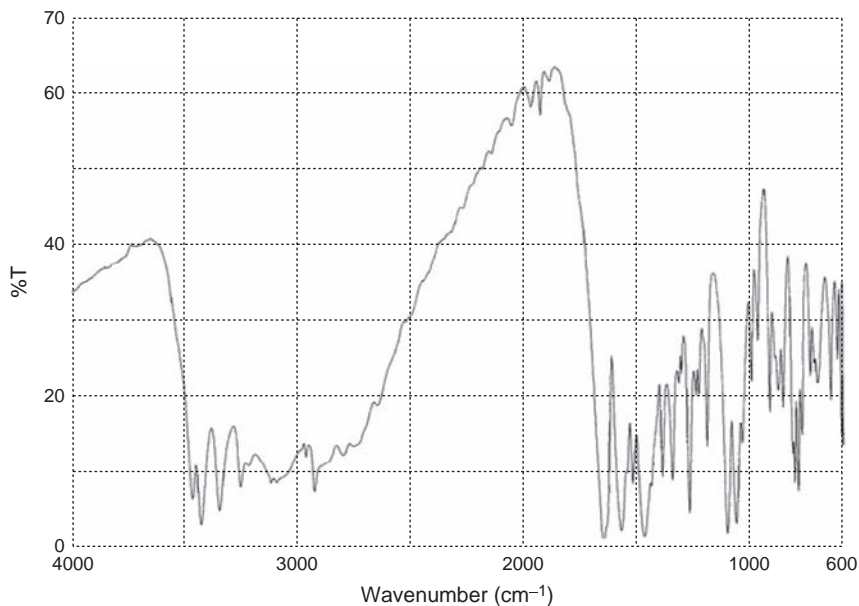
FIGURE 2.4   The infrared absorption spectrum of cytarabine (KBr pellet).

TABLE 2.2   Assignments for the infrared absorption bands of cytarabine

Frequency (cm^{-1})	Assignments
3477, 3441, 3357, 3264	NH and OH stretching
2938, 2656	CH stretching
1656	C=O stretching
1581, 1529, 1480	C=N and C=C stretching
1280, 1111, 1071	C-O stretching
798	C-H bonding

of the 1D and 2D spectra. The sample was dissolved in DMSO-d_6 and all resonance bands were referenced to tetramethylsilane (TMS) as internal standard. The ^{1}H NMR spectra of cytarabine are shown in Figs. 2.5–2.7. The ^{1}H NMR assignments of cytarabine are shown in Table 2.3.

The entire proton spectrum of cytarabine is shown in Figs. 2.5 and 2.6. Based on chemical shift consideration the doublets at δ 7.59 and 5.68 ppm are assigned for protons at positions 6 and 5 of the cytosine ring, respectively. The distorted doublet at δ 7.09–7.12 ppm is assigned for the 4-amino function. Anomeric proton resonated at δ 6.04 ppm. Protons of the 2′, 3′, 4′ and 5′ are listed in Table 2.3, in addition to three exchangeable

7.620
7.605
7.203

6.052
6.044
5.736
5.722
5.489
5.456
5.110

3.983
3.904
3.757
3.601
3.572

2.506

X

10   9   8   7   6   5   4   3   2   1   0

1.00
1.98

1.00
1.00
2.01
0.98
1.00
1.03
1.04
4.37

Chemical shift (ppm)
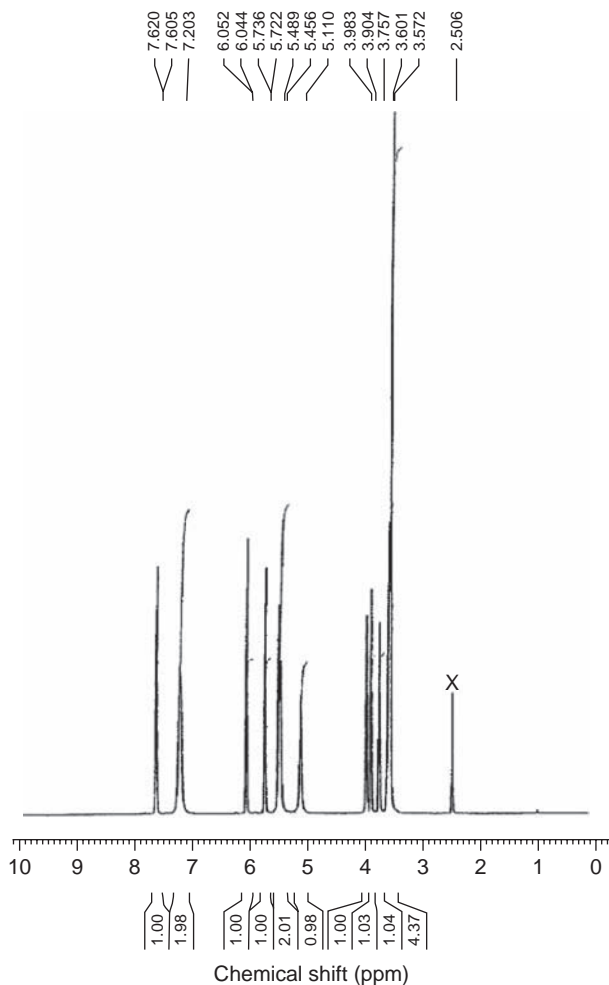
FIGURE 2.5   The ^{1}H-NMR spectrum of cytarabine in DMSO-d_6.

protons belong to the hydroxyl groups. All ^{1}H-NMR assignments were confirmed by means of 2D COSY experiment (Fig. 2.7).

3.6.3.2. ^{13}C-NMR Spectra   A noise-modulated, broadband decoupled ^{13}C-NMR spectrum (Fig. 2.8) showed nine resonance bands which is in accordance with what would be anticipated for the nine carbons of cytarabine (Table 2.4). Carbon resonance bands at 74.8, 76.4, 84.8, 85.1, 92.4, and 142.1 were assigned to 6 CH groups, also absorption at 61.2 ppm
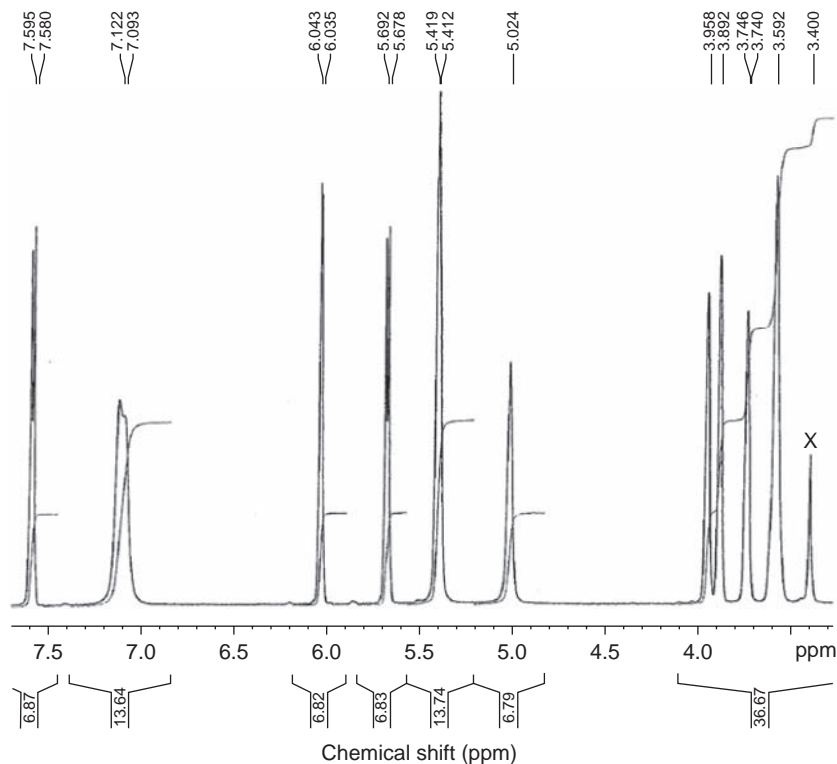
FIGURE 2.6   The expanded ^{1}H-NMR spectrum of cytarabine in DMSO-d_6.

was assigned to the only CH_2 group of this structure. Bands at 155.2, and 165.6 ppm are assigned to the two quaternary carbons at the cytosine heterocycle.

A DEPT experiment (Fig. 2.9) permitted the identification and confirmation of the methine and methylene carbons. Another confirmation was obtained through the HSQC (Fig. 2.10) and the long-range coupling experiment HMBC (Fig. 2.11).

3.6.4. Mass spectrometry

The mass spectrum of cytarabine was obtained using a Shimadzu PQ 5006 mass spectrometer. The parent ion was collided with helium as a carrier gas. Fig. 2.12 shows the detailed mass fragmentation pattern for cytarabine. Table 2.5 shows the proposed mass fragmentation pattern of the drug.
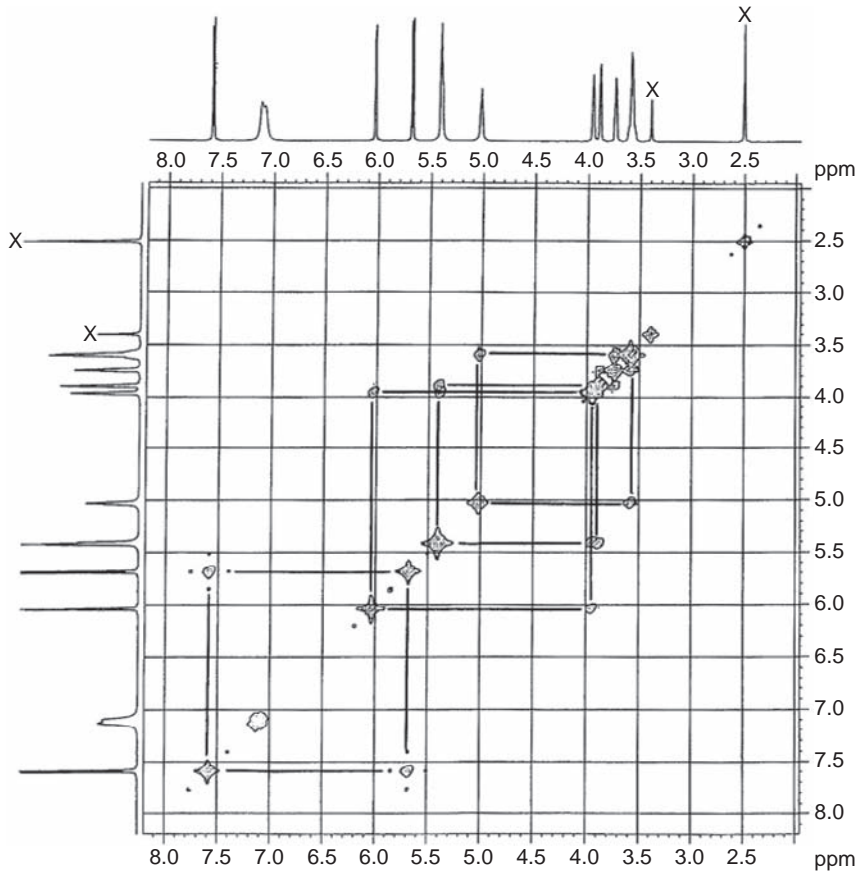
FIGURE 2.7   The COSY ^{1}H-NMR experiment of cytarabine in DMSO-d_6.

4. METHODS OF ANALYSIS

4.1. Compendial methods

4.1.1. British pharmacopoeia methods [5]
4.1.1.1. Cytarabine   Cytarabine contains not less than 99% and not more than the equivalent of 100.5% of 4-amino-1-β-D-arabinofuranosyl-1*H*-pyrimidin-2-one, calculated with referece to the dried substance.

TABLE 2.3 ¹H-NMR resonance band assignments for cytarabine
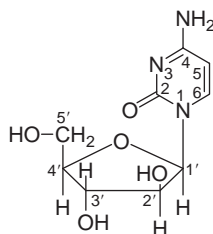
Chemical sifts (δ, ppm)	No. of protons	Multiplicity* (J Hz)	Assignments
7.59	1	d (7.5 Hz)	H-6
7.09–7.12	2	m	NH₂
6.04	1	d (4 Hz)	H-1′ (anomeric)
5.68	1	d (7.5 Hz)	H-5
5.41–5.42	2	m	2′-OH or 3′-OH
5.02	1	brs	5′-OH
3.96	1	brs	H-2′ or H-3′
3.89	1	s	H-3′ or H-2′
3.74–3.75	1	m	H-4′
3.58–3.59	2	m	H-5′

* s = singlet, brs = broad singlet, d = doublet, m = multiplet.

Identification

Test 1: Dissolve 20 mg of cytarabine in 0.1 M *hydrochloric acid* and dilute to 100 ml with the same acid. Dilute 5 ml of the solution to 100 ml with 0.1 M *hydrochloric acid.* Examine between 230 and 350 nm according to the general method (*2.2.25*), the solution shows an absorption maximum at 281 nm. The specific absorbance at the maximum is 540–570 nm.

Test 2: According to the general procedure (*2.2.24*), examine by infrared absorption spectrophotometry, comparing with the spectrum obtained with *cytarabine CRS*. Examine the substances prepared as discs.

Test 3: Examine the chromatograms obtained in the test for related substances in ultraviolet light at 254 nm. The principal spot in the chromatogram obtained with test solution (b) is similar in position and size to the principal spot in the chromatogram obtained with reference solution (a).
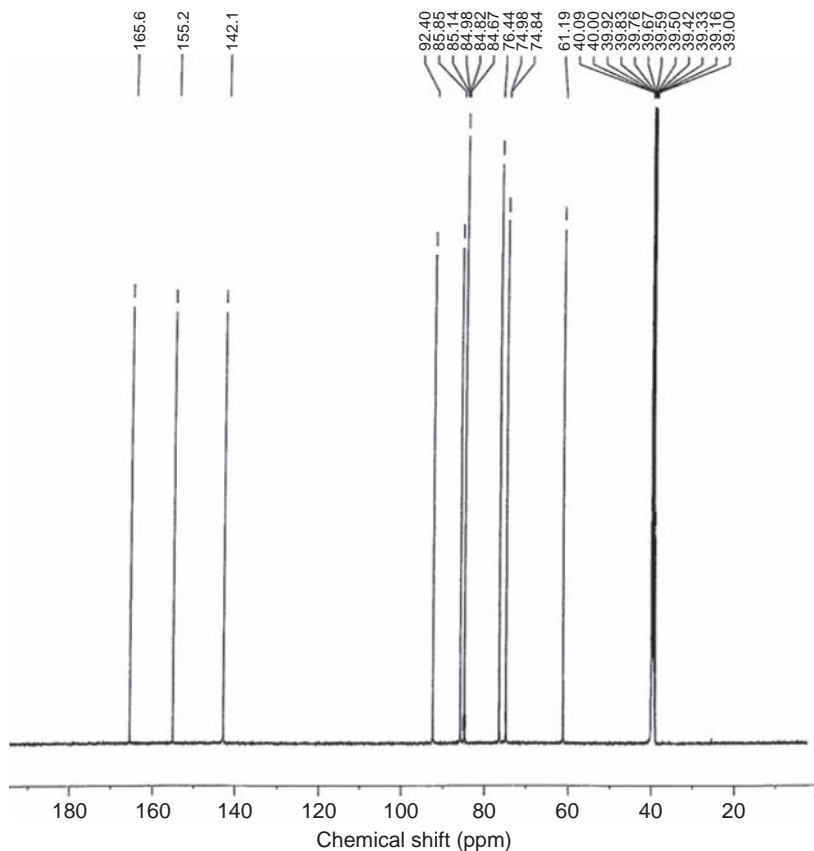
FIGURE 2.8   The ^{13}C-NMR spectrum of cytarabine in DMSO-d_6.

Tests

Appearance of solution: Dissolve 1 g of cytarabine in *water R* and dilute to 10 ml with the same solvent. According to the general procedure (2.2.1), the solution is clear and not more intensely colored than reference solution Y_5, as directed in the general method (*Method 2, 2.2.2*).

Specific optical rotation: According to the general method (2.2.7), dissolve 0.25 g of cytarabine in *water R*, and dilute to 25 ml with the same solvent. The specific optical rotation is $+154°$ to $+160°$, calculated with reference to the dried substance.

Related substances: Examine cytarabine by thin-layer chromatography, as directed in the general procedure (2.2.27), using *silica gel GF$_{254}$ R* as the coating substance.

Test solution (a): Dissolve 0.25 g of cytarabine in *water R* and dilute to 5 ml with the same solvent.

TABLE 2.4   ^{13}C-NMR resonance band assignments for cytarabine
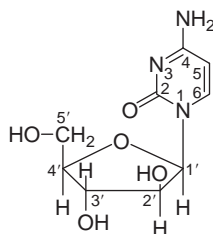
Chemical sifts (δ, ppm)	Assignments	Chemical sifts (δ, ppm)	Assignments
74.8	C-2′ or C-3′	92.4	C-5
76.4	C-3′ or C-2′	142.1	C-6
84.8	C-4′	155.2	C-NH$_2$
85.1	C-1′	165.6	C=O
61.2	C-5′		

Test solution (b): Dilute 2 ml of test solution (a) to 50 ml of *water R*.
Reference solution (a): Dissolve 10 mg of *cytarabine CRS* in *water R* and dilute to 5 ml with the same solvent.
Reference solution (b): Dilute 0.5 ml of test solution (a) to 100 ml with *water R*.
Reference solution (c): Dissolve 20 mg of *uridine R* and 20 mg of *uracil arabinoside CRS* in *methanol R* and dilute to 10 ml with the same solvent.

Apply separately to the plate 5 μl of each solution. Develop over a path of 15 cm using a mixture of 15 volumes of *water R*, 20 volumes of *acetone R* and 65 volumes of *methyl ethyl ketone R*. Allow the plate to dry in air and examine in UV light at 254 nm. Any spot in the chromatogram obtained with test solution (a), apart from the principal spot, is not more intense than the spot in the chromatogram obtained with reference solution (b), (0.5%). The test is not valid unless the chromatogram obtained with reference solution (c) shows two clearly separated spots.

Loss on drying: When cytarabine is tested according to the general procedure (2.2.32), not more than 1%, determined on 0.25 g by dyring over *diphosphorus pentoxide R* at 60 °C at a pressure of 0.2–0.7 kPa for 3 h.

Sulfated ash: When cytarabine is tested according to the general method (2.4.14), not more than 0.5%, determined on 1 g.
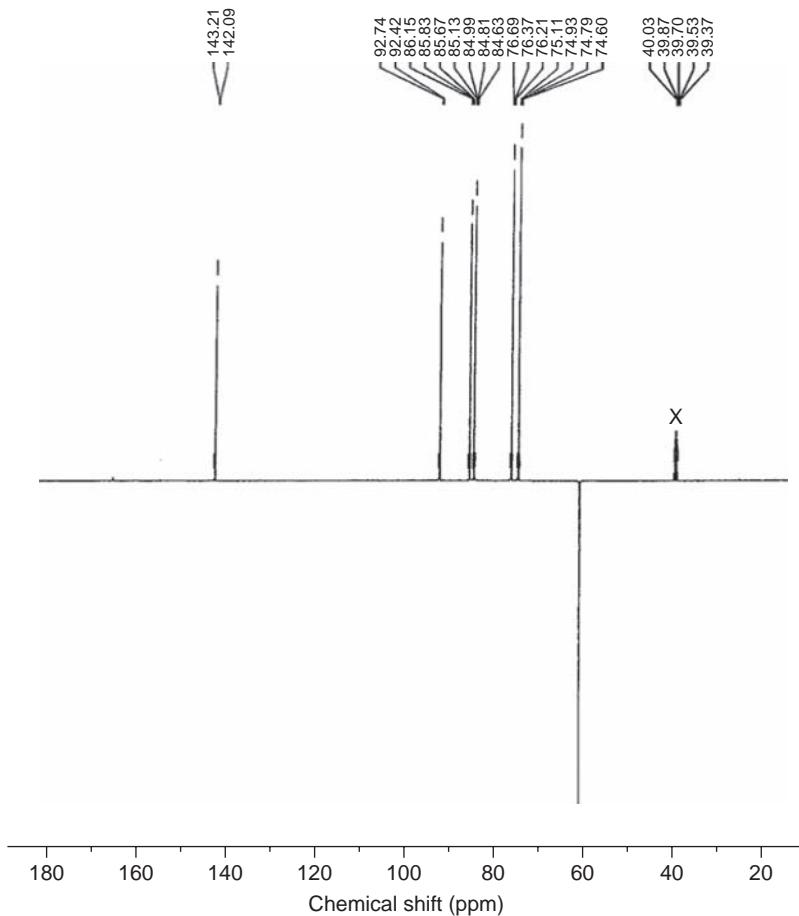
FIGURE 2.9   The DEPT 135 ^{13}C-NMR experiment of cytarabine in DMSO-d_6.

Assay   Dissolve 0.2 g of cytarabine in 60 ml of *anhydrous acetic acid R*, warming if necessary. Titrate with *0.1 M perchloric acid* determining the endpoint potentiometrically as directed in the general procedure (2.2.20). 1 ml of *0.1 M perchloric acid* is equivalent to 24.32 mg of $C_9H_{13}N_3O_5$.

Storage   Store in an airtight container, protected from light.
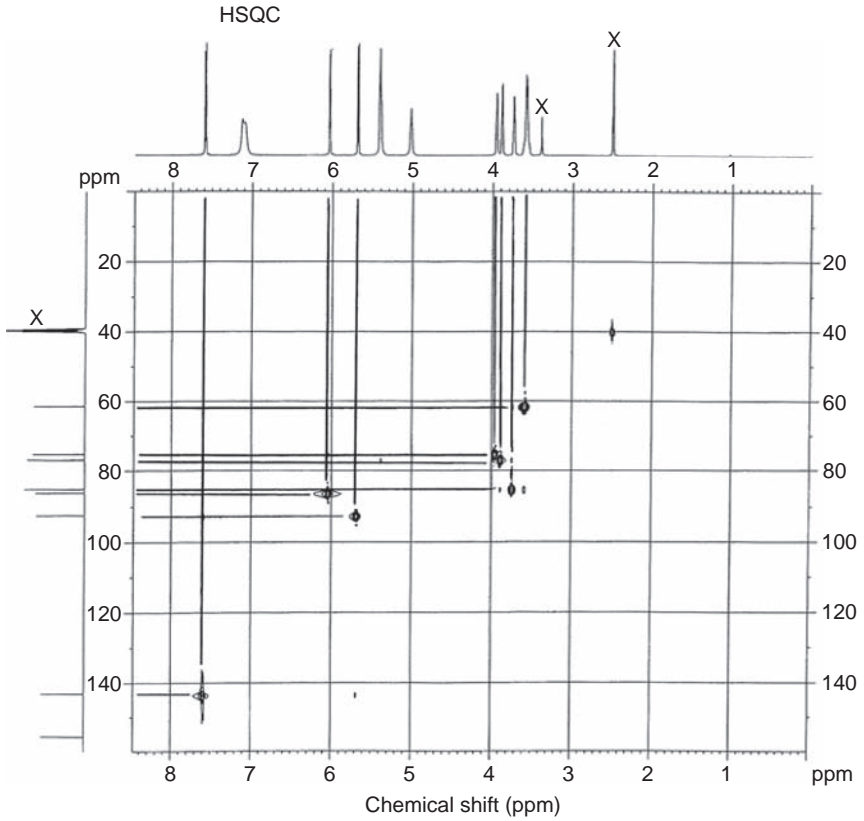
FIGURE 2.10   The HSQC NMR experiment of cytarabine in DMSO-d_6.

Impurities

A. Uracil arabinoside.
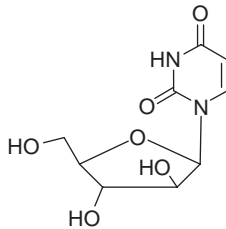
B. Uridine
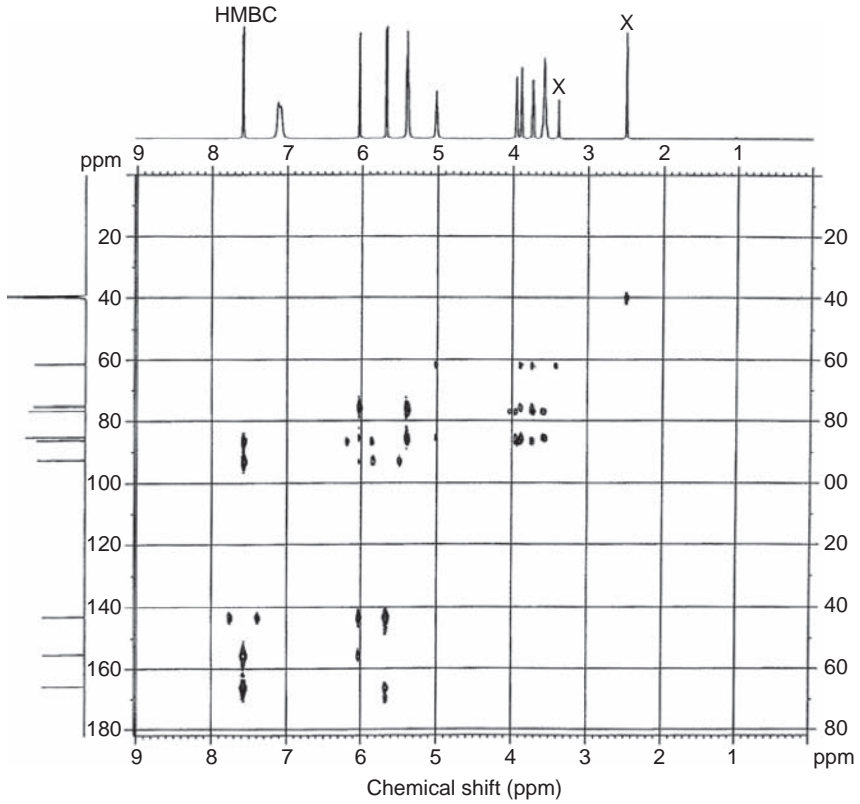
FIGURE 2.11   The HMBC NMR experiment of cytarabine in DMSO-d_6.
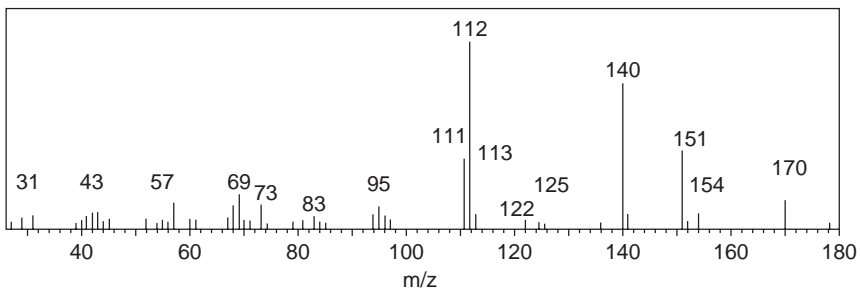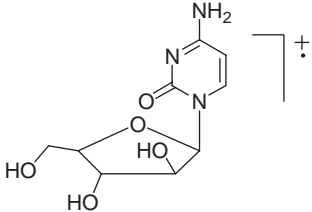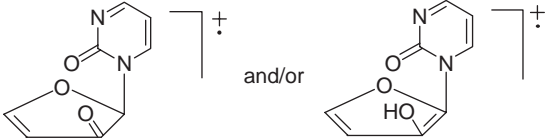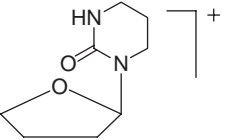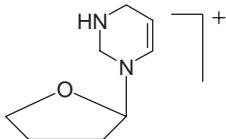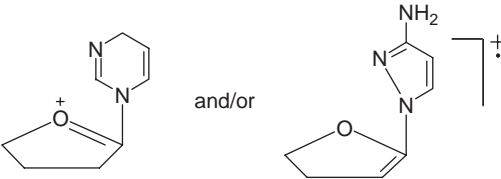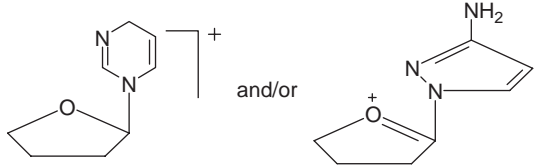
FIGURE 2.12   The mass spectrum of cytarabine.

TABLE 2.5 Summary of assignments for the fragmentation ions observed in the mass spectrum of cytarabine

		Fragment	
m/z	Relative intensity	Formula	Structure
243	–	$C_9H_{13}N_3O_5$	
178	2.4%	$C_8H_6N_2O_3$	and/or
170	12.4%	$C_8H_{14}N_2O_2$	

TABLE 2.5 (*continued*)

		Fragment	
m/z	Relative intensity	Formula	Structure
154	6.8%	$C_8H_{14}N_2O$	
151	35.6%	$C_8H_{11}N_2O$ or $C_7H_9N_3O$	and/or
152	3.6%	$C_8H_{12}N_2O$ $C_7H_{10}N_3O$	and/or
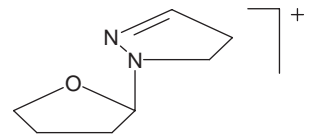
140	64.4%	$C_7H_{12}N_2O$	
136	2%	$C_7H_8N_2O$ $C_5H_{12}O_4$	
113	7.2%	$C_5H_5O_3$	
112	100%	$C_5H_4O_3$	
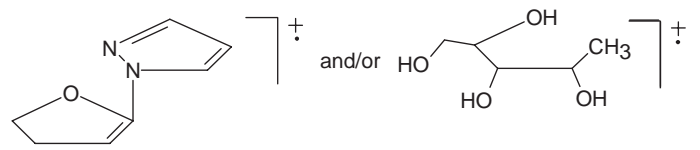
TABLE 2.5 (*continued*)

		Fragment	
m/z	Relative intensity	Formula	Structure
111	33.2%	C$_5$H$_3$O$_3$ and/or C$_4$H$_5$N$_3$O	
97	3.2%	C$_5$H$_5$O$_2$	
96	4.8	C$_5$H$_4$O$_2$ and/or C$_4$H$_4$N$_2$O	
95	10.4%	C$_5$H$_3$O$_2$	
85	3.2%	C$_4$H$_9$N$_2$ and/or C$_3$H$_7$N$_3$	
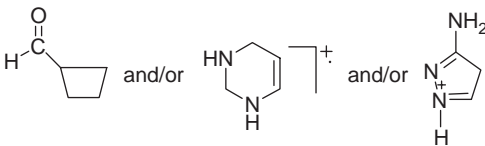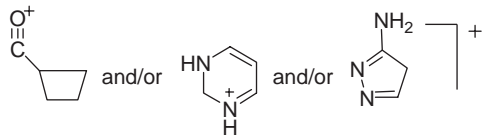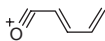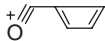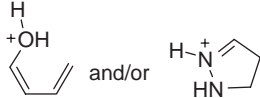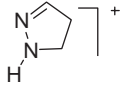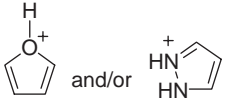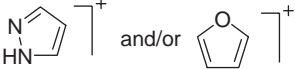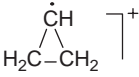
84	2.4%	C_5H_8O and/or $C_4H_8N_2$ and/or $C_3H_6N_3$	
83	4.4%	C_5H_7O and/or $C_4H_7N_2$ and/or $C_3H_5N_3$	
81	2.4%	C_5H_5O	
79	2.4%	C_5H_3O	
71	4.4%	C_4H_7O and/or $C_3H_7N_2$	
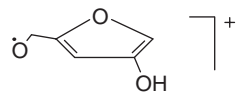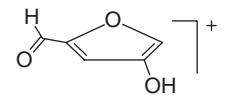
TABLE 2.5 (*continued*)

m/z	Relative intensity	Fragment	
		Formula	Structure
70	4.4%	C₃H₆N₂	
69	16%	C₄H₅O and/or C₃H₅N₂	
68	11.2%	C₃H₄N₂ and/or C₄H₄O	
57	11.6%	C₄H₉	
56	2.8%	C₄H₈	

54	2%	C_4H_6	

$$\left[\quad \right]^{+}$$

| 44 | 3.2% | C_3H_8 | |

$$\left[H_3C-CH_2-CH_3 \right]^{+}$$

| 43 | 8% | C_3H_7 | |

$$\left[H_3C-CH_2\overset{\cdot}{C}H_2 \right]^{+}$$

| 42 | 7.6% | C_3H_6 | |

$$\left[\underset{H_2C-CH_2}{\overset{\overset{H_2}{C}}{}} \right]^{+} \text{ and/or } \left[H_3C-\underset{H}{C}=CH_2 \right]^{+}$$

| 41 | 6% | C_3H_5 | |

$$\left[\underset{H_2C-CH_2}{\overset{\overset{\cdot}{C}H}{}} \right]^{+}$$

| 40 | 4% | C_3H_4 | |

$$\left[\triangle \right]^{+}$$

TABLE 2.5 (*continued*)

		Fragment	
m/z	Relative intensity	Formula	Structure
31	6%	C_2H_6	$\left[H_3C-CH_3 \right]^+$
29	4.8%	C_2H_5	$\left[H_3C-\overset{\bullet}{C}H_2 \right]^+$
27	3.2%	C_2H_3	$\left[H\overset{\bullet}{C}=CH_2 \right]^+$
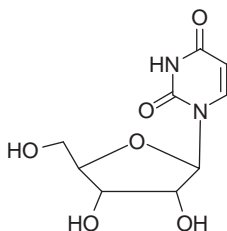
4.1.1.2. Cytarabine injection   Cytarabine injection is a sterile solution of Cytarabine in Water for Injection. It is supplied as a ready-to-use injection or it is prepared immediately before use by dissolving Cytarabine for Injection in the requisite amount of liquid stated on the label.

The injection complies with the requirements stated under Parenteral Preparations.

When supplied as a ready-to-use injection, the injection complies with the following requirements:

Content of cytarabine: $C_9H_{13}N_3O_5$ 95 to 105% of the prescribed or stated amount.

Identification: Evaporate a volume of the injection containing 0.1 g of cytarabine to dryness at 60 °C at a pressure of 0.7 kPa, mix the residue with a minimum amount of hot *ethanol (96%)*, filter, allow the filtrate to cool and induce crystallization if necessary. Filter, wash the crystals with 2 ml of *ethanol (96%)* and dry at 60 °C at a pressure of 0.7 kPa. The *infrared absorption spectrum* of the dried crystals, Appendix II A, is concordant with the *reference spectrum* of cytarabine (RS 081).

Acidity or Alkalinity: pH 7–9.5, Appendix V L.

Related Substances: Carry out the method for *thin-layer chromatography*, Appendix III.A, using a silica gel 60 F_{254} precoated plate (Merck plates are suitable) and a mixture of 15 volumes of *water*, 20 volumes of *acetone* and 65 volumes of *butan-2-one* as the mobile phase. Apply separately to the plate 10 µl of each of the following solutions in *water*. For solution (1) dilute, if necessary, a volume of the injection to produce a solution containing 2% (w/v) of Cytarabine. For solution (2) dilute 1 volume of solution (1) to 200 volumes. Solution (3) contains 0.04% (w/v) of *uracil arabinoside EPCRS*. Solution (4) contains 0.02% (w/v) each of *uridine* and *uracil arabinoside* EPCRS. After removal of the plate, allow it to dry in air and examine under *ultraviolet light (254 nm)*. In the chromatogram obtained with solution (1) any spot corresponding to uracil arabinoside

is not more intense than the spot in the chromatogram obtained with solution (3) (2%). Any other *secondary spot* in the chromatogram obtained with solution (1) is not more intense than the spot in the chromatogram obtained with solution (2) (0.5%). The test is not valid unless the chromatogram obtained with solution (4) shows two clearly separated spots.

Assay: Carry out the method for *liquid chromatography*, Appendix III.D, using the following solutions. For solution (1) dissolve 20 mg of *cytarabine BPCRS* in *water* and dilute to 100 ml with the same solvent. Dilute 10–100 ml with *water*. For solution (2) dilute a volume of the injection to produce a solution containing 0.002% of Cytarabine.

The chromatographic procedure may be carried out using (a) a stainless steel column (25 cm × 4.6 mm) packed with *stationary phase C* (5 µm) (Spherisorb ODS 2 is suitable) and maintained at 30 °C, (b) a mixture of 7.5 volumes of *methanol* and 100 volumes of 0.005 m *sodium pentanesulfonate* adjusted to pH 2.8 using *glacial acetic acid* as the mobile phase with a flow rate of 1 ml/min, and (c) a detection wavelength of 280 nm.

Calculate the content of $C_9H_{13}N_3O_5$ using the declared content of $C_9H_{13}N_3O_5$ in *cytarabine BPCRS*.

4.1.1.3. Cytarabine for injection

Cytarabine for Injection is a sterile material consisting of Cytarabine with or without excipients. It is supplied in a sealed container.

The contents of the sealed container comply with the requirements for Powders for Injection stated under Parenteral Preparations and with the following requirements:

Content of cytarabine: $C_9H_{13}N_3O_5$ 95–105% of the prescribed or stated amount.

Identification: Mix a quantity of the contents of the sealed container containing 0.1 g of Cytarabine with 10 ml of hot *ethanol (96%)*, filter, allow the filtrate to cool and induce crystallization if necessary. Filter, wash the crystals with 2 ml of *ethanol (96%)* and dry at 60 °C at a pressure of 0.7 kPa. The *infrared absorption spectrum* of the crystals, Appendix II.A, is concordant with the *reference spectrum* of cytarabine.

Acidity: pH of a solution containing 2% (w/v) of Cytarabine in the solvent stated on the label, 4–6, Appendix V.L.

Related substances: Carry out the method of *thin-layer chromatography*, Appendix III.A, using *silica gel GF₂₅₄* as the coating substance and a mixture of 15 volumes of *water*, 20 volumes of *acetone* and 65 volumes of *butan-2-one* as the mobile phase. Apply separately to the plate 10 µl of each of the following four solutions in *water*. For solution (1) dissolve the contents of the sealed container in a sufficient volume to produce a solution containing 2% (w/v) of Cytarabine. For solution (2) dilute 1

volume of solution (1) to 200 volumes. Solution (3) contains 0.02% (w/v) of *uracil arabinoside EPCRS.* Solution (4) contains 0.02% (w/v) each of *uridine* and *uracil arabinoside EPCRS*. After removal of the plate, allow it to dry in air and examine under *ultraviolet light (254 nm)*. In the chromatogram obtained with solution (1) any spot corresponding to uracil arabinoside is not more intense than the spot in the chromatogram obtained with solution (3) (1%). Any other *secondary spot* in the chromatogram obtained with solution (1) is not more intense than the spot in the chromatogram obtained with solution (2) (0.5%). The test is not valid unless the chromatogram obtained with solution (4) show two clearly separated spots.

Water: Not more than 3% w/w, Appendix IX C. Use 0.8 g.

Assay: Determine the weight of the contents of each of 10 containers as described in the test for Uniformity of weight under Parenteral Preparations, Powders for Injections. Carry out the assay described for the ready-to-use injection but using the following solution as solution (2). Dissolve sufficient of the mixed contents of the 10 containers in *water* to produce a solution containing 0.002% (w/v) of Cytarabine.

Calculate the content of $C_9H_{13}N_3O_5$ in a container of average content weight using the declared content of $C_9H_{13}N_3O_5$ in *cytarabine BPCRS*.

4.1.2. United States Pharmacopoeia methods [6]

4.1.2.1. Cytarabine   Cytarabine contains not less than 98% and not more than 102% of $C_9H_{13}N_3O_5$, calculated on the dried basis.

Packaging and Storage—Preserve in well-closed, light-resistant containers.

Labeling—Where it is intended for use in preparing injectable dosage forms, the label states that it is sterile or must be subjected to further processing during the preparation of injectable dosage forms.

USP Reference Standard <**11**>**—***USP Cytarabine RS, USP Uracil Arabinoside RS USP Endotoxin RS*.

Identification

Test 1: Carry out the infrared test according to the general procedure <197 *M*>: Spectrum of potassium bromide dispersion of it, previously dried at a pressure of not more than 5 mm of mercury at 60 °C for 3 h, exhibits maxima only at the same wavelength as that a similar preparation of *USP Cytarabine RS*.

Test 2: The retention time of the major peak in the chromatogram of the *Assay preparation* corresponds to that in the chromatogram of the *Standard preparation* as obtained in the *Assay*.

Specific rotation: When the test is carried out according to the general procedure <**781S**>, *Test solution*: 10 mg/ml, in water, the specific rotation of cytarabine is between $+154°$ and $+160°$.

Loss on drying: Carry out the test according to the general procedure <**731**>—Dry cytarabine in vacuum at a pressure not exceeding 5 mm of mercury at $60°$ for 3 h. Cytarabine loses not more than 1% of its weight.

Residue on ignition: When the test is carried out according to the general method <**281**>, residue on ignition of cytarabine is not more than 0.5%.

Heavy metals: When the test is carried out as directed in *Method II* of the general procedure <**231**>, heavy metals in cytarabine is not more than 0.001%.

Chromatographic purity

Phosphate buffer—Prepare a solution containing 0.01 *M* monobasic sodium phosphate and 0.01 *M* dibasic sodium phosphate in a suitable container. Adjust with 0.1 *M* sodium hydroxide or 0.1 *M* phosphoric acid to a pH of 7.

Solution A—Prepare a filtered and degassed mixture of *Phosphate buffer* and methanol (49:1). Make adjustments if necessary (see *System Suitability* under *Chromatography*, in the general procedure <621>). Prepare this solution fresh daily.

Solution B—Prepare a filtered and degassed mixture of *Phosphate buffer* and methanol (7:3). Make adjustments if necessary (see *System Suitability* under *Chromatography*, in the general procedure <621>). Prepare this solution fresh daily.

Mobile phase—Use variable mixtures of *Solution A* and *Solution B* as directed under *Chromatographic system*.

System Suitability Solution—Dissolve suitable quantities of uridine, *USP Uracil Arabinoside RS*, and *USP Cytarabine RS* in water to obtain a solution containing about 0.02, 0.02, and 5 mg/ml, respectively.

Standard Solution—Dissolve an accurately weighed quantity of *USP Cytarabine RS* in water, and dilute quantitatively, and stepwise if necessary, with water to obtain a solution having a known concentration of about 4 µg/ml.

Test Solution—Transfer about 25 mg of Cytarabine, accurately weighed, to a 5 ml volumetric flask, dissolve in and dilute with water to volume, and mix. (NOTE: Prepare this solution fresh daily).

Chromatographic system (see *Chromatography*, in the general procedure <621>)—the liquid chromatograph is equipped with a 254-nm detector and a 4.6 mm × 25 cm column that contains packing L1. The flow rate is about 1 ml/min. The chromatograph is programmed to provide variable mixtures of *Solution A* and *Solution B*, the percentage of *Solution B* being 0% at the time of injection. This composition is held for

10 min. *Solution B* is then linearly increased to 100% over a period of 10 min. After maintaining this composition for 5 min, the percentage of *Solution B* is then linearly decreased to 0% over a period of 5 min. This composition is maintained for 20 min to equilibrate the system. chromatograph the *System suitability solution*, and record the peak responses as directed under *Procedure*: the relative retention times are about 0.55 for uracil, 1.14 for uridine, 1.62 for uracil arabinoside, and 1 for cytarabine; and the resolution, *R*, between cytarabine and uridine is not less than 1.25. Chromatograph the *Standard solution*, and record the peak responses as directed under *Procedure*: the relative standard deviation for replicate injections is not more than 3%.

Procedure: Inject equal volumes (about 20 μl) of the *Standard solution* and the *Test solution* into the chromatograph, record the chromatograms, and measure the peak responses. Calculate the percentage of uracil arabinoside in the portion of Cytarabine taken by the formula:

$$500 \times \frac{C}{W} \times \frac{r_i}{1.34\, r_s},$$

in which *C* is the concentration, in mg/ml, of *USP Cytarabine RS* in the *Standard solution*, *W* is the weight, in mg, of the specimen, 1.34 is the relative response factor for uracil arabinoside, r_i is the peak response of uracil arabinoside in the *Test solution*, and r_s is the peak response of *USP Cytarabine RS* in the *Standard solution*: not more than 0.3% is found.

Calculate the percentage of all other impurities in the portion of Cytarabine taken by the formula:

$$500 \times \frac{C}{W} \times \frac{r_i}{F\, r_s}$$

in which *C* is the concentration, in mg/ml, of *USP Cytarabine RS* in the *Standard solution*, *W* is the weight, in mg, of the specimen, r_i is the peak response of each impurity in the *Test solution*, r_s is the peak response of *USP Cytarabine RS* in the *Standard solution*, and *F*, the relative response factor, equals 2.5 for the uracil peak, with a relative retention time of 0.55; 1.5 for peaks with relative retention times of 0.38, 0.43, and 1.14; and 1 for all other peaks. Not more than 0.1% of any individual impurity is found, and not more than 0.3% of total impurities are found (including uracil arabinoside).

Other requirement—Where the label states the Cytarabine is sterile, it meets the requirements for *Sterility Test* in the general procedure <71> and for *Bacterial endotoxins* under *Cytarabine for Injection*. Where the label states that cytarabine must be subjected to further processing during the preparation of injectable dosage forms, it meets the requirements for *Bacterial endotoxins* under *Cytarabine for Injection*.

Assay

Phosphate Buffer—Dissolve 0.73 g of monobasic sodium phosphate and 1.4 g of dibasic sodium phosphate in 1 l of water, mix, and filter.

Mobile Phase—Prepare a filtered and degassed mixture of *Phosphate buffer* and methanol (95:5). Make adjustments if necessary (see *System Suitability* under *Chromatography*, in the general procedure <621>).

Standard preparation—Dissolve an accurately weighed quantity of *USP Cytarabine RS* in water, and dilute quantitatively, and stepwise if necessary, with water to obtain a solution having a known concentration of about 0.1 mg/ml.

Resolution Solution—Dissolve an accurately weighed quantity of *USP Uracil Arabinoside RS* in *Standard preparation,* and dilute quantitatively, and stepwise if necessary, with *Standard preparation* to obtain a solution having a known concentration of about 0.1 mg/ml.

Assay Preparation—Transfer about 10 mg of Cytarabine, accurately weighed, to a 100-ml volumetric flask, dissolve in and dilute with water to volume, and mix.

Chromatographic System (see *Chromatography*, in the general procedure <621>)—the liquid chromatograph is equipped with a 254-nm detector and a 4.6 mm × 25 cm column that contains packing L1. The flow rate is about 1 ml/min. Chromatograph the *Resolution solution*, and record the peak responses as directed under *Procedure*: the relative retention times are about 1 for cytarabine and 1.3 for uracil arabinoside, and the resolution, *R*, between cytarabine and uracil arabinoside is not less than 2.5. Chromatograph the *Standard preparation*, and record the peak responses as directed under *Procedure*: the relative standard deviation for replicate injections is not more than 2% (NOTE—After chromatography has been completed, flush the column with a mixture of water and methanol (7:3)).

Procedure—Separately inject equal volumes (abut 10 μl) of the *Standard preparation* and the *Assay preparation* into the chromatograph, record the chromatograms, and measure the responses for the major peaks. Calculate the quantity, in mg, of $C_9H_{13}N_3O_5$ in the portion of cytarabine taken by the formula:

$$100 \times C \times \frac{r_U}{r_S},$$

in which *C* is the concentration, in mg/ml, of *USP Cytarabine RS* in the *Standard preparation*, and r_U and r_S are the peak responses obtained from the *Assay preparation* and the *Standard preparation*, respectively.

4.1.2.2. Cytarabine for injection   Cytarabine for injection contains not less than 90% and not more than 110% of the labeled amount of cytarabine ($C_9H_{13}N_3O_5$).

Packaging and storage—Preserve in *Containers for Sterile Solids as described under injections as directed in the general method <1>.*

Constituted solution—At the time of use, it meets the requirements for *Constituted Solutions* under *Injection <1>.*

USP Reference Standards <11>—*USP Cytarabine RS. USP Uracil Arabinoside RS. USP Endotoxin RS.*

Identification: The retention time of the major peak in the chromatogram of the *Assay preparation* corresponds to that in the chromatogram of the *Standard Preparation*, as obtained in the *Assay*.

Bacterial endotoxins <85>—It contains not more than 0.07 USP Endotoxin Unit/mg of cytarabine.

pH <791>: Between 4 and 6, in a solution containing the equivalent of 10 mg of cytarabine/ml.

Water, Method 1 <921>: Water content in cytarabine is not more than 3%.

Other requirements: Cytarabine meets the requirements for *Stability Test <71>, Uniformity of Dosage Units <905>,* and labeling under *Injections <1>.* The drug substance in vial meets the requirements of *Cytarabine.*

Assay

*Phosphate buffer, Mobile phase, Standard preparation, Resolution solution, and Chromatographic system—*Proceed as directed in the Assay under Cytarabine.

*Assay preparation—*Separately constitutes 5 vials of *Cytarabine for Injection* in volume of water, accurately measured, corresponding to the volume specified in the labeling. Pool and mix the constituted solutions in a suitable container. Transfer an accurately measured volume of the constituted solution, equivalent to about 100 mg of cytarabine, to a 100-ml volumetric flask, dilute with water to volume, and mix.

*Procedure—*Separately inject equal volumes (about 10 µl) of the *Standard preparation* and the *Assay preparation* into the chromatograph, record the chromatograms, and measure the responses for the major peaks. Calculate the quantity, in mg, of $C_9H_{13}N_3O_5$ in the portion of constituted solution taken by the formula:

$$1000 \times C \times \frac{r_U}{r_S},$$

In which C is the concentration, in mg/ml, of *USP Cytarabine RS* in the *Standard preparation*; and r_U and r_S are the peak responses obtained from the *Assay preparation* and the *Standard preparation*, respectively.

4.2. Reported methods of analysis

4.2.1. Titrimetric method

Zaharans and Fridmanis [17] titrimetrically determined cytarabine by a periodate oxidation method. The stoichiometry of cytarabine periodate oxidation depends on the pH and duration of reaction. This titrimetric method is based on the oxidation of cytarabine with 2.5–6-fold excess of sodium peroxide in water during 21–48 h at room temperature.

4.2.2. Ultraviolet spectrometric methods

Tuncel *et al.* [18] used a rapid, accurate, and practical second-derivative UV spectrophotometric method for the determination of cytarabine. The unstable metabolite of cytarabine did not interfere at 299.4 nm. The calibration graph was rectilinear for 10–50 µM cytarabine, the determination limit was 2 µg/ml. The coefficients of variation were 19.96 and 19.80% in the analysis of ampoules by second-derivative and UV spectrophotometry, respectively.

Mahrous *et al.* [19] described a first- and second-derivative differential ultraviolet spectrophotometric methods for the analysis of cytarabine and acyclovir in their dosage forms. Acidic solution of the drugs in 0.1 *M* hydrochloric acid were measured at 290 nm (for the differential method) against the corresponding alkaline solution in 0.1 *M* sodium hydroxide as blanks. Similarly, the peak-trough amplitude were measured at 290/268 nm for cytarabine and 290/272 nm for acyclovir in the first-derivative method and at 298/276 nm for cytarabine and 296/276 nm for acyclovir in the second-derivative method. The calibration graphs showed rectilinear relationships obeying Beer's law in the concentration range 0.2–1 mg%.

Subramanian and Murthy [20] developed two simple spectrophotometric methods for the determination of cytarabine and its injection formulation. The estimation was carried out in distilled water and methanol and the methods were compared with the high-performance liquid chromatographic method reported in the United States Pharmacopoeia. Analytical parameter such as stability, accuracy, and precision have been established for both the methods and evaluated statistically to assess the applications of the two methods. Both the methods were found to have the advantages for simplicity, stability, reproducibility, and accuracy for using as an alternate to the existing nonspectrophotometric methods for the routine analysis of the drug in pharmaceutical formulations.

4.2.3. Chemiluminescence method

Chen *et al.* [21] used a flow-injection chemiluminescence method for the determination of cytarabine hydrochloride with online electrogenerated hypochlorite. A solution of 10 mM disodium hydrogen phosphate-sodium hydroxide buffer of pH 10 containing 0.12 *M* potassium chloride was electrolyzed at 200 µA in the setup until stable output of hypochlorite was reached. A 20 µl portion of 10 mM luminol was injected directly into a carrier stream of 0.1 *M* sodium hydroxide was mixed in a reactor (16 cm

long) and the chemiluminescence intensity was measured. When portions of a standard solution of cytarabine hydrochloride were injected into the flow-injection system as well as the reagents, an inhibition of the chemiluminescence intensity was detected. The calibration graph was linear from 10 ng/l to 0.1 μg/l of cytarabine hydrochloride with a detection limit of 8 ng/l for this chemiluminescence intensity reduction. The relative standard deviation was 3%. The method is applied to the analysis of the drug in injection solutions, with recoveries of 98.5−101.2%. Only Fe^{3+}, Cr^{3+}, and Co^{2+} produced negative interference.

4.2.4. Polarographic methods

Marin and Teijeiro [22] described a differential-pulse polarographic method for the determination of cytarabine and its isomer the nucleoside cytidine. Conditions for the differential-pulse polarography of the epimers cytarabine and cytidine were adjusted to determine either cytarabine or cytarabine-cytidine mixtures. Polarography was performed with a dropping mercury electrode, saturated calomel electrode, and a platinum counter electrode. For cytarabine alone, optimum conditions were pH 7, a scan rate of 2 mV/s, a pulse amplitude of 75 mV, a drop time of 1 s and a drop surface area of 0.88 mm^2. Rectilinear calibration graphs were obtained for 3–400 μM cytarabine, with a detection limit of 0.4 μM. For mixtures of cytarabine and cytidine, optimum conditions were pH 5.3, with a temperature of 5 °C, a scan rate of 1 mV/s, an amplitude of 50 mV and a drop time of 1 s. Calibration graphs of similar slopes were obtained for 1–60 μM cytarabine or cytidine. In the presence of cytarabine, the peak current of cytidine was increased by 16%. When allowance was made for this effect, good recoveries from mixtures of 10–60 μM cytarabine and cytidine were obtained. This method may be applicable to biological media after high-performance liquid chromatography separation.

Dogrukol and Tuncel [23] determined cytarabine in ampoules by polarographic techniques. Pharmaceutical liquid (1 ml) was diluted to 100 ml with water and a 10 ml portion was suitably diluted with 0.2 M potassium chloride-0.2 M phosphate buffer of pH 6 as supporting electrolyte. The electrolyte was deoxygenated with nitrogen and the direct current polarograms were recorded at a mercury drop electrode with a platinum wire auxiliary electrode versus silver/silver chloride with a drop time of 1 s, a pulse height of 50 mV and a scan speed of 4 mV/s. Both superimposed increasing amplitude pulse and differential pulse polarographic techniques were used. Relative standard deviation ($n = 6$) were 0.9 and 1%, respectively, for superimposed increasing amplitude pulse and differential pulse polarography at 20 mg of cytarabine. The results agreed well with those obtained by ultraviolet spectrophotometry.

Dogrukol and Tuncel [24] carried out an electroanalytical study on the cytarabine reduction process at a dropping mercury electrode in aqueous

supporting electrolyte solution using direct current polarography technique. The optimum parameters were found as 1000 dyne/cm^2 pressure on the mercury reservoir, 1 s drop time, 4 mV/s scan rate and 5.50–6.60 pH range. The reversibility of the reduction of the mercury electrode was ascertained as quasi-reversible and the polarographic current was mainly diffusion controlled. The results obtained by direct current stripping ion polarography, and differential pulse polarography allowed a method developed for the determination of cytarabine in the 1×10^{-4}–5×10^{-4} mol/l concentration range. Good results were obtained by applying the direct current polarography technique to the determination of cytarabine in pharmaceutical preparation.

Teijeiro and Marin [25] studied cytarabine systematically using polarography, cyclic voltammetry, and coulometry in buffered aqueous media in the pH range 4–11. The reduction mechanism proposed for cytarabine is also valid for cytosine and cytidine. Either an overall 4e$^-$ or 3e$^-$ process takes place, depending on the medium characteristics, pH, presence of surface-active substances, and a higher or lower concentration of an organic acid.

Teijeiro and Marin [26] also studied some aspects of the mechanism of reduction of cytarabine on a mercury electrode. Tafel slopes are obtained in the pH range 4–11 at potential corresponding to the foot of the wave. The mechanism at pH values below 6 is as follows: $[A + H^+ \rightleftharpoons HA^+]$ $[HA^+ + e^- \rightleftharpoons HA]$ $[HA^+ + H^+ \rightleftharpoons H_2A^+]$ $[H_2A^+ + e^- \rightleftharpoons H_2A]$ where the second electron-transfer step is the rate-determining step at the lower overpotentials, and the second protonation step is the rate-determining at the higher overpotentials. At pH values higher than 6 the mechanism is $[A + H^+ \rightleftharpoons HA^+]$ $[HA^+ + e^- \rightleftharpoons HA]$ $[HA + e^- \rightarrow HA^-]$ and the third step is the rate determining step.

Novotny and Vachalkova [27] determined the conditions for the polarographic reduction of cytarabine and several other nucleic acid components. Polarographic reduction, its character, and mechanism were studied in aqueous conditions of Britton Robinson buffer at different pH and in nonaqueous conditions of dry dimethylformamide. The polarographic wave of all compound had a diffuse character and the whole process was a 2-electron event which in dependence on pH may consist of two 1-electron steps. It was demonstrated on the hydrolysis reaction of cyclocytidine hydrochloride to arabinosylcytosine at alkaline pH that the polarographic method may be used for the documentation of structural changes of pyrimidine nucleoside going on in the polarographic chamber.

4.2.5. Voltammetric method

Abd El-Hady *et al.* [28] studied the electrochemical oxidation and reduction behavior of absorbed species of cytarabine in Sorensen buffer solution of pH values at an *in situ* mercury film electrode using cyclic voltammetry and Osteryoung square-wave stripping voltammetry. Optimal experimental and operational parameters have been selected for the drug preconcentration and determination in aqueous medium. Based on the adsorption and accumulation of cytarabine using Osteryoung square-wave anodic stripping voltammetry at mercury film electrode, the drug is easily detected as 0.134 ng/ml (5.51×10^{-10} M). Calibration plots have been constructed at different accumulation times. The standard deviation ($n = 10$) at a concentration level of 6×10^{-8} M cytarabine is 0.062. The interaction of ssDNA with the drug under the optimal conditions at pH 7.7 has been studied. The formal potential E° and $E^{\circ\prime}$ and the equilibrium constants K_1 and K_2 have been calculated for the free form of cytarabine and the bonded form with ssDNA, respectively. It was found that K_2 value for the bonded oxidized form is 298 times than that of K_1 for the bonded reduced form. Therefore, ssDNA has been found to interact strongly with the oxidized form of the drug. The method has been used for the nanogram determination of ssDNA with 1.9% variation coefficient. Detection limit of 3 ng/ml ssDNA has been achieved. Possible interfering organic compounds, cations, and anions have been tested. The method has been applied for the drug determination in urine samples, down to 0.23 ng/ml could be easily achieved in such samples.

4.2.6. Chromatographic methods

4.2.6.1. Thin layer chromatography   Paw and Misztal [29] determined cytarabine in human plasma by a thin-layer chromatographic method. Human plasma (1 ml) was diluted to 3 ml with methanol and the mixture was centrifuged. The supernatant (1.5 ml) was subjected to solid phase extraction on a Bakerbond C-18 column, the eluate was evaporated to dryness under nitrogen and the residue was redissolved in 500 µl methanol. Portions (5−15 µl) were spotted onto thin-layer chromatographic plate (20 × 10 cm) coated with 0.25 mm silica gel containing a fluorescent indicator, and the plates were developed in *n*-butanol-water-isopropanol (7:2:1). The analytes were visualized using UV light. The detection limits were 200 ng cytarabine. R_f values are tabulated for drug or the drug metabolite in seven mobile phases.

Clarke [1] recommended the following three TLC systems [30]:

System 1

Plates: Silica gel G, 250 µm thick, dipped in, or sprayed with, 0.1 M
   potassium hydroxide in methanol, and dried.
Mobile Phase: Methanol: strong ammonia solution (100:1.5).
Reference compounds:

| Diazepam | $R_f = 75$ | Chlorprothixene | $R_f = 56$ |
| Codeine | $R_f = 33$ | Atropine | $R_f = 18.$ |

R_f 05.

System 2

Plates: This system uses the same plates as in system 1 with which it may
   be used because of the low correlation of R_f values.
Mobile Phase: Cyclohexane: toluene: diethylamine (75:15:10).
Reference compounds:

| Diazepam | $R_f = 66$ | Pethidine | $R_f = 37$ |
| Desipramine | $R_f = 20$ | Codeine | $R_f = 06.$ |

R_f 00.

System 3

- *Plates:* This system uses the same plates as in systems 1 and 2 with
  which it may be used because of the low correlation of R_f values.
- *Mobile Phase:* Chloroform: methanol (90: 10).
- Reference compounds:

| Meclozine | $R_f = 79$ | Caffeine | $R_f = 58$ |
| Dipipanone | $R_f = 33$ | Desipramine | $R_f = 11.$ |

- $R_f = 01$ (acidified potassium permanganate solution, positive).

4.2.6.2. High-performance liquid chromatography   Pallavicini and Mazri-
mas [31] developed two analytical procedures to measure cytarabine and
its metabolite levels in biological samples. One method uses a quaternary
ammonium type anion-exchange resin to achieve isocratic separation in
less than 1 h. The second method utilizes a boronate-derivatized poly-
acrylamide column which binds cis-diols to selectively retain cytosine
and uridine, while arabinose compounds are eluted with recovery
approaching 100%. The eluted compounds are then easily quantitated
on a reversed-phase C-13 column. The sensitivity of both procedures was
sufficient to obtain pharmacokinetic data on cytarabine and uracil-
arabinose levels in serum and urine and on cytarabine triphosphate levels
in tumor cells. A Beckman chromatographic unit (Model 330) with a
variable-wavelength UV detector set at 270 nm to detect cytarabine and

metabolites. Aminex A-27 or A-29 (13.5 µm and 9.0 µm, respectively), strong anion-exchange resins were used for isocratic separation of cytarabine and its metabolites from naturally occurring compounds. The A-27 was slurry-packed at 140 bar into a stainless-steel column (500 nm × 4 mm) and nucleosides were eluted with 0.025 M sodium citrate and 0.08 M sodium tetraborate buffer, pH 9.3 at a pressure of 105 bar, a flow rate of 0.7 ml/min and at temperature of 65 °C. Nucleosides can also be eluted on a reversed-phase µBondapak (10 µm) C_{18} column (300 mm × 3.9 mm) with 0.01 M potassium phosphate, pH 5.6 at a flow rate of 0.6 ml/min. A guard column (7 cm) packed with Co: pell ODS was used when analyzing biological samples to protect the column from absorbing compounds. Cytarabine triphosphate was eluted from a slurry-packed Aminex A-29 resin (200 mm × 4 mm) using 0.25 M sodium citrate, pH 8.2 at a flow rate of 0.7 ml/min and temperature of 65 °C.

Plunkett *et al.* [32] described a sensitive high-performance liquid chromatographic method for the detection of cytarabine triphosphate in bone marrow and tissue samples obtained from patients receiving therapy with cytarabine. The method is rapid and sensitive and is useful for evaluating the biochemical and pharmacological bases of the therapeutic efficacy of treatment regimens that combine cytarabine and 3-deazauridine that require intracellular phosphorylation to their respective 5′-triphosphate for activity. A Waters Associates high-performance liquid chromatograph equipped with two pumps and a gradient programmer was used to analyze cytarabine triphosphate in perchloric acid-soluble cell extract. Samples of 0.01–2 ml were injected onto a column of Partisil 10 SAX anion-exchange resin with an injection system. Optimum separation of the nucleotides from normal cellular constituents was obtained by the following gradient scheme. Starting with the initial conditions of 65% buffer A, 0.005 M ammonium dihydrogen phosphate, pH 2.8 and 35% buffer B, 0.75 M ammonium dihydrogen phosphate, pH 3.7, a concave gradient was run at 3 ml/min for 30 min to the final condition of 100% buffer B. The eluted compounds were detected by their absorbance at 280 nm.

Linssen *et al.* [33] described a reversed-phase high-performance liquid chromatographic method for the determination of cytarabine and its metabolite uracil arabinoside in human plasma. After deprotonization of the plasma sample, separation is performed by reversed-phase high-performance liquid chromatography. For the cytarabine concentration exceeding 0.05 mg/l, injection volumes of 100 µl are applied. For lower concentrations an injection volume of 500 µl is used. Cytarabine is detected at 280 nm with a lowest detection limit of 0.002 mg/l in plasma. Cytarabine is detected at 264 nm with a lowest detection limit varying from 0.01 to 0.1 mg/l in plasma. This variation is caused by an unknown substance with the same elution properties as uracil arabinoside and

which appears to be present in plasma in variable concentrations. The coefficient of variation of the whole procedure is about 6% for cytarabine concentrations above 0.005 mg/l and for uracil arabinoside concentrations above 0.1 mg/l. For lower concentrations the coefficient of variation is about 14%. The chromatographic system used for this analysis consists of a Pye Unicam LC 3-XP pump, an injection valve equipped with a 500-µl loop, and two reversed-phase columns (Nucleosil 10 C_{18}, 250 × 4.6 mm, 10 µm) linked together to improve separation. Two UV detectors are used: a UV III monitor LDC 1203 with a 10-µl low cell and a fixed wavelength of 280 nm for cytarabine and a Pye Unicam LC-UV with an 8-µl flow cell and variable wavelength set at 264 nm for uracil arabinoside.

Tuncel *et al.* [34] developed a rapid stability-indicating isocratic reversed-phase high-performance liquid chromatographic assay method for the analysis of the hydrolysis products of cyclocytidine; cytarabine, and uracil arabinoside. The analysis employs a 4.6 cm column together with a low methanol mobile phase containing 1-heptane sulfonic acid at pH 2.9. The ion-pairing of cyclocytidine, a cation, was independent of pH. However, ion-pairing of cytarabine was controlled by adjusting the pH to 2.9 which is below its pKa of 4.2. The retention time of neutral uracil arabinoside (pKa = 9.2) was not affected by either pH or the ion-pairing agent. Its separation was achieved by using a primarily aqueous mobile phase with the minimum methanol required for the other components. The time courses for cyclocytidine and its hydrolysis products were successfully defined under a variety of aqueous conditions. An isocratic separation was employed using one pump of a gradient liquid chromatograph having a 20 µl loop on the injection port and a 254 nm ultraviolet detector with 8 µl analytical cuvet and pump. An all-glass 250 µl syringe was used to fill the loop throughout the study. A 4.6 cm × 4.2 mm column was packed with Spherisorb (5 µm) ODS C-18 under 4000 psi using a Haskell pump. The mobile phase is 0.005 M aqueous 1-heptane sulfonic acid and 30 ml of methanol, degassed, and adjusted to pH 2.9 with glacial acetic acid.

Breithaupt [35] described a high-performance liquid chromatographic method for the determination of cytarabine and its main metabolite uracil arabinoside. Complete separation from endogenous constituents was achieved by isocratic reversed-phase chromatography using phosphate buffer (0.05 M, pH 7) as eluent. The limit of detection was 50 ng/ml. Day-to-day coefficients of variation were below 10%. The applicability of this rapid, simple, and specific method for pharmacokinetic studies and monitoring of therapy was demonstrated. This study were performed using a stainless-stell tube (30 cm × 4 mm) filled with Spherisorb ODS (5 µm). The chromatograph was operated at a flow-rate of 1.6 ml/min and a pressure of 210 bar at room temperature. The eluent was monitored at

270 nm, the absorption maximum of cytarabine in 0.05 M phosphate buffer at pH 7.

Danks [36] described two simple high-performance liquid chromatographic methods for the simultaneous determination of 2'-deoxycytidine-5'-triphosphate and cytarabine-5'-triphosphate concentrations in biological samples. The ratio of the cytarabine metabolite to the andogenous nucleotide may be important in determining the effectiveness of cytarabine therapy. The high-performance liquid chromatograph used was a Beckmann Model 332, with a Partisil SAX 10 anion-exchange column (25 cm $\times$ 4.6 mm). In the first method, the mobile phase was 500 mM ammonium dihydrogen phosphate (pH 3.5) with 2% methanol. The flow rate was 0.5 ml/min. The methanol was added to the buffer at the beginning of each day and was used for 1 day only. The solution was filtered and kept under vacuum for 30 min if the most sensitive scale, 0.005 absorbance units full scale was used, or baseline drift interpretation of the graphs difficult. In the second method, a gradient system was used and the separated 2'-deoxycytidine-5'-triphosphate and cytarabine-5'-triphosphate peaks by greater than 2 min. The buffers used were: Buffer A, 150 mM ammonium dihydrogen phosphate (pH 3.5); Buffer B, 750 mM ammonium dihydrogen phosphate (pH 3.5) with 5% methanol. The flow rate was 0.5 ml/min. The gradient was programmed as follow: (1) 0–10 min, 0–5% buffer B, (2) 10–20 min, 50–10% buffer B, (3) 20–50 min, 10–100% buffer B, and (4) 50–60 min, 100–0% buffer B. The elution profiles obtained by both methods were monitored at 254-nm and at 280 nm and the peak areas of the output of the 254-nm detector were quantitated by an integrator.

Linssen *et al.* [37] described a rapid and sensitive isocratic high-performance anion-exchange column chromatographic method for the determination of cytarabine triphosphate in leukemic cell. A Pye-Unicam pump, equipped with an automatic injection valve, a 100-μl loop, and a column (250 $\times$ 4.6 mm) packed with Partisil-10 SAX anion-exchange resin (10 μm) was used for the separation. A guard column (30 $\times$ 4.6 mm), Partisil-10 SAX is incorporated in the system to protect the analytical column. Two UV detectors were used: an UV III monitor LDC 1203 (10-μl flowcell, wavelength 280 nm) and a Pye-Unicam LC-UV (8-μl flowcell, wavelength 254 nm). Samples of 100 μl of cell extract are injected into the column. Elution is carried out at a constant temperature (35 °C) and at a constant flow-rate of 2.5 ml/min with 0.125 M potassium dihydrogen phosphate solution, containing 0.075 M trisodium citrate as counter-ion, adjusted to pH 4.6 (at 35 °C) with phosphoric acid. Helium gas is led through the eluent to prevent development of air bubbles at the low pressure side. Detection of cytarabine triphosphate is optimal at 280 nm. Peak heights are used for quantitation, whereas ratios of the absorbance at 280 nm and at 254 nm are used for purity control of the peaks.

Sinkule and Evan [38] developed a novel, dual-column high-performance liquid chromatographic method for the determination of cytarabine and its major metabolite uracil arabinoside. This analytical procedure is sensitive (25 ng/ml) and specific for cytarabine, uracil arabinoside and the endogenous nucleoside that may influence response to cytarabine therapy, cytidine, and deoxycytidine. Conventional and high dose calibration curves were linear and the method precise with the assay coefficient of variation for cytarabine and uracil arabinoside not greater than 9.1% over the range of 0.1–10 µg/ml. Accuracy was determined to be within ± 3–9% over this concentration range. Using this method, patient plasma samples from both conventional dose (100–200 mg/m^2 per day) and the high dose (3500–6500 mg/m^2 per day) cytarabine, can be simultaneously analyzed for cytarabine and uracil arabinoside and nucleosides so that comparative pharmacokinetic and pharmacodynamic studies can be conducted. The chromatographic conditions used a mobile phase of 2.5 mM potassium dihydrogen phosphate (pH 3.2) with 2.5% methanol. Waters Associates Model M-45 high-performance liquid chromatographic pump, a Rheodyne Model 7125 injector with a 100-µl sample loop, and a 5-µm reversed-phase Ultrasphere-ODS column (15 cm × 4.6 mm), connected in series with a 10-µm cation-exchange column (Partisil PXS 10/25 SCX; 25 cm × 4.6 mm). The column effluent was monitored for UV absorbance at 280 nm. The mobile phase flow-rate was about 0.8 ml/min at a pressure of 17 MPa (2500 p.s.i.).

An et al. [39] developed a high-performance liquid chromatographic method for the determination of cytarabine and its metabolite uracil arabinoside in plasma of leukemia patients. A reversed-phase ion-pairing technique using the free amino group of the pyrimidine ring of cytarabine was used to determine the plasma concentration of cytarabine and its metabolite uracil arabinoside in patient samples. Chromatographic separation was achieved on C_{18} column with acetonitrile-methanol-0.01 mol/l phosphate buffer. The standard curve was linear at 0.25–25 mg/l for cytarabine, 5–100 mg/l for the metabolite uracil arabinoside. The minimum detection concentration was 0.1 mg/l for cytarabine, 0.2 mg/l for uracil arabinoside. Intra- and inter-day assay precision were <9% and 11% for cytarabine, 1% and 3% for uracil arabinoside, respectively. The recovery was between 99 and 105%. The simple method offers accuracy, precision, sensitivity, and efficiency for plasma cytarabine and its metabolite uracil arabinoside determination.

Burk et al. [40] described an ion-pair high-performance liquid chromatographic method for the determination of cytarabine and uracil arabinoside in human plasma. Complete separation is achieved within 10 min using a reversed stationary phase and an isocratic eluent containing 0.4 mmol/l heptane sulfonic acid as modifier. Detection by ultraviolet absorption occurs at 270 nm. Quantification of cytarabine and its main

plasma metabolite, uracil arabinoside is achieved by means of internal standardization using adenine arabinoside. Retention times of uracil arabinoside, cytarabine, and adenine arabinoside are 3.9, 5.9, and 9.4 min, respectively. Detection limit of cytarabine and uracil arabinoside are 10 and 15 ng/ml, respectively. During a pharmacokinetic study of high-dose cytarabine treatment no interference could be observed in plasma samples.

Gao *et al.* [41] established a high-performance liquid chromatographic method for the determination of cytarabine hydrochloride for injection. The contents of cytarabine hydrochloride were detected by high-performance liquid chromatography with C_{18} column, phosphate buffer solution-methanol (90:10) as mobile phase. The results showed that the calibration curves were linear in the range from 10 to 25 µg/ml, $r = 0.9997$, recovery 99.9%, and relative standard deviation 0.62%. The results indicated that this method was feasible. Other high performance liquid chromatographic methods [42–63] are listed in Table 2.6.

4.2.6.3. Gas chromatography-mass spectrometry   Boutagy and Harvey [64] used gas chromatography and gas chromatography-mass spectrometric methods for the analysis of cytarabine and related pyrimidine nucleoside. Acetyl methyl derivatives of cytarabine and six other pyrimidine nucleosides were prepared and examined by gas-liquid chromatography using a nitrogen-sensitive flame ionization detector and by gas chromatography-mass spectrometry. The derivatives gave symmetrical gas chromatographic peaks and could be separated on SE-30 or OV-17. Detection limit for cytarabine was approximately 500 pg using both the nitrogen-sensitive flame ionization detector and single-ion monitoring $((M-15)^+$ ion). Methyl trimethylsilyl and three homologous alkyl oxime trimethylsilyl derivatives of cytarabine and cytidine were also prepared and examined by gas chromatography-mass spectrometry. Retention indices reported on four phases and the mass spectra of these derivatives discussed. The methyl trimethylsilyl derivatives gave a lower detection limit than the methyl acetyl derivatives ($\sim$50 pg), but the oxime derivatives were less sensitive. Allyl and propyl dimethylsilyl derivatives of cytarabine were also examined.

Boutagy and Harvey [65] also determined cytarabine in human plasma by gas chromatography with a nitrogen-sensitive detector and by gas chromatography-mass spectrometry. To increase volatility, a double derivative of cytarabine was used, prepared by acetylation and subsequent methylation. Cytidine was used as internal standard for the gas chromatographic procedure and the column was packed with either 3% SE-30 on Chromosorb W or 3% OV-17 on Gas-Chrom Q, Helium was used as the carrier gas. For the gas chromatography-mass spectrometry the column was packed with either 3% OV-17 or SE-30. Gas

TABLE 2.6 High-performance liquid chromatographic conditions of the method used for the determination of cytarabine

Column	Mobile phase and (flow rate)	Detection	Remarks	Ref.
Precolumn (3 cm × 4.6 mm) of Ranin OD-MP RP-18 Spheri 5 and (10 cm × 4.6 mm) of the same packing.	Aqueous ammonia, formic acid, formic acid buffer solution and/or acetonitrile.	254 nm	Analysis of cytarabine and uracil arabinoside in biological samples. Recovery was 98–113%. Cefmetazole was used as internal standard.	[42]
25 cm × 4.6 mm of Nucleosil 5 C_{18}	Potassium dihydrogen phosphate (13.6 g/l) of pH 3 [1.5 ml/min]	254 nm	Cytarabine injection, formulation, quality assessment and shelf-life prediction. 2-Deoxy uridine was used as internal standard.	[43]
Radial-Pak C_{18} (5 µm) cartridge in a RCM 100 radial compression module.	Gradient elution by 0–10% acetonitrile (over 30 min) in 100 mM potassium dihydrogen phosphate containing 5 mM tetrabutylammonia phosphate (pH 4.5), followed by 14 min of isocratic elution with 10% acetonitrile in the phosphate solution.	280 nm	Simultaneous assay of the drug and its nucleotides and metabolites by ion-pair high-performance liquid chromatography. Detection limits were 5–10 pmol for cytarabine and cytosine arabinonfuronside-5′-triphosphate, respectively.	[44]

Precolumn 2 cm × 4.6 mm of Spherisorb ODS (10 μm) and analytical column 25 cm × 4.6 mm of Hypersil ODS (5 μm)	2.5 mM potassium dihydrogen phosphate buffer, adjusted with phosphoric acid to pH 3.1, containing 5 mM sodium hexane sulphonate (mobile phase A). Sample was then transferred to the analytical column using mobile phase A-methanol (22:3) [1.5 ml/min]	280 nm	Determination of the drug in plasma. Calibration graph was rectilinear for 0.05–10 mg/l of the drug in plasma. Recovery averaged 100.2%. Detection limit was 25 μg/l.	[45]
30 cm × 3.9 mm of μ Bondapak C_{18}	Aqueous 5% methanol containing disodium hydrogen phosphate-sodium dihydrogen phosphate buffer pH 7 [1 ml/min].	254 nm	Determines cytarabine and azacitidine and their degradation products by high-performance liquid chromatography.	[46]
25 cm × 4 mm steel column of Bondapak C_{18}	10–100 mM phosphate buffer of pH 4.8–5.3 containing 0.1–2.5 M ammonium sulphate.	265 nm	Reversed-phase high-performance liquid chromatography of abnormal antitumor nucleosides.	[47]

TABLE 2.6 (*continued*)

Column	Mobile phase and (flow rate)	Detection	Remarks	Ref.
25 cm × 4.6 mm of Partisil-10 SAX (10 μm)	Concave gradient elution with 5 mM ammonium dihydrogen phosphate (pH 2.8) containing 30–100% of 0.75 M ammonium dihydrogen phosphate (pH 3.5) [3 ml/min].	262 nm	Separation of cytarabine triphosphate in human leukemia cells by high-performance liquid chromatography. Calibration graphs were rectilinear for 50–800 pmol.	[48]
25 cm × 4.6 mm of Ultrasphere ODS (5 μm)	5 mM sodium dihydrogen phosphate and 1 mM disodium hydrogen phosphate containing 5% of methanol.	254 nm	Substituent effect on degradation rates and pathways of cytosine nucleosides	[49]
15 cm × 3.9 mm of μBondapak C_{18} (10 μm) with a precolumn of Corasil II	0.5 M Ammonium acetate (pH 6.5) [1.5 ml/min].	280 nm	High-performance liquid chromatography monitoring of cytarabine and its metabolite uracil arabinoside in serum.	[50]
25 cm × 4.9 mm of Partisil SAX (10 μm) anion-exchange resin with a guard column of	2 mM potassium dihydrogen phosphate (pH 2.85), 500 mM potassium dihydrogen phosphate (pH 3.4) and	254 nm	Determination of ^{3}H-labeled cytarabine and eight metabolites in cell extracts by high-performance liquid	[51]

pellicular anion-exchange silica.	acetonitrile−2 mM potassium dihydrogen phosphate of pH 2.85 (4:1) [1 ml/min].		chromatography and scintillation spectrometry.	
25 cm × 4.65 mm of Ultrasphere ODS (5 μm) and Brownlee C_{18} guard column	3.5 mM potassium dihydrogen phosphate (pH 3.3)-methanol (49:1) [1 ml/min]	280 nm	Analysis of cytarabine and uracil arabinoside in cereprospinal fluid and plasma.	[52]
25 cm × 4.6 mm of Nucleosil C_{18} (5 μm) equipped with a guard column (3 cm × 4 mm) of the same material and a precolumn (25 cm × 4.6) of C_{18} material (40 μm).	0.1 M potassium dihydrogen phosphate (pH 2.7) containing 5 mM tetrabutylammonium phosphate and 0.5% of acetonitrile. [0.8 ml/min for 16 min followed by back flushing at 1.4 ml/min for further 9 min].	280 nm	Detection and separation of intracellular cytarabine 5′-triphosphate by ion-pair high-performance liquid chromatography.	[53]
25 cm × 4.6 mm of octadecyl Si 100 Polyol (5 μm)	0.1 M phosphate buffer (pH 5.05).	265 nm	Determination of cytarabine and 6-azacytidine and their deamination products in blood by high-performance liquid chromatography.	[54]

(*continued*)

TABLE 2.6 (*continued*)

Column	Mobile phase and (flow rate)	Detection	Remarks	Ref.
25 cm × 4.6 mm of Octadecyl Polyol Si 100 (5 μm) operated at 35 °C	0.1 M phosphoric acid adjusted to pH 5.1 with 0.1 M sodium hydroxide [0.5 ml/min].	265 nm	Simultaneous analysis of cytarabine, 6-aza-cytidine, 6-azauridine, and uracil arabinoside in blood by high-performance liquid chromatography.	[55]
12 cm × 4.6 mm of EnCaPharm 100 RP 18 (5 μm) reversed-phase packing.	Phosphate buffer solution of pH 7.	260 nm	Determination of cytarabine and four of its decomposition products by high-performance liquid chromatography.	[56]
4 × 4 mm of C_{18} cartridge (5 μm). Retained analyte was transferred to the analytical Nucleosil 120−7 phenyl column (25 cm × 4 mm) operated at 8 °C.	15 mM disodium hydrogen phosphate, 5 mM tetrabutylammonium sulphate, 25 mM sodium dihydrogen phosphate (buffer A) containing 30% acetonitrile [2 ml/min]. Retained analytes eluted by buffer A of pH 6.8 containing 50% acetonitrile [0.6 ml/min].	275 nm	Highly sensitive high-performance liquid chromatography method for analysis of cytarabine ocfostate with a detection limit of 2 ng/ml and calibration graph was linear from 5–500 ng/ml. Recoveries were 56.4–64.1%.	[57]
15 cm × 3.9 mm of C_{18} Nova-Pak radial	Methanol-acetonitrile-10 mM potassium	280 nm	Determines plasma or cerebrospinal fluid	[58]

compression column (4 μm) with a C_{18} Nova-Pak Guard-Pak precolumn in a Waters Z compression module.	phosphate buffer (1:3:96) containing 27.5 mM 1-pentanesulphonic acid adjusted to pH 4 with potassium hydroxide [1.8 ml/min]		cytarabine in paediatric pharmacokinetic analysis. Calibration graphs were linear for 250 μM cytarabine. Detection limit: 0.1 μM.	
Teicoplanin stationary phase.	Reversed mobile phase of Methanol: buffer pH 4.05 (20:80)	285 nm	Simultaneous micellar electrokinetic chromatography and liquid chromatography of Tarapine PFS and adriblastina in biological fluids.	[59]
25 cm × 4.6 mm of C_{18} column (5 μm) protected by a 5 μm C_{18} precolumn (30 cm × 5 mm).	Aqueous 2.5 mM tetrabutyl-ammonium phosphate-acetonitrile (494:1) [0.8 ml/min]. After 13.5 ml eluent had passed through it was followed by 0.1 M potassium dihydrogen phosphate, 5 mM tetrabutyl ammonium phosphate and 0.5% acetonitrile.	Radioactivity measured in a 250 μl detector cell containing CaF_2 as a solid scintillator	Detection and analysis of the major metabolite of ^3H cytosine arabinoside by high-performance liquid chromatography. The detection limit for seven major metabolites were 40–110 pg.	[60]
25 cm × 4 mm of Nucleosil C_{18} (5 μm)	Phosphate buffer-methanol	UV and fluorimetry	Trace enrichment high-performance liquid	[61]

(*continued*)

TABLE 2.6 (*continued*)

Column	Mobile phase and (flow rate)	Detection	Remarks	Ref.
with a 11-mm guard column of the same packing.			chromatography separation and biodegradation of cytostatic compounds in surface water.	
Five silica columns:15 cm × 4.6 mm of Zorbax SIL (two columns), 25 cm × 4 mm of Silasorb 600, 25 cm × 4.6 mm of Supelcosil LC-SI and 15 cm × 3.9 mm of Nova-Pak Silica.	Hexane-isopropanol-ethanediol.	—	Five silica columns used for the analysis of cytarabine and nine other compounds in ternary mobile phase systems.	[62]
3 μm Supelguard column (1 cm × 4.6 mm) and a 3 μm Supelcosil LC-18 analytical column (3.3 cm × 4.6 mm)	10 mM Aqueous ammonium acetate buffer (pH 6.9). [0.8 ml/min]	272 nm	Measurement of surface contamination from nucleoside analog antineoplastic drugs by high-performance liquid chromatography in occupational hygiene studies for oncologic hospital departments. 5-Bromo uracil was used as an internal standard.	[63]

chromatography-mass spectrometry was performed with either cytidine as internal standard and detection by single-ion monitoring or by the use of $[^2H_3]$-acetate-methyl derivative of cytarabine as internal standard and subsequent multiple-ion monitoring. Attempted extraction of cytarabine from plasma with various organic solvents was unsuccessful, but protein precipitation with ethanol or trichloroacetic acid followed by washing the aqueous residue with organic solvents to remove as many of the interfering substances as possible gave satisfactory results. The minmum detectable quantity of pure cytarabine was similar for both techniques ($\sim$500 pg). However, with gas chromatography using a nitrogen-sensitive detector, the lower limit of detection from plasma was approximately 40–70 ng/ml plasma, whereas gas chromatography-mass spectrometry showed greater analytical selectivity with a detection limit in some cases as low as 1 ng/ml plasma.

Makino *et al.* [66] used a mass fragmentographic method for the simultaneous determination of cytarabine and uracil arabinoside, the urinary metabolites of N^4-behenoyl-1-β-D-arabinofuranosylcytosine. Acetyl methylated cytarabine and acetylated uracil arabinoside were prepared and examined by gas chromatography-mass fragmentography. Each derivative was separated on 3% SE-30 column at 250°. The contents of cytarabine and uracil arabinoside were estimated from the calibration curve with papaverine as an internal standard. The urinary metabolites of N^4-behenoyl-1-β-D-arabinofuranosylcytosine could be analyzed by this method without any extraction or separation procedure. The method is suitable for the selective analysis of cytarabine and uracil arabinoside from the urinary metabolites of N^4-behenoyl-1-β-D-arabinofuranosylcytosine.

4.2.6.4. Miceller electrokinetic capillary chromatography

Abd El-Hady *et al.* [59] described an analytical procedure for the simultaneous determination of cytarabine and adriblastina by micellar electrokinetic chromatography and liquid chromatography. For the micellar electrokinetic chromatography analysis, separation, and identification were accomplished using uncoated fused-silica capillary with hydrodynamic injectins in the presence of 50 mM borate/phosphate pH 8.7 and 100 mM of sodium dedecyl sulphate. The migration times of cytarabine and adriblastina were found to be 2.70 and 6.40 min, respectively. Calibration curves were established for 10–300 ng/ml ($r = 0.998$) cytarabine. The methods were applied for the determination of the analytes in urine samples.

Houze *et al.* [67] described a miceller electrokinetic capillary chromatographic method for the quantification of cytarabine and its metabolite uracil arabinoside, in human serum. Cytarabine is widely used to induce remission in adult granulocytic leukemia. High doses can be infused in refractory leukemia or in relapse. After injection, cytarabine

is quickly metabolized to uracil arabinoside, the main inactive metabolite. This method describes an miceller electrokinetic capillary chromatographic method to determine simultaneously cytarabine and uracil arabinoside in human serum using 6-O-methylguanine as an internal standard. The assay was linear from 6.25 to 200 μg/ml with a quantification limit between 3 and 6 μg/ml. The analytical precision was satisfactory at between 2 and 4.3 (within-run) and 3.7% and 7.3% (between runs). This assay was applied to the analysis of serum from an acute granulocytic leukemia patient treated by high dose of cytarabine (3 g/m² body surface).

4.2.6.5. Electrophoresis   Lloyd *et al.* [68] described a validated assay method for the determination of cytarabine in human serum by capillary electrophoresis using the P/ACE system 2000. Cytarabine was extracted from serum (200 μl) with use of C-18 solid-phase extraction cartridges and acetonitrile as eluent. The eluate was reduced to dryness and the residue was dissolved in water. The resulting solution was centrifuged and a portion of the supernatant solution was analyzed by the cited system with use of a fused-silica capillary (26 cm × 50 μm; 20 cm to the detector), 20 mM citrate buffer (pH 2.5), a separation potential of 8 kV and detection at 280 nm. Intra- and inter-day coefficients of variation were 15.2 and 12%, respectively. Cytarabine eluted in 5 min with no observed interference. Injection was by pressure for 10 s resulting in a total injected volume of 28 nl. The detection limit was 0.5 μM cytarabine and response was rectilinear from 1 to 10 μM.

Lloyd *et al.* [69] also determined cytarabine in plasma using capillary electrophoresis method. Plasma sample was applied to a Bond Elut C-18 cartridge prewashed with acetonitrile and water; the cartridge was washed with water before elution of cytarabine with acetonitrile. The eluent was evaporated at room temperature under nitrogen and an aqueous solution of the residue was analyzed by electrophoresis in fused-silica capillary (26 cm × 50 μm) with use of 40 mM citrate buffer of pH 2.5 and on-capillary detection at 280 nm. By using peak stacking, a symmetrical peak for cytarabine was obtained and the calculated separation efficiency was 71,000 plates. The detection limit was 0.5 μM cytarabine and the calibration graph was rectilinear from 1 to 10 μM cytarabine in plasma. At 2 μM cytarabine, the intra- and inter-day coefficients of variation were 15.2% ($n = 10$) and 12.0% ($n = 13$), respectively.

Krivankova *et al.* [70] separated cytarabine and cytidine by capillary-electrophoretic techniques. Cytarabine and cytidine were separated in a fused-silica capillary (80 cm × 100 μm: 60 cm to detector), with 10 mM *N,N*-bis-(2-hydroxyethyl)-2-aminoethane sulphonic acid adjusted to pH 7 with sodium borate containing 40 mM sodium dedecyl sulfate and

detection at 275 nm. Separation was also achieved in a fused-silica capillary (43.2 cm $\times$ 100 μm; 35.2 cm to detector) coated with polyacrylamide at 30 °C and 15 kV with 0.1 M acetate buffer pH 4.2 as running buffer and detection at 275 nm. Under these conditions, the calibration graphs were linear for 1.3 (detection limit) to 37 μg/ml cytarabine and cytidine and the relative standard deviation ($n = 6$) was 1%. Separation was also achieved under alkaline solutions at 10 kV in uncoated capillaries with 50 mM boric acid of pH 9 (adjusted with sodium hydroxide) containing 60 mM sodium dedecyl sulfate as run buffer. Calibration graphs were linear for 0.47 (detection limit) to 300 μg/ml. The last method was used to determine cytarabine and cytidine in serum. The relative standard deviation was 5–3% at 2.4 μg/ml of cytarabine.

4.2.6.6. Isotachophoresis   Liliemark *et al.* [71] described an isotachophoresis method for the determination of cytarabine 5′-triphosphate in leukemic cells incubated with cytarabine. After incubation with cytarabine at 37 °C, the cells were rapidly washed and suspended in perchloric acid (0.7 M): methanol (80:20) at −10 °C to precipitate proteins. After centrifugation, portions (2–12 μl) of the supernatant were injected into the LKB Tachophor 2127. Hydrochloric acid (5 mM) buffered to pH 4 with ε-aminocaproic acid was used as the leading ion and glutamic acid (10 mM) was the terminating ion. Quantification was done by UV absorption. Cytarabine 5′-triphosphate could be separated from endogenous nucleoside triphosphates. When cytarabine 5′-triphosphate was added to a homogenate of untreated leukemic cells and portions were injected into the Tachophor, a linear relation was observed between the amount of cytarabine 5′-triphosphate and the peak hight from 15 pmol. After incubation of the isolated leukemic cells with 50 μM of cytarabine for 1 h, the intercellular concentration of cytarabine-5′-triphosphate was about 100 pmol/10^6 cells.

5. RADIOIMMUNOASSAY

Piall *et al.* [72] developed a radioimmunoassay method for the determination of cytarabine using antiserum raised in a sheep to cytarabine monophosphate—ovalbumin conjugate. The antibody shows only 0.008% cross-reactivity with uracil arabinoside and low (0.023%) cross-reactivity with other commonly coadministered drugs such as cytotoxic and antibacterial agents, and also a number of naturally occurring nucleoside and nucleotides. It does, however, cross-react by 125% with cytarabine monophosphate and by 109% with cytarabine triphosphate. As little as 1 ng/ml of cytarabine can be detected in plasma, serum, urine, and cerebrospinal fluid with no need for prior extraction.

This radioimmunoassay has been used to follow the disappearance of cytarabine from the plasma of patients receiving the drug.

Sato *et al.* [73] established a sensitive and specific radioimmunoassay method for cytarabine or uracil arabinoside, by using ^{3}H-cytarabine and anticytarabine antiserum or ^{3}H-uracil arabinoside and antiuracil arabinoside antiserum. The antiserum was prepared by immunizing rabbits with cytarabine or uracil arabinoside hapten conjugated to human albumin. In this assay, as low as 2.5 ng/ml (0.01 µM) of cytarabine or 5 ng/ml (0.02 µM) of uracil arabinoside in blood plasma samples could be detected. The cross-reaction of cytarabine or uracil arabinoside structurally related compounds with each antiserum was so small that the nucleosides could be determined without any purification procedure. The plasma concentration of cytarabine and uracil arabinoside in mice following oral administration of an antileukemic agent, cytosine arabinoside-5′-stearylphosphate (100 mg/kg), or cytarabine (48 mg/kg) was determined by using this method. In case of cytosine arabinoside-5′-stearylphosphate administraton, cytarabine was detectable in blood for at least 24 h longer than in the case of cytarabine administration. This method is suitable for the analysis of cytarabine and uracil arabinoside, the metabolites of depot drugs of cytarabine such as cytosine arabinoside-5′-stearylphosphate.

Shimada *et al.* [74] developed a sensitive and specific radioimmunoassay method for the determination of the blood level of cytarabine using anticytarabine serum, [5–3 H] cytarabine and a dextran-coated charcoal. The anticytarabine serum obtained from a guinea pig was hardly cross-reactive with uracil arabinoside, tetrahydrouridine, and other cytarabine analogs. The radioimmunoassay system for cytarabine could detect concentrations as low as 60 pg/ml in plasma. Average intra- and interassay variations at 5, 10, and 20 ng/ml were 4.3% and 5.6%, respectively. Cytarabine in blood samples obtained from human patients who orally received N^4-palmitoyl-1-β-D-arabinofuranosyl cytosine was determined by the present radioimmunoassay system.

A radioimmunoassay method for cytarabine and other arabino nucleoside in blood plasma was described in which radiolabeled arabino-nucleoside and anti-arabino-nucleoside antibody are mixed with a sample, and radioactivity of free or antibody-bound arabino nucleoside is counted [75]. Arabino nucleoside antigen was prepared by binding arabino nucleoside to carrier protein through dicarboxylic acid groups in the protein and the hydroxyl group at the 3′ position in the arabino nucleoside. Thus for the determination of cytarabine in blood plasma, antigen was prepared as follows: 3′-O-succinylarabinofuranosyl cytosine was prepared by mixing 2,2′-cyclocytidine-5′-monophosphate and anhydrous succinic acid in dioxane and triethylamine, and hydrolyzing the reaction product with phospho-monoesterase and treating with anion-exchange resin. The human blood serum albumin with conjugated with 3′-O-succinylarabinofuranosyl

cytosine and 3'-*O*-succinylarabinofuranosyl cytosine-albumin (mol. ratio = 11.6) was obtained. Antibody to this antigen was obtained from rabbits. This antibody was specific to cytarabine and it could distinguish the derivative of cytarabine at the 5' position and other derivatives. Known amounts of ^{3}H-labeled cytarabine and antibody were mixed in a blood plasma sample. After 1 h incubation at 0 °C, free ^{3}H-labeled cytarabine was separated by centrifugation with activated carbon. The radioactivity of the supernatant was counted with a liquid scintillation counter, and concentrations of cytarabine were calculated based on a calibration curve which was with standard cytarabine.

Okabayashi and Moffatt [76] described a radioimmunoassay method for the analysis of cytarabine in plasma. 1-(5-*O*-Succinyl-β-D-arabinofuranosyl)cytosine is prepared and coupled to serum albumin for use as an antigen to prepare antibodies in rabbits. The limit of sensitivity for cytarabine was 0.7 pmol, the calibration curve was linear for values $\leq$3 pmol, and the assay precision was 0.10 at 1 pmol. The assay was used to determine the plasma levels of cytarabine in mice after injection of 1-(3-*O*-octanoyl-β-D-arabinofuranosyl)cytosine. The relationship between the chain length of the acyl group and the susceptibility to plasma esterase of 3'-*O*-acylated cytarabine derivatives was determined. The affinity of the antibody for cytarabine metabolites and analogs is described. A radioimmunoassay for arabinofuranosyluracil is also described.

Okabayashi *et al.* [77] developed a rapid and reliable radioimmunoassay method for the analysis of cytarabine using antibody induced in rabbits ^{3}H-labeled cytarabine and a Millipore filtration technique. The sensitivity of this assay was such that cytarabine, 0.02 µg/ml, in plasma could be detected, and the assay was practically free from interference by deoxycytidine, cytidine, 1-β-D-arabinofuronosyluracil, and other nucleosides, as well as from various antibiotics. Blood level of cytarabine in (C57BL $\times$ DBA/2) F1 were determined after injection of 1-(3-*O*-octanoyl-β-D-arabinofuranosyl)cytosine. Relatively, high cytarabine levels could be maintained for a fairly long period. Plasmas of mouse, rat, and rabbit contained high esterase activity which hydrolyzed the 3'-octanoyl group in 1-(3-*O*-octanoyl-β-D-arabinofuranosyl)cytosine, whereas this activity was relatively low in dog and human plasmas.

Okabayashi *et al.* [78] used a radioimmunoassay method for the analysis of uracil arabinoside using antibodies directed against cytarabine. Above pH 7 uracil arabinoside showed marked pH-dependent cross-reactivity with antibodies directed towards cytarabine. Since this peculiar phenomenon has not been observed with other nucleoside and nucleotides thus far tested, it is probably the result of base-catalyzed tautomerism of uracil arabinoside to its enolic form which renders it more structurally similar to cytarabine. By performing the radioimmunoassay at both pH 6.2 and 8.6, cytarabine, and uracil arabinoside were

determined simultaneously. This method for the assay of uracil arabinoside is simple fairly reliable and applicable to blood level studies.

Yamauchi *et al.* [79] established a new sensitive method for the determination of intracellular cytarabine-5′-triphosphate, an intracellular active metabolite of cytarabine, in human materials *in vivo*. An acid soluble fraction containing cytarabine-5′-triphosphate was extracted from blastic cells by treatment of cytarabine with trichloroacetic acid (final concn., 0.3 *M*) neutralized with an equal volume of cold freon containing 0.5 *M* tri-*n*-octylamine. The cytarabine-5′-triphosphate fraction was separated from the acid-soluble fraction by high-performance liquid chromatography (TSK gel diethylaminoethyl-2 SW column) eluted with pH 6.9, 0.05 *M* phosphate buffer, and 20% acetonitrile. Cytarabine-5′-triphosphate was lypholized, dephosphorylated to cytarabine by incubation with 10 units alkaline phosphatase for 12 h at 55 °C, and measured by radioimmunoassay using anticytarabine serum. Recovery through the whole procedure was 92%. In the human chronic myelogenous leukemia cell line K562, the intracellular cytarabine-5′-triphosphate levels produced when cells were incubated with cytarabine were assayed as above, and they showed a linear increase depending on cytarabine concentrations from 0.01 to 10 μM, demonstrating a very close correlation with the labeled cytarabine-5′-triphosphate levels yielded by cells on incubation with radiolabeled cytarabine ($r^2 = 0.99$). The detection limit was 0.1 pmol/5×10^6 cells and a sample amount of only 5×10^6 cells was enough for each assay. In the clinical applications, this method was capable of detecting a wide concentration range of cytarabine-5′-triphosphate produced when patients were treated with cytarabine or its derivatives from very low to intermediate doses. No radiolabeled drug was necessary. The method was very useful for *in vivo* pharmacodynamic studies of cytarabine therapy.

6. BIOLOGICAL ANALYSIS

Hanka *et al.* [80] developed an improved microbiological assay method for cytarabine which detected drug concentrations as low as 0.1 μg/ml in biological fluid, a sensitivity adequate for studies of cytarabine distribution in animals and man. Cytarabine was deaminated by *Streptococcus faecalis* ATCC 8043 to the inactive uracil arabinoside. 1-β-D-Ribofuranosylhydrouracil inhibited this degradation and, when added to the assay medium, significantly increased this sensitivity of the organisms towards cytarabine. Neither 1-β-D-ribofuranosylhydrouracil nor uracil arabinoside inhibited the test organism, nor did uracil arabinoside affect the activity of cytarabine when a mixture was assayed.

Hanka [81] reported that only methotrexate and actinomycin D out of 12 of common antitumor drugs, inhibited *S. faecalis/ACB*, useful for the

assay of cytarabine in biological samples containing other antitumor or antibacterial drugs. The activity of methotrexate was reversed in the presence of folinic acid which did not alter the organism's sensitivity to cytarabine. The interference of penicillin or ampicillin was eliminated by the application of penicillinase. Deoxycytidine reversed the inhibition of *S. faecalis/ACB* by cytarabine, but did not change the inhibition by the common antibacterial drugs. Cytarabine was inactive at 1 mg/ml against twenty one common organism cultivated in common agar media. Actinomycin D was detected in the presence of cytarabine by chromatographic separation of the two.

Neil *et al.* [82] described a *S. faecalis* bioassay method for the detection of cyclocytidine and cytarabine in biological fluids. Cyclocytidine and cytarabine levels <0.1 mg/ml could be detected by the method. Application of the assay method in the study of cyclocytidine and cytarabine pharmacokinetics in mice, indicated that cyclocytidine represents a molecular depot form of cytarabine. The pharmacokinetic data was discussed in relation of the antitumor activity of the two compounds.

Mehta *et al.* [83] developed a microbiological assay method capable of detecting cytarabine in the presence of methotrexate and 6-mercaptopurine in body fluids using a strain of *Streptococcus faecium* variety durans resistant to methotrexate and 6-mercaptopurine. The assay can also be used to detect cytarabine in the presence of 6-thioguanine.

Mehta and Hutchison [84] found that the microorganism, *S. faecium* variety durans, was sensitive to cytarabine but not methotrexate, 6-mercaptopurine, or 6-thioguanine, and thus is useful in detecting cytarabine in the presence of these and other pyrimidine nucleosides. The inhibition of this microorganism by 22 pyrimidine nucleosides is given.

Mellett *et al.* [85] developed a bioassay method for the estimation of cytarabine in biological samples which utilizes laser light scattering from suspensions of drug-sensitive bacteria. The species employed in the assay was *S. faecium* durans resistant to methotrexate and 6-mercaptopurine. In less than 4 h, serum and urine levels of cytarabine can be reproducibly measured using the method. A sample volume of 0.1 ml containing 30 ng/ml may be assayed with a precision of 10%. These studies further confirm the utility of the method as a rapid and relatively inexpensive assay methodology of broad application. Time variations of drug serum levels and urinary excretion rates in dogs are compared via the differential light scattering assay, standard disk diffusion assay, and radioisotopic assay. The results obtained by the various methods are in excellent agreement.

Wright and Matsen [86] reported that patients receiving cytarabine and other antitumor chemotherapy are at increased risk of developing nosocomial infections, and the antibacterial therapy of such infections is often monitored by bioassay. The effect of antitumor agents on seven bioassay procedures using strains of *Sarcina*, *Klebsiella*, *Clostridium*,

Pseudomonas, *Staphylococcus aureus*, and *Staphylococcus epidermidis* or *Bacillus* was evaluated. The minimal inhibitory concentrations of antitumor drugs, cytarabine, and five other drugs were determined for each of the test organisms.

7. STABILITY

The increased use of high-dose cytarabine in the treatment of neoplasms prompted Munson *et al.* [87] to carry out a study on the reconstituted stability of cytarabine in intravenous admixtures with sodium bicarbonate in plastic syringes. The study of the effect of sodium bicarbonate was prompted by the frequent use of this agent in patients being treated with cytarabine as means of achieving systemic alkalinization in order to manage hyperuricemia. The stability of reconstituted cytarabine in plastic syringes was measured to determine whether cytarabine could be reconstituted and stored prior to use. The results of this study indicate that sodium bicarbonate 50 mEq/l in the intravenous solution containing cytarabine has no effect on the chemical stability of cytarabine for at least 1 week at room temperature or in the refrigerator. Consequently, sodium bicarbonate and cytarabine can be coadministered in one intravenous solution. The reconstituted stability of cytarabine at 20 and 50 mg/ml is not affected by storage in plastic syringes.

Molina *et al.* [88] used spectrophotometry, pH changes, osmolarity, and thin-layer chromatography at different times (0 and 4 h, 1 and 7 days) to study the stability of a mixture of cytarabine and methotrexate, dissolved in either Ringer's lactate solution, 0.9% sodium chloride, or Elliot's B solution. Apparently, Elliot's B solution was the most suitable solvent for this mixture intended for intrathecal administration. In saline solution, the methotrexate spectrum was markedly altered.

Cheung *et al.* [89] developed a high-performance liquid chromatographic method for the simultaneous determination of cytarabine, methotrexate sodium, and hydrocortisone sodium succinate, and the stability of the three drugs mixed together in four infusion fluids was assessed. Solutions were prepared with two concentrations of the three drugs similar to those administered intrathecally. Admixtures were prepared in Elliott's B solution, 0.9% sodium chloride injection, 5% dextrose injection, and lactated Ringer's injection. Solutions were filtered and kept in a disposable syringe in a 25 °C water bath for 24 h. An high-performance liquid chromatography assay capable of separating the three drugs and their degradation products was developed and validated. With one exception, all three drugs were stable in all four solutions for 24 h. Admixtures of these three drugs in the four solutions tested are stable for at least 10 h at 25 °C. Intrathecal and administration of such

admixtures within several hours of preparation is encouraged since none contains antibacterial preservatives.

Quock and Sakai [90] studied the stability of cytarabine in a commonly used parenteral nutrient solution. From each of 2 l of parenteral nutrient solution for pediatric patients, two 200 ml aliquots containing cytarabine 50 µg/ml were prepared. One aliquot from each litre was stored at each of two temperatures (25 and 8 °C). At 0, 1, 2, 8, 24, 48, and 96 h, 1 ml from each sample was mixed with internal standard and the cytarabine concentration was determined by high-performance liquid chromatography. Samples were also tested for pH and visually inspected for particulate matter and color change. No particulate matter or color change was noted, and no pH changes occurred during 48 h of testing. Cytarabine concentrations during 96 h of testing were 90–104.4% of initial concentration. Cytarabine at a concentration of 50 µg/ml was stable for at least 48 h in the parenteral nutrient solution studied.

Zhou and Shang [91] used spectrophotometry to study the stability of acyclovir, cyclocytidine, and cytarabine in intravenous infusions (glucose, saline, and other solutions). The three drugs were stable in the intravenous infusions tested ($\geq$12 h at 25 °C and $\geq$4 h at 40 °C).

Rochard *et al.* [92] investigated the stability of cytarabine, fluorouracil, and doxorubicin hydrochloride in admixtures stored in portable infusion-pump reservoir. Admixtures containing cytarabine 25 or 1.25 mg/ml, fluorouracil 50 or 10 mg/ml, or doxorubicin hydrochloride 1.25 or 0.5 mg/ml in 0.9% sodium chloride injection or 5% dextrose injection were placed in 80-ml ethylene vinylacetate drug reservoirs protected from light, and 1 ml quantities were withdrawn immediately after preparation and after storage for 1, 2, 3, 4, 7, 14, and 28 days at 4, 22, or 33 °C. For each condition, three samples from each admixture were tested for drug concentration by stability-indicating high-performance liquid chromatography. The admixtures were also monitored for precipitation, color change, and pH. Evaporative water loss from the containers was measured. Cytarabine was stable for 28 days at 4 and 22 °C and for 7 days at 35 °C. No color change or precipitation was observed, and pH values were stable. Loss of water through the reservoirs was substantial only at 35 °C for 28 days. When stored in ethylene vinylacetate portable infusion-pump reservoirs, cytarabine, and the other two drugs were each stable for at least 1 week at temperatures up to 35 °C. Cytarabine and doxorubicin hydrochloride showed decreasing stability at longer storage times at higher temperatures.

Aoki *et al.* [93] studied the physical and chemical properties; appearance, melting point, solubility, stability of cytarabine ocfosfate, and its capsules. The results indicated that cytarabine ocfosfate and its capsules are stable for more than 42 months at room temperature.

Smirnov *et al.* [94] determined the stability of cytarabine in aqueous solutions during a preset storage time. High-performance liquid chromatography and spectrochemical methods were used in this study. A comparative study of the kinetics of cytarabine hydrolytic deamination in aqueous solution was carried out.

Trissel *et al.* [95] studied the physical and chemical stability of cytarabine, methotrexate, and hydrocortisone in Elliott's B solution for intrathecal use. The existing stability information on these drug combinations is inadequate due to the clinical use of increased doses of the drugs, as well as a change in the formulation of Elliott's B solution. This study was carried out to evaluate the physical and chemical stability of simulated high intrathecal doses of the subject drugs in the current formulation of Elliott's B solution. Methotrexate sodium, 6, 12, and 15 mg was combined with cytarabine 100 mg with and without hydrocortisone sodium succinate 100 mg using Elliott's B solution as the intrathecal vehicle. Samples were stored at 4 and 23 °C and evaluated for physical and chemical stability over 48 h. No precipitation or other evidence of physical instability was observed in any sample. Measured pH was 7.2–7.5 in the samples and was sufficient to prevent methotrexate precipitation. High-performance liquid chromatography analysis found little or no loss of methotrexate and cytarabine in any sample and hydrocortisone at 4 °C. At room temperature, hydrocortisone losses of 6–8% occurred in 48 h. The high doses of methotrexate sodium and cytarabine with or without hydrocortisone sodium succinate evaluated in this study are physically and chemically stable for 48 h at 4 and 23 °C in Elliott's B solution.

8. PHARMACOKINETICS, METABOLISM, AND EXCRETION

Cytarabine is not effective by mouth due to rapid deamination in the gastrointestinal tract; less than 20% of an oral dose is absorbed. After intravenous injection it disappears rapidly from the plasma with an initial half-life of about 10 min; the terminal elimination half-life ranges from 1 to 3 h. It is converted by phosphorylation to an active form which is rapidly deaminated, mainly in the liver and the kidneys, to inactive 1-*β*-D-arabinofuranosyluracil (uracil arabinoside, ara-U). The majority of an intravenous dose is excreted in the urine within 24 h, mostly as the inactive metabolite with about 10% as unchanged cytarabine. There is only moderate diffusion of cytarabine across the blood-brain barrier following intravenous injection, but, because of low deaminase activity in the cerebrospinal fluid, concentrations achieved after continuous intravenous infusion or intrathecal injection are maintained for longer in the cerebrospinal fluid than are those in plasma, with a terminal elimination half-life of 3.5 h. After intrathecal administration of the liposomal

formulation, a terminal elimination half-life of 100–263 h was seen. Cytarabine also crosses the placenta [2, 4, 7, 96–102].

Cytarabine pharmacokinetics varies markedly from patient to patient and that there is a wide range in the plasma concentrations associated with therapeutic response [103]. The rapid deamination of cytarabine is the reason for the ongoing search for effective formulations and derivatives that cannot be deaminated and exhibit better pharmacokinetic parameters. Protection of cytarabine from fast degradation and elimination has been investigated by encapsulating the drug into pharmaceutically acceptable carriers. Cytarabine derivatives have shown promise *in vitro* and in animal models, as cyclocytidine, enocitabine, and cytarabine ocfosfate have been used clinically [104].

The pharmacokinetics of cytarabine in patients with acute myeloid leukemia was determined. The obtained results indicated that variability in cytarabine disposition in plasma at the used dosage level does not correlate with remission status or toxicity in those patients [105]. It was also observed that there is similarity of cellular accumulation of cytarabine among patients of acute myelogenous leukemia and acute lymphoblastic leukemia which support the prolonged infusion duration for cytarabine as an alternative to the intensification by high-dose schedules with short-term infusion [106].

Cytarabine is interacellularly activated and correlations have been established between the pharmacokinetic behavior of active metabolite and their antileukemic effect. A good response to high-dose treatment of leukemias has additional been attributed to a so-called low deamination phenotype of cytarabine inactivation. Consequently, these findings would support plasma level monitoring of cytarabine and its metabolite uracil arabinoside in high dose regimens. Patients were treated with high dose infusions, a fast deamination phenotype of cytarabine was not observed [107].

The liposomal formulation of cytarabine pharmacokinetics was studied in comparison to cytarabine itself. The pharmacokinetics demonstrated significant differences. The liposome distribution was wider and the area under the curve in liver, spleen, kidney, lung, and heart was larger. The liposome exhibited protective effect on cytarabine metabolism in liver and the median recognition threshold in liver was prolonged [108, 109].

Previous *in vitro* investigations demonstrated that human leukemia cells, when incubated with hematopoietic growth factors such as granulocyte-colony-stimulating factor, augment the accumulation of the triphosphate of 1-β-D-arabinofuranosylcytosine (ara-C cytarabine). To test whether granulocyte-colony-stimulating factor infusion prior to ara-C incusion would biologically modulate the accumulation of ara-9-β-D-arabinofuranosylcytosine 5'-triphosphate (ara-CTP) and other ara

nucleotides in the leukemia blasts during therapy, protocols were designed to infuse granulocyte-colony-stimulating factor prior to ara-C to increase the accumulation of the active triphosphates (9-β-D-arabino-furanosyl-2-fluoroadenine 5′-triphosphate (F-ara-ATP) and (ara-CTP) in acute myelogenous leukemia blasts during therapy. To complement these *in vivo* studies, *ex vivo* accumulation of ara-CTP was also investigated before and after granulocyte-colony-stimulating factor infusion. Based on these investigations it could be concluded that investigation (a) granulocyte-colony-stimulating factor did not increase ara-CTP accumulation, rather it may have caused it to decrease; and (b) these data imply that when granulocyte-colony-stimulating factor and ara-C are used in combination, may maintain the ara-CTP area under the curve [110]

Antifungal prophylaxis is an important component of the induction therapy for patients with acute myeloid leukemia. Azole antifungal agents are increasingly used in this context. *In vitro* assays were performed to assess whether cytochrome P450 enzymes were affected by combinations of cytarabine with itraconazole or caspofungin. Cytarabine is a substrate of CYP 450 3A4. Cytarabine, itraconazole, and caspofungin inhibit CYP 450 3A4. Cytarabine metabolism was significantly decreased when combined with those antifungal agents, which might lead to important clinical implications [111].

Cytarabine metabolism was modulated in human promyelocytic leukemia cell line HL-60 by two ribonucleotide reductase inhibitors. 3,4,5-Trihydroxybenzohydroxamic acid and 3,4-dihydroxybenzohydroxamic acid were investigated for their ability to modulate the cellular pharmacology of ara-C. The trihydroxy analog enhanced the incorporation of cytarabine metabolite into DNA by 3.6 fold, while the dihydroxy derivative produced 5.6-fold increase [112].

9. PHARMACOLOGY

Cytarabine, a pyrimidine nucleoside analog, is an antimetabolite antineoplastic which inhibits the synthesis of deoxyribonucleic acid. Its actions are specific for the S phase of the cell cycle. It also has antiviral and immunosuppressant properties. Cytarabine is one of the mainstays of the treatment of acute myeloid leukemias, together with an anthracycline, and is used for the prophylaxis of meningeal leukemia, as well as in regimens for consolidation, in patients with acute lymphoblastic leukemia. It has also been investigated in the blast crisis of chronic myeloid leukemia and the myelodysplasias. It may also be used in salvage regimens for Hodgkin's disease as part of the complex regimens sometimes employed in aggressive intermediate- and high-grade non-Hodgkin's lymphomas and for meningeal lymphoma. Cytarabine is usually given

by the intravenous route. Higher doses can be tolerated when given by rapid injection rather than slow infusion, because of the rapid clearance of cytarabine, but there is little evidence of clinical advantage either way. Cytarabine may be given by the intrathecal route for leukaemic or lymphomatous meningitis. For the induction of remission in adults and children with acute leukemia a wide variety of dosage regimens have been used: 100 mg/m^2 twice daily by rapid intravenous injection, or 100 mg/m^2 daily by continuous intravenous infusion, have often been employed. These doses are generally given for 5–10 days, depending on therapeutic response and toxicity. Children reportedly tolerate high doses better than adults. For maintenance 1–1.5 mg/kg once or twice weekly have been given intravenously or subcutaneously; other regimens have been used [7].

In the treatment of refractory disease high-dose regimens have been employed, with cytarabine given in doses of up to 3 g/m^2 every 12 h for up to 6 days. These doses should be given by intravenous infusion over at least 1 h. In leukemia meningitis cytarabine has been given intrathecally, often in a dose of 10–30 mg/m^2 every 2–4 days; it has also been used prophylactically. A liposomal formulation is available in some countries for intrathecal administration and permits less frequent dosing because of its longer duration of action. The recommended dose for lymphomatous meningitis is 50 mg intrathecally every 2 weeks for 5 doses then every 4 weeks for 5 doses. White cell and platelet counts should be determined regularly during treatment with cytarabine and therapy should be stopped immediately if the count falls rapidly or to low values. Cytarabine ocfosate is an orally active prodrug of cytarabine used for chronic myeloid leukemia [7].

9.1. Leukemias

9.1.1. Acute myeloid leukemia

Cytarabine is used principally as a component of various chemotherapeutic regimens for remission induction in acute myeloid (myelogenous, nonlymphocytic) leukemia (AML, ANLL) [113]. Acute myeloid leukemia includes acute promyelocytic, monocytic, myelomonocytic, megakaryoblastic, and erythroid leukemias [114]. Induction regimens are used to rapidly reduce the tumor burden in order to achieve complete remission [114, 115] which generally is defined as less than 5% leukemic blast cells in the bone marrow and normalization of peripheral blood counts (including hemoglobin concentration, hematocrit, granulocyte count, and platelet count) [115]. Cytarabine used alone has produced complete remissions in 25–40% of patients, but combination therapy for induction of

remissions is superior to single-agent therapy and is preferred. Although maintenance regimens (with lower doses) previously were administered for prolonged periods (e.g., years) in the treatment of acute myeloid leukemia, most current treatment regimens in the United States of America no longer employ maintenance therapy [115] but instead use intensive consolidation therapy that is administered for a shorter period of time at higher doses and then discontinued since there is no evidence of superior disease-free survival with prolonged maintenance [114, 116, 117].

Remission rates in adult acute myeloid leukemia are inversely related to age, with expected rates exceeding 65% in those younger than 60 years of age. In addition, some evidence suggests that, once attained, duration of remission may be shorter in older patients and increased morbidity and mortality during induction also appear to be directly related to age. Other adverse prognostic factors include leukemic central nervous system involvement, systemic infection at diagnosis, elevated leukocyte count (exceeding $100,000/mm^3$) treatment-induced acute myeloid leukemia, and a history of myelodysplastic syndrome. In addition, leukemias that express the progenitor cell antigen CD34 and/or P-glycoprotein (MDR-1 gene product) have an inferior outcome. Cytogenetic analysis, although not readily available, provides the strongest prognostic information for newly diagnosed acute myeloid leukemia, with abnormalities that indicate a good prognosis including t (8; 21), inv (16), and t (15; 17) normal cytogenetics generally indicate average-risk acute myeloid leukemia. Patients with acute myeloid leukemia that is characterized by deletions of the long arms or monosomies of chromosomes 5 or 7; by translocations or inversions of chromosome 3, t (6; 9), t (9; 22); or by abnormalities of chromosome 11q23 exhibit particularly poor prognoses with chemotherapy [114].

Cytarabine and an anthracycline (usually daunorubicin) have been principal components of induction regimens, but various regimens have been used in combination therapy and comparative efficacy is continually being evaluated. Cytarabine has been used with agents such as daunorubicin, doxorubicin, idarubicin, thioguanine, or vincristine. The two-drug regimen of cytarabine and daunorubicin generally results in a complete response rate of approximately 65% in patients with previously untreated acute myeloid leukemia. The results of randomized trials comparing combined mitoxantrone and cytarabine therapy with combined daunorubicin and cytarabine therapy have shown the two regimens to have similar efficacy and toxicity as induction therapy in patients with previously untreated acute myeloid leukemia [114–118]. There is some evidence that dose intensity of cytarabine as a component of induction therapy may affect disease-free survival [114, 119–122]. In one study, high-dose rapid cytarabine administration combined with daunorubicin and etoposide produced similar complete response rate but superior

disease-free survival compared with conventional-dose continuous-infusion cytarabine combined with these drugs [114, 119]. In another study in which the second course of induction therapy was administered after hematopoietic recovery or in a planned sequence beginning on day 10 of therapy (i.e., during aplasia), both regimens produced similar remission rates but the time sequential regimen produced superior disease-free survival regardless of the postremission therapy (e.g., consolidation chemotherapy, allogenetic, or autologous bone marrow transplantation). Some clinicians have used thioguanine or mercaptopurine in addition to intensive therapy with cytarabine and daunorubicin for remission induction; complete remissions occurred in 60–85% of patients [114, 120–122].

Cytarabine has also been used with other antineoplastic agents in regimens of consolidation therapy for acute myeloid leukemia following induction of a complete remission; however, the role of such therapy in the prolongation of remissions is not firmly established. Cytarabine-containing consolidation chemotherapy regimens that do not employ bone marrow transplantation are associated with treatment-related death rates that usually are less than 10–20% and have produced disease-free survival rates of 20–50% [114, 120, 123, 124]. There is some evidence that high-dose cytarabine consolidation regimens provide a clear benefit in survival in patients younger than 60 years of age [114, 123], but dose-intensive cytarabine-based chemotherapy can be complicated by severe neurologic and/or pulmonary toxicity and therefore should be administered under the direction of clinicians experienced in the use of such regimens in facilities equipped to manage potential complications [114, 125–127]. Consolidation therapy has ranged in duration from 1–4 or more cycles, but the optimal doses, schedules, and duration of consolidation chemotherapy remain to be established. Cytarabine also has been used with other antineoplastic agents in the treatment of erythroleukemia. Cytarabine has been used alone in high-dose regimens to induce remissions in some patients with refractory acute myeloid leukemia, or with secondary acute myelolid leukemia [114, 125–127].

9.1.2. Acute lymphocytic leukemia

Cytarabine has been used alone or with other antineoplastic agents for remission induction in acute lymphocytic leukemia, however, combinations containing other antineoplastic agents are more effective. Cytarabine has generally been limited to use with other antineoplastic agents for remission induction in some patients who do not achieve a complete remission with combinations containing other agents or who relapse during maintenance therapy. Cytarabine has also been used occasionally in regimens of consolidation and/or maintenance therapy following induction of a complete remission by combinations containing other agents. Although long-term survivors may eventually experience a

recurrence or relapse, a substantial number of children with acute lymphocytic leukemia have achieved long-term complete remissions following induction and maintenance combination therapy. Cytarabine has been used alone in high-dose regimens to induce remissions in some patients with refractory acute lymphocytic leukemia [113].

9.1.3. Meningeal leukemia and other meningeal neoplasms

Cytarabine has been used effectively alone or with other chemotherapeutic agents in the treatment and maintenance therapy of meningeal leukemia and other meningeal neoplasms (e.g., lymphoma). Although therapeutic concentrations of cytarabine in the cerebrospinal fluid have apparently been attained during continuous intravenous or subcutaneous infusions of the drug, cytarabine is usually administered intrathecally to ensure therapeutic concentrations of the drug. Many clinicians consider intrathecal cytarabine and intrathecal methotrexate to have similar efficacy in the treatment of these conditions; however, intrathecal cytarabine produces less systemic toxicity than intrathecal methotrexate. Intrathecal cytarabine may be useful in patients whose central nervous system disease does not respond to intrathecal methotexate or in patients with methotrexate-related neurotoxicity. Focal leukemic involvement of the central nervous system may not respond to intrathecal cytarabine or intrathecal methotrexate and may better be treated with radiation therapy. The value of intrathecal cytarabine in the prophylaxis of meningeal leukemia has not been established [113].

9.1.4. Chronic myelogenous leukemia

Cytarabine is used with other antineoplastic agents such as daunorubicin in the treatment of patients with chronic myelogenous leukemia who are in the accelerated or blastic phase of the disease; however, the prognosis for patients receiving standard therapy remains poor and other therapies are continually being evaluated [113, 128, 129].

Cytarabine also is used in combination with interferon alfa for the treatment of the chronic phase of chronic myelogenous leukemia [113, 128]. Concomitant administration of cytarabine with interferon alfa-2b has been associated with increased survival in patients with chronic myelogenous leukemia [130, 131]. Results of a randomized controlled study in previously untreated patients with chronic myelogenous leukemia demonstrate a longer survival in patients receiving interferon alfa-2b (5 million units/m^2 given subcutaneously daily) in combination with cytarabine (20 mg/m^2 daily for 10 days given subcutaneously 2 weeks after initiation of interferon alfa-2b therapy and monthly thereafter) versus those receiving interferon alfa-2b without cytarabine; patients from both groups also received hydroxyurea 50 mg/kg daily until a

complete hematologic remission was achieved [130]. After 3 years, median survival rate of about 86 or 79%, respectively, reportedly was observed in patients receiving combined interferon alfa-2b therapy with cytarabine or interferon alfa-2b without cytarabine while overall hemotologic response rate was 66 or 55% in patient receiving combined interferon alpha-2b therapy with cytarabine or interferon alfa-2b without cytarabine, respectively [130, 131]. Major cytogenetic response rate after 12 months was 41 or 24% in patients receiving combined interferon alfa-2b therapy with cytarabine or interferon alfa-2b without cytarabine, respectively. Longer survival was observed in patients with cytogenetic response [130]. Some patients underwent allogeneic or autologous bone marrow transplantation, and the 2-year survival rate after allogeneic bone marrow transplantation was 56 or 59% in patients receiving combined interferon alfa-2b therapy with cytarabine or interferon alfa-2b without cytarabine, respectively, while 2-year survival rate after autologous bone marrow transplantation was 61 or 68% in patients receiving combined interferon alfa-2b therapy with cytarabine or interferon alfa-2b without cytarabine, respectively [130]. Patients who did not have complete hematologic or major cytogenetic responses within six or 12 months, respectively, were allowed to cross over to combined treatment with interferon alfa-2b and cytarabine [130, 132]. Among patients who received initial therapy with interferon alfa-2b without cytarabine, but then crossed-over to receive combined treatment with interferon alfa-2b and cytarabine, complete, and partial responses of 2 and 6%, respectively, were observed [130, 132].

9.2. Other uses

Cytarabine has been used with other antineoplastic agents in regimens of maintenance therapy in the treatment of non-Hodgkin's lymphomas in children. Cytarabine has also been used with other antineoplastic agents for remission induction and/or maintenance therapy in adults with non-Hodgkin's lymphomas, principally advanced diffuse histiocytic lymphoma. It has been suggested, but is not clearly established, that cytarabine decreases the incidence of central nervous system relapse in patients with advanced diffuse histiocytic lymphoma because the drug crosses the blood-brain barrier. However, the best combination or sequential therapy in the treatment of advanced diffuse histiocytic lymphoma has not been established and comparative efficacy is continually being evaluated. Cytarabine has also been used alone in high-dose regimens with some success for the treatment of refractory non-Hodgkin's lymphomas [7].

ACKNOWLEDGMENTS

REFERENCES

[1] A. C. Moffat (ed.), *Clarke's Isolation and Identification of Drugs*, 2nd edn., The Pharmaceutical Press, London, 1986, p. 506.

[2] S. C. Sweetman (ed.), *Martindale, The Complete Drug Reference*, 33rd edn., The Pharmaceutical Press, Chicago, USA, 2002, p. 525.

[3] S. Budavari (ed.), *The Merck Index*, 12th edn., Merck and Co., NJ, 1996, p. 471.

[4] A. R. Gennaro (ed.), *Remington's: The Science and Practice of Pharmacy*, 18th edn., Mack Publishing Co., Pennsylvania, USA, 1995, p. 1247.

[5] *British Pharmacopoeia* 2000 CD-ROM, Vol. 1. Her Majesty's Stationary Office, London, 2000.

[6] *United States Pharmacopoeia*, 24th edn., USP24-NF 19 through Supplement 3, United States Pharmaceutical Convention, Inc., Rockville, MD, USA, 2001, p. 491–492.

[7] J. H. Harman and L. E. Limbirt (chief Eds.), *Goodmann and Gilman's Pharmacological Basis of Therapeutics*, 9th edn., International edn., McGraw-Hill, Health Profession Division, New York, 1996, p. 1251.

[8] J. H. Hunter *US Patent 3116282*, 1963.

[9] T. Y. Shen, H. M. Lewis, and W. V. Ruyle *J. Org. Chem.*, 1965, **30**, 835.

[10] H. P. M. Fromageot, and C. B. Reese *Tetrahedron Lett.*, 1966, **29**, 3499.

[11] W. K. Roberts, and C. A. Dekker *J. Org. Chem.*, 1967, **32**, 816.

[12] J. Nagyvary, and C. M. Tapiero *Tetrahedron Lett.*, 1969, **40**, 3481.

[13] D. H. Shannahoff, and R. A. Sanchez *J. Org. Chem.*, 1973, **38**, 593.

[14] E. J. Hessler *J. Org. Chem.*, 1976, **41**, 1828.

[15] T. Kanai, C. Yamashita, and M. Ichino *Jpn. Tokkyo Koho*, 1971, pp. 4, Patent number JP 46027463.

[16] C. Jin, Z. Wu, G. Jia, H. Li, and X. Wu *Faming Zhuanli Shenqing Gongkai Shuomingshu*, 2005, pp.10, Patent number CN 1583776.

[17] V. Zaharans, and J. Fridmanis *Latvijas Kimijas Zurnals*, 1994, **2**, 203.

[18] M. Tuncel, D. Dogrukol, S. Ficicioglu, and Z. Senturk *FABAD Farm Bilimler Derg*, 1991, **16**, 195.

[19] M. S. Mahrous, M. M. Abdel-Khalek, H. G. Daabees, and Y. A. Beltagy *Anal. Lett.*, 1992, **25**, 1491.

[20] N. Subramanian, and R. S. R. Murthy *Ars. Pharm.*, 2004, **45**, 319.

[21] X. N. Chen, C. X. Zhang, and J. R. Lu *Fenxi Shiyanshi*, 2000, **19**, 62.

[22] D. Marin, and C. Teijeiro *Bioelectrochem. Bioenerg.*, 1992, **28**, 417.

[23] D. Dogrukol, and M. Tuncel *Pharmazie*, 1994, **49**, 928.

[24] D. Dogrukol, and M. Tuncel *Portugaliae Electrochimica Acta*, 1991, **9**, 331.

[25] C. Teijeiro, and D. Marin *J. Electroanal. Chem. Interfacial Electrochem.*, 1991, **316**, 119.

[26] C. Teijeiro, and D. Marin *J. Electroanal. Chem.*, 1992, **337**, 175.

[27] L. Novotny, and A. Vachalkova *Neoplasma*, 1993, **40**, 369.

[28] D. Abd El-Hady, M. I. Abdel-Hamid, M. M. Seliem, V. Andrisano, and N. Abo-El-Maali *J. Pharm. Biomed. Anal.*, 2004, **34**, 879.

[29] B. Paw, and G. Misztal *Chem. Anal.*, 1997, **42**, 37.

[30] A. H. Stead, R. Gill, T. Wright, J. P. Gibbs, and A. C. Moffat *Analyst*, 1982, **107**, 1106.

[31] M. G. Pallavicini, and J. A. Mazrimas *J. Chromatogr.*, 1980, **183**, 449.

[32] W. Plunkett, S. Chubb, and B. Barlogie *J. Chromatogr.*, 1980, **221**, 425.

[33] P. Linssen, A. Drenthe-Schonk, H. Wessels, and C. Haanen *J. Chromatogr.*, 1981, **223**, 371.

[34] M. Tuncel, R. E. Notari, and L. Malspeis *J. Liq. Chromatogr.*, 1981, **4**, 887.

[35] H. Breithaupt, and J. Schick *J. Chromatogr.*, 1981, **225**, 99.

[36] M. K. Danks *J. Chromatogr.*, 1982, **233**, 141.

[37] P. Linssen, A. Drenthe-Schonk, H. Wessels, G. Wierwinden, and C. Haanen *J. Chromatogr.*, 1982, **232**, 424.

[38] J. A. Sinkule, and W. E. Evans *J. Chromatogr.*, 1983, **274**, 87.

[39] F. An, Y. Fei, J. Yuan, D. Zhu, L. Sun, P. Wang, and H. Cao *Zhongguo Linchuang Yaolixue Zazhi*, 2001, **17**, 228.

[40] M. Burk, M. Volmer, K. Fartash, and W. Schneider *Arzneimittel-Forschung*, 1995, **45**, 616.

[41] C. Gao, H. Dai, F. Su, and H. Gao *Zhongguo Shenghua Yaowu Zazhi*, 2003, **24**, 141.

[42] G. G. Liversidge, T. Nishihata, T. Higuchi, R. Shaffer, and M. Cortese *J. Chromatogr.*, 1983, **276**, 375.

[43] A. Bakker, H. Bloemhof, and E. K. Juul-Christensen *Pharm. Weekbl.*, 1984, **119**, 1181.

[44] R. L. Schilsky, and F. S. Ordway *J. Chromatogr.*, 1985, **337**, 63.

[45] K. Maurer, H. Schmidt, H. E. Keller, and F. C. Sitzmann *Fresenius'Z. Anal. Chem.*, 1986, **324**, 329.

[46] L. D. Kissinger, and N. L. Stemm *J. Chromatogr.*, 1986, **353**, 309.

[47] S. V. Galushko, I. P. Shishkina, and A. T. Pilipenko *Zh. Anal. Khim.*, 1987, **42**, 1684.

[48] V. Gandhi, L. Danhauser, and W. Plunkett *J. Chromatogr.*, 1987, **413**, 293.

[49] N. AT. Nguyen, and R. E. Notari *J. Pharm. Sci.*, 1989, **78**, 802.

[50] J. R. Wermeling, J. M. Pruemer, F. M. Hassan, A. Warner, and A. J. Pesce *Clin. Chem.*, 1989, **35**, 1011.

[51] L. M. Wang, C. N. Woodward, J. C. White, and R. L. Capizzi *J. Chromatogr.*, 1989, **491**, 331.

[52] A. Riccardi, T. Servidei, A. Lasorella, and R. Riccardi *J. Chromatogr.*, 1989, **497**, 302.

[53] E. Schleyer, G. Ehninger, G. Zuehlsdorf, M. Proksch, B. Proksch, and W. Hiddemann *J. Chromatogr.*, 1989, **497**, 109.

[54] S. V. Galushko, and I. P. Shishkina *Khim Farm. Zh*, 1990, **24**, 85.

[55] S. V. Galushko, and I. P. Shishkina *J. Pharm. Biomed. Anal.*, 1992, **10**, 1093.

[56] P. G. Dietrich, B. Buechele, and I. Molnar *Pharmazie*, 1992, **47**, 868.

[57] B. Ramsauer, J. Braess, M. Unterhalt, C. C. Kaufmann, W. Hiddemann, and E. Schleyer *J. Chromatogr.*, 1995, **665**, 183.

[58] M. L. Stout, and Y. Ravindranath *J. Chromatogr.*, 1995, **692**, 59.

[59] D. Abd El-Hady, N. Abo-El-Maali, R. Gotti, and V. Andrisano *Talanta*, 2005, **66**, 253.

[60] J. Braess, J. Pfoertner, C. C. Kaufmann, B. Ramsauer, M. Unterhalt, W. Hiddemann, and E. Schleyer *J. Chromatogr.*, 1996, **676**, 131.

[61] T. Kiffmeyer, H. J. Goetze, M. Jursch, and V. Lueders *Fresenius' J. Anal. Chem.*, 1998, **361**, 185.

[62] H. Kazoka *J. Chromatogr.*, 1999, **836**, 235.

[63] L. Floridia, A. M. Pietropaolo, M. Tavazzani, F. M. Rubino, and A. Colombi *J. Chromatogr.*, 1999, **724**, 325.

[64] J. Boutagy, and D. J. Harvey *J. Chromatogr.*, 1978, **156**, 153.

[65] J. Boutagy, and D. J. Harvey *J. Chromatogr.*, 1978, **146**, 283.

[66] Y. Makino, Y. Matsubara, K. Watanabe, and M. Hirobe *Yakugaku Zasshi*, 1982, **102**, 49.

[67] P. Houze, F. Deschamps, H. Dombret, B. Bousquet, and B. Gourmel *J. Chromatogr.*, 2001, **754**, 185.

[68] D. K. Lloyd, A. M. Cypess, and I. W. Wainer *Beckman Appl. Brief*, 1991, **DS-792**, 2.

[69] D. K. Lloyd, A. M. Cypess, and I. W. Wainer *J. Chromatogr.*, 1991, **568**, 117.

[70] L. Krivankova, A. Kostalova, G. Vargas, J. Havel, and P. Bocek *Electrophoresis*, 1996, **17**, 1954.
[71] J. Liliemark, A. Baldesten, and C. Peterson *Curr. Chemother. Immunother., Proc. Int. Congr. Chemother.*, 1982, **2**, 1312, 12th meeting date 1981.
[72] E. M. Piall, G. W. Aherne, and V. M. Marks *Br. J. Cancer*, 1979, **40**, 548.
[73] T. Sato, M. Morozumi, K. Kodama, A. Kuninaka, and Y. Yoshino *Cancer Treat. Rep.*, 1984, **68**, 1357.
[74] N. Shimada, T. Ueda, T. Yokoshima, J. Oh-Ishi, and T. Oh-Oka *Cancer Lett.*, 1984, **24**, 173.
[75] Anonymous, Patent to ''Yamasa Shoyu Co., Ltd., Japan,'' *Jpn Kokai Tokkyo Koho*, 1983, pp. 8, Patent No. JP 58221168 A2 1983 12 22 Showa.
[76] T. Okabayashi, and J. G. Moffatt *Method Enzymol.*, 1982, **84**, 470.
[77] T. Okabayashi, S. Mihara, D. B. Repke, and J. G. Moffatt *Cancer Res.*, 1977, **37**, 619.
[78] T. Okabayashi, S. Mihara, and J. G. Moffatt *Cancer Res.*, 1977, **37**, 625.
[79] T. Yamauchi, T. Ueda, and T. Nakamura *Cancer Res.*, 1996, **56**, 1800.
[80] L. J. Hanka, S. L. Kuentzel, and G. L. Neil *Cancer Chemother. Rep.,* Part I, 1970, **54**, 393.
[81] L. J. Hanka *Cancer Chemother. Rep.* Part I, 1971, **55**, 557.
[82] G. L. Neil, S. L. Kuentzel, and A. E. Berger *Res. Commun. Chem. Pathol. Pharmacol.*, 1973, **5**, 561.
[83] B. M. Mehta, M. B. Meyers, and D. J. Hutchison *Cancer Chemother. Rep.*, 1975, **59**, 515.
[84] B. M. Mehta, and D. J. Hutchison *Ann. N. Y. Acad. Sci.*, 1975, **255**, 559.
[85] L. B. Mellett, P. J. Wyatt, and C. Woolley *Res. Commun. Chem. Pathol. Pharmacol.*, 1978, **20**, 379.
[86] D. N. Wright, and J. M. Matsen *Antimicrob. Agents Chemother.*, 1980, **17**, 417.
[87] J. W. Munson, E. J. Kubiak, and M. S. Cohon *Drug Intell. Clin. Pharm.*, 1982, **16**, 765.
[88] M. J. Molina, M. Martinez de Lecea, A. Garde, A. Vinuales, J. Alfaro, A. Iruin, and V. Napal *Revista de la Asociacion Espanola de Farmaceuticos de Hospitales*, 1983, **7**, 87.
[89] Y. W. Cheung, B. R. Vishnuvajjala, and K. P. Flora *Am. J. Hosp. Pharm.*, 1984, **41**, 1802.
[90] J. R. Quock, and R. I. Sakai *Am. J. Hosp. Pharm.*, 1985, **42**, 592.
[91] X. Zhou, and R. Zhang *Zhongguo Yiyuan Yaoxue Zazhi*, 1992, **12**, 32.
[92] E. B. Rochard, D. M. Barthes, and P. Y. Courtois *Am. J. Hosp. Pharm.*, 1992, **49**, 619.
[93] M. Aoki, M. Nakada, T. Terada, H. Ohata, Y. Takei, T. Saino, M. Morozumi, Y. Hasegawa, and T. Takahashi *Kagaku Ryoho no Ryoiki*, 1993, **9**, 722.
[94] I. V. Smirnov, G. G. Zav'yalov, and S. V. Eremin *Pharm. Chem. J.*, 2000, **34**, 451.
[95] L. A. Trissel, K. M. King, Y. Zhang, and A. M. Wood *J. Oncol. Pharm. Pract.*, 2002, **8**, 27.
[96] AHFS Drug Information, *Online Computer Version*, 2006.
[97] M. L. Slevin, E. M. Piall, G. W. Aheme, A. Johnston, M. C. Sweatman, and T. A. Lister *Br. J. Clin. Pharmacol.*, 1981, **12**, 507.
[98] L. M. DeAngelis, W. Kreis, K. Chan, E. Dantis, and S. Akerman *Cancer Chemother. Pharmacol.*, 1992, **29**, 173.
[99] A. Hamada, T. Kawaguchi, and M. Nakano *Clin. Pharmacol.*, 2002, **41**, 705.
[100] N. Takayama, Y. Nakagawa, H. Ochiai, M. Morozumi, Y. Esumi, M. Takaichi, Y. Tin, H. Seki, and S. Gunji *Yakubutsu Dotai*, 1993, **8**, 1229.
[101] P. Skiekowski, J. C. Murphy, E. S. Watson, R. M. Folk, and C. L. Litterst *Gov. Rep. Announce, Index (U.S.)*, 1979, **79**, 63.
[102] S. M. ElDareer, V. M. White, D. Tillery, F. P. Chen, L. B. Mellett, and D. L. Hill *Cancer Treat. Rep.*, 1977, **61**, 805.
[103] Y. Ono, N. Tatewaki, A. Okita, and Y. Katsura *Yakug. Zas.*, 1972, **92**, 592.
[104] A. L. Harris, C. Potter, C. Bunch, J. Boutagy, J. D. Harvey, and D. G. Grahame-Smith *Br. J. Clin. Pharm.*, 1979, **8**, 219.
[105] R. A. Fleming, R. L. Capizzi, G. L. Rasner, L. K. Oliver, S. J. Smith, A. C. Schiffer, R. T. Silver, B. A. Peterson, and R. B. Wiess *Cancer Chemother. Pharmacol.*, 1995, **36**, 425.

[106] J. Boos, B. Hohenlackter, P. S. Westhoff, M. Schiller, M. Zimmermann, U. Creutzig, J. Ritter, and H. Jurgens *Med. Ped. Oncol.*, 1996, **26**, 397.

[107] M. Burk, A. Heyll, M. Arning, M. Volmer, K. Fartash, and W. Schneider *Leuk. Lymphoma*, 1997, **27**, 321.

[108] B. Liu, and D. Xia *Zhong. Yao. Za.*, 1995, **30**, 615.

[109] K. K. Assil, and R. N. Weinreb *Arch. Ophthalm.*, 1987, **105**, 400.

[110] V. Gandhi, E. Estey, M. Du, B. Nowak, M. J. Keating, and W. Plunkett *Clin. Cancer Res.*, 1995, **1**, 169.

[111] D. E. Colburn, F. J. Giles, D. Oladouich, and J. A. Smith *Hematology*, 2004, **9**, 217.

[112] S. B. Howell, S. Gill, and L. H. Elford *Cancer Treat. Rep.*, 1982, **66**, 1825.

[113] Anonymous, *Med. Lett. Drugs Ther.*, 2000, **42**, 83.

[114] Adult acute myeloid leukemia, From: PDQ. Physician data query (database): Bethesda, MD, National Cancer Institute, 1996.

[115] D. L. McCauley *Clin. Pharm.*, 1992, **11**, 767.

[116] Z. Arlin, D. C. Case, Jr., J. Moore, P. Wiernik, E. Feldman, S. Saletan, P. Desai, L. Sia, and K. Cartwright *Leukemia*, 1990, **4**, 177.

[117] S. Pavlovsky, L. J. Garcia Gonzalez, M. A. Martinez, P. Sobrevilla, M. Eppinger-Helft, A. Marin, M. Lopes-Hernandez, I. Fernandiz, M. E. Rubio, S. Ibarra, M. Lluesma, G. R. Arguelles, and F. J. de Diego *Ann Hematol.*, 1994, **69**, 11.

[118] A. Wahlin, P. Hornsten, M. Hedenus, and C. Malm *Cancer Chemother. Pharmacol.*, 1991, **28**, 480.

[119] J. F. Bishop, J. P. Matthews, G. A. Young, J. Szer, A. Gillett, D. Joshua, K. Bradstock, A. Enmo, M. M. Wolf, R. Fox, R. Coberoft, R. Herrmann, *et al. Blood*, 1996, **87**, 1710.

[120] R. B. Geller, P. J. Burke, J. E. Karp, R. L. Humphrey, H. G. Braine, R. W. Tucker, M. G. Fox, M. Zahurak, L. Morrell, and K. L. Hall *Blood*, 1989, **74**, 1499.

[121] W. G. Woods, N. Kobrinsky, J. D. Buckley, J. W. Lee, J. Sanders, S. Neudot, S. Gold, D. R. Barnard, J. DeSwarte, K. Dusenbergy, D. Kalousek, D. C. Arthur, and B. J. Lange *Blood*, 1996, **87**, 4979.

[122] W. G. Woods, S. Neudorf, S. Gold, S. Sanders, N. Kobrinsky, D. Bernard, J. DeKwarte, D. Arthur, and B. J. Lange *Proc. Am. Soc. Clin. Oncol.*, 1996, **15**, 368.

[123] R. J. Mayer, R. B. Davis, C. A. Schiffer, D. T. Berg, B. L. Powell, P. Schulman, G. A. Omura, J. O. Moore, O. R. Mclntyre, and E. Frei 3rd *N. Engl. J. Med.*, 1994, **331**, 896.

[124] R. Champlin, J. Gajewski, S. Nimer, S. Vollset, E. Landaw, D. Winston, G. Schiller, and W. Ho *J. Clin. Oncol.*, 1990, **8**, 1199.

[125] F. X. Mahaney, Jr. *J. Natl. Cancer Inst.*, 1990, **82**, 259.

[126] W. J. Baker, G. L. Royer, and R. B. Weiss *J. Clin. Oncol.*, 1991, **9**, 679.

[127] H. M. Haupt, G. M. Hutchins, and G. W. Moore *Am. J. Med.*, 1981, **70**, 256.

[128] Chronic Myelogenous Leukemia, From: PDQ. Physician Data Query (Database): Bethesda, MD, National Cancer Institute, 2002.

[129] H. M. Kantarjian, M. Talpaz, D. Kontoyiannis, J. Gutterman, M. J. Keating, E. H. Estey, S. O'Brien, M. B. Rios, M. Beran, and A. Deisseroth *J. Clin. Oncol.*, 1992, **10**, 398.

[130] F. Guilhot, C. Chastang, M. Michallet, A. Guerci, J. L. Harousseau, F. Maloisel, R. Bouabdallah, D. Guyotat, N. Cheron, F. Nicolini, J. F. Abgrall, and J. Tanzer *N. Engl. J. Med.*, 1997, **337**, 223.

[131] J. M. Goldman *N. Engl. J. Med.*, 1997, **337**, 270.

[132] T. Patel, D. F. Roychowdhury, F. Guilhot, J. Guilhot, and C. Chastang *N. Engl. J. Med.*, 1997, **337**, 1634.

This page intentionally left blank

CHAPTER **3**

Famotidine

Mohamed A. Al-Omar* and **Abdullah M. Al-Mohizea[†]**

* Department of Pharmaceutical Chemistry, College of Pharmacy, King Saud University, Riyadh-11451, Saudi Arabia
† Department of Pharmaceutics, College of Pharmacy, King Saud University, Riyadh-11451, Saudi Arabia

1. GENERAL INFORMATION

1.1. Nomenclature

1.1.1. Systemic chemical names

3-[[2-[(Aminoiminomethyl)amino]-4-thiazolyl]methyl]thio]-
  N-(aminosulfonyl) propanimidamide.
[1-amino-3-[[2-[(diaminomethylene)amino]-4-thiazolyl]-methyl]thio]pro-
  pylidene]sulfamide.
N-sulfamoyl-3-[(2-guanidinothiazol-4-yl)methylthio]propionamide [1, 2].

1.1.2. Nonproprietary names
Famotidine.

1.1.3. Proprietary names
Amfamox, Apo-Famotidine, Blocacid, Brolin, Confobos, Cronol, Cuantin, Dispromil, Famodil, Famodine, Famosan, Famoxal, Fanosin, Fibonel, Ganor, Gaster, Gastridin, Gastropen, Ifada, Lecedil, Motiax, Muclox,

Nulcerin, Pepcid, Pepcidina, Pepcidine, Pepdine, Pepdul, Peptan, Ulcetrax, Ulfamid, Ulfinol [2, 3, 4].

1.1.4. Synonyms
YM-11170, MK-208, L-643341 [2, 3].

1.2. Formulae

1.2.1. Empirical formula, molecular weight, CAS number [3, 4]
$C_8H_{15}N_7O_2S_3$, 337.45, [0076824-35-6].

1.2.2. Structural formula
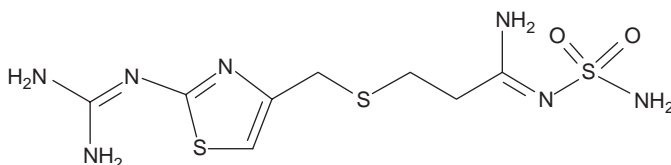
1.3. Elemental analysis

C, 28.47%; H, 4.48%; N, 29.06%; O, 9.48%; S, 28.51%.

1.4. Appearance

A white to pale yellowish-white crystalline powder or crystals [1, 3].

2. PHYSICAL CHARACTERISTICS

2.1. Solution pH

Famotidine solution has a pH of 5.0–5.6; homogenous suspensions of the drug have a pH of 6.5–7.5 [3].

2.2. Solubility characteristics

Freely soluble in glacial acetic acid; slightly soluble in methanol; very slightly soluble in water; practically insoluble in ethanol [1].

2.3. Optical activity

Famotidine has no optical activity.

2.4. X-ray powder diffraction pattern

The crystal structure of famotidine form B has been solved directly from powder diffraction data by the application of simulated annealing. The molecule crystallizes in the monoclinic space group $P2_1/c$ with refined

TABLE 3.1 Atomic coordinates ($\times 10^4$) and equivalent isotropic displacement parameters ($\mathring{A}^2 \times 10^3$) of famotidine. U(eq) is defined as one third of the trace of the orthogonalized U_{ij} tensor [5]

	Form A				Form B			
	x	*y*	*z*	*U*(eq)	*x*	*y*	*Z*	*U*(eq)
S1	6443.7(3)	437.3(9)	3693.2(3)	37(1)	6836.1(5)	2629.8(7)	8226.0(4)	40(1)
C2	6953(1)	2989(3)	3533(1)	27(1)	6134(2)	1353(3)	8497(1)	30(1)
N3	6584.7(9)	3545(3)	2703.7(9)	29(1)	6230(2)	2803(2)	8035(1)	35(1)
C4	5897(1)	1907(3)	2164(1)	30(1)	6858(2)	2361(3)	7435(1)	34(1)
C5	5728(1)	110(4)	2574(1)	36(1)	7261(2)	613(3)	7456(1)	39(1)
N6	7663(1)	4120(3)	4258.6(9)	35(1)	5581(2)	1177(2)	9133(1)	35(1)
C7	8095(1)	5986(4)	4155(1)	34(1)	4920(2)	2544(3)	9317(1)	34(1)
N8	7901(1)	6860(3)	3393(1)	33(1)	4750(2)	4145(3)	8926(1)	44(1)
N9	8781(2)	7081(5)	4876(1)	71(1)	4389(2)	2264(3)	9943(1)	52(1)
C10	5387(1)	2280(4)	1191(1)	37(1)	7009(2)	3841(3)	6845(1)	41(1)
S11	6087.4(3)	2308.2(8)	754.4(3)	33(1)	8105.9(5)	5529.6(8)	7222.3(3)	43(1)
C12	6537(1)	2843(3)	1030(1)	29(1)	9382(2)	4204(3)	7231(1)	36(1)
C13	7275.2(6)	21177(2)	860.6(6)	31(1)	9870(2)	4285(3)	6441(1)	37(1)
C14	8118.8(6)	335(2)	1486.0(6)	24(1)	9135(2)	3299(3)	5768(1)	28(1)
N15	8441.5(6)	1747(2)	1128.6(6)	31(1)	8474(2)	4324(2)	5241(1)	43(1)
N16	8436.4(9)	40(3)	2319.7(9)	29(1)	9193(1)	1470(2)	5781(1)	28(1)
S17	9342.0(2)	1353.8(8)	3106.1(2)	23(1)	8340.8(4)	216.2(6)	5160.7(3)	28(1)
N18	9281(1)	4353(3)	3065(1)	35(1)	8525(2)	834(3)	4264(1)	38(1)
O19	9389.7(9)	607(3)	3883.0(7)	38(1)	7174(1)	630(2)	5195(1)	43(1)
O20	10113.0(8)	768(3)	3067.2(8)	34(1)	8710(2)	21654(2)	5336(1)	47(1)

unit-cell dimensions $a = 17.6547$ (4) Å, $b = 5.2932$ (1) Å, $c = 18.2590$ (3) Å and $\beta = 123.558$ (1)° at $T = 130$ K. The core of this work is a systematic investigation of the influence of algorithmic, crystallographic, and molecular factors on the structure solution process. With an appropriate choice of annealing schedule, molecular description, and diffraction data range, the overall number of successes in solving the crystal structure is close to 100%. Other factors, including crystallographic search space restrictions and parameter sampling method, have little effect on the structure solution process. Table 3.1 shows the atomic coordinates ($\times 10^4$) and equivalent isotropic displacement parameters ($\text{Å}^2 \times 10^3$) U(eq) for famotidine which were obtained from Ref. [5]. Figure 3.1A shows the X-ray powder diffraction pattern of famotidine, which was obtained using a pure sample of the drug and Fig. 3.1B shows the projection of the famotidine modifications in the plane of the thiazole ring. (a) form A; (b) form B [5].

2.5. Thermal methods of analysis

2.5.1. Melting behavior
Famotidine melts at about 163–164 °C [1, 3].

Scattering angle
(degrees 2-θ)
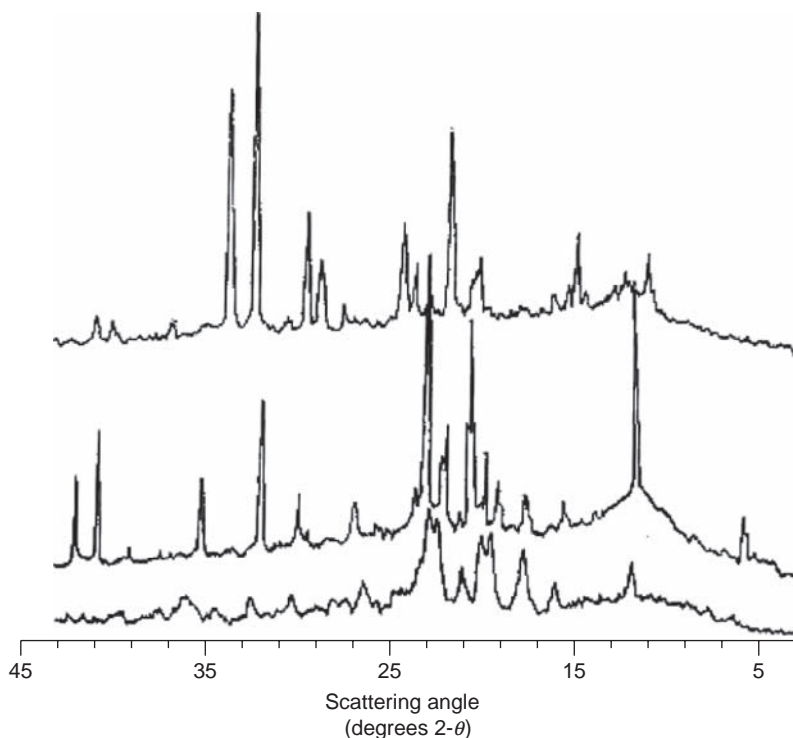
FIGURE 3.1 (Continued)

2.5.2. Differential scanning calorimetry

The differential scanning calorimetry (DSC) thermogram of famotidine was obtained using thermal analyzer model 785 (Stanton Redcroft, England) in an open pan system equipped with a data acquisition station as reported by Hassan *et al.* [6]. The thermogram shown in Fig. 3.2 was
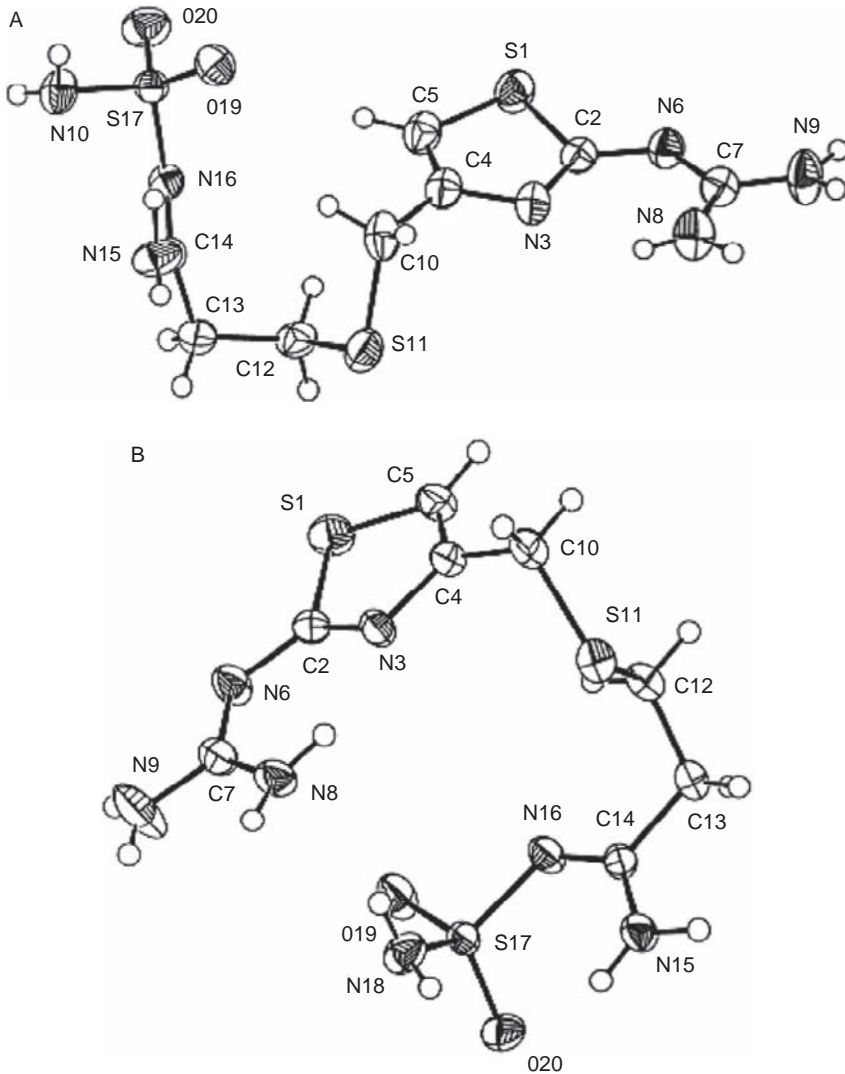
FIGURE 3.1 (A) X-ray powder diffraction pattern of famotidine. (B) Projection of the famotidine modifications in the plane of the thiazole ring. (a) form A; (b) form B [5].
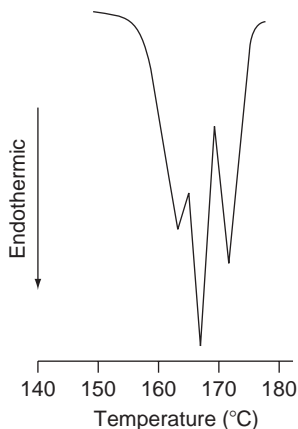
FIGURE 3.2 Differential scanning calorimetry thermogram of famotidine [6].

obtained at a heating rate of 10 °C/min, and was run from 100 to 190 °C. The compound was found to melt at 166.4 °C [6].

2.6. Spectroscopy

2.6.1. Ultraviolet spectroscopy

The UV spectrum of famotidine (5 µg/ml) in methanol is shown in Fig. 3.3. The spectrum was recorded using a Shimadzu UV–vis Spectrophotometer 1601 PC. Famotidine exhibited three maxima wavelengths:

λ_{max}(nm)	A (1%, 1 cm)	Molar absorptivity (l mol^{-1} cm^{-1})
288.0	4.94	166.7
211.0	6.52	220.0
205.1	5.98	201.8

2.6.2. Vibrational spectroscopy

The infrared absorption spectrum of famotidine was obtained in a KBr disc using a Perkin Elmer infrared spectrophotometer. The infrared spectrum is shown in Fig. 3.4. Famotidine molecule consists of guanidine, thiazole, thioether, and sulfamoyl parts. Due to the presence of these parts in its structure, vibrational assignment is very difficult. The spectral position of NH_2 groups in guanidine and sulfamoyl depends upon bonded atom or groups to NH_2 group. However, its stretching vibrations generally give rise to bands in the region 3550–3250 cm^{-1}. The bands observed in the range at 3506–3234 cm^{-1} of famotidine are assigned to the stretching vibrations of NH_2 groups. The region of IR spectrum of SO_2–NH_2 moiety exhibiting the NH_2 stretching modes is around 3390–3230 cm^{-1}. The NH_2 scissoring (δ, bending) vibration gives rise to strong
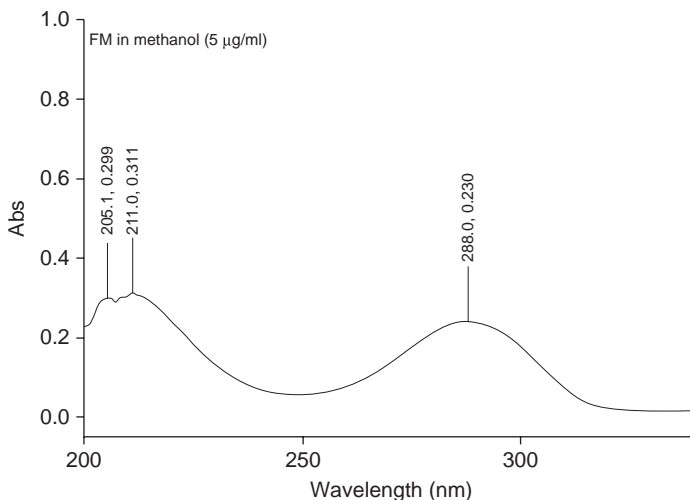
FIGURE 3.3   The UV absorption spectrum of famotidine in methanol.
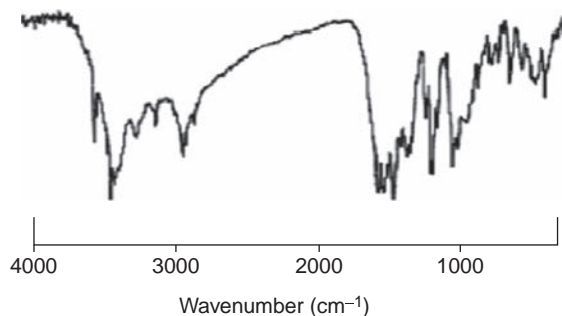
FIGURE 3.4   The infrared absorption spectrum of famotidine obtained in a KBr pellet [8].

band in the region 1650 ± 50 cm^{-1}. The very strong bands observed at 1639, 1604, and 1535 cm^{-1} are assigned to NH$_2$ bending vibrations. The band at 1562 cm^{-1} is assigned as ν(N–C=N) $^+\delta$(NH$_2$). The medium intensity band at 1118 cm^{-1} corresponds to the p(NH$_2$) vibration of guanidine. Guanidines show the C=N stretching in the general ranges 1690–1550 cm^{-1}. The identification of C=N vibration in ring systems is very difficult by the interaction with other double bonds. The bands found in the 1600–1480 cm^{-1} region can be associated with the ring stretching modes. The asymmetric and symmetric stretching modes of SO$_2$ group are generally assigned in the range 1335 ± 25 and 1150 ± 15 cm^{-1}, respectively. The observed bands at 1321 and 1146 cm^{-1} are assigned to the ν_{as} (SO$_2$) and ν_s (SO$_2$) modes, respectively. The band observed at 942 cm^{-1} is assigned to the ν(N–S) stretching mode. The band observed

at 904 cm^{-1} is not pure which assigned to the $\upsilon(\text{S–N}) + \gamma(\text{CH})$. The scissors and wagging vibrations of this group are observed at 603 and 543 cm^{-1}, respectively [7]. The assignment of infrared absorption bands for famotidine is abridged in Table 3.2.

2.6.3. Nuclear magnetic resonance spectrometry

The NMR spectra of famotidine were measured using a Bruker model AMX operating 500 MHz spectrometer. The sample was dissolved in deuterated water (D_2O) and measured at room temperature as reported by Barańska $et\ al.$ [8]. The ^{1}H-NMR spectrum was obtained with tetramethylsilane (TMS) was used as the internal standard. The ^{13}C NMR spectrum was recorded with a resonance frequency of 125.77 MHz. ^{15}N NMR spectrum was recorded with no proton decoupling in a 10-mm tube as indicated Baranska $et\ al.$ [8]. The ^{1}H-NMR, ^{13}C NMR, and ^{15}N NMR spectra are shown in Figs. 3.5A–C–3.11, respectively. The assignments for the ^{1}H-NMR, ^{13}C NMR, and ^{15}N NMR spectra of famotidine are shown in Tables 3.3–3.5, respectively [8].

TABLE 3.2   Assignments for the infrared absorption bands of famotidine [7]

Frequency (cm^{-1})	Assignments
3506-strong	$\upsilon_a(\text{NH}_2)_{\text{gua}}$, $\upsilon_a(\text{NH}_2)_{\text{sulfo}}$
3401-strong	$\upsilon_s(\text{NH}_2)_{\text{gua}}$, $\upsilon_s(\text{NH}_2)_{\text{sulfo}}$
3337-strong	$\upsilon(\text{NH}_2)_{\text{sulfo}}$, $\upsilon_s(\text{NH}_2)_{\text{sulfo}}$, $\upsilon(\text{C–H})_{\text{thiazole}}$, $\upsilon_a(\text{CH}_2)$, $\upsilon_a(\text{CH}_2)$, $\upsilon_{as}(\text{CH}_2)$, $\upsilon_s(\text{CH}_2)$
2911-weak	$\upsilon(\text{CH}_2\text{–S})$, $\upsilon_s(\text{CH}_2)$, $\upsilon(\text{C=N})_{\text{gua+sulfo}}$
1639-strong	$\upsilon(\text{C=N})_{\text{gua}}$
1601-strong	$\delta(\text{NH}_2)_{\text{gua}}$, $\upsilon(\text{N–C=N}) + \delta(\text{NH}_2)$
1533-strong	$\delta(\text{NH}_2)_{\text{sulfo}}$ $\upsilon_{\text{(thiazole)}}$, $\delta(\text{CH}_2)$
1427-medium	$\delta(\text{CH}_2) + \upsilon_{\text{(thiazole)}}$, $\upsilon(\text{C–N})_{\text{gua}}$, $\upsilon_{\text{(thiazole)}}$, $\delta(\text{CH}_2)$ $+(\text{C–C–C})_{\text{thioether}}$, $\omega(\text{CH}_2) + \upsilon_{\text{(thiazole)}}$, $\delta(\text{CH}_2)$, $\upsilon_{as}(\text{SO}_2)$, δ_{thiazole}, $\omega(\text{CH}_2)$
1286-strong	$\delta_{\text{thiazole}}+ \gamma(\text{CH}_2\text{–S})$, $\delta(\text{C}_{\text{thioether–thiazole}})$, $\upsilon(\text{C–C})$
1147-strong	$\upsilon_s\ (\text{SO}_2)$, $\rho(\text{NH}_2)_{\text{gua}}$, $\text{CH}_2+ \rho(\text{NH}_2)_{\text{sulfo}}$, $\rho(\text{CH}_2)$, $\rho(\text{CH})+ \delta_{\text{thiazole}}$, $\upsilon(\text{C–N})_{\text{gua}}+ \delta_{\text{(thiazole)}}$, $\omega(\text{NH}_2)$, δ_{thiazole}, $\delta(\text{N–C–N})_{\text{sulfo}}+ \omega(\text{SO}_2)$, γ_{thiazole} $+ \gamma(\text{C–N})_{\text{gua}}$, $t(\text{SO}_2)$, $\tau(\text{NH}_2)$, $\rho(\text{SO}_2)$

a, asymmetric; s, symmetric; υ, stretching; δ, in-plane deformation; γ, out-of-plane deformation; ω, wagging; ρ, rocking; τ, torsional relative intensity.
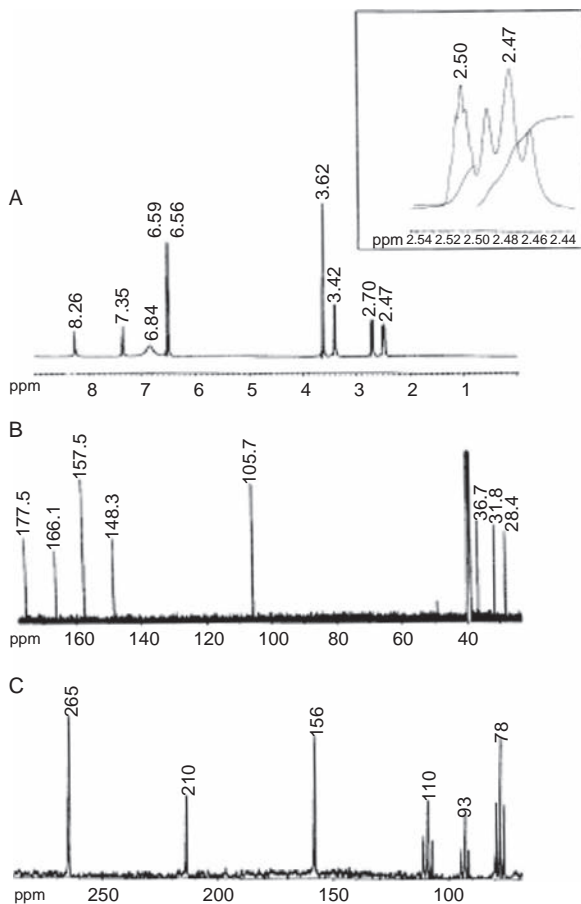
FIGURE 3.5 Summary NMR spectra of famotidine (A) ^{1}H (B) ^{13}C (C) ^{15}N (the insert shows the triplet at 2.47 ppm overlaps with quintet at 2.50 ppm) [7].

2.7. Mass spectrometry

The electron impact (EI) spectrum of famotidine is presented in Fig. 3.12. The mass spectrum was recorded using a Shimadzu PQ-5000 GC-Ms spectrometer. The spectrum shows a mass peak (M·) at 276 m/z and a base peak at 44 m/z resulting from the loss of the group. These and other proposed fragmentation patterns of the drug are presented in Table 3.6.
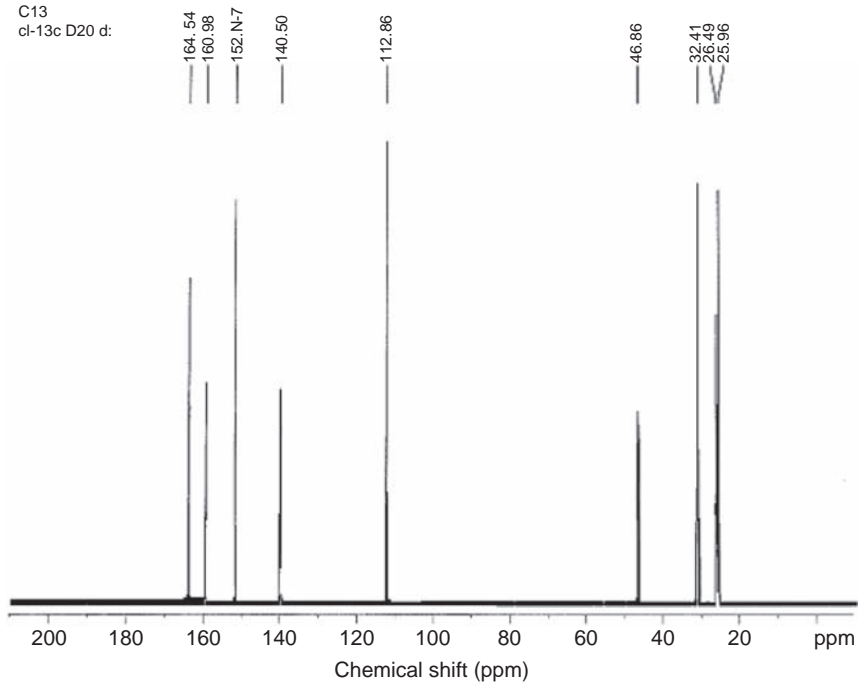
FIGURE 3.6   The ^{13}C-NMR spectrum of famotidine in D_2O.

3. STABILITY AND STORAGE [3, 9]

The solution of famotidine is light sensitive and should be protected from light [3]. Commercially available famotidine tablets should be stored in well-closed, light resistant containers at temperature of 40 °C or less. The tablets have an expiration date of 30 months following the date of manufacture when stored under these conditions.

Commercially available famotidine powder for oral suspension should be stored in tight containers at temperature of 40 °C or less. Oral suspensions of the drug, should be stored at less than 30 °C, freezing should be avoided. Any unused suspension should be discarded after 30 days of reconstitution [9]. Commercially available famotidine injection should be refrigerated at 2–8 °C and has an expiration date of 24 months. After dilution of commercially available injection with intravenous solutions, resulting solutions are stable for 48 h at room temperature [9]. Recently, Değim and Ağabeyoğlu have compared the stability of famotidine and nizatidine using isothermal and nonisothermal techniques [10]. The results of both techniques indicate that famotidine is a stable compound in comparison to nizatidine.
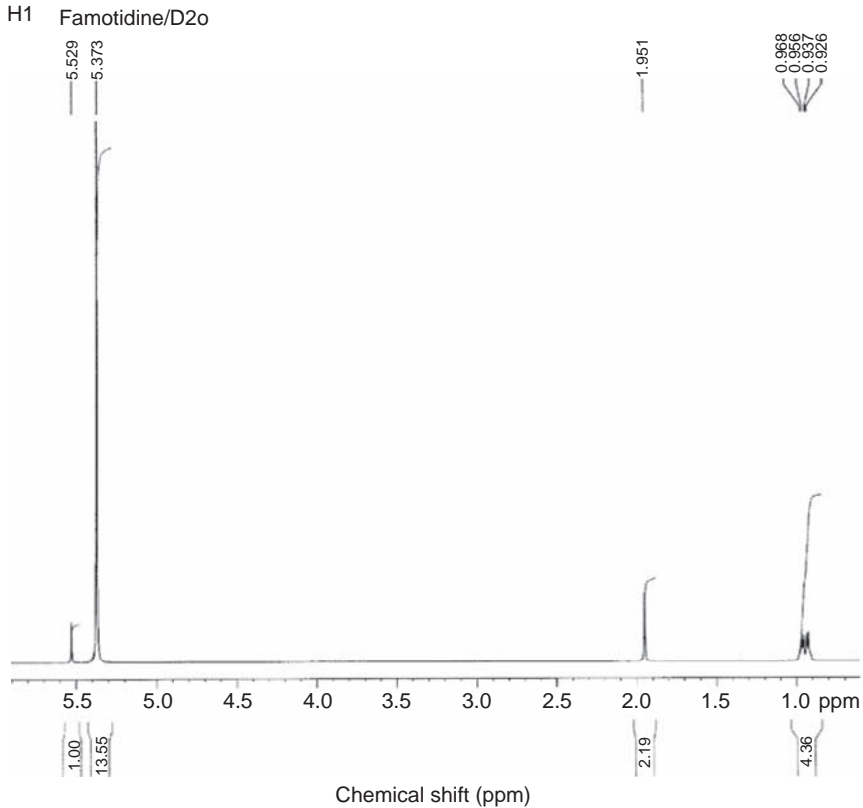
FIGURE 3.7   The expanded ^{1}H-NMR spectrum of famotidine in D_2O.

4. ANALYTICAL PROFILES OF FAMOTIDINE

4.1. Compendial methods of analysis

4.1.1. Identification

The European Pharmacopoeia [11] recommends the use of following methods for the identification of the pure drug.

First identification: **B**.

Second identification: **A, C, and D**.

A. Dissolve 25.0 mg of famotidine in buffer solution pH 2.5 R1 and dilute to 100.0 ml with the same solution. Dilute 10.0 ml of this solution to 100.0 ml with buffer solution pH 2.5 R1. Examined between 230 and 350 nm, the solution shows one absorption maximum at 265 nm. The specific absorbance at the maximum is 297–315 nm, calculated with reference to the dried substance.
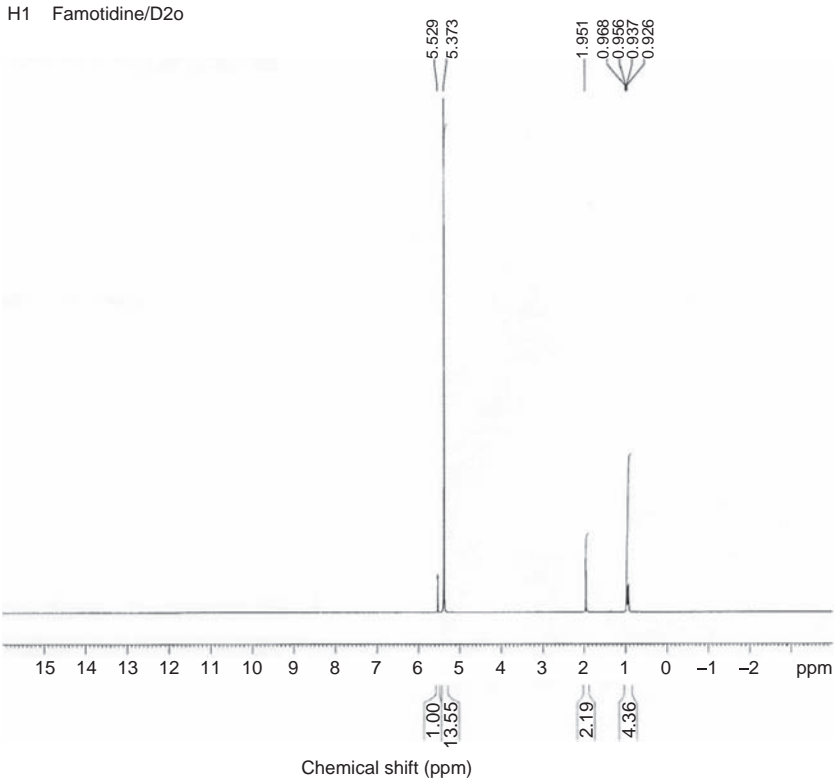
FIGURE 3.8   The ^{1}H-NMR spectrum of famotidine in D_2O.

B. Examine by infrared absorption spectrophotometry, comparing with the spectrum obtained with famotidine CRS. Examine the substances prepared as discs. If the spectra obtained show differences, suspend 0.10 g of the substance to be examined and the reference substance separately in 5 ml of water R. Heat to boiling and allow to cool, scratching the wall of the tube with a glass rod to initiate crystallization. Filter, wash the crystals with 2 ml of iced water R, and dry in an oven at 80 °C at a pressure not exceeding 670 Pa for 1 h. Record new spectra using the residues.

C. Examine the chromatograms obtained in the test for related substances. The principal spot in the chromatogram obtained with test solution (b) is similar in position and size to the principal spot in the chromatogram obtained with reference solution (f).

D. Dissolve with shaking about 5 mg of the substance to be examined and about 3 mg of p-phenylenediamine dihydrochloride R in 5 ml of a
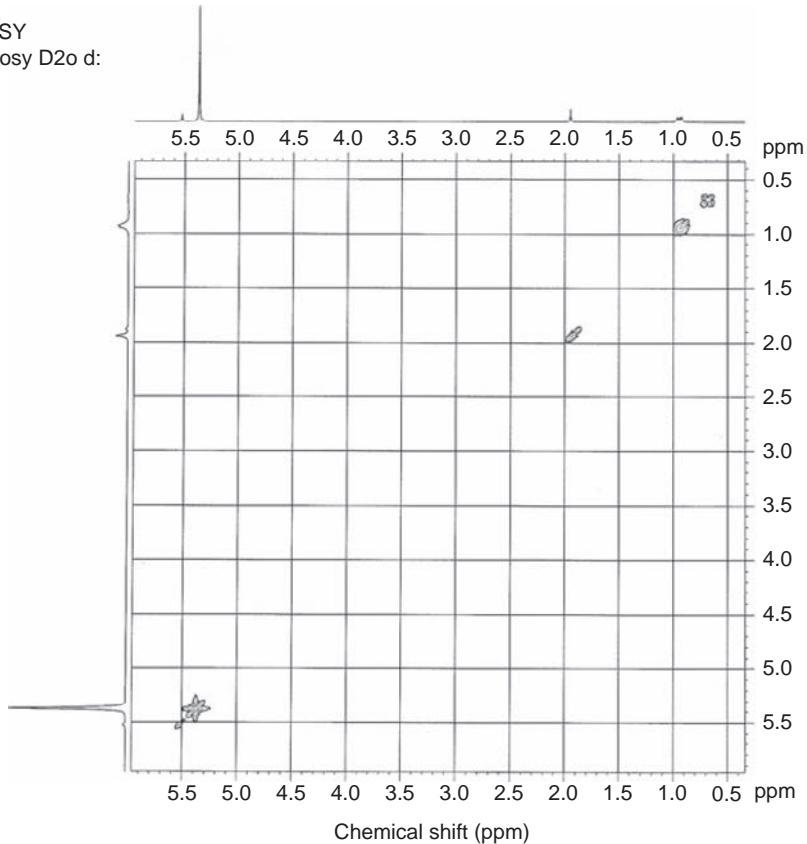
FIGURE 3.9 The COSY ^{1}H-NMR spectrum of famotidine in D_2O.

10 g/l solution of hydrochloric acid R. Add about 0.1 g of zinc powder R, mix and allow to stand for 2 min. Add 5 ml of ferric ammonium sulphate solution R6 and mix. A blue or violet-blue color develops.

4.1.2. Tests [11, 12]

4.1.2.1. Appearance of solution   Dissolve 0.20 g of famotidine in a 50 g/l solution of hydrochloric acid R, heating to 40 °C if necessary, and dilute to 20 ml with the same acid. The solution is clear and not more intensely colored than reference solution BY$_7$.

4.1.2.2. Impurities and related substances   Examine by thin-layer chromatography (TLC), using a plate coated with a suitable silica gel (5 mm) containing a fluorescent indicator having an optimal intensity at 254 nm.

HSQC
cl-13c-hsqc D2o d:
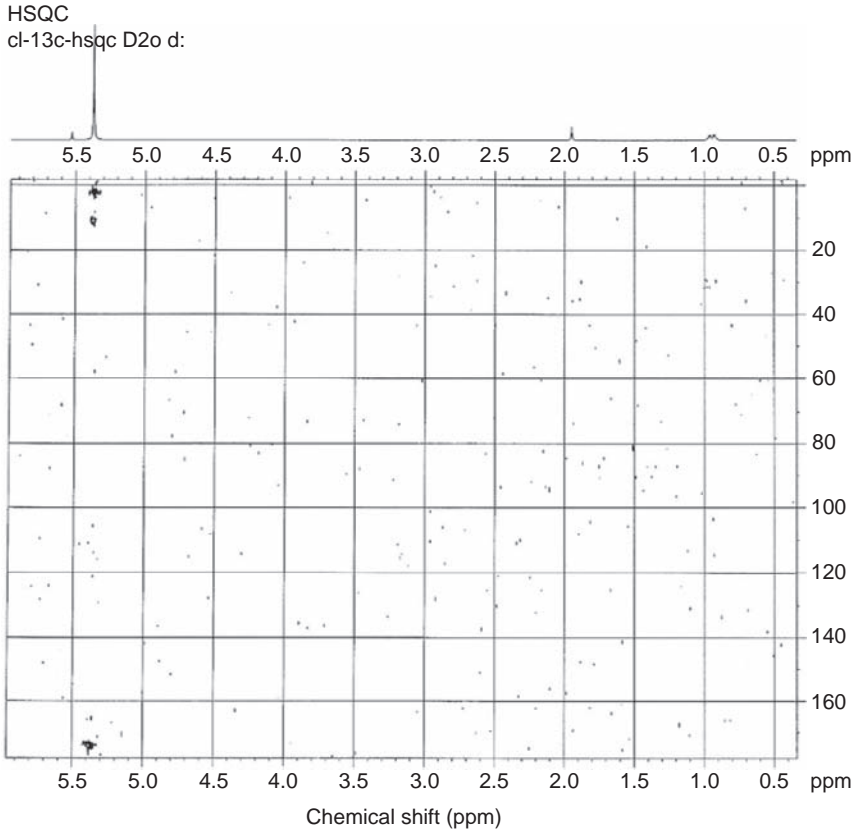
FIGURE 3.10   The HSQC NMR spectrum of famotidine in D_2O.

Test solution (a): Dissolve 0.20 g of the substance to be examined in glacial acetic acid R and dilute to 10 ml with the same acid.

Test solution (b): Dilute 1 ml of test solution (a) to 10 ml with glacial acetic acid R.

Reference solution (a): Dilute 3 ml of test solution (b) to 100 ml with glacial acetic acid R.

Reference solution (b): Dilute 1 ml of test solution (b) to 100 ml with glacial acetic acid R.

Reference solution (c): Dilute 5 ml of reference solution (b) to 10 ml with glacial acetic acid R.

Reference solution (d): Dissolve 4 mg of famotidine impurity A CRS in glacial acetic acid R and dilute to 10 ml with the same acid. Dilute 1 ml of this solution to 10 ml with glacial acetic acid R.
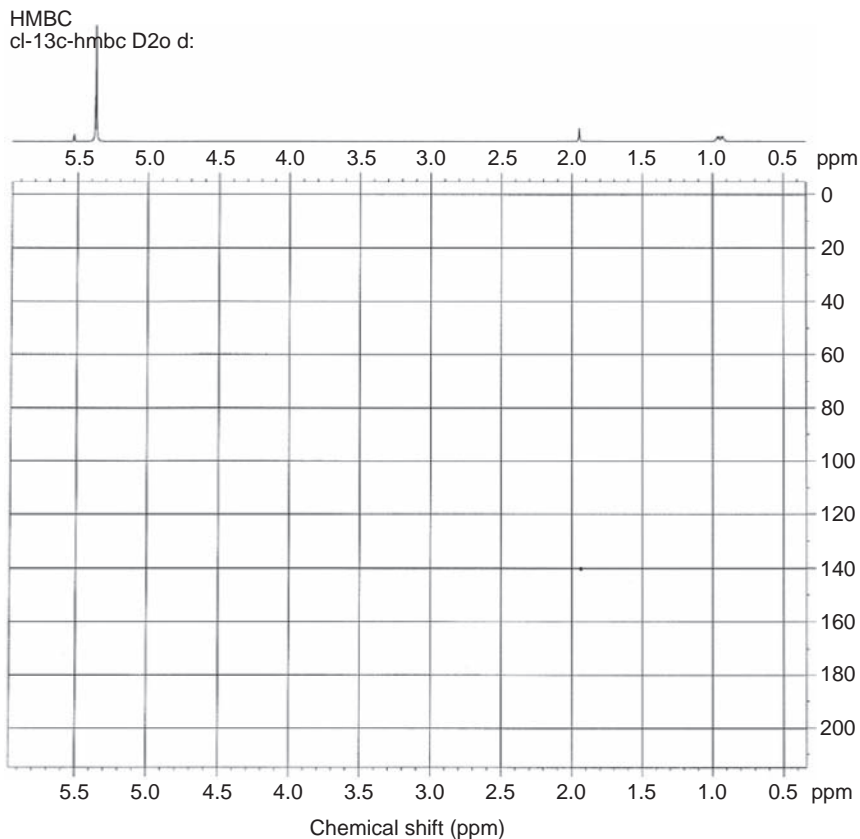
FIGURE 3.11   The HMBC spectrum of famotidine in D_2O.

Reference solution (e): Dissolve 4 mg of famotidine impurity B CRS in glacial acetic acid R and dilute to 10 ml with the same acid. Dilute 1 ml of this solution to 10 ml with reference solution (a).

Reference solution (f): Dissolve 20 mg of famotidine CRS in glacial acetic acid R and dilute to 10 ml with the same acid.

Apply separately to the plate 5 ml of each solution in aliquots of 1 ml, drying with a current of nitrogen R after application of each aliquot. Place the plate in a desiccator for 2 h and develop over a path of 8 cm using a freshly prepared mixture of 2 volumes of concentrated ammonia R, 20 volumes of toluene R, 25 volumes of methanol R, and 40 volumes of ethyl acetate R. Allow the plate to dry in air until the odor of the solvent is no longer perceptible and examine in UV light at 254 nm. In the chromatogram obtained with test solution (a): any spot corresponding to

TABLE 3.3   Assignments of the protons chemical shifts of famotidine [8]
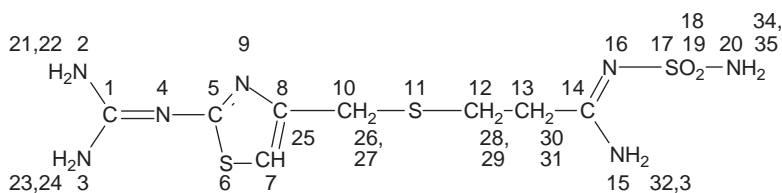
Proton atoms	Chemical shift, δ, (ppm relative to TMS)	Multiplicity s: singlet, t: triplet	Number of proton atoms
H 30, H 31	2.68	t	2
H 28, H 29	2.90	t	2
H 26, H 27	3.82	s	2
H 32, H 33	7.04	s	2
H 25	6.95	s	1
H 21, H 22, H 23, H 24	6.83	s	4
H 34	8.78	s	1
H 35	9.18	s	1

TABLE 3.4   Assignments of Carbon-13 chemical shifts of famotidine [8]
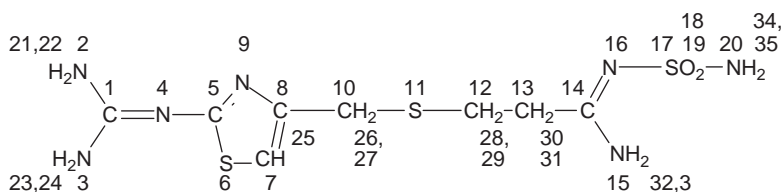
Carbon atoms	Chemical shift, δ, (ppm relative to TMS)	Number of carbon atoms
C 13	25.0	1
C 12	28.2	1
C 10	29.1	1
C 7	105.5	1
C 8	137.9	1
C 1	157.9	1
C 14	166.8	1
C 5	182.9	1

TABLE 3.5   Assignments of ^{15}N NMR spectrum chemical shifts of famotidine [8]
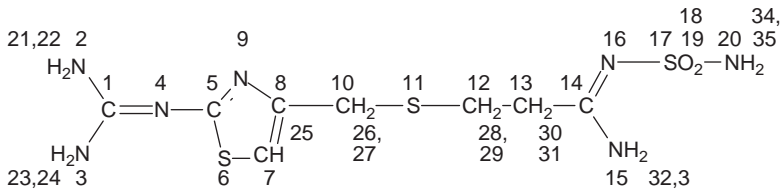
Nitrogen atoms	Chemical shift, (ppm relative to TMS)	Multiplicity s: singlet, t: triplet	Number of nitrogen atoms
N 9	265	s	1
N 16	215	s	1
N 4	163	s	1
N 20	107	t	1
N 15	95	t	1
N 2, N 3	72.79	t	2

Scan # : 313
Mass peak # : 276 Ret. Time : 4.700
Base peak : 44.00 (5491864)
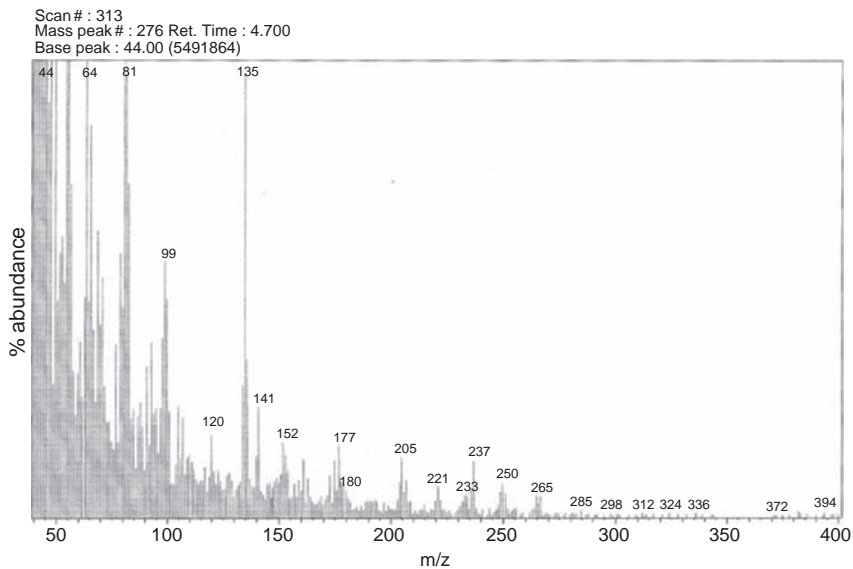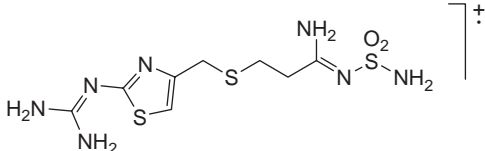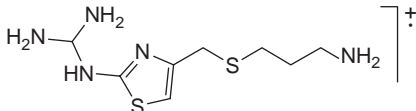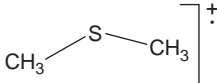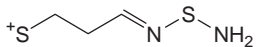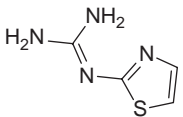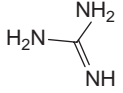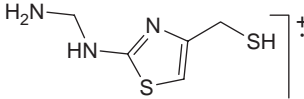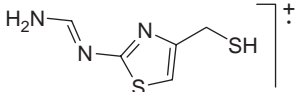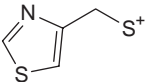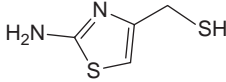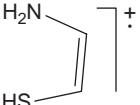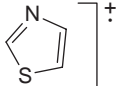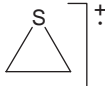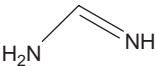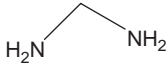
FIGURE 3.12   Mass spectrum of famotidine.

TABLE 3.6 Assignments for the fragmentation pattern observed in the mass spectrum of famotidine

Mass number (m/z)	Structural assignment	Mass number (m/z)	Structural assignment
M-1 336, 0.1%		m/z 73, 1.0%	
m/z 247, 02% Frag. +2 249, 04%		m/z 62, 2.0% Frag. +1 63, 3.0% Frag. +2 64, 48.0%	
m/z 135, 7.3% Frag. +1 136, 2.2%		m/z 141, 1.5% Frag. +1 142, 0.4%	
m/z 59, 1.4% Frag. +1 60, 2.0% Frag. +2 61, 2.4%		m/z 175, 0.8% Frag. +1 176, 0.4%	

(continued)

TABLE 3.6 (*continued*)

Mass number (*m/z*)	Structural assignment	Mass number (*m/z*)	Structural assignment
m/z 173, 0.6%		*m/z* 129, 0.5% Frag. +1 130, 0.3%	
m/z 146, 0.5%		*m/z* 75, 1.0%	
m/z 85, 1.5%		*m/z* 43, 20.0% Frag. +1 44, 100.0%	
m/z 60, 2.0%		*m/z* 44, 100.0% Frag. +1 45, 25.0% Frag. +2 46, 24.0%	
m/z 46, 24.0%		*m/z* 75, 1.0%	

m/z 41, 11.0%
Frag. +1 42, 10.0%
Frag. +2 43, 20.0%
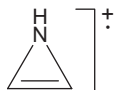
m/z 42, 10.0%
Frag. +1 43, 20.0%
Frag. +2 44, 100.0%
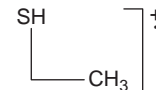
NH=C=NH

m/z 62, 2.0%
Frag. +1 63, 3.0%
Frag. +2 64, 48.0%

famotidine impurity A is not more intense than the principal spot in the chromatogram obtained with reference solution (d) (0.2%); any spot, apart from the principal spot and any spot corresponding to famotidine impurity A, is not more intense than the principal spot in the chromatogram obtained with reference solution (a) (0.3%); and not more than three such spots are more intense than the principal spot in the chromatogram obtained with reference solution (b) (0.1%). The test is not valid unless the chromatogram obtained with reference solution (e) shows two clearly separated spots and the chromatogram obtained with reference solution (c) shows a visible spot.

4.2. Impurities
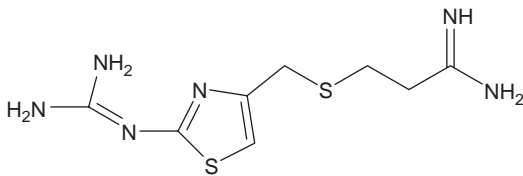
A.   3-[[[2-[(diaminomethylene)amino]thiazol-4-yl]methyl]thio]propanamidine,
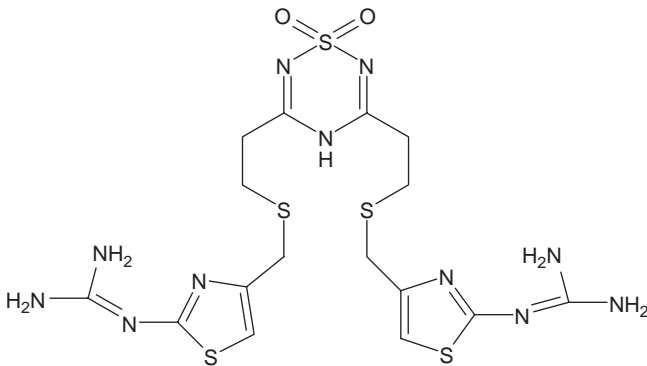
B. 3,5-bis[2-[[[2-[(diaminomethylene)amino]thiazol-4-yl]methyl]thio]-ethyl]-4 H-1,2,4,6-thiatriazine1,1-dioxide,
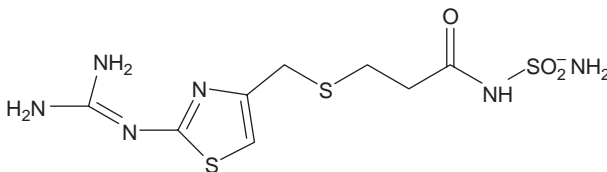
C.   *N*-(aminosulphonyl)-3-[[[2-[(diaminomethylene)amino]thiazol-4-yl]methyl] thio]propanamide,
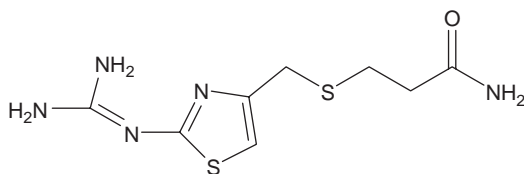
D.   3-[[[2-[(diaminomethylene)amino]thiazol-4-yl]methyl]thio] propanamide.

4.3. Heavy metals

2.0 g of famotidine complies with limit test D for heavy metals (10 ppm). Prepare the standard using 2 ml of lead standard solution (10 ppm Pb) R.

4.4. Loss on drying

Not more than 0.5% of famotidine, determined on 1.000 g by drying in an oven at 80 °C at a pressure not exceeding 670 Pa for 5 h.

4.5. Sulphated ash

Not more than 0.1% of famotidine, determined on 1.0 g.

4.6. Assay

Dissolve 0.120 g of famotidine in 60 ml of anhydrous acetic acid R. Titrate with 0.1 M perchloric acid, determining the end-point potentiometrically.
    1 ml of 0.1M perchloric acid is equivalent to 16.87 mg of $C_8H_{15}N_7O_2 S_3$.

4.7. Reported methods of analysis

Several methods were reported in literature for the determination of famotidine in pharmaceutical formulation and biological fluids.

4.7.1. Colorimetric methods

Ayad *et al.* [13] developed two sensitive and simple spectrophotometric methods for the determination of trazodone HCl, famotidine, and diltiazim HCl in pure and pharmaceutical preparations. The methods are based on the oxidation of the cited drugs with iron(III) in acidic medium.

The librated iron(II) reacts with 1,10-phenanthroline (method A) and the ferroin complex is colorimetrically measured at 510 nm against reagent blank. Method B is based on the reaction of librated iron(II) with 2,2-bipyridyl to form a stable colored complex with λ_{max} at 520 nm. Beer's law was obeyed in the concentration range of 1–5, 2–12, and 12–32 μg/ml for trazodone, famotidine, and diltiazem with method A, and 1–10, 8–16 μg/ml for trazodone and famotidine with method B. The apparent molar absorptivity for method A is 1.06×10^5, 2.9×10^4, 1.2×10^4 and for method B is 9.4×10^4 and 1.6×10^4, respectively. This method could be used for the determination of the three drugs, both in pure and dosage forms without interference from common excipients [13].

Quantitative determination of famotidine and its dosage forms was carried out spectrophotometrically, analyzing the colored complex resulting from a charge-transfer interaction between the drug as an electron-donor and chloranilic acid as an electron-acceptor [14]. Famotidine–Chloranilic acid complex displayed one maximum at 525 nm. Conditions and time for complex formation have been optimized. The stoichiometry of the complex is 3:2 donor to acceptor mole ratio. Calibration graph of the complex was found to be linear at a working concentration range of 1.60–11.g% (w/v). Excellent quantitative recoveries (99.01–100.71%) was obtained for the drugs in both its pure and standard dosage forms.

A simple and fast spectrophotometric procedure has been developed for the determination of famotidine in tablet [15]. The method is based on the interaction of ninhydrin with primary amines present in the famotidine. This reaction produces a blue colored product which absorbed maximally at 590 nm. The effects of variables such as reagent concentration and reaction time were investigated to optimize the procedure. Beer's law was obeyed in the concentration range of 5–30 μg/ml with molar absorptivity of $6.99 \times 10^3 \, l \, mol^{-1} \, cm^{-1}$. The results were validated statistically. The proposed method has been applied to the determination of famotidine in tablets with satisfactory results.

Kamath *et al*. [16] have developed colorimetric methods for the determination of diclofenac sodium, famotidine, and ketorolac tromethamine in pharmaceutical formulations by flow injection analysis. The sample solutions (5–50 μg/ml of diclofenac sodium, 10–80 μg/ml of famotidine, and 10–120 μg/ml of ketorolac tromethamine) in methanol were injected into a flow system containing 0.01% (w/v) of 2,4-diciloro-6-nitrophenol (DCNP) in methanol. The color produced is due to the formation of a charge transfer complex was measured with a spectrophotometric detector set at 451 nm. A sampling rate of 40 per hour was achieved with high reproducibility of measurements (RSD < 1.6%).

More identification methods are mentioned in Section 2.5, by Kelani *et al*. [25].

4.7.2. Potentiometric method

Two potentiometric methods for the determination of famotidine in pure form and in its pharmaceutical tablet form were developed by Ayad *et al.* [17]. In the first method, the construction of plasticized poly(vinyl chloride) (PVC) matrix-type famotidine ion-selective membrane electrode and its use in the potentiometric determination of the drug in the pharmaceutical preparations are described. It is based on the use of ion-associated species, formed by famotidine cation and tetraphenyl borate (TPB) counterion. The electrode exhibited a linear response for 1×10^{-3}–1×10^{-5} M of famotidine solutions over the pH range 1–5 with an average recovery of 99.26% and mean standard deviation of 1.12%. Common organic and inorganic cations showed negligible interference. In the second method, the conditions for the oxidimetric titration of the thioether contained in famotidine have been studied. The method depends on using Pb(IV) acetate for oxidation of the thioether contained in famotidine. The titration takes place in the presence of catalytic quantities of potassium bromide (KBr). Direct potentiometric determination of 1.75×10^{-2} M famotidine solution showed an average recovery of 100.51% with a mean standard deviation of 1.26%. The two methods have been applied successfully to commercial tablet.

4.7.3. Voltammetric method

An electrochemical behavior for the analysis of famotidine in urine has been studied recently by Skrzypek *et al.* [18]. The best results for the determination of famotidine were obtained in MOPS buffer solution at pH 6.7. This electroanalytical procedure enable to determine famotidine in the concentration range 1×10^{-9}–4×10^{-8} mol/l by linear sweep adsorptive stripping voltammetry (LS AdSV) and 5×10^{-10}–6×10^{-8} mol/l by square wave adsorptive stripping voltammetry (SW AdSV). The detection and quantification limits were found to be 1.8×10^{-10} and 6.2×10^{-10} mol/l for LS AdSV and 4.9×10^{-11} and 1.6×10^{-10} mol/l for SW AdSV, respectively [18].

4.7.4. Capillary electrophoresis (CE)

A simple and sensitive capillary electrophoresis (CE) method using UV detection has been developed for the direct determination of ranitidine and famotidine in serum, urine, and pharmaceutical formulations. A buffer consisting of 60 mM phosphate buffer adjusted to pH 6.5 was found to provide a very efficient and stable electrophoretic system for the analysis of both drugs. The detection limits obtained were 0.088 µg/ml for ranitidine and 0.16 µg/ml for famotidine [19].

Five drugs (including famotidine) were determined simultaneously in urine by CE [20]. The analysis was carried out in uncoated capillary (48 cm effective length, 50 or 75 μm i.d.) at 22 kV with detection at 220 nm and 32 mM 6-aminohexanoic acid/18 mM adipic acid buffer of pH 4.5 containing 5% (v/v) of methanol, 5% of dextran 18 300 plus 0.02% of poly(ethylene oxide) 300 000 gave the best results. The optimum buffer additives for determination of famotidine in urine were 4% of dextran 73 000, 0.04% of poly(ethylene oxide) 300 000 and 2% (v/v) of methanol. Further improvement was achieved by adding 7.5 mM heptakis-(2,6-di-O-methyl)-β-cyclodextrin [20].

A simple capillary zone electrophoresis (CZE) method was described for the simultaneous determination of cimetidine, famotidine, nizatidine, and ranitidine in tablets [21]. The analysis of these drugs was performed in a 100 mM phosphate buffer, pH 3.5. Several parameters were studied, including wavelength for detection, concentration and pH of phosphate buffer, and separation voltage. The quantitative ranges were 100–1000 μM for each analyte. The intra- and interday relative standard deviations (RSDs) ($n = 5$) were all less than 4%. The detection limits were found to be about 10 μM for cimetidine, 20 μM for ranitidine, 20 μM for nizatidine, and 10 μM for famotidine (S/N = 3, injection 1 s) at 214 nm. All recoveries were greater than 92%. Applications of the method to the assay of these drugs in tablets proved to be feasible [21].

In a sensitive study, low concentrations of histamine-2-receptor (H_2) antagonists were effected across a water plug, with separation taking place in a binary buffer comprising ethylene glycol and NaH_2PO_4 (pH 5.0), and detection at 214 nm [22]. Liquid–liquid extraction with ethyl acetate–isopropanol is shown to provide extracts that are sufficiently clean. The calibration curves were linear over a concentration range of 0.1–2.00 μg/ml cimetidine, 0.2–5.0 μg/ml ranitidine–HCI, 0.3–5.0 μg/ml nizatidine, and 0.1–3.0 μg/ml famotidine. Mean recoveries were >82%, while the intra- and interday RSDs and relative errors (REs) were all <13%. The method is sensitive with a detection limit of 3 ng/ml cimetidine, 30 ng/ml ranitidine HCI, 50 ng/ml nizatidine, and 10 ng/ml famotidine (S/N = 3, electric-driven injection 90 s). This developed CE method was applied for the determination of analytes extracted from plasma taken from a volunteer dosing a cimetidine, ranitidine, and nizatidine tablet simultaneously. These three H_2-antagonists can be detected in real samples by this method, excluding the low dosing of famotidine tablet.

4.7.5. Spectrophotometric methods

El-Bayoumi *et al*. [23] developed a synchronous spectrofluorimetric method for the determination of famotidine, fluconazole, and ketoconazole in bulk powder and in pharmaceutical dosage forms. Famotidine

was dissolved in methanol and the fluorimeter incorporated a 7 μl fused-silica flow cell, and all scanning speeds were 600 nm/min. The relevant excitation range was 230–360 nm, the emission range was 330–460 nm, the intensity was measured at 384 nm and the linear range was 15–50 μg/ml for famotidine.

Famotidine was also determined by extinction coefficient method [24]. An appropriate amount of solid sample was dissolved in and diluted to 100 ml with 0.1 M HCl and a 3 ml portion of the solution was diluted to 50 ml with 0.1 M HCl. The absorbance of the solution was measured at 166 nm versus 0.1 M HCl. Beer's law was obeyed from 8 to 24 μg/ml of famotidine. The absorption coefficient of the drug at 266 nm was 315. Average recovery ($n = 5$) was 100.2% with RSD of 0.68%.

Three different spectrophotometric methods for the determination of cimetidine (I), ranitidine hydrochloride (II), and famotidine (III) in pharmaceutical formulations were developed by Kelani *et al.* [25]. The first was colorimetric method (Section 2.2.1) and was based on the reaction of the three drugs with sodium nitroprusside to produce red complexes. The zero-order spectrum was used to determine III at 500 nm, while the first-derivative spectra were used to determine I and II at 523 and 510 nm, respectively. Beer's law was obeyed over the concentration ranges 25–150 μg/ml for I and 50–500 μg/ml for II and III. The recoveries were quantitative. The second method was also a colorimetric method and was applied to the determination of III. It was based on the reaction of III with 3-methyl-2-benzothiazolinone hydrazone and measurement of the absorbance at 536 or 620 nm. The method was applicable over the concentration range 20–120 μg/ml III and the recovery was quantitative. The third method was a spectrophotometric method and was applied to the determination famotidine. It was based on the reaction of III with Co (II) to form a complex with an absorption maximum at 319 nm. The method was applicable over the concentration range 10–60 μg/ml and the recovery was quantitative [25].

Li and Xuan [26] have designed a spectrophotometric method for the determination of famotidine in tables. Sample was ultrasonically dissolved in methanol and the absorbance of the solution was measured at 288 nm. The mean recovery ($n = 8$) was 100.2% with a RSD of 0.6%. Results agree with those obtained by HPLC.

A flow-injection analysis of famotidine tablets with spectrophotometric detector has been reported [27]. Powdered tablets equivalent to 40 mg of the drug were shaken with 60 ml of 0.2 M acetate buffer of pH 5 (buffer A) for 5 min. After dilution to 100 ml with buffer A, the mixture was filtered and a 100 μl portion of the filtrate was injected into a carrier stream of buffer A at 1.6 ml/min. This stream merged with a stream through a 2 m reaction coil before the absorbance was measured at 630 nm. A 5 ml portion of the initial filtrate was further diluted to 50 ml

and then subjected to analysis as above with the absorbance being monitored at 314 nm. Calibration graphs were linear for 10–50 µg/ml of famotidine with detection at 314 nm and 50–500 µg/ml with detection at 630 nm. Up to 60 samples an hour could be analyzed with a RSD of <1.4%. Recoveries were 98–100.6% and the results are comparable with those obtained by official methods [27].

A spectrophotometric method for the determination of famotidine in tablets or bulk powder was reported [28]. In this assay, a methanolic extracts of the drug were mixed with 0.2% chloranil in toluene–methanol (2:3; 2 ml), methanolic 0.2% 2,3-dichloro-5,6-dicyano-6-nitrophenol (1 ml), diluted to 10 ml with methanol, and set aside at 28 °C for 30 min. Absorbance were measured at 458, 460, and 425 nm, respectively. Rectilinear ranges for the three reagents were 50–500, 40–450, and 10–100 µg/ml of the compound in final solution, respectively. Results with all three reagents on four tablet lots agreed with those obtained by USP (1990) nonaqueous titration method.

A simple kinetic spectrophotometric method is described for the determination of famotidine in commercial dosage forms [29]. The method is based on the oxidation of the drug with alkaline potassium permanganate. The reaction is followed spectrophotometrically by measuring the rate of change of absorbance at 610 nm. The initial-rate and fix-time (at 12 min) methods are adopted for determining the drug concentration. The calibration graphs are linear in the ranges of 2–10 and 1–8 µg/ml using the initial-rate and fixed-time methods, respectively. The method has been applied to the determination of famotidine in tablet formulations. The obtained results are compared statistically with those given by a reference spectrophotometric method.

Simple, sensitive, and rapid spectrophotometric techniques have been established for the determination of cimetidine (I), famotidine (II), and ranitidine hydrochloride (III) in presence of their S-oxide derivatives in both raw materials and in pharmaceutical formulations. Hydrogen peroxide was used to enhance the formation of S-oxide compounds (oxidative derivatives) [30]. Linear calibration curves were obtained for the determination of I and II at 220 and 230 nm in the concentration range of 2–20 and 4–40 µg/ml with the mean percentage recoveries of 99.88 ± 0.943 ($n = 10$) and $99.88 \pm 0.824\%$ ($n = 10$) for compound I and II, respectively. The concentration range was 2–20 µg/ml with the corresponding mean percentage recoveries of $(100.13 \pm 0.464)\%$, $(100.01 \pm 0.428)\%$, and $(99.94 \pm 0.439)\%$ for I, II, and III, respectively. The results obtained by the proposed methods were statistically analyzed and compared with those obtained by official BP methods.

Spectrophotometric and spectrofluorimetric methods were adopted for the analysis of famotidine and ranitidine depending on their reaction with 1,4-benzoquinone reagent at pH 5.2 and 5.6, respectively [31]. The

absorbances of the resulting condensation products were measured at 502 and 508 nm for famotidine and ranitidine, respectively. Concentrations adhering to Beer's law were from 40 to 160 µg/ml for famotidine and from 20 to 100 µg/ml for ranitidine. Furthermore, the resulting condensation products exhibited fluorescence at 665 nm when excited at 290 nm and the calibration graphs were rectilinear from 0.4 to 1.4 µg/ml for famotidine and from 0.21 µg/ml for ranitidine. Different parameters affecting these reactions were thoroughly studied. Also these methods were applied to the pharmaceutical preparations and the results were satisfactory. The validities of the methods were ascertained by the standard addition technique revealing fine results in consideration to the mean recovery percent and standard deviation. The spectrofluorimetric method was a hundred times more sensitive than the spectrophotometric method. The proposed methods were sensitive, accurate, and precise as statistically compared with the official methods of analysis of famotidine and ranitidine [31].

A spectrophotometric method for the determination of famotidine in pharmaceutical preparations based on the formation of a 1:1 ion-pair complex with both bromocresol green (BCG) and bromothymol blue (BTB), and its subsequent extraction with an organic solvent was developed [32]. Commercial tablets, containing 20 and 40 mg of the drug were weighted, finely powdered and mixed. Portions (equivalent to 20 or 40 mg) were dissolved in 100 ml H_2O and portions of the solution were mixed with 5 ml Britton–Robinson buffer of pH 3.7 and 5 ml 1 mM BCG in ethanolic NaOH. The yellow organic phase was separated, dried over anhydrous sodium sulfate, and diluted to 25 ml with more solvent. The absorbance of the diluted solution was measured at 420 nm. Beer's law obeyed from 2.0 (detection limit) to 23.6 µg/ml and 0.7 (detection limit) to 8.1 µg/ml of famotidine, respectively, for BCG and BTB reagents. The average recoveries of five analysis were 97.6%, 95.4%, and 98.2%, respectively, of labeled values, for BCG, BTB, and the official method.

Three simple, accurate, sensitive and selective spectrophotometric methods (A, B, and C) for the determination of famotidine in bulk samples [33]. The first method A is based on oxidation of the drug by *N*-bromosuccinimide (NBS) and determination of the unreacted NBS by measuring the decrease in absorbance of Amaranth dye at a suitable λ_{max} (521 nm). The methods B and C involve addition of excess of cerium(IV) sulfate and determination of the unreacted Ce(IV) by measuring the decrease in the red color of chromotrope 2R at λ_{max} 528 nm for method B or the decrease in the orange-pink color of rhodamine 6G at λ_{max} 526 nm for method C. Regression analysis of Beer's-Lambert plots showed good correlation in the concentration ranges 0.1–2.4 µg/ml for method A and 0.1–2.2 µg/ml for method B and C. Ringbom optimum concentration ranges were 0.2–2.2 µg/ml for methods A and 0.2–2.0 µg/ml for methods B and C.

4.7.6. Thin-layer chromatography

Pharmaceutical raw material is dissolved in and diluted with glacial acetic acid to a concentration of 0.4 mg/ml famotidine [34]. A 10 μl portion of the solution is loaded onto a silica gel GF_{254} plate alongside standard famotidine for TLC with ethyl acetate/methanol/toluene/NH_4OH (40:25:20:2) as mobile phase. The developed chromatogram was examined under UV (254 nm). An impurity spot was clearly visible at an R_f lower than that of the parent drug.

Novakovic [35] described separate methods for famotidine and ranitidine hydrochloride in pharmaceuticals. For famotidine, samples containing ~20 mg famotidine were dissolved in acetic acid/methanol (1:9), the solution was diluted to 25 ml with the same solvent and filtered. Portions (0.3 μl) were applied to the plates as before, with development for 5 cm with ammonium hydroxide/toluene/methanol/ethyl acetate (4:40:50:80) and the spots were scanned at 276 nm. The calibration graph was linear from 165 to 413 ng of famotidine. Recoveries of added drug were 98.09–102.66% ($n = 10$). The intra-assay RSD ($n = 6$) was 0.93%.

A quantitative method using silica gel high-performance TLC (HPTLC) plates with fluorescent indicator, automated sample application, and UV absorption videodensitometry was developed for the determination of famotidine tablets [36]. Precision was evaluated by replicate analyses of samples and accuracy by analysis of a sample, fortification with standard, and reanalysis (standard addition). The percent famotidine in the tablets ranged from 92.5% to 140% compared to label values, precision from 1.25% to 2.55% RSD, and the error in standard addition analysis was 1.76% compared to the fortification level.

4.7.7. High-performance liquid chromatographic methods

Several high-performance liquid chromatography (HPLC) methods have been reported, and the salient features of these are summarized in Table 3.7.

5. DRUG METABOLISM AND PHARMACOKINETIC PROFILES OF FAMOTIDINE

5.1. Uses and application and associated history

In the mid-1970s, cimetidine, the first histamine H_2-receptor antagonist has been discovered in United Kingdom. Ten years later famotidine has been introduced, and since its introduction, more than 30 million patients worldwide have been treated with the drug. Famotidine is potent histamine H_2-receptor antagonist, which differs structurally from its

TABLE 3.7 Reported HPLC methods for famotidine

No.	Material	Column	Mobile phase	Internal standard	Flow rate	Detection wavelength	Ref.
1	Human plasma and urine	C18 RP	Water-saturated ethyl acetate	Cimetidine	1 ml/min	267 nm	[37]
2	Human plasma	Reverse phase C18	Acetonitrile/10 mM phosphate with heptanesulphonic acid, pH 7.5	Molsidomine	NA	286 nm	[38]
3	Human plasma	Inertsil C4/BDS hypersil C8	Acetonitrile/phosphate aqueous sol.	Cimetidine	NA	267 nm	[39]
4	Bulk drugs and formulations	Reverse phase C8	Acetonitrile/0.01 M aqueous potassium dihydrogenphosphate (25:75, v/v, pH 3.15)	NA	1.5 ml/min	NA	[40]
5	Human plasma	ODS hypersil (5 μm)	Acetonitrile/water (12:88, v/v) containing 20 mM disodium hydrogenphosphate and 50 mM sodium dodecyl sulphate, pH 3	Clopamide	NA	267 nm	[41]
6	Human plasma and urine	TSK-gel ODS-80-Tm (25 cm × 4.6 mm)	100 mM-H_3PO_4 (containing 10 mM-Na dodecyl sulfate)-acetonitrile (13:7)	YAS-423	NA	266 nm	[42]
7	Dosage form	Hypersil C18 (15 cm × 4.6 mm, i.d) (5 μm)	Acetonitrile/0.1 M sodium acetate of pH 6 (7:93)	NA	1 ml/min	270 nm	[43]
8	Plasma	YWG-C18 (20 cm × 4.6 mm, i.d) (10 μm)	Acetonitrile/aqueous 19 mM-H_3PO_4 (1:9)	External standard	1 ml/min	267 nm	[44]

TABLE 3.7 (*continued*)

No.	Material	Column	Mobile phase	Internal standard	Flow rate	Detection wavelength	Ref.
9	Serum	Merck RP-8 (25 cm × 4.6 mm, i.d)	10 mM-Phosphoric acid containing 10 mM-n-heptane sulfonic acid, acetonitrile and H_2O (20:23:57) pH 4.5 with 10% KOH	Ranitidine	2 ml/min	267 nm	[45]
10	Pharmaceutical dosage forms	LiChrospher RP-18 (25 cm × 4 mm, i.d) (5 μm)	Methanol/0.1 M-ammonium acetate (3:7)	NA	1 ml/min	254 nm	[46]
11	Human plasma	Inertsil C4 (5 cm × 4.6 mm, i.d) (5 μm)	33% acetonitrile/15 mM phosphate buffer/20 mM-SDS (pH 3.5)	NA	1 ml/min	267 nm	[47]
12	Plasma and urine	Novapak C18 (15 cm × 3.9 mm, i.d) (4 μm)	Methanol/phosphate buffer of pH 6.3 (1:4)	Cimetidine	1.5 ml/min	282 nm	[48]
13	Commercial dosage forms	Inertsil ODS-2 (15 cm × 4.6 mm, i.d) (5 μm)	0.04 M-NaH_2PO_4/ acetonitrile/methanol / triethylamine (3450:200:350:7)	Procaine HCl	1 ml/min	230 nm	[49]

TABLE 3.7 (*continued*)

No.	Material	Column	Mobile phase	Internal standard	Flow rate	Detection wavelength	Ref.
14	Human plasma	Phenomenex Prodigy ODS analytical (25 cm × 3.9 mm, i.d) (5 μm)	Acetonitrile/0.25% heptanesulfonic acid in 20 mM-acetate buffer (23:77) pH 4.7 with HCl	Cimetidine	1 ml/min	267 nm	[50]
15	Human plasma	BDS Hypersil silica column (5 cm × 3 mm, i.d) (3μm)	H_2O-acetonitrile (2:3, v/v) containing 0.1% TFA	[4-({[2-(5-amino-4H-1,2,4,6-thiatriazin-3-yl)ethyl]thio}-methyl-2-thiazolyl] guanidine S,S-thiatriazine dioxide	0.2 ml/min	NA	[51]
16	Human plasma	Zobax SD C8 column (15 cm × 4.6, i.d) (5 μm)	Acetonitrile/H_2O/formic acid (30:70:1)	Salbutamol	0.4 ml/min	NA	[52]
17	Human plasma	Supelcosil LC-8-DB column (25 cm × 4.6 mm, i.d) (5 μm)	Acetonitrile/0.1% triethylamine (2:23) oh pH 2.3	3-[({2-[(aminoiminomethyl) amino]-4-thiazole} methyl]propanamide	1 ml/min	NA	[53]

NA: Not Available

predecessors cimitidine and ranitidine in having a guanidine-substituted thiazole ring rather than an imidazole or furan ring. In humans, famotidine inhibits basal and stimulated gastric acid secretion from parietal cells and has no apparent clinically significant activity at histamine H_2-receptors outside the gastrointestinal tract. Through the inhibition of gastric acid secretion, famotidine promote the healing of duodenal and gastric ulcers and erosive esophagitis. Famotidine is given by mouth or parenterally by the intravenous route [54]. It has an excellent tolerability profile and have the lowest incidence of side effects [55].

The drug is recommended for the short-term treatment of acute duodenal ulcer, gastric ulcer, and gastroesophageal reflux. It is also indicated for maintenance therapy of benign gastric ulcer and duodenal ulcer and management of pathological hypersecretory conditions, such as Zollinger–Ellison syndrome and multiple endocrine adenomas [56, 57]. The recommended famotidine dose to achieve those gastrointestinal effects is 40 mg daily at bedtime for 4–8 weeks, and these doses produced peak plasma concentrations of 75–100 ng/ml. Plasma famotidine concentrations that inhibit 50% of stimulated gastric acid secretion, that is, IC_{50}, are estimated to be 13 ng/ml [58]. Inhibition of gastric secretion is apparent within 1 h following intravenous or oral administration of famotidine. The duration of inhibition of basal and nocturnal acid secretion following an oral dose of the drug is 10–12 h. Inhibition of food-stimulated secretion generally persists for 8–10 h [56]. Famotidine also has been reported to moderately ameliorate psychotic symtomatology of Schizophrenia in doses ranging from 40 to 100 mg daily [59, 60].

5.2. Absorption and bioavailability

Orally administered famotidine is incompletely absorbed from gastrointestinal tract, and it undergoes minimal first-pass metabolism. The bioavailability of famotidine following oral doses is 40–45%, this is slightly affected by food or antacid. After oral doses, peak plasma level is 75–100 ng/ml which occur in 1–3 h [54]. The peak plasma level is not altered by chronic administration, and elimination half-life is 2.5–3.5 h which is prolonged in renal failure. The drug is 15–20% bound to plasma proteins. The apparent volume of distribution of famotidine is reported to be 1.1–1.4 l/kg in normal renal function and does not appear to be altered substantially in patients with renal dysfunction [56, 58]. It is widely distributed into kidney, liver, pancreas, and submandibular gland. In rats, it is distributed into central nervous system [54, 56].

5.3. Metabolism

Famotidine is metabolized in the liver to famotidine S-oxide. The metabolite has no pharmacological activity on gastric acid secretion. It is eliminated largely as unchanged drug and only 30–35% undergo metabolic routes. Orally administered drug undergoes minimal first-pass metabolism [56].

Famotidine

Famotidine-S-oxide
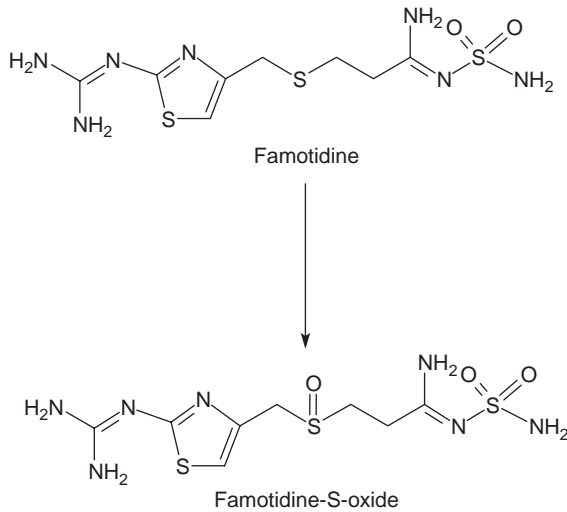
5.4. Excretion

Famotidine is excreted markedly, 25–30% or 65–80%, unchanged by renal route, primarily by active tubular secretion and glomerular filtration within 24 h after oral or intravenous administration, respectively. The remaining drug is excreted via metabolic routes [56]. Total body clearance of the drug averages 381–483 ml/min, and renal clearance of the drug averages 250–450 ml/min [56]. As a result, famotidine should be used in a lower dosage and at longer dosing intervals when used in patients with sever renal insufficiency. In rats, the drug is found in breast milk, and does not cross the placenta [54, 56]. It is not known whether the drug crosses the placenta or distributes into milk in humans. The elimination of famotidine does not appear to be affect by age in adults.

REFERENCES

[1] A. R. Gennaro (ed.), *Remington's: Pharmaceutical Sciences*, 20th edn., Mack Publishing Co., Pennsylvania, chapter 66, 2000, p. 1282.
[2] S. Budavari (ed.), *The Merck Index*, 12th edn., Merck and Co., NJ, 1996, p. 3976.
[3] S. C. Sweetman (ed.), *Martindale, The Complete Drug Reference*, 33rd edn., The Pharmaceutical Press, Chicago, 2002, p. 1225.
[4] Swiss Pharmaceutical Society, *Index Nominum 2000: International Drug Directory*, 17th edn., Medpharm Scientific Publishers, 2000, p. 425.
[5] G. G. Ferenczy, L. Parkanyi, J. G. Angyan, A. Kalman and B. Hegedus, *J. Mol. Struct. (Theochem).*, 2000, **503**, 73.
[6] M. A. Hassan, , M. S. Salem, M. S. Sueliman and N. M. Najib, *Int. J. Pharmaceut.*, 1997, **149**, 227.
[7] S. Sagdinc and S. Bayrai, *J. Mol. Struct.*, 2005, **369**, 744–747.
[8] M. Barańska, K. Czarnieki and L. M. Proniewicz, *J. Mol. Struct.*, 2001, **563**, 347.
[9] G. K. McEvoy (ed.), *Drug Information*, 95 edn., American Society of Helth-System Pharmacists, 1995, p. 2029.
[10] Z. Değim and I. Ağabeyoğlu, *II Farmaco*, 2002, **57**, 729.
[11] *European Pharmcopeia*, 4th edn., Council of Europe, Strasbourg, 2002, p. 1169.
[12] *British Pharmacopeia*, Vol. I, 16th edn., on line, HMSO Publication, Ltd., London, 2000, CD.
[13] M. M. Ayad, A. Shalaby, H. E. Abdellatef and M. M. Hosny, *Anal. Bioanal. Chem.*, 2003, **376**, 710.
[14] U. Ajali and B. K. C. Chukwurah, *Boll. Chim. Farm.*, 2001, **140**, 354.
[15] N. Rahman and M. Kashif, *II Farmaco*, 2003, **58**, 1045.
[16] B. V. Kamath, K. Shivram and A. C. Shah, *J. Pharm. Biomed. Anal.*, 1994, **12**, 343.
[17] M. M. Ayad, A. Shalaby, H. E. Abdellatef and H. M. Elsaid, *J. Pharm. Biomed. Anal.*, 2002, **29**, 247.
[18] S. Skrzypek, W. Ciesielski, A. Sokolowski, S. Yilmaz and D. Kazmierczak, *Talanta*, 2005, **66**, 1146.
[19] T. Perez-Ruiz, C. Marinez-Lozano, V. Tomas, E. Bravo and R. Galera, *J. Pharm. Biomed. Anal.*, 2002, **30**, 1055.
[20] H. Soini, M. L. Riekkola and M. V. Novotny, *J. Chromatogr. A.*, 1994, **680**, 623.
[21] S. M. Wu, Y. S. Ho, H. L. Wu, S. H. Chen and H. S. Ko, *Electrophoresis*, 2001, **22**, 2758.
[22] H. S. Ko, S. H. Chen, H. L. Wu and S. M. Wu, *Electrophoresis*, 2001, **22**, 2717.
[23] El-Bayoumi, A. A, El-Shanawany, M. E. El-Sadek and A. Abd El-Sattar, *Spectrosc. Lett.*, 1997, **30**, 25.
[24] Y. X. Zhao, Y. Song and M. Zhu, *Zhongguo Yiyao Gongye Zazhi*, 2002, **33**, 348.
[25] K. M. Kelani, A. M. Aziz, M. A. Hegazy and L. S. Abdel Fattah, *Spectrosc. Lett.*, 2002, **35**, 543.
[26] H. Li and J. Xuan, *Zhongguo Yiyao Gongye Zazhi*, 1993, **24**, 319.
[27] B. V. Kamath, K. Shivram and S. Vangani, *Anal. Lett.*, 1993, **26**, 2183.
[28] B. V. Kamath, K. Shivram and S. Vangani, *Anal. Lett.*, 1992, **25**, 2239.
[29] N. Rahman and M. Kashif, *Anal. Sci.*, 2003, **19**, 907.
[30] K. M. Kelani, A. A. M. Moustafa, M. A. Hegazy and L. Abdel Fattah, *Anal. Lett.*, 2002, **35**, 1055.
[31] A. K. S. Ahmad, M. A. Kawy and M. Nebsen, *Anal. Lett.*, 1999, **32**, 1403.
[32] A. Z. Abu Zuhri, R. M. Shubiertah and G. M. Badah, *J. Pharm. Biomed. Anal.*, 1999, **21**, 459.
[33] A. S. Amin, S. A. Shama, I. S. Ahmed and E. A. Gouda, *Anal. Lett.*, 2002, **35**, 1851.
[34] Y. Y. Peng, *Yaowu Fenxi Zazhi*, 1998, **18**, 116.
[35] J. Novakovic, *J. Chromatogr. A.*, 1999, **846**, 193.

[36] J. Sherma and A. N. Campbell, *J. Liq. Chromatogr. Rel. Tech.*, 2003, **26**, 2719.
[37] R. F. Frye and T. C. Dowling, *J. Chromatogr. B: Biomed. Sci. Appl.*, 1999, **732**, 239.
[38] E. Anzenbacher, M. Nobilis, K. Filipova and E. Anzenbacherva, *J. Separ. Sci.*, 2003, **26**, 722.
[39] L. Zhong and K. C. Yeh, *J. Pharm. Biomed. Anal.*, 1998, **16**, 1051.
[40] S. Husain, S. Khalid, V. Nagaraju and N. Rao, *J. Chromatogr. A.*, 1996, **743**, 328.
[41] A. R. Zoest, S. Wanwimolruk and C. T. Hung, *J. Chromatogr.: Biomed. Appl.*, 1991, **572**, 227.
[42] Y. Imai and S. Kobayashi, *Biomed. Chromatogr.*, 1992, **6**, 222.
[43] X. Z. Qun, D. P. Ip, K. H. C. Chang, P. M. Brooks and T. Sakuma, *J. Pharm. Biomed. Anal.*, 1994, **12**, 221.
[44] Z. Lu and J. M. Chen, *Yaowu Fenxi Zazhi*, 1997, **17**, 107.
[45] Y. R. Tahboub, M. F. Zaater and N. M. Najib, *Quim. Anal. (Barcelona)*, 1998, **17**, 117.
[46] B. Cakir, A. U. Tosun and M. F. Sahin, *Pharm. Sci.*, 1997, **3**, 493.
[47] L. Zhong and K. C. Yeh, *J. Pharm. Biomed. Anal.*, 1998, **16**, 1051.
[48] H. Zarghi, Komeilizadeh, M. Amini and L. Kimiagar, *Pharm. Pharmacol. Commun.*, 1998, **4**, 77.
[49] H. M. Ho, Haung, S. Y. Hsu, C. Y. Shaw and B. L. Chang, *Drug Dev. Ind. Pharm.*, 1999, **25**, 379.
[50] T. C. Dowling and R. F. Frye, *J. Chromatogr. B: Biomed. Sci. Appl.*, 1999, **732**, 239.
[51] L. Zhong, R. Eisenhandler and K. C. Yeh, *J. Mass Spectrom.*, 2001, **36**, 736.
[52] Y. Zhang, X. Y. Chen, H. Y. Yang and D. F. Zhong, *Shenyang Yaoke Daxue Xuebao*, 2002, **19**, 340.
[53] D. Zendelovska, S. Simeska, S. Petrov and P. Milosevski, *Acta Pharma.*, 2002, **52**, 113.
[54] S. C. Sweetman (ed.), *Martindale, The Complete Drug Reference*, 33rd edn., The Pharmaceutical Press, Chicago, 2002, p. 1226.
[55] C. W. Howden and G. N. J. Tytgat, *Clin. Therapeut.*, 1996, **18**, 36.
[56] G. K. McEvoy (ed.), *Drug Information*, 95 edn., American Society of Helth-System Pharmacistsp. 2031.
[57] A. R. Gennaro (ed.), *Remington's: Pharmaceutical Sciences*, 20th edn., Mack Publishing Co., Pennsylvania, 2000, p. 1283.
[58] M. A. Campanero, I. Bueno, M. A. Arangoa, M. Escolar, E. G. Quetglas, A. Lopez-Ocariz and J. R. Azana, *J. Chromatog. B.*, 2001, **763**, 21.
[59] P. N. Dannon, E. Lepkifher, I. Iancu, R. Ziv, N. Horesh and M. Kotler, *Eur. Psych.*, 1997, **12**, 263.
[60] R. B. Rosse, , K. Kendrick, , L. C. Tsui, M. McCarthy, J. P. Collins Jr., P. Rosenberg, T. Peace, R. J. Wyatt and S. I. Deutsch, *Biol. Psych.*, 1995, **37**, 666.

This page intentionally left blank

CHAPTER 4

Fexofenadine Hydrochloride

Lokesh Kumar,* Md. Shahnwaj Alam,* Chhuttan Lal Meena,† Rahul Jain,† and Arvind K. Bansal*

* Department of Pharmaceutical Technology (Formulations), National Institute of Pharmaceutical Education and Research (NIPER), Punjab 160062, India
† Department of Medicinal Chemistry, National Institute of Pharmaceutical Education and Research (NIPER), Punjab 160062, India

1. DESCRIPTION

1.1. Nomenclature

1. Systematic chemical name
    (±)-2-[4-[1-hydroxy-4-[4-(hydroxydiphenylmethyl)piperidino]butyl]
       phenyl]-2-methylpropanoic acid, hydrochloride
    α,α-dimethyl-4-[4(hydroxydiphenylmethyl)-1-piperidinyl]butyl]ben-
       zeneaceticacid, hydrochloride
    (±)-*p*-[1-hydroxy-4-[4-(hydroxydiphenylmethyl)-1-piperidinyl]
       butyl]α-methylhydratropic acid, hydrochloride
2. Nonproprietary names
    Carboxyterfenadine, MDL-16455, MDL-16455A, Terfenadine carboxyl-
       ate hydrochloride
3. Proprietary names
    Allegra®, Telfast®

1.2. Formulae

1. Empirical formula, molecular weight, CAS number
    Fexofenadine (FEX) free base $C_{32}H_{39}NO_4$ (MW $= 501.56$); CAS number:
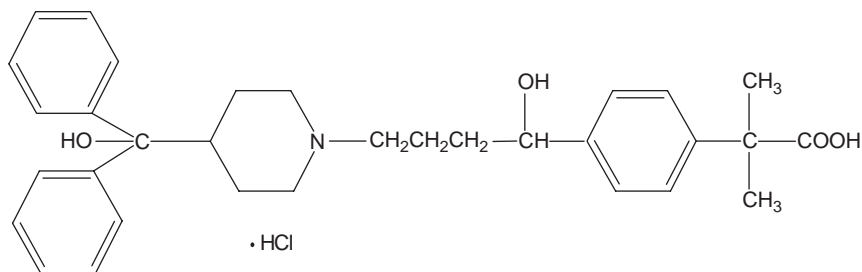   83799-24-0

FIGURE 4.1   Chemical structure of fexofenadine hydrochloride.

TABLE 4.1   Elemental analysis of fexofenadine base and hydrochloride salt

Element	Free base	Hydrochloride salt
Carbon	76.62	71.42
Hydrogen	7.84	7.49
Oxygen	12.76	11.89
Nitrogen	2.79	2.60
Chloride	–	6.59

Fexofenadine hydrochloride (FEX-HCL) $C_{32}H_{39}NO_4 \cdot HCl$ (MW = 538.12); CAS number: 138452-21-8

2. Structural formula see Fig. 4.1

1.3. Elemental analysis

The calculated elemental composition is as in Table 4.1.

1.4. Appearance

FEX is obtained as a white to off-white crystalline powder.

1.5. Uses and applications

FEX is a nonsedating, second-generation H_1 antihistamine, which acts as a reversible and competitive inhibitor at H_1 histamine receptor sites. The drug is an active carboxylic acid metabolite of terfenadine, and provides all the therapeutic benefits of terfenadine, while avoiding the serious cardiotoxic and drug interaction risks of the parent drug, and is therefore, considered as a relatively safe alternative to terfenadine [3, 4].

FEX is indicated for the relief of symptoms associated with seasonal allergic rhinitis in children 12 years of age, and older. It is effective in the treatment of allergic conditions, including sneezing, rhinorrhea, itchy nose/palate/throat, and itchy/watery/red eyes. Extended-release tablets containing FEX, in fixed combination with pseudoephedrine hydrochloride, also provide a symptomatic relief of nasal congestion. FEX is also

indicated for the treatment of uncomplicated skin manifestations of chronic idiopathic urticaria in adults and children of 6 years of age and older, where it reduces pruritus and the number of wheals. The drug shows high selectivity for peripheral H_1 histamine receptors and does not readily penetrate blood–brain barrier, which may account for the lack of sedation associated with its use [5]. FEX is also indicated as a potential alternative for the treatment of asthma and atopic dermatitis [6].

2. METHODS OF PREPARATION

In general, the synthetic approach for preparation of FEX involves the reduction of a carboxylate derivative, 4-[4-[4-(hydroxybiphenylmethyl)-1-piperidinyl]-1-oxobutyl]-α,α-dimethyl benzene acetate; followed by hydrolysis with a base, for example alkali metal hydroxides, to get the carboxylic acid derivative FEX. The sequence of synthesis is depicted in Fig. 4.2 [10].

A number of patents, including US patent numbers 5,578,610, 5,589,487, 5,581,011, 5,663,412, 5,750,703, 5,994,549, 5,618,940, 6,631,375, 5,644,061, 5,650,516, 5,652,370, 5,654,433, 5,633,353, 5,675,009, 5,375,693, and 6,147,216, describe the synthesis of FEX. US patent 5,750,703 suggests

FIGURE 4.2   (*continued*).

Ethylene glycol, pTsOH,
PhH, reflux, 24 h

68%

NaOH, MeOH, r.t., 30 min

99%

Jones oxidation

89%

CH$_2$N$_2$, Et$_2$O, 0°C

92%

2% HCl, THF, r.t., 1.5 h

81%

NaBH$_4$, MeOH/THF, 0°C, 30 min

93%

FIGURE 4.2   (*continued*).

Azacyclonol, K₂CO₃, KI, PhMe-DMF
(8:2, v/v), reflux, 7 h

56%

10% NaOH, MeOH, reflux, 2 h
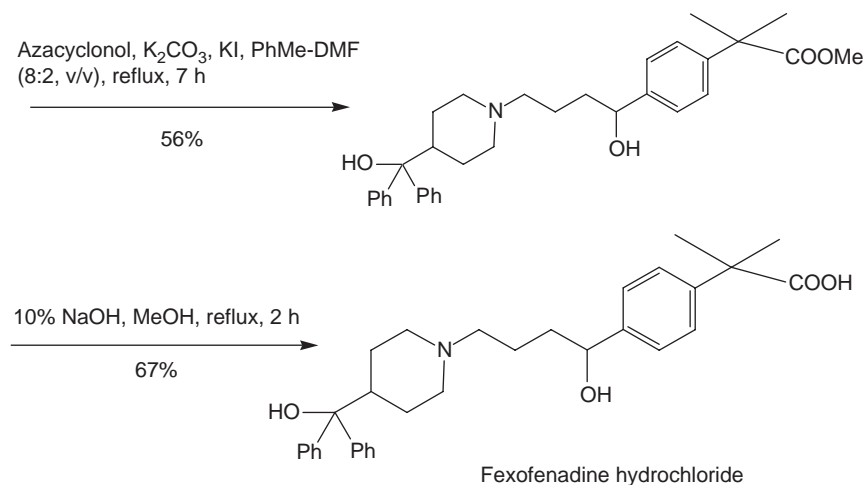
67%
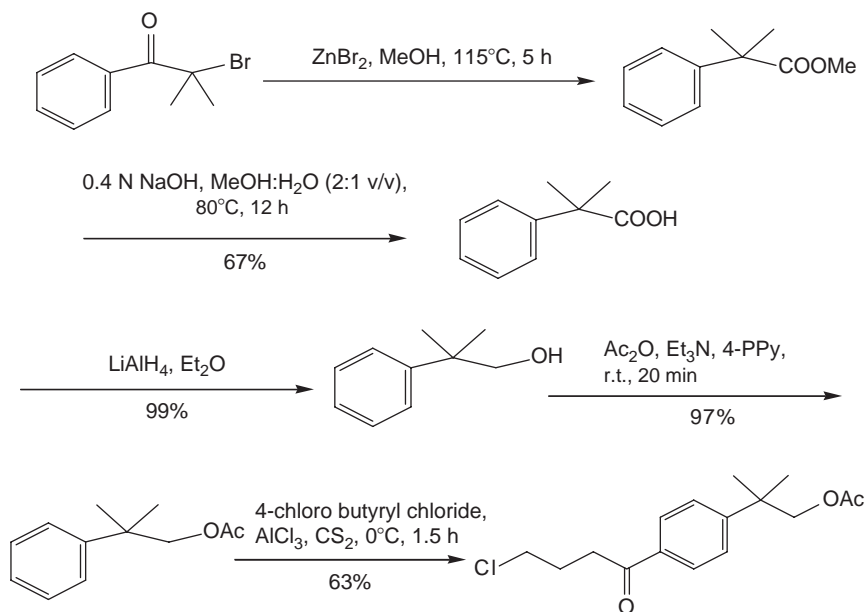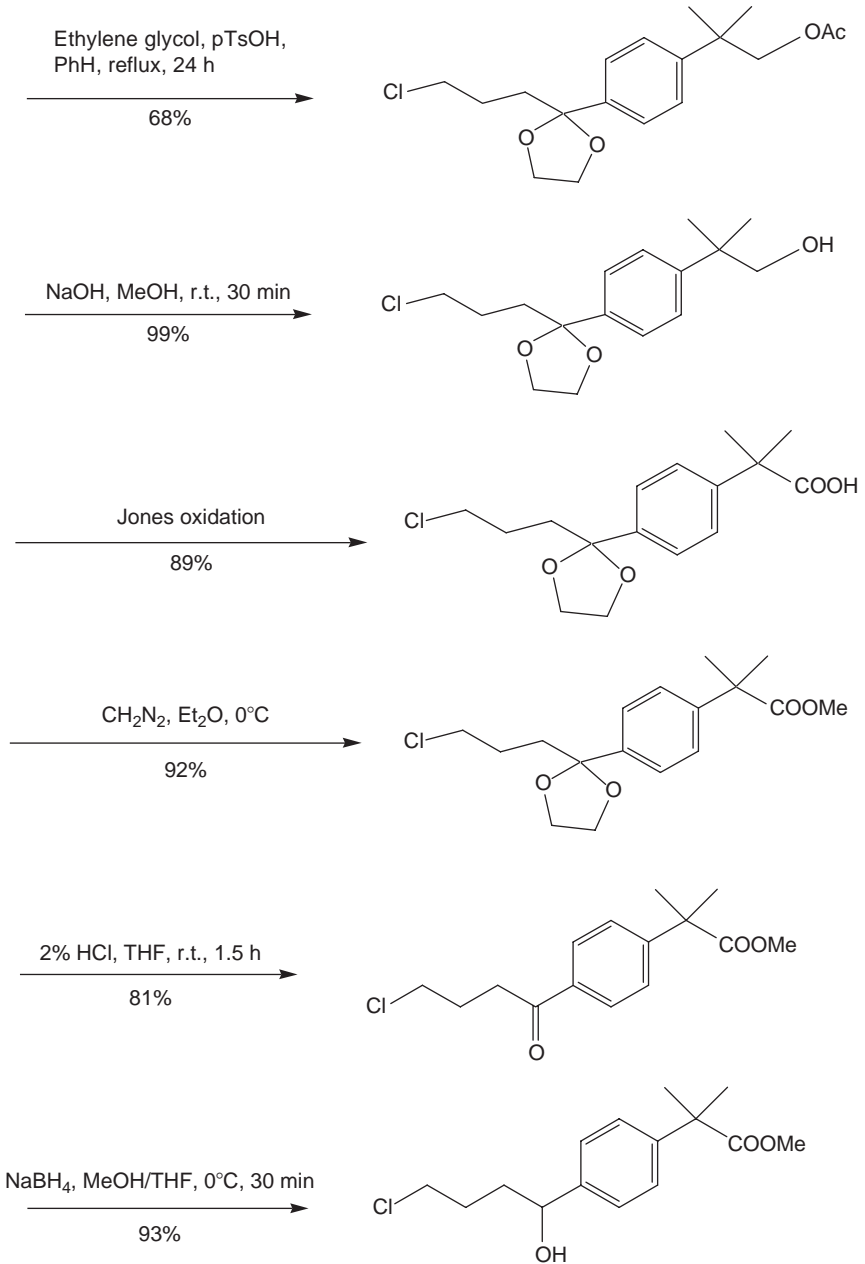
Fexofenadine hydrochloride

FIGURE 4.2   Scheme I for synthesis of fexofenadine hydrochloride.

a process involving the reaction of azacyclonol with a cyclopropyl ketone derivative. However, the method requires a substantially pure cyclopropyl regioisomer to react with azacyclonol. The cyclopropyl ketone derivative is prepared by the acylation, for example, of an aromatic ester derivative with an acid chloride in the presence of a Lewis acid catalyst. The resulting benzyl derivative comprises a mixture of ortho and para isomers. After formation of a mixture of cyclopropyl ketone isomers, the desired para isomer is isolated via recrysallization in a low yield. Another strategy for synthesis of (S) or (R)-FEX utilizes enantiomeric-enriched benzyl alcohol. Optically active precursor is prepared by the asymmetric reduction of phenyl ketone using oxazaborolidine-based catalysts. The optically active alcohol is then further treated to yield (S)-FEX, with no detectable epimerization by chiral high performance liquid chromatography (HPLC) assay.

Chemical synthesis of FEX is laborious and the products are obtained in low yields in comparison with that obtained for the synthesis of terfenadine. Microbial oxidation of terfenadine to FEX has been achieved using bacteria *Streptomyces platensis*, *Streptoymces risomus*, or the fungi *Cunninghamella blakesleeana*, and *Absidia corymbifera*. US Patent 6558931 B1 describes a microbiological process of preparation of FEX using a microorganism culture of *A. corymbifera* genus or a microorganism culture of the *Streptomyces* genus, at a pH between 5.0 and 8.0. The microbiological process is amenable to industrial use, by giving a concentration of starting product of 0.5 g/l, with a yield in excess of 70% relative to the starting product.
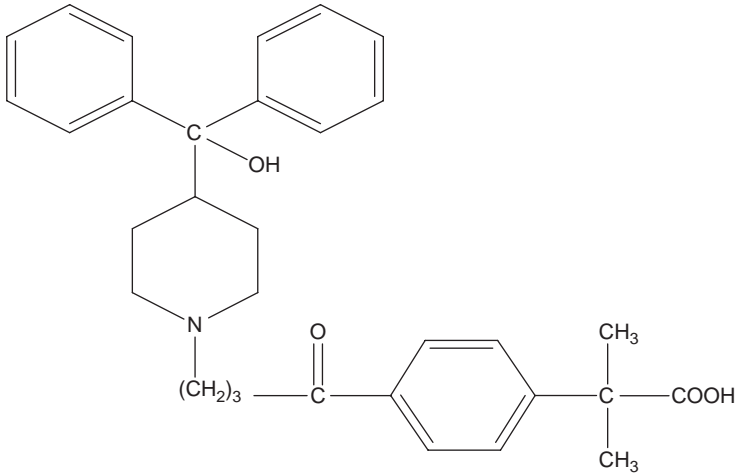
FIGURE 4.3   Keto isomer of fexofenadine hydrochloride.
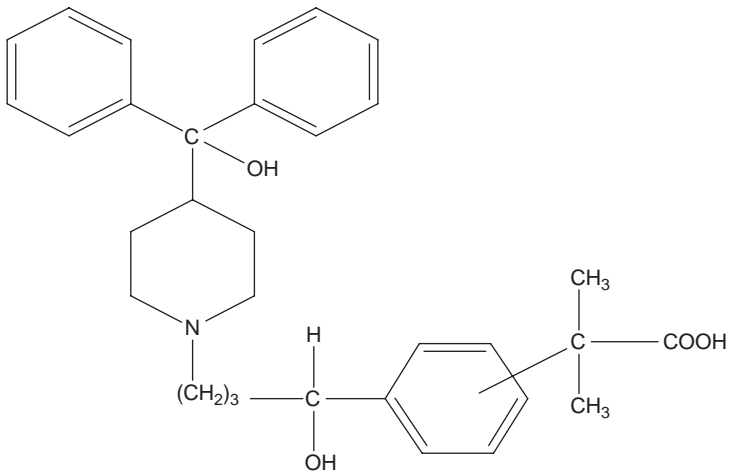

FIGURE 4.4   Meta isomer of fexofenadine hydrochloride.

2.1. Impurities

1. Keto isomer of FEX (keto ester intermediate obtained during FEX synthesis) (Fig. 4.3).
2. Meta isomer of FEX (arising from the reduction of keto ester intermediate; a stereoisomer of FEX) (Fig. 4.4).

FIGURE 4.5   Isopropyl derivative of fexofenadine hydrochloride.
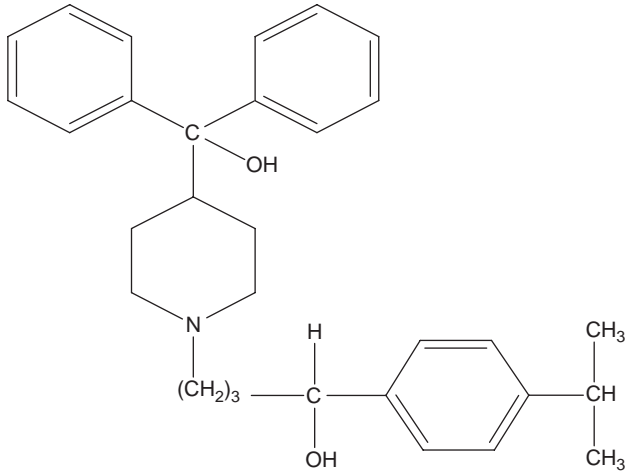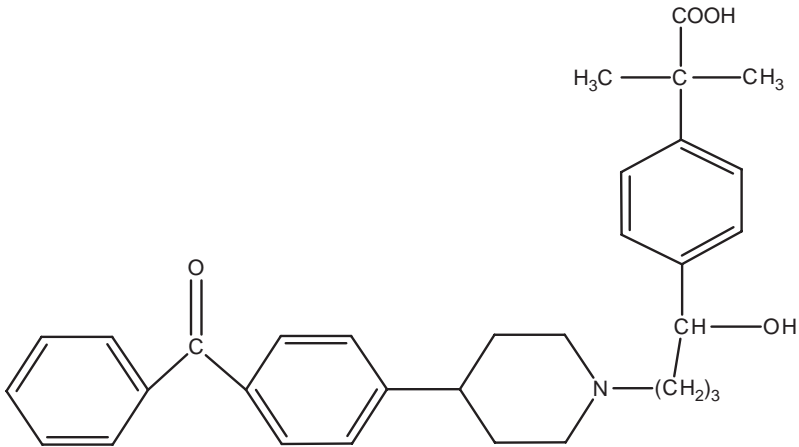

FIGURE 4.6   Benzophenone derivative of fexofenadine hydrochloride (reproduced with permission from Elsevier).

3. Decarboxylated degradant (isopropyl derivative) of FEX hydrochloride [7] (reproduced with permission from Elsevier) (Fig. 4.5).
4. Benzophenone derivative of FEX [7] (reproduced with permission from Elsevier) (Fig. 4.6).
5. Dehydro impurity of FEX.

TABLE 4.2   Solubility of fexofenadine hydrochloride in different solvents

Solvent	Quantity dissolved at 25 °C (mg/ml)
Water	~1
Methanol	>400
Ethanol	85
Acetone	<0.1
Chloroform	<0.1
Diethyl ether	<0.1
n-Hexane	<0.1
Dimethyl formamide	>400
Polyethylene glycol 200	<0.1
Acetonitrile	<0.1
Ethyl acetate	<0.1

3. PHYSICAL PROPERTIES

3.1. Ionization constants

FEX exists as a zwitterion in aqueous media at physiological pH. The drug have two ionization groups corresponding to free carboxylic group on the side chain and the substituted ring nitrogen, contributing to a pK_a value of 4.25 and 9.53, respectively [8].

3.2. Solubility characteristics

The approximate solubility of FEX was determined in a variety of solvents. An excess of FEX was kept in screw capped vials with 10 ml of solvent and analyzed for the dissolved fraction after 24 h, using HPLC (Table 4.2).

Aqueous solution of FEX is acidic and the pH of a 0.1% (w/v) aqueous solution falls in the range of 3.2–3.3.

3.3. Partition coefficients

The partition coefficient ($\log P$, octanol/water) of FEX base is reported to be 2.81 [1]. Lin *et al.* studied the apparent 1-octanol/water ($\log P$) partition coefficient of FEX at room temperature. The concentration of the compound in each phase was determined by HPLC after appropriate dilution with methanol. Apparent partition coefficient of FEX was found to be 0.49 ± 0.01 [8].

3.4. Optical activity

FEX contains one chiral center and can be resolved into two enantiomers. The pharmacological studies with (*R*) and (*S*)-enantiomer in humans showed a higher plasma concentration for (*R*)-FEX than that of the corresponding isomer. The area under the plasma concentration–time curve ($AUC_{0-infinity}$), and the maximum plasma concentration (C_{max}) of *R*-(+)-FEX were also significantly greater than those of the *S*-(−)-enantiomer [9].

An enantioselective synthesis of bioisosteric tetrazole analog of FEX was undertaken by Giacomo *et al.*, based on the conversion of a α-halo-alkylarylketone into the corresponding substituted 2-arylalkanoic ester [10]. Optical resolution of chiral (+)- and (−)-FEX is described in Chinese patent CN 144207, mentioning the optical resolution of racemic FEX alkyl esters with chiral tartaric acid derivatives, such as dibenzoyltartaric acids, diacetyltartaric acids, or their hydrates in organic solvent at −20 to 100 °C to obtain chiral (+)- and (−)-FEX alkyl ester, that can be hydrolyzed to provide FEX.

3.5. X-ray powder diffraction pattern

Powder X-ray diffraction pattern of FEX Form I was recorded at room temperature on Bruker's D8 Advance diffractometer (Karlsruhe, Germany) with Cu Kα radiation (1.54 Å), at 40 kV, 40 mA passing through a nickel filter, equipped with a 2θ compensating slit. Sample was subjected to X-ray powder diffraction analysis in polymethylmethacrylate (PMMA) sample holder and analyzed in a continuous mode with step size of 0.01° and step time of 1 s over an angular range of 3–40° 2θ. Obtained diffracto-gram was analyzed with DIFFRAC^{plus} EVA (ver 9.0) diffraction software.

FEX occurs in multiple solid-state forms. US Patent 5,738,872, 5,932,247, and 5,855,912 describe four crystal forms of FEX designated as Forms I–IV. Form II and IV are hydrates and Form I and III are anhydrous. FEX Forms V, VI, and VIII–XV are disclosed in US patents 20030021849 and US20020177608. FEX Form XVI is disclosed in US patent 20040044038. FEX is also discovered as Form XIX, XX, XXI, and XVI (Tables 4.3–4.5, Figs. 4.7 and 4.8).

3.6. Hygroscopicity

Hygroscopicity of FEX Form I was determined by exposing the samples to controlled relative humidity conditions (20–92% RH) at ambient tempera-ture, and the percent weight change after 7 days was recorded. The drug was found to show <0.1% weight gain at all conditions of relative humidity ranging from 21% to 92% RH, signifying its nonhygroscopic nature.

TABLE 4.3 Scattering angles, interplanar *d*-spacing and relative intensities in the X-ray powder diffraction of Form I of fexofenadine hydrochloride

Scattering angle (deg 2θ)	d-spacing (Å)	Relative intensity (I∕I$_0$)
18.273	4.851	100
14.099	6.276	88
17.877	4.957	57
19.947	4.447	46
19.430	4.564	45
5.914	14.933	36
23.490	3.784	33
7.448	11.859	32
17.557	5.047	31
15.982	5.541	30
14.993	5.904	27
22.565	3.937	26
23.941	3.713	25
19.220	4.614	23

3.7. Thermal method of analysis

3.7.1. Melting behavior

The melting point range of FEX free base Form II was found to be 225–230 °C by differential scanning calorimetry (DSC). Hydrochloride salt of FEX Form I has been reported to have a melting point of 193–199 °C [11].

3.7.2. Differential scanning calorimetry

DSC analysis of Form I of FEX was performed using Mettler Toledo 821^e DSC (Mettler Toledo, Switzerland) operating with Stare software version Solaris 2.5.1. Temperature axis and cell constant were calibrated using indium. Sample (~4 mg) was heated at 10 °C/min over the temperature range of 25–500 °C under dry nitrogen purging (80 ml/min) in pinholed aluminum pan (Fig. 4.9).

DSC thermogram of FEX shows a melting point in the range of 199–206 °C, with peak maxima at 202 °C. Melting of drug is followed by a major baseline shift in DSC pattern that is attributed to the thermal degradation of FEX.

3.7.3. Thermogravimetric analysis

TGA of FEX Form I (sample weight ~ 7.54 mg) was performed using Mettler Toledo 851^e TGA/SDTA in pinholed aluminum crucibles at a heating rate of 10 °C/min from 25 to 500 °C under nitrogen purging (10 ml/min) (Fig. 4.10).

TABLE 4.4 Crystal forms of fexofenadine hydrochloride

Name	Patent Number	State	Melting range/endothermic peak (°C)
Form A	WO 02/102777 A3	Crystalline-anhydrous	230.38
Form B	EP 1614681; A1 US 2005/ 0282860 A1	Crystalline-hydrate (1:1)	80.27, 109.27, 149.14
Form C	EP 1614681; A1 US 2005/ 0282860 A1	Crystalline–solvate (acetonitrile, 1:1)	n.d.*
Form C	US 2007/0191428 A1	Crystalline-anhydrous	192–194
Form I	US 5738872	Crystalline-anhydrous	195–199
Form II	US 5738872	Crystalline-hydrate (1:0.1–5)	124–126
Form III	US 5738872	Crystalline-anhydrous	166
Form IV	US 5738872	Crystalline-hydrate (1:0.1–5)	146
Form V	US 2002/0177608 A1	Crystalline-hydrate (variable hydration states)	n.d.
Form VI	US 2002/0177608 A1	Crystalline	n.d.
Form VIII	US 2002/0177608 A1	Crystalline	84, 142
Form IX	US 2002/0177608 A1	Crystalline	138.6
Form IX	US 2002/0177608 A1	Crystalline-solvate (methyl-t-butyl ether)	–
Form IX	US 2002/0177608 A1	Crystalline-solvate (cyclohexane)	–
Form X	US 2002/0177608 A1	Crystalline-hydrate	–
Form X	WO 2002/102777 A3	Crystalline-anhydrous	186.6
Form XI	US 2002/0177608 A1	Crystalline	n.d.
Form XII	US 2002/0177608 A1	Crystalline	n.d.
Form XIII	US 2002/0177608 A1	Crystalline	185–195

Form XIV	US 2002/0177608 A1	Crystalline-solvate (ethyl-acetate)	100
Form XV	US 2002/0177608 A1	Crystalline-solvate (ethyl-acetate)	140
Form XVI	US 2004/0044038 A1	Crystalline	67, 125, 135
Form XIX	US 2005/0256163 A1	Crystalline	90–100, 148–155
Form XX	WO 2007/052310 A2	Crystalline	142–152
Form XX	US 2005/0256163 A1	Crystalline-hydrate	50–55, 100–140
Form XXI	US 2005/0256163 A1	Crystalline	n.d.
Form IXX	WO 2007/052310 A2	Crystalline	145–155
Novel form	US 2004/0248935 A1	Crystalline	196.56
Amorphous form	US 2005/0256163 A1	Amorphous	–
Amorphous form	US 2004/0167168 A1	Amorphous	–

* n.d.—not defined

TABLE 4.5 Characteristic diffraction peaks of polymorphs of fexofenadine hydrochloride

| Form type	Characteristic powder X-ray diffraction peaks
Form A	4.15, 4.20, 4.44, 5.07, 5.33, 5.43, 6.16, 6.67 8.29, 23.11 Å (d spacings)
Form B	4.4, 4.7, 5.2, 7.9, 10.1, 23.6 (deg. 2θ)
Form C (mono solvate)	7.0, 11.6, 15.4, 17.3, 18.0, 20.5 (deg. 12θ)
Form C	8.97, 14.82, 16.05, 17.07, 18.34, 19.30, 19.77, 21.13, 21.52, 23.07, 23.82 (deg. 2θ)
Form I	3.7, 3.8, 3.9, 4.4, 4.8, 5.0, 5.9, 6.3, 7.3, 11.8 Å (d spacings)
Form II	3.5, 3.6, 3.7, 4.1, 4.2, 4.4, 4.7, 4.9, 5.2, 6.4, 7.8 Å (d spacings)
Form III	3.7, 4.5, 4.6, 4.8, 4.9, 9.0 Å (d spacings)
Form IV	3.5, 3.8, 4.0, 4.1, 4.3, 5.2, 5.3, 6.4, 7.0, 10.4 Å (d spacings)
Form V	15.9, 16.8, 17.2, 20.9, 21.5, 21.8 (deg. 2θ)
Form VI	15.7, 16.1, 17.0, 17.3, 18.6, 18.8 (deg. 2θ)
Form VIII	8.5, 11.0, 11.4, 13.4, 13.8, 17.1, 20.0, 21.5 (deg. 2θ)
Form IX	4.7, 9.3, 17.4, 18.2, 19.4, 19.6, 21.6 24.0 (deg. 2θ)
Form X (hydrate)	4.2, 8.0, 9.3, 14.2, 16.0, 16.8, 17.2, 17.6, 18.8, 20.0, 20.6, 21.7, 22.9, 23.8, 24.2, 25.4 (deg. 2θ)
Form X (anhydrous)	3.80, 4.03, 4.55, 4.70, 4.89, 5.54, 6.25, 8.29, 12.98, 16.05 Å (d spacings)
Form XI	8.7, 14.5, 14.9, 16.6, 17.2, 18.3, 19.5, 21.2, 22.1, 23.3 (deg. 2θ)
Form XII	5.2, 7.9, 8.1, 12.1, 18.5, 19.0 (deg. 2θ)
Form XIII	5.5, 6.8, 16.0, 16.3 (deg. 2θ)
Form XIV	5.4, 5.7, 10.9, 11.4, 11.6 (deg. 2θ)
Form XV	5.5, 5.8, 16.4, 16.9, 18.4 (deg. 2θ)
Form XVI	10.1, 15.2, 18.6, 19.2, 20.1 (deg. 2θ)
Form XIX	3.8, 8.8, 11.3, 18.8, 20.2 (deg. 2θ)
Form XX	11.18, 11.14, 13.56, 13.84, 16.18, 17.04, 18.28, 18.84, 20.08, 21.4, 21.96, 23.48, 23.84, 24.72 (deg. 2θ)
Form XX (hydrate)	5.4, 10.7, 14.0, 14.7, 15.8, 17.0, 19.0, 20.0, 21.6, 23.2 (deg. 2θ)
Form XXI	7.2, 11.7, 14.1, 15.4, 16.9, 18.5, 23.1, 23.9 (deg. 2θ)
Form IXX	4.68, 9.32, 9.56, 15.08, 17.08, 17.9, 18.54, 19.28, 19.74, 21.02, 23.96 (deg. 2θ)
Novel form	4.98, 5.13, 6.32, 6.77, 7.73, 3.87, 3.49, 3.64, 4.85, 4.88 Å (d Spacings)
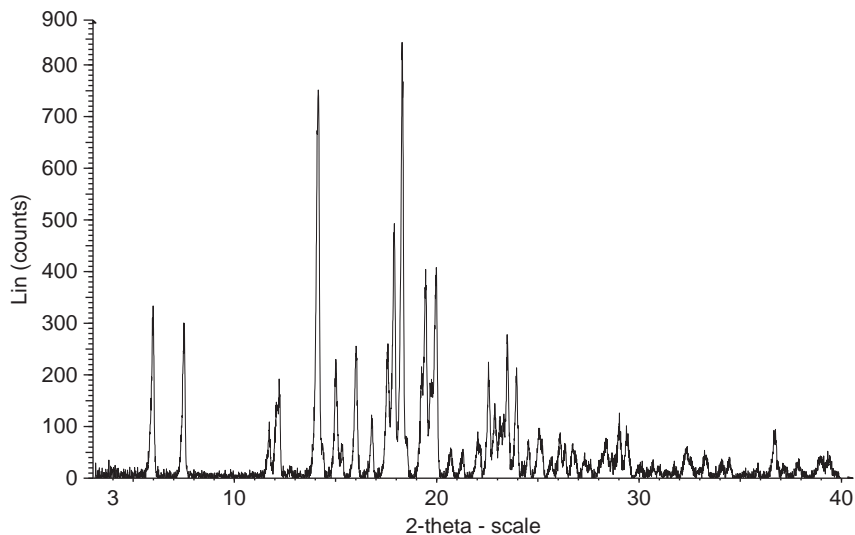
FIGURE 4.7   Powder X-ray diffractogram of fexofenadine hydrochloride Form I.
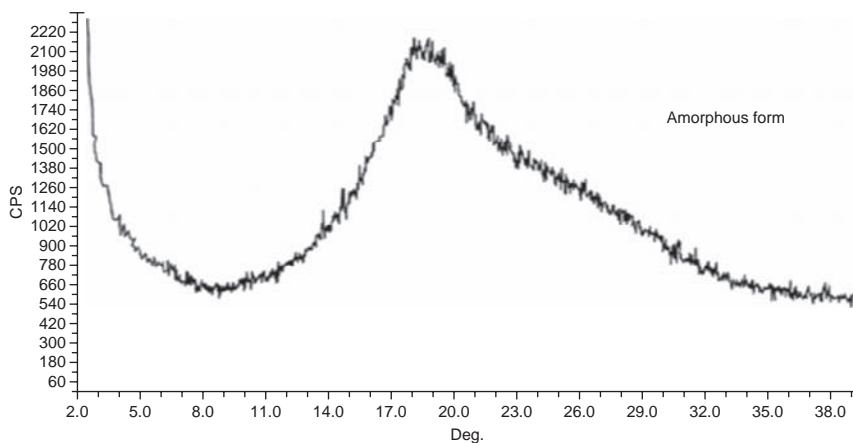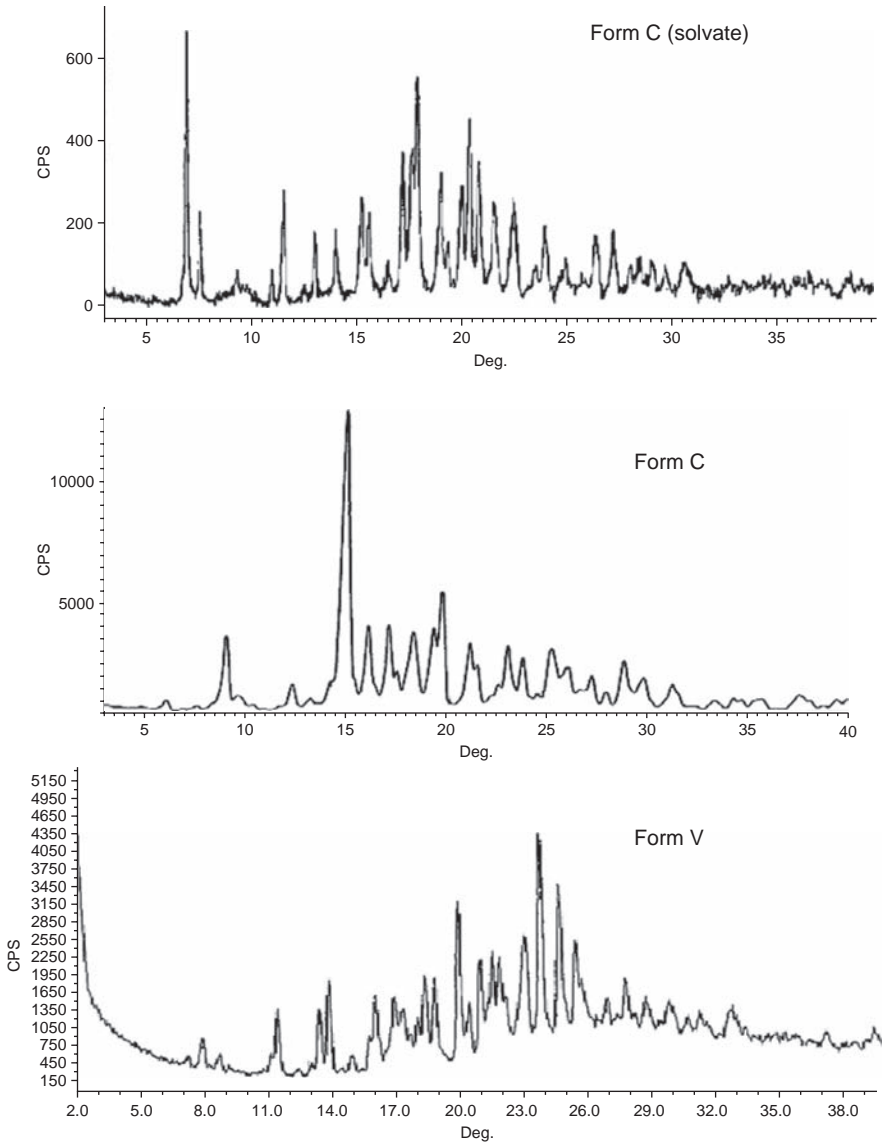

FIGURE 4.8   (*continued*).

TGA thermogram showed a 12% weight loss corresponding to the melting temperature of FEX at 200–202 °C. No weight loss was observed prior to melting temperature, indicating its anhydrous nature. The melting peak is further followed by degradation peak, showing major drug weight loss starting at a temperature of about 280 °C.
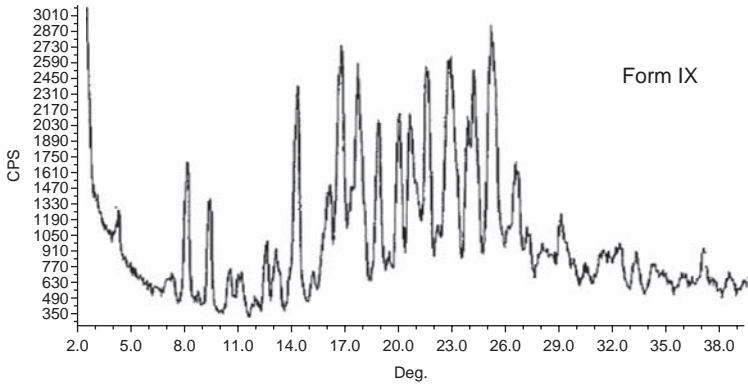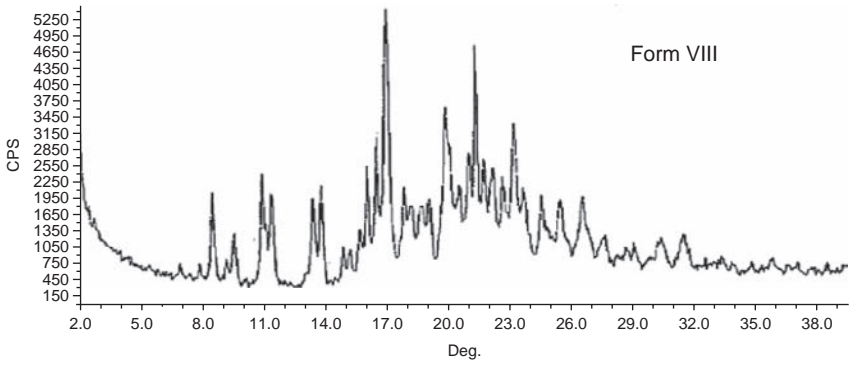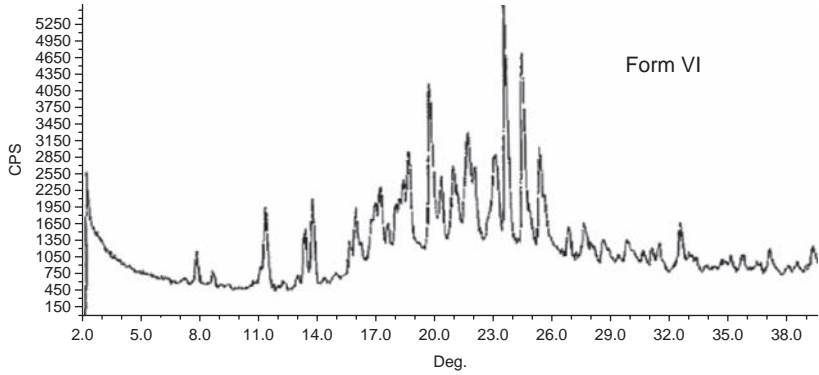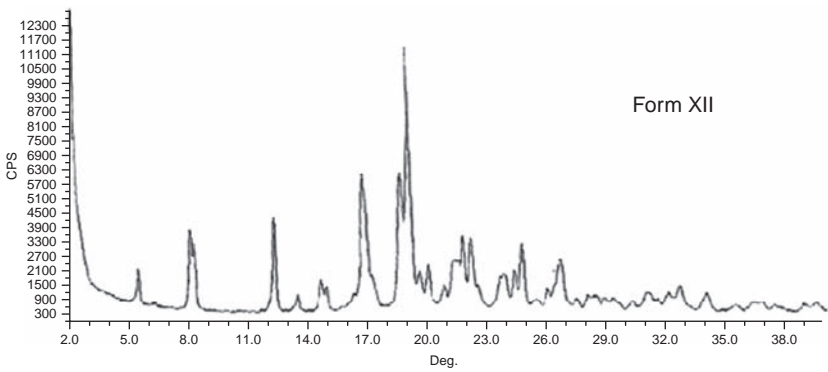
FIGURE 4.8 (*continued*).

FIGURE 4.8   (*continued*).

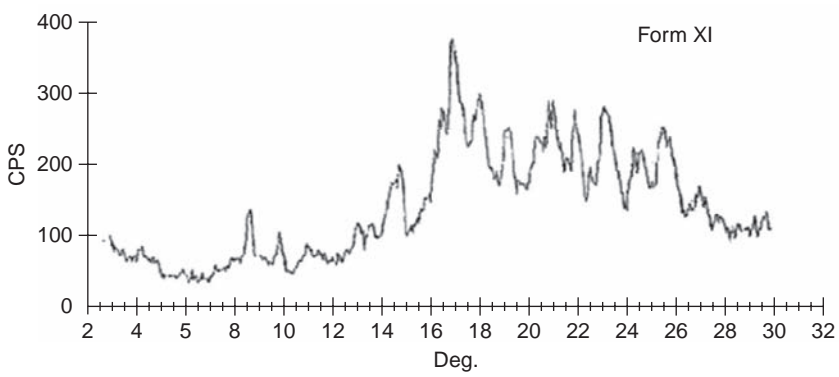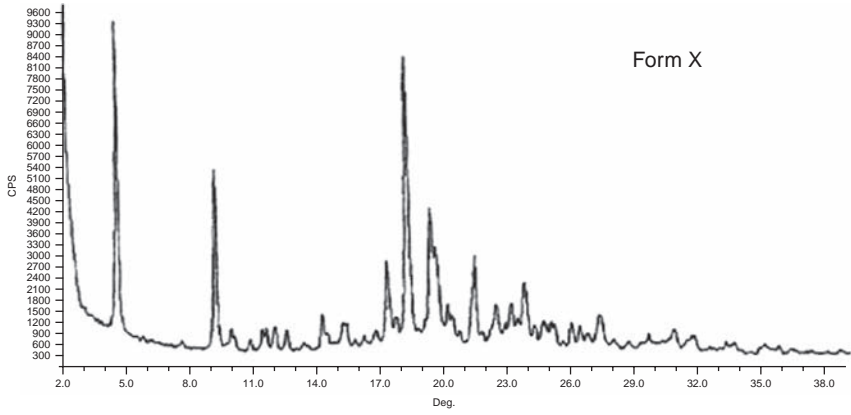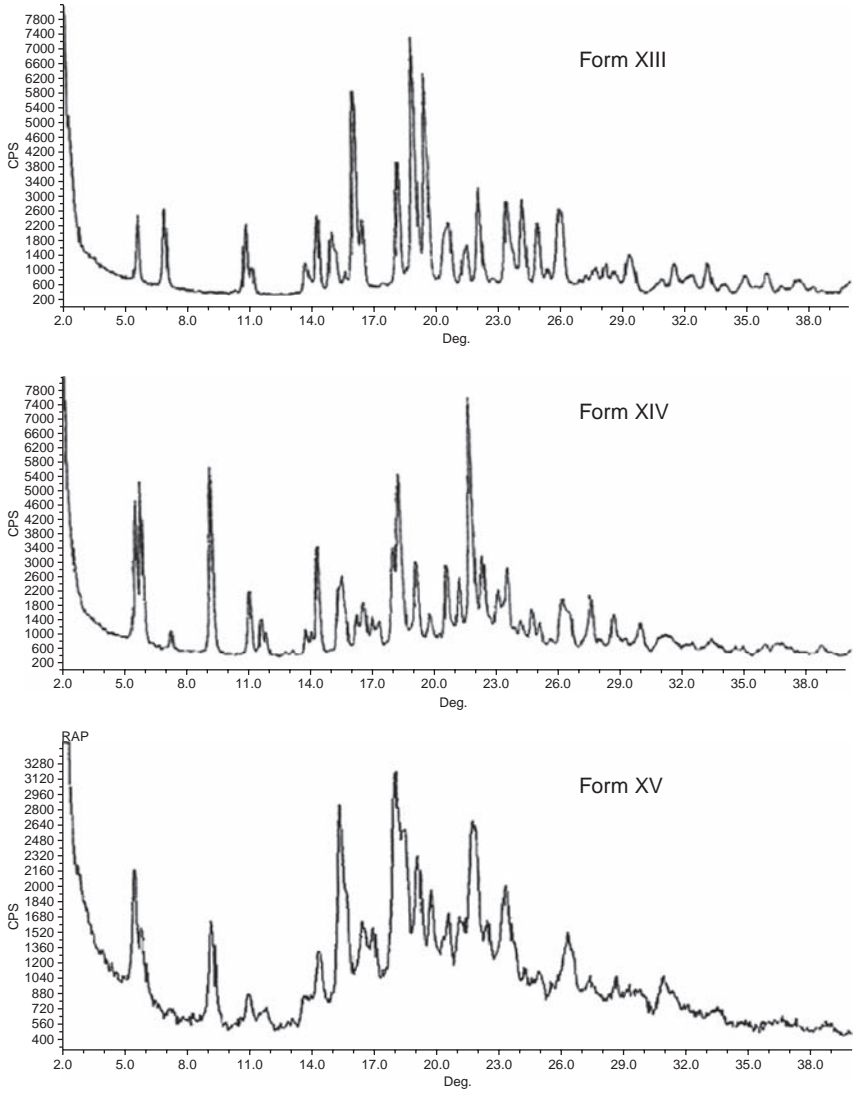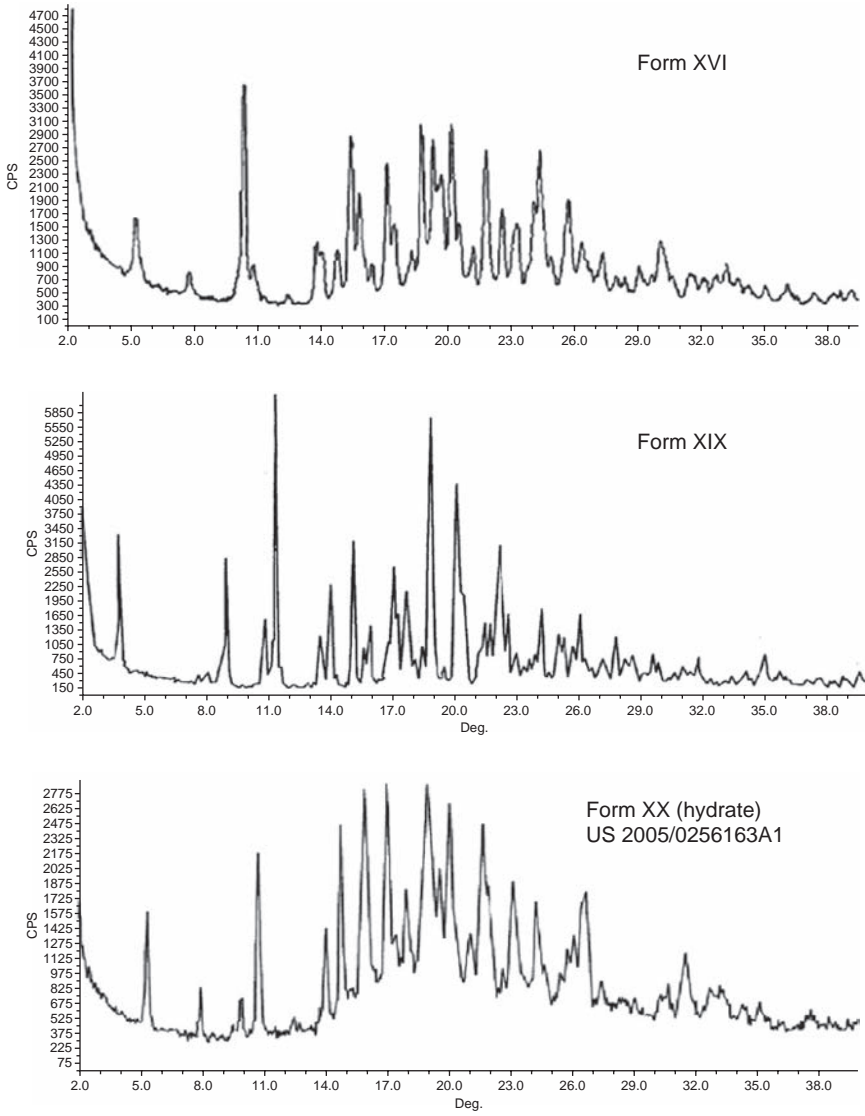**FIGURE 4.8** (*continued*).

FIGURE 4.8   (*continued*).

FIGURE 4.8 (*continued*).
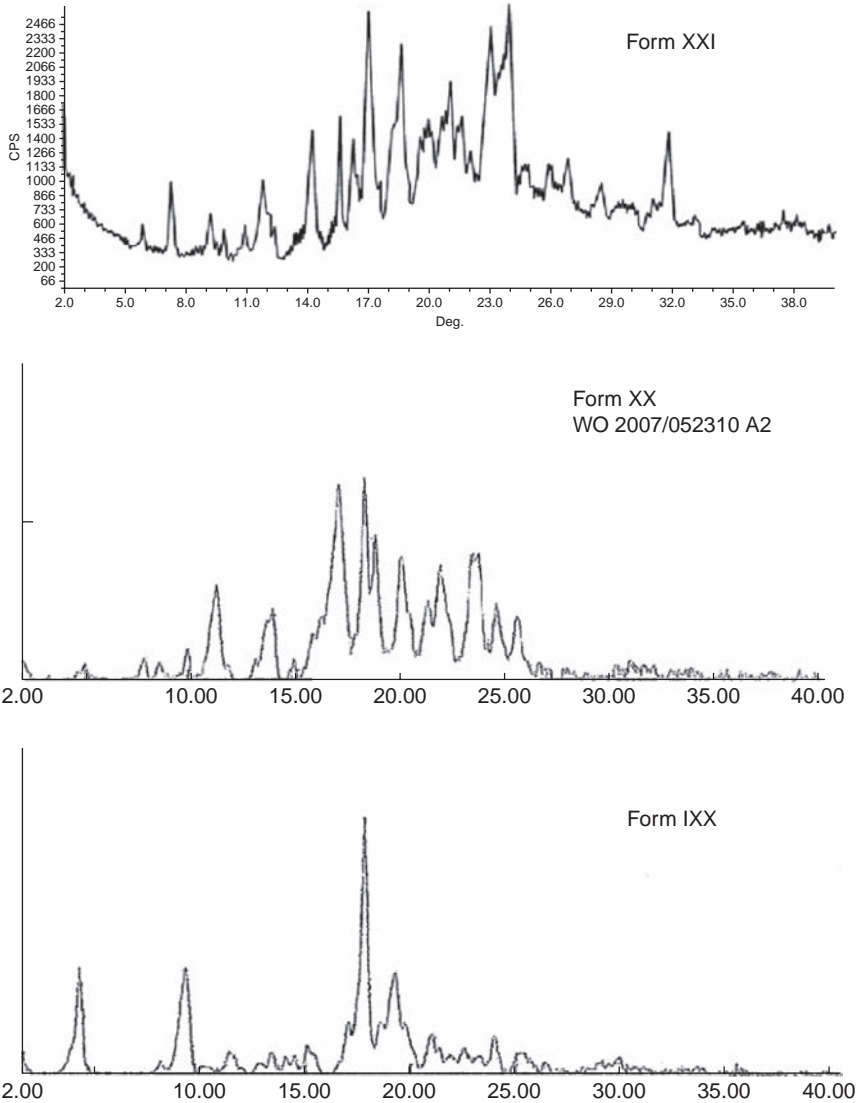
FIGURE 4.8   PXRD scans of polymorphic forms of fexofenadine hydrochloride.

3.8. Spectroscopy

3.8.1. UV–vis spectroscopy

FEX was dissolved in water (5 µg/ml) to obtain the UV absorbance maxima. The λ_{max} of FEX is observed in water at a wavelength of approximately 190 and 220 nm (Fig. 4.11).
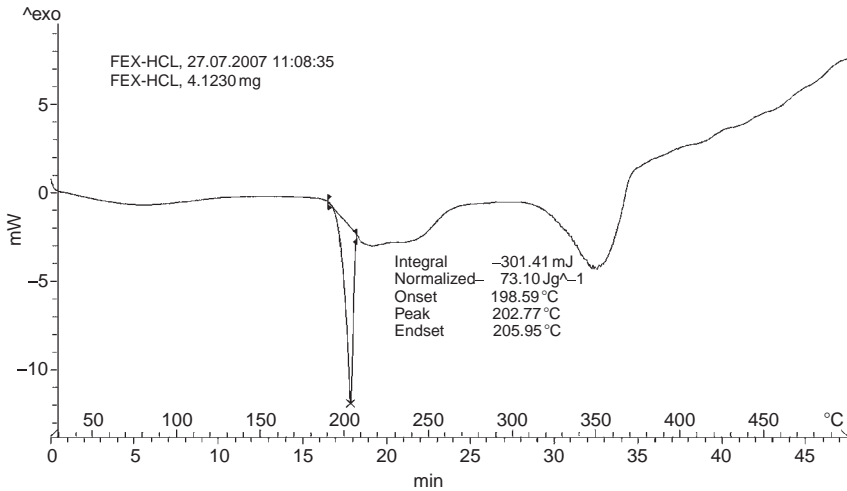
FIGURE 4.9   DSC thermogram of fexofenadine hydrochloride Form I.
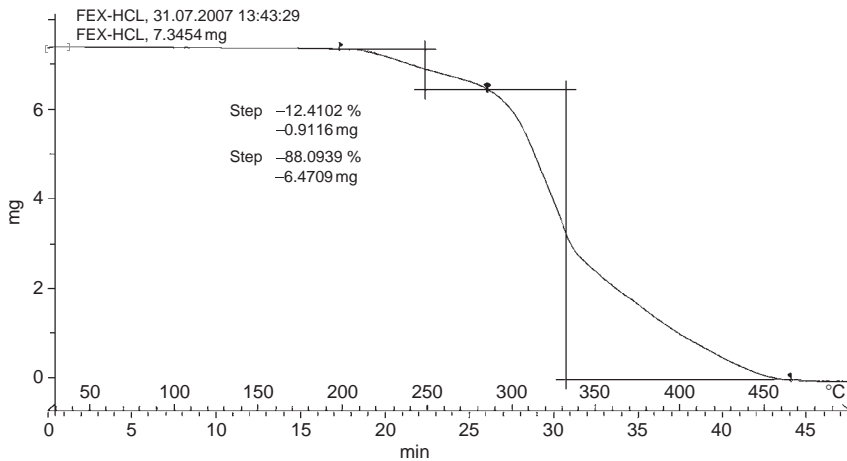
FIGURE 4.10   TGA thermogram of Form I of fexofenadine hydrochloride.

3.8.2. Vibrational spectroscopy

FTIR spectra of FEX Form I was obtained using Nicolet FTIR Impact 410 spectrophotometer (Nicolet, USA) equipped with deuterated triglycine sulfate detector. Potassium bromide pellet method was employed and the background spectrum was collected under identical conditions. Each spectrum was derived from averaging 16 single scans collected in the region 4000–400 cm^{-1} at a spectral resolution of 2 cm^{-1}. Spectra were analyzed using Omnic 5.1a software (Nicolet, USA) (Table 4.6, Fig. 4.12).
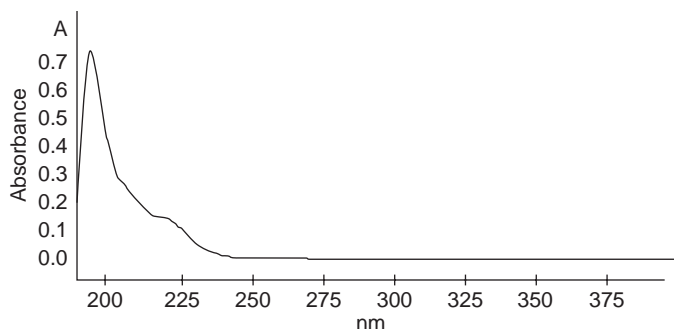
FIGURE 4.11   UV absorption scan of aqueous solution of fexofenadine (5 μg/ml).

TABLE 4.6   Assignment for the characteristic Infrared absorption bands of fexofenadine hydrochloride

Energy (cm^{-1})	Assignment
3296	Broad, OH stretching vibrations
3088–3024	Aromatic =CH stretching vibration
1705	Carbonyl (C=O) stretching of carboxylic acid
1440–1490	Aromatic C=C stretching
1403	In plane, OH deformation vibrations of tertiary alcohol
1168	C–O stretching vibrations of tertiary alcohol
1068	C–O stretching vibrations of secondary alcohol

3.8.3. Nuclear magnetic resonance spectrometry

1. ^{1}H NMR spectrum (see Figs. 4.13 and 4.14, Table 4.7).
2. ^{13}C-NMR spectrum (see Figs. 4.15 and 4.16, Table 4.8).

3.9. Mass spectrometry

See Figs. 4.17 and 4.18, Table 4.9.

4. METHODS OF ANALYSIS

4.1. Identification

FEX may be identified as such on the basis of its characteristic infrared absorption spectrum (Section 3.8.2), HPLC (Section 4.3.2), and thin layer chromatography (Section 4.3.1). Supportive evidence for identification can be obtained by DSC (Section 3.7.2) and thermogravimetric analysis (Section 3.7.3).
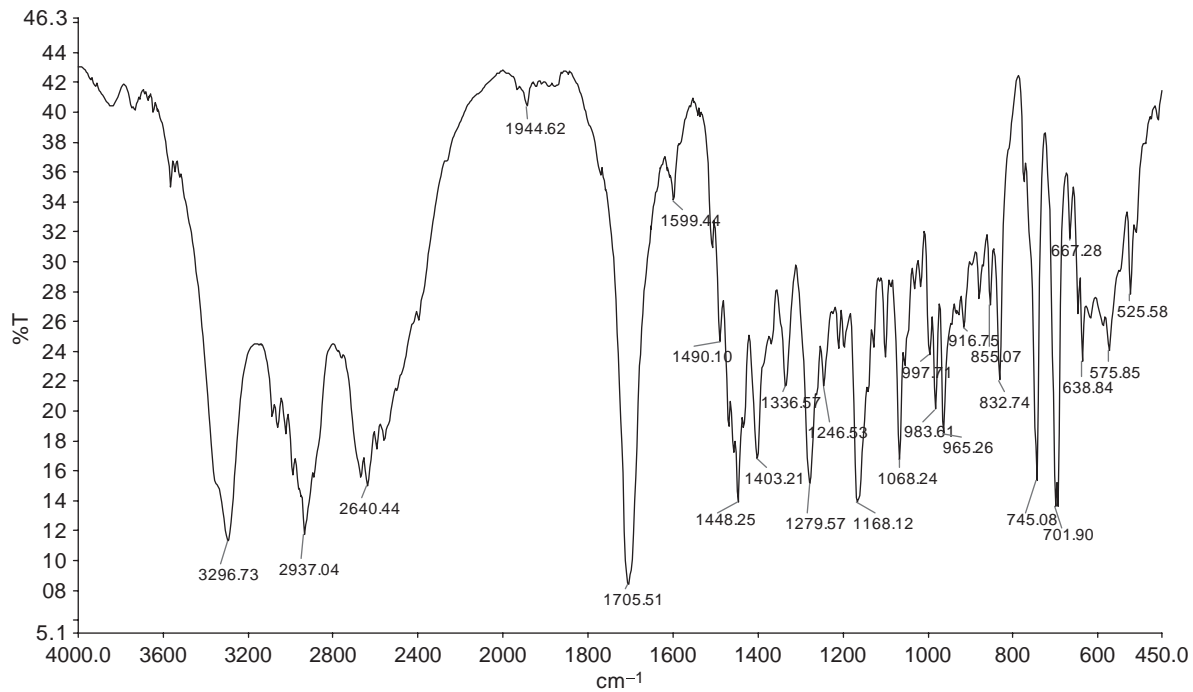
FIGURE 4.12   FT-IR spectra of Form I of fexofenadine hydrochloride.
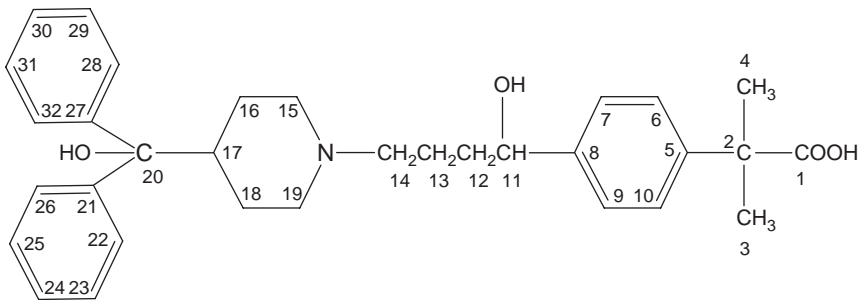
FIGURE 4.13   Structure of fexofenadine hydrochloride.
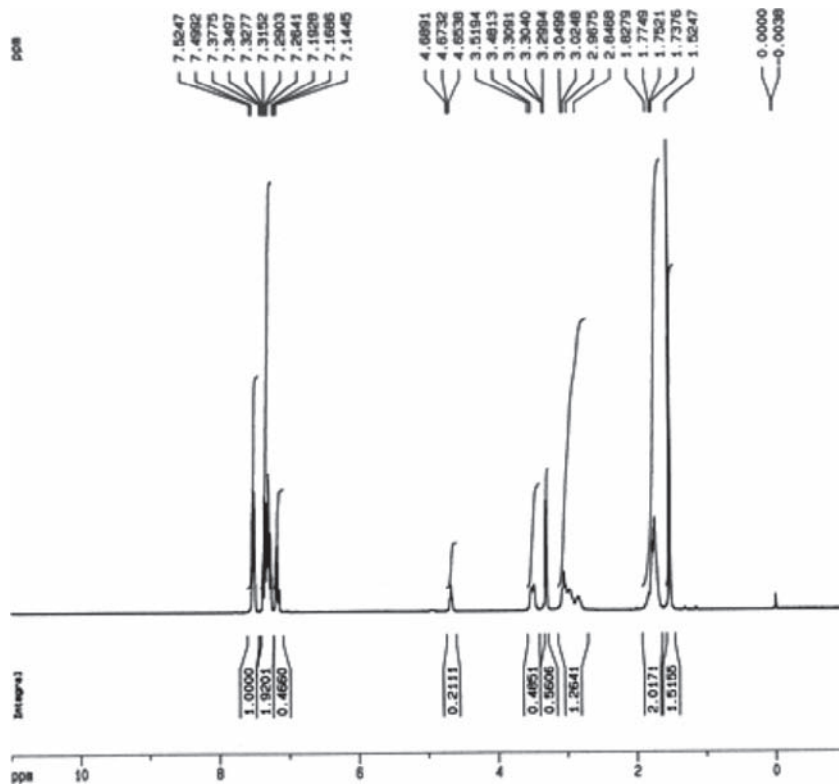
FIGURE 4.14   NMR spectra of fexofenadine hydrochloride.

TABLE 4.7 Assignment for the resonance bands in ^{1}H NMR spectrum of fexofenadine hydrochloride (solvent—CH_3OH-*d3*)

Chemical shift (ppm)	Number of hydrogen atoms	Position of hydrogen atoms
1.52 (s)	6	3, 4
1.74 (m)	8	12, 13, 16, 18
2.85 (t)	1	17
2.84–3.04 (m)	6	14,15,19
3.48 (s)	1	11
7.14	2	24, 30
7.26 (J = 7.2)	4	23, 25, 29, 31
7.29–7.49	4	6, 10, 7, 9
7.52 (J = 7.2)	4	22, 26, 28, 32
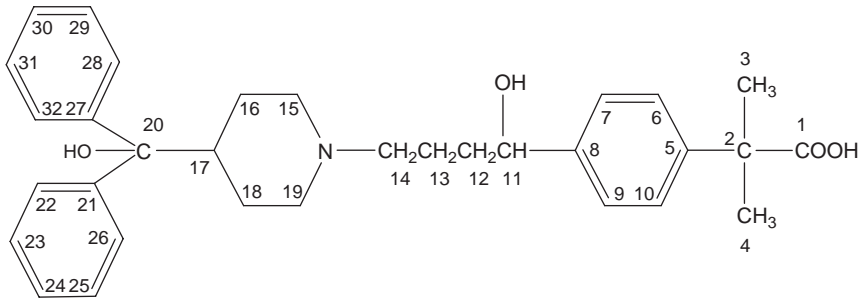
FIGURE 4.15 Structure of fexofenadine hydrochloride showing positions of different carbon atoms.
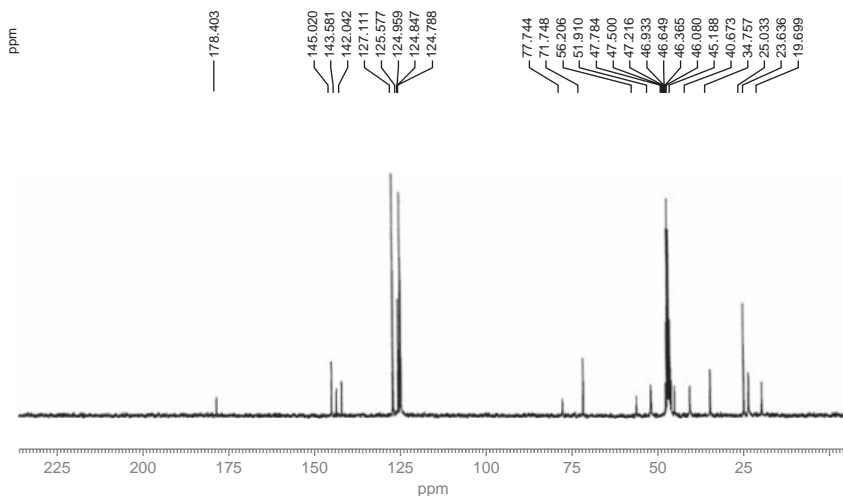
FIGURE 4.16 CMR spectra of fexofenadine hydrochloride.

TABLE 4.8 Assignment for the resonance bands in ^{13}C-NMR spectrum of fexofenadine hydrochloride (solvent—CH$_3$OH-*d3*)

Chemical shift (ppm)	Assignment	Chemical shift (ppm)	Assignment
19.69	C3, C4	124.96	C22, C26, C28, C32
23.64	C13, C16, C18	125.58	C6, C10
47.22	C2	127.11	C24, C30
51.91	C19, C15	142.04	C5
56.21	C14	143.58	C8
71.75	C11	145.02	C21, C27
77.74	C20	178.40	C1
124.85	C23, C25, C29, C31		

4.2. Spectroscopic analysis

4.2.1. Colorimetry and spectrophotometry

Rajput and Parekh developed three simple analytical methods based on derivative spectroscopy, difference spectrophotometry, and colorimetry for the estimation of FEX in bulk drug and film coated tablet formulations. Derivative spectroscopic method was adapted to obtain a linear calibration curve in the range of 5–20 µg/ml. The method gave maxima and minima of second derivative spectrum curve at 233 and 222 nm. Difference spectrum was generated between 200 and 300 nm having a maxima and minima at 223–208.5 nm respectively. In the colorimetric method, FEX was treated with potassium iodide in acidic medium to get a yellow chromogen that was extracted in chloroform and determined at 363 nm. The colorimetric method showed linearity in the range of 20–70 µg/ml of FEX. The methods were successfully applied to film coated tablet formulations of FEX with a relative standard deviation (RSD) of 0.324, 0.522, and 0.0401 for method I, II, and III respectively [12].

Suresh *et al.* developed a spectrophotometric method for the determination of FEX, based on the chloroform-extractable pale yellow color complex formed by the reaction of FEX with bromothymol blue at pH 2.6, followed by estimation at 412 nm against a reagent blank. The method showed linearity in the concentration range of 10–50 µg/ml of FEX. The proposed method was successfully applied to the analysis of bulk drugs and their dosage forms [13].

Saleh *et al.* demonstrated a colorimetric method for the determination of FEX, along with some skeletal muscle relaxants. The method involved formation of a charge transfer complex with 4-chloro-7-nitro-2,1,3-ben-zoxadiazole (NBD-Cl) in nonaqueous medium. The orange color products were measured at 472, 465, 475, and 469 nm for drugs I, II, III, and IV,
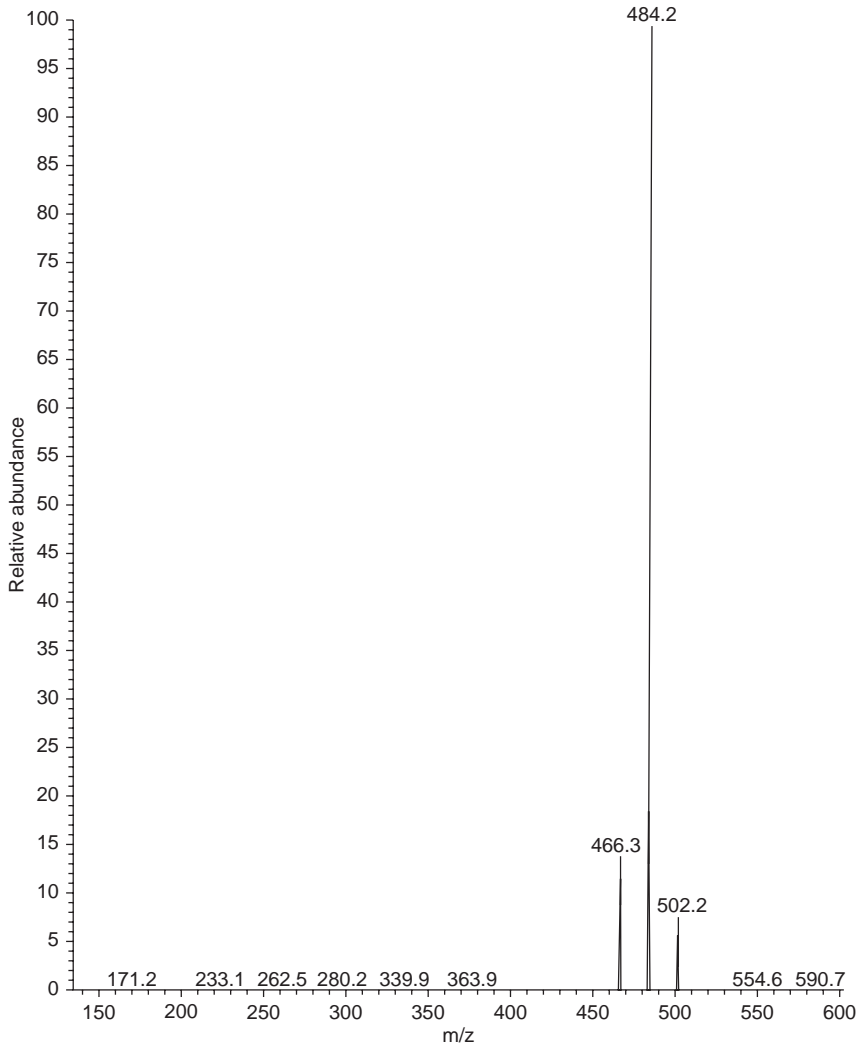
FIGURE 4.17   MS spectra of fexofenadine hydrochloride (ESI mode).

respectively. The method compared well with the pharmacopoeial method for determination of FEX [14].

4.3. Chromatographic methods of analysis

4.3.1. Thin layer chromatography

Meyyanathan *et al.* developed a HPTLC method for determination of simvastatin and FEX. Chromatography was performed on aluminum-backed silica gel 60 F254 HPTLC plates prewashed with methanol, followed by
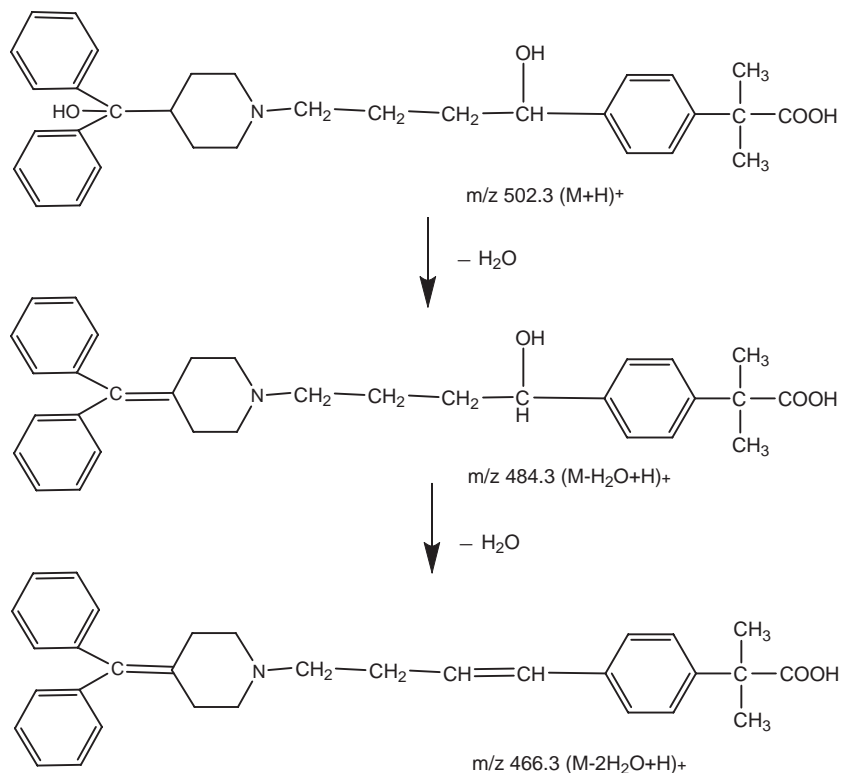
FIGURE 4.18 Fragmentation pattern of fexofenadine hydrochloride.

TABLE 4.9 Assignment for the fragment ions in the mass spectrum of fexofenadine hydrochloride

m/z	Assignment	Relative intensity (%)
502.3	$(M + H)^+$	~10
484.3	$(M-H_2O + H)^+$	100
466.3	$(M-2H_2O + H)^+$	~15

development with ethyl acetate–methanol–ammonia solution 25% (7:1.5:0.5, v/v/v), and analyzed at 220 nm. The R_f values for simvastatin and FEX were 0.89 and 0.20 respectively [15]. TLC method for two degradation product of FEX, *viz.* isopropyl (decarboxylate) degradant and the benzophenone derivative, were analyzed with chloroform: methanol (85:15, v/v) as eluent [7].

4.3.2. High performance liquid chromatography

A number of HPLC methods are reported for FEX, both as single components, as well as in combination with pseudoephedrine and/or other antihistaminic agents. Radhakrishna and Reddy suggested a simple reversed phase liquid chromatography for determination of FEX and its related compounds A and B. The method utilized an Eclipse XDB column (C8, 4.6 × 150 mm, 5 μm) and a mobile phase comprising 1% triethylamine phosphate (pH 3.7), acetonitrile, and methanol in the ratio 60:20:20 (v/v/v), over a range of 0.7–18.7 μg/ml for related compounds A and B and 60–750 μg/ml for assay of FEX. Limits of detection (LOD) and quantification (LOQ) for the related compounds A and B were 0.18, 0.12, and 0.56, 0.48 μg/ml, respectively [16].

Gregov *et al.* developed a liquid chromatography-tandem mass spectrometry (LC-MS/MS) for simultaneous screening and quantitation of FEX in along with 17 other antihistaminics. Sample pretreatment included liquid–liquid extraction of the basic antihistaminics followed by a second extraction of the acidic antihistamines. The combined extract was run by LC on a reversed phase C18 column using acetonitrile-ammonium acetate mobile phase at a pH of 3.2. Screening was performed using MRM followed by subsequent MS/MS run. A LOQ of 0.0005 mg/l was achieved with the proposed method [17].

Gazy *et al.* suggested three simple HPLC methods for determination of cetirizine, FEX, loratadine, and acrivastine in pure form as well as commercial dosage forms. The first method utilized a reaction with bromocresol purple dye to form ion-pair complex extractable with chloroform and subsequently measured spectrophotometrically. The second method employed formation of an ion-pair complex with eosin, measurable directly without extraction both spectrophotometrically and spectrofluorimetrically. The last method involves the base-catalyzed condensation of mixed anhydrides of organic acids (citric acid/acetic anhydride). The products of condensation were measured spectrophotometrically [18].

Zarapkar *et al.* suggested a HPLC method for simultaneous determination of FEX and pseudoephedrine by reverse phase HPLC. A 5 μm Inertsil C8 column was utilized in an isocratic mode with a mobile phase of pH 3.5 0.025 M H_3PO_4–MeCN (60:40). The flow rate was 1.0 ml/min and the effluent was monitored at 215 nm. Methylparaben was used as an internal standard. The LOD was 0.5 and 5 mg/ml of pseudoephedrine and FEX, respectively [19].

Golcu *et al.* performed a cyclic, linear sweep, differential pulse, and square wave voltammetric study of oxidation of FEX by glassy carbon electrode, wherein, a dependence of intensity of current and potential on pH, concentration, scan rate, and nature of the buffer was investigated. Different parameters were tested to optimize the conditions for the determination of FEX. A linear response was obtained in supporting electrolyte

in the ranges of 1.0×10^{-6}–2.0×10^{-4} M with a LOD of 6.6×10^{-9} M and 5.76×10^{-8} M, and in serum samples in the range of 2.0×10^{-6}–1.0×10^{-4} M with LOD of 8.08×10^{-8} M and 4.97×10^{-8} M for differential pulse and square wave voltammetric techniques, respectively. Based on this study, a simple, rapid, selective, and sensitive voltammetric methods were developed for the determination of FEX in dosage forms and biological fluids. The precision and accuracy of the developed methods was ascertained from recovery studies, utilizing standard addition method. No electroactive interferences were found in biological fluids from the endogenous substances and additives present in tablets [20].

Oliveira *et al.* developed a simple reversed phase HPLC method for the analysis and dissolution studies of FEX in dosage forms. The method utilized a mobile phase of triethylamine phosphate 1% (pH 3.2):acetonitrile:methanol (50:30:20) and a wavelength of 210 nm for detection, and was successfully applied to the determination of the drug in commercial tablet preparations [21].

Rustichelli *et al.* developed a HPLC method for stereoselective separations of terfenadine and its active metabolite FEX. Racemic FEX was derivatized with diazomethane and *R*-(+)-1-phenylethylisocyanate, subjected to achiral LC on a reversed-phase analytical column. Complete enantioseparation was achieved in short analysis times; excess reagent eluted before the diastereoisomeric pair and did not interfere in the analysis [22].

Chan *et al.* developed an enantioselective method for determination of FEX using BSA-7 column (Resolvosil, 150×4 mm, 5 μm), with a mobile phase of 2-propanol:sodium phosphate (0.08 M, pH 8.0) (1.5:98.5 v/v) at a flow rate of 0.4 ml/min. Sample were analyzed at 210 or 254 nm, with an average retention time of 10.2 and 14.4 min for (*S*)- and (*R*)-FEX respectively [23].

Sui-wei *et al.* proposed a method for determination of FEX in presence of related substances using a Hypersil pH 2 column (250×4.6 mm, 5 μm) using a mobile phase of 0.5% monobasic sodium phosphate in water (pH 4.0)–acetonitrile (60:40 v/v) having 2 ml/l of triethylamine and a flow rate of 1.5 ml/min. The detection wavelength employed was 220 nm [24].

Breier *et al.* developed a liquid chromatographic method for the determination of the antihistamine FEX using LiChrospher 100 RP-18 (250×4.0 mm, 5 μm) column with acetonitrile–5 mM ammonium acetate buffer (50:50, v/v) at pH 3.2 as the mobile phase. The method is linear ($r^2 = 0.9999$) at concentrations ranging from 20.0 to 80.0 μg/ml, precise (intraday RSD = 0.85, 0.40, and 0.81%; interday RSD = 0.77%), accurate (mean recovery = 99.05%), robust and specific. The LOD and LOQ were 0.3409 and 1.033 μg/ml, respectively [25].

Aiqin *et al.* developed a HPLC method for the determination of FEX tablets in the conditions as follows: Spherisorb C18 (4.6×250 mm) as the column, potassium dihydrogen phosphate (0.01 mol/l)–methanol (75:25) as

the mobile phase (pH adjusted by 10% phosphoric acid to 3.5) and the detection wavelength of 220 nm. It was shown that FEX could be separated from related compounds effectively with a LOD of 2 ng. The method was fast, simple, accurate, and suitable for the quality control of FEX [26].

Lin *et al.* proposed a HPLC method for simultaneous determination of FEX and pseudoephedrine using a Hypersil CN (4.6 × 200 mm, 5 μm) column and acetonitrile–5 mM $NH_4H_2PO_4$ buffer (pH 3.5, 53:47) as the mobile phase, with detection at 210 nm. The flow rate was 1.0 ml/min. The method had linearity in the range of 20.28–101.4 mg/l for FEX and 39.66–198.3 mg/l for pseudoephedrine. Recoveries were 99.9% and 99.8%, with RSD of 0.51% and 0.38% for FEX and pseudoephedrine respectively [27].

Abbas *et al.* developed a novel membrane sensor for FEX based on ion exchange with reineckate, tetraphenylborate, and tetraiodomercurate. The novel sensor based on reineckate exchange showed a stable, potentiometric response for FEX in the concentration range of 1×10^{-2}–2.5×10^{-6} M at 25 °C, independent of pH in the range of 2.0–4.5. The sensor possesses a Nernstian cationic slope of 62.3 ± 0.7 mV/concentration decade and a lower LOD of 1.3×10^{-6} M with a fast response time of 20–40 s. Selectivity coefficients for a number of interfering ions and excipients relative to FEX were investigated. A negligible interference from almost all studied cations, anions, and pharmaceutical excipients, was observed. However, cetirizine that has a structure homologous to that of FEX was found to interfere. The determination of FEX in aqueous solution shows an average recovery of 99.83% with a mean RSD of 0.5%. Direct potentiometric determination of FEX in tablets gave results that compare favorably with those obtained by standard spectrophotometric methods. Potentiometric titration of FEX with phosphomolybdic acid as a titrant was monitored with the proposed sensor as an end point indicator electrode [28].

Thomas and Schmitt developed a method for separation of FEX, pseudoephedrine, potential impurities and their degradation products using an ion exchange chromatography. Because of uncharged/cationic nature of analyte in FEX-D tablets, a dual mechanistic system was developed for HPLC so that the charged and neutral components are retained and separated. An ion interaction liquid chromatographic system that contains an anionic surfactant, such as sodium dodecyl sulfate (SDS), meets both of these requirements: a reversed stationary phase for a hydrophobic analyte and a fixed anionic charge site for a positively charged analyte. Effect of variables including concentration of SDS, ionic strength, pH, concentration of phosphoric acid, concentration of organic modifier, column temperature, and different gradients was evaluated [29].

Emara *et al.* developed a simple liquid chromatographic technique for simultaneous determination of loratadine and terfenadine, and their major active metabolites, desloratadine, and FEX respectively. Serum samples

were enriched on a protein-coated RP8 silica precolumn (10 × 4.6 mm), and the serum constituents, including proteins and salts, were eluted to waste. An online column switching system was utilized for transferring drugs and their metabolites on a second analytical column (Shim pack cyanopropyl column, 250 × 4.6 mm, 5 μm) for separation, followed by UV detection at 243 and 220 nm for loratadine and terfenadine respectively. High precision, accuracy, and linearity was obtained over the range of 10–1000 ng/ml for loratadine and desloratadine, 10–500 ng/ml for terfenadine, and 10–3000 ng/ml for FEX in human serum [30].

Mahgoub et al. developed a derivative spectrophotometric method for the assay of three binary mixtures of pseudoephedrine with FEX (mix I), cetirizine (mix II), and loratadine (mix III) based on the use of the first derivative of the ratio spectrum. The ratio spectrum was obtained by dividing the absorption spectrum of the mixture by that of one of the components. Concentration of the other component was determined from its respective calibration graph treated similarly. Moreover, the influence of $\Delta\lambda$ for obtaining the first derivative of the ratio spectra and the effect of the divisor concentration on the calibration graphs were studied. The described method was successfully applied for determination of these combinations in synthetic mixtures and dosage forms [31].

Kakarus et al. developed a simple, accurate, precise, and rapid reversed-phase RP-HPLC method for the determination of antihistaminic–decongestant pharmaceutical dosage forms containing binary mixtures of pseudoephedrine hydrochloride (PSE) with FEX or cetirizine dihydrochloride (CET). Separation was achieved on a Zorbax C8 (150 × 4.6 mm, 5 μm) column using UV detection at 218 and 222 nm. The optimized mobile phase consisted of triethylamine solution (0.5%, pH 4.5)–methanol–acetonitrile (50:20:30, v/v/v). Retention times were 1.099, 2.714, and 3.808 min for PSE, FEX, and CET, respectively. A linear response was achieved within the concentration ranges 30–240 and 1.25–10 μg/ml with LOD values of 1.75 and 0.10 μg/ml for PSE and CET, respectively. Linearity range for PSE–FEX binary mixtures were 10–80 and 5–40 μg/ml with LOD values of 0.75 and 0.27 μg/ml for PSE and FEX, respectively. No interference from any components of pharmaceutical dosage forms or degradation products was observed. The proposed method could be applied to the quantitative analysis of these drugs in capsules containing PSE–CET or extended-release tablets containing PSE–FEX binary mixtures [32].

Maggio et al. developed a RPLC method for the determination of FEX and PSE in their combined tablet formulation. The method was validated, and was found to be linear for both the analyte, over the range of 160.6–301.2 mg/l for FEX ($r^2 = 0.9993$) and between 325.6 and 610.5 mg/l for PSE ($r^2 = 0.9992$), accurate exhibiting 99.8% and 99.9% drug recoveries for FEX and PSE, respectively ($n = 9$). The contents of both analyte were assayed in commercial tablets employing this method and the results

were found to be in good statistical agreement with the data generated by HPLC method [33].

4.3.3. Capillary chromatography

Breier *et al.* developed a capillary electrophoresis (CE) method with UV absorbance detection for the quantitation of the antihistamine FEX in capsules. Separation was performed with an uncoated fused-silica capillary operated at 20 kV potential. Temperature was maintained at 25 °C. Running buffer was prepared with 20 mM $Na_2B_4O_7 \cdot 10H_2O$. The method was linear ($r^2 = 0.9999$) in the range of 20–100 mg/ml, precise (RSD intra-assay = 1.2, 1.6, and 1.8% and inter-assay = 1.5%), accurate (98.1% recovery), and specific. The LOD and LOQ were 0.69 and 2.09 mg/ml respectively [34].

Mikus *et al.* suggested a CE method for the determination of FEX in tablets in free solution and in solution with cyclodextrins (CDs) as analyte carriers. It was demonstrated that FEX could be effectively analyzed in free solution cationic CE at low pH. Another analytical approach studied was based on CD modified CE, where the highly charged CD derivatives served as analyte carriers. In this way, the separation range was spread to physiological pH region and CE analysis of FEX, present actually in its zwitterionic form could be accomplished. The method was successfully applied to the determination of FEX in tablets [35].

4.4. Determination in biological fluids

Uno *et al.* developed a HPLC method for determination of FEX utilizing fluorescence detection. The mobile phases utilized was a linear gradient from 0.05 M KH_2PO_4 buffer/acetonitrile/methanol (60:35:10, v/v/v) to 0.05 M KH_2PO_4 buffer/acetonitrile (40:60, v/v) in 10 min. Chromatographic separation was achieved on an ODS-80A column (150 × 4.6 mm, 5 μm). The peak was detected using a fluorescence detector set at excitation and emission wavelength of 220 and 290 nm respectively. The method was validated for a linear range of 1.0–500 ng/ml and applied successfully to therapeutic drug monitoring in patients treated with clinical doses of FEX and for analysis within the pharmacokinetic studies [36].

Miura *et al.* developed a simple and sensitive HPLC method for assay of FEX enantiomers in human plasma, using a mobile phase of 0.5% KH_2PO_4– acetonitrile (65:35, v/v) on a Chiral CD-Ph column at a flow rate of 0.5 ml/ min and measurement at 220 nm. The lower LOQ was 25 ng/ml for (*R*)- and (*S*)-FEX. The linear range of this assay was between 25 and 625 ng/ml (regression line $r^2 > 0.993$). This method was applied effectively to measure FEX enantiomer concentrations in clinical samples [37].

Naidong *et al.* developed a bioanalytical method for FEX using an automated 96-well solid-phase extraction (SPE) and liquid chromatography with electrospray tandem mass spectrometry (LC/MS/MS) method. SPE

methods typically require manual steps of drying of the eluates and recon-stituting of the analytes with a suitable injection solvent possessing elution strength weaker than the mobile phase. In this study, a novel approach of eliminating these two steps in 96-well SPE by using normal-phase LC/MS/MS methods with low aqueous/high organic mobile phases was demon-strated, which consisted of 70–95% organic solvent, 5–30% water, and small amount of volatile acid or buffer. Analytical methods for a range of polar pharmaceutical compounds including omeprazole, metoprolol, FEX, pseu-doephedrine as well as rifampin and its metabolite 25-desacetyl-rifampin, in biological fluids, were developed and optimized [38].

Hofmann *et al.* suggested a sensitive method for determination of FEX in human plasma and urine by HPLC-electrospray mass spectrometry, utilizing a mobile phase of (A) 12 mM ammonium acetate in water and (B) acetonitrile. Separation was achieved on a cyano column (10 cm × 2.0 mm, 3 mm) using a linear gradient from 40% B to 60% B in 10 min. The mass spectrometer was operated in the selected ion monitoring mode using the respective MH^+ ions, m/z 502.3 for FEX. The LOQ achieved with this method was 0.5 ng/ml in plasma and 1.0 ng in 50 ml of urine. The method described was successfully applied to the determination of FEX in human plasma and urine in pharmacokinetic studies [39].

Fu *et al.* described a fast and sensitive HPLC–MS/MS method, utilizing atmospheric pressure chemical ionization, for determination of FEX in human plasma. Plasma samples were prepared using 96-well SPE with plates containing Waters Oasis HLB sorbent and the analysis was per-formed using a Restek Ultra IBD column (3.2 × 50 mm, 3 μm) with a mobile phase consisting of a mixture of 90% acetonitrile and 10% 10 mM ammo-nium acetate buffer with 0.1% formic acid. Quantitation of the analyte was performed in a range of 1–200 ng/ml by the response from the MRM of the precursor to product ion pairs for FEX (m/z 502→466). The method was found to be suitable for the analysis of human plasma samples obtained 24 h after the administration of a single 60 mg dose of FEX [40].

Ramenskaya *et al.* developed a sensitive and reproducible HPLC pro-cedure for quantitation of FEX in blood plasma. Separation was achieved by a reverse phase HPLC mode on a μ-bondapak phenyl column and reliably detected by spectrophotometry at 220 nm [41].

Teng *et al.* developed a validated rapid and sensitive liquid chromatography–tandem mass spectrometry method (LC–MS/MS) for the quantification of FEX in human plasma to conduct comparative human bioavailability studies. Human plasma was extracted with a mix-ture of dichloromethane–diethyl ether (volume ratio 2:3) in a basic envi-ronment and the extract was separated on a C18 column with acetonitrile–methanol–10 mmol/l ammonium acetate (volume ratio 45:45:10) as the mobile phase. The analytes were detected *via* electrospray ionization (ESI) tandem mass spectrometry in the MRM mode. The linearity was within a

range of 1–1000 ng/ml. The intra and interday precision were <4.1% and <4.8%, respectively, and the accuracy was in the range of 95.0–105%. The method was successfully applied to the quantification of FEX human plasma from 20 healthy male Chinese volunteers [42].

5. STABILITY

5.1. Solid-state stability

FEX Form I was stable when stored for 1 month in open containers at 40 °C and 75% relative humidity, and at 65 °C.

The stability data obtained during the course of these studies for FEX and related impurities are shown in Table 4.10.

FEX is stable under normal storage conditions, but the substance should be stored in tight containers and protected from light and humidity. Photodegradation of FEX was studied using a stability indicating HPLC method. Degradation was performed in methanol and water, and analyzed by UV light at 254 nm. The kinetic parameters of order of reaction and the rate constants of degradation were determined for both the solvents. Degradation progress was described as second order kinetics under the experimental conditions [43]. Two new degradation products *viz.* isopropyl derivative and the benzophenone derivative of FEX were elucidated during the photodegradation study of FEX [7].

5.2. Solution-state stability

The pH stability profile for FEX was studied in buffered solutions (10 mM concentration adjusted to 0.15 M ionic strength with NaCl) in the pH range of 1–12 at 37 °C, and the percentage of original drug left after 24 h was determined. It was observed that no significant loss of potency of FEX occurred in the pH range 1–12.

5.3. Drug-excipient interactions

FEX Form I was separately mixed in 1:1 ratios with sodium carbonate, mannitol, magnesium stearate, colloidal anhydrous silica, povidone K90, crospovidone, and hydroxypropyl methyl cellulose. The blends were

TABLE 4.10   Solid-state stability of Form I of fexofenadine hydrochloride

Test required	Initial	40 °C/75% RH	65 °C
Assay (%)	100	100.5	99.5
Water content	0.15%	0.05%	0.05%

stored at 40 °C/75% relative humidity, and 65 °C for 30 days. In case of drug–sodium carbonate mixture at 40 °C/75% RH, a liquefaction tendency was observed, with reduction in enthalpy value (ΔH) of FEX peak at 200–205 °C in DSC, and a concomitant decrease in assay value. No evidence for instability was noted with other excipients, indicating their compatibility with FEX.

6. DRUG METABOLISM AND PHARMACOKINETICS

6.1. Absorption

FEX is rapidly absorbed following an oral administration of a single dose of two 60 mg capsules to healthy male volunteers with a mean time to plasma concentration occurring at 2.6 h post dose. After administration of a single dose of 60 mg as an oral solution to healthy subjects, the mean plasma concentration was observed to be 209 ng/ml. However, the mean maximum plasma concentration after single 60 mg capsule administration to healthy subjects was 131 ng/ml. Following single dose oral administrations of either the 60 or 180 mg tablet to healthy, adult male volunteers, mean maximum plasma concentrations were 142 and 494 ng/ml, respectively. FEX pharmacokinetics was linear for oral dose up to 120 mg twice daily. The pharmacokinetics of FEX in seasonal allergic rhinitis patients was similar to those in healthy subjects. Peak FEX plasma concentrations were similar between adolescent (12–16 years of age) and adult patients.

6.2. Distribution

FEX is 60%–70% bound to plasma proteins, primarily to the albumin and α_1-acid glycoprotein plasma proteins.

6.3. Metabolism

Only 5% of a dose is metabolized by intestinal mucosa, 0.5–1.5% undergoes hepatic biotransformation.

6.4. Elimination

The drug is mainly excreted in feces unchanged (80%) and 10% in urine. FEX is a metabolite of terfenadine and therefore has been detected in breast milk after administration of terfenadine. The drug does not cross the blood brain barrier. The mean elimination half-life of FEX was 14.4 h following administration of 60 mg, twice daily, in normal volunteers, that

may be prolonged in patients with renal impairment. Human mass balance studies documented a recovery of approximately 80% and 11% of the [^{14}C]FEX dose in the feces and urine, respectively. The absolute bioavailability of FEX has not been established, which makes it unclear whether the fecal component represents unabsorbed drug or the result of biliary excretion.

6.5. Toxicity

FEX usage may lead to a prolongation of QT interval, especially in elderly patients, leading to chances of arrhythmia. An abnormally long QT time was observed on the electrocardiogram (ECG) of a 67-year old man, who was taking 180 mg daily FEX. On stopping the FEX treatment, the QTc time was shortened. When the treatment was restarted, the QTc time was seen to increase again. After 11 days of continued treatment with FEX, the patient suffered tachycardia and fibrillation, and had to be defibrillated. Treatment with FEX was permanently stopped for decrease in QT time [44].

ACKNOWLEDGMENTS

REFERENCES

[1] A. C. Moffat, M. D. Osselton and B. Widdop (eds.), *Clarke's Analysis of Drugs and Poisons in Pharmaceuticals, Body Fluids and Postmortem Material*, 3rd edn., Pharmaceutical Press, London, UK, 2004, pp. 1033–1034.
[2] *Physicians' Desk Reference*, 61st edn., MDR Thomson, New Jersey, USA, 2007, pp. 2844–2851.
[3] S. C. Sweetman (ed.), *Martindale—The Complete Drug Reference*, 35th edn., Pharmaceutical Press, London, UK, 2007, p. 524.
[4] A. Markham and A. J. Wagstaff, *Drugs*, 1998, **55**, 269–274.
[5] FDA, Allegra®—Patient information, 2005.
[6] P. S. Borade, C. C. Bellary, G. P. Currie and D. K. C. Lee, Modern H$_1$ antihistamines in asthma, *Drug Discov. Today*, 2006, **3**, 253–259.
[7] A. R. Breier, N. S. Nudelman, M. Steppe and E. E. S. Schapoval, Isolation and structure elucidation of photodegradation products of fexofenadine, *J. Pharm. Biomed. Anal.*, 2008, **46**, 250–257.
[8] H. Lin, J. W. Yoo, H. J. Roh, M. K. Lee, S. J. Chung, C. K. Shim and D. D. Kim, Transport of anti-allergic drugs across the passage cultured human nasal epithelial cell monolayer, *Eur. J. Pharm. Sci.*, 2005, **26**, 203–210.

[9] M. Miura, T. Uno, T. Tateishi and T. Suzuki, Pharmacokinetics of fexofenadine enantiomers in healthy subjects, *Chirality*, 2007, **19**, 223–227.

[10] B. D. Giacomo, D. Coletta, B. N. Natalini, M. H. Ni and R. Pellicciari, A new synthesis of carboxyterfenadine (fexofenadine) and its bioisosteric tetrazole analogs, *Il Farmaco*, 1999, **54**, 600–610.

[11] USP29–NF24, United States Pharmacopeial Convention, Rockville, MD, USA, 2006, pp. 905–907.

[12] S. J. Rajput and P. R. Parekh, Spectrophotometric determination of fexofenadine hydrochloride in bulk drug and in its dosage form, *Eastern Pharmacist*, 2001, **44**, 101–103.

[13] K. S. Kumar, V. Ravichandran, M. R. M. K. Mohan and R. D. Thyagu, Spectrophotometric determination of fexofenadine hydrochloride, *Indian J. Pharm. Sci.*, 2006, **68**, 841–842.

[14] H. M. Saleh, M. M. El-Henawee, G. H. Ragab and S. S. A. El-Hay, Utility of NBD-Cl for the spectrophotometric determination of some skeletal muscle relaxant and antihistaminic drugs, *Spectrochim. Acta Part A*, 2007, **67**, 1284–1289.

[15] S. N. Meyyanathan, G. V. S. Ramasarma and B. Suresh, Analysis of simvastatin in pharmaceutical preparations by high performance liquid chromatography, *Ars. Pharm.*, 2004, **45**, 121–129.

[16] T. Radhakrishna and G. Om Reddy, Simultaneous determination of fexofenadine and its related compounds by HPLC, *J. Pharm. Biomed. Anal.*, 2002, **29**, 681–690.

[17] M. Gergov, I. Ojanpera and E. Vuori, Simultaneous screening for 238 drugs in blood by liquid chromatography-ionspray tandem mass spectrometry with multiple-reaction monitoring, *J. Chromatogr. B*, 2003, **795**, 41–53.

[18] A. A. Gazy, H. Mahgoub, F. A. El-Yazbi, M. A. El-Sayed and R. M. Youssef, Determination of some histamine H_1-receptor antagonists in dosage forms, *J. Pharm. Biomed. Anal.*, 2002, **30**, 859–867.

[19] S. S. Zarapkar, N. P. Bhandari and U. P. Halkar, Simultaneous determination of Fexofenadine Hydrochloride and Pseudoephedrine Sulfate in pharmaceutical dosage by reverse phase high performance liquid chromatography, *Indian Drugs*, 2000, **37**, 421–425.

[20] A. Golcu, B. Dogan and S. A. Ozkan, Anodic voltammetric behavior and determination of antihistaminic agent: Fexofenadine HCl, *Anal. Lett.*, 2005, **38**, 1913–1931.

[21] D. C. Oliveira, A. Weich and C. M. B. Rolim, Simple and reliable HPLC analysis of fexofenadine hydrochloride in tablets and its application to dissolution studies, *J. AOAC Int.*, 2007, **62**, 96–100.

[22] C. Rustichelli, M. C. Gamberini, V. Ferioli and G. Gamberini, Enantioselective analyses of antihistaminic drugs by high-performance liquid chromatography, *Chromatographia*, 2004, **60**, 99–103.

[23] K. Y. Chan, R. C. George, T. M. Chen and R. A. Okerholm, Direct enantiomeric separation of terfenadine and its major acid metabolite by high-performance liquid chromatography, and the lack of stereoselective terfenadine enantiomer biotransformation in man, *J. Chromatogr.*, 1991, **571**, 291–297.

[24] A. Sui-wei and L. Wei-kang, Establishment of analytical method to determine related substances for fexofenadine hydrochloride, *Guangdong Yaoxue*, 2005, **15**, 22–24.

[25] A. R. Breier, C. S. Paim, J. Menegola, M. Steppe and E. E. S. Schapoval, Development and validation of a liquid chromatographic method for fexofenadine hydrochloride in capsules, *J. AOAC Int.*, 2004, **87**, 1093–1097.

[26] W. Aiqin, L. Man, W. Zhaoyi, Z. Zhihao, L. Yi and L. Ying, HPLC determination of fexofenadine hydrochloride and related compounds in fexofenadine hydrochloride tablets, *Guangdong Yaoxueyuan Xuebao*, 2004, **20**, 478–479.

[27] L. Wang, T. Zhang and R. Jiang, Simultaneous determination of fexofenadine hydrochloride and pseudoephedrine hydrochloride in their sustained-release two-layer tablets by HPLC, *Shenyang Yaoke Daxue Xuebao*, 2003, **20**, 266–268, 271.

[28] M. N. Abbas, A. A. Abdel Fateh and E. Zahran, A novel membrane sensor for histamine H_1-receptor antagonist fexofenadine'' *Anal. Sci.*, 2004, **20**, 1137.

[29] T. A. Walker and G. L. Schmitt, Separation of fexofenadine, pseudoephedrine, potential impurities, and degradation products using ion interaction chromatography, *J. Liq. Chromatogr. Related Technol.*, 2006, **29**, 25–43.

[30] S. Emara, A. El-Gindy, M. K. Mesbah and G. M. Hadad, Direct injection liquid chromatographic technique for simultaneous determination of two antihistaminic drugs and their main metabolites in serum, *J. AOAC Int.*, 2007, **90**, 384–390.

[31] H. Mahgoub, A. A. Gazy, F. A. El-Yazbi, M. A. El-Sayed and R. M. Youssef, Spectrophotometric determination of binary mixtures of pseudoephedrine with some histamine H1-receptor antagonists using derivative ratio spectrum method, *J. Pharm. Biomed. Anal.*, 2003, **31**, 801–809.

[32] S. Karakus, I. Kucukguzel and S. G. Kucukguzel, Development and validation of a rapid RP-HPLC method for the determination of cetirizine or fexofenadine with pseudoephedrine in binary pharmaceutical dosage forms, *J. Pharm. Biomed. Anal.*, 2008, **46**, 295–302.

[33] R. M. Maggio, P. M. Castellano, S. E. Vignaduzzo and T. S. Kaufman, Alternative and improved method for the simultaneous determination of fexofenadine and pseudoephedrine in their combined tablet formulation, *J. Pharm. Biomed. Anal.*, 2007, **45**, 804–810.

[34] A. R. Breier, S. S. Garcia, A. Jablonski, M. Steppe and E. E. S. Schapoval, Capillary electrophoresis method for fexofenadine hydrochloride in capsules, *J. AOAC Int.*, 2005, **88**, 1059–1063.

[35] P. Mikuš, I. Valášková and E. Havránek, Determination of fexofenadine in tablets by capillary electrophoresis in free solution and in solution with cyclodextrins as analyte carriers, *Drug Dev. Ind. Pharm.*, 2005, **31**, 795–801.

[36] T. Uno, N. Yasui-Furukori, T. Takahata, K. Sugawara and T. Tateishi, Liquid chromatographic determination of fexofenadine in human plasma with fluorescence detection, *J. Pharm. Biomed. Anal.*, 2004, **35**, 937–942.

[37] M. Miura, T. Uno, T. Tateishi and T. Suzuki, Determination of fexofenadine enantiomers in human plasma with high-performance liquid chromatography, *J. Pharm. Biomed. Anal.*, 2007, **43**, 741–745.

[38] W. Naidong, W. Z. Shou, T. Addison and S. M. Xiangyu Jiang, Liquid chromatography/tandem mass spectrometric bioanalysis using normal-phase columns with aqueous/organic mobile phases - a novel approach of eliminating evaporation and reconstitution steps in 96-well SPE, *Rapid Commun. Mass Spectrom.*, 2002, **16**, 1965–1975.

[39] U. Hofmann, M. Seiler, S. Drescher and M. F. Fromm, Determination of fexofenadine in human plasma and urine by liquid chromatography-mass spectrometry, *J. Chromatogr. B Analyt. Technol. Biomed. Life Sci.*, 2002, **766**, 227–233.

[40] I. Fu, E. J. Woolf and B. K. Matuszewski, Determination of fexofenadine in human plasma using 96-well solid phase extraction and HPLC with tandem mass spectrometric detection, *J. Pharm. Biomed. Anal.*, 2004, **35**, 837–846.

[41] G. V. Ramenskaya, E. A. Skuridina and L. M. Krasnykh, Developing a method for the quantitative determination of the P-glycoprotein activity marker fexofenadine in blood plasma, *Pharm. Chem. J.*, 2006, **40**, 686–689.

[42] T. Guo-sheng, T. Le-sheng, W. Yi, T. Yun-biao, L. Lan-ying and G. Jing-kai, Rapid and sensitive lc-ms/ms method for quantification of fexofenadine in human plasma - application to a bioequivalence study in chinese volunteers, *Chem. Res. Chinese U.*, 2007, **23**, 514–517.

[43] A. R. Breier, M. Steppe and E. E. S. Schapoval, Photodegradation kinetics of fexofenadine hydrochloride using a lc method, *Chromatographia*, 2006, **64**, 725–729.

[44] Y. M. Pinto, I. C. van Gelder, M. Heeringa and H. J. Crijns, QT lengthening and life-threatening arrhythmias associated with fexofenadine, *Lancet*, 1999, **353**, 980.

Itraconazole: Comprehensive Profile

Abdullah A. Al-Badr and **Hussein I. El-Subbagh**

Department of Pharmaceutical Chemistry, College of Pharmacy, King Saud University, Riyadh 11451, Kingdom of Saudi Arabia

1. DESCRIPTION

1.1. Nomenclature

1.1.1. Systematic chemical name

(±)-1-[(*R**)-sec-Butyl]-4-[*p*-[4-[*p*-[[(2*S**, 4*R**)-2-(2,4-dichlorophenyl)-2-(1*H*-1,2,4-triazol-1-ylmethyl)-1,3-dioxolan-4-yl]methoxy]phenyl]-1-piperazinyl]-phenyl]-2–1,2,4-triazolin-5-one.

(±)-4-[4-[4-[4-[[2-(2,4-Dichlorophenyl)-2-(1*H*-1,2,4-triazol-1-yl-methyl)-1,3-dioxolan-4-yl]-methoxy]-phenyl]-1-piperazinyl]-phenyl]-2,4-dihydro-2-(1-methylpropyl)-3*H*-1,2,4-triazol-3-one.

(±)-1-*sec*-Butyl-4-[*p*-[4-[*p*-[[(2*R**,4*S**)-2-(2,4-dichlorophenyl)-2-(1*H*-1,2,4-tirazol-1-yl-methyl)-1,3-dioxolan-4-yl]-methoxy]-phenyl]-1-piperazinyl]-phenyl]Δ^2-1,2,4-triazolin-5-one.

(±)-2-*sec*-Butyl-4-[4-(4-[4[[2*R*(*), 4*S*(*)-2-(2,4-dichlorophenyl)-2-(1*H*-1,2,4,-triazol-1-yl-methyl)1,3-dioxolan-4-yl]-methoxy]-phenyl]-piperazin-1-yl)-phenyl]-2,4-dihydro-1,2,4-triazol-3-one.

(±)-2-*sec*-Butyl-4-[4-(4-{4-[[(2*R*,4*S*)-2-(2,4-dichlorophenyl)-2-(1*H*-1,2,4-triazol-1-ylmethyl)-1,3-dioxolan-4-yl]-methoxy]-phenyl}-piperazin-1-yl)-phenyl]2,4-dihydro-1,2,4-triazol-3-one.

3*H*-1,2,4-Triazol-3-one, (±)-4-[4-[4-[4-[[2-(2,4-dichlorophenyl)-2-(1*H*-1,2,4-triazol-1-ylmethyl)-1,3-dioxolan-4-yl]-methoxy]-phenyl]-1-piperazinyl]-phenyl]-2,4-dihydro-2-(1-methylpropyl).

4-[4-[4-[[*cis*-2-(2,4-Dichlorophenyl)-2-(1*H*-1,2,4-triazol-1-ylmethyl)-1,3-dioxolan-4-yl]methoxy]phenyl]piperazin-1-yl]phenyl]-2-(1*RS*)-1-methylpropyl]-2,4-dihydro-3*H*-1,2,4-triazol-3-one.

(±)-*cis*-4-[4-[4-[[2-(2,4-Dichlorophenyl)-2-(1*H*-1,2,4-triazol-1-yl-methyl)-1,3-dioxolan-4-yl]methoxy]phenyl]piperazin-1-yl]phenyl]-2,4-dihydro-2-(1-methylpropyl)-3*H*-1,2,4-triazol-3-one.

cis-2-*sec*-Butyl-4-{4-[4-(4-{[2-(2,4-dichlorophenyl)-2-(1*H*-1,2,4-triazol-1-ylmethyl)-1,3-dioxolan-4-yl]methoxy}phenyl)-1-piperazinyl]phenyl}-2,4-dihydro-3*H*-1,2,4-triazol-3-one [1–7].

1.1.2. Nonproprietary names

Itraconazolum, Itraconazol, Itraconazole, R-51211, Itrizole [1, 7].

1.1.3. Proprietary names

Canadiol, Carexan, Fulzoltec, Funit, Hongoseril, Isox, Itraflux, Itranax, Itraspor, Itrazol, Itrizole, Kanazol, Oriconazole, Orungal, Polantral, Salimidin, Sempera, Siros, Sporacid, Sporal, Sporanox, Sporex, Spozol, Traconal, Tranazol, Tirasporin, Trisporal, Zolken [1–7].

1.1.4. Synonyms

Oriconazole, R-51211.

1.2. Formula

1.2.1. Empirical formula, molecular weight, CAS number

$C_{35}H_{38}Cl_2N_8O_4$, 705.64, [84625-61-6] [1–3].

1.2.2. Structural formula
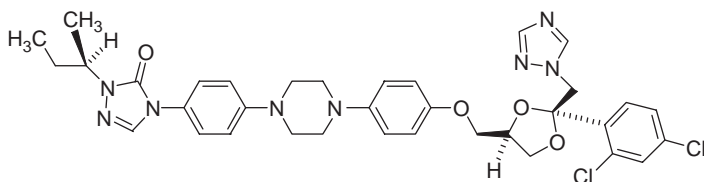
1.3. Elemental analysis

C, 59.57%; H, 5.43%, Cl, 10.05%, N, 15.88%, O, 9.07% [1].

1.4. Appearance

Crystals from toluene. White or almost white powder [2, 7].

2. PHYSICAL CHARACTERISTICS

2.1. Ionization constants

pK_a value $= 3.7$ [1, 3]

2.2. Solubility characteristics

Practically insoluble in water and dilute acidic solutions. Freely soluble in methylene chloride, sparingly soluble in tetrahydrofuran, very slightly soluble in alcohol [2, 7].

2.3. Partition coefficients

n-Octanol/aqueous buffer of pH 8.1 $= 5.66$ [1].

2.4. Crystallographic properties

2.4.1. X-ray powder diffraction pattern
The X-ray powder diffraction pattern of itraconazole was obtained using a Simmons XRD-5000 diffractometer, and the powder pattern is shown in Fig. 5.1. A summary of the crystallographic data deduced from the powder pattern of itraconazole is shown in Table 5.1.
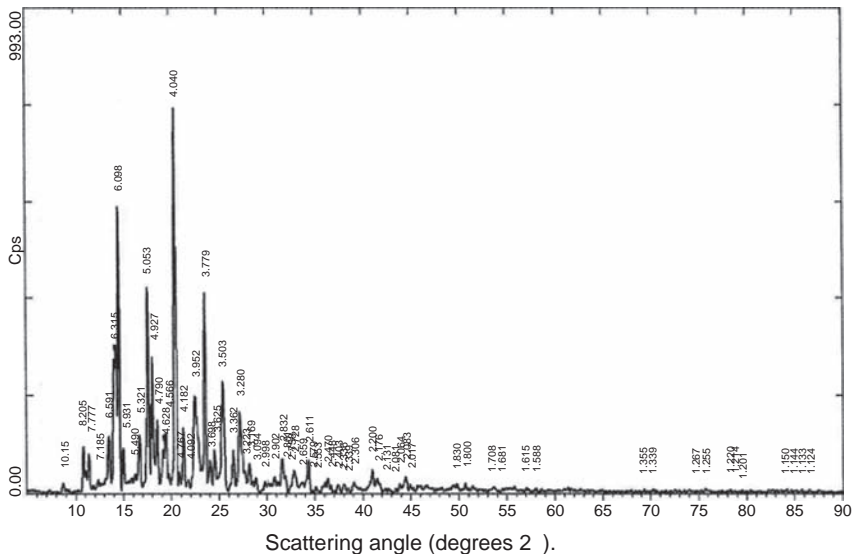

FIGURE 5.1   X-ray powder diffraction pattern of itraconazole.

TABLE 5.1   The X-ray powder diffraction pattern for itraconazole

Scattering angle 2θ	d-spacing (Å)	Relative intensity (%)	Scattering angle 2θ	d-spacing (Å)	Relative intensity (%)
8.702	10.1533	2.54	33.684	0.6586	2.71
10.773	8.2054	12.01	34.317	2.6110	8.41
11.369	7.7766	10.09	34.759	2.5788	0.62
12.309	7.1850	3.41	35.115	2.5534	1.46
13.424	6.5906	14.52	36.337	2.4704	3.65
14.011	6.3155	34.57	36.680	2.4480	1.87
14.514	6.0977	74.33	37.3.92	2.4030	2.07
14.925	5.9306	11.57	38.019	2.3648	2.32
16.131	5.4900	4.83	38.457	2.3389	1.17
16.636	5.3244	14.79	39.027	2.3060	2.73
17.536	5.0531	53.16	40.986	2.2002	5.83
17.987	4.9274	35.12	41.455	2.1764	3.55
18.507	4.7903	18.59	42.378	2.1311	1.06
19.160	4.6284	11.21	43.406	2.0830	1.09
19.426	4.5657	17.06	43.818	2.0643	2.31
20.420	4.3455	100.00	44.415	2.0380	3.99
20.800	4.2670	5.29	44.904	2.0169	2.13
21.226	4.1823	16.46	49.778	1.8303	2.29
21.699	4.0923	3.40	50.669	1.8001	2.54
22.481	3.9517	24.82	53.610	1.7081	1.42
23.520	3.7794	51.87	54.532	1.6814	1.11
24.047	3.6977	8.10	56.979	1.6149	1.30
24.540	3.6246	11.24	58.016	1.5884	1.10
25.406	3.5029	28.61	69.268	1.3553	0.90
26.487	3.3624	11.04	70.233	1.3391	0.93
27.163	3.2802	20.93	74.862	1.2673	0.60
27.653	3.2231	5.58	75.738	1.2548	1.08
28.134	3.1691	7.48	48.291	1.2202	0.78
28.833	3.0939	3.85	78.727	1.2145	0.50
29.774	2.9982	2.88	79.513	1.2045	0.68
30.788	2.9017	4.09	84.132	1.1497	0.95
31.569	2.8317	8.96	84.626	1.1442	0.66
31.920	2.8014	4.27	85.689	1.1327	0.79
32.440	2.7576	1.85	86.486	1.1243	0.79
32.801	2.7281	5.59			

2.4.2. Single crystal structure

Peeters *et al.* determined the molecular structure of itraconazole from single-structure X-ray diffraction data [8]. The two molecules in the asymmetric unit differ mainly in the conformation of the methoxyphenylpiperazine moiety. Apart from a 180° rotation of the triazole ring, the geometry of the dichlorophenylethoxytriazole moiety is almost the same as the dichlorophenylethoxyimidazole geometry found in miconazole, econazole, and ketoconazole. The crystal structure of itraconazole was determined for comparison with the structures of ketoconazole [9], miconazole [10], and econazole [11]. The asymmetric unit contains two molecules (**A** and **B**) partly related by a pseudo-inversion center at ∼0.25, 0.49, 0.25 (Fig. 5.2). The *sec*-butyl side chain is statistically disordered in both molecules implying that both the *R* and *S* configurations are present. The main difference between the two molecules is the orientation of the methoxy phenylpiperazine moiety. In molecule **A**, the methoxy group is almost perpendicular to the phenyl ring, whereas in molecule **B**, it is almost coplanar with the phenyl ring. As a consequence, the C70−O71−C72 and O71−C72−C77 angles are enlarged by ∼4°.

Each molecule contains seven rings of which the triazole and benzene rings are essentially planar with a maximum deviation of 0.014(5) Å. The dioxolane rings have conformations close to envelope, with the flap at atoms O11 and O61 [puckering parameters $q_2 = 0.326(4)$ and 0.350(5) Å, and $\Psi_2 = -41.4(8)$ and 134.3(8)° for molecules **A** and **B**, respectively]. The piperazine rings have chair conformations although that of molecule **B** is markedly flattened ($Q = 0.421(6)$ Å) with shorter bond lengths, enlarged internal angles and smaller torsion angles. All other bond lengths and angles agree within 3σ and are close to accepted values. There are no intermolecular contacts significantly shorter than the sum of the corresponding van der Waals radii. r.m.s fits [12] of the dichlorophenylethoxytriazole moiety of itraconazole with the dichlorophenylethoxyimidazole moiety of miconazole, econazole, and ketoconazole give r.m.s error values of 0.23, 0.12, and 0.14 Å, respectively. Apart from the 180° rotation of the triazole ring in itraconazole, the orientation of the nitrogen heterocycle is almost the same in the crystal structures of all four antifungal agents. This suggests that the differentiation in potency is not due to a different orientation of the nitrogen heterocycle.

Crystals of itraconazole were obtained from the Janssen Research Foundation, Beerse, Belgium. The density D_m was measured by flotation in aqueous potassium iodide solution.

Crystal data, data collection and refinement are shown in table 5.2, while Fractional atomic coordinates and equivalent isotropic displacement parameters are lisetd in table 5.3 and Geometric parameters are presented in table 5.4.

The *sec*-butyl moieties are statistically disordered. Both *R* and *S* configurations are present at the same location and were refined isotropically
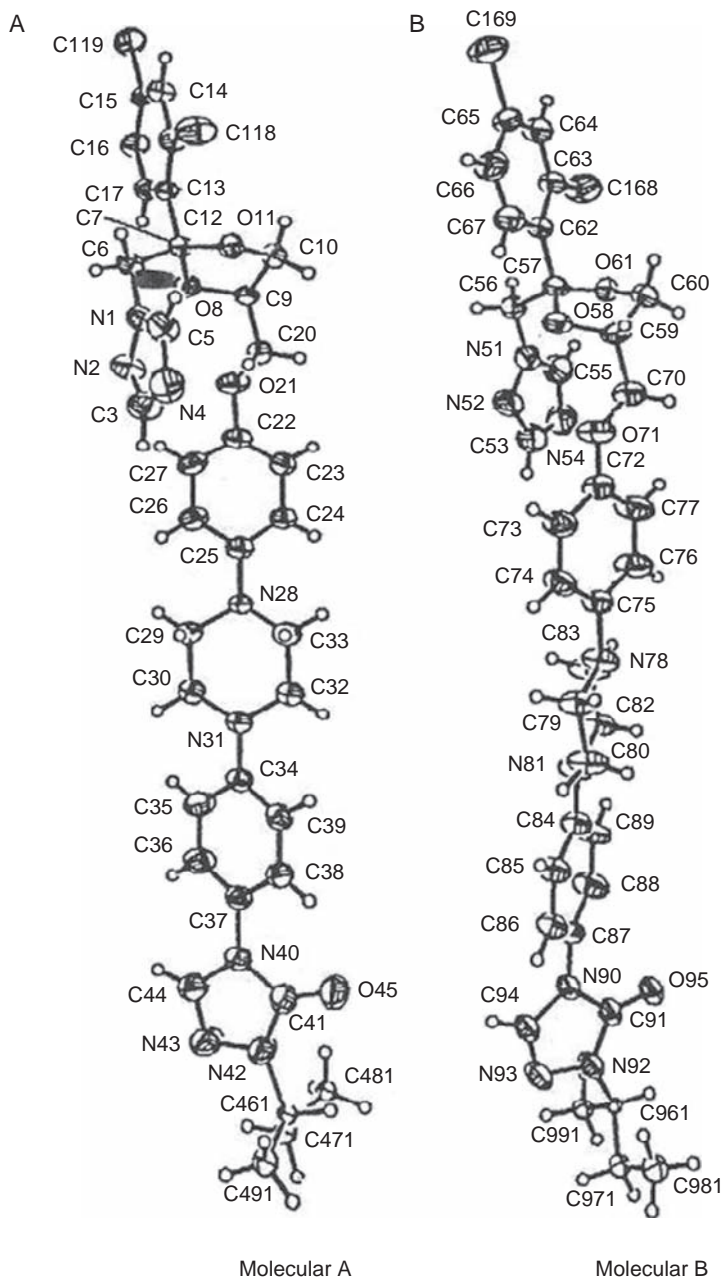
FIGURE 5.2   Perspective view of molecules **A** and **B** of itraconazole with the atomic numbering schemes. For clarity, only one configuration of the disordered *sec*-butyl moieties is shown in each case. Displacement ellipsoids are drawn at the 40% probability level [8].

with geometric restraints. The sum of the occupancy factors was con-strained to 1. The refined occupancy factors for atoms C461–C491 and C961–C991 are 0.43(1) and 0.68(1), respectively.

2.5. Thermal methods of analysis

2.5.1. Melting behavior
Itraconazole is observed to melt at 166.2 °C [1].

2.5.2. Differential scanning calorimetry
Differential scanning calorimetry (DSC) of itraconazole was performed using A Dupont TA-9900 thermal analyzer attached to Dupont Data unit. The data were obtained at a scan rate of 10 °C/min, over the range of 80–220 °C. The thermogram is shown in Fig. 5.3, where it may be observed that the compound melts at 169.60 °C.

2.6. Spectroscopy

2.6.1. UV–vis spectroscopy
The UV spectrum of itraconazole was recorded using Shimadzu model 1601-PC UV–vis spectrophotometer. Itraconazole was dissolved in meth-anol at a concentration of 20 μg/ml, and the ultraviolet spectrum was obtained. As shown in Fig. 5.4, the spectrum consisted of a one maximum at 264 nm characterized by $A_{1\%,\ 1cm} = 436.2$.
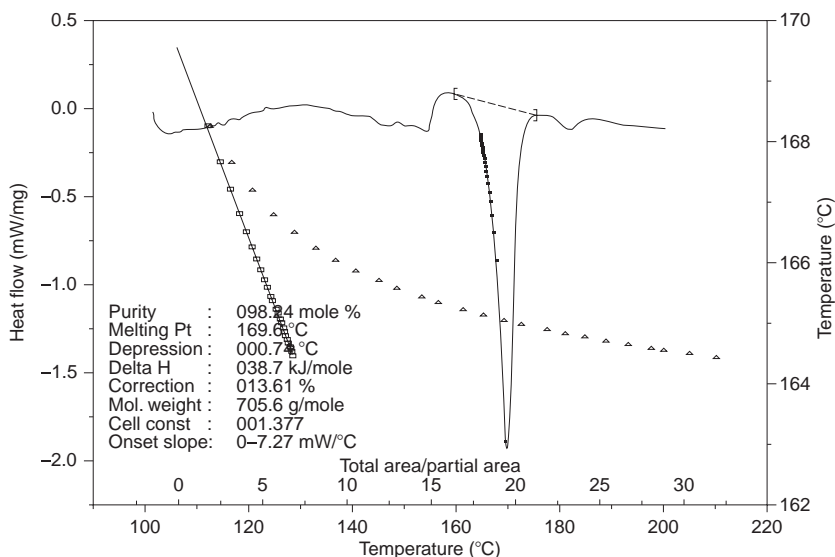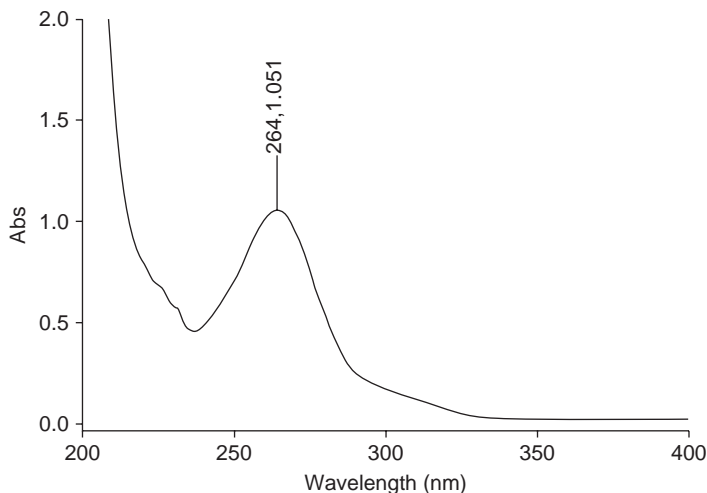

FIGURE 5.3   DSC thermogram of itraconazole.

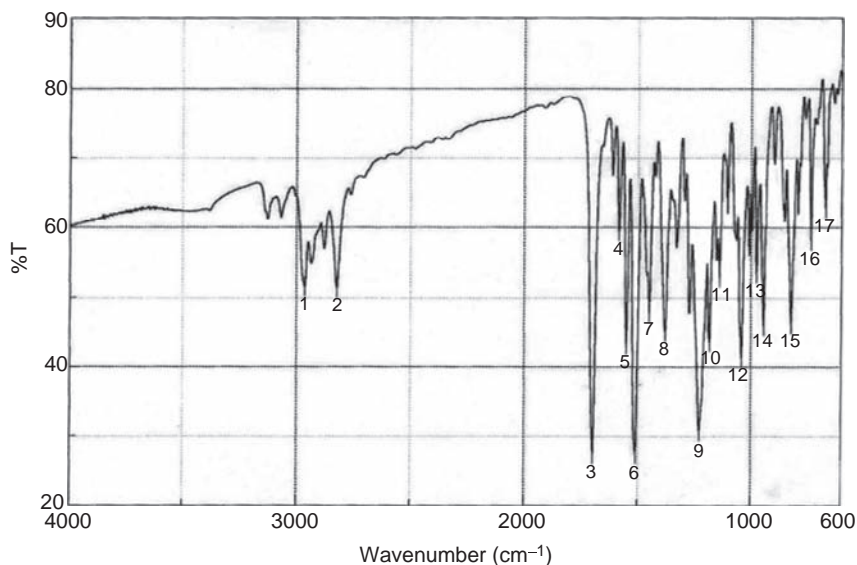**FIGURE 5.4**   Ultraviolet spectrum of itraconazole.

FIGURE 5.5   Infrared absorption spectrum of itraconazole (KBr pellet).

2.6.2. Vibrational spectroscopy

The infrared absorption spectrum of itraconazole was obtained using a Perkin–Elmer infrared spectrophotometer, with the substance being pressed in a KBr pellet. As shown in Fig. 5.5, the principle absorption bands were observed at 3130, 3068, 2964, 2823, 1698, 1585, 1551, 1510, 1451, 1381, 1228, 1184, 1139, 1043, 976, 944, 824, 736 cm^{-1}. The assignment of the infrared absorption bands are shown in Table 5.5.

TABLE 5.2 Crystal data, data collection and refinement [8]

Crystal data	Data collection	Refinement
$C_{35}H_{38}Cl_2N_8O_4$	Siemens *P4 four-circle*	Refinement on F^2
$M_r = 705.64$	diffractometer	$R(F) = 0.0594$
Triclinic	$\omega/2\theta$ scans	$wR(F^2) = 0.2000$
$P\bar{1}$	Absorption correction:	$S = 1.020$
$a = 8.6202$ (3) Å	empirical *via* ψ scans	9213 reflections
$b = 20.154$ (1) Å	(*XEMP*; Siemens,	886 parameters
$c = 21.0425$ (9) Å	1989) $T_{min} = 0.383$,	H-atom parameters not
$\alpha = 73.497$ (4)°	$T_{max} = 0.554$	refined
$\beta = 89.067$ (3)°	11 393 measured	$w = 1/[\sigma^2(F_o^2)$
$\gamma = 79.781$ (4)°	reflections	$+ (0.0777P)^2$
$V = 3447.3$ (3) Å^3	9215 independent	$+ 6.1836P]$
$Z = 4$	reflections	where $P = (F_0^2 + 2F_c^2)/3$
$D_x = 1.360$ Mg	5083 observed	$(\Delta/\sigma)_{max} = 0.001$
m^{-3}	reflections	$\Delta\rho_{max} = 0.44$ e Å^{-3}
$D_m = 1356$ Mg	$[I > 3.0\sigma(I)]$	$\Delta\rho_{min} = -0.43$ e Å^{-3}
m^{-3}	$R_{int} = 0.0286$	Extinction
Cu Kα radiation	$\theta_{max} = 57.06$ °	correction:
$\lambda = 1.54184$ Å	$h = -1 \rightarrow 9$	*SHELXL93*
Cell parameters	$k = -20 \rightarrow 20$	(Sheldrick, 1993)^a
from 40	$l = -22 \rightarrow 22$	Extinction coefficient:
reflections	3 standard reflections	0.00058 (9)
$\theta = 22$–56 °	monitored every	Atomic scattering
$\mu = 2.120$ mm^{-1}	100 reflections	factors from
$T = 293$ K	intensity decay:	*International Tables for*
Plate	17.0%	*X-ray Crystallography*
0.36 × 0.18 ×		(1974, Volume IV,
0.04 mm		Tables 2.2B,
Colorless		and 2.3.1).

^{a} G.M. Sheldrick (1993). *SHELXL 93*. Program for the refinement of crystal structures. University of Göttingen, Germany.

2.6.3. Nuclear magnetic resonance spectrometry

2.6.3.1. ^{1}H-NMR spectrum The ^{1}H-NMR spectrum of itraconazole dissolved in CDCl$_3$ is shown in Figs. 5.6–5.9. The aliphatic region of the ^{1}H-NMR spectrum showed two methyl absorptions, a triplet and a doublet, each integrated for three protons at δ 0.83 and δ 1.32 ppm, respectively. A doublet of multiplets resonate at δ 1.61–1.83 ppm integrated for two protons of a methylene group, all of the previous absorptions belong to the isobutyl residue of the structure, Fig. 5.7. Another set of doublet of multiplets resonate at δ 3.14–3.15 and 3.26–3.27 ppm, each integrated for four protons, a typical position for the piperazine moiety of the structure Fig. 5.8. A mutliplet extended from δ 3.41 to 3.45 ppm integrated for two
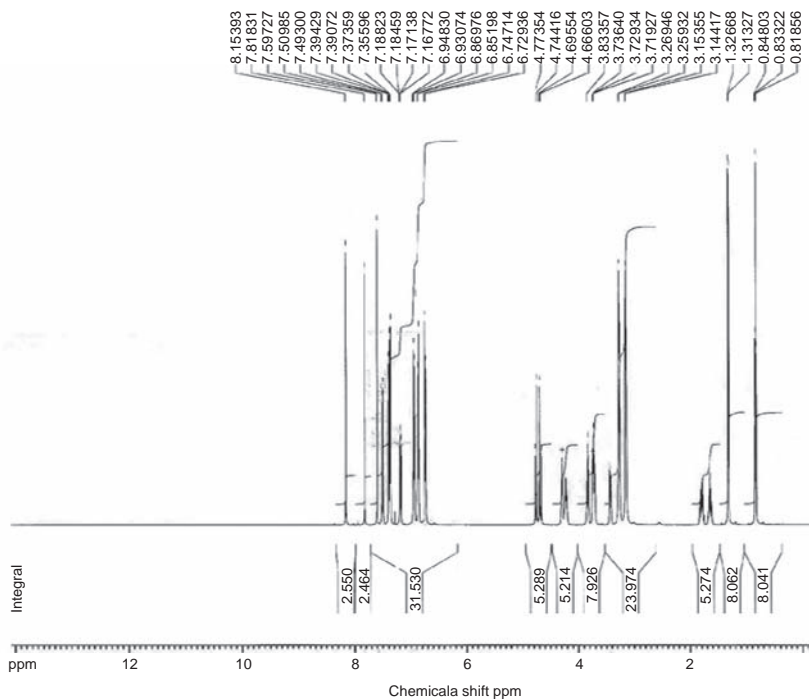
FIGURE 5.6 ¹H-NMR spectrum of itraconazole in CDCl₃.

protons, in addition to a multiplet at δ 3.70–3.85 ppm and another at δ 4.27–4.31 ppm integrated for two protons and one proton, respectively, represent the O–CH₂–CH–CH₂–O part of the dioxolan heterocyclic ring. The isobutyl methine showed a multiplet resonates at δ 4.20–4.24 ppm. The methylene bridge connecting the triazole and the dioxolan hetero-cycles showed an ABq at δ 4.67–4.77 ppm (Fig. 5.8).

The aromatic region of the ¹H spectrum (Fig. 5.9) showed two sets of ABq represent the 1,4-disubstituted aromatic patterns at δ 6.73–6.87 and δ 6.93–7.39 ppm each integrated for four protons. Two multiplets at δ 7.17–7.19 and δ 7.39–7.40, in addition to a doublet at δ 7.49–7.51 ppm each integrated for one proton represents the trisubstituted phenyl ring. Three singlets resonate at δ 7.60, 7.82, and 8.15 ppm represent the triazole ring protons. Confirmation of these assignments was derived from a two dimensional COSY experiment (Fig. 5.10). Table 5.6 shows a summary of the ¹H-NMR bands assignment of itraconazole.

2.6.3.2. ¹³C-NMR spectrum   The noise modulated broadband decoupled ¹³C-NMR spectrum of itraconazole is shown in Fig. 5.11. A total of 29 absorptions represent the 35 carbons of the structure which contain six symmetric carbons. A DEPT experiment (Figs. 5.12–5.14), identified two
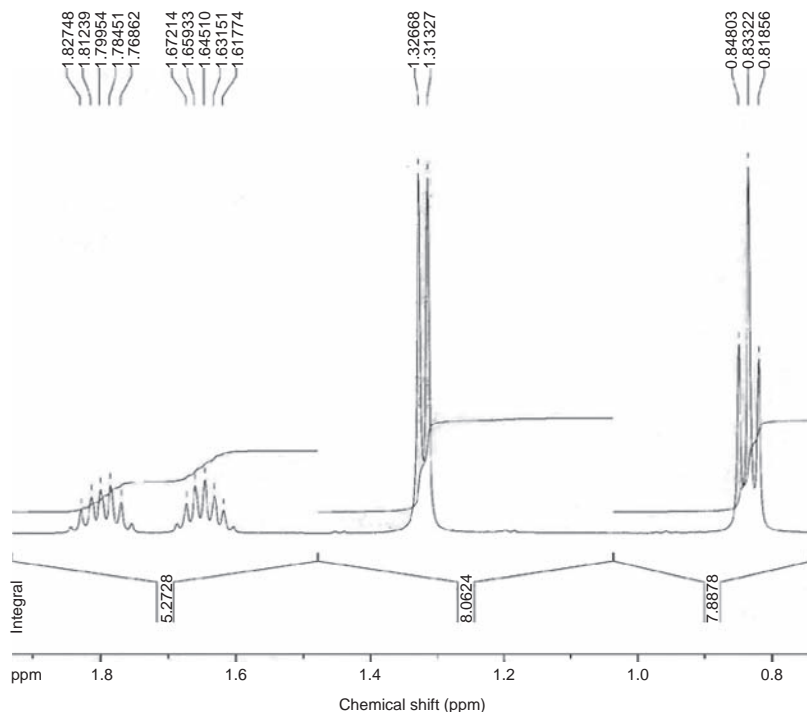
FIGURE 5.7   Expanded ^{1}H-NMR spectrum of itraconazole in CDCl$_3$.

methyl, six methylene, and twelve methine absorptions. Eight quaternary carbon signals could easily be detected by exclusion. Confirmation of these assignments was attained by a δ value gradient HMQC experiment (Fig. 5.15). Table 5.7 shows a summary of the ^{13}C bands assignment of itraconazole.

Inkmann and Holzgrabe [13] conducted a ^{1}H- and ^{13}C-NMR studies of the sites of protonation in itraconazole and fluconazole. The spectra were measured in neutral solution, and upon addition of varying amounts of deuterated hydrochloric acid. The comparison of the chemical shift in the different solutions revealed the high proton affinity on the piperazine nitrogen N26. Upon addition of a surplus of acid, the triazole ring was protonated. Corresponding observations were made for fluconazole.

2.6.3. Mass spectrometry

The detailed mass fragmentation pattern [14] is shown in Fig. 5.16, where a base peak was observed at $m/z = 392.3$. The molecular ion peak appeared at $m/z = 705$. The proposed mass fragmentation pattern of the drug is summarized in Table 5.8.
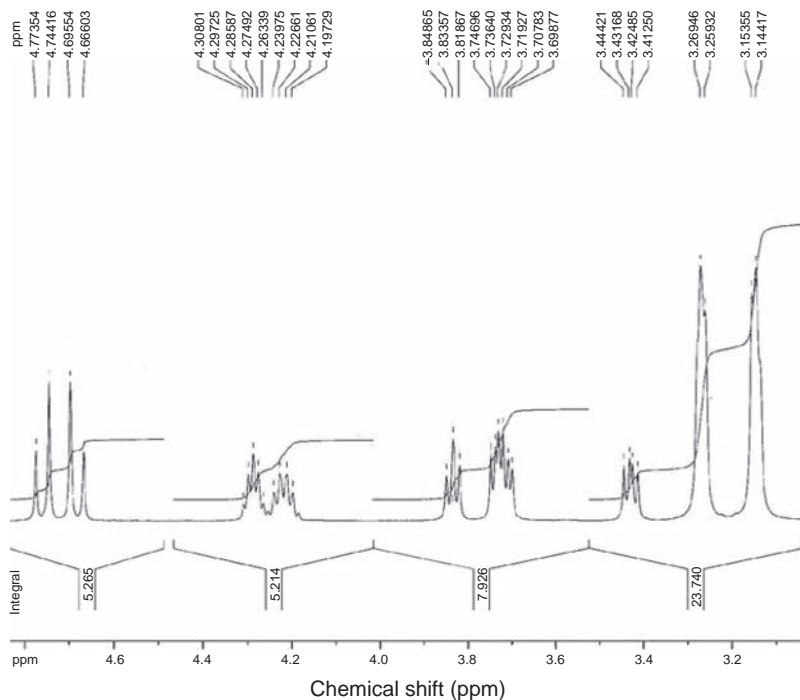
FIGURE 5.8   Expanded ^{1}H-NMR spectrum of itraconazole in CDCl$_3$.

3. USES AND APPLICATIONS

Itraconazle is an antifungal given by mouth for the treatment of aropharyngeal and vulvogaginal candidiasis, for pityriasis versicolor, for dermatophytosis unresponsive to topical treatment, for mychomycosis, and for systemic infections, including aspergillosis, blastomycosis, candidiasis, chromoblastomycosis, coccidioidomycosis, cryptococcosis, histoplasmosis, paracoccidioidomycosis, and sparotrichosis. It is also given for the prophylaxis of fungal infections in immunocompromised patients [15–17]. Itraconazole has been suggested for Acanthamoeba keratitis, when it is given orally in combination with topical miconazole, also itraconazole has been reported for the treatment of cutaneous leishmaniasis, but infections with leishmania aethiopica may not respond [18–21].

4. METHODS OF CHEMICAL SYNTHESIS

Heeres *et al.* [22–26] reported the synthetic method for the preparation of itraconazole as follows:
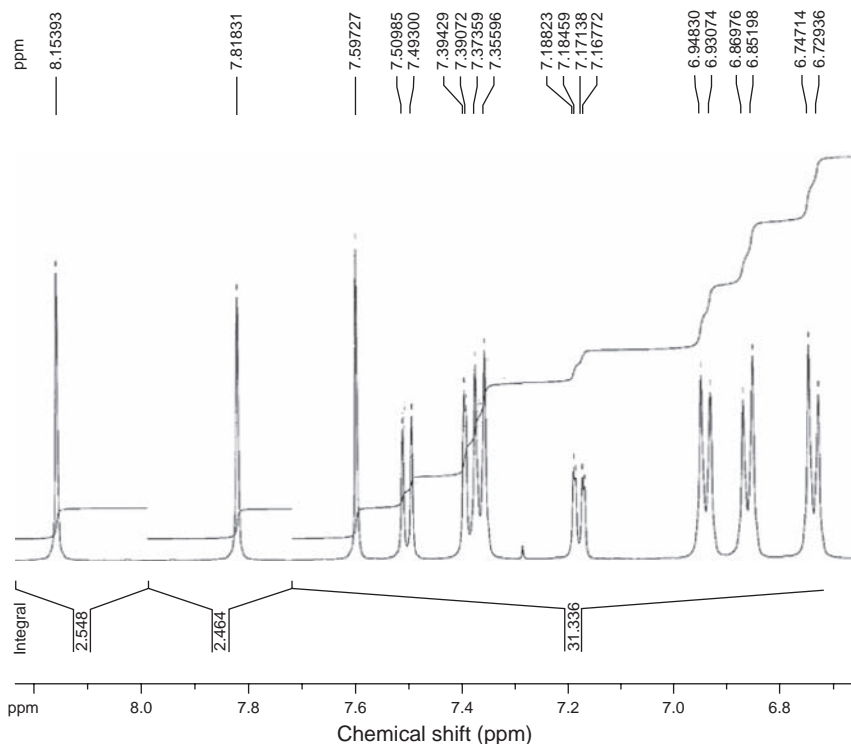
FIGURE 5.9 Expanded ^{1}H-NMR spectrum of itraconazole in CDCl$_3$.

Method A

Starting from 2,4-dichloroacetophenone **1**. Ketalization of **1** with glycerin was performed in a benzene/1-butanol medium with azeotropic removal of water in the presence of a catalytic amount of *p*-toluene sulphonic acid gives the ketal **2**. Without isolation, the ketal **2** was brominated at 30 °C to the bromoketal **3**. Benzoylation of **3** in pyridine affords the ester as a *cis/trans* mixture, from which the *cis* form **4** was isolated by crystallization from ethanol. The pure *trans* isomer was obtained by liquid chromatography of the mother liquor. The sodium salt of 1,2,4-triazole, generated *in situ* from 1,2,4-triazole and NaH dispersion (50%), in mineral oil is coupled with the bromomethyl ketal **4** in dimethyl sulphoxide at 130 °C to give a mixture of 1,2,4-triazole derivatives, which were saponified at reflux temperature with NaOH in dioxane–water to the alcohol **5**. Pure **5** was obtained after chromatography on silica gel. Alcohol **5** was converted to the corresponding methane sulphonate **6**. Compound **6** was allowed to interact with 1-*p*-hydroxyphenyl-4-acetyl piperazine **7** to yielded compound **8**. Compound **8** was deacylated at reflux temperature
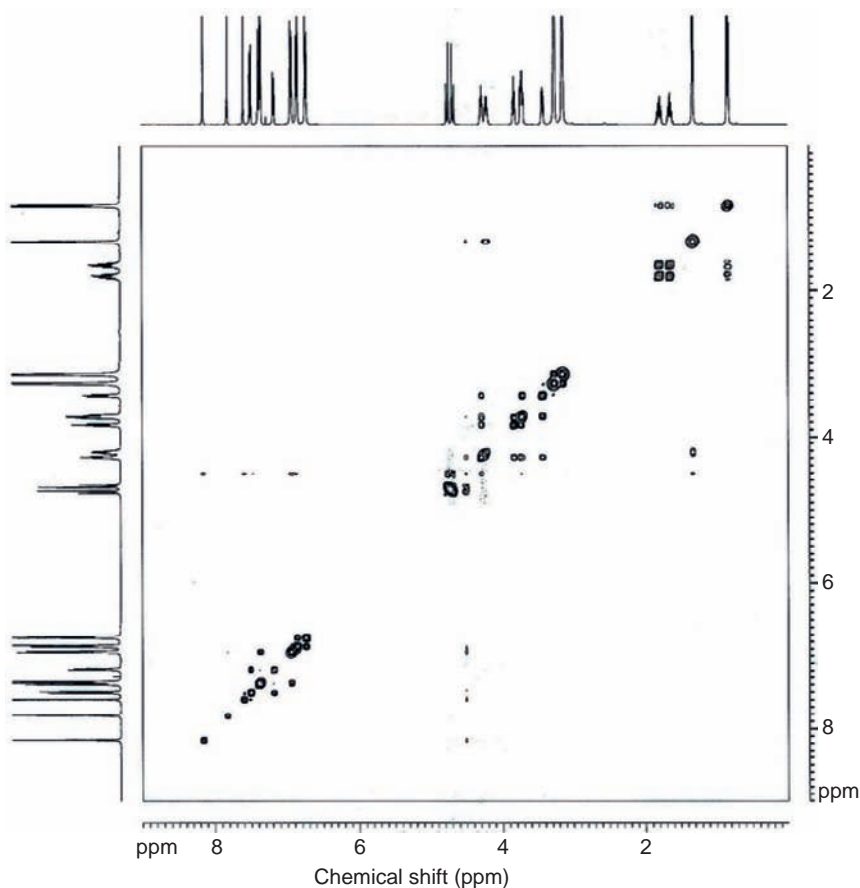
FIGURE 5.10   Expanded COSY ^{1}H-NMR spectrum of itraconazole in CDCl$_3$.

with NaOH in *n*-butanol to the piperazine **9**. Compound **9** was arylated with 1-chloro-4-nitrobenzene to the corresponding nitroaryl compound **10**. Catalytic reduction of compound **10** with 5% Pt/C afforded the anilino derivative **11** which was acylated with phenyl chloroformate to the phenyl carbamate **12**. Conversion of the carbamate **12** with hydrazine hydrate at reflux temperature yielded the semicarbazide **13** which was cyclized to the 1,2,4-triazole-3-one **14**. The alkylation of the triazole **14** with isobutyl bromide give the target compound, itraconazole **15**.

Method B

1-(4-Methoxyphenyl)-piperazine **16**, was reacted with 1-chloro-4-nitro-benzene to give the nitroaryl compound **17**. Catalytic reduction with 5% Pt/C afforded the aniline derivative **18**. The latter was acylated with phenylchloroformate to the phenyl carbamate **19**. This carbamate was

SCHEME 1   Method A:

SCHEME 1   (*continued*)

11

12

13

14

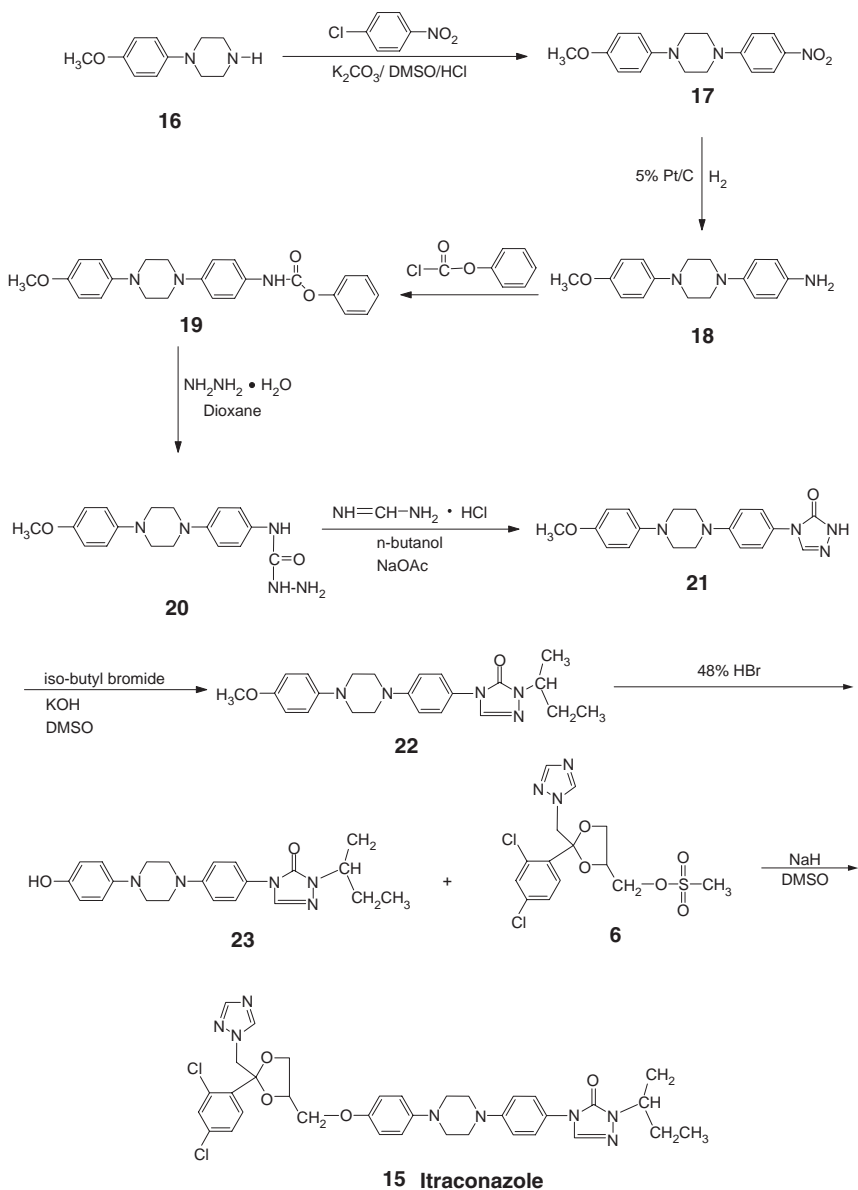**15   Itraconazole**

SCHEME 2   Method B:

15 Itraconazole
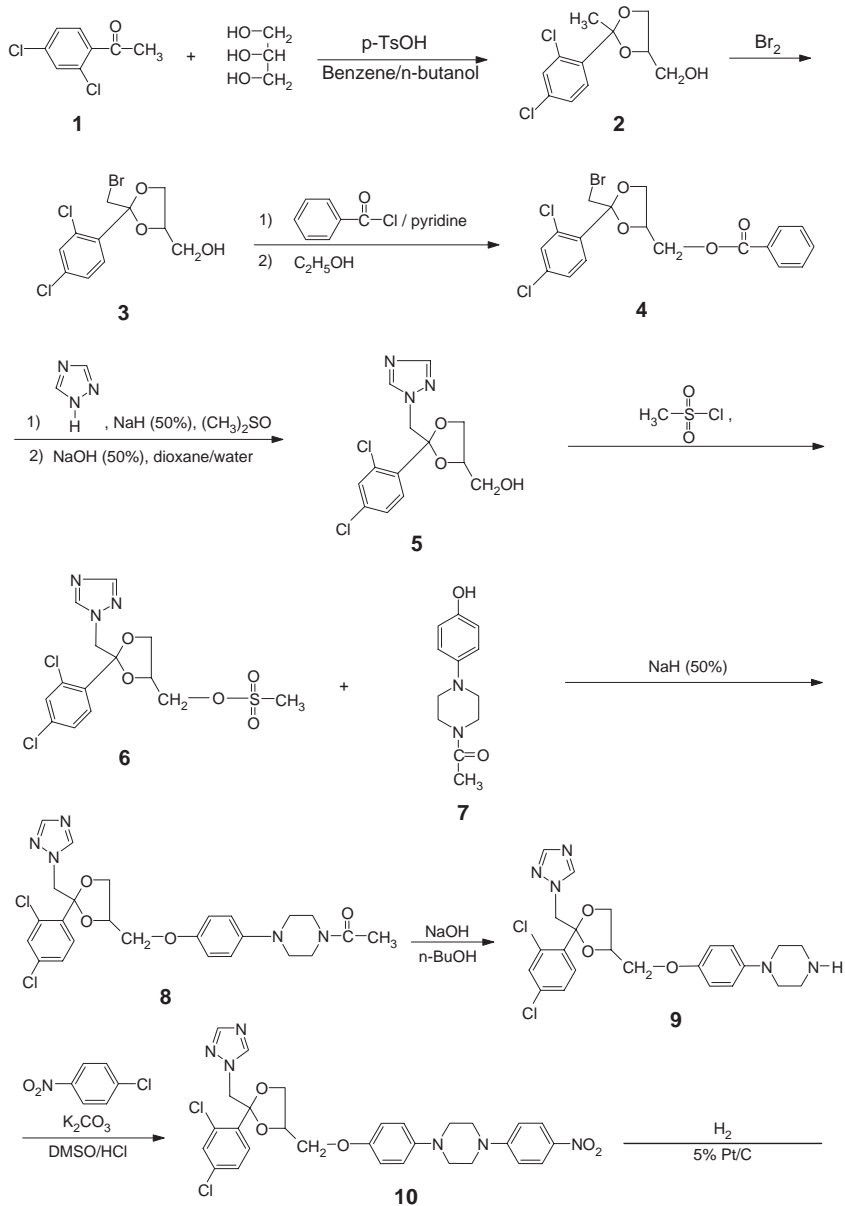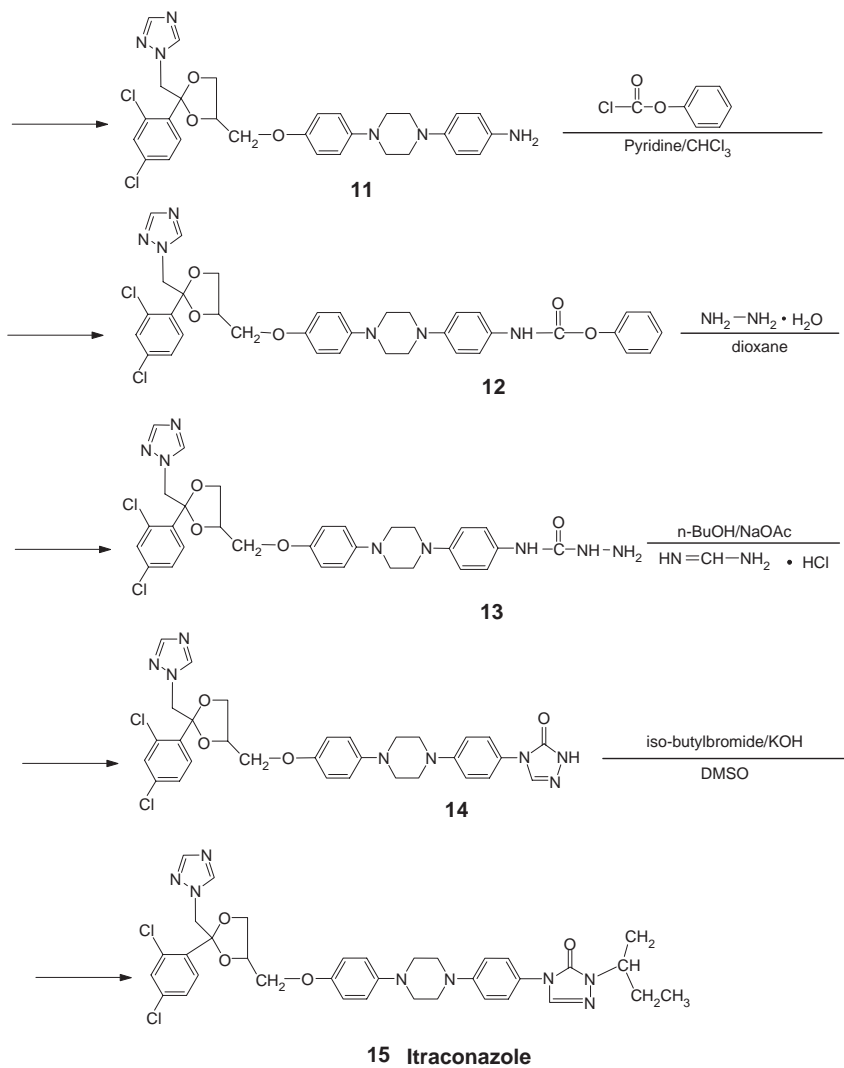
TABLE 5.3   Fractional atomic coordinates and equivalent isotropic displacement-parameters ($Å^2$) $U_{eq} = (I/3)\sum_i\sum_j U_{ij}a_i * a_j^* a_i.a_j$[8].

	X	Y	Z	U_{eq}
N1	0.2817 (5)	0.1063 (2)	0.3690 (2)	0.050 (2)
N2	0.3469 (5)	0.1625 (3)	0.3373 (2)	0.064 (2)
C3	0.4573 (7)	0.1600 (4)	0.3811 (4)	0.075 (3)
N4	0.4392 (6)	0.1075 (4)	0.4371 (3)	0.082 (3)
C5	0.3553 (7)	0.0746 (4)	0.4275 (3)	0.068 (3)
C6	0.1487 (5)	0.0880 (3)	0.3399 (3)	0.048 (2)
C7	−0.0103 (6)	0.1251 (2)	0.3572 (2)	0.040 (2)
O8	−0.0262 (4)	0.1984 (2)	0.3283 (2)	0.046 (1)
C9	−0.0933 (6)	0.2322 (3)	0.3770 (3)	0.046 (2)
C10	−0.1220 (6)	0.1719 (3)	0.4357 (3)	0.052 (2)
O11	−0.0145 (4)	0.1138 (2)	0.4256 (2)	0.045 (1)
C12	−0.1411 (6)	0.0965 (2)	0.3297 (2)	0.038 (2)
C13	−0.1869 (6)	0.0328 (3)	0.3613 (2)	0.046 (2)
C14	−0.3078 (6)	0.0103 (3)	0.3342 (3)	0.053 (2)
C15	−0.3804 (6)	0.0506 (3)	0.2752 (3)	0.048 (2)
C16	−0.3337 (6)	0.1126 (3)	0.2413 (3)	0.053 (2)
C17	−0.2158 (6)	0.1346 (3)	0.2691 (2)	0.048 (2)
C118	−0.0971 (2)	0.02376 (7)	0.43381 (7)	0.0711 (6)
C119	−0.5325 (2)	0.02357 (9)	0.24243 (8)	0.0764 (7)
C20	0.0202 (7)	0.2736 (3)	0.3945 (3)	0.054 (2)
O21	0.0413 (5)	0.3287 (2)	0.3370 (2)	0.062 (1)
C22	0.1620 (7)	0.3638 (3)	0.3465 (3)	0.053 (2)
C23	0.1348 (6)	0.4160 (3)	0.3784 (3)	0.052 (2)
C24	0.2532 (6)	0.4531 (3)	0.3816 (3)	0.053 (2)
C25	0.3991 (6)	0.4387 (3)	0.3549 (3)	0.049 (2)
C26	0.4230 (7)	0.3850 (3)	0.3249 (3)	0.069 (3)
C27	0.3042 (7)	0.3490 (3)	0.3201 (3)	0.064 (3)
N28	0.5129 (5)	0.4821 (2)	0.3553 (2)	0.048 (2)
C29	0.6531 (7)	0.4712 (3)	0.3176 (3)	0.067 (3)
C30	0.7419 (7)	0.5316 (3)	0.3087 (3)	0.065 (3)
N31	0.7843 (5)	0.5383 (2)	0.3726 (2)	0.051 (2)
C32	0.6447 (7)	0.5489 (3)	0.4104 (3)	0.063 (3)
C33	0.5524 (7)	0.4895 (3)	0.4185 (3)	0.062 (3)
C34	0.8977 (6)	0.5815 (3)	0.3730 (3)	0.048 (2)
C35	0.9610 (7)	0.6184 (3)	0.3152 (3)	0.064 (3)
C36	1.0796 (7)	0.6559 (3)	0.3184 (3)	0.063 (3)
C37	1.1378 (6)	0.6572(3)	0.3776 (3)	0.047 (2)
C38	1.0760 (6)	0.6206 (3)	0.4356 (3)	0.053 (2)

(continued)

TABLE 5.3 (*continued*)

	X	Y	Z	U_{eq}
C39	0.9574 (6)	0.5840 (3)	0.4324 (3)	0.051 (2)
N40	1.2604 (5)	0.6959 (2)	0.3794 (2)	0.052 (2)
C41	1.2974 (7)	0.7205 (3)	0.4316 (3)	0.064 (3)
N42	1.4146 (6)	0.7567 (3)	0.4074 (2)	0.080 (3)
N43	1.4502 (7)	0.7568 (3)	0.3438 (2)	0.086 (3)
C44	1.3574 (7)	0.7197 (3)	0.3287 (3)	0.068 (3)
O45	1.2403 (6)	0.7126 (3)	0.4858 (2)	0.088 (2)
C461[a]	1.532 (1)	0.7757 (6)	0.4481 (6)	0.048 (4)
C471[a]	1.527 (2)	0.8515 (7)	0.4109 (7)	0.072 (5)
C481[a]	1.356 (2)	0.8906 (8)	0.418 (1)	0.058 (5)
C491[a]	1.688 (2)	0.730 (1)	0.468 (1)	0.085 (6)
C462[a]	1.456 (1)	0.8131 (5)	0.4367 (5)	0.050 (3)
C472[a]	1.633 (1)	0.8094 (6)	0.4284 (6)	0.075 (4)
C482[a]	1.731 (2)	0.7400 (8)	0.4487 (8)	0.093 (5)
C492[a]	1.377 (2)	0.8881 (6)	0.3989 (8)	0.080 (5)
N51	0.2556 (6)	0.8512 (3)	0.1432 (2)	0.063 (2)
N52	0.1978 (6)	0.7929 (3)	0.1776 (3)	0.075 (3)
C53	0.0910 (8)	0.7899 (4)	0.1353 (4)	0.085 (3)
N54	0.0745 (7)	0.8409 (4)	0.0777 (3)	0.087 (3)
C55	0.1811 (8)	0.8783 (4)	0.0851 (3)	0.078 (3)
C56	0.3861 (6)	0.8731 (3)	0.1706 (3)	0.058 (2)
C57	0.5449 (6)	0.8412 (3)	0.1491 (3)	0.050 (2)
O58	0.5653 (4)	0.7668 (2)	0.1733 (2)	0.060 (2)
C59	0.6247 (7)	0.7384 (3)	0.1212 (3)	0.061 (3)
C60	0.6537 (7)	0.8019 (3)	0.0660 (3)	0.065 (3)
O61	0.5435 (4)	0.8573 (2)	0.0800 (2)	0.056 (2)
C62	0.6769 (6)	0.8676 (3)	0.1778 (3)	0.051 (2)
C63	0.7219 (7)	0.9316 (3)	0.1483 (3)	0.060 (3)
C64	0.8434 (7)	0.9522 (4)	0.1761 (3)	0.070 (3)
C65	0.9184 (7)	0.9098 (4)	0.2335 (3)	0.065 (3)
C66	0.8738 (7)	0.8464 (4)	0.2651 (3)	0.071 (3)
C67	0.7547 (7)	0.8255 (3)	0.2367 (3)	0.063 (2)
Cl68	0.6279 (2)	0.99237 (9)	0.07767 (9)	0.0938 (8)
Cl69	1.0712 (2)	0.9357 (1)	0.2670 (1)	0.104 (1)
C70	0.5038 (7)	0.7033 (3)	0.0979 (3)	0.065 (3)
O71	0.4723 (5)	0.6474 (2)	0.1530 (2)	0.073 (2)
C72	0.3502 (7)	0.6145 (3)	0.1441 (3)	0.060 (3)
C73	0.3085 (7)	0.5675 (3)	0.1991 (3)	0.067 (3)
C74	0.1891 (7)	0.5304 (3)	0.1949 (3)	0.068 (3)

(*continued*)

TABLE 5.3   (*continued*)

	X	Y	Z	U_{eq}
C75	0.1090 (7)	0.5412 (3)	0.1354 (3)	0.057 (2)
C76	0.1525 (8)	0.5893 (3)	0.0807 (3)	0.082 (3)
C77	0.2739 (8)	0.6257 (3)	0.0847 (3)	0.087 (3)
N78	−0.0098 (6)	0.5024 (2)	0.1283 (2)	0.9065 (2)
C79	−0.0096 (7)	0.4373 (3)	0.1778 (3)	0.065 (3)
C80	−0.1232 (7)	0.3959 (3)	0.1637 (3)	0.070 (3)
N81	−0.2768 (5)	0.4348 (2)	0.1421 (2)	0.064 (2)
C82	−0.2790 (7)	0.5017 (3)	0.0932 (3)	0.068 (3)
C83	−0.1620 (8)	0.5417 (3)	0.1076 (4)	0.082 (3)
C84	−0.3971 (6)	0.3974 (3)	0.1387 (3)	0.051 (2)
C85	−0.4003 (7)	0.3325 (3)	0.1856 (3)	0.057 (2)
C86	−0.5196 (6)	0.2957 (3)	0.1836 (3)	0.056 (2)
C87	−0.6382 (6)	0.3220 (3)	0.1361 (3)	0.049 (2)
C88	−0.6407 (7)	0.3861 (3)	0.0908 (3)	0.072 (3)
C89	−0.5202 (7)	0.4230 (3)	0.0924 (3)	0.074 (3)
N90	−0.7611 (5)	0.2826 (2)	0.1350 (2)	0.051 (2)
C91	−0.8193 (7)	0.2702 (3)	0.0791 (3)	0.055 (2)
N92	−0.9180 (6)	0.2246 (3)	0.1045 (2)	0.068 (2)
N93	−0.9247 (7)	0.2081 (3)	0.1730 (2)	0.076 (3)
C94	−0.8301 (7)	0.2437 (3)	0.1890 (3)	0.062 (3)
O95	−0.7890 (5)	0.2945 (2)	0.0215 (2)	0.071 (2)
C961[a]	−1.030 (1)	0.2007 (4)	0.0644 (4)	0.048 (3)
C971[a]	−0.996 (1)	0.1209 (5)	0.0923 (5)	0.070 (3)
C981[a]	−0.836 (2)	0.0881 (9)	0.085 (1)	0.100 (6)
C991[a]	−1.200 (1)	0.2298 (6)	0.0743 (6)	0.068 (3)
C962[a]	−0.949 (2)	0.1715 (8)	0.0694 (7)	0.041 (5)
C972[a]	−1.108 (2)	0.153 (1)	0.089 (1)	0.077 (7)
C982[a]	−1.237 (3)	0.216 (2)	0.068 (2)	0.18 (2)
C992[a]	−0.829 (4)	0.101 (2)	0.090 (3)	0.15 (2)

[a] Partial occupancies (see below).

treated with hydrazine hydrate at reflux temperature to yield the semi-carbazide **20**. This semicarbazide **20** was cyclized to the 1,2,4-triazole-3-one **21**. Alkylation of the triazole-3-one **21** with isobutyl bromide gives compound **22**. Treatment of this methoxy compound **22** with 48% HBr gives the corresponding phenol **23**. Reaction of compound **23** with the methane sulphonates **6** in the presence of NaH (50%) gives the target compound, itraconazole **15**.

TABLE 5.4 Geometric parameters (Å, °) [8].

N1–N2	1.353 (7)	N51–N52	1.365 (8)
N1–C5	1.326 (7)	N51–C55	1.315 (8)
N1–C6	1.458 (7)	N51–C56	1.461 (8)
N2–C3	1.320 (9)	N52–C53	1.31 (1)
C3–N4	1.333 (8)	C53–N54	1.339 (9)
N4–C5	1.33 (1)	N54–C55	1.32 (1)
C6–C7	1.531 (7)	C56–C57	1.524 (7)
C7–O8	1.411 (5)	C57–O58	1.420 (6)
C7–O11	1.392 (6)	C57–O61	1.398 (6)
C7–C12	1.543 (8)	C57–C62	1.536 (9)
O8–C9	1.444 (7)	O58–C59	1.424 (8)
C9–C10	1.518 (7)	C59–C60	1.520 (8)
C9–C20	1.507 (9)	C59–C70	1.52 (1)
C10–O11	1.423 (6)	C60–O61	1.428 (7)
C12–C13	1.390 (7)	C62–C63	1.384 (8)
C12–C17	1.387 (6)	C62–C67	1.390 (7)
C13–C14	1.395 (8)	C63–C64	1.39 (1)
C13–Cl18	1.722 (5)	C63–Cl68	1.737 (5)
C14–C15	1.366 (7)	C64–C65	1.360 (8)
C15–C16	1.377 (8)	C65–C66	1.38 (1)
C15–Cl19	1.729 (6)	C65–Cl69	1.729 (8)
C16–C17	1.378 (8)	C66–C67	1.38 (1)
C20–O21	1.426 (6)	C70–O71	1.430 (7)
O21–C22	1.404 (8)	O71–C72	1.381 (8)
C22–C23	1.384 (9)	C72–C73	1.360 (8)
C22–C27	1.358 (8)	C72–C77	1.363 (9)
C23–C24	1.382 (9)	C73–C74	1.39 (1)
C24–C25	1.386 (8)	C74–C75	1.382 (8)
C25–C26	1.384 (9)	C75–C76	1.373 (8)
C25–N28	1.427 (8)	C75–N78	1.427 (8)
C26–C27	1.38 (1)	C76–C77	1.40 (1)
N28–C29	1.452 (7)	N78–C79	1.425 (7)
N28–C33	1.434 (8)	N78–C83	1.411 (7)
C29–C30	1.52 (1)	C79–C80	1.479 (9)
C30–N31	1.447 (8)	C80–N81	1.423 (7)
N31–C32	1.449 (7)	N81–C82	1.442 (6)
N31–C34	1.421 (8)	N81–C84	1.400 (8)
C32–C33	1.521 (9)	C82–C83	1.48 (1)
C34–C35	1.392 (7)	C84–C85	1.401 (7)
C34–C39	1.377 (8)	C84–C89	1.376 (8)

(*continued*)

TABLE 5.4 (*continued*)

C35–C36	1.388 (9)	C85–C86	1.379 (9)
C36–C37	1.360 (8)	C86–C87	1.365 (7)
C37–C38	1.388 (7)	C87–C88	1.367 (7)
C37–N40	1.428 (8)	C87–N90	1.436 (8)
C38–C39	1.376 (8)	C88–C89	1.39 (1)
N40–C41	1.390 (9)	N90–C91	1.389 (8)
N40–C44	1.374 (7)	N90–C94	1.378 (7)
C41–N42	1.360 (9)	C91–N92	1.357 (8)
C41–O45	1.213 (8)	C91–O95	1.214 (6)
N42–N43	1.368 (7)	N92–N93	1.387 (6)
N42–C461	1.50 (1)	N92–C961	1.47 (1)
N42–C462	1.53 (1)	N92–C962	1.52 (2)
N43–C44	1.29 (1)	N93–C94	1.284 (9)
C461–C471	1.50 (2)	C961–C971	1.52 (1)
C461–C491	1.48 (2)	C961–C991	1.49 (1)
C471–C481	1.56 (2)	C971–C981	1.45 (2)
C462–C472	1.52 (1)	C962–C972	1.50 (2)
C462–C492	1.53 (1)	C962–C992	1.56 (3)
C472–C482	1.45 (2)	C972–C982	1.50 (4)
C5–N1–C6	128.5 (5)	N42–C461–C471	100.5 (9)
N2–N1–C6	121.8 (4)	C471–C461–C491	118 (1)
N2–N1–C5	109.6 (5)	C461–C471–C481	106 (1)
N1–N2–C3	101.5 (5)	N42–C462–C492	113.4 (9)
N2–C3–N4	116.4 (6)	N42–C462–C472	104.9 (8)
C3–N4–C5	101.6 (6)	C472–C462–C492	106.8 (9)
N1–C5–N4	110.9 (5)	C462–C472–C482	117 (1)
N1–C6–C7	112.4 (4)	C55–N51–C56	129.4 (5)
C6–C7–C12	107.4 (4)	N52–N51–C56	121.0 (5)
C6–C7–O11	109.3 (4)	N52–N51–C55	109.5 (5)
C6–C7–O8	109.7 (4)	N51–N52–C53	101.7 (5)
O11–C7–C12	112.9 (4)	N52–C53–N54	115.8 (6)
O8–C7–C12	110.4 (4)	C53–N54–C55	102.1 (6)
O8–C7–O11	106.8 (4)	N51–C55–N54	111.0 (6)
C7–O8–C9	107.4 (3)	N51–C56–C57	111.6 (5)
O8–C9–C20	109.9 (4)	C56–C57–C62	109.2 (4)
O8–C9–C10	104.4 (4)	C56–C57–O61	109.3 (4)
C10–C9–C20	112.2 (4)	C56–C57–O58	108.9 (4)
C9–C10–O11	102.3 (4)	O61–C57–C62	113.2 (4)
C7–O11–C10	106.1 (3)	O58–C57–C62	110.0 (4)
C7–C12–C17	119.2 (4)	O58–C57–O61	106.2 (4)

(*continued*)

TABLE 5.4   (*continued*)

C7–C12–C13	123.8 (4)	C57–O58–C59	108.0 (4)
C13–C12–C17	117.0 (4)	O58–C59–C70	110.7 (5)
C12–C13–C118	122.9 (4)	O58–C59–C60	104.3 (5)
C12–C13–C14	121.0 (5)	C60–C59–C70	110.1 (5)
C14–C13–C118	116.1 (4)	C59–C60–O61	101.8 (5)
C13–C14–C15	119.8 (5)	C57–O61–C60	105.2 (4)
C14–C15–C119	119.8 (4)	C57–C62–C67	118.7 (5)
C14–C15–C16	120.7 (5)	C57–C62–C63	123.3 (5)
C16–C15–C119	119.5 (4)	C63–C62–C67	118.0 (5)
C15–C16–C17	118.8 (5)	C62–C63–C168	123.5 (4)
C12–C17–C16	122.6 (5)	C62–C63–C64	120.7 (6)
C9–C20–O21	108.7 (4)	C64–C63–C168	115.7 (5)
C20–O21–C22	112.3 (4)	C63–C64–C65	120.0 (6)
O21–C22–C27	118.7 (5)	C64–C65–C169	119.5 (5)
O21–C22–C23	121.1 (5)	C64–C65–C66	120.7 (6)
C23–C22–C27	120.1 (5)	C66–C65–C169	119.8 (5)
C22–C23–C24	118.9 (5)	C65–C66–C67	119.1 (6)
C23–C24–C25	121.8 (5)	C62–C67–C66	121.4 (6)
C24–C25–N28	119.4 (5)	C59–C70–O71	107.5 (5)
C24–C25–C26	117.5 (5)	C70–O71–C72	116.4 (4)
C26–C25–N28	122.9 (5)	O71–C72–C77	124.3 (5)
C25–C26–C27	120.9 (6)	O71–C72–C73	116.0 (5)
C22–C27–C26	120.7 (6)	C73–C72–C77	119.8 (6)
C25–N28–C33	116.3 (4)	C72–C73–C74	120.3 (5)
C25–N28–C29	116.6 (4)	C73–C74–C75	121.0 (6)
C29–N28–C33	111.1 (4)	C74–C75–N78	122.9 (5)
N28–C29–C30	110.2 (5)	C74–C75–C76	117.6 (6)
C29–C30–N31	110.4 (5)	C76–C75–N78	119.5 (5)
C30–N31–C34	116.6 (4)	C75–C76–C77	121.4 (6)
C30–N31–C32	110.5 (4)	C72–C77–C76	119.9 (6)
C32–N31–C34	116.6 (4)	C75–N78–C83	116.6 (5)
N31–C32–C33	111.0 (5)	C75–N78–C79	116.7 (5)
N28–C33–C32	110.9 (4)	C79–N78–C83	113.9 (5)
N31–C34–C39	119.9 (5)	N78–C79–C80	114.1 (5)
N31–C34–C35	122.6 (5)	C79–C80–N81	115.1 (5)
C35–C34–C39	117.3 (5)	C80–N81–C84	118.1 (5)
C34–C35–C36	120.5 (5)	C80–N81–C82	114.5 (5)
C35–C36–C37	121.2 (5)	C82–N81–C84	118.3 (5)
C36–C37–N40	119.9 (5)	N81–C82–C83	113.7 (5)
C36–C37–C38	119.0 (5)	N78–C83–C82	115.8 (5)

TABLE 5.4 (*continued*)

C38–C37–N40	121.0 (4)	N81–C84–C89	122.8 (5)
C37–C38–C39	119.7 (5)	N81–C84–C85	120.2 (5)
C34–C39–C38	122.2 (5)	C85–C84–C89	116.9 (5)
C37–N40–C44	126.8 (4)	C84–C85–C86	120.9 (5)
C37–N40–C41	126.1 (4)	C85–C86–C87	120.6 (5)
C41–N40–C44	107.0 (5)	C86–C87–N90	119.6 (5)
N40–C41–O45	129.5 (6)	C86–C87–C88	119.9 (5)
N40–C41–N42	103.0 (5)	C88–C87–N90	120.5 (5)
N42–C41–O45	127.5 (6)	C87–C88–C89	119.6 (6)
C41–N42–C461	125.8 (6)	C84–C89–C88	122.1 (6)
C41–N42–C462	121.9 (6)	C87–N90–C94	126.9 (4)
C41–N42–N43	113.1 (5)	C87–N90–C91	125.6 (4)
N43–N42–C461	118.4 (6)	C91–N90–C94	107.1 (4)
N43–N42–C462	121.3 (6)	N90–C91–O95	128.3 (5)
N42–N43–C44	104.4 (5)	N90–C91–N92	103.1 (4)
N40–C44–N43	112.5 (5)	N92–C91–O95	128.6 (5)
N42–C461–C491	121.0 (1)	C91–N92–C961	127.4 (5)
C91–N92–C962	120.8 (7)	N92–C961–C971	105.3 (6)
C91–N92–N93	113.2 (5)	C971–C961–C991	111.7 (8)
N93–N92–C961	118.8 (5)	C961–C971–C981	115.2 (9)
N93–N92–C962	119.6 (7)	N92–C962–C992	114 (2)
N92–N93–C94	103.8 (4)	N92–C962–C972	108 (1)
N90–C94–N93	112.8 (4)	C972–C962–C992	106 (2)
N92–C961–C991	114.6 (7)	C962–C972–C982	112 (2)
N2–N1–C6–C7	−88.5 (6)	N52–N51–C56–C57	91.8 (6)
N1–C6–C7–O8	65.2 (5)	N51–C56–C57–O58	−61.3 (6)
N1–C6–C7–O11	−51.6 (5)	N51–C56–C57–O61	54.2 (6)
N1–C6–C7–C12	−174.6 (4)	N51–C56–C57–C62	178.5 (4)
C6–C7–C12–C13	80.3 (6)	C56–C57–C62–C63	−83.1 (6)
O8–C9–C20–O21	64.0 (5)	O58–C59–C70–O71	−60.9 (6)
C9–C20–O21–C22	−171.7 (4)	C59–C70–O71–C72	172.2 (5)
C20–O21–C22–C27	102.7 (6)	C70–O71–C72–C77	8.8 (8)
C36–C37–N40–C41	158.5 (6)	C86–C87–N90–C91	−133.9 (6)

5. METHODS OF ANALYSIS

5.1. Compendial methods

5.1.1. European pharmacopoeia [7]

Itraconazole contains not less than 98.5% and not more than the equivalent of 101.5% of 4-[4-[4-[4-[[*cis*-2-(2,4-dichlorophenyl)-2-(1*H*-1,2,4-triazol-1-ylmethyl)-1,3-dioxolan-4-yl]methoxy]phenyl]piperazin-1-yl]phenyl]-2-

TABLE 5.5   Assignment of the infrared characteristic bands of itraconazole.

Frequency (cm^{-1})	Assignment
3130, 3068	Aromatic C—H stretching
2964, 2823	Aliphatic C—H stretching
1698	C=O stretching
1585, 1551	C=N stretching
1510, 1451, 1381	Aromatic C=C stretching
1228, 1183, 1139	C—O and C—N stretching
1043	Aromatic C—Cl stretching
976, 944, 824, 736	C—H bending
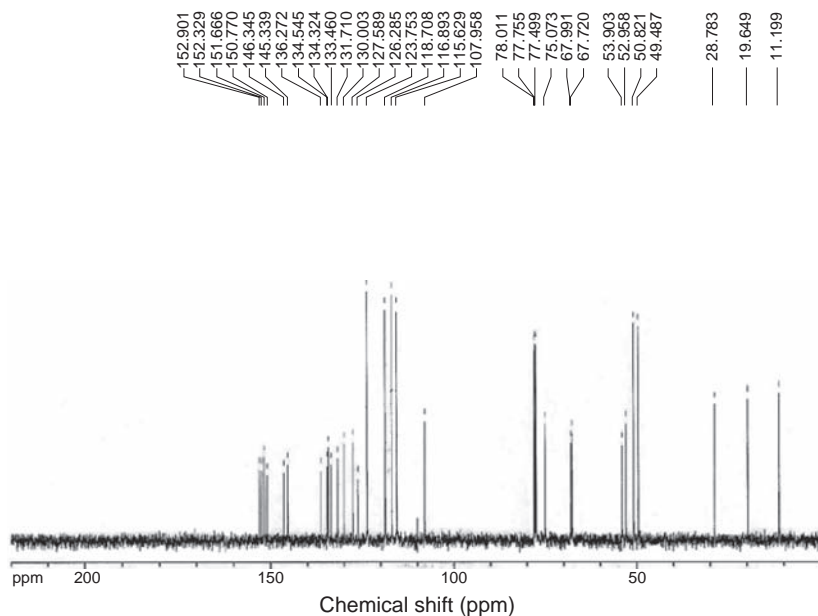
FIGURE 5.11 ^{13}C-NMR spectrum of itraconazole in CDCl₃.

[(1*RS*)-methylpropyl]-2,4-dihydro-3*H*-1,2,4-triazol-3-one, calculated with reference to the dried substance.

Identification

Test 1. When tested according to the general procedure (2.2.14); itraconazole melts at 166–170 °C.

Test 2. Examine itraconazole by infrared spectrophotometry according to the general procedure (2.2.24), comparing with the spectrum obtained with *itraconazole CRS*. Examine the substance prepared as discs.
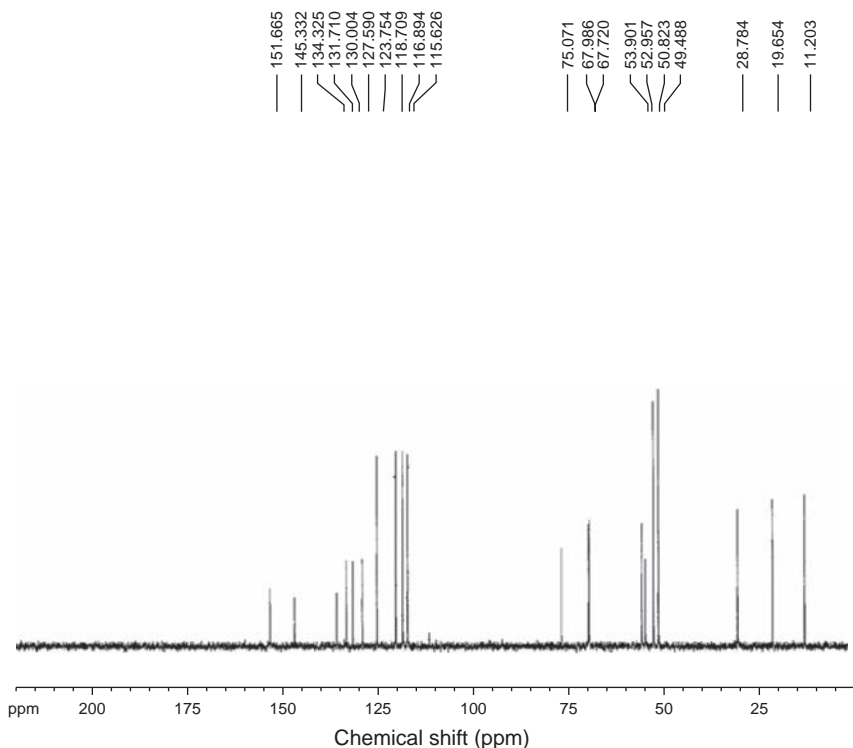
FIGURE 5.12   DEPT 45 ^{13}C-NMR spectrum of itraconazole in CDCl$_3$.

Test 3. Examine itraconazole by thin-layer chromatography according to the general procedure (2.2.27), using a suitable octadecylsilyl silica gel as the coating substance:

Test solution: Dissolve 30 mg of itraconazole in a mixture of equal volumes of methanol R and methylene chloride R and dilute to 5 ml with the same mixture of solvents.

Reference solution (a): Dissolve 30 mg of itraconazole CRS in a mixture of equal volumes of methanol R and methylene chloride R and dilute to 5 ml with the same mixture of solvents.

Reference solution (b): Dissolve 30 mg of itraconazole CRS and 30 mg of ketoconazole CRS in a mixture of equal volumes of methanol R and methylene chloride R and dilute to 5 ml with the same mixture of solvents.

Apply to the plate 5 µl of each solution. Develop in an unsaturated tank over a path of 10 cm using a mixture of 20 volumes of ammonium acetate solution R, 40 volumes of dioxan R and 40 volumes of methanol R. Dry the plates in a current of warm air for 15 min and expose it to iodine vapor until spots appear. Examine in daylight. The principal spot in the
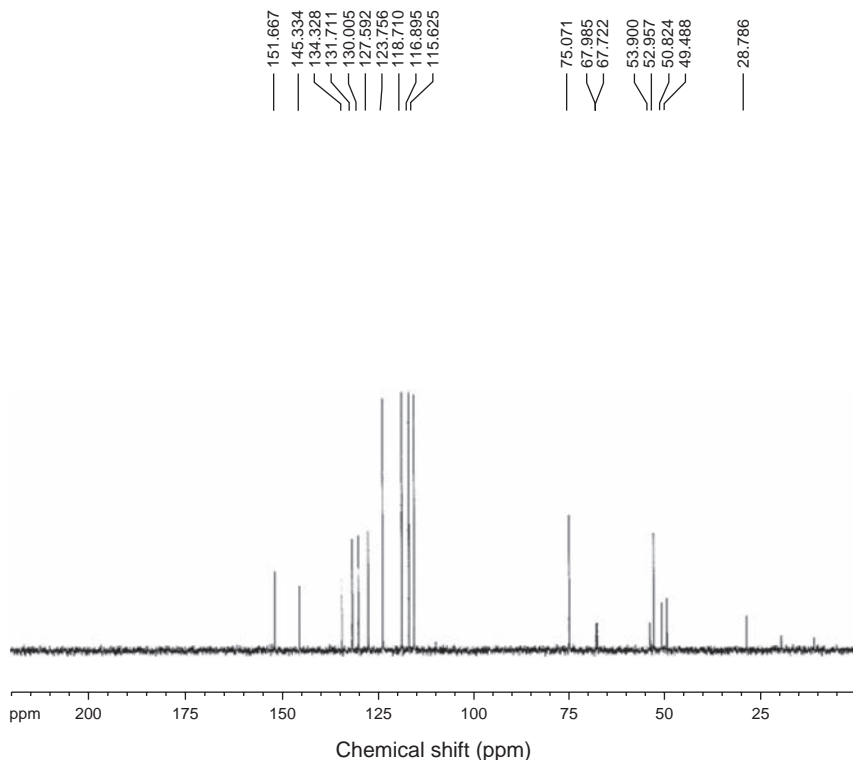
FIGURE 5.13   DEPT 90 ^{13}C-NMR spectrum of itraconazole in CDCl$_3$.

chromatogram obtained with the test solution is similar in position, color, and size to the principal spot in the chromatogram obtained with reference solution (a). The test is not valid unless the chromatogram obtained with reference solution (b) shows two clearly separated spots.

Test 4. To 30 mg of itraconazole in a porcelain crucible add 0.3 g of anhydrous sodium carbonate R. Heat over an open flame for 10 min. Allow to cool. Take up the residue with 5 ml of dilute nitric acid R and filter. To 1 ml of the filtrate add 1 ml of water R. The solution gives reaction (a) of chloride as in the general procedure (2.3.1).

Tests

Solution S. Dissolve 2 g of itraconazole in methylene chloride R and dilute to 20 ml of the same solvent.

Appearance of solution. Solution S, according to the general procedure (2.2.1), is clear and not intensely colored than reference solution BY$_6$ according to the general procedure (2.2.2, Method II).

151.667
145.333
134.327
131.710
130.004
127.591
123.755
118.709
116.894
115.623

67.984
67.720
53.899
52.955
50.823
49.488

28.785
19.656
11.205

ppm   200   175   150   125   100   75   50   25

Chemical shift (ppm)
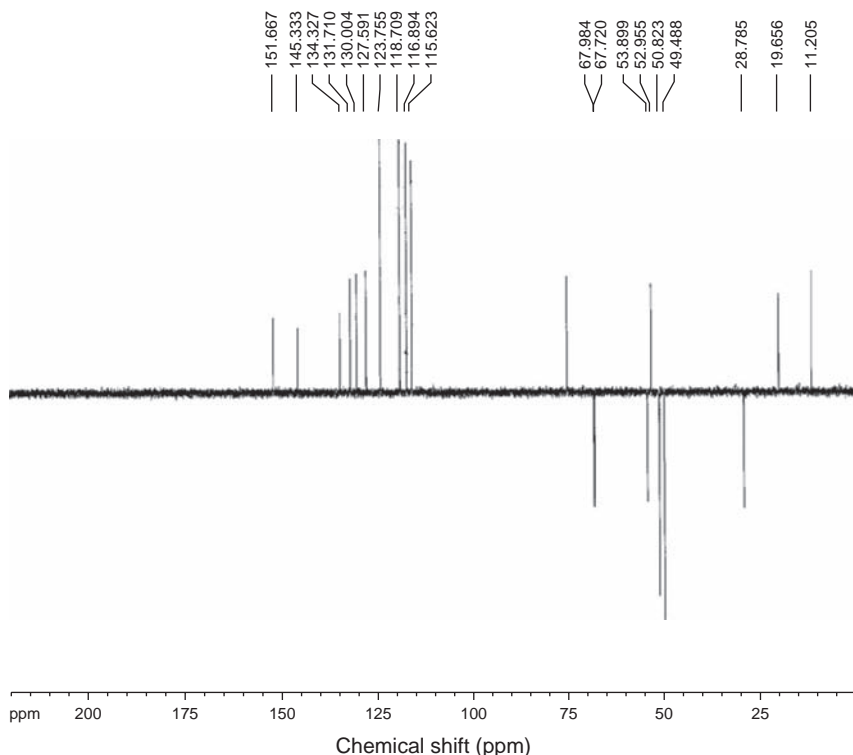
FIGURE 5.14   DEPT 135 ^{13}C-NMR spectrum of itraconazole in CDCl$_3$.

Optical rotation. When the test is carried out according to the general procedure (2.2.7), the angle of rotation for itraconazole is −0.10° to +0.10, determined on solution S.

Related substances. Examine by liquid chromatography according to the general procedure (2.2.29):

Test solution. Dissolve 0.1 g of the substance to be examined in a mixture of equal volumes of methanol R and tetrahydrofuran R and dilute to 10 ml with the same mixture of solvents.

Reference solution (a). Dissolve 5 mg of itraconazole CRS and 5 mg of miconazole CRS in a mixture of equal volumes of methanol R and tetrahydrofuran R and dilute to 100 ml with the same mixture of solvents.

Reference solution (b): Dilute 1 ml the test solution to 100 ml with a mixture of equal volumes of methanol R and tetrahydrofuran R. Dilute to 5 ml of this solution to 10 ml with the same mixture of solvents.

The chromatographic procedure may be carried out using:

- A stainless steel column 0.1 m long and 4 mm in internal diameter packed with base-deactivated octadecylsilyl silica gel for chromatography R (3 μm).
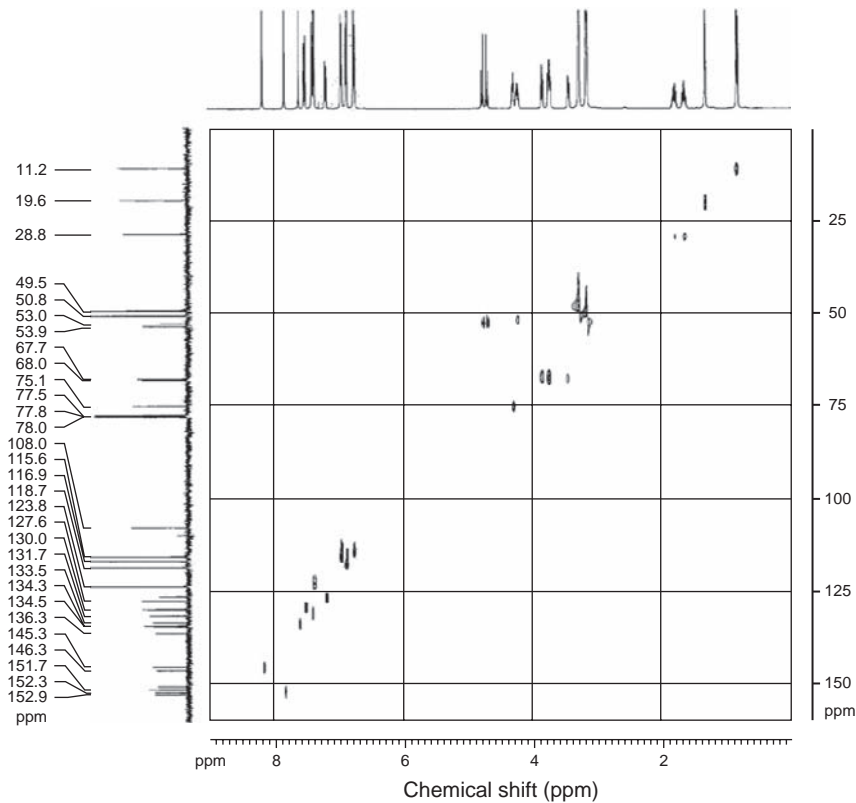
FIGURE 5.15   Gradient HMQC-NMR spectrum of itraconazole in CDCl₃.

- As mobile phase at a flow-rate of 1.5 ml/min a gradient program using the following conditions:
  Mobile phase A : A 27.2 g/l solution of tetrabutylammonium hydrogen sulphate R.
  Mobile phase B: Acetonitrile R.

Time (min)	Mobile Phase A (Per cent v/v)	Mobile phase (Per cent v/v)	Comment
0–20	80 → 50	20 → 50	linear gradient
20–25	50	50	isocratic elution
25–30	80	20	switch to initial eluent composition
30 = 0	80	20	restart gradient

- As detector a spectrophotometer set at 225 nm.

TABLE 5.6   Summary of assignments for the ¹H nuclear magnetic resonance bands of itraconazole.
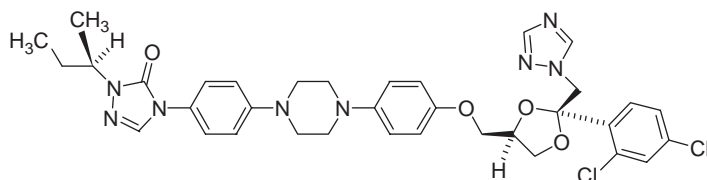
Chemical shift, relative to TMS (ppm)	Number of protons	Multiplicity and coupling constants (Hz)	Assignment
0.83	3	*t* (7.5)	CH$_3$CH$_2$-
1.32	3	*d* (7.5)	CH$_3$CH-
1.61–1.83	2	M	CH$_3$CH$_2$-
3.14–3.15	4	M	(CH$_2$)$_2$-N-
3.26–3.27	4	M	(CH$_2$)$_2$-N-
3.41–3.45	2	M	CH$_2$-O-Ph
3.70–3.85	2	M	O-CH$_2$-CH-
4.20–4.24	1	M	CH$_3$-CH
4.27–4.31	1	M	O-CH$_2$-CH-
4.67–4.77	2	ABq (15)	N-CH$_2$-C
6.73–6.87	4	ABq (9)	ArH
6.93–7.39	4	ABq (8.5)	ArH
7.17–7.19	1	M	ArH
7.39–7.40	1	M	ArH
7.49–7.51	1	*d* (8.5)	ArH
7.60	1	S	ArH
7.82	1	S	ArH
8.15	1	S	ArH

s = singlet, *d* = doublet, *m* = multiplet, *ABq* = AB quartet.

Equilibrate the column for at least 30 min with acetonitrile R at a flow-rate of 1.5 ml/min and then equilibrate at the initial eluent composition for at least 5 min.

Adjust the sensitivity of the system so that the height of the principal peak in the chromatogram obtained with 10 μl of reference solution (b) is at least 50% of the full scale of the recorder.

Inject 10 μl of reference solution (a). When the chromatogram is recorded in the prescribed conditions, the retention times are: miconazole, about 10.5 min and itraconazole about 11 min. The test is not valid unless the resolution between the peaks corresponding to miconazole and itraconazole is at least 2. If necessary, adjust the concentration of acetonitrile in the mobile phase or adjust the time program for the linear gradient elution.
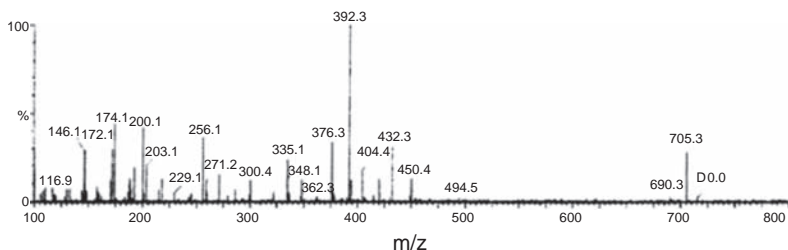
FIGURE 5.16   Mass spectrum of itraconazole [14].

TABLE 5.7   Summary of assignments for the ^{13}C nuclear magnetic resonance bands of itraconazole
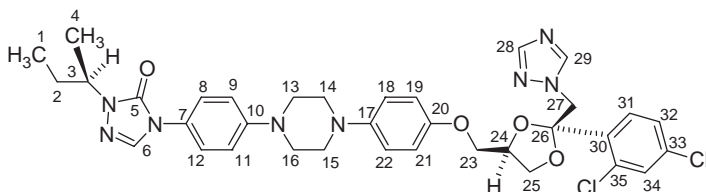
Chemical shifts, relative to TMS (ppm)	Assignment (carbon number)	Chemical shift, relative to TMS (ppm)	Assignment (carbon number)
11.2	1	115.6, 118.7	Ar–C
19.6	4	116.9, 131.7	Ar–C
28.8	2	123.8	Ar–C
49.5	13, 16	127.6	Ar–C
50.8	14, 15	130.0	Ar–C
52.9	24	134.3	Ar–C
53.9	27	145.3	Ar–C
67.7 or 67.9	23	151.7	Ar–C
67.7 or 67.9	25	152.9	5
75.1	3		

Inject separately 10 μl of the mixture of equal volumes of methanol R and tetrahydrofuran R as a blank, 10 μl of the test solution and 10 μl of reference solution (b). In the chromatogram obtained with the test solution: the area of any peak, apart from the principal peak, is not greater than that of the principal peak in the chromatogram obtained with reference solution (b) (0.5%); the sum of the areas of all the peaks, apart from the principal peak, is not greater than 2.5 times the area of the principal peak in the chromatogram obtained with reference solution (b) (1.25%).

Disregard any peak obtained with the blank run and any peak with an area less than 0.1 times the area of the principal peak in the chromatogram obtained with reference solution (b).

   Loss on Drying: When test is carried out according to general procedure (2.2.32), not more than 0.5%, determined on a 1 g of itraconazole by drying in an oven at 100–105 °C for 4 h.

   Sulphated ash: When test is carried out according to the general procedure (2.4.14), not more than 0.1%, determined on 1 g of itraconazole.

Assay

Dissolve 0.3 g itraconazole in 70 ml of a mixture of 1 volume of anhydrous acetic acid R and 7 volumes of methyl ethyl ketone R. Titrate with 0.1 M perchloric acid, determining the end point potentiometrically at the second point inflexion, according to the general procedure (2.2.20).

   1 ml of 0.1 M perchloric acid is equivalent to 35.3 mg of $C_{35}H_{38}Cl_2N_8O_4$.

Storage

Store in a well-closed container, protected from light.

Impurities
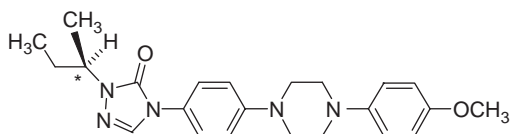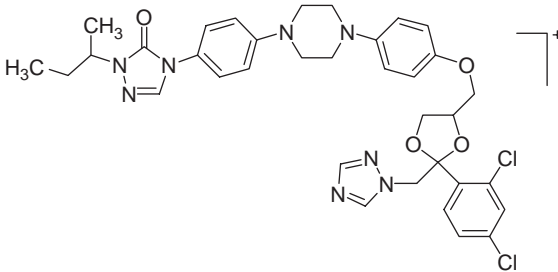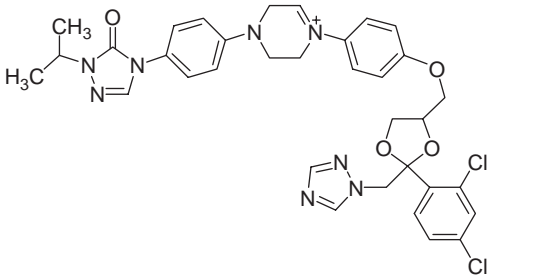
and enantiomer

A) 4-[4-[4-(4-methoxyphenyl)-piperazin-1-yl]-phenyl]-2-[(1*RS*)-1-methyl propyl]-2,4-dihydro-3*H*-1,2,4-triazol-3-one.
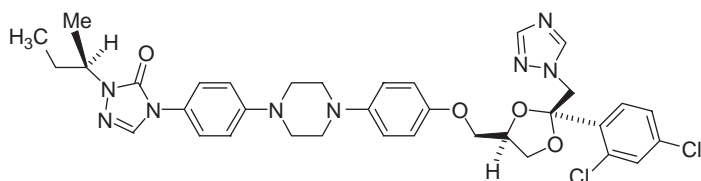
mixture of stereoisomers

TABLE 5.8 Summary of assignments for the fragmentation ions observed in the mass spectrum of itraconazole

| m/z | Relative intensity (%) | Fragment | |
		Formula	Structure
705	30	$C_{35}H_{38}Cl_2N_8O_4$	
690	1	$C_{34}H_{35}Cl_2N_8O_4$	
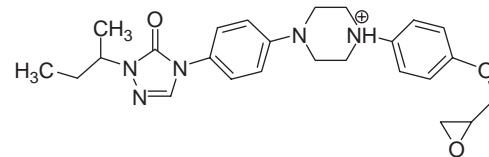
450	15	$C_{25}H_{32}N_5O_3$	
432	35	$C_{25}H_{30}N_5O_2$	
404	20	$C_{23}H_{26}N_5O_2$	
392	100	$C_{22}H_{26}N_5O_2$	
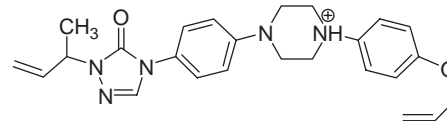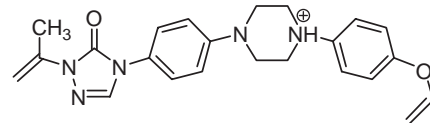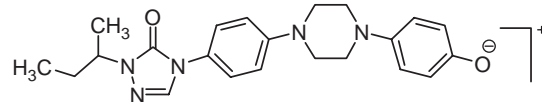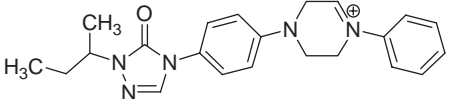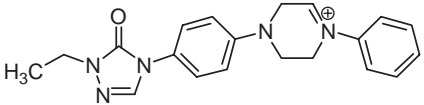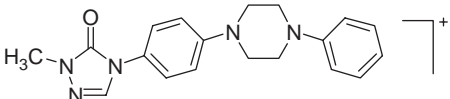
TABLE 5.8 (*continued*)

m/z	Relative intensity (%)	Fragment Formula	Structure
376	35	$C_{22}H_{26}N_5O$	
348	12	$C_{20}H_{22}N_5O$	
335	20	$C_{19}H_{21}N_5O$	

300	12	$C_{12}H_{11}Cl_2N_3O_2$	
256	40	$C_{10}H_7Cl_2N_3O$	
174	50	$C_{10}H_{12}N_3$	
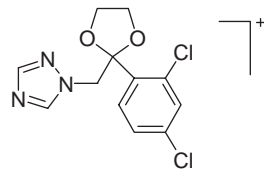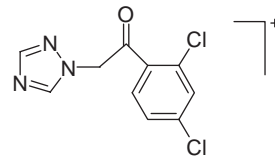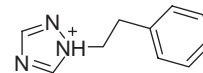
B) 4-[4-[4-[4-[[*cis*-2-(2,4-dichlorophenyl)-2-(1*H*-1,2,4-triazol-4-yl-methyl)-1,3-dioxolan-4-yl]methoxy]phenyl]piperazin-1-yl]phenyl]-2-[(1*RS*)-1-methylpropyl]-2,4-dihydro-3*H*-1,2,4-triazol-3-one.

and enantiomer
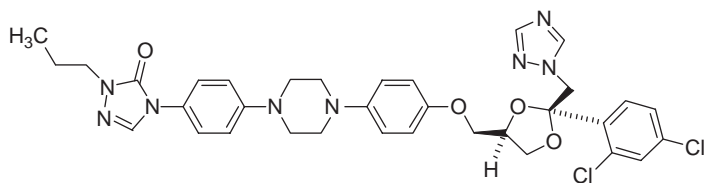
C) 4-[4-[4-[4-[[*cis*-2-(2,4-dichlorophenyl)-2-(1*H*-1,2,4-triazol-1-yl-methyl)-1,3-dioxolan-4-yl]methoxy]phenyl]piperazin-1-yl]phenyl]-2-(1-propyl)-2,4-dihydro-3*H*-1,2,4-triazol-3-one.

and enantiomer
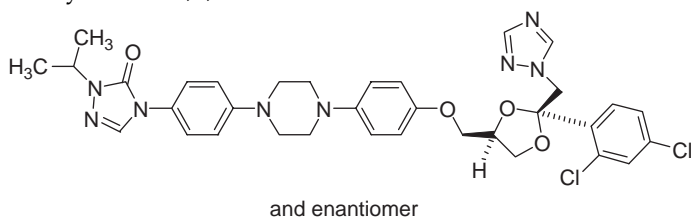
D) 4-[4-[4-[4-[[*cis*-2-(2,4-dichlorophenyl)-2-(1*H*-1,2,4-triazol-1-yl-methyl)-1,3-dioxolan-4-yl]methoxy]phenyl]-piperazin-1-yl]phenyl[-2-(1-methylethyl)-2,4-dihydro-3*H*-1,2,4-triazol-3-one.

mixture of the stereoisomers
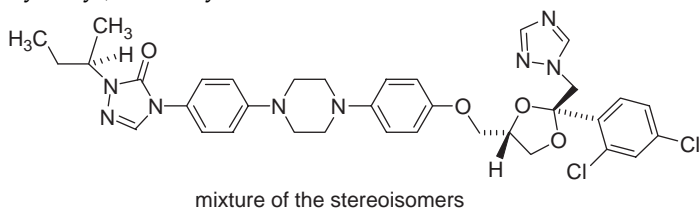
E) 4-[4-[4-[4-[[*trans*-2-(2,4-dichlorophenyl)-2-(1*H*-1,2,4-triazol-1-yl-methyl)-1,3-dioxolan-4-yl]methoxy]phenyl]piperazin-1-yl]phenyl]-2-(1*RS*)-1-methylpropyl]-2,4-dihydro-3*H*-1,2,4-triazol-3-one.
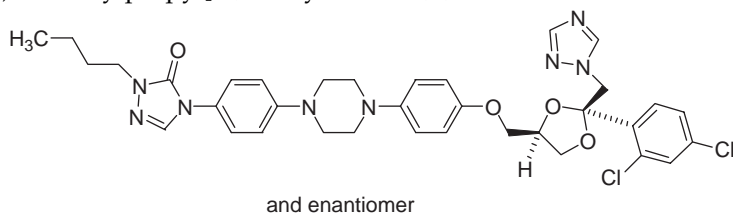
and enantiomer

F) 2-Butyl-4-[4-[4-[4-[[*cis*-2-(2,4-dichlorophenyl)-2-(1*H*-1,2,4-triazol-1-yl-methyl)-1,3-dioxalan-4-yl]methoxy]phenyl]piperazin-1-yl]phenyl]-2,4-dihydro-3*H*-1,2,4-triazol-3-one.
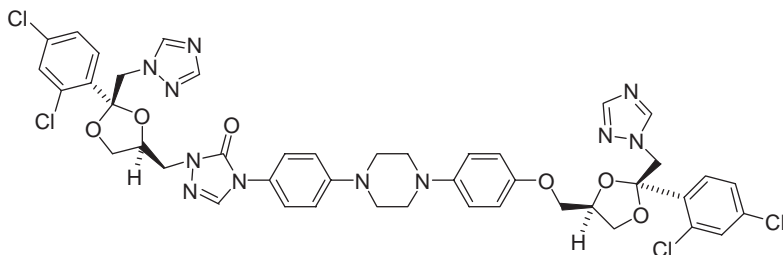
and enantiomer

G) 4-[4-[4-[4-[[*cis*-2-(2,4-dichlorophenyl)-2-(1*H*-1,2,4-triazol-1-yl-methyl)-1,3-dioxolan-4-yl]methyl]phenyl]piperazin-1-yl]-phenyl]-2-[[*cis*-2-(2,4-dichlorophenyl)-2-(1*H*-1,2,4-triazol-1-yl-methyl)-1,3-diox-olan-4-yl]metyl]-2,4-dihydro-3*H*-1,2,4-triazol-3-one.

5.2. Reported methods of analysis

5.2.1. Spectrophotometric methods

Devi *et al.* [27] described two simple and sensitive visible spectrophoto-metric methods for the assay of itraconazole and lisinopril in bulk sam-ples and in pharmaceutical formulations, based on their ability to produce color species with acid dyes.

Devi *et al.* [28] described four simple spectrophotometric methods for the assay of itraconazole, based on its ability to form water insoluble complexes. These methods involve the quantitative precipitation of itra-conazole with phosphomolybdic acid (method A), ammonium molybdate (method B), iodine (method C), and tannic acid (method D), followed by the second step procedure, estimation of either released precipitant from the adduct (precipitate) through acetone addition (methods A, B, or D) or the unreacted precipitant in the filtrate (method C) with the chromo-genic reagents such as Co(II)–EDTA (for phosphomolybdic acid), potas-sium thiocyanate for ammonium molybdate, *p*-N-methyl aminophenol sulfate-sulphanilamide (for iodine) and *p*-N-methylaminophenol–Cr(VI) (for tannic acid). These methods obey Beer's law and give reproducible results. The percentage recoveries were 99.67%.

5.2.2. Chromatographic methods

5.2.2.1. Thin layer chromatography   Clarke [6] reported the following thin-layer chromatographic system:

System 1:
Plates: Silica gel G, 250 µm thick, dipped in, or sprayed with 0.1 M potassium hydroxide in methanol, and dried.
Mobile phase: Cyclohexane: toluene: diethylamine (75 : 15 : 10).
Reference compounds: Codeine R_f = 0.06, Desipramine R_f = 20.
Prazepam R_f = 36, trimipramine R_f = 62.
R_f = 01

System 2:
Plates: Silica gel G, 250 µm thick.
Mobile phase: Ethyl acetate: methanol: strong ammonia solution (85:10:5).
Reference compounds: Sulfadimidine R_f = 13, hydrochlorothiazide R_f = 34.
Temazepam: R_f = 63, Prazepam R_f = 81.
R_f = 79

System 3:
Plates: Silica gel 6, 250 µm thick.
Mobile phase: Ethyl acetate.
Reference compounds: Sulfathiazole R_f = 20, Phenacetin R_f = 38,
Salicylamide R_f = 55, Secobarbital R_f 68.
R_f = 11

System 4:
Plates: Silica gel G, 250 µm thick.
Mobile phase: Methanol.
Reference compounds: Codeine R_f = 20, Trimipramine R_f = 36
Hydroxyzine R_f = 56, Diazepam R_f = 85.
R_f = 87

5.2.2.2. High-performance liquid chromatographic methods Clarke [6] reported the following three high-performance liquid chromatographic systems [29, 30]:

System 1:
Column: Lichrospher 60 RP-Select B (125 × 4 mm, 5 µm) with precolumn Lichrospher 60 RP-Select B (4 × 4 mm, 5 µm).
Mobile phase: (A : B) triethylammonium phosphate buffer (25 mM, pH 3): acetonitrile.
Elution program: (A : B) (100 : 0) to (30 : 70) in 30 min, hold 10 min, back to initial condition in 3 min with equilibration for 10 min before next injection.
Flow-rate: 1 ml/min.
Detection: UV diode-array.
Standards: Nitro-*n*-alkanes (C_1–C_{11}) 10 µl in 10 ml acetonitrile.
R_I values = 725.

System 2:
Column: RP C_{18} (Rsil C_{18} HL, 150 × 2.1 mm, 5 μm).
Mobile phase: Water–acetonitrile (40 : 60), 0.5 ml/min flow-rate.
Internal standard: R 51012.
Detection: UV at 254 nm.
Retention time: Itraconazole, 4.3 min., Internal standard, 5.8 min [29].

System 3:
Column: RP C_{18} (Hypersil, 100 × 4.5 mm, 3 μm).
Mobile phase: Water–acetonitrile (40 : 60) containing 0.03% diethylamine,
    pH 7.8 with dilute orthophosphoric acid, 1 ml/min flow-rate.
Internal standard: R 51012.
Detection: UV at 254 nm.
k value: Itraconazole, 7.4, hydroxyitraconazole 2.7, internal standard,
    10.8 [30].

Woestenborghs *et al.* [29] determined itraconazole in plasma and in animal tissues by a high-performance liquid chromatographic method. The homogenized animal tissue or plasma was mixed with internal standard [the 5-methyl-2-(2-methylbutyl)triazol-3-one analog of itraconazole], and extracted with heptane–isoamyl alcohol (197:3) after adjustment of the pH to 7.8 with 0.05 M phosphate buffer. The organic phase was back-extracted with 0.05 M sulfuric acid. The acidic phase was adjusted to pH 9 and re-extracted with heptane–isoamyl alcohol, and the organic phase was evaporated to dryness. The residue was dissolved in the mobile phase (aqueous 60% acetonitrile) and subjected to high-performance liquid chromatography on a column (15 cm × 2.1 mm i.d.) of RSIL C18 HL (5 μm) with a mobile phase flow-rate of 0.5 ml/min and detection at 263 or 254 nm. The calibration graph was rectilinear for 0.001–10.0 μg/ml and coefficient of variation was 0.3–13.9%.

Warnock *et al.* [31] compared the high-performance liquid chromatographic method with the microbiological methods used for the determination of itraconazole. The drug in the serum was determined by high-performance liquid chromatography on a column of Hypersil ODS, protected by a guard column of Chrompack C18, with aqueous acetonitrile as the mobile phase. The calibration graph was rectilinear from 10 μg/l to 10 mg/l. The detection limit was 10 μg/l. In the determination of 20–1600 μg/l of itraconazole, coefficient of variation ranged from 2.2% to 7.8%. An agar diffusion method was also described, by which the detection limit was 100 μg/l and coefficient of variation ranged from 11.1% to 17.1% and the determination of 100–1600 μg/l of itraconazole. Results by high-performance liquid chromatography were found to be lower than those by the latter method.

Babhair [32] used a high-performance liquid chromatographic method for the assay of itraconazole in human plasma. The plasma (1 ml)

containing 10 µg of itraconazole and 1 µg of ketoconazole (internal standard) was vortex-mixed with sodium chloride (1 g) and acetonitrile (2 ml). After centrifugation at 2500 rpm for 5 min, a 20 µl portion of the organic layer was analyzed by high-performance liquid chromatography on a column (10 cm × 8 mm i.d.) of Radial-Pak C18, with methanol–water–anhydrous acetic acid (80:2:1) as mobile phase (2 ml/min) and detection at 261 nm. The calibration graph was rectilinear for up to 10 µg/ml of itraconazole. Recoveries were 97–98.8% and coefficients of variation were 12% and the detection limit was 250 ng/ml.

Remmel *et al.* [33] reported the assay of itraconazole in leukemic patient plasma by a reversed phase small-bore liquid chromatographic method. Plasma was treated with R51012 as an internal standard, and was diluted (1:1) with 0.5 M ammonium phosphate buffer (pH 7.8) and applied to a C18 solid-phase extraction column. The drug was eluted with acetonitrile, the eluate was evaporated to dryness and the residue was dissolved in mobile phase. A 25 µl portion was analyzed by high-performance liquid chromatography on a column (15 cm × 2 mm i.d.), of Spherisorb ODS-2 (5 µm) with aqueous 65% acetonitrile as mobile phase (0.25 ml/min). The detection limit of itraconazole was 10 ng/ml. The calibration graph was rectilinear up to 10 µg/ml. Recovery of the drug was 93.4%. Within- and between-day coefficients of variation were 1.1–7.7 and 6.3–13.8% for 10–1000 ng/ml of itraconazole.

Badcock [34] used a microscale method for the analysis of itraconazole in plasma by a reversed-phase high-performance liquid chromatographic method. The drug was extracted from the sample with methanol. High-performance liquid chromatography was performed on a column (15 cm × 4.6 mm i.d.) of Ultrasphere ODS (5 µm) with acetonitrile–water (3:2) containing 0.05% diethylamine as mobile phase (1.5 ml/min) and detection at 261 nm. Calibration graphs were rectilinear for 0.01–6 µM of itraconazole. Within-run coefficient of variation for 100 nM of itraconazole was 3.8% ($n = 10$).

Allenmark *et al.* [35] determined itraconazole in serum with a high-performance liquid chromatographic method and fluorescence detection. The serum samples were mixed with the internal standard (R 51012) and were cleaned up on a Bond Elut solid-phase extraction column. The extracts were then analyzed by high-performance liquid chromatography on a column (10 cm × 4.6 mm i.d.) of MPLC RP-18 Spheri-5 with aqueous 60% acetonitrile–10 mM triethylamine as mobile phase (pH 2.3, 1 ml/min) and fluorescence detection at 365 nm (excitation at 260 nm). The calibration graph was rectilinear from 10 to 250 ng/ml. The limit of detection was 4 ng/ml. Recoveries were 95–100%. The method is rapid, specific, and sensitive enough for use in therapeutic monitoring.

Badcock and Davies [36] recommended a reversed-phase high-performance liquid chromatographic method for the determination of

itraconazole in nail clippings. Nail clipping were hydrolyzed by incuba-
tion with 4 M potassium hydroxide at 80° for 15 min, after addition of
sodium chloride and acetonitrile containing a dimethyl analog of itraco-
nazole as an internal standard and centrifugation of the mixture, portions
of the supernatant solution was analyzed by high-performance liquid
chromatography on an Ultrasphere ODS (5 μm) column (15 cm ×
4.6 mm i.d.) equipped with a guard column (4.5 cm × 4.6 mm i.d.) with
mobile phase (1.5 ml/min) of water–acetonitirle–ethylamine (800:1200:1)
and detection at 261 nm. Calibration graphs were rectilinear from 10 to
200 pmol of itraconazole in 100 μl of potassium hydroxide solution. The
detection limit was 0.1 pmol of itraconazole per mg of nail and recovery of
the drug was 92.5%. Intra and interassay coefficient of variation were 4.1–
8.3% and 4.2–9.4%, respectively.

Persat *et al.* [37] used a high-performance liquid chromatographic
method to measure plasma itraconazole concentrations in neutropeic
patients after repeated high-dose treatment. The chromatograph used
consisted of a M 45 pump, a U6K universal detector and a 441 absorbance
detector. The eluate was monitored at 254 nm and absorbance was
recorded. The analytical column was a reversed-phase Nucleosil C18,
5 μm (15 cm × 4.6 mm) equipped with a μBondapak C-18 Corasil precol-
umn. The elution system consisted of 0.5% diethylamine in acetonitrile–
water (70:30). The flow-rate was constant at 0.7 ml/min. Itraconazole and
internal standard were prepared in methanol and stored at 4 °C. Plasma
specimens and standard (1 ml) were usually spiked with 10 μl of internal
standard at 0.1 g/l, then once extracted by a liquid–liquid method. After
extraction, the samples were evaporated, the residue redissolved in 100 μl
mobile phase and 40 μl was injected. Itraconazole was quantitated by
comparison of the peak height ratio of the drug to the internal standard.
The standard solutions contained 100, 250, 500, and 1000 μg of itracona-
zole per liter of plasma. The lower limit of detection was 50 μg/l.
The intraassay coefficients of variation were between 4.7% and 5.8% and
the interassay coefficients of variation were between 3.8% and 8.2% as a
function of the itraconazole concentrations.

Law *et al.* [30] described an high-performance liquid chromatographic
method for the determination of serum itraconazole concentrations using
hydroxyl itraconazole standards. The chromatograph consisted of a
Waters Model 6000 A pump connected to a C_{18} guard column and a
steel cartridge (100 cm × 4.5 mm) containing Hypersil octyldecyl silane
(3 μm). The mobile phase consisted of water–acetonitrile (40:60) contain-
ing 0.03% diethylamine, adjusted to pH 7.8 with dilute orthophosphoric
acid and then filtered and degassed under reduced pressure before use.
The flow-rate of the mobile phase was 1 ml/min, and 20 μl aliquots of
sample or standard were injected on to the column *via* a rheodyne valve.
A fixed wavelength UV absorbance detector (254 nm) was used.

Poirier *et al.* [38] determined the drug and its active metabolite in plasma by a column liquid chromatographic method. To 500 µl of plasma was added 500 µl of borate buffer (pH 10) and 4 ml of diethyl ether. The sample were mixed for 5 min and the organic phase was removed after centrifugation for 5 min at 2000 *g* then back-extracted with 500 µl 1 M hydrochloric acid, centrifuged, and the organic phase was discarded. The acetic phase was alkalinized with 500 µl M sodium hydroxide and 500 µl of pH 10 borate buffer and reextracted for 5 min with 4 ml diethyl ether. After centrifugation, the organic layer was evaporated to dryness at room temperature and the residue was dissolved in 200 µl mobile phase. A portion (100 µl) was analyzed by high-performance liquid chromatography on an Ultremex C18 column (15 cm × 4.6 mm i.d.) equipped with a 1 cm precolumn packed with the same material, methanol–water–14.7 M phosphoric acid–triethylamine (825:165:10:2) adjusted to pH 3 with 10 M sodium hydroxide as mobile phase (1 ml/min) and fluorimetric detection at 355 nm (excitation at 265 nm). The calibration graph was linear from 20 (detection limit) to 4000 ng/ml for hydroxyitraconazole and itraconazole. Within-day and day-to day relative standard deviation ($n = 5$) were 1.3–8.8% and 1.6–10.9% for the hydroxy metabolite and the drug, respectively. Recoveries were 80% with no interference for 45 coadministered drugs occurred.

A high-performance liquid chromatographic assay method was used by Rifai *et al.* [39] for the determination of itraconazole concentration using solid-phase extraction and small sample volume. The internal standard R051012 (50 µl, 4 µg/ml) and 3 ml of 15% acetonitrile were added to 100 µl plasma. After vortexing for 30 s, the mixture was applied to a Bond-Elut C18 extraction column. After washing with 9 ml 40% acetonitrile, the drug was eluted with 500 µl dichloromethane–methanol (1:1). After evaporation to dryness, the residue was reconstituted with 100 µl mobile phase. A 100 µl portion was analyzed on a 5 µm LC-1 column (5 cm × 4.6 mm i.d.), 25 mM dipotassium hydrogen phosphate of pH 6.3–methanol–acetonitrile (4:3:3) as mobile phase (2 ml/min) and detection at 263 nm. The calibration graph was linear from 50 (detection limit) to 5000 ng/ml. Relative standard deviations were 5.8–12% and recoveries were 99–102%. Forty-eight of commonly prescribed drugs did not interfere.

Itraconazole and its metabolite in plasma and serum were determined by Brandsteterova *et al.* [40] using solid-phase extraction high-performance liquid chromatographic method. Serum (0.5 ml) was shaken with 1.5 ml methanol (solvent A) for 5 min and the mixture was centrifuged. The supernatant was decanted, evaporated to dryness and the residue was dissolved in 100 µl of solvent A. Plasma (1 ml) was mixed with 1 ml water and applied to a Bakerbond (or Separcol) C18 SPE cartridge. The cartridge was washed with 2 ml water and itraconazole and its hydroxy metabolite were eluted with 2 ml acetonitrile (or solvent A). The eluate was

evaporated to dryness and the residue was dissolved in 200 μl of solvent A. Portions (20 μl) of the reconstituted plasma and serum extracts were analyzed by high-performance liquid chromatography on 5 μm Separon SGX C-18 column (15 cm × 3 mm i.d.) with methanol–water–triethylamine (72:28:0.05) as mobile phase (1.1 ml/min) and detection at 263 nm. The detection limits were 10 and 6 μg/ml, respectively for the drug and its hydroxy metabolite. Average recoveries were 86% and 96.1%, and 83.9% and 91.3%, respectively, for 0.4 μg/ml of added itraconazole and hydroxy itraconazole to plasma, from the Separcol and Bakerbond SPE cartridges, respectively. The method was applied to therapeutic monitoring in leukemic patients.

Darouiche *et al.* [41] developed a simplified high-performance liquid chromatographic assay method for the determination of itraconazole levels in plasma and esophageal tissue of four patients with AIDS who had been receiving daily oral doses of 100 mg of itraconazole in solution for at least 3 weeks for therapy of esophageal candidiasis. Itraconazole levels were about three times higher in esophageal tissues than in plasma (means standard errors of 0.69 ± 0.5 μg/g and 0.24 ± 0.16 μg/ml, respectively; $P = 0.04$). This method is quick (requires only 1 h for completion), and sensitive (the limit of detectability of itraconazole in plasma and esophageal tissues are 0.005 μg/ml and 0.01 μg/g, respectively), and it can be reliably used in clinical and research setting (accuracy, >95%; absolute recovery from biological samples 80–90%, coefficient of variation, 3.3–6.6%).

Lacroix *et al.* [42] described a fast and specific assay method for the simultaneous determination of itraconazole, hydroxyitraconazole, and amphotericin B in human plasma by high-performance liquid chromatography with photodiode array detection. The method is based on methanolic extraction of the compounds from plasma, followed by reversed-phase high-performance liquid chromatography with two detection wavelengths (263 and 405 nm). The extraction step provides ≥94% recovery and the response of the detection system is linear from 50 to 5000 ng/ml. No other drugs have been found to interfere with the assay.

Hulsewede *et al.* [43] determined the concentrations of itraconazole and its active metabolites, hydroxyitraconazle in the sera of 49 patients having received itraconazole for therapeutic or prophylaxis purposes. Measurements by high-performance liquid chromatography were compared with a biological assay using a strain of *Paecilomyces variotii* as test organism and itraconazole as standard. The concentration of hydroxyitraconazole in serum was on average 1.6 times higher than the concentration of itraconazole. The sum of itraconazole and hydroxyitraconazole concentrations determined by high-performance liquid chromatography showed a linear relationship with the concentrations obtained by the bioassay ($r = 0.94$). The biological method gives approximately 20%

higher values than the high-performance liquid chromatographic method indicating that hydroxyitraconazole is biologically more active than itraconazole. As the values of *Paecilomyces variolii* bioassay are in the same range as the high-performance liquid chromatographic measurements, it is concluded that both methods are suitable for the monitoring of itraconazole medication.

Ng *et al.* [44] assayed itraconazole and six other antifungal agents using a single step sample preparation and an isocratic high-performance liquid chromatographic procedure based on three mobile phases of similar components. The method was simple, flexible, and rapid, the assays being completed within half an hour. The method showed high reproducibility, good sensitivity with detection limit of 0.078–0.625 mg/l and high recovery rates of 86–105%. High-performance liquid chromatographic assay is useful in the clinical laboratory for monitoring patients on antifungal therapy.

The analysis of itraconazole and its hydroxy derivative in plasma by an high-performance liquid chromatographic method was described by Compas *et al.* [45]. Ketoconazole (1 μg, internal standard) and 1 M carbonate buffer (200 μl) were added to 1 ml serum and the sample mixed, then 7 ml heptane–isoamyl alcohol (9:1) added. After mixing and centrifuging, the organic layer was removed and evaporated to dryness and the residue was dissolved in 125 μl of the mobile phase. High-performance liquid chromatography was performed on a Lichrospher 10 RP8 column (25 cm × 5.6 mm i.d.), acetonitrile–water (31:19) containing 0.05% diethylamine and adjusted to pH 6 with 30% acetic acid as mobile phase, detection at 258 nm. Recoveries for the drug were 77 ± 5% and for hydroxyitraconazole 83 ± 3% over the range 0.1–3.2 mg/l. Day-to-day precision ($n = 5$) was 3.7–7.9% coefficient of variation for itraconazole and 3.4–6% for hydroxyitraconazole. The respective detection limits were 10 and 7 μg/l.

An example of a quick liquid chromatographic assay method used for the determination of itraconazole in serum was presented by Cociglio *et al.* [46]. A prevalidation design for the optimization of assays was described and includes a spreadsheet program (Valplan) which allows evaluation, in a single run, of linearity, matrix effect on recovery, repeatability of analysis, and extraction. The validation design was used to devise an assay for itraconazole in serum. When analyzing unknown samples, extraction of itraconazole, its main metabolite hydroxyitraconazole and its 2-(3-methylbutyl)-5-methyl analog (R 51012) as internal standard, would be with acetonitrile containing potassium chloride (demixing extraction). Supernatants were analyzed by high-performance liquid chromatography on a 5 μm column (25 cm × 4 mm i.d.) of Lichrospher with aqueous 55% acetonitrile as mobile phase (1.5 ml/min) and detection at 263 nm. The performance of this method was acceptable for

0.06–5.0 mg/l of itraconazole and hydroxy itraconazole and detection limits were 0.03 mg/l for both analytes.

A rapid and specific liquid chromatographic assay method for the determination of itraconazole and hydroxyitraconazole in plasma was described by Poirier and Cheymol [47]. The plasma (500 µl) was treated with 100 µl internal standard (R 51012; 1000 ng), 500 µl borate buffer of pH 10 and 4 ml diethyl ether. After mixing for 5 min and centrifuging, the organic phase was evaporated under air. The dry extract was dissolved in 300 µl of the mobile phase and vortexed for 1 min. A 100 µl portion of the resulting solution was analyzed by high-performance liquid chromatography on a 5 µm Symmetry C8 column (15 cm × 4.6 mm i.d.) equipped with a precolumn (2 cm) of similar material, with methanol–water–14.7 M phosphoric acid (145:54:1) adjusted to pH 3 with 10 M sodium hydroxide as mobile phase (0.8 ml/min) and fluorescence detection at 355 nm (excitation at 265 nm). The peaks of hydroxyitraconazole, itraconazole, and the internal standard were well separated with retention times of 3.2, 4.9, and 7 min, respectively. The daily relative standard deviation ($n = 14$) were 3 and 1.5% for hydroxyitraconazole and itraconazole, respectively.

Cox *et al.* [48] recommended an high-performance liquid chromatographic microassay method for the determination of itraconazole and hydroxyitraconazole in plasma and in tissue biopsies. The drug and its hydroxy metabolite were extracted from tissue (5–100 mg) and plasma (0.1 ml) samples, containing internal standard (R 51012), by extraction into methanol. High-performance liquid chromatography was performed on a 4 µm Novapak C18 column (10 cm × 8 mm i.d.) equipped with a Novapak Guard-Pak precolumn with water–acetonitrile–diethylamine (42:58:0.05) adjusted to pH 2.45 with 85% phosphoric acid as mobile phase (1.5 ml/min) and fluorescence detection at 365 nm (excitation at 260 nm). Calibration graphs were linear from 10 to 1000 ng/ml for itraconazole and its hydroxymetabolite and detection limits of itraconazole were 5 ng/ml in tissue, plasma, and serum. Intraday relative standard deviations were <2% and <4.5% for itraconazole and its hydroxyl metabolite respectively in tissue, and intraday relative standard deviation were <12% and ≤10% for both analytes in tissue and plasma, respectively. Recoveries were ≥79% and >80% for both analytes in tissues and plasma, respectively.

A rapid and sensitive high-performance liquid chromatographic assay method used for the determination of itraconazole and its hydroxyl metabolite in human serum, was described by Gubbins *et al.* [49]. Human serum (250 µl) was mixed with 50 µl of 0.3 N barium hydroxide and 50 µl of 0.4 N zinc sulphate heptahydrate. The mixture was extracted with 1 ml acetonitrile with centrifugation and the supernatant was evaporated to dryness. The residue was dissolved in 250 µl acetonitrile containing 45% 0.05 M phosphate buffer of pH 6.7 and 8% methanol (mobile

phase) and the solution was centrifuged. A portion (50 µl) of the supernatant was analyzed on an analytical 5 µm Alltech Alltima C-18 base-deactivated column (25 cm × 4.6 mm, 5 µm) at 37 °C with mobile phase flowing at 1 ml/min and detection at 263 nm. The calibration graphs were linear from 0.02 to 1.5 µg/ml for both the drug and its hydroxy metabolite, and the detection limit was 10 ng/ml. Absolute recoveries of itraconazole and its metabolite were 93.3% and 92.9%, respectively. The intraday relative standard deviations were <12% and interday relative standard deviations were <14%.

Bai *et al.* [50] described an high-performance liquid chromatographic method for the determination of itraconazole in serum. The method was carried out by using ODS column and acetonitrile–water (67.5:32.5) as the mobile phase. The detection wavelength was 263 nm. Itraconazole was extracted from serum with *n*-heptane–isoamyl alcohol (98.5:1.5) and evaporated to dryness. The linear range was 5–600 ng/ml, $r = 0.9995$. The recovery rate of high, middle, low concentrations was 105.05%, 100.57%, 97.91% ($n = 6$), respectively. Coefficient of interday and intraday variations were 3.83%, 4.05%, 3.09%, and 6.00%, 4.90%, 4.72% ($n = 6$), respectively. The method is rapid and accurate.

Thienpont *et al.* [51] studied the resolution of ketoconazole and itraconazole enantiomers in high-performance liquid chromatography and supercritical fluid chromatography on chiral stationary phases based upon substituted polysaccharides with different groups such as 3,5-dimethylphenylcarbamates and (R)-phenylethylcarbamate. The separations have been studied particularly in supercritical fluid chromatography (influence of pressure, temperature, as well as type and percentage of organic modifier). This study shows the advantage of supercritical fluid chromatography over high-performance liquid chromatography for the enantiomeric separation of ketoconazole and itraconazole. Chromatographic separations were carried out with an high-performance liquid chromatographic system including a Jasco Ultraviolet – 975 ultraviolet/visible detector and a Jasco P-980 high-performance liquid chromatography pump. The supercritical fluid chromatographic separations were performed on a Gilson SF3 system equipped with a Rainin Dynamax model ultraviolet visible detection during liquid chromatographic analyses was carried out with a Jasco OR 990 chiral detector. The drugs were dissolved in ethanol at a concentration of 1% and 3% for analysis by high-performance liquid chromatography and supercritical fluid chromatography. The separation was achieved using a mobile phase of hexane–methanol–ethanol (75:12:13), plus octanoic acid (10 mmol) with a flow-rate of 1 ml/min and ultraviolet detection at 254 nm.

Odds *et al.* [52] used high-performance liquid chromatography in a bioassay for the determination of itraconazole blood levels. Concentrations as low as 0.005 mg/l were measured and the mean coefficient of variation for 15 duplicate samples was 2.3%.

Al-Rawithi *et al.* [53] described a useful and rapid high-performance liquid chromatographic micromethod for the analysis of itraconazole and its active metabolite hydroxyitraconazole in human plasma. After a simple deprotonization of 100 ml plasma with acetonitrile, the drug, its metabolite, and internal standard (ketoconazole) were separated on a 10 cm × 8 mm Novapak C-18 (4 μm) radial compression cartridge. The compounds of interest were detected using a fluorescence detector with the excitation wavelength set at 260 nm and the emission at 365 nm. The mobile phase consisted of 420 ml water adjusted to a pH 2.5 with phosphoric acid, 580 ml acetonitrile, and 100 μl triethylamine, which was delivered at a flow-rate of 3 ml/min. This expedient and rugged method is being used to monitor therapeutic levels in bone marrow transplant recipients who are taking the drug for prophylaxis.

Kubalec and Brandsteterova [54] described a column-switching high-performance liquid chromatographic assay method for the determination of itraconazole and its main metabolite hydroxyitraconazole in serum samples. Three precolumns packed with alkyl-diol silica sorbents differing in alkyl chain length are compared in the simple cleanup step. Chromatographic separation is achieved with a Symmetry C8 column. The assay presented shows a robust and selective analytical procedure with low requirements for sample quantity, no manual sample treatment and high sample throughput. The columns used are: LiChrosorb RP-8, 25 cm × 4 mm (10 μm), symmetry C8 and symmetry Shield C8, 15 cm × 3.9 mm (5 μm) with symmetry C8 and Symmetry Shield C8 guard columns 2 cm × 4 mm (5 μm). LiChrospher ADS RP-4, RP-8, and RP-18, 25 cm × 25 mm were used as precolumns in the column-switching system. The washing mobile phase was 50 mM phosphate buffer (pH 7.2), the flow-rate was 1.4 ml/min. Mobile phase II-the eluting mobile phase—consisted of 75% methanol and 25% water and the flow-rate was 0.8 ml/min. The separation was detected at 263 nm.

Koks *et al.* [55] developed and validated a sensitive and selective reversed-phase liquid chromatographic assay method for the determination of itraconazole and hydroxyitraconazole in human plasma. The drug and its hydroxy metabolite were extracted from the matrix using solid-phase extraction on a strong cation-exchange sorbent. All the compounds were detected using fluorescence at 265 and 363 nm for excitation and emission, respectively. The assay has been validated over the range 10–1000 ng/ml for both compounds, 10 ng/ml being the lower limit of quantification. Accuracies ranged from 104% to 113% for itraconazole and from 91% to 103% for hydroxyitraconazole. The intraassay precisions were all below 9% for itraconazole and below 8% for hydroxyitraconazole. The selectivity has been evaluated with respect to all registered antihuman immunodeficiency virus (HIV) drugs and other potential comedications and a few of their metabolites, commonly used by

HIV-infected individuals. Both itraconazole and hydroxyitraconazole were stable under relevant conditions of HIV-inactivation and storage samples. The applicability of the assay was demonstrated for samples collected from a treated HIV-infected patient.

Wong *et al.* [56] developed a sensitive and selective high-performance liquid chromatographic method for the determination of itraconazole and its metabolite, hydroxyitraconazole, in human plasma. Prior to the analysis, both compounds together with the internal standard were extracted from alkalinized plasma samples using a 3:2 (v/v) mixture of 2,2,4-trimethylpentane and dichloromethane. The mobile phase comprised 0.02 M. potassium dihydrogen phosphate–acetonitrile (1:1, v/v) adjusted to pH 3. Analysis was run at a flow-rate of 0.9 ml/min with excitation and emission wavelengths set at 260 and 365 nm, respectively. Itraconazole was found to adsorb on glass or plastic tubes, but could be circumvented by prior treating the tubes using 10% dichlorodimethylsilane in toluene. Moreover, rinsing the injector port with acetonitrile helped to overcome any carryover effect. This problem was not encountered with hydroxyitraconazole. This method was sensitive with limit of quantification of 3 ng/ml of itraconazole and 6 ng/ml for hydroxyitraconazole. The calibration curve was linear over a concentration range of 2.8–720 ng/ml for itraconazole and 5.6–720 ng/ml for the hydroxyl metabolite. Mean recovery value of the extraction procedure for both compounds was about 85%, while the within-day and between-day coefficient of variation and percent error values of the assay method were all less than 15%. The method is suitable for use in pharmacokinetic and bioavailability studies of intraconazole.

Srivatsan *et al.* [57] developed and validated a high-performance liquid chromatographic method for the simultaneous determination of itraconazole and its metabolite, hydroxyitraconazole, in human plasma. The method involved liquid-phase extraction of itraconazole and hydroxyitraconazole using a hexane–dichloromethane (70:30) mixture, after addition of loratadine as internal standard. Separation was achieved with reversed-phase C-18 column (25 cm × 4.6 mm) employing fluorescence detection (excitation: 264 nm, emission: 380 nm). The mobile phase consisted of 0.01% triethylamine adjusted to pH 2.8 with orthophosphoric acid–acetonitrile (46:54)–isopropanol (90 : 10, v/v) at a flow-rate of 1 ml/min. For both the drug and metabolite, the standard curve was linear from 5 to 500 ng/ml with goodness of fit (r^2) greater than 0.98 observed with four precision and accuracy batches during validation. An observed recovery was more than 70% for drug, metabolite, and internal standard. The applicability of this method to pharmacokinetic studies was established after successful application during 35 subjects bioavailability study. The method was found to be precise, accurate, and specific during the study.

Li *et al.* [58] performed a study on the preparation and stability of intraconazole gel. Carbopol 940 was used as gel matrix to prepare itraconazole gels. A high-performance liquid chromatographic method was established to determine itraconazole concentration in the preparation. The preliminary stability experiments were carried out. A uniform preparation was obtained. The calibration curves were linear in the range 2.4–24 mg/l (r = 0.999). The average recovery for itraconazole with 100.7%. The result of stability experiments showed that no flocculation, coalescence, or breaking was found under high temperature, light, or centrifugation. In the meanwhile, the drug content of the gels was not obviously changed. The preparation process is simple and quality controllable. Physical and chemistry properties of the itraconazole gels are stable.

Shin *et al.* [59] described a high-performance liquid chromatographic method for the analysis of itraconazole and/or 7-hydroxy itraconazole. To a 2.2 ml Eppendorf tube containing a 50 ml aliquot of the biological sample, a 50 ml aliquot of an internal standard (R 510912) (0.2 mg/ml dissolved in acetonitrile) and a 250 ml aliquot of 0.1 M carbonate buffer (pH 10) were added. After vortexing for 30 s, the mixture was extracted with 1 ml of *tert*-butyl methyl ether. The organic layer was evaporated under nitrogen at 65 ml. The residue was then reconstituted with a 100 ml aliquot of the mobile phase, and a 75 ml aliquot was injected directly to the high-performance liquid chromatography column. The analysis was carried out in a column (10 cm × 4.6 mm) of MPLC RP-18 Spheri-s. The mobile phase, 20 mM potassium dihydrogen phosphate (pH 2)-acetonitrile-85% phosphoric acid (50:50:0.15), was run at a flow-rate of 2 ml/min and the column effluent was monitored by a fluorescence detector set at an excitation wavelength of 260 nm and an emission wavelength of 364 nm. The retention times of 7-hydroxy itraconazole, itraconazole, and the internal standard were approximately 3, 6.2, and 9.3 min, respectively. The detection limit of itraconazole and 7-hydroxyitraconazole in plasma and urine were both 50 ng/ml. The coefficient of variation were generally low (below 8.21%).

Khoschsorur *et al.* [60] presented a simple and specific method for the simultaneous determination of voriconazole and itraconazole and its metabolite, hydroxyitraconazole, in human serum using one-step liquid–liquid extraction and high-performance liquid chromatography. Linearity tests ranged from 0.1 to 8 μg/ml; the minimum detectable concentration was 0.03 μg/ml. The chromatographic system consisted of an isocratic pump with a wavelength detector. The separation was carried out on a 250 mm × 4.6 mm reversed-phase column Zorbax SB C_{18} (5 μm) maintained at 40 °C. The mobile phase consisted of 50 mM phosphate buffer, pH 6 (adjusted with 1 M potassium hydroxide), acetonitrile, and methanol (35:45:20); the flow-rate was 1.7 ml/min. Detection was 255 nm, and injected volume was 30 μl. Ketoconazole was used as the internal standard.

Ohkubo and Osanai [61] described a practical, simple high-performance chromatographic method for the determination of itraconazole in clinical plasma samples. Itraconazole and bifonazole (internal standard) were extracted from plasma using a C8-bonded solid-phase cartridge, separated by C8 reversed-phase high-performance liquid chromatography and quantified by ultraviolet absorption at 263 nm. This method enabled the determination of itraconazole in the concentration range of 10–500 µg/l. The detection limit of itraconazole was 5 µg/l. The mean recovery of itraconazole was 5 µg/l. The mean recovery of itraconazole added to plasma was more than 89.1%, with a coefficient of variation of less than 6.9%. The method was applied for the determination of plasma itraconazole in volunteers treated daily with a 200 mg oral capsule of itraconazole for 4 days. Plasma level of itraconazole was monitored for the following 24 h and the mean area under the plasma concentration-time curve from 0 to 24 h value of 4358.9 ± 1933.4 µg h/l was obtained.

Redmann and Charles [62] described a rapid high-performance liquid chromatographic method with fluorometric detection for the determination of plasma itraconazole and hydroxyitraconazole concentrations in cystic fibrosis children with allergic bronchopulmonary aspergillosis. The mobile phase of methanol (75%) and water (25%) was pumped at 1 ml/min through a C_{18} symmetry (3.9 mm $\times$ 150 mm) cartridge. Using a protein-precipitation method, 100 µl internal standard solution (R051012, 555 µg/l in acetonitrile) were added to 100 µl of plasma followed by 10 µl zinc sulfate solution (20%). Itraconazole, hydroxyitraconazole, and internal standard eluted at 4.7, 8.3, and 12.5 min, respectively and were detected spectrofluorometrically at 250 nm (excitation) and 380 nm (emission). Recoveries were 87.1–96.7%. Calibrations in drug-free plasma were linear ($r^2 > 0.99$) from 50 to 2000 µg/l, using $1/C^2$ (C = concentration) weighting. Intraday and Interday imprecision (CV%) was 4.8–17.3 and 6.3–16.6% for itraconazole, and 4.6–17.9% and 7.02–18.4% for hydroxyitraconazole. Inaccuracy was -7.1% to -14.7% for itraconazole and -0.1 to 9.7% for hydroxyitraconazole. The clinical application of the method was demonstrated by measurement of itraconazole and hydroxyitraconazole in plasma samples drawn from pediatric cystic fibrosis patients, who were prescribed itraconazole for treatment of allergic bronchopulmonary aspergillosis.

Orosz et al. [63] used a high-performance liquid chromatographic method for the analysis of itraconazole and hydroxyitraconazole in plasma and tissues. The analytical system consisted of a 600E solvent delivery system, a model 700W/SP autosampler, an RCM 8 mm $\times$ 10 cm cartridge holder equipped with a Novapak C8 cartridge (4 µm), and a Novapak GuardPak precolumn insert, a model 470 fluorescence detector, and a NEC Powermate computer. Itraconazole and hydroxylitraconazole were extracted from plasma and tissue with methanol. The mobile phase was an isocratic mixture of water: acetonitrile: diethylamine

(42 : 58 : 0.005). Fluorescence of the parent drug and metabolite were measured using an excitation of 245 nm and emission of 380 nm. The sensitivity of the assay was 10 ng/ml for itraconazole and hydroxyitraconazole. The assay was validated by measuring blank plasma and tissues and plasma and tissues spiked with known amounts of itraconazole and hydroxyitraconazole. The interassay and interassay coefficients of variation were less than 5% and less than 10%, respectively.

5.2.2.3. Liquid chromatography-mass spectrometry Carrier and Parent [64] developed a validated fast, reliable, and sensitive liquid chromatography–mass spectrometric assay method for the determination of itraconazole and its metabolite, hydroxy itraconazole in dog plasma. The analysis involves a simple liquid–liquid extraction followed by liquid chromatography–mass spectrometric analysis using electrospray ionization in the positive mode. Total separation of the drug, its metabolite and the internal standard, miconazole was achieved on a C_{18} column in 3.5 min using an isocratic mixture of acetonitrile and 10 mM ammonium acetate. The response was linear over four-orders of magnitude, allowing reliable quantification of each species. The analysis was performed on a Zorbax SB-C_{18} column (3 cm $\times$ 4.6 mm, 3.5 µm) maintained at 25 °C. The mobile phase consisted of acetonitrile–10 mM ammonium acetate, pH 3.5 (60:40). The mobile phase was filtered through a 0.45-µm polypropylene filter and degassed under vacuum. The mobile phase was pumped at 1 ml/min and the injection volume was 5 µl. Mass spectrometry was carried out on the Agilent 1100 mass spectrometer equipped with an electrospray ionization source in the positive ionization mode. Data handling was performed with a Chemistation VA 06.01 data handling system. Full scan of the spectra were obtained by scanning masses between m/z 200 and 800. In the electrospray experiment the chromatographic effluent entered the mass spectrometer through an electospray capillary set at 3.5 kV. Nitrogen was used both as drying gas (11 l/h) and as nebulizing gas (50 psi.). The temperature of the drying gas was set at 350 °C. All the experiments were conducted at a fragmintor voltage of 140 V. Quantitative analyses were conducted in single-ion monitoring mode scanning the quasi-molecular ions $[M + H]^+$ of itraconazole, hydroxyitraconazole, and miconazole with a dwell time of 100 ms. Protonated molecules were detected as the major peaks for all compounds except for hydroxyitraconazole where the natriated peak was larger. The spectra were obtained with a fragmentor voltage set at 140 V.

Yao *et al.* [65] developed and validated a liquid chromatographic–mass spectrometric assay method for the determination of itraconazole in rat heparinized plasma using reversed-phase high-performance liquid chromatographic combined with positive atmospheric pressure ionization mass spectrometry. After protein precipitation of plasma samples

(0.1 ml) with acetonitrile containing nefazodone as an internal standard, a 50-μl aliquot of the supernatant was mixed with 100 μl of 10 mM ammonium formate (pH 4). An aliquot of 25 μl of the mixture was injected onto a BDS Hypersil C-18 column (5 cm × 2 mm, 3 μm) at a flow-rate of 0.3 ml/min. The mobile phase comprising of 10 mM ammonium formate (pH 4) and acetonitrile (60:40, v/v) was used in an isocratic condition, and itraconazole was detected in single-ion monitoring mode. Standard curves were linear ($r^2 \geq 0.994$) over the concentration range of 4–1000 ng/ml. Both itraconazole and the internal standard were stable in the injection solvent at room temperature for at least 24 h. The extraction recovery of itraconazole was 96%. The validated assay was applied to a pharmacokinetic study of itraconazole in rats following administration of a single dose of itraconazole (15 mg/kg). Mass spectrometric detection was carried out using a PE Sciex API 100 single stage quadrupole instrument, operating in the positive atmospheric pressure ionization mode. The mass spectrometer was programd to admit the protonated molecule at the mass to charge ratios (m/z) of 705.2 (itraconazole), and 470.4 (Nefazodone). The positive turbo-ionspray voltage (V) was 4450 mV. The orifice and ring voltages were set at 56 and 395 mV, respectively. The dwell time was 200 ms. Curtain gas and nebulizing gas (nitrogen) pressure were set at 8.26 and 4.82 kPa, respectively. The flow-rate of heated gas was operated at 5 l/min. Turbolon Spray temperature was set at 35 °C. Analytical data were acquired by the PE Sciex Software (LC Tune 1.3) and the peak areas measured using MacQuan Software (MacQuan 1.6).

Vogeser *et al.* [66] used a liquid chromatography-tandem mass spectrometry, with online solid-phase extraction, for the determination of itraconazole and hydroxyitraconazole in plasma. The method proved rugged, enables short turn-around times, and is highly specific. A Waters Alliance 2690 high-performance liquid chromatography module was used, coupled to a Micromass Quattro liquid chromatography-tandem mass spectrometry system with a split of approximately 1:10. Compound R51012 (dimethyl homolog of itraconazole) was used as the internal standard for itraconazole and hydroxyitraconazole. The analytical column, a LiCrospher C-18 end-capped 12.5 cm × 4 mm; 5 μm, was equilibrated with acetonitrile–2 mM ammonium acetate (80:20) delivered at a flow-rate of 0.85 ml/min. The mobile phase was water–methanol (95:5) delivered at a flow-rate of 3 ml/min. The retention times of itraconazole, hydroxyitraconazole, and the internal standard were approximately 3.6, 2.9 and 3.9 min, respectively. Electrospray atmospheric pressure ionization in the positive mode was used. The quasimolecular ions ([M + H$^+$]) of itraconazole, hydroxyitraconazole and the internal standard compound are m/z 705, 721, and 733, respectively.

Kunze *et al.* [67] developed a stereoselective high-performance liquid chromatographic-mass spectrometric assay method to analyze the

concentrations of itraconazole stereoisomers in plasma and to determine the absolute configuration of formed metabolites. The stereoisomers were separated using Chiralpak AS-RH (5 µm) column (15 cm × 2.1 mm) with a mobile phase flow-rate of 0.2 ml/min. The initial mobile phase was 30% acetonitrile:70% aqueous 5 mM ammonium acetate. The acetonitrile concentration increased linearly to 70% between 4 and 50 min, then to 80% over additional two min. Ions monitored were m/z 705 for itraconazole and m/z 721 for hydroxyitraconazole, m/z 719 for keto-itraconazole and m/z 649 for N-desalkylitraconazole, all [MH$^+$]-ions. The drying gas flow was set at 10 l/min, nebulizer pressure at 25 psig, gas temperature at 300 °C and the capillary voltage at 5500 V. The fragmentor was set at 160 V for all ions. The incubation samples were prepared identically to the nonchiral assay. For plasma samples, 300 µl of acetonitrile was added to 100 µl of plasma and the samples were centrifuged at 10,000 g for 10 min and then transferred to autosampler vials. A 20 µl sample was injected on column.

Choi *et al.* [68] developed a highly sensitive high-performance liquid chromatographic-tandem mass spectrometric method to quantify itraconazole in human plasma for the purpose of pharmacokinetic studies. Sample preparation was carried out by liquid–liquid extraction using loratadine as an internal standard. Chromatographic separation used a YMC C$_{18}$ column giving an extremely fast total run time of 3 min. The method was validated and used for the bioequivalence study of itraconazole tablets in healthy male volunteers ($n = 31$). The lower limit detection proved to be 0.2 ng/ml for itraconazole. The column used was a YMC C$_{18}$ (5 × 2 mm, 3 µm). The mobile phase consisted of acetonitrile: 10 mM ammonium formate (85:15) and was set at a flow-rate of 0.2 ml/min. Mass spectrometric detection was performed using: Applied Biosystem MDS SCIEX API 3000 triple-quadrupole mass spectrometry. Electrospray ionization–mass spectrometry was performed in the positive mode using: nebulizing gas, nitrogen, collision gas, nitrogen; ion spray temperature, 350 °C and an ion spray voltage of 5.5 kV System control and data evaluation were carried out using Analyst$^®$ (ver. 1.3). Multiple reaction monitoring was used to quantify itraconazole (m/z 705.2→392.5) and loratadine (m/z 383.1 → 336.8).

Kousoulus *et al.* [69] developed a high-throughput method for the simultaneous determination of itraconazole and its hydroxyl metabolite in human plasma, employing automated liquid–liquid extraction based on 96-well format plates and liquid chromatography-tandem mass spectrometry. The plasma samples underwent liquid–liquid extraction in 2.2 ml 96 deepwell plates. Itraconazole and its hydroxyl metabolite and the internal standard R51012 were extracted from plasma, using a mixture of acetonitrile, and methyl tertiary butyl ether as the organic solvent. This specific mixture, due to its composition, had a significant impact on the

performance of the assay. All liquid transfer steps, including preparation of calibration standards and quality control samples as well as the addition of the internal standard were performed automatically using robotic liquid handling workstations for parallel sample processing. After vortexing, centrifugation, and freezing, the supernatant organic solvent was evaporated. The analytes and internal standard were dissolved in a small volume of a reconstitution solution, an aliquot of which was analyzed by combined reversed-phase liquid chromatography-tandem mass spectrometry, with positive ion electrospray ionization and a Turbolon Spray interface, using multiple reactions monitoring. The method was shown to be sensitive and specific to both itraconazole and hydroxyl Itraconazole. It revealed excellent linearity for the range of concentrations 2–500 ng/ml for itraconazole and 4–1000 ng/ml for hydroxyitraconazole. It was very accurate at it gave very good inter and intraday precisions. The method was employed in a bioequivalence study after per os administration of two 100 mg tablets of itraconazole and it allowed this study to be completed in under 4 days. The isocratic high-performance liquid chromatographic elution mobile phase was composed of 80% acetonitrile and 20% mM ammonium acetate. The pH of the 10 mM ammonium acetate solution was adjusted to 3.5 by adding glacial acetic acid. A flow-rate of 0.6 ml/min was used for sample analysis on a YMC-Pack ODS-A C18 analytical column (5 cm × 4 mm). The column was maintained at ambient temperature (23 °C) whilst the autosampler temperature was set at 10 °C. The injection volume was 50 µl and the total run time was set at 2 min.

5.2.2.4. Electrokinetic chromatography   Castro-Puyana *et al.* [70] used an electrokinetic chromatographic method for the separation and quantitation of four stereoisomers of itraconazole in pharmaceutical formulation. The four isomers were resolved by electrokinetic electrophoresis using a cyclodextrin as a chiral selector. A study on the enantiomeric separation ability of different neutral cyclodextrins was carried out: Heptakis-2,3,6-tri-*O*-methyl-β-cyclodextrin was shown to provide the highest values for the enantiomeric resolution. The influence of some experimental conditions, such as pH, chiral selector concentration, and temperature, on the enantiomeric separation was also studied. The use of a 100 mM phosphate buffer (pH 2.5), 30 mM in heptakis-2,3,6-tri-*O*-methyl-β-cyclodextrin with an applied voltage of 30 kV and a temperature of 20 °C enabled the separation of the enantiomers of itraconazole with high resolutions ($R_s > 3$). The method was validated and applied to the quantitative analysis of itraconazole in three pharmaceutical formulations.

Breadmore *et al.* [71] studied the electrokinetic separation of the hydrophobic antimycotic drug itraconazole and its major metabolite, hydroxyitraconazole, by a binary aqueous–organic solvent medium containing

sodium dodecyl sulphate, by microemulsion electrokinetic chromatography and by miceller electrokinetic chromatography. The results suggest that the first approach is difficult to apply and that there is no substantial difference between separations performed using microemulsion electrokinetic chromatography and miceller electrokinetic chromatography modified with *n*-butanol. The simpler miceller electrokinetic chromatography method is more than adequate and was thus employed for the analysis of itraconazole and hydroxyitraconazole in human serum and plasma. Separation was achieved in plain fused-silica capillaries having a low-pH buffer (pH 2.2) and sodium dodecyl sulphate micelles and reversed polarity. The addition of 2-propanol and *n*-butanol enhanced analyte solubility and altered the selectivity of the separation by influencing the magnitude of the electrophoretic component in the separation mechanism. Under optimized conditions and using head-column field-amplified sample stacking, an internal standard, itraconazole, and two forms of hydroxyitraconazole could be separated in under 9 min, with detection limit less than 0.01 μg/ml. Analysis of samples from patients currently prescribed itraconazole revealed a different hydroxyitraconazole peak area ratio to that of the standard, suggesting a stereoselective component of itraconazole metabolization. Comparison of miceller electrokinetic chromatography data with those of a high-performance liquid chromatographic method employed on a routine basis showed excellent agreement, indicating the potential of this approach for therapeutic drug monitoring of itraconazole.

5.2.2.5. Capillary electrophoresis   Zhang *et al.* reported the separation of hydrophobic, positively chargeable substances by a capillary electrophoresis method [72]. Capillary electrophoresis at +20 or 20 kV with 220 nm detection was carried out (a) on a Biofocus 3000 System (Bio-Rad, Hercules, CA, USA) at 20 °C, or (b) on a Prince apparatus (Polymicro Technologies, Phoenix, AZ, USA) at 35 °C with the use of a fused-silica capillary (40 cm × 50 μm i.d.), or 55.5 cm × 50 μm i.d., respectively). Phosphate running buffers of pH 2–11 were used: aqueous, mixed with organic solvents, or containing surfactants (0.5 μM–75 mM) or other additives. Systems containing micelle-forming or ion-pairing reagents gave unsatisfactory results. Capillary zone electrophoresis in systems containing 40% or 60% of propanol or 60% of tetrahydrofuran or capillary electrophoresis in presence of β-cyclodextrin (20 mM) or other neutral complexing agents afforded good separation. Itraconazole could be determined in aqueous buffer containing β-cyclodextrin at pH 2–3. The methods were extended to the analysis of the drugs in serum.

Breadmore and Thormann developed a chiral capillary electrophoretic method, for the separation of itraconazole stereoisomers and those of its metabolite hydroxyitraconazole, to determine the stereoselective nature

of itraconazole and hydroxyitraconazole biotransformation [73]. The method is based on the formation of inclusion complexes of the target analytes with the negatively charged sulphated β-cyclodextrin in the presence of moderate concentrations of methanol in a low pH phosphate buffer. The addition of polyethylene glycol 4000 was found to be critical in obtaining baseline resolution of eight peaks, two form itraconazole, four from hydroxyitraconazole and two from R0 51012 (internal standard), in under 20 min. Application of the developed procedure to serum samples from patients being treated with itraconazole showed clearly the presence of a stereoselective component in the metabolism of this antimycotic drug. This could be shown from *in vitro* incubations with single enzyme. Super-somes to be in part due to the stereoselective formation of hydroxyitraco-nazole by the human CYP3A4 enzyme. For 1 patient, monitoring of the itraconazole and hydroxyitraconazole and peak ratios over a 103-day period of treatment with itraconazole showed a strong dependency of the chiral itraconazole ratio to the concentration of itraconazole, while the dominant enantiomeric ratio of hydroxyitraconazole was largely inde-pendent of the total hydroxyitraconazole concentration.

Crego *et al.* [74] developed a simple and robust solid-phase extraction procedure for the cleanup and sample preconcentration of itraconazole and four other antifungal agents and their metabolites after incubation with human liver microsomes, as well as a simplified capillary-zone electrophoresis method for their rapid analysis, to determine the stability of these compounds in *in vitro* samples. Three different sample pretreat-ment procedures using solid-phase extraction with reversed-phase sor-bents (100 mg C-8, 100 mg C-18, and 30 mg Oasis-HLB) were studied. The highest and most reproducible recoveries were obtained using a 30 mg Oasis-HLB sorbent and methanol containing 2% acetic acid as eluent. Enrichment by a factor of about four times was achieved by reconstituting the final solid-phase extraction eluates to a small volume. For the capillary-zone electrophoresis, good separations without interfering peaks due to the *in vitro* matrix were obtained with a simple running electrolyte using a fused-silica capillary. The best separation for all com-ponents originated by each tested drug after incubation with human liver microsomes (unmetabolized parent drug and its metabolites) was obtained using 0.05 M phosphate running buffer (pH 2.2) without addi-tives. The effect of the injection volume was also investigated in order to obtain the best sensitivity. Performance levels in terms of precision, linearity, limit of detection, and robustness were determined.

5.2.3. Biological methods

Law *et al.* [30] used a bioassay method for measuring serum itraconazole concentrations using hydroxyitraconazole standards. Low concentrations of itraconazole in serum have been associated with therapeutic failure.

Variable interpatient bioavailability and detrimental drug interactions with P450 enzyme-inducing agents are well documented. The routine monitoring of serum itraconazole concentrations in patients with life-threatening mycoses is essential for patient care. Present high-performance liquid chromatographic methods measure only concentrations of itraconazole and not its active metabolite, hydroxyitraconazole. Bioassay methods using itraconazole standards overestimate concentrations in serum as measured by high-performance liquid chromatography. This bioassay method measures the total serum itraconazole and hydroxyitraconazole concentrations using hydroxyitraconazole standards. Itraconazole and hydroxyitraconazle concentrations in forty clinical samples were assayed by high-performance liquid chromatography. Total drug concentrations were measured in the same samples by bioassay with itraconazole or hydroxyitraconazole standards. The correlation of concentrations measured by the last bioassay method with high-performance liquid chromatographic determinations of both compounds was excellent ($r = 0.98$, slope $= 0.5$), with acceptable reproducibility. Small errors were seen at extremes of concentrations. The ratio of hydroxyitraconazole to itraconazole in serum varied from 0.76 to 3.2. The use of hydroxyitraconazole standards rather than itraconazole standards for determination of total itraconazole and hydroxyitraconazole concentrations in serum by bioassay gives accurate and reproducible results that correlate well with total itraconazole and hydroxyitraconazole concentrations as measured by high-performance liquid chromatography. The data show that although hydroxyitraconazole gives larger inhibition zones than itraconazole in bioassay standards, this is not true for patient samples, in which the two compounds make equivalent contributions.

Odds *et al.* [52] carried out an interlaboratory collaborative study on the bioassays for itraconazole blood levels. Duplicate bioassays for itraconazole and hydroxyitraconazole were run with 30 serum samples in five laboratories, each using a different method. Both itraconazole and hydroxyitraconazole were used as standards. Despite quantitative variations, the results of the bioassays correlated sufficiently to indicate the relative level of antifungal activity in the test samples.

6. FOOD AND DRUG INTERACTION

Yeates *et al.* [75] examined the oral pharmacokinetics of 100 mg doses of fluconazole and itraconazole in separate but identically designed studies in Japanese and German subjects (both $n = 12$), both fasting and concomitant to a heavy breakfast. With fasting subjects, no significant difference was found with either antimycotic for any parameter. The mean area under the curve for itraconazole in Japanese subjects after the meal was only 54.9% of the value with Germans; the corresponding C_{max} was only

54.7%. As itraconazole is normally administered together with food, this suggests that there is a possibility of underdosage in Japanese subject.

Wishart [76] studied the influence of food on the pharmacokinetics of itraconazole in patients with superfacial fungal infection. The results showed that taking the drug with breakfast gives much better results than taking the drug before breakfast.

Barones *et al.* [77] evaluated the influence of food on itraconazole pharmacokinetics for twenty seven healthy volunteers in a single dose (200 mg) crossover study with capsules containing itraconazole-coated sugar spheres. The results of the food interaction segment showed that a meal significantly enhances the amount of itraconazole absorbed.

Cavalier *et al.* [78] evaluated the pharmacokinetics of itraconazole and ceftriaxone alone and in combination in a chronic model of catheterized miniature pigs. Itraconazole does not influence ceftriaxone kinetic behavior. Ceftriaxone was shown to alter the disposition of the triazole.

Kawakami *et al.* [79] examined the effect of grapefruit juice on the disposition of oral administered itraconazole in healthy subjects. Twenty two healthy male subjects received a single 100 mg dose of itraconazole with either 350 ml grapefruit juice, orange juice or mineral water. Plasma concentration of itraconazole were measured by high-performance liquid chromatography, and pharmacokinetics parameter; C_{max}, T_{max}, $T_{1/2}$, AUC, and AUC corrected by human body surface areas: AUC/s, were calculated. Grapefruit juice had no effect on any pharmacokinetic parameter of itraconazole, while that of orange juice decreased the parameters of $T_{1/2}$, AUC, and AUC/s of the drug.

Barone *et al.* [80] evaluated the effect of food on the bioavailability of itraconazole hydroxyl propyl-β-cyclodextrin solution under multiple-dose to steady-state conditions and to determine the pharmacokinetics of itraconazole solution at steady-state. The bioavailability of itraconazole and hydroxyitraconazole is enhanced when itraconazole oral solution is given in the fasted state; this was true for both single and multiple dosing to steady state.

Jaruratanasirikul and Sriwiriyajan [81] investigated the effects rifampicin on the pharmacokinetics of itraconazole in humans. The study was conducted with six healthy normal volunteers and three AIDS patients. All subjects received a 200 mg single dose of oral itraconazole on day one and day 15 and 600 mg of oral rifampicin once daily from day 2 to day 15. Itraconazole pharmacokinetics studies were carried out on day 1 and on day 15. Results showed that concentrations itraconazole were higher when it was administered alone than when it was administered with rifampicin. Rifampicin has a very strong inducing effect on the metabolism of itraconazole. These two drugs could not be administered concomitantly.

The authors [82] also studied the effect of omeprazole on the pharmacokinetics of itraconazole. Eleven healthy volunteers received a single

dose of oral itraconazole (200 mg) on days 1 and 15 and oral omeprazole (40 mg) once daily from day 2 to day 15. The concentrations of itraconazole were higher when it was taken alone than when it was taken with omeprazole. With concomitant omeprazole treatment, the mean AUC 0–24 and C_{max} of itraconazole were significantly reduced by 64% and 66%, respectively. Omeprazole affects itraconazole kinetics leading to a reduction in bioavailability and C_{max}. Itraconazole should not be used together with omeprazole.

Mizutani and Tabata [83] studied the effects of a high fat content of the coadministered meal and low pH liquid in pharmacokinetic parameters following itraconazole capsule administration. Healthy volunteers were given the drug with either a light meal or a high fat meal, or with either a glass of water or low pH liquid (cranberry juice) but without meal in crossover methods, and their pharmacokinetics parameter following each administration were evaluated respectively. The C_{max} and AUC showed increased following administration of the drug with either a high fat meal or with a glass of low pH liquid. It was revealed that administration of a high fat meal or with a glass of low pH liquid promoted absorption of itraconazole.

Shin *et al.* [59] reported that the dose-dependent pharmacokinetics of itraconazole after intravenous (10, 20, or 30 mg/kg) and oral (10, 30, or 50 mg/kg) administration and the first-pass effects of itraconazole after intravenous, intraportal, intragastric, and intraduodenal administration at a dose of 10 mg/kg were evaluated in rats. The hepatic and gastric first-pass effects were almost negligible in rats. The intestinal first-pass effect was approximately 70% of that of an oral dose of 10 mg/kg. The low bioavailability after oral administration of itraconazole at dose of 10 mg/kg could be mainly due to the considerable intestinal first-pass effect.

7. STABILITY

Carrier and Parent [64] performed a study on the stability of itraconazole and hydroxyitraconazole in dog plasma at ambient temperature. Spiked samples at 100 and 1000 ng/ml were lift at ambient temperature for 18 h. They were extracted and the results obtained were compared to freshly prepared extracted material at the same level. The results showed that itraconazole and hydroxyitraconazole were stable for at least 18 h in plasma kept at room temperature. After that period of time, 105 ± 3% of the expected concentration was recovered for both compounds. This indicated that dog plasma could be kept at ambient temperature for at least 18 h without altering the integrity of the samples. The stability of the extracted and reconstituted samples at ambient temperature was investigated. Samples spiked at 100 ng/ml were extracted and reconstituted.

Reconstituted samples were left for 3, 4.5, or 8 h on the bench at ambient temperature and then analyzed and compared to the freshly prepared extracted material at the same concentration. Results obtained showed that all three points tested, $108 \pm 7\%$, and $100 \pm 6\%$ of itraconazole and hydroxyitraconazole, respectively, of the expected concentration was recovered. This indicates that samples could be left on the injector tray for at least 8 h without altering the integrity of the analysis. Typically, the analysis of 100 samples will take less than 6 h.

Shin et al. [59] reported that itraconazole was stable in buffer solutions of pH 1 or 2 for up to a 48-h incubation; 98.2% and 114% of spiked amount of itraconazole were recovered after a 48-h incubation for buffer solutions having pHs of 1 and 2, respectively. The stability of itraconazole in buffer solutions having pH of 3–14 could not be determined due to solubility problems. Itraconazole was also stable in human gastric juices for up to a 4-h incubation; 100%, 102%, 110%, and 94% of the spiked amount of itraconazole were recovered after a 4-h incubation for human gastric juices having pHs of 3.9, 5.82, 3.19, 2.9, and 4.55, respectively. This indicates that itraconazole is stable in acidic conditions, and that enzymatic degradation of itraonazole in human gastric juices is almost negligible.

Jacobson et al. [84] studied the stability of itraconazole in an extemporaneously compounded oral liquid formulation. A suspension was prepared from beads contained in commercially available 100 mg itraconazole capsules and sufficient Simple Syrup, NF, to make a final volume of 60 ml. The final concentration of itraconazole in the suspension was 40 mg/ml. The final concentration of itraconazole in the suspension was 40 mg/ml. Three identical volumes of each suspension were prepared and stored in 2-oz capped, amber glass prescription bottles and refrigerated at 4 °C (range, 2–6 °C). Immediately after preparation and at 7, 14, 21, 28, and 35 days, samples were visually inspected and assayed in duplicate by high-performance liquid chromatography; the pH of samples was also determined. On day 35, the mean standard deviation percentage of initial itraconazole concentration remaining in the three suspensions was $95.3 \pm 2.2\%$. The color, odor, and pH of the samples did not change appreciably over the study period. Itraconazole 40 mg/ml in an oral liquid compounded from simple syrup and beads from capsules, stored in amber glass bottles, was stable for 35 days at 4 °C.

8. PHARMACOKINETICS

Hardin et al. [85] evaluated the pharmacokinetics of itraconazole in five healthy male volunteers. Each subject was studied on day 1 and 15 at the following dosages: 100 mg once daily (regimen A), 200 mg once daily (regimen B) and 200 mg twice daily (regimen C). On each study day,

itraconazole was administered with a standardized meal. Plasma samples were collected for 72 h post dose, and 24-h urine specimens were obtained. On day 1 of regimen C, plasma samples were collected following the second dose. Samples were assayed for itraconazole by a sensitive, reversed-phase high-performance liquid chromatography method. Wide intersubject variation in itraconazole concentration in plasma versus time profiles were observed in all study days.

Boelaert *et al.* [86] studied the single-dose pharmacokinetics of 200 mg of oral itraconazole in seven uremic patients, seven patients treated for hemodialysis, and five patients treated by continuous ambulatory peritoneal dialysis. Plasma concentration *versus* time profile showed wide intersubject variation. This study could not demonstrate any significant effect of renal dysfunction and hemodialysis or continuous ambulatory peritoneal dialysis treatment upon the pharmacokinetics of itraconazole.

Heykants *et al.* [87] presented an overview on the clinical pharmacokinetics of itraconazole. The pharmacokinetics of the drug in man are characterized by a good oral absorption, an extensive tissue distribution with tissue concentrations many times higher than in plasma, a relatively long elimination half-life of about 1 day and a biotransformation into a large number of metabolites. One of the metabolites hydroxyitraconazole, is antifungally active and explains why antifungal plasma levels, when measured by bioassay, are about three times the itraconazole levels measured by a specific high-performance liquid chromatographic method. Distribution studies have shown that therapeutically active levels of itraconazole are maintained much longer in some infected tissues than in plasma.

Negroni and Arechavala [88] presented a review on the pharmacokinetics and indications of itraconazole. The drug is a highly lipophilic compound, scarcely soluble in acidified polyethylene glycol and soluble in hydroxypropyl-β-cyclodextrin, it possesses an excellent digestive absorption and its peak plasma level after oral administration of 100 mg is 0.16 µg/ml at 3 or 4 h after drug intake. Half-life of the drug ranges between 17 and 21 h and 99.8% bind to plasma proteins, especially albumin. Metabolization is mainly done in the liver where inactive metabolites are formed with the exception of hydroxyitraconazole, which exhibits a discrete antifungal activity.

Cauwenbergh [89] reported that itraconazole is suitable for treatment of variety of systemic mycoses, as aspergillosis, cryptococcosis, candidiasis as well as non-European endemic mycosis. The lipophilicity of the drug molecule is the reason for the pronounced tissue affinity meaning that the tissue levels of the drug usually are substantially higher than the corresponding plasma levels.

Prentice *et al.* [90] measured the pharmacokinetics of itraconazole oral solution in seven patients receiving chemotherapy followed by

autologous bone marrow transplantation for leukemia or lymphoma. Patients received 5 mg/kg/day itraconazole either as once or twice daily dose. Drug concentration reached steady state by day 15, in both groups. The mean predose itraconazole serum concentration at h 0, day 8 was 385 ng/ml in the od group and 394 ng/ml in the bd group, rising to 762 and 845 ng/ml by day 15, respectively. The serum concentration of itraconazole suitable for antifungal prophylaxis can be attained in neutropenic patients, with the administration of an oral solution in a dosage of 5 mg/kg as either an od or bd schedule, following preautograft high dose cytotoxic chemotherapy.

De Doncker *et al.* [91] investigated the pharmacokinetics and pharmacodynamics of monthly cycles of 1 week pulse therapy with itraconazole. The efficacy and nail kinetics of intermittent pulse-dosing therapy with oral itraconazole in patients who were suffering from onychomycosis. Fifty patients with confirmed onychomycosis of toenails, predominantly *Trichophyton rubrum*, were recruited and randomly assigned to three ($n = 25$) or four ($n = 25$) pulses of 1 week itraconazole therapy (200 mg twice daily for each month). Clinical and mycological evaluation of the infected toenails, and determination of the drug levels in the distal nail ends of the fingernails and toenails, were performed at the end of each month up to month 6 and then every 2 months up to 1 year. In the three-pulses treatment group, the mean concentration of itraconazole in the distal ends of the toenails ranged from 67 (month 1) to 471 (month 6) ng/g, and in the distal ends of the fingernails, it ranged from 103 (month 1) to 424 (month 6) ng/g. At month 11, the drug was still present in the distal ends of the toenails at average concentrations of 186 ng/g. the highest individual concentrations of 1064 and 1166 ng/g were reached at month 6 for toenails and fingernails, respectively. The data suggest that pulse therapy with itraconazole is an effective and safe treatment option for onychomycosis.

Song *et al.* [92] reviewed the pharmacokinetic profile of itraconazole and its use in treatment of onychomycosis, *in vitro* antifungal activities and pharmacokinetics of itraconazole, and treatment of onychomycosis.

Vandewoude *et al.* [93] assessed the pharmacokinetics and safety of a hydroxyl-β-propyl solution of itraconazole in sixteen patients in an intensive care unit. One the first 2 days, four 1 h infusions of 200 mg were given at 0, 8, 24, and 32 h. From day 3 to 7, inclusive, a single 1 h infusion of 200 mg of itraconazole was given daily. The intravenous treatment was directly followed by repeated administration of an oral solution of itraconazole at a dosage of either 200 mg once daily or 200 mg twice daily. During the intravenous treatment, steady-state concentrations of itraconazole and hydroxylitraconazole in plasma were reached within 48 h and 96 h, respectively. The results of this study suggest that plasma itraconazole levels above 0.250 μg/ml may be achieved and maintained with the 1

week intravenous schedule followed by twice daily oral dose administration, whereas the once daily oral follow up seems to be a suboptimal treatment.

Reynes *et al.* [94] determined the pharmacokinetics of itraconazole formulated in a hydroxypropyl-β-cyclodextrin oral solution for two groups of human immunodeficiency virus (HIV)-infected adults with oral candidiasis. Patients received 100 mg of itraconazole every 12 h for 14 days. Concentrations of itraconazole and hydroxyitraconazole were measured in plasma and saliva by high-performance liquid chromatography. Pharmacokinetic parameters determined at day 1 and day 14 were comparable in both groups. The results of this study indicate that itraconazole generates effective levels in plasma and in saliva in HIV-infected patients; its relative bioavailability is not modified by the stage of HIV infection.

De Repentigny *et al.* [95] investigated the safety, tolerability, and pharmacokinetics of an oral solution of itraconazole and its active metabolites hydroxyitraconazole in an open multicenter study of 26 infants and children aged 6 months to 12 years with documented mucosal fungal infections or at risk for the development of invasive fungal disease. The patients were treated with itraconazole at a dosage of 5 mg/kg of body weight once daily for 2 weeks. Blood samples were taken after the first dose, during treatment, and up to 8 days after the last itraconazole dose. On day 1, the mean peak concentrations in plasma after the first and last doses and area under the concentration-time curve from 0 to 24 h for itraconazole and hydroxyitraconazole were lower in the children aged 6 months to 2 years than in the children aged 2–12 years but were comparable on day 14. It is concluded that an itraconazole oral solution given at 5 mg/kg/day provides potentially therapeutic concentrations in plasma, which are substantially lower than dose attained in adult cancer patients, and is well tolerated and safe in infants and children.

Michallet *et al.* [96] performed a prospective study of the pharmacokinetics of itraconazole solution in 11 patients who underwent allogeneic BMT (day of BMT = day 0) after a conditioning regimen including total body irradiation. Itraconazole solution (400 mg once a day) was given 7 days before BMT and continued up to the end of neutropenia unless another antifungal treatment was necessary. Blood samples were collected before itraconazole intake (C_{min}) and 4 h later (C_{max}) every other day for assays of itraconazole and its active metabolite hydroxyitraconazole. The mean values of C_{min} itraconazole and hydroxyitraconazole, respectively, were 287 ± 109 and 629 ± 227 ng/ml at day -1 and 378 ± 147 and 725 ± 242 ng/ml at day $+1$. The maximum C_{min} values were observed at day $+3$. Six patients at day -1 (54%) and eight patients at day $+1$ (72%) had satisfactory residual plasma concentrations of at least 250 ng/ml of unchanged itraconazole. These results show a good

bioavailability of itraconazole oral solution during the early phase after allogeneic BMT, but more data are needed for the late phases.

Gupta et al. [97] reported that the pharmacokinetics of itraconazole in nail results in drug remaining at therapeutic levels for 6–9 months after completion of the treatment of fingernail and toenail onychomycosis. Following continuous therapy at 200 mg/day for 3 months for toenail onychomycosis ($n = 1741$), the rate of clinical cure, clinical response and mycologic cure were: (meta-average $\pm$ 95% SE) 52 $\pm$ 9%, 86 $\pm$ 2%, and 74 $\pm$ 3%, respectively, at follow up 12 months following start of therapy. In fingernail onychomycosis ($n = 211$), the duration of therapy was 6 weeks and the corresponding efficacy rates at follow up, 9 months after start of the therapy, were meta-average ($\pm$SE) 82$\pm$5%, 90 $\pm$ 2%, and 86 $\pm$ 3%, respectively. Both the continuous and pulse therapy regiments are safe with a few adverse effects. Compared to continuous therapy, the pulse regimen has an improved adverse-effect profile, is more cost-effective and is preferred by many patients.

Schmitt et al. [98] investigated the pharmacokinetics and safety of an oral solution of itraconazole in two groups of neutropenic children stratified by age. Effective concentrations of itraconazole in plasma were reached quickly and maintained throughout treatment. The results indicate a trend toward higher concentrations of itraconazole in plasma in older children.

Debruyne and Coquerel [99] presented a review on the pharmacokinetics of itraconazole and other antifungal agents in onychomycoses. Itraconazole is well absorbed orally and can be detected in nails 1–2 weeks after the short therapy. The nail: plasma ratio stabilizes at around one by week 18 of treatment. Itraconazole is still detectable in nails 27 weeks after stopping administration. Nail concentrations are higher than the minimum inhibitory concentration for most dermatophytes and Candida species from the first month of treatment. The elimination half-life of Itraconazole from nails is long, ranging from 32 to 147 days.

Willems et al. [100] reviewed the pharmacokinetics and pharmacodynamics of itraconazole oral solution and intravenous formulation. Two new formulations of itraconazole, an oral solution and an intraverous formulation which combine lipophilic itraconazole with cyclodextrin. These formulations have improved the solubility of itraconazole, leading to enhanced absorption and bioavailability compared with the original capsule formulation, without having an impact on the tolerability profile of itraconazole. The oral solution and the intravenous formulations of the drug produce consistent plasma concentration and are ideal for the treatment of systemic fungal infections in a wide range of patient populations.

Koks et al. [101] described the development of a population pharmacokinetic model using NONMEM for itraconazole and its hydroxyitraconazole metabolite in a Thai cohort of HIV-infected patient who were using

itraconazole as an addition to their antiretroviral therapy. The data were described with an open two-compartment model for both itraconazole and hydroxyitraconazole. The model adequately described the data and provided population pharmacokinetic parameters which were not different from those described for other populations. It was found that concomitant use of co-trimoxazole leads to a reduced formation rate (-51%) of hydroxyitraconazole.

Conte *et al.* [102] determined the steady-state intrapulmonary pharmacokinetic and pharmacodynamic parameters of orally administered itraconazole, 200 mg every 12 h on an empty stomach, for a total of 10 doses, in 26 healthy volunteers. Five subgroups each underwent standardized bronchoscopy and bronchoalveolar lavage at 4, 8, 12, 16, and 24 h after administration of the last dose. Itraconazole and hydroxyitraconazole were measured in plasma, bronchoalveolar fluid and alveolar cells using high-performance liquid chromatography. Half-life and area under the concentration-time curves in plasma, epithelial lining fluid and alveolar cells were derived using noncompartmental analysis. Itraconazole and hydroxyitraconazole maximum concentrations of drug (C_{max}) in plasma epithelial lining fluid, and alveolar cells were 2.1 ± 0.8 and 3.3 ± 1, 0.5 ± 0.7 and 1 ± 0.9, and 5.5 ± 2.9 and 6.6 ± 3.1 µg/ml, respectively.

Conway *et al.* [103] assessed the pharmacokinetics of itraconazole and hydroxyitraconazole in patients with cystic fibrosis. Patients were divided into those who are less than sixteen and those who are equal or more than 16 years of age. All received itraconazole oral solution 2.5 mg/kg twice daily for 14 days. Serial blood samples were taken for itraconazole and hydroxyitraconazole plasma level measurements. Safety was assessed from biochemistry and hematology data and reported adverse events. Seventeen patients entered the study. Steady-state concentrations were achieved after maximally 8 days of dosing. On day 14 average peak plasma concentrations were 404 ± 268 ng/ml (<16 year, $n = 5$) and 779 ± 470 ng/ml (≥ 16 years, $n = 11$). A high intersubject variability in itraconazole pharmacokinetics was seen. Intrasubject variability was low. All younger patients and 50% of the older patient failed to achieve a plasma steady-state trough concentration of >250 ng/ml. The pharmacokinetics showed marked intersubject variability. The dosage regimen was safe and well tolerated.

Van Cauteren *et al.* [104] conducted several pharmacological studies on itraconazole in humans and animals. In dogs and rats, no significant toxic effects were seen at doses up to 40 mg/kg. Endocrinological studies demonstrated that itraconazole does not significantly affect human testicular and Adrenol steroidogenesis. The drug has a high tissue affinity and a longer half-life than ketoconazole. Itraconazole has a broader spectrum of activity and a lower potential for producing adverse effects.

De Beule [105] reported that itraconazole has a higher affinity for fungal cytochrome P-450 than ketoconazole but a low affinity for

mammalian cytochrome P-450. Inaconazole has a broad spectrum of activity than other azole antifungals and shows interesting pharmacokinetic features in terms of its tissue distribution. These properties have resulted in reduced treatment times for a number of diseases such as vaginal candidiasis, as well as effective oral treatment for several deep mycosis, including aspergillosis and candidiasis.

Kim *et al.* [106] investigated the absorption characteristics of itraconazole from the intestinal segments in the anesthesized rat *in situ* in order to design an effective oral drug delivery system. The pH–solubility profile of itraconazole, the rate and the extent of its absorption, the optimal absorption site(s), and the absorption enhancing effect of sodium chlorate were examined. *In situ* single-pass perfusion method and recirculating perfusion technique using duodenum, jejunum, and ileum were employed for the calculation of apparent permeability and apparent first-order rate constant, respectively. Itraconazole showed appreciable aqueous solubility, only at pH values of <2 apparent permeability (cm/s) decreased in the following order: duodenum (10.24×10^{-4}) > jejunum (8.86×10^{-4}) ileum (3.78×10^{-4}). The apparent first-order rate constant/min decreased in the following order: Jejunum (17.12×10^{-3}) > duodenum (13.37×10^{-3}) > ileum (11.05×10^{-3}). The solubility of itraconazole markedly increased with the increase of the concentration of sodium cholate. The addition of 10 mM sodium cholate increased the apparent first-order rate constant of itraconazole in the ileum by a factor of 6.8.

Gamble *et al.* [107] assessed the plasma and tissues concentrations of itraconazole after oral dosing in reptiles, a 23.5 mg/kg itraconazole dose was administered orally with a standard food bolus once daily for 3 days to 10 groups of three or four spiny lizard (*Sceloporus sp.*). On days 0, 1, 2, 3, 4, 6, 9, 12, and 18, group samples of blood, liver, and muscle were collected. Microbiologic assay of itraconazole concentration was performed on these pooled samples. Values from an elimination graph of the concentrations of area under the curve (377.31 μg h/ml) and terminal elimination half-life (48.3 h) were obtained for itraconazole in spiny lizard plasma. With this dosing regimen, itraconazole plasma and liver concentrations would persist within reported minimum inhibitory concentrations for many fungal pathogens for 6 days beyond the peak concentration.

9. ABSORPTION, METABOLISM, AND EXCRETION

Itraconazole is slowly but well absorbed after oral administration with peak concentrations reached in approximately 4 h. Absorption is enhanced in the presence of food and in acidic intragasic environment. Itraconazole is metabolized, mainly *via* oxidative pathways, to inactive metabolites which are excreted *via* bile and urine. Over thirty metabolites

have been isolated and most are biologically inactive including a hydroxyl metabolite (bioactive) and hydroxyitraconazole. Both the drug and hydroxyitraconazole are inhibitors of CYP3A4 enzyme system. The drug is widely distributed throughout the body with small amounts detected in most body fluid and accumulation occurring in tissues. Itraconazole has also been detected in skin hair and nail but it does not easily redistribute in these tissues. Three to eighteen percent is excreted in the feces and unchanged drug [6].

Itraconazole blood level vary considerably among patients and are reduced by more than half in patients who are fasting [108], who have reduced gastric acid, or who have advanced AIDS [109, 110]. Itraconazole is more than 90% bound to serum proteins. Extensive binding to tissues also occurs. No detectable drug appears in cerebrospinal fluid, and little or no intact drug appears in urine. Azotemia and hemodialysis do not affect plasma levels. Itraconazole is metabolized in the liver, although modes liver disease does not change drug catabolism. A biologically active metabolite, hydroxyitraconazole, appears in blood in concentrations almost twice that of unaltered drug [111]. Many fungi are equally susceptible to the parent drug and the hydroxylated metabolite. One commonly used bioassay uses an organism that is more susceptible to the metabolite than parent drug. The contribution of hydroxyitraconazole to the chemotherapeutic effect is unclear. Neither itraconazole nor hydroxyitraconazole penetrates well into the cerebrospinal fluid, and neither is excreted into the urine. Steady-state levels are reached only after several days, so loading dose often is used for 3 days. The half-life at steady state is approximately 30 h [5].

ACKNOWLEDGEMENT

REFERENCES

[1] S. Budavari (Ed.), *The Merck Index*, 12th edn., Merck and Co., Inc. Rahway, NJ, 1996, p. 916.

[2] J. E. F. Reynold (Ed.), *Martindale, The Extra Pharmacopeia*, 32nd edn., Royal Pharmaceutical Society, London, 1999, pp. 381–82.

[3] R. G. Alfonso (Ed.), *Remington, Practice of the Science and Pharmacy*, 19th edn., Mack Publishing Co., Easton PA, 1995, p. 1330.

[4] Swiss Pharmaceutical Society (Ed.), *Index Nominum 2000, International Drug Directory*, 17th edn., Medpharm GmbH Scientific Publishers, Stuttgart, 2000, p. 580.

[5] J. G. Hardman, and L. E. Limbirt (Eds.), *Goodman and Gilman's Pharmacological Basis of Therapeutics*, 9th edn., International Edition, McGraw Hill Health Profession Division, New York, 1996, p. 1182.

[6] A. C. Moffat, D. Osselton, and B. Widdop (Eds.), *Clarke's Analysis of Drugs and poisons*, 3rd edn., Pharmaceutical Press, London, 2004, p. 1151.

[7] *European Pharmacopoeia*, 4th edn., The Council of Europe, Strasburg, 2002, p. 1416.

[8] O. M. Peeters, N. M. Blaton, and C. J. De Ranter *Acta Crystallogr.*, 1996, **C52**, 2225.

[9] O. M. Peeters, N. M. Blaton, and C. J. De Ranter *Acta Crystallogr.*, 1979, **B35**, 2461.

[10] O. M. Peeters, N. M. Blaton, and C. J. De Ranter *Bull Soc. Chim. Belg.*, 1979, **88**, 265.

[11] A. A. Freer, A. Peerson, and E. G. Salole *Acta Crystallogr.*, 1986, **C42**, 1350.

[12] Hypercube (1993), *Chemplus: Extensions for Hyperchem.* Hypercube Inc., Waterloo, Ontario, Canada.

[13] E. Inkmann, and U. Holzgrabe *J. Pharm. Biomed. Anal.*, 1999, **20**, 297.

[14] N. Isoherranen, K. L. Kunze, K. E. Allen, W. L. Nelson, and K. E. Thummel *Drug Metab. Dispos.*, 2004, **32**, 1121.

[15] M. Haria, H. M. Bryson, and K. L. Goa *Drugs*, 1996, **51**, 585.

[16] G. Garber *Drugs*, 2001, **61**, 1.

[17] D. Slain, P. D. Rogers, J. D. Cleary, and S. W. Chapman *Ann. Pharmacother.*, 2001, **35**, 720.

[18] G. Albanese, P. Giorgetti, L. Santagostino, D. Crippa, and C. Sala *Arch. Dermatol.*, 1989, **125**, 1540.

[19] G. Pialoux, C. Hennequin, B. Dupont, and P. Ravisse *J. Infect. Dis.*, 1990, **162**, 1221.

[20] J. Dogra, and V. N. Saxena *Int. J. Parasitol.*, 1996, **26**, 1413.

[21] H. Akuffo, M. Dietz, S. Teklemariam, T. Tadesse, G. Amare, and T. Y. Berhan *Trans. R. Soc. Trop. Med. Hyg.*, 1990, **84**, 532.

[22] J. Heeres, and L. J. J. Backx 1980, *Eur. Pat. Appl.* **6**, 711.

[23] J. Heeres, and L. J. J. Backx 1981, *U.S. Pat.* **4 267**, 179.

[24] J. Heeres, L. J. J. Backx, and J. Van Cutsem *J. Med. Chem.*, 1984, **27**, 894.

[25] J. Heeres, L. J. J. Backx, J. H. Mostmans, and J. Van Cutsem *J. Med. Chem.*, 1979, **22**, 1003.

[26] J. Heeres, R. Hendrickx, and J. Van Cutsem *J. Med. Chem.*, 1983, **26**, 611.

[27] P. A. Devi, G. P. V. M. Rao, K. M. M. K. Prasad, and C. S. P. Sastry *Acta Ciencia Indica Chem.*, 2002, **28**, 127.

[28] P. A. Devi, G. P. V. M. Rao, K. M. M. K. Prasad, and C. S. P. Sastry *Asian J. Chem.*, 2002, **14**, 771.

[29] R. Woestenborghs, W. Lorreyne, and J. Heykants *J. Chromatogr.*, 1987, **413**, 332.

[30] D. Law, C. B. Moore, and D. W. Denning *Antimicrob. Agents Chemother.*, 1994, **38**, 1561.

[31] D. W. Warnock, A. Turner, and J. Burke *J. Antimicrob. Chemother.*, 1988, **21**, 93.

[32] S. A. Babhair *J. Liq. Chromatogr.*, 1988, **11**, 3261.

[33] R. P. Remmel, D. Dombrovskis, and D. M. Canafax *J. Chromatogr.*, 1988, **432**, 388.

[34] N. R. Badcock *J. Chromatogr.*, 1990, **525**, 478.

[35] S. Allenmark, A. Edebo, and K. Lindgren *J. Chromatogr.*, 1990, **532**, 203.

[36] N. R. Badcock, and A. Davies *Ann. Clin. Biochem.*, 1990, **27**, 506.

[37] F. Persat, C. Marzullo, D. Guyotat, M. J. Rochet, and M. A. Piens *Eur. J. Cancer*, 1992, **28A**, 838.

[38] J. M. Poirier, M. Lebot, P. Descamps, M. Levy, and G. Cheymol *Ther. Drug Monit.*, 1994, **16**, 596.

[39] N. Rifai, M. Sakamoto, O. Platt, and C. Brugnara *Ther. Drug Monit.*, 1995, **17**, 522.

[40] E. Brandsteterova, P. Kubalec, A. Rady, and V. Krcmery *Pharmazie*, 1995, **50**, 597.

[41] R. O. Darouiche, A. Setoodeh, and E. J. Anaissie *Antimicrob. Agents Chemother.*, 1995, **39**, 757.

[42] C. Lacroix, F. Wojciechowski, and P. Danger *Ann. Biol. Clin.*, 1995, **53**, 293.

[43] J. W. Huelsewede, H. Dermoumi, and R. Ansorg *Zentralbl Bakkeriol*, 1995, **282**, 457.

[44] T. K. C. Ng, R. C. Y. Chan, F. A. B. Adeyemi-Doro, S. W. Cheung, and A. F. B. Cheng *J. Antimicrob. Chemother.*, 1996, **37**, 465.

[45] D. Compas, D. J. Touw, and P. N. F. C. de-Goede *J. Chromatogr.*, 1996, **687**, 453.
[46] M. Cociglio, D. Hillaire-Buys, and R. Alric *J. Chromatogr.*, 1997, **698**, 225.
[47] J. M. Poirier, and G. Cheymol *Ther. Drug Monit.*, 1997, **19**, 247.
[48] S. K. Cox, S. Orosz, J. Burnette, and D. Frazier *J. Chromatogr.*, 1997, **702**, 175.
[49] P. O. Gubbins, B. J. Gurley, and J. Bowman *J. Pharm. Biomed. Anal.*, 1998, **16**, 1005.
[50] L. Bai, X. Y. Lu, X. L. Chen, *et al. Yiyuan Xaoxue Zazhi*, 1999, **19**, 7.
[51] A. Thienpont, J. Gal, C. Aeschlimann, and G. Félix *Analusis*, 1999, **27**, 713.
[52] F. C. Odds, B. Dupont, M. G. Rinaldi, D. A. Stevens, D. W. Warnock, and R. Woestenborghs *J. Antimicrob. Chemother.*, 1999, **43**, 723.
[53] S. Al-Rawithi, R. Hussein, I. Al-Mohsen, and D. Raines *Ther. Drug Monit.*, 2001, **23**, 445.
[54] P. Kubalec, and E. Brandsteterova *Pharmazie*, 2001, **56**, 397.
[55] C. H. Koks, R. W. Sparidans, G. Lucassen, K. M. Crommentuyn, and J. H. Beijnen *J. Chromatogr.*, 2002, **767**, 103.
[56] J. W. Wong, U. R. Nisar, and K. H. Yuen *J. Chromatogr.*, 2003, **798**, 355.
[57] V. Srivatsan, A. K. Dasgupta, P. Kale, R. R. Datla, D. Soni, M. Patel, R. Patel, and C. Mavadhiya *J. Chromatogr.*, 2004, **1031**, 307.
[58] F. Li, X. Qi, L. Li, M. Ma, S. Wang, and D. Su *Chin. J. Pharm.*, 2004, **6**, 134.
[59] J. H. Shin, K. Y. Choi, Y. C. Kim, and M. G. Lee *Antimicrob. Agents Chemother.*, 2004, **48**, 1756.
[60] G. A. Khoschsorur, F. Fruehwirth, and S. Zelzer *Antimicrob. Agents Chemother.*, 2005, **49**, 3569.
[61] T. Ohkubo, and T. Osanai *Ann. Clin. Biochem.*, 2005, **42**, 94.
[62] S. Redmann, and B. G. Charles *Biomed. Chromatogr.*, 2006, **20**, 343.
[63] S. E. Orosz, E. C. Schroeder, S. K. Cox, S. Doss and D. L. Frazier, http://www.lafeber.com/lafeber-library/ppi_in_amazons.asp.
[64] A. Carrier, and J. Parent *J. Chromatogr.*, 2000, **745**, 413.
[65] M. Yao, L. Chen, and N. R. Srinivas *J. Chromatogr.*, 2001, **752**, 9.
[66] M. Vogeser, U. Spohrer, and X. Schiel *Clin. Chem. Lab. Med.*, 2003, **41**, 915.
[67] K. L. Kunze, W. L. Nelson, E. D. Kharasch, K. E. Thummel, and N. Isoherranen *Drug Metab. Dispos.*, 2006, **34**, 583.
[68] Y. W. Choi, D. Nam, K. H. Kang, K. W. Ha, I. H. Han, B. K. Chang, M. Yoon, and J. Lee *Bull. Korean Chem. Soc.*, 2006, **27**, 291.
[69] C. Kousoulos, G. Tastsou, C. Apostolou, Y. Dotsikas, and Y. L. Loukas *Anal. Bioanal. Chim.*, 2006, **384**, 199.
[70] M. Castro-Puyana, A. L. Crego, and M. Luisa Marina *Electrophoresis*, 2006, **27**, 887.
[71] M. C. Breadmore, A. Prochazkova, R. Theurillat, and W. Thormann *J. Chromatogr.*, 2003, **1014**, 57.
[72] C. X. Zhang, F. von-Heeren, and W. Thormann *Anal. Chem.*, 1995, **67**, 2070.
[73] M. C. Breadmore, and W. Thormann *Electrophoresis*, 2003, **24**, 2588.
[74] A. L. Crego, J. Gomez, M. L. Marina, and J. L. Lavandera *Electrophoresis*, 2001, **22**, 2503.
[75] R. A. Yeates, T. Zimmermann, H. Laufen, M. Albrecht, and A. Wildfeuer *Int. J. Clin. Pharmacol. Ther.*, 1995, **33**, 131.
[76] J. M. Wishart *J. Am. Acad. Dermatol.*, 1987, **17**, 220.
[77] J. A. Barone, J. G. Koh, R. H. Bierman, J. L. Colaizzi, K. A. Swanson, M. C. Gaffar, B. L. Moskovitz, W. Mechlinski, and V. Van de Velde *Antimicrob Agents Chemother.*, 1993, **37**, 778.
[78] A. Cavalier, D. Leveque, J. D. Peter, J. Salmon, H. Elkhaili, Y. Salmon, P. Nobelis, J. Geisert, H. Monteil, and F. Jehl *Antimicrob. Agents Chemother.*, 1997, **41**, 2029.
[79] M. Kawakami, K. Suzuki, T. Ishizuka, T. Hidaka, Y. Matsuki, and H. Nakamura *Int. J. Clin. Pharmacol. Ther.*, 1998, **36**, 306.
[80] J. A. Barone, B. L. Moskovitz, J. Guarnieri, A. E. Hassell, J. L. Colaizzi, R. H. Bierman, H. Robert, and L. Jessen *Pharmacotherapy*, 1998, **18**, 295.

[81]   S. Jaruratarasirikul, and S. Sriwiriyajan *Eur. J. Clin. Pharmacol.*, 1998, **54**, 155.

[82]   S. Jaruratanasirikul, and S. Sriwiriyajan *Eur. J. Clin. Pharmacol.*, 1998, **54**, 159.

[83]   T. Mizutani, and H. Tabata *Kagaku Ryoho no Ryoiki*, 2003, **19**, 441.

[84]   P. A. Jacobson, C. E. Johnson, and J. R. Walters *Am. J. Health Syst. Pharm.*, 1995, **52**, 189.

[85]   T. C. Hardin, J. R. Graybill, R. Fetchick, R. Woestenborghs, M. G. Rinaldi, and J. G. Kuhn *Antimicrob. Agents Chemother.*, 1988, **32**, 1310.

[86]   J. Boelaert, M. Schurgers, E. Matthys, R. Daneels, A. Van Peers, K. De Beule, R. Woestenborghs, and J. Heykants *Antimicrob. Agents Chemother.*, 1988, **32**, 1595.

[87]   J. Heykants, A. Van Peers, V. Van del Velde, P. Van Rooy, W. Meuldermans, K. Lavrijsen, R. Woestenborghs, J. Van Cutsem, and G. Cauwenbergh *Mycoses*, 1989, **32**(Suppl. 1), 67.

[88]   R. Negroni, and A. I. Arechavala *Arch. Med. Res.*, 1993, **24**, 387.

[89]   G. Cauwenbergh *Mycoses*, 1994, **37**(Suppl. 2), 27.

[90]   A. G. Prentice, D. W. Warnock, S. A. Johnson, M. J. Phillips, and D. A. Oliver *J. Antimicrob. Chemother.*, 1994, **34**, 247.

[91]   P. De Doncker, J. Decroix, G. E. Pierard, D. Roelant, R. Woestenborghs, P. Jacqmin, F. Odds, A. Heremans, P. Dockx, and D. Roseeuw *Arch. Dermatol.*, 1996, **132**, 34.

[92]   S. Song, R. Li, and D. Wang *Zhongguo Linchuang Yaolixue Zazhi*, 1997, **13**, 120.

[93]   K. Vandewoude, D. Vogelaers, J. Decruyenaere, P. Jaqmin, K. De Beule, A. Van Peer, R. Woestenborghs, K. Groen, and F. Colardyn *Antimicrob. Agents Chemother.*, 1997, **41**, 2714.

[94]   J. Reynes, C. Bazin, F. Ajana, A. Datry, J. P. Le Moing, E. Chwetzoff, and J. C. Levron *Antimicrob. Agents Chemother.*, 1997, **41**, 2554.

[95]   L. De Repentigny, J. Ratelle, L. Johanne, J. M. Leclerc, G. Cornu, E. M. Sokal, P. Jacqmin, and K. De Beule *Antimicrob Agents Chemother.*, 1998, **42**, 404.

[96]   M. Michallet, F. Persat, N. Kranzhofer, J. C. Levron, C. Prat, A. Belhabri, E. Chwetzoff, J. P. Le Moing, D. Fiere, and M. A. Piens *Bone Marrow Transplant.*, 1998, **21**, 1239.

[97]   A. K. Gupta, P. De Doncker, R. K. Scher, E. Haneke, C. R. Daniel 3rd, J. Andre, and R. Baran *Int. J. Dermatol.*, 1998, **37**, 303.

[98]   C. Schmitt, Y. Perel, J. L. Harousseau, S. Lemerle, E. Chwetzoff, J. P. Le Moing, and J. C. Levron *Antimicrob. Agents Chemother.*, 2001, **45**, 1561.

[99]   D. Debruyne, and A. Coquerel *Clin. Pharmacokinet.*, 2001, **40**, 441.

[100] L. Willems, R. Van der Geest, and K. De Beule *J. Clin. Pharm. Ther.*, 2001, **26**, 159.

[101] C. H. W. Koks, A. D. R. Huitema, D. M. B. Eugene, T. Chuenyam, R. W. Sparidans, J. M. A. Lange, and J. H. Beijnen *Ther. Drug Monit.*, 2003, **25**, 229.

[102] J. E. Conte Jr., J. A. Golden, J. Kipps, M. Mclver, and E. Zurlinden *Antimicrob. Agents Chemother.*, 2004, **48**, 3823.

[103] S. P. Conway, C. Etherington, D. G. Peckham, K. G. Brownlee, A. Whitehead, and H. Cunliffe *J. Antimicrob. Chemother.*, 2004, **53**, 841.

[104] H. Van Cauteren, J. Heykants, R. De Coster, and G. Cauwenbergh *Rev. Infect. Dis.*, 1987, **9**(Suppl. 1), S43.

[105] K. De Beule *Int. J. Antimicrob. Agents*, 1996, **6**, 175.

[106] Y. H. Kim, Y. S. Lee, G. P. Park, and K. P. Lee *Yakche Hakhoechi*, 1991, **21**, 215.

[107] K. C. Gamble, A. P. Alvarado, and C. L. Bennett *J. Zoo Wildlife Med.*, 1997, **28**, 89.

[108] D. Smith, V. Van de Velde, R. Woestenborghs, and B. G. Gazzard *J. Pharm. Pharmacol.*, 1992, **44**, 618.

[109] S. G. Lim, A. M. Sawyerr, M. Hudson, J. Sercombe, and R. E. Pounder *Aliment Pharmacol. Ther.*, 1993, **7**, 317.

[110] J. S. Hostetler, J. Heykants, K. V. Clemons, R. Woestenborghs, L. H. Hanson, and D. A. Stevens *Antimicrob. Agents Chemother.*, 1993, **37**, 2224.

[111] S. M. Grant, and S. P. Clissold *Drugs*, 1989, **37**, 310.

CHAPTER **6**

Ofloxacin

Mohammed A. Al-Omar

Department of Pharmaceutical Chemistry, College of Pharmacy, King Saud University, Riyadh-11451, Kingdom of Saudi Arabia

1. PHYSICAL PROFILES OF OFLOXACIN

1.1. General information

1. Nomenclature

Systemic chemical names [1, 2]

(±)-9-Fluoro-2,3-dihydro-3-methyl-10-(4-methyl-1-piperazinyl)-7-oxo-7H-Pyridol[1,2,3,-de]-1,4-benzoxazine-6-carboxylic acid.

Nonproprietary names

Ofloxacin.

Proprietary names [2–4]

Apazix; Bactocin; Exocin; Flobacin; Floxal; Floxil; Floxin; Girasid; Monoflocet; Ocuflox; Oflocet; Oflocin; Oxaldin; Tarivid; Urosin; Visiren; Zanocin.

Synonyms [3]

DL-8280; HOE-280; Ofloxacinum.

2. Formulae

Empirical formula, molecular weight, CAS number [3, 4]

$C_{18}H_{20}FN_3O_4$, 361.388, 0082419-36-1.

Structural formula
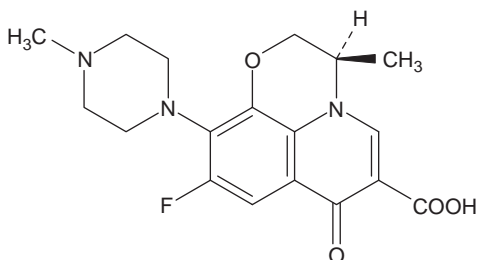
3. Elemental analysis

C, 59.83%; H, 5.5%; F, 5.26%; N, 11.63%; O, 17.71%.

4. Appearance [1, 3]
   A pale yellow or bright yellow crystalline powder, colorless needles
   from ethanol.

1.2. Physical characteristics

1.2.1. Solution pH
The concentrate solution of the drug has a pH of 3.8–5.5 in aqueous [5].

1.2.2. Solubility characteristics
Slightly soluble in water, alcohol, dichloromethane, and methyl alcohol;
sparingly soluble in chloroform. The solubility of ofloxacin varies
depending upon pH [3].

1.2.3. Optical activity
R-(+)-form, isomer, $[\alpha]^{23}$ + 76.9 (c = 0.385 in 0.5 N NaOH) rotation: +7.9°.
S-(–)-form, isomer, (levofloxacin): $[\alpha]^{23}$ − 76.9 (c = 0.385 in 0.5 N NaOH)
rotation: −7.9° [2].
   The angle of optical rotation, determined on solution S, is –0.10 ° to
+ 0.10°.

1.2.4. X-ray powder diffraction pattern
Crystal data were collected at 291 K using a Bruker Smart CCD 1000
diffractometer as described by Macías *et al.* [6]. Graphite monochromated
MoKa radiation (λ = l50.71073 Å) was used throughout. The data were
processed with SAINT and corrected for absorption using SADABS
(transmissions factors: 1.000–0.644). The structure was solved by direct
methods using the program SHELXS-86 and refined by full-matrix least-
squares techniques against F^2 using SHELXL-97. Positional and aniso-
tropic atomic displacement parameters were refined for all non-hydrogen
atoms. Atomic scattering factors were from the International Tables for
X-ray Crystallography. Molecular graphics were from Ref. [6], Fig. 6.1.
A summary of the crystal data, experimental details, and refinement
results are listed in Table 6.1.

1.2.5. Thermal methods of analysis
1.2.5.1. Melting behavior   The racemate ofloxacin mixture melts at
250–257 °C; S-(–)-form, levofloxacin melts at 225–227 °C [1, 2].

1.2.5.2. Differential scanning calorimetry   The differential scanning calo-
rimetry (DSC) thermogram of ofloxacin was obtained using a DuPont
TA-9900 thermal analyzer attached to DuPont Data Unit. The
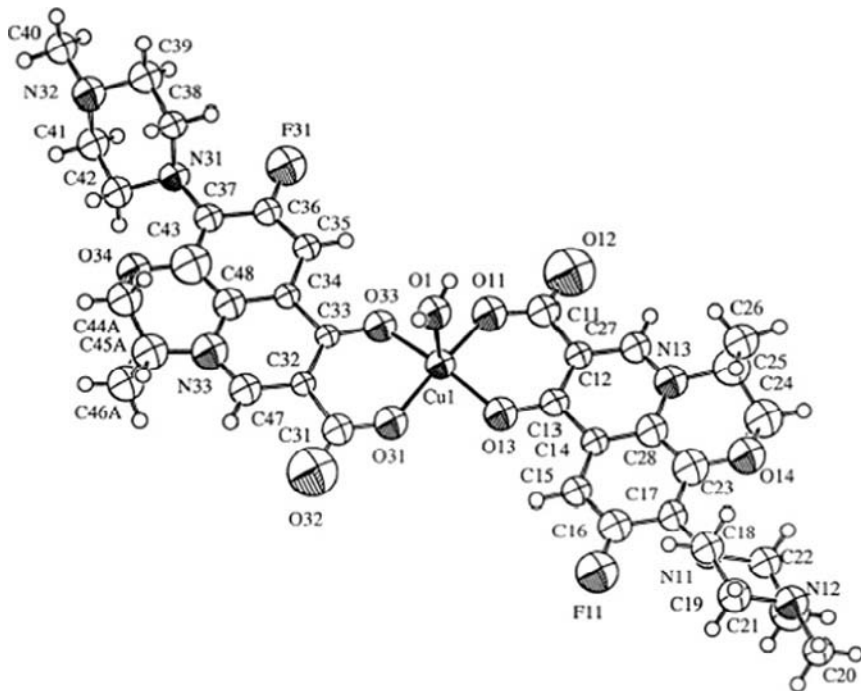
FIGURE 6.1 Projection of the ofloxacin modifications in the plane. Adapted from Ref. [6].

thermogram shown in Fig. 6.2 was obtained at a heating rate of 10 °C/min, and was run from 40 to 400 °C. The compound was found to melt at 256.51 °C.

1.2.6. Spectroscopy

1.2.6.1. Ultraviolet spectroscopy   The UV spectrum of ofloxacin (10 µg/µl) in ethanol is shown in Fig. 6.3. The spectrum was recorded using a Shimadzu UV–visible Spectrophotometer 1601 PC. Ofloxacin exhibited two maxima at 225.6 and 299.4 nm and shoulder at 328.8 nm:

λ_{max} (nm)	A (1%, 1 cm)	Molar absorptivity (L mol^{-1} cm^{-1})
225.6	477	1.72×10^4
299.4	996	3.59×10^4
328.8	385	1.39×10^4

1.2.6.2. Vibrational spectroscopy   The infrared absorption spectrum of ofloxacin was obtained in a KBr disc using a Perkin Elmer infrared spectrophotometer. The infrared spectrum is shown in Fig. 6.4 and the principal peaks are at 3428, 3071, 2967, 2786, 1714, 1550, and 1460 cm^{-1}.

TABLE 6.1 Atomic coordinates ($\times 10^4$) and equivalent isotropic displacement parameters ($\mathring{A}^2 \times 10^3$) of ofloxacin

	x	y	z	U(eq)		x	y	z	U(eq)
F(11)	3367(4)	2153(2)	6647(2)	63(1)	C(23)	2988(7)	−836(5)	5854(3)	51(2)
F(31)	−3017(4)	2497(2)	−510(2)	60(1)	C(24)	2266(8)	−2925(5)	5609(4)	79(2)
O(1)	2361(7)	2472(5)	2513(4)	77(2)	C(25)	2477(7)	−2752(4)	4823(3)	51(2)
O(11)	−136(4)	751(3)	2649(2)	50(1)	C(26)	4007(9)	−2812(6)	4664(5)	116(3)
O(12)	−95(5)	−1189(3)	2574(2)	79(2)	C(27)	1884(6)	−1372(4)	3958(3)	39(1)
O(13)	999(4)	1818(3)	4024(2)	45(1)	C(28)	2284(6)	−609(4)	5140(3)	43(2)
O(14)	3315(6)	−1963(3)	6044(2)	95(2)	C(31)	−40(6)	4906(5)	3240(3)	44(2)
O(31)	437(4)	3928(3)	3048(2)	44(1)	C(32)	−720(6)	4944(4)	2444(3)	35(1)
O(32)	41(5)	5835(3)	3625(2)	76(2)	C(33)	−1042(6)	3918(4)	1958(3)	36(1)
O(33)	−847(4)	2852(3)	2139(2)	43(1)	C(34)	−1655(6)	4130(4)	1202(3)	34(1)
O(34)	−2553(7)	6623(3)	−13(2)	126(3)	C(35)	−2042(6)	3168(4)	681(3)	40(1)
N(11)	4143(5)	−20(4)	7089(2)	43(1)	C(36)	−2608(6)	3420(4)	−14(3)	40(1)
N(12)	6133(6)	−647(4)	8300(2)	55(1)	C(37)	−2857(6)	4568(5)	−284(3)	41(1)
N(13)	1954(5)	−1557(3)	4625(2)	45(1)	C(38)	−2459(6)	4433(5)	−1599(3)	49(2)
N(31)	−3466(5)	4665(4)	−1029(2)	41(1)	C(39)	−3265(6)	4292(5)	−2371(3)	51(2)

(*continued*)

TABLE 6.1 (*continued*)

	x	y	z	U(eq)		x	y	z	U(eq)
N(32)	−4092(5)	5343(4)	−2546(2)	48(1)	C(40)	−4807(8)	5255(5)	−3306(3)	78(2)
N(33)	−1516(5)	6236(3)	1471(2)	47(1)	C(41)	−5125(6)	5488(5)	−1993(3)	47(2)
C(11)	185(6)	−243(5)	2928(3)	45(2)	C(42)	−4333(6)	5704(4)	−1208(3)	44(2)
C(12)	888(6)	−274(4)	3708(3)	36(1)	C(43)	−2421(7)	5491(5)	224(3)	56(2)
C(13)	1246(6)	740(4)	4192(3)	33(1)	C(44A)	−1279(11)	7415(8)	376(5)	49(4)
C(14)	1941(6)	536(4)	4936(3)	35(1)	C(44B)	−3356(17)	7418(11)	743(8)	50(5)
C(15)	2315(6)	1478(4)	5464(3)	39(1)	C(45A)	−1620(50)	7370(30)	1140(20)	56(13)
C(16)	3007(6)	1237(4)	6143(3)	45(2)	C(45B)	−1900(40)	7550(30)	1261(17)	31(8)
C(17)	3391(6)	96(5)	6371(3)	42(1)	C(46A)	−3170(20)	7759(9)	1286(7)	73(5)
C(18)	5671(7)	321(5)	7118(3)	51(2)	C(46B)	−680(20)	7966(17)	904(10)	54(7)
C(19)	6333(7)	443(5)	7913(3)	60(2)	C(47)	−1001(6)	6052(4)	2176(3)	42(1)
C(20)	6791(9)	−531(6)	9087(4)	105(3)	C(48)	−1879(6)	5280(4)	967(3)	43(2)
C(21)	4610(7)	−929(5)	8286(3)	57(2)	O(2)	9251(10)	411(6)	1050(4)	192(4)
C(22)	3923(7)	−1103(5)	7495(3)	53(2)	O(3)	1851(7)	4361(4)	5045(3)	120(2)

U(eq) is defined as one third of the trace of the orthogonalized U_{ij} tensor [6].
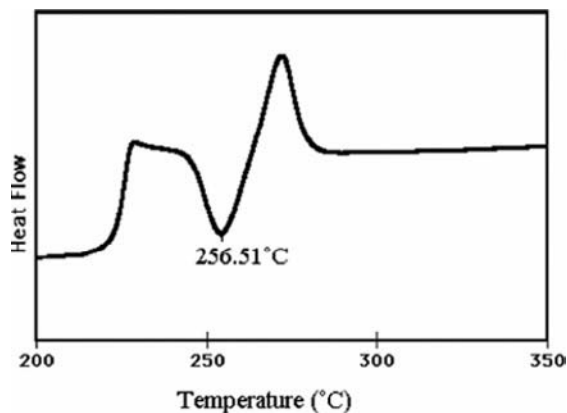
FIGURE 6.2   Differential scanning calorimetry thermogram of ofloxacin.

The assignment of infrared absorption bands for ofloxacin are abridged in Table 6.2 [7].

1.2.7. Nuclear magnetic resonance spectrometry

1.2.7.1. ^{1}H-NMR spectrum   The proton NMR spectrum of ofloxacin was obtained using a Bruker Avance Instrument operating at 300, 400, and 500 MHz. Standard Bruker Software was used to obtain COSY and HET-COR spectra. The sample was dissolved in D_2O and tetramethylsilane (TMS) was used as the internal standard. The proton NMR spectra are shown in Figs. 6.5 and 6.6. The COSY ^{1}H-NMR spectra are shown in Figs. 6.7 and 6.8 and the gradient HSQC- and HMBC-NMR spectra are shown in Figs. 6.9–6.13. The assignments for the ^{1}H-NMR spectral of ofloxacin are shown in Scheme 6.1.

1.2.7.2. ^{13}C-NMR spectrum   The carbon-13 NMR spectrum of ofloxacin was obtained using a Bruker Advance Instrument operating at 75, 100, and 125 MHz. Standard Bruker Software was used to obtain DEPT spectra. The sample was dissolved in D_2O and TMS was used as the internal standard. The carbon-13 NMR spectrum of ofloxacin is shown in Fig. 6.10. The DEPT 135-NMR spectra are shown in Figs. 6.14 and 6.15. The assignments for the various carbons of ofloxacin are shown in Scheme 6.2.

1.2.8. Mass spectrometry

The electron impact (EI) spectrum of ofloxacin is presented in Fig. 6.16. The mass spectrum was recorded using a Shimadzu PQ-5000 GC-MS spectrometer. The spectrum shows a mass peak (*M*) at *m/z* 362 and a base peak at *m/z* 318 resulting from the loss of the nitrophyl group. The mass spectrum of ofloxacin shows a protonated molecular ion $[M + H]^+$. Two
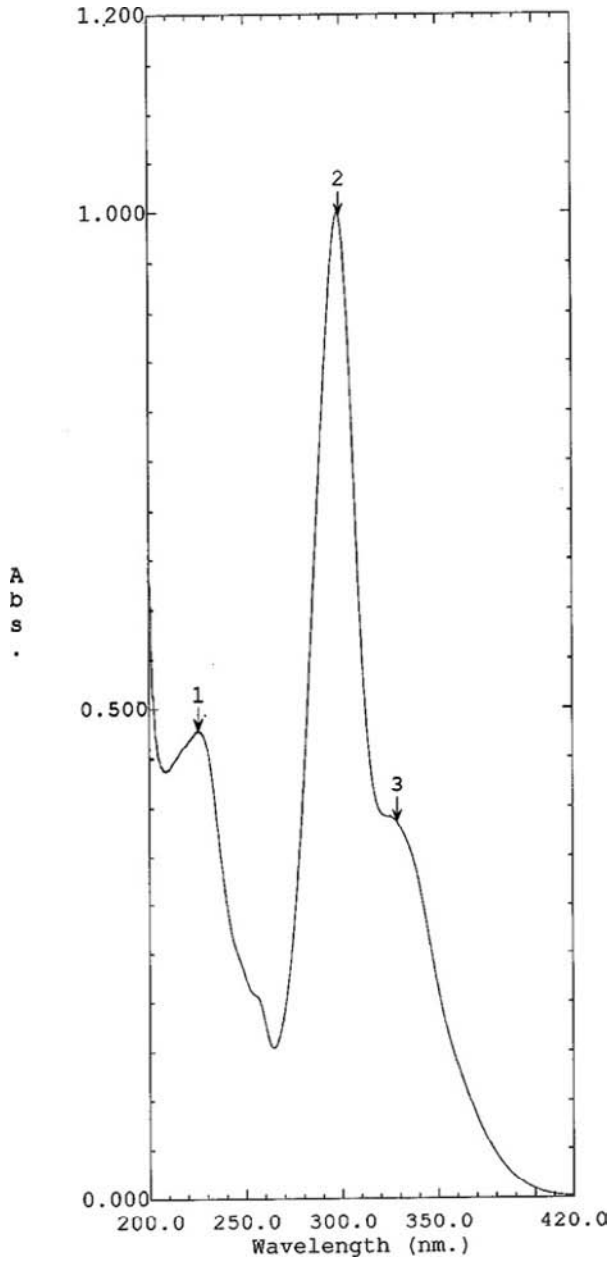
FIGURE 6.3   The ultraviolet absorption spectrum of ofloxacin in ethanol.
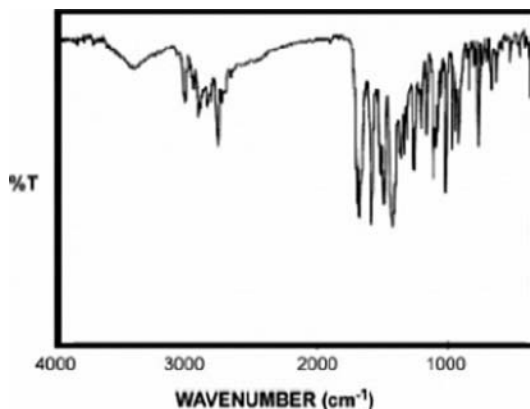
FIGURE 6.4   The infrared absorption spectrum of ofloxacin obtained in a KBr pellet.

SCHEME 6.1   Assignments of the protons chemical shifts of ofloxacin.
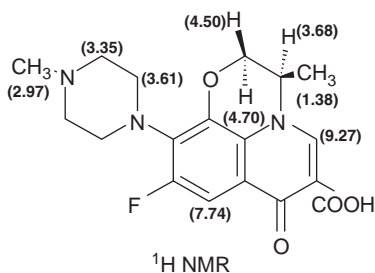
major fragmentation pathways were observed in the full scan spectra for this fluoroquinolone: (a) Loss of H_2O from the carboxyl function at C-3 and (b) Initial loss of CO_2 from the carboxyl group, followed by loss of C_3H_7N. These fragmentation patterns of the drug are presented in Table 6.3.

1.3. Stability and storage [5, 8]

The manufacturer recommends that ofloxacin tablets should be stored below 30 °C (86 °F) in a well-closed container [5]. Ofloxacin injection in single-use vials and premixed bottles should be stored at controlled room temperature (59–86 °F, 15–30 °C) and protected from freezing and light; brief exposure up to 104 °F (or 40 °C) does not adversely affect the product. When diluted in a compatible intravenous fluid to a concentration between 0.4 and 4 mg/ml, the solution is stable for 72 h at or below 75 °F (24 °C). The solution is stable for 14 days if stored under refrigeration at 41 °F or 5 °C in glass or plastic intravenous container. Solutions that are

SCHEME 6.2   Assignments of carbon-13 chemical shifts of ofloxacin.

^{13}C NMR
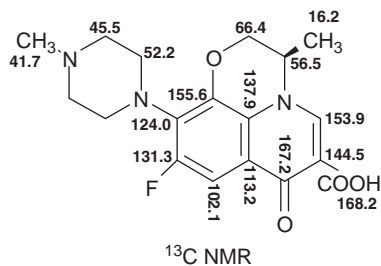
TABLE 6.2   Assignments for the infrared absorption bands of ofloxacin [7]

Frequency (cm^{-1})	Assignments
3043	$\upsilon_s(CH_2) + \upsilon(CH)$
3071	$\upsilon(CH)$
2936	$\upsilon_s(CH_2)$, $\upsilon(CH_2\text{-}S)$
2786	$\upsilon_s(CH_2)$
1714	$\upsilon(C=O)_{carboxylate}$, $\upsilon(C=O)_{gua\,+\,sulfo}$
1622	$\upsilon(C=O)_{ring}$, $\upsilon_s(COO^-)$, $\delta(NH_2)_{gua}$, $\delta(N-C=N) +$ $\delta(NH_2)$, $\delta(NH_3^+)$
1550	$\upsilon(CC) + \upsilon(CF)$, $\delta(NH_2)_{sulfo}$
1523	υ_{ring}, $\upsilon_{(thiazole)}$, $\upsilon_s(COO^-)$
1468	$\delta_s(CH_2) + \upsilon(CC)$
1460	$\delta_s(CH_3)$, υ_{ring}, $\delta_s(CH_2)$, $\delta(CH_2) + \upsilon_{(thiazole)}$, $\upsilon_{(thiazole)}$
1407	$\delta(N-CH_3)$
1397	$\upsilon(C-O) + \delta(OH)$
1371	$\delta(C-CH_3) + \upsilon(CC)$
1350	$\upsilon(CC) + \tau(CH_2)$, $\omega(CH_2) + \upsilon_{(thiazole)}$, $\upsilon_{as}(SO_2)$,
1306	$\omega(CH_2) + \delta(CH)$
1289	$\upsilon(C-F) + \upsilon(COOH)$, $\delta_{(thiazole)} + \gamma(CH_2\text{-}S)$
1254	$\upsilon(CC)$, $\delta(C_{thiazole-thiazole})$
1199	$\delta(OH) + \upsilon(C-O)$
1146	$\delta(CH)$
1132	$\delta(CH) + ring$, $\rho(NH_2)_{gua}$
1117	$\upsilon(C-N) + CH_3 + CH_2$
1056	$\delta(CH) + ring$, $\rho(NH_2)_{sulfo} + \upsilon(C-S)_{thioet}$
1011	$\delta ring$, $C-N_{gua} + \delta_{(thiazole)}$, $\omega(NH_2)$
980	$\gamma(CH)$
956	$\gamma(CH) + \rho(CH_2)$, $\upsilon(S-N)_{sulfo}$

(*continued*)

TABLE 6.2   (*continued*)

Frequency (cm^{-1})	Assignments
877	$\gamma(C=O)_{carboxylate}$
804	$\gamma(CH)$
782	$\delta(COOH)$
710	CH_2 rock + $\gamma(CH)$, $\omega(NH_2)_{sulfo}$
669	$\gamma(O–C=O) + \gamma(OH)$, $(C_{10-thiazole})$, $CCN + SO_2 + CS$
415	$\gamma(C=O)_{ring\ carbonyl}$

a, asymmetric; s, symmetric; υ, stretching; δ, in-plane deformation; γ, out-of-plane deformation; ω, wagging; ρ, rocking; τ, torsional relative intensity.
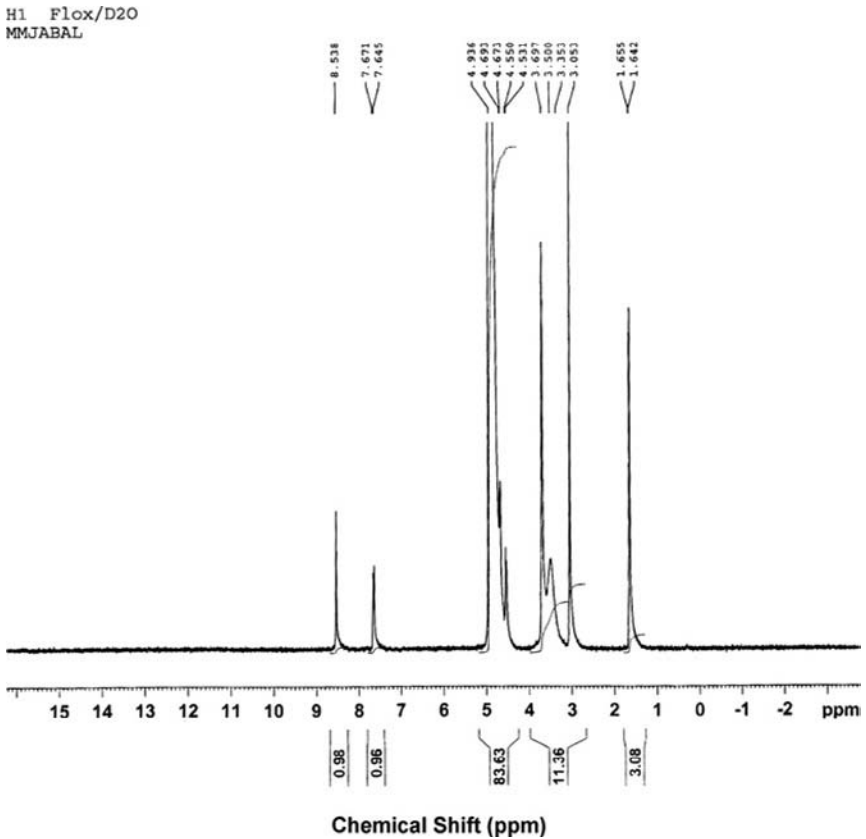
FIGURE 6.5   The ^{1}H-NMR spectrum of ofloxacin in D_2O.

H1   Flox/D2O
MMJABAL
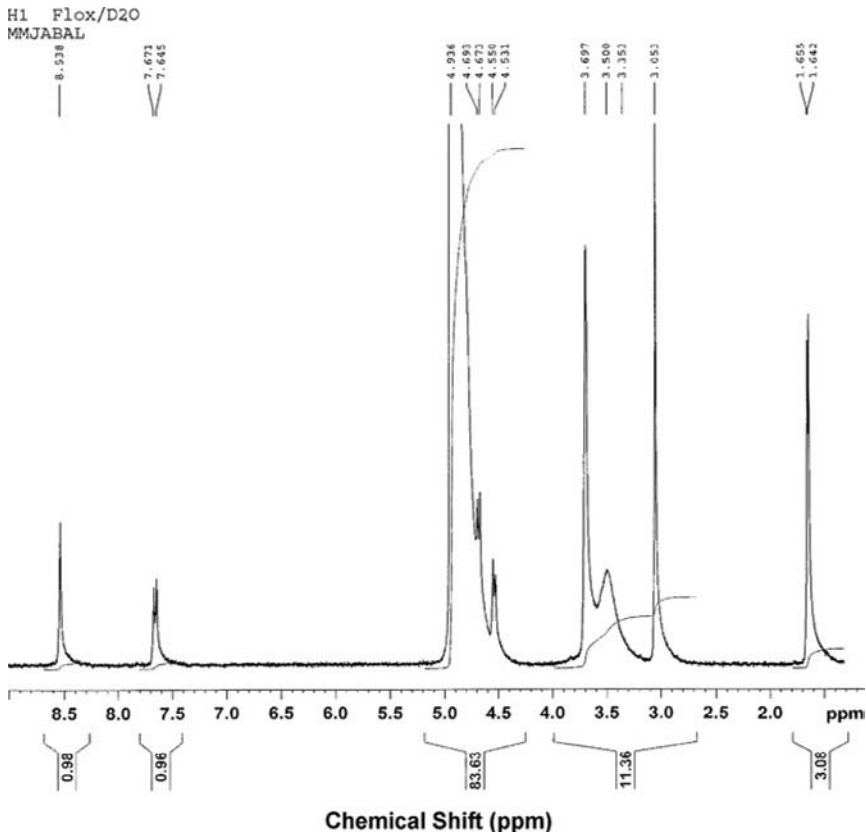
FIGURE 6.6   Expanded ^{1}H-NMR spectrum of ofloxacin in D$_2$O.

diluted as described above are stable for 6 months when stored at -4 °F or -20 °C. Once thawed, this solution is stable for 14 days if refrigerated at 36–46 °F (2–8 °C) [8]. It is not recommended to force thaw by microwave or water bath immersion.

Because of limited data on the compatibility of ofloxacin and other drugs, the manufacturer state that the drug should not be admixed with other drugs.

2. ANALYTICAL PROFILES OF OFLOXACIN

2.1. Compendial methods of analysis

2.1.1. Identification methods for the drug substances
The European Pharmacopoeia [9] recommends the use of infrared absorption spectrophotometry for the identification of the pure drug.
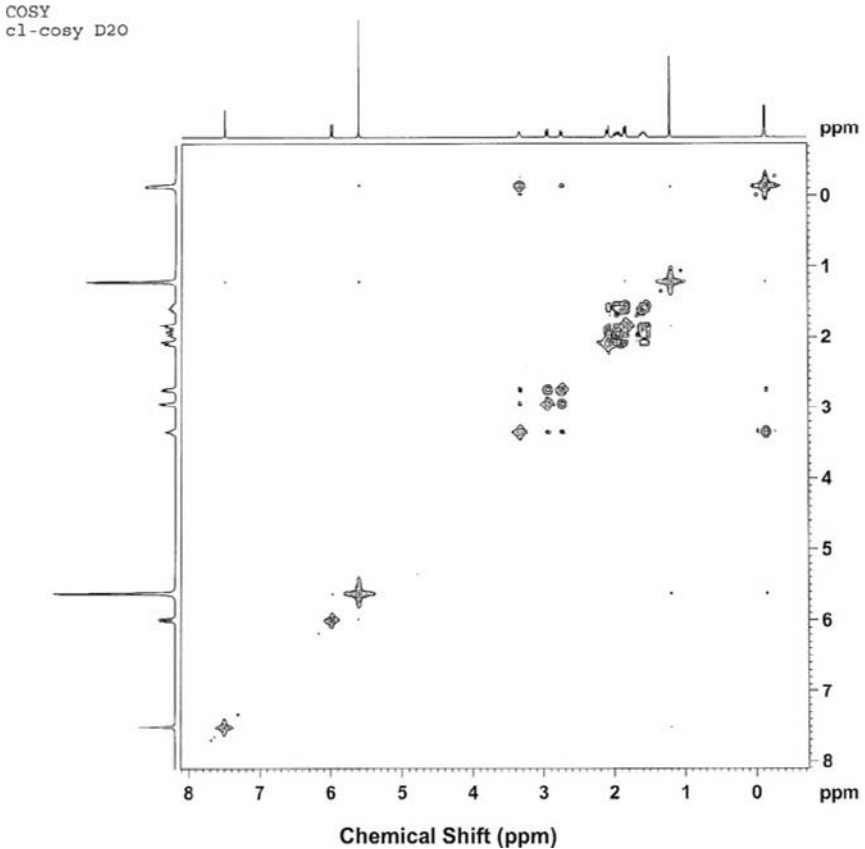
COSY
cl-cosy D20

FIGURE 6.7   COSY ^{1}H-NMR spectrum of ofloxacin in D$_2$O.

Examine by infrared absorption spectrophotometry, comparing with the spectrum obtained with ofloxacin CRS. Examine the substances prepared as discs.

2.1.2. Tests

2.1.2.1. Absorbance   Dissolve 0.5 g in 0.1 M hydrochloric acid and dilute to 100 ml with the same solvent. The absorbance of the solution measured at 440 nm is not greater than 0.25.

2.1.2.2. Optical rotation   Dissolve 0.300 g in a mixture of 10 volumes of methanol R and 40 volumes of methylene chloride R and dilute to 10 ml with the same mixture of solvents. The angle of optical rotation is $-0.10°$ to $+0.10°$.
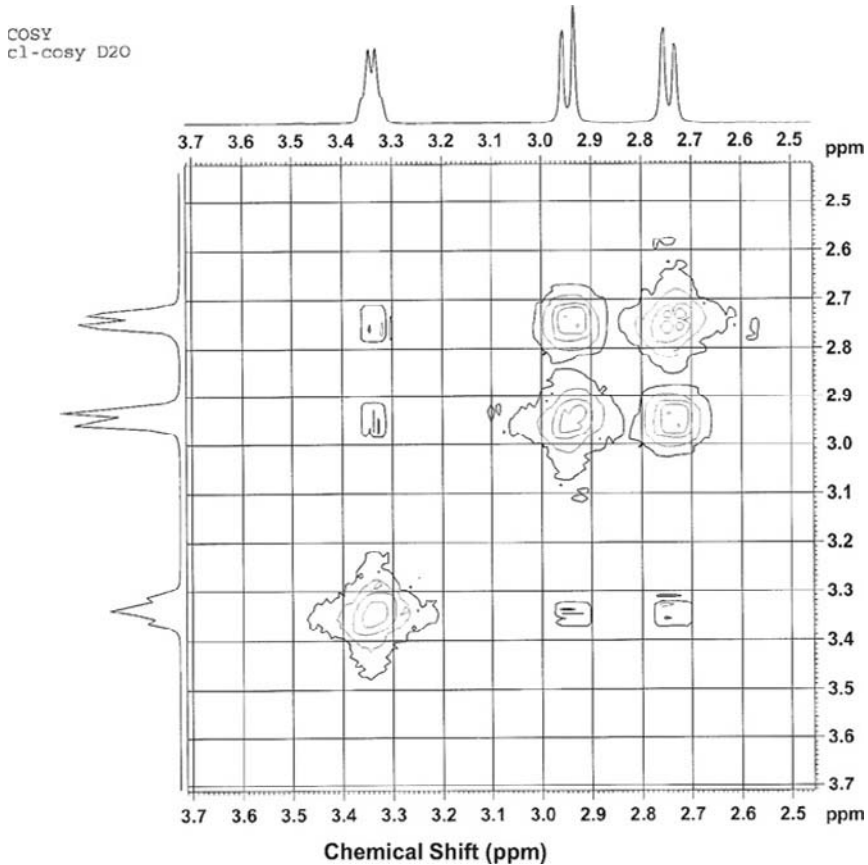
COSY
cl-cosy D2O

FIGURE 6.8 Expanded COSY ^{1}H-NMR spectrum of ofloxacin in D_2O.

2.1.3. Impurities and related substances [9, 10]

2.1.3.1. Impurity A   Examine by thin-layer chromatography, using a TLC silica gel GF$_{254}$ plate R (2–10 μm).

Test solution: Dissolve 0.250 g of the substance to be examined in a mixture of 10 volumes of methanol R and 40 volumes of methylene chloride R and dilute to 5.0 ml with the same mixture of solvents.

Reference solution: Dissolve 10 mg of ofloxacin impurity A CRS in a mixture of 10 volumes of methanol R and 40 volumes of methylene chloride R and dilute to 100.0 ml with the same mixture of solvents.

Apply to the plate 10 μl of each solution. Develop over a path of 10 cm using a mixture of 1 volume of glacial acetic acid R, 1 volume of water R, and 2 volumes of ethyl acetate R. Allow the plate to dry in air and examine in ultraviolet light at 254 nm. Any spot because of impurity A in the

HSQC
cl-13c-hsqc D2O d: mmjabal 1
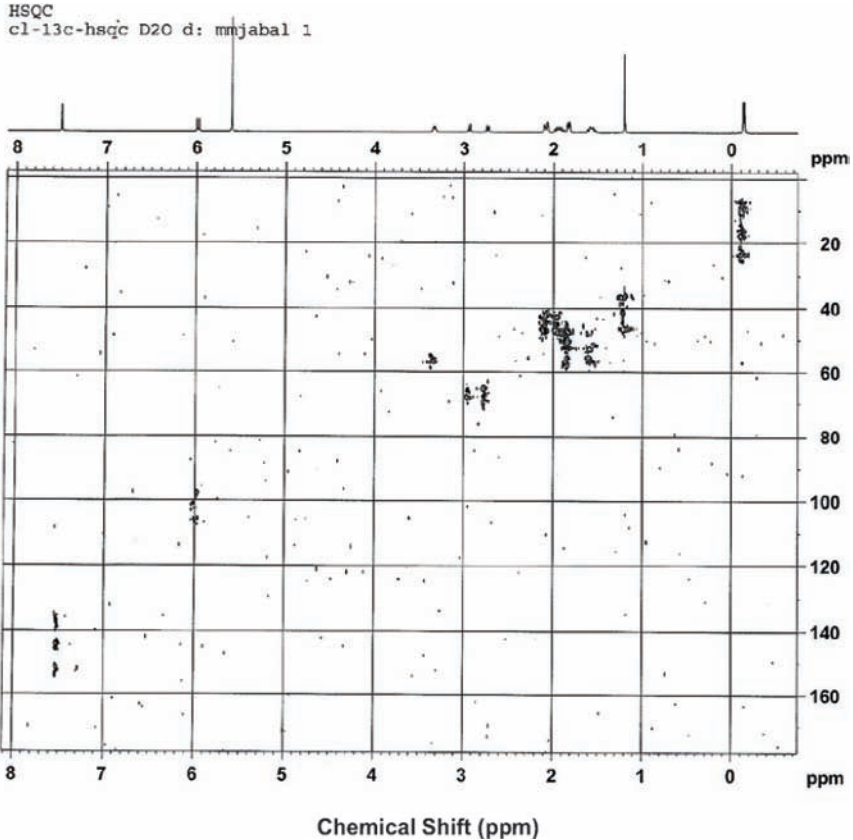
FIGURE 6.9   The HSQC NMR spectrum of ofloxacin in D$_2$O.

chromatogram obtained with the test solution is not more intense than the spot in the chromatogram obtained with the reference solution (0.2%).

2.1.3.2. Related substances   Examine by liquid chromatography. Prepare the solutions immediately before use.

Test solution: Dissolve 10.0 mg of the substance to be examined in a mixture of 10 volumes of acetonitrile R and 60 volumes of water R and dilute to 50.0 ml with the same mixture of solvents.

Reference solution (a): Dilute 1.0 ml of the test solution to 50.0 ml with a mixture of 10 volumes of acetonitrile R and 60 volumes of water R. Dilute 1.0 ml of this solution to 10.0 ml with a mixture of 10 volumes of acetonitrile R and 60 volumes of water R.

Reference solution (b): Dissolve 10.0 mg of ofloxacin impurity E CRS in a mixture of 10 volumes of acetonitrile R and 60 volumes of water R and dilute to 100.0 ml with the same mixture of solvents. Mix 10.0 ml of this
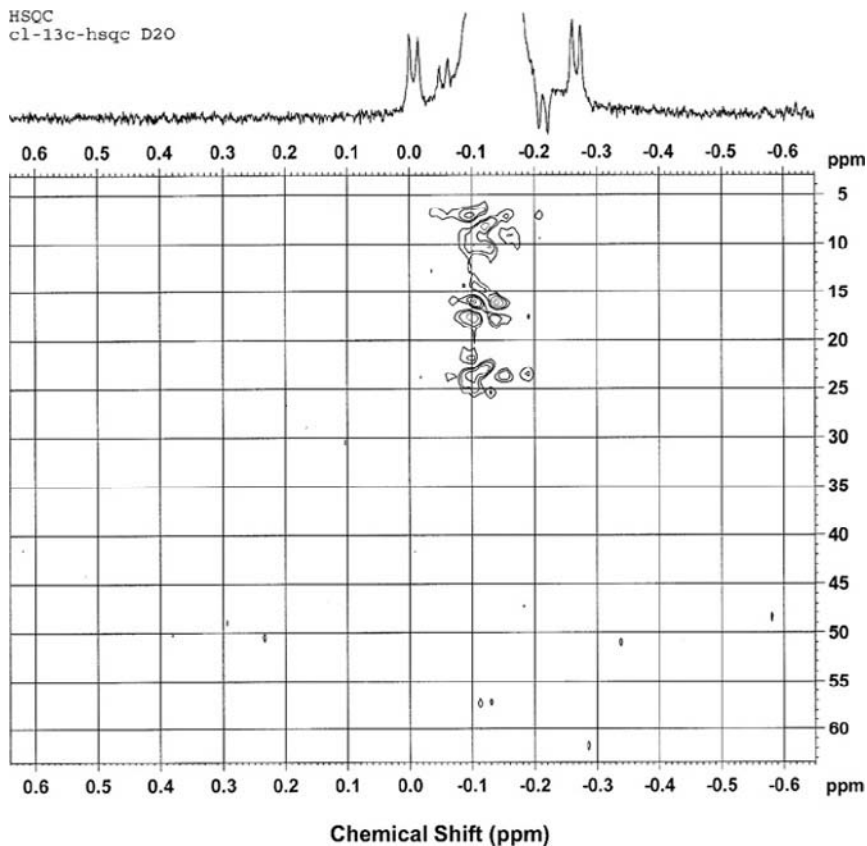
HSQC
cl-13c-hsqc D2O

FIGURE 6.10   Expanded HSQC NMR spectrum of ofloxacin in D$_2$O.

solution with 5.0 ml of the test solution. Dilute to 50.0 ml with a mixture of 10 volumes of acetonitrile R and 60 volumes of water R. Dilute 1.0 ml of this solution to 50.0 ml with a mixture of 10 volumes of acetonitrile R and 60 volumes of water R.

The chromatographic procedure may be carried out using:

- a stainless steel column 0.15 m long and 4.6 mm in internal diameter packed with octadecylsilyl silica gel for chromatography R (5 µm)
- as mobile phase, a mixture prepared as follows: dissolve 4.0 g of ammonium acetate R and 7.0 g of sodium perchlorate R in 1300 ml of water R. Adjust to pH 2.2 with phosphoric acid R. Add 240 ml of acetonitrile R. Adjust the flow rate of the mobile phase so that a retention time of about 20 min is obtained for ofloxacin
- as detector, a spectrophotometer set at 294 nm, maintaining the temperature of the column at 45 °C
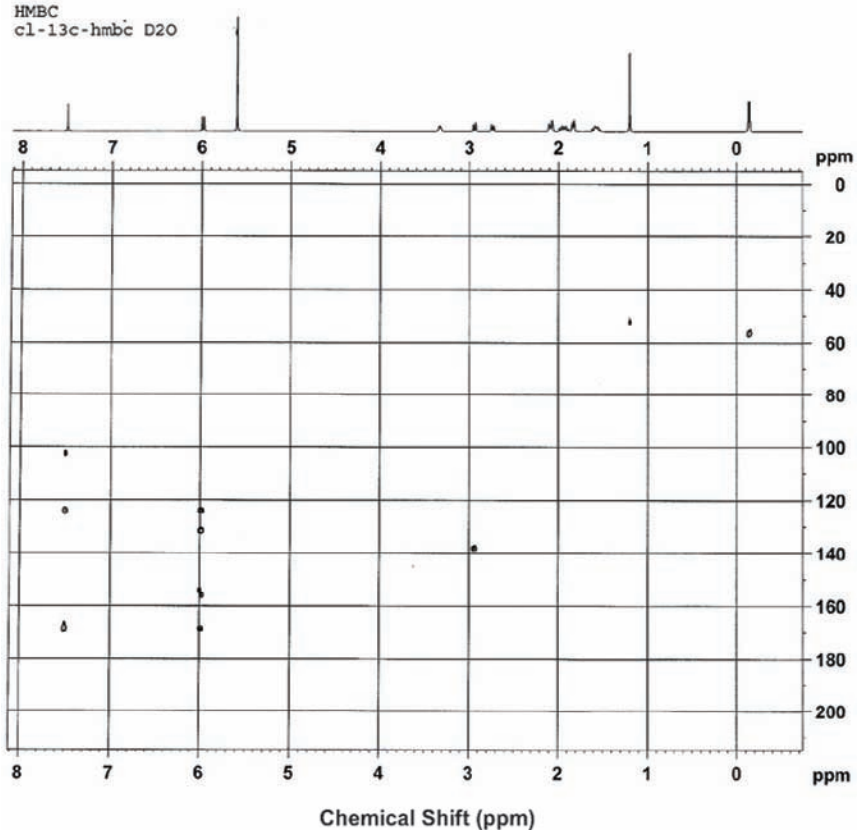
FIGURE 6.11   The HMBC NMR spectrum of ofloxacin in D_2O.

Inject 10 µl of reference solution (b). Adjust the sensitivity of the system so that the heights of the two principal peaks in the chromatogram obtained are at least 50% of the full scale of the recorder. The test is not valid unless: in the chromatogram obtained, the resolution between the peaks corresponding to impurity E and ofloxacin is at least 2.0. Inject 10 µl of the test solution and 10 µl of reference solution (a). Continue the chromatography for 2.5 times the retention time of the principal peak. In the chromatogram obtained with the test solution, the area of any peak, apart from the principal peak, is not greater than the area of the principal peak in the chromatogram obtained with reference solution (a) (0.2%); the sum of the areas of all the peaks is not greater than 2.5 times the area of the principal peak in the chromatogram obtained with reference solution (a) (0.5%). Disregard any peak with an area less than 0.1 times the area of the principal peak in the chromatogram obtained with reference solution (a).
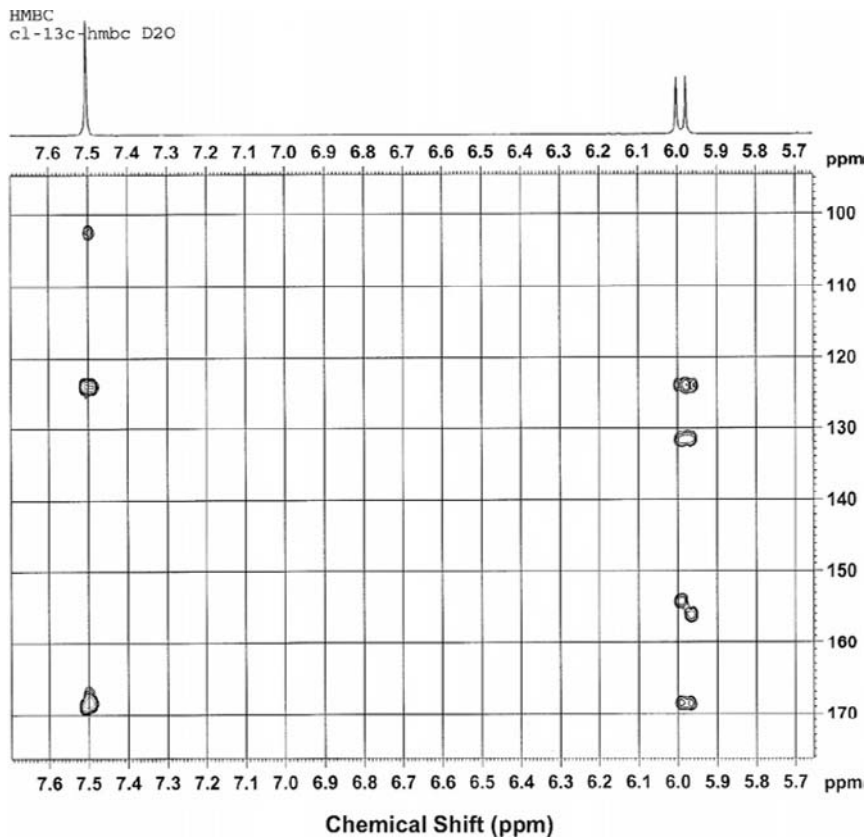
FIGURE 6.12 Expanded HMBC NMR spectrum of ofloxacin in D_2O.

2.1.3.3. Impurities

A. (RS)-9,10-difluoro-3-methyl-7-oxo-2,3-dihydro-7H-pyrido[1,2,3-de]-1,4-benzoxazine-6-carboxylic acid (FPA),
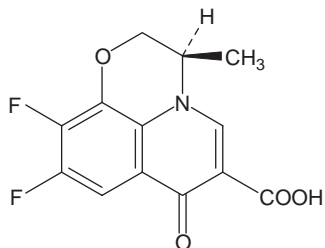
and enantiomer

B. $R_1 = H$, $R_2 = F$, $R_3 = CH_3$: (RS)-9-fluoro-3-methyl-10-(4-methylpiper-azin-1-yl)-2,3-dihydro-7H-pyrido[1,2,3-de]-1,4-benzoxazin-7-one,
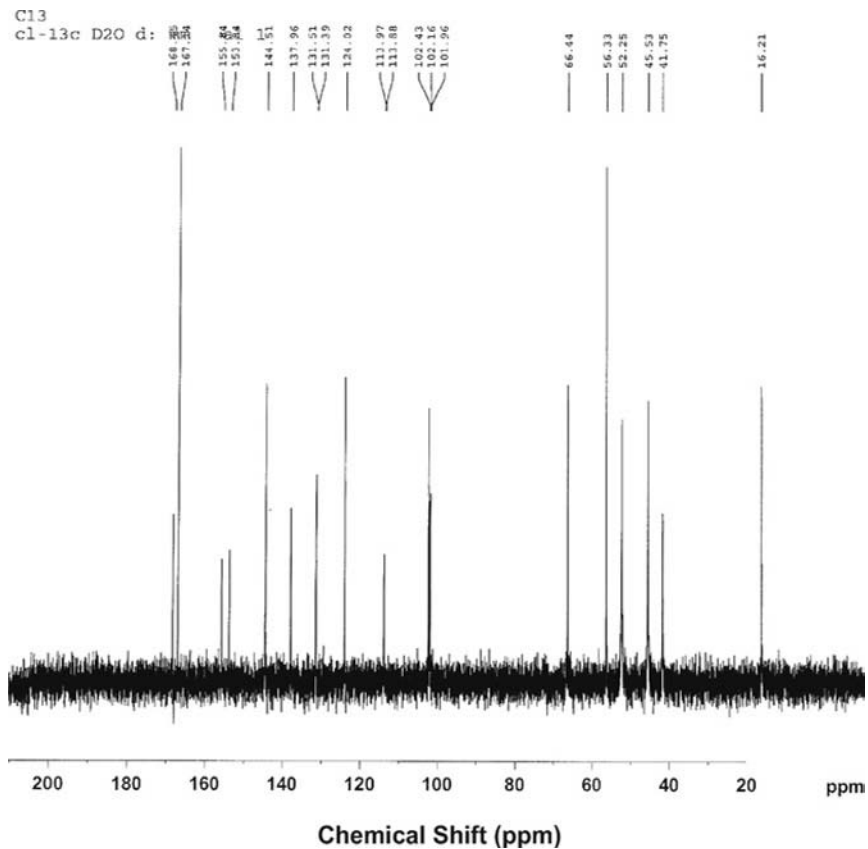
FIGURE 6.13 ¹³C-NMR spectrum of ofloxacin in D₂O.

C. $R_1 = CO_2H$, $R_2 = H$, $R_3 = CH_3$: (*RS*)-3-methyl-10-(4-methylpiperazin-1-yl)-7-oxo-2,3-dihydro-7*H*-pyrido[1,2,3-*de*]-1,4-benzoxazine-6-carboxylic acid,
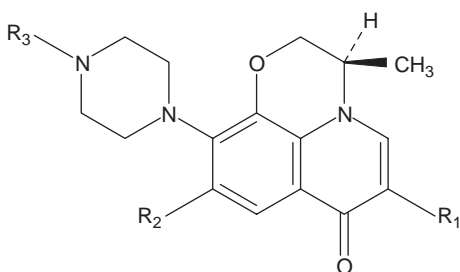
and enantiomer

D. (*RS*)-10-fluoro-3-methyl-9-(4-methylpiperazin-1-yl)-7-oxo-2,3-dihydro-7*H*-pyrido[1,2,3-*de*]-1,4-benzoxazine-6-carboxylic acid,

C13
cl-13c D2O
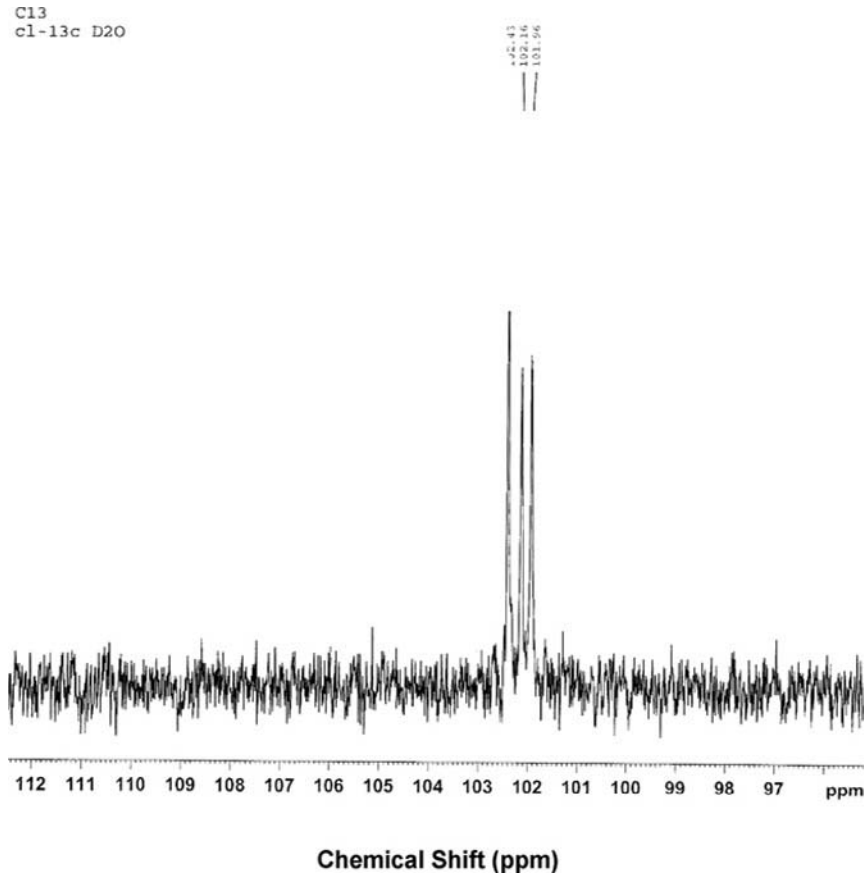
FIGURE 6.14   Expand ed^{13}C-NMR spectrum of ofloxacin in D$_2$O.

E. R$_1$ = CO$_2$H, R$_2$ = F, R$_3$ = H: (RS)-9-fluoro-3-methyl-7-oxo-10-(piperazin-1-yl)-2,3-dihydro-7H-pyrido[1,2,3-de]-1,4-benzoxazine-6-carboxylic acid,

and enantiomer

DEPT 135
cl-dept135-bbo D2O
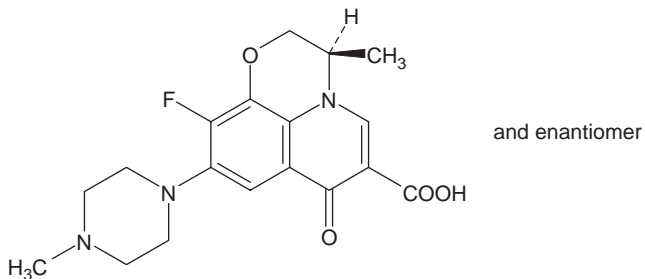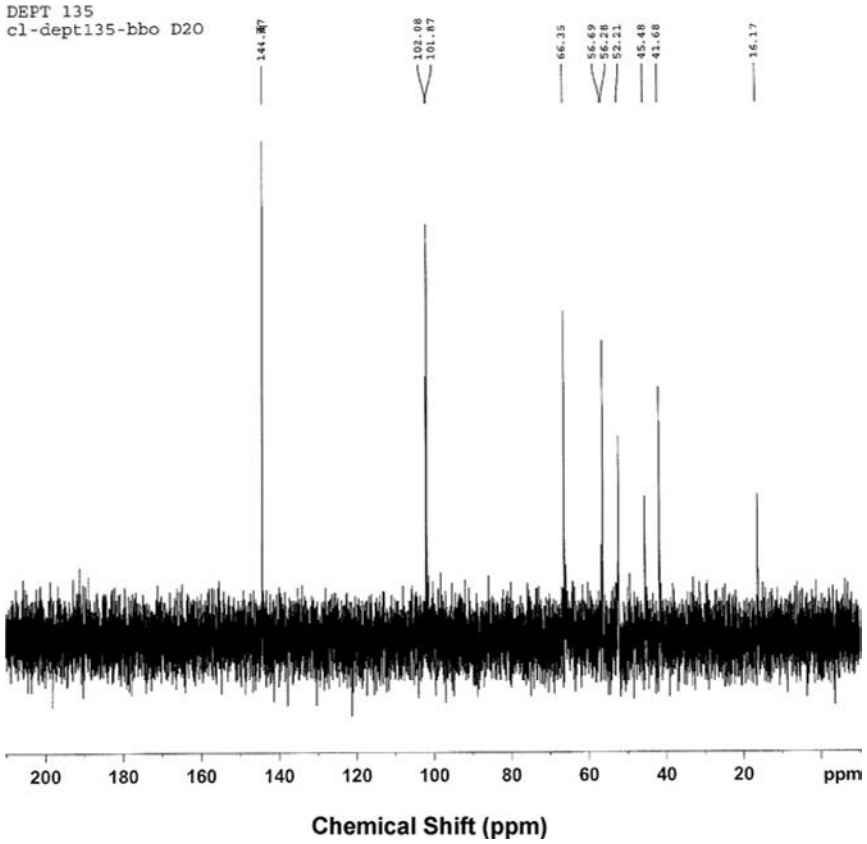
FIGURE 6.15   The DEPT 135 ^{1}H-NMR spectrum of ofloxacin in D_2O.
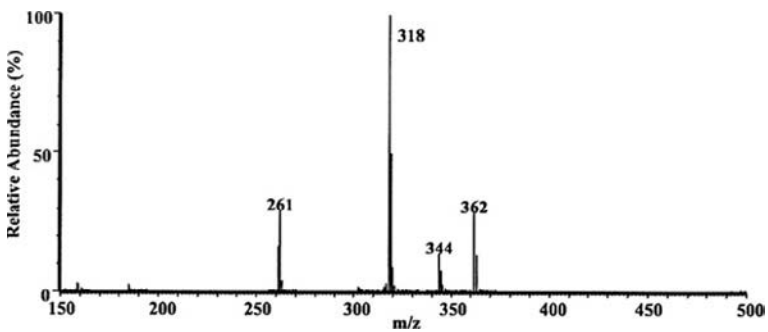
FIGURE 6.16   Mass spectrum of ofloxacin.

TABLE 6.3   Assignments for the fragmentation pattern observed in the mass spectrum of ofloxacin

Structural assignment	Mass number (m/z)	Relative abundance
$[M + H]^+$	362	30
$[M–H_2O + H]^+$	344	15
$[M–CO_2 + H]^+$ (A)	318	100
(A)–Pip	261	30

F. 4-[(RS)-6-carboxy-9-fluoro-3-methyl-7-oxo-2,3-dihydro-7H-pyrido [1,2,3-de]-1,4-benzoxazine-10-yl]-1-methylpiperazine 1-oxide.

and enantiomer
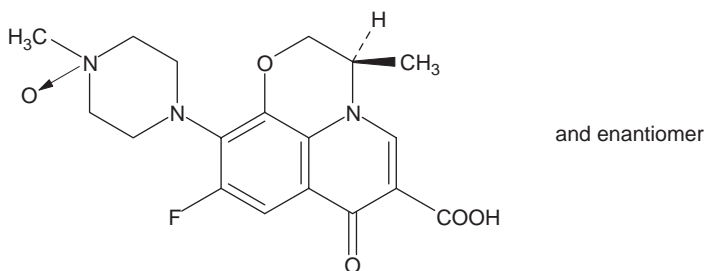
2.1.4. Heavy metals

2.0 g complies with limit test C for heavy metals (10 ppm). Prepare the standard using 2 ml of *lead standard solution* (10 ppm Pb) R.

2.1.5. Loss on drying

Not more than 0.2%, determined on 1.000 g by drying at 100–105 °C for 4 h.

2.1.6. Sulfate ash

Not more than 0.1%, determined on 1.0 g.

2.1.7. Assay

Dissolve 0.300 g in 100 ml of anhydrous acetic acid R. Titrate with 0.1 M perchloric acid determining the end-point potentiometrically.

   1 ml of 0.1 M perchloric acid is equivalent to 36.14 mg of $C_{18}H_{20}FN_3O_4$.

2.2. Reported methods of analysis

2.2.1. Titration method

Four DNA topisomerase (gyrase) inhibitors, including ofloxacin (alone or in mixture with other drugs), were determined by titration method [11]. Tablets containing ofloxacin was extracted for 3 times with 30 ml methanol. A portion of the solution was mixed with 2 ml water and the resulting solution was titrated with aqueous 5 mM NaOH, 5 mM tetrabutylammonium hydroxide, or 5 mM $AgNO_3$ by adding 0.1 ml increments at 2 min intervals. The end point was detected by conductimetry.

2.2.2. Spectrophotometric methods

An extractive spectrophotometric method was developed for determination of ofloxacin in bulk and pharmaceutical dosage form [12]. These methods are based on the formation of yellow ion-pair complexes between the basic nitrogen of the drug and bromophenol blue and bromocresol purple as sulfophthalein dyes in phthalate buffer pH 3.0 and 3.1, respectively. The formed complexes were extracted with chloroform and measured at 414 nm for ofloxacin–bromophenol blue and 408 nm for ofloxacin–bromocresol purple. Beer's law was obeyed in the range 0.87–17.35 and 0.58–14.46 µg/ml for ofloxacin–bromophenol blue and ofloxacin–bromocresol purple, respectively.

Quan *et al.* have reported a new charge-transfer complex that formed by reaction of ofloxacin with *p*-nitrophenol [13]. This complex had strong absorbance at 302 nm while ofloxacin had no absorbance at the same wavelength. The linear calibration range was 2–80 µg/ml for the drug.

Ballesteros *et al.* have developed a method for the determined of trace amounts of ofloxacin in human urine and serum sample based on solid-phase spectrofluorimetry [14]. The relative fluorescence intensity of ofloxacin fixed on Sephadex SP C-25 gel was measured and emission was 294 and 494 nm, respectively. The linear concentration range of application was 0.5–16.0 ng/ml of ofloxacin, with relative standard deviation (RSD) of 1.1% and detection limit of 0.14 ng/ml. Recovery level of the method reached 100% in all cases.

A simple, rapid, accurate and sensitive spectrophotometric method for the determination of ofloxacin in pharmaceutical formulations was described by Amin [15]. This method is based on the formation of an ion pair with Sudan III in aqueous acetone medium (40% acetone (v/v)). The colored products are measured at 565 nm. Beer's law is obeyed in the range 0.4–8.8 µg/ml. The results obtained showed good recoveries of ±1.5% with RSD of 0.83%.

Four fluoroquinolone antibiotics (including ofloxacin) were studied by spectroflurimetry [16]. The fluoroquinolones formed fluorescent complexes with Sc^{3+} at pH 4.2 in aqueous media. A mixture of 2 ml

0.33 mM Sc^{3+}/5.6 mM SDS in 0.05 M acetate buffer at pH 4.25. After 30 s, the fluorescence intensity was measured at 430 nm or at 480 nm (excitation at 280 nm). Calibration graph was linear for up to 1 µM and the detection limits of 1.1 nM with RSD ($n = 3$) of 5.7% at 5 nM.

Sastry et al. [17] presented two spectrophotometric methods for the determination of ofloxacin. In the first method, 0.5–6 ml (50 µg/ml) of the drug was added to 2 ml Supracene Violet 3B and 6 ml buffer (pH 1.3; 7.505 g glycine and 5.85 g NaCl dissolved in 1 l H_2O and 774 ml 0.1 M HCl), and the solution made up to 15 ml with H_2O. The mixture was shaken with 10 ml $CHCl_3$ for 2 min then the absorbance of the $CHCl_3$ layer was read at 575 nm. In the second method, 0.5–6 ml (50 µg/ml) of the drug was added to 6 ml 0.1 M HCl and 2 ml Troaeolin 000 and the volume adjusted to 15 ml with H_2O. The mixture was shaken with 10 ml $CHCl_3$ for 2 min then the absorbance of the $CHCl_3$ layer was read at 485 nm. Beer's law was obeyed and the detection limits were 2.5 µg/ml for ofloxacin in both methods.

2.2.3. Chemiluminescence methods

A flow-injection chemiluminescence (CL) method was described for the determination of three fluoroquinolones, including ofloxacin [18]. The method is based on these compounds of the weak CL from peroxynitrous acid. The linear range is 3×10^{-7} to 3×10^{-5} mol l^{-1} for ofloxacin. The detection limit ($S/N = 3$) is 1.1×10^{-7} mol l^{-1}. The recoveries were 96–106% ($n = 5$).

Aly et al. [19] reported a rapid and sensitive CL method for determination of three fluoroquinolone derivatives, including ofloxacin, in both pharmaceuticals and biological fluids. The method is based on the CL reaction of the drugs with tris(2,2'-bipyridyl)ruthenium(II) and cerium (IV) in sulfuric acid medium. The CL intensity was proportional to the concentration of ofloxacin in solution over the range 0.003–0.7 µg/ml. The limit of detection (signal-to-noise ratio = 3) was 5.5 nM.

A flow-injection CL method was developed by Rao et al. [20] for determination of fluoroquinolones, including ofloxacin, based on the CL reaction of sulfite with cerium(IV) sensitized by these compounds. The linear range for ciprofloxacin CL was 0.4–4 µg/ml and the detection limit was 0.016 µg/ml for ofloxacin with RSD of 2.1–2.6% ($n = 10$).

2.2.4. High-performance liquid chromatographic methods (HPLC)

Several high-performance liquid chromatography (HPLC) methods were reported for the determination of ofloxacin in biological and pharmaceutical forms as summarized in Table 6.4.

TABLE 6.4 Reported HPLC methods for ofloxacin

No.	Material	Column	Mobile phase	Internal standard	Flow rate	Detection wavelength	Ref.
1	Plasma	RP Novapack C_{18} column (5 μm) 15 cm × 3.9 mm i.d.	Acetonitril/aqueous phosphate solution (1:4)	Sarafloxacin		338/425 nm	[21]
2	Ophthalmic suspension	Waters Spherisorb (5 μm ODS) 15 cm x 4.6 mm i.d.	0.5 M-Phosphate buffer/ acetonitrile (65:35; pH adjusted to 2.7 with orthophosphoric acid)	Propylparaben (254 nm)	1.2 ml/ min	210 nm	[22]
3	Raw material	Waters C18 (5μm) 15 cm × 4.6 mm i.d.	Phosphate buffer—0.98 mg/ml sodium heptanesulfonat pH 2.4/methanol (13:7)	p-Aminobenzoic acid	1 ml/ min	277 nm	[23]
4	Tablete and serum	Shim-pack CLS-ODS (5μm) 15cm x 4.6 mm i.d.	50 mM Citric acid containing 0.01 M ammonium acetate/ methanol (75:25; pH adjusted to 4.5 with triethylamine)	NA	1 ml/ min	294 nm	[24]
5	Dosage forms and bulk drug	LiChrospher C18 (5 μm) 25 cm × 4 mm i.d.	Water/acetonitrile/ triethylamine (80:20:0.6) pH 3 with orthophosphoric acid	Cephalexin	1.5 ml/ min	280 nm	[25]
6	Dosage forms	Lichrospher 100 RP-18 (5 μm) 25 cm × 4.6 mm i.d.	100 mM-tertrabutylammonium hydroxide in acetonitrile/ water (93:7)/25 mM H_3PO_4 in acetonitrile/water (93/7)	NA	1 ml/ min	444/491 nm	[26]
7	Clinical specimens	Alltech Adsorbospher HS C18 7U (7 μm) 15 cm × 4.6 mm i.d.	0.02 M Sodium phosphate buffer/acetonitrile (13:7; pH adjusted to 3 with 0.2% triethylamine and 0.2% SDS)	Marbofloxacin	1.75 ml/ min	280 nm	[27]
8	Human serum	Lichrosorb RP-18 (5 μm) 25 cm × 4 mm i.d.	Acetonitrile/methanol/0.4 M citric acid (1:3:6)	Theophylline	NA	275 nm	[28]

TABLE 6.4 (*continued*)

No.	Material	Column	Mobile phase	Internal standard	Flow rate	Detection wavelength	Ref.
9	Aqueous humour and plasma	Hypersil ODS column (5 μm) 30 cm × 4.6 mm i.d.	0.01 M NaH$_2$PO$_4$ comtaining 15% acetonitrile and 6% DMF of pH 3	Ciprofloxacin	1 ml/min	285 nm	[29]
10	Tablets and capsules	Nacalai Cosmosil 5C18 MS (25 cm × 4.6 mm i.d.)	Methanolic 3 mM SDS/40 mM-phosphate buffer/acetonitrile (5:11:4) pH 3.5	Piroxicam	0.8 ml/min	257 nm	[30]
11	Raw material	LiChrospher 100 C18 (5 μm) 25 cm × 4 mm i.d.	0.1 M-tetrabutylammonium bromide in 25 mM- H$_3$PO$_4$ of pH 3.89/acetonitrile (93:7)	NA	NA	278 nm	[31]
12	Human aqueous humor	Novapak C18 cartridge (4 μm) 10 cm × 8 mm i.d.	Methanol/acetonitrile/0.4 M citric acid (3:1:10)	Pipemidic acid	1 ml/min	278/450 nm	[32]
13	Urine	HP Hypersil C18 (5 μm) 10 cm × 4 mm i.d.	Gradient elution: 100 ml/l acetonitrile in 1 M ammounium acetate; pH 5.1 and 100 ml/l acetonitrile in methanol	NA	1 ml/min	404/615 nm	[33]
14	Dosage forms	Shimpack CLC-ODS (15 cm × 6 mm i.d.)	Tetrabutylammonium hydroxide buffer/acetonitrile (9:1)	NA	1 ml/min	280 nm	[34]

15	Dosage forms	LiChrospher C18 (5 μm) 25 cm × 4.6 mm i.d.	Methanol/phosphate buffer (1:1)	Difloxacin	NA	254 nm	[35]
16	Clinical specimens	Ultropac LiChrosorb RP-18 (10 μm) 25 cm × 4 mm)	Acetonitrile/0.4 M-citric acid (1:5)	Pipemidic acid	1 ml/ min	340 or 275 nm	[36]
17	Human serum and prostatic tissue	Micro Bondapak C18 in radial compressed polyethylene	0.1 M citric acid containing 15–25% of methanol	NA	1 ml/ min	NA	[37]
18	Serum, urine and sputum	Micr-Pak MCH 10 (10 μm) 30 cm × 4 mm i.d.	Acetonitrile/0.1 M KH$_2$PO$_4$ (pH 2.5; 19:81)	NA	0.8 ml/ min	NA	[38]
20	Human serum and urine	Nucleosil 5 C18 (20 cm × 4.6 mm)	Water/acetonitrile/methanol (18:1:1) pH 3 adjusted with tetrabutylammonium hydroxide	NA	1 ml/ min	278/446 nm	[39]
21	Human serum	Nucleosil C18 (5 μM) 25 cm × 4.6 mm i.d.	Water/85% H$_3$PO$_4$/ tetrabutylammonium iodide/ methanol (7000:19:14:3000; v/v/w/v)	NA	NA	294 nm	[40]

NA: Not Available.

2.2.5. Capillary electrophoresis (CE)

Ofloxacin, a chiral fluoroquinolone, possesses two optical isomers [41]. A capillary zone electrophoresis method has been developed to quantify the enantiomers of ofloxacin in high diluted samples (20–700 ng/ml of each enantiomer). After fluid–fluid extraction of the drug from physiological solution electrokinetic injection was employed to improve the sensitivity. The quantification limit is 11.4 ng/ml for *S*-(−)-ofloxacin and 10.8 ng/ml for *R*-(+)-ofloxacin. The method has shown good validation data.

A capillary electrophoresis method for the simultaneous separation and enantio-separation of the antibacterial drug ofloxacin and its metabolites desmethylofloxacin and N-oxide in human urine has been developed by Horstkötter and Blaschke [42]. Enantio-separation was achieved by adding 0.65 mg/ml sulfobutyl β-cyclodextrin to 100 mM phosphate–TEA buffer, pH 2.0 as running buffer. Separation was carried out by applying a voltage of 25 kV on fused-silica capillary of 50 μm i.d. × 375 μm o.d. with total length of 37 cm and a detection length of 30 cm. The detection of analytes was performed by laser-induced fluorescence detection using a HeCd-laser with an excitation wavelength of 325 nm.

First and second generation of quinolones (including ofloxacin) were separated by capillary electrophoresis [43]. The compound were hydrostatically injected (10 cm for 10 s) on fused-silica capillary (60 cm × 75 μm i.d.; 52.5 cm to detector), operated at an applied voltage of 22 kV, with 125 mM phosphate buffer of pH 7.0 as running buffer and detection at 214 nm.

The potential of CZE and MEKC have been investigated for the separation and quantitative determination of ten quinolone antibiotics (including ofloxacin) [44]. Buffer consisting of 40 mM sodium tetraborate at pH 8.1 containing 10% (v/v) methanol was found to be a highly effective electrophoretic system for separating ofloxacin and other nine quinolones. A SPE method to remove the sample matrix (pig plasma sample) was developed on a C18 cartridge using a mixture of water/methanol (3:7). The method was specific and reproducible and mean recoveries were in the range (94 ± 4.2)% and (123.3 ± 4.1)% for pig plasma samples. The detection limits were between 1.1 and 2.4 mg/l and a linear graph was obtained in the concentration range 5–20 mg/l.

Six quinolone antibiotics (including ofloxacin) were separated and determined by CZE on fused-silica capillaries (57 cm × 75 μm i.d.; 50 cm to detector) at 25 °C with injection on the anode side, an applied voltage of 10 kV and detection at 280 nm. The buffer was 100 mM HEPES/acetonitrile (9:1). The calibration graphs were linear from 0.25–40 μg/ml and detection limits were ∼0.25 ng/ml [45].

Sun and Wu [46] described a capillary electrophoresis method for determination of seven fluoroquinolones, including ofloxacin, in pharmaceutical formulations. Pipemidic acid (10 mg) was added as internal

standard to 25 mg active ingredient of the drugs in 100 ml methanol. The clear solutions (4.1 nl) were hydrodynamically injected at 60 mbar for 3 s on fused-silica capillary (67 cm × 50 μm i.d.; effective length = 52 cm). The compounds were well separated in <8.5 min with 65 mM sodium borate/35 mM sodium dihydrogen phosphate/60 mM sodium cholate of pH 7.3 in acetonitrile (72:28) as running buffer with an applied voltage of +27 kV and detection at 275 nm. The calibration graphs were linear from 25 to 300 μg/ml of the fluoroquinolones with recoveries within 95–105% oh their label claims.

A mixture of four fluoroquinolones, including ofloxacin, was determined by high-performance capillary electrophoresis using caffeine as internal standard [47]. A portion of the solution was introduced by pressure-differential sampling at 10 cm for 10 s and the drugs were separated and determined by high-performance CZE on fused-silica capillary column (60 cm × 0.75 μm i.d.; effective length 55 cm) operated at an applied voltage of 18 kV with 50 mM $Na_2B_4O_7/NaH_2PO_4$ buffer of pH 8.5 as running buffer, and detection at 214 nm. The calibration graph for ofloxacin was linear from 20 to 100 mg/l. The detection limits and RSD were 0.40–0.48 mg/l and <2%, respectively.

Fourteen quinolone antibacterials (including ofloxacin) were separated by fused-silica column (59 cm × 50 μm i.d.; 43 cm to detector) at 30 kV in less than 8 min and monitored at 260 nm [48]. In this method, a background electrolyte of pH 7.3 containing 32 mM borate, 39 mM cholate, 8 mM heptanesulfonate, and 18 mM phosphate (as sodium salts) modified with 28% acetonitrile was used as running buffer.

3. DRUG METABOLISM AND PHARMACOKINETIC PROFILES OF OFLOXACIN

3.1. Uses and application and associated history

Ofloxacin is a fluoroquinolone carboxylic acid antibacterial showing bactericidal effects by inhibition of DNA gyrase [49]. This inhibition leads to promotion of double strand DNA breakage in susceptible organisms. Because of the substitution of ofloxacin by a methyl group at the C-3 position of the oxazine ring, the drug is chiral. It is well known that the S-(–)-enantiomer is 8–128 times more potent than the R-(+)-enantiomer and about twice as potent as racemic ofloxacin [50, 51]. Since 1998, the drug is used therapeutically in its S-(–)-isomer, levofloxacin [52, 53].

Ofloxacin is given orally or intravenously as the base or hydrochloride form, respectively. Ofloxacin and other quinolone antibiotics are not currently considered first line agents for most of the approved indications. It is recommended for the treatment of mild to moderate urinary

tract infections, prostatitis, lower respiratory tract infections, and skin and skin structure infections caused by susceptible gram-negative and gram-positive aerobic bacteria [54–57]. It is also recommended for the treatment of acute, uncomplicated gonorrhea and nongonococcal urethritis and cervicitis caused by *Chlamydia* [54]. The drug is inactive against most anaerobic bacteria; therefore, it should not be used alone in mixed aerobic–anaerobic bacterial infection.

Oral doses of ofloxacin up to 400 mg daily preferable in the morning and may increase to 400 mg twice daily. By intravenous infusion a 0.2% solution is infused over 30 min or a 0.4% solution over 60 min [55]. Because ofloxacin absorption is rapid and almost complete, the intravenous formulation of ofloxacin does not provide a higher degree of efficacy or increased antimicrobial activity than the oral formulation. Patients should be started on or switched to, the oral formulation at the same dose as soon as possible. It is also employed as 0.3% eye drops and 0.3% ear drops.

3.2. Absorption and bioavailability

Oral dose of ofloxacin is rapidly and well absorbed from the gastrointestinal tract and oral bioavailability is almost complete in health-fasting adults. The piperazinyl group at position 7 of the 4-quinolone nucleus is methylated, which may contribute to the great bioavailability of ofloxacin compared with other fluoroquinolones. The peak plasma concentration of 3–4 µg/ml is achieved 1–2 h after single 400 mg dose by mouth [54, 55]. It undergoes minimal first pass metabolism. Absorption time but not the extent may be delayed by the presence of food or when complexed with minerals such as ferrous, ferric, or calcium [55, 58, 59]. Following intravenous infusion of 400 mg dose of ofloxacin over 60 min, peak plasma concentration average 4 µg/ml. The plasma half-life ranges from 5 to 8 h in normal healthy human. About 20–32% of ofloxacin is bound to plasma proteins [59, 60].

Ofloxacin is widely distributed into body tissues and fluids following oral administration [61]. The apparent volume of distribution of the drug averages 2.4–3.5 l/kg following oral or intravenous administration [60, 62]. It is distributed into bone, cartilage, bile, skin, sputum, bronchial secretions, pleural effusions, tonsils, saliva, gingival mucosa, nasal secretions, aqueous humor, tears, sweat, lung, blister fluid, pancreatic fluid, ascitic fluid, pertioneal fluid, gynecologic tissue, vaginal fluid, cervix, ovary, semen, prostatic fluid, prostatic tissue, and cerebrospinal fluid [54, 60, 62]. Ofloxacin concentrations in the tissues or fluids are more than that of serum concentrations. The drug crosses the placenta and found in amniotic fluid. It also found in mammalian milk in a moderate concentration after oral administration [63, 64].

3.3. Metabolism

Ofloxacin is metabolized in liver at the piperazinyl moiety following oral doses. Unlike other fluoroquinolones, ofloxacin structure contains an oxazine ring linking the nitrogen at position 1 and carbon at position 8 of the quinolone nucleus. This fused ring results in low metabolism of the drug in vivo. Nearly 90% of the administered dose is excreted unchanged in the urine within 48 h following single oral of ofloxacin doses and less than 10% of the compound is excreted as metabolites [65–68]. Two metabolites of ofloxacin, desmethylofloxacin, and ofloxacin N-oxide (Scheme below) have been identified at low concentrations in human urine [69, 70]. Desmethylofloxacin represents 3–6% of the metabolites and 1–5% is ofloxacin N-oxide [54, 71]. The former metabolite has moderate antibacterial activity, while other has only minimal microbiological activity. A third metabolite, ofloxacin β-D-glucuronide, is eliminated by biliary excretion in humans and recently, it has been found in urine, which does not has any activity [72].

Ofloxacin

Desmethylofloxacin

Ofloxacin *N-oxide*
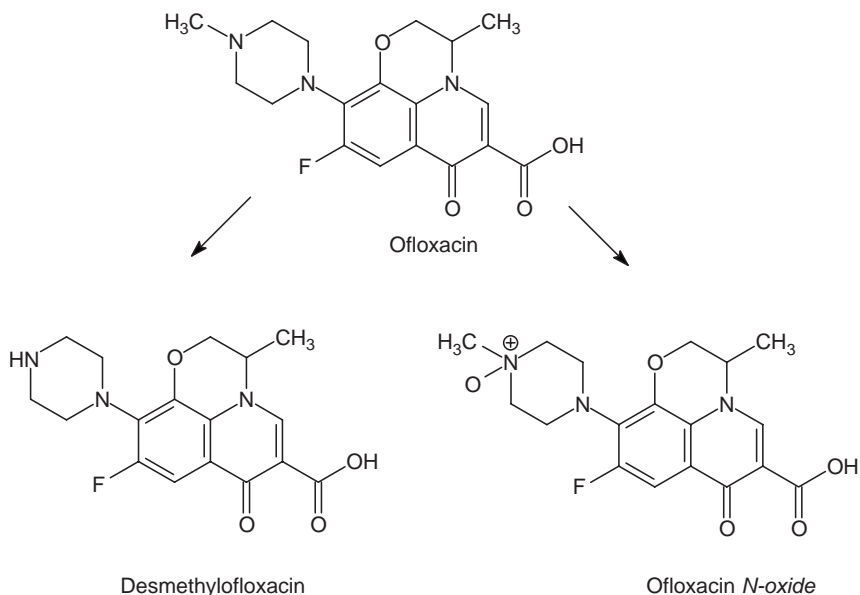
3.4. Excretion

Ofloxacin is excreted mainly (90%) unchanged by the kidney via active tubular secretion and glomerular filtration with an elimination half-life of 5–7.5 h [59, 73]. The elimination half-life of ofloxacin following a single

200 mg intravenous dose was reportedly 5.37 h in healthy male volunteers. Following multiple doses of 200 mg intravenous every 12 h for 9 doses, the half-life did not change significantly (4.76 h) [74]. The renal clearance of ofloxacin averages 133–200 ml/min healthy adult volunteers. In patients with renal impairment the half-life of ofloxacin increases to 15–37 h [75]. Approximately 4–8% of the dose is excreted in the feces. Ofloxacin is found in breast milk [54, 63]. The American Academy of Pediatrics considers ofloxacin to be usually compatible with breastfeeding [63]; however, the manufacturer states that lactating mothers receiving ofloxacin should not breast feed infants [60]. The drug crosses the placenta and found in relatively high concentration in cord blood and amniotic fluid [64].

REFERENCES

[1] A. R. Gennaro (Ed.), *Remington's: Pharmaceutical Sciences*, 18th edn., Mack, Pennsylvania, 1990, p. 1540.
[2] S. Budavari (Ed.), *The Merck Index*, 12th edn., Merck, New Jersey, 1996, p. 6875.
[3] S. C. Sweetman (Ed.), *Martindale, The Complete Drug Reference*, 33th edn., The Pharmaceutical Press, Chicago, 2002, p. 232.
[4] *Index Nominum 2000: International Drug Directory*, 17th edn., Swiss Pharmaceutical Society, Medpharm Scientific Publishers, Stuttgart, 2000, p. 757.
[5] G. K. McEvoy (Ed.), *Drug Information*, 95th edn., American Society of Health-System Pharmacists, Bethesda, 1995, p. 520.
[6] B. Macías, M. V. Villa, I. Rubio, A. Castineras and J. Borras, *J. Inorg. Biochem.*, 2001, **84**, 163.
[7] S. Sagdinc and S. Bayrai, *J. Mol. Struct.*, 2005, **369**, 744–747.
[8] *Thomson MICROMEDEX*$^{(R)}$ *Healthcare Series*, Vol. 116, 2002, DE0858.
[9] *European Pharmcopeia*, 4th edn., Council of Europe, Strasbourg, 2002, p. 1661.
[10] *British Pharmacopeia*, Vol. I, 16th edn., on line, HMSO, London, 2000, CD.
[11] F. Belal, M. Rizk, F. A. Aly and N. M. El-Enany, *Chem. Anal.*, 1999, **44**, 763.
[12] I. Suslu and A. Tamer, *Anal. Lett.*, 2003, **36**, 1163.
[13] H. Quan, X. H. Bai and Y. H. Song, *Fenxi-Shiyanshi*, 2002, **21**, 64.
[14] O. Ballesteros, J. L. Vilchez and A. Navalon, *J. Pharm. Biomed. Anal.*, 2002, **30**, 1103.
[15] A. S. Amin, *Mikrochim*, 2000, **134**, 89.
[16] A. I. Drakopoulos and P. C. Ioannou, *Anal. Chim. Acta.*, 1997, **354**, 197.
[17] C. S. P. Sastry, K. Rama-Rao and D. S. Prasad, *Talanta*, 1995, **42**, 311.
[18] Y-D. Liang, J-F. Song and X-F. Yang, *Anal. Chim. Acta.*, 2004, **510**, 21.
[19] F. A. Aly, S. A. Al-Tamimi and A. A. Alwarthan, *Talanta*, 2001, **53**, 885.
[20] Y. Rao, Y. Tong, X. R. Zhang, G. A. Luo and W. R. G. Baeyens, *Anal. Lett.*, 2000, **33**, 1117.
[21] M. A. Garcia, C. Solans, A. Calvo, M. Royo, E. Hernandez, R. Rey and M. A. Bregante, *Chromatographia*, 2002, **55**, 431.
[22] M. S. Ali, M. Ghori and A. Saeed, *J. Chromatogr. Sci.*, 2002, **40**, 429.
[23] Y. J. Niu and S. X. Zhang, *Yaown-Fenxi-Zazhi.*, 2001, **21**, 204.
[24] P. Liang, Y. C. Qin, Z. C. Jiang and C. M. Xiong, *Fenxi-Shiyanshi*, 2000, **19**, 56.
[25] S. O. Thoppil and P. D. Amin, *J. Pharm. Biomed. Anal.*, 2000, **22**, 699.
[26] J. A. Hernandez-Arteseros, J. Barbosa, R. Compano and M. D. Prat, *Chromatographia*, 1998, **48**, 251.
[27] D. H. Wright, V. K. Herman, F. N. Konstantinides and J. C. Rotschafer, *J. Chromatogr. B: Biomed.*, 1998, **709**, 97.

[28] I. N. Papadoyannis, V. F. Samanidou and K. A. Georga, *Anal. Lett.*, 1998, **31**, 1717.
[29] H. J. Kraemer, R. Gehrke, A. Breithaupt and H. Breithaupt, *J. Chromatogr. B: Biomed.*, 1997, **700**, 147.
[30] Y. P. Chen, C. Y. Shaw and B. L. Chang, *Yaowu. Shipin. Fenxi.*, 1996, **4**, 155.
[31] J. Barbosa, R. Berges and V. Sanz-Nebot, *J. Chromatogr. A.*, 1996, **719**, 27.
[32] N. E. Bssci, A. Bozkurt, D. Kalayci and S. O. Kayaalp, *J. Pharm. Biomed. Anal.*, 1996, **14**, 353.
[33] N. Schoenfeld and R. Mamet, *Clin. Chem.*, 1994, **40**, 417.
[34] R. Jain and C. L. Jain, *LC. GC.*, 1992, **10**, 707.
[35] Z. Budvari-Barany, G. Szasz, K. Takacs-Novak, I. Hermecz and A. Lore, *J. Liq. Chromatogr.*, 1991, **14**, 3411.
[36] C. Y. Chan, A. W. Lam and G. L. French, *J. Antimicrob. Chemother.*, 1989, **23**, 597.
[37] L. O. White, H. M. Bowyer, C. H. McMullin and K. Desai, *J. Antimicrob. Chemother.*, 1988, **21**, 512.
[38] C. M. Myers and J. L. Blumer, *J. Chromatogr. Biomed. Appl.*, 1987, **66**, 153.
[39] W. Schoenfeld, J. Knoeller, K. D. Bremm, A. Dahlhoff, B. Weber and W. Koenig, *Zentralbl. Bakteriol. Mikrobiol. Hyg. Ser. A.*, 1986, **261**, 338.
[40] A. J. N. Groeneveld and J. R. B. J. Brouwers, *Pharm. Weekbl,. Sci. Ed.*, 1986, **8**, 89.
[41] B. Awadallah, P. C. Schmidt and M. A. Wahl, *J. Chromatogr. A.*, 2003, **988**, 135.
[42] C. Horstkötter and G. Blaschke, *J. Chromtogr. B.*, 2001, **754**, 169.
[43] C. Fierens, S. Hillaert and W. van-den-Bossche, *J. Pharm. Biomed. Anal.*, 2000, **22**, 763.
[44] M. Hernandez, F. Borrull and M. Calull, *J. Chromatogr. B: Biomed. Appl.*, 2000, **742**, 255.
[45] T. Perez-Ruiz, C. Martinez-Lozano, A. Sanz and E. Bravo, *Chromatographia.*, 1999, **49**, 419.
[46] S. W. Sun and A. C. Wu, *J. Liq. Chromatogr. Relat. Technol.*, 1999, **22**, 281.
[47] C. Yin and Y. T. Wu, *Yaown. Fenxi. Zazhi.*, 1997, **17**, 371.
[48] S. W. Sun and L. Y. Chen, *J. Chromatogr. A.*, 1997, **766**, 215.
[49] J. T. Smith, *Infection*, 1986, **14**(Suppl. I), S3.
[50] T. Fujimoto and S. Mitsuhashi, *Chemotherapy*, 1990, **36**, 268.
[51] I. Hayakawa, S. Atarashi, S. Yokohama, M. Imamura, K. Sakano and M. Furukawa, *Antimicrob. Agents Chemother.*, 1986, **29**, 163.
[52] H. Dabernat, *Int. J. Antimicrob. Agents*, 1999, **11**, 139.
[53] K. J. Madaras-Kelly and T. A. Demasters, *Diagn. Microbiol. Infect. Dis.*, 2000, **37**, 253.
[54] G. K. McEvoy (Ed.), *Drug Information*, 95th edn., American Society of Health-System Pharmacists, Bethesda, 1995, p. 522.
[55] S. C. Sweetman (Ed.), *Martindale, The Complete Drug Reference*, 33th edn., The Pharmaceutical Press, Chicago, 2002, p. 947.
[56] S. Nouira, M. Marghil, M. Belghith, L. Besbes, S. Elatrous and F. Abroug, *Lancet*, 2001, **358**, 2020.
[57] R. Fünfstück, M. Wolfram and J. Gerth, *et al., Int. J. Antimicrob. Agents*, 1999, **11**, 297.
[58] A. I. Azcurra, I. M. Yudi and A. M. Baruzzi, *et al.,* J. Electroanal. Chem., 2001, **506**, 138.
[59] C. J. Eboka, R. S. Okor and J. O. Akerele, *et al., J. Clin. Pharm. Ther*, 1997, **22**, 217.
[60] Thomson *MICROMEDEX*[(R)] *Healthcare Series*, Vol. 116, 2002, DE0858.
[61] H. Nomura, M. Tsumura and H. Tachizawa, *et al.,* Ofloxacin: A new quinolone antibacterial agent, in *Proceedings of a Workshop held at the 14th International Congress of Chemotherapy* (eds. Mitsuhaski and Daikos), University of Tokyo Press, Kyoto, Tokyo, 1985, p. 49.
[62] E. Buonpane, *Hosp. Forum.*, 1990, **25**, 389.
[63] Anon, *Pediatrics*, 2001, **108**, 776.
[64] Anon, *Med. Lett. Drugs Ther.*, 1991, **33**, 71.
[65] H. Lode, A. Kirch and P. Olschewski, *et al., 26th Interscience Conference on Antimicrobial Agents and Chemotherapy*, New Orleans, 1986, Abstract 484.

[66] M. Verho, V. Malerczyk and E. Dagrosa, *et al., Curr. Med. Res. Opin.*, 1986, **10**, 166.
[67] M. Verho, V. Malerczyk and E. Dagrosa, *et al., Pharmatherapeutica*, 1985, **4**, 376.
[68] N. Ichihara, H. Tachizawa and M. Tsumura, *et al., Chemotherapy*, 1984, **32**, 118.
[69] F. A. Wong and S. C. Flor, *Drug Metab. Dispos.*, 1990, **18**, 1103.
[70] D. N. Fish and A. T. Chow, *Clin. Pharmacokinet.*, 1997, **32**, 101.
[71] C. Horstkötter and G. Blaschke, *J. Chromtogr. B.*, 2001, **754**, 169.
[72] M. Verho, E. E. Dagrosa and V. Malerczyk, *Infection*, 1986, **14**(Suppl. 1), S47.
[73] E. E. Dagrosa, M. Verho and V. Malerczyk, *et al., Clin. Ther.*, 1986, **8**, 632.
[74] R. Farinotti, J. H. Trouvin and V. Bocquet, *et al., Antimicrob. Agents Chemother.*, 1988, **32**, 1590.
[75] E. Buonpane, *Hosp. Forum*, 1990, **25**, 389.

CHAPTER **7**

Paclitaxel

Saurabh Jauhari, Somnath Singh, and **Alekha K. Dash***

* Department of Pharmacy Sciences, School of Pharmacy and Health Professions, Creighton University, Omaha, NE 68178, USA

1. INTRODUCTION

1.1. History

In 1958, the National Cancer Institute (NCI) commissioned Department of Agriculture botanists to collect samples of over 30,000 plants to test for anticancer properties. One of those botanists, Arthur S. Barclay, collected 15 lbs of twigs, needles, and bark from Pacific yew trees, *Taxus brevifolia,* in a forest near Mount St. Helens. In 1963, Monroe E. Wall discovered that bark extract from the Pacific yew possessed antitumor activities. In 1967, Monroe E. Wall and Mansukh C. Wani isolated the active ingredient, paclitaxel, from bark extract of *T. brevifolia* and they reported its structure in 1971 [1–5]. However, there was a problem in obtaining paclitaxel from bark of Pacific yew because a 40-ft long plant, which may have taken 200 years to reach that height, yielded only a half gram of paclitaxel. Robert A. Holton's research group addressed this problem and developed a four-step procedure to convert 10-deacetylbaccatin, a related compound found in various nonthreatened yew species, *Taxus*, and which can be harvested without destruction of the entire tree, into paclitaxel [6–8].

1.2. Mode of action

Paclitaxel, the first of a new class of microtubule stabilizing agents, evolved from the National Cancer Institute as the most significant advance in chemotherapy of the past two decades. Microtubules are structures made up of tubulin and perform functions such as mitosis, spindle formation, and shape of cells [9]. Drugs interfering with the function of microtubule are called as antimicrotubule drugs. These drugs, depending upon their mode of action on microtubule, can be divided into two groups, one of which leads to destabilization of micro-tubules and the other group in which they lead to stabilize the micro-tubules. Paclitaxel has a unique mode of action: it binds to microtubules, preferentially to β-tubulin. Paclitaxel stimulates phosphorylation of β-tubulin in both differentiated and undifferentiated N115 cells [10] and stabilizes microtubules by the prevention of depolymerization [11–13]. The stabilized microtubules formed lead to cell death. In 1971, Wani and coworkers [1] concluded that paclitaxel acts by preventing somatic cell division, and later Horwitz *et al.* 1992 [14] established that paclitaxel stabilizes microtubules and arrests somatic cell mitosis at the G_2/M stage of the replication.

1.3. Pharmacokinetics

After IV infusion, the initial and final elimination half-lives of paclitaxel (Fig. 7.1) were reported to be 0.29 ± 0.13 and 6.95 ± 5.40 h, respectively [15]. Ninety percent of the drug is hydroxylated by the CYPs 3A4, 3A5, 1A2, and CYP2C8 enzymes in the liver and excreted in feces [16–19]. Less than 10% of the drug is eliminated unchanged through the kidney. Adults who received a 24-h infusion of paclitaxel achieved a C_{max} of 0.053–0.077 µmol/l [16, 20–25]. When the duration of intravenous infusion was decreased from 24 to 3 h, the pharmacokinetic profile of paclitaxel became nonlinear because drug elimination and tissue binding was saturated [16, 23]. The volume of distribution of paclitaxel is greater than total body water, indicating that more than 95% of the drug is bound to tissue protein. The extensive binding of paclitaxel was due to the association of drug with microtubules [16].

1.4. Resistance development

Resistance to paclitaxel is very common, and an increase in dose is necessary to maintain efficacy. Paclitaxel develops resistance by one of the following mechanisms: multidrug resistance-1 (MDR-1)/P-glycoprotein (PgP) expression, effect of drug efflux transporter (PgP (ABCB1) and breast cancer resistance protein (BRCP), β-tubulin expression, overexpression of oncogene c-erb-B-2, modification of apoptosis signaling sensitivity, and paclitaxel detoxification mediated by CYP.
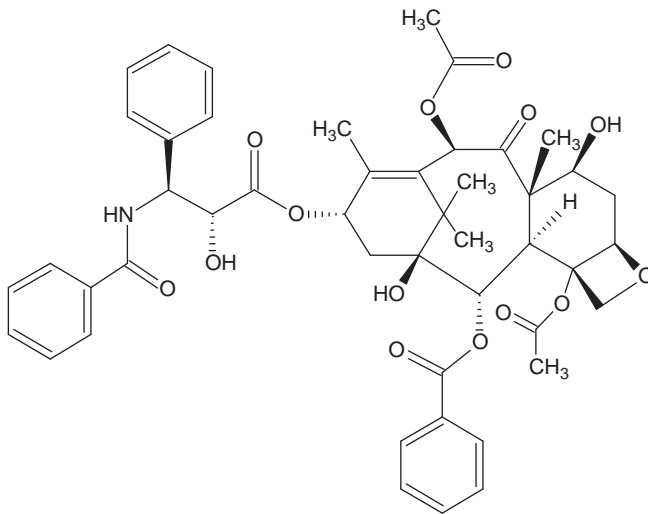
FIGURE 7.1   Molecular structure of paclitaxel.

Paclitaxel resistance is mainly governed by PgP expression. PgP, earlier known as MDR1, was the first ATP binding cassette (ABC) transporter discovered. PgP is an integral membrane protein, present on the apical surface of the epithelia of cells [26, 27]. Expression of PgP leads to development of multidrug resistance cells. Both the PgP and BCRP act as a drug efflux pump and share the common characteristics, which include localization on the apical surface, ATP dependent, and their substrates are mostly hydrophobic and amphipathic in nature [28, 29]. Paclitaxel binds to β-tubulin, inducing tubulin polymerization and bundling, ultimately resulting in mitotic arrest and apoptosis [30]. Paclitaxel resistance has been associated with increased microtubule dynamics and increased expression of the βIII-tubulin isotype [31]. A very recent report showed that overexpression of βIII-tubulin resulted in paclitaxel resistance by reducing the ability of paclitaxel to suppress microtubule dynamics thus providing a link between βIII-tubulin expression, tubulin dynamics, and paclitaxel resistance [32].

1.5. Therapeutic application

Paclitaxel is used in combination with other drugs, some of which have been discussed below. Combination therapy of paclitaxel with etoposide was investigated by Hahn *et al.* 1992 [33] using human MCF-7 breast and A549 lung carcinoma cells. Cytotoxicity of the drugs was studied by using clonogenic assay. The results of this study revealed that cytotoxicity was antagonistic. Hahn *et al.* 1992 [33], have also investigated the combination therapy of paclitaxel with Amsacrine in human MCF-7 breast and A549 lung carcinoma cell line. The results showed antagonistic cytotoxicity of paclitaxel with topotecan.

The combination of paclitaxel with topotecan was investigated in human (MCF-7) or mouse (MAM 16/C) breast cancer cell lines by Waud *et al.* 1992 [34]. The cell growth inhibition was determined by neutral red dye uptake. The results of this study showed a synergistic toxicity. Taniki *et al.* 1993 [35], have reported the synergistic toxicity of both paclitaxel and Tiazofurin. Tiazofurin inhibits inosine monophosphate dehydrogenase and causes disruption of guanosine triphosphate (GTP) metabolism [36]. The combination of these drugs was evaluated in human pancreatic (PANC-1), ovarian (OVCAR-5), and lung (H 125) carcinoma cells and a rat hepatoma cell line (3924A). Vinblastine is an anticancer drug that inhibits tubulin assembly. When both paclitaxel and vinblastine were combined, the association did not increase the levels of cytotoxicity beyond the effects of individual drug. A phase II study of carboplatine–paclitaxel combination therapy in elderly patients with advanced non-small-cell lung cancer was reported as a feasible treatment option with a favorable toxicity profile [37].

Chou *et al.* 1993 [38], has investigated the combination therapy of paclitaxel with Edatraxate using human breast adeno carcinoma cell line SKBR-3. The results showed synergism for 3 h, but after that, mild antagonism was observed. Interferon is a biological response modifier. Scmid *et al.* 1992 [39], has reported synergistic cytotoxicity when the combination therapy was studied using five human carcinoma cell lines: ACHN, MCF-7 breast, UO-31 renal, OVCAR-4, and OVCAR-5 ovarian. A weekly docetaxel and paclitaxel regimen was reported as a valuable therapeutic option for women with metastatic breast cancer [40].

1.6. Administration

Challenges encountered in the delivery of paclitaxel are its hydrophobicity, poor aqueous solubility, and low oral bioavailability [41]. To enhance the solubility of paclitaxel in the commercial available formulation, Cremphor EL is used as a solubilizer. Cremphor EL is a viscous, liquid surfactant with a molecular weight of approximately 3 kDa [42, 43]. Presence of the Cremphor EL in the formulation has led to hypersensitivity reactions which include rash, chest pain, flushing, hypotension, tachycardia, angioedema, and generalized urticaria [20, 42, 44, 45]. Cremphor EL causes hyperlipidemia and peripheral neuropathy, including axonal degeneration and demyelination [42, 46–48]. After the use of Cremphor EL, there is an enhancement of cell association of Paclitaxel in cancer cells by reversing the activity of PgP [49–52].

The other toxicities of paclitaxel include hepatoxicity, hypersensitivity, neurotoxicity, alopecia, myopathy, fatigue, and pulmonary lipid embolism [53]. Low solubility, low bioavailability, and side effects of paclitaxel therapy have led to the need for a delivery system which reduces systemic toxicity and increases safety and efficacy. To overcome the disadvantages of Cremphor EL in the formulation, various delivery systems for paclitaxel without Cremphor EL have been investigated which include pastes, liposomes, micelles, nanospheres, cyclodextrins complexes, emulsions, microspheres, prodrugs, and macromolecular adducts.

1.6.1. Pastes

The purpose of formulating paclitaxel into pastes was to obtain higher concentrations of water insoluble drug in a fatty base [54]. The bases (polycaprolactone or methoxy polyethylenglycol) were dissolved in dichloromethane. The rate of drug release was concentration-dependent and sustained up to 20 days [55]. The release rate can be increased by using gelatin, dextrin, and sodium chloride [56]. The use of topical pastes

is limited in the treatment of breast cancer because of the toxicity of dichloromethane and low percutaneous absorption.

1.6.2. Liposomes

Liposomes have been used to prolong drug release, enhance cellular association, and eliminate Cremophor EL from the formulation. It has been observed that liposomes are better tolerated and reduce tumor size in nude mice [57, 58]. In spite of its reduction of toxicity, the physical instability of liposomes limits their use.

1.6.3. Nanospheres

Most nanospheres are prepared with biodegradable, biocompatible, and synthetic polymers. Because of the small size of nanospheres, they can be administered orally, locally, and systemically. Feng *et al.* 2000 [59] discovered that nanospheres formed with PVA are more uniform. Feng *et al.* 2001 [60] also found a good amount of an emulsifier on the surface of nanospheres. They are commonly prepared with emulsion evaporation technique with PLA and PLGA [61, 62].

Scientists have observed that the release rate depends on the properties of the polymer. Feng *et al.* 2001 [60], has investigated the effect of different polymers by using the same concentration of emulsifier. Results have shown that the smallest paclitaxel nanospheres were obtained with PLA, then PLGA 75:25 and then PLGA 50:50. Perkins *et al.* 2000 [63] showed that nanospheres coated with distearoyl phosphatidylethanolamine and PEG 5000 increased circulation time. Sharma *et al.* 1996 [64], has reported that polyvinylpyrrolidone nanospheres increase the survival time in a cancer induced mice model. Nanospheres containing paclitaxel produce higher tissue levels, rapid distribution, and slower metabolism [65]. The main objective of using nanospheres as a delivery system is to enhance complete entrapment of the drug and the release properties of the drug.

1.6.4. Cyclodextrin complexes

Cyclodextrin complexes were prepared in order to increase paclitaxel solubility by formation of water soluble inclusion complexes [66]. The use of cyclodextrin is limited because of the high drug loading required [67].

1.6.5. Emulsions

The aim of emulsions as a drug delivery system is to solubilize the drug, make it stable in the organic phase, and eliminate the need of Cremophor EL.

For example, the oil in water (o/w) emulsion of taxol was more stable than its solution in human plasma at room temperature [68]. However,

there is a disadvantage of droplet aggregation and there can be a blockade of capillaries which makes this delivery system unacceptable.

1.6.6. Microspheres

The rate of drug release is slower in the case of microspheres, as compared to nanospheres. Demetrick *et al.* 1997 [69] showed that PLA microspheres released paclitaxel at a constant rate for 15 days and doses of 50, 150, 350 mg of particles reduced tumor volume. When 30% (w/w) isopropyl myristate was incorporated into PLGA microspheres, the release of paclitaxel increased from 10% to 70% in 21 days while the particle size was not affected [70]. The coating of microspheres with PEG did not increase the release rate [71]. Sato *et al.* 1996 [72] have shown that PLGA microspheres of taxol can be distributed into the lungs and only 10% excreted unchanged in the urine. According to Bragdon *et al.* 2001 [73], an ethylenevinylacetate (EVA) microsphere containing paclitaxel was used as an angiogenic inhibitor, and drug release was slower as compared to PLGA [74]. Poly(anhydride-*co*-imide) microspheres containing paclitaxel were used as radiosensitizer [75]. Although microspheres were found to increase efficacy, act as a protectant for the drug, and reduce toxicity of paclitaxel, but did not release the incorporated drug completely.

1.6.7. Prodrugs

The aim of prodrugs is to increase aqueous solubility, improve efficacy, and eliminate the use of Cremophor EL. Prodrugs are ester derivatives synthesized using the alcoholic functional group at the C-2 or the C-7 position of paclitaxel. Studies have shown that the use of prodrugs can reduce the tumor size. The 2-methyl PEG esters of paclitaxel, formulated into liposomes were more stable in aqueous forms [76]. The other prodrugs which have been used as a delivery system for paclitaxel include: disulfides, *N*-methylpyridinum acetate, cephalosporin, hyaluronic acid, sialic acid, cathepsin-B, and polyethyleneglycol [77–83].

1.6.8. Macromolecular adducts

It has been known that macromolecular adducts increase the permeability and the drug retention time. According to Dosio *et al.* 2001 [84], there has been an increase in the retention time of anticancer drugs in the body and macromolecular adducts can also target the cancer cells [83–90]. When conjugation was done to an antibody specific for tumor p75 receptor specificity was enhanced, resulting in reduced tumor volume in female mice [85]. The drawback of macromolecules is that their activity is not uniform, cannot be predicted, and in some cases is lower than paclitaxel alone.

1.6.9. Mucoadhesive gel

A mucoadhesive *in situ* gel forming delivery system has been reported for the sustained delivery of paclitaxel specifically targeted to mucin producing cells [91]. The delivery system consisted of chitosan and glyceryl monooleate (GMO) in 0.33 M citric acid containing paclitaxel. The *in vitro* release study of paclitaxel from the gel indicated a controlled release profile dependent on its loading and presence of a surfactant in the release medium. The transport of paclitaxel from the gel across Caluc-3 cell line was lower than Caco-2 cell line which was 2–4 times higher in basolateral-apical direction than apical-basolateral direction. Calu-3 cells produces mucin higher than the Caco-2 cells which indicate that transport of paclitaxel from mucoadhesive gels was influenced by the mucin-producing capability of cell.

2. DESCRIPTION

2.1. Nomenclature

2.1.1. Systematic chemical name

2aR-(2a a, 4b, 4 6b,9a (a R*S*)11a,12a,12aa,12ba]-B(Benzoylamino)-a-hydroxy-benzenepropanoic acid 6, 12b-bis(acetyloxy)-12-(benzoyloxy)-2a, 3,4 4a, 5,6,9,10,11,12,12a, 12b-dodecahydro-4,11-dihydroxy 4a, 8 13,13-tetra-methyl-5-oxo-7, 11-methano-1H-cyclodeca[3,4]benz[1,2-b] oxet-9-yl-ester.

2.1.1.1. Nonproprietary name Taxol.

2.1.1.2. Proprietary names [92] Abitaxel (Teva, Rus.), Abraxane (Abraxis, USA), Anzatax (Mayne, Austral.), Asotax (Asofarma, Mex.), Biopaxel (Biosintetica, Braz.), Biotax (Faulding, Israel), BrisTaxol (BMS, Mex.), Britaxol (BMS, Chile), Clitaxel (Pfizer, Arg.), Dalys (Dosa, Arg.), Drifen (Richmond, Arg.), Ebetaxel (Ebewe, Austria), Formoxol (YSP, Malaysia),Genexol (Samyang, Singapore), Ifaxol (Andromaco, Mex.), Intaxel (Dabur, India), Magytax (BMS, Hung.), Medixel (Taro, Israel), Mitotax (Reddy, Malaysia), NeoTaxan (Neocorp, Ger.), Oncotaxel (Sun, Thai.), Onxel (Darrow, Braz.), Onxol (Zenith Goldline, USA), Paclikebir (Aspen, Arg.), Paclisan (Sanfer, Mex.), Paclitax (Cipla, India), Paclitax (Eurofarma, Braz.), Paclitaxel Injection USP 29, Paclitaxin (Pharmachemie, Neth.), Pacliteva (Teva Tuteur, Arg.), Paklitaxfil (Filaxis, Arg.), Panataxel (Bioprofarma, Arg.), Parexel (Zodiac, Braz.), Paxel (Cristalia, Braz.), Paxene (Combino, Spain), Petaxel (Biochem, India), Praxel (Laboratorios Chile, Chile), Ribotax (Ribosepharm, Ger.),Taclipaxol (Biochimico, Braz.), Taclix (Cellofarm, Braz.), Tarvexol (Sandoz, Arg.), Taxilan (Bergamo, Braz.), Taxocris (LKM, Arg.), Taxodiol (Tecnofarma, Chile), Taxol (BMS Oncology, USA), Taycovit (Ivax, Arg.), Yewtaxan (Pharmachemie, S.Afr.).

2.2. Formulae

1. Empirical formula, molecular weight, CAS number
   $C_{47}H_{51}NO_{14}$, Molecular weight $= 853.92$ g/mol, CAS number $= 33069$-62-4
2. Structural formula (see Fig. 7.1)

2.3. Elemental analysis [93]

The calculated elemental composition of paclitaxel is as follows:

Carbon	66.11%
Hydrogen	6.02%
Oxygen	1.64%
Nitrogen	26.23%

2.4. Appearance

Paclitaxel is available as a white to off-white crystalline powder.

2.5. Uses and applications [94]

Paclitaxel is an antineoplastic agent that is highly effective against ovarian and breast cancer. It was approved by US Food and Drug Administration (FDA) for the treatment of ovarian cancer in 1992; for advanced breast cancer in 1994; and for early stage breast cancer in 1999. Various stages in the development of this drug are depicted below [95].

1962–1966	NCI screening of cytotoxic agents from natural product.
1967	Antitumor activity detected.
1969	Pure Paclitaxel isolated.
1971	Structure was elucidated.
1983	Phase 1 studies initiated.
1986	Hypersensitive reaction observed.
1988	NCI suggests premedication regimen.
1989	Proved effective against ovarian cancer.
1991	Proved effective against breast cancer.
1992	Proved effective against non-small-cell lung cancer.
1992	Approved by FDA for ovarian cancer.
1994	Approved by FDA for breast cancer.

Paclitaxel, in combination with the platinum containing compound (cisplatin or carboplatin), is used for the initial treatment of advanced ovarian carcinoma (stage III or IV) in patients who have already undergone surgery.

Paclitaxel alone is used for metastatic ovarian cancer refractory to conventional therapy. It is used as a second line drug for the palliative treatment of recurrent or refractory ovarian carcinoma.

Paclitaxel is used as monotherapy for the treatment of breast cancer in patients who have metastatic disease refractory to conventional combination therapy, or who have relapsed within 6 months of adjuvant therapy. Paclitaxel alone is used as second line therapy for the palliative treatment of advanced or refractory AIDS-related Kaposi's sarcoma.

Paclitaxel monotherapy, as well combinational therapy is used for the treatment of non-small-cell and small-cell lung cancers. Paclitaxel appears to be one of the most active single agents in patients with non-small-cell lung carcinomas who have not received prior chemotherapy. Paclitaxel is active against both squamous cell carcinoma and adeno carcinoma. It has been used alone or in combination with cisplastin or fluorouracil for the treatment of advanced esophageal cancer.

3. METHODS OF PREPARATION

3.1. Old extraction method

Paclitaxel is mainly extracted from the bark of a slow growing Western (Pacific) yew, and yields are about 0.01% of the dry weight of bark [96].

3.2. New extraction method

Newer methods of extraction of paclitaxel in large-scale application using chloroform from a single reverse-phase column has increased yields to 0.04% [97]. The chloroform extractable fraction of the bark of *T. brevifolia* is applied directly on to a C-18 bonded silica column in 25% acetonitrile/water, with elution using a step gradient: 30–50% acetonitrile/water. On standing, eight different taxanes, including taxol, crystallize out directly from different fractions. The crystals are filtered and purified further by recrystallization. Taxol and four other taxanes are purified this way. The other three require a short silica column. Taxol is freed from cephalomannine by selective ozonolysis. Approximately 3000 trees must be sacrificed in order to obtain 1 kg of paclitaxel, which is sufficient to treat about 500 patients. Present-day protocol prescribes about 2 g of paclitaxel for complete treatment [98].

3.3. Semisynthetic method

An alternative method allowing preparation of the drug in larger yields (i.e., a semisynthetic method using a precursor extracted from needles and twigs of a more prevalent yew) has also been developed [99].

3.3.1. Docetaxel [100]

Docetaxel, a semisynthetic taxoid, is synthesized by attaching a semisynthetic side-chain to 10-deacetylbaccatin III, which is readily available.

3.3.2. Cell culture-based method

Taxus cell culture, by a fungal endophyte, *Taxomyces andreanae*, for biosynthesis of paclitaxel was tested a viable solution [101], even though the amount produced was very low. A recent report indicated the possibility of increasing the production of paclitaxel and baccatin III in Taxus cell suspension cultures by addition of methyl jasmonate, which plays an important role in signal transduction processes [102].

Sustained production of paclitaxel by semicontinuous perfusion nodule cultures appears to be another approach to produce large quantities of the drug [103, 104].

3.4. Total paclitaxel synthesis

Three approaches have been utilized for the total syntheses of paclitaxel. The Holton group [105, 106] and Nicolaou group [107] published their approaches in 1994, and more recently, Danishefsky and coworkers have reported another method of total taxol synthesis in 1996 [108].

3.4.1. Holton's method

(–)-Borneol was used as the starting material, which was converted to an unsaturated ketone over 13 chemical steps. This ketone was converted into β-patchouline oxide. This was epoxidized and underwent skeletal rearrangement to a tertiary alcohol in presence of a Lewis acid. The tertiary alcohol is further epoxidized and undergoes fragmentation reaction to produce the A and B rings of taxol.

(–) Borneol   Homocamphor
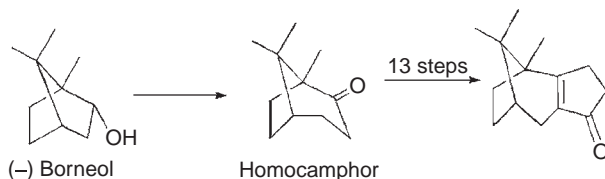
The C-ring was then added finally to the structure using the Robinson–Stork annulation methodology.

Tertiary alcohol

Taxol A, B rings   Taxol A, B, C rings
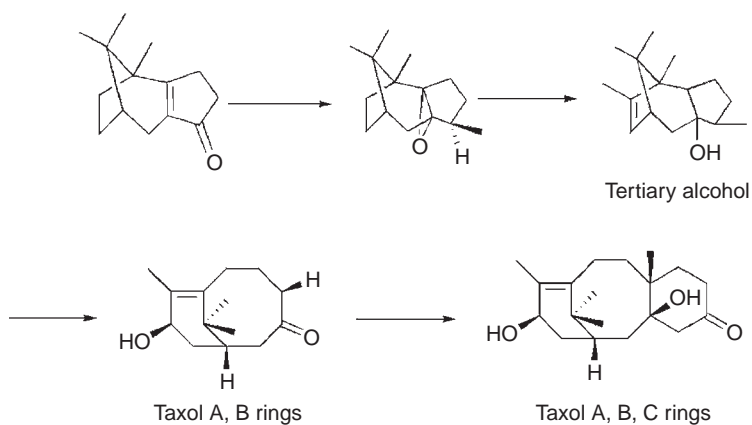
The full synthesis of paclitaxel is reported elsewhere [105, 106].

3.4.2. Nicolaou's method

Nicolaou *et al.* 1994 [99] have reported another route of synthesis of paclitaxel. According to this method of synthesis, both A- and C-rings were constructed separately, and then linked together using a Shapiro reaction to connect the southern part, and a McMurray coupling reaction to complete the B-ring.
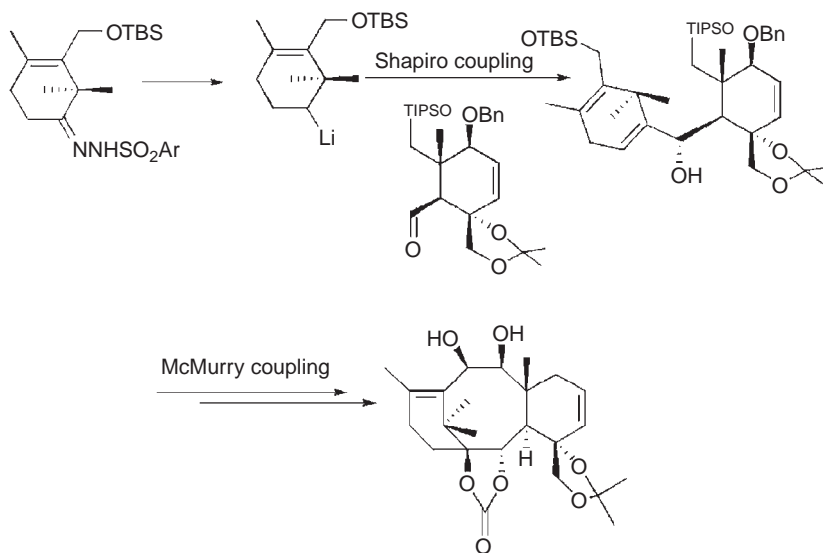
3.4.3. Danishefsky's method

Danishefesky *et al.* 1996, [108] have published a different method of synthesis for paclitaxel. Wieland–Miescher ketone was used as the starting material. This was elaborated to a complex enol triflate, bearing an olefin on the C-ring for development to taxol via an intramolecular Heck reaction.
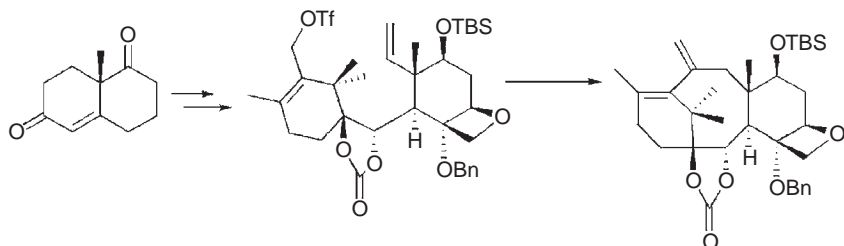
4. PHYSICAL PROPERTIES

4.1. X-ray powder diffraction pattern

The sample was sprinkled on a zero-ground holder and exposed to Cu-K$_\alpha$ radiation (45 kV $\times$ 40 mA) in a wide-angle powder X-ray diffractometer (model D5005, Siemens, Madison, WI). The instrument was operated in the step-scan mode, in increments of 0.05 ° 2θ over 5–50 ° 2θ and the counts were accumulated for 1 s at each step. The data collection and analyses were performed with commercially available software (Jade, version 7.0, Materials Data Inc., Livermore, CA). Fig. 7.2 shows the XRD patterns of paclitaxel. The *d*-spacing and 2θ value are shown in Table 7.1.

4.2. Thermal analysis

4.2.1. Melting behavior

The melting range of Paclitaxel has been reported to be within 213–220 °C with decomposition [41].

4.2.2. Differential scanning calorimetry (DSC)

Paclitaxel sample (2–4 mg) was heated under a nitrogen purge from 30 to 350 °C in a nonthermatically crimped aluminum pan at a rate of 10 °C/min in a Shimadzu DSC-50 thermal analysis system. The DSC thermogram of paclitaxel is shown in Fig. 7.3 [109]. The endothermic peak at 217.5 °C was attributed to the melting of paclitaxel followed by decomposition. The enthalpy of fusion for this melting event was calculated to be 55.35 J/g.
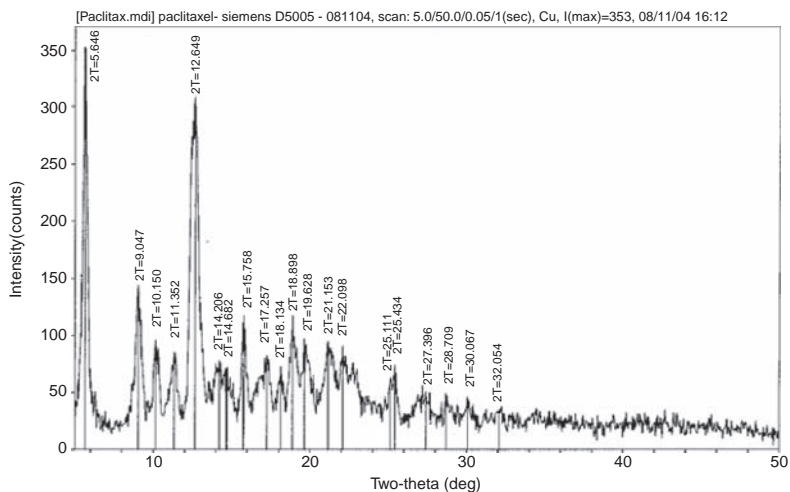
FIGURE 7.2 X-ray powder diffraction pattern of paclitaxel.

TABLE 7.1 X-ray powder diffraction patterns data for paclitaxel

Scattering angle (degrees 2-Θ)	d-spacing (Å)	Relative intensity (%)	FWHM
5.646	15.6395	79.4	0.328
9.047	9.7667	29.5	0.353
10.15	8.7076	10.1	0.234
11.352	7.7881	13	0.341
12.649	6.9926	100	0.498
14.206	6.2296	12.7	0.555
14.682	6.0286	13.2	0.571
15.758	5.6194	13	0.22
17.257	5.1344	13.7	0.452
18.134	4.8879	2	0.101
18.898	4.6922	10.8	0.233
19.628	4.5192	8.8	0.306
21.153	4.1966	12.6	0.395
22.098	4.0193	9.3	0.385
25.111	3.5435	12.3	0.626
25.434	3.4992	10.6	0.326
27.396	3.2529	10.7	0.622
28.709	3.1071	2.8	0.169
30.067	2.9698	3.5	0.229
32.054	2.79	1.9	0.264
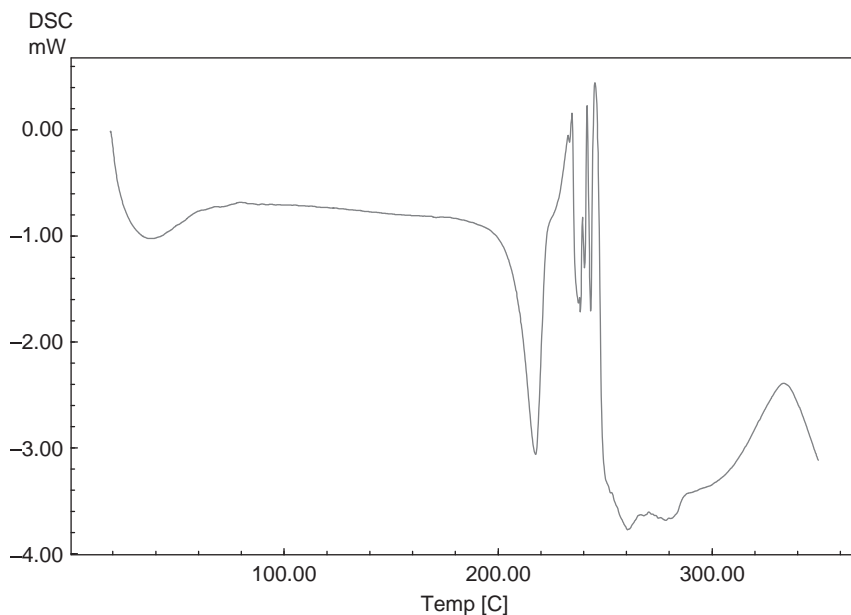
FIGURE 7.3   DSC thermogram of paclitaxel.

4.2.3. Thermogravimetric analysis

TG analysis of paclitaxel was conducted using a Shimadzu Thermogravimetric Analyzer (model TGA-60). Approximately 15.5 mg sample was subjected to a constant heating rate (10 °C/min) and heated from room temperature to 350 °C in presence of an inert atmosphere (nitrogen). The TG thermogram of paclitaxel is shown in Fig. 7.4 and the weight loss above 220 °C was believed to be due to the sample decomposition that takes place after the melting step [109].

4.3. Solubility characteristics

Paclitaxel is highly lipophilic and practically insoluble in water. There are wide variations in the published values of the aqueous solubility of paclitaxel, with values of 0.6 mM [41], 35 µM [110], 0.7 µg/ml, 6 µg/ml [111], and less than 0.01 mg/ml [46] having been reported. Paclitaxel solubility in various solvent systems at room temperature has also been reported and is summarized in Table 7.2. Various approaches have been utilized and investigated to enhance the aqueous solubility of paclitaxel, and the results of these studies are summarized in Table 7.3.
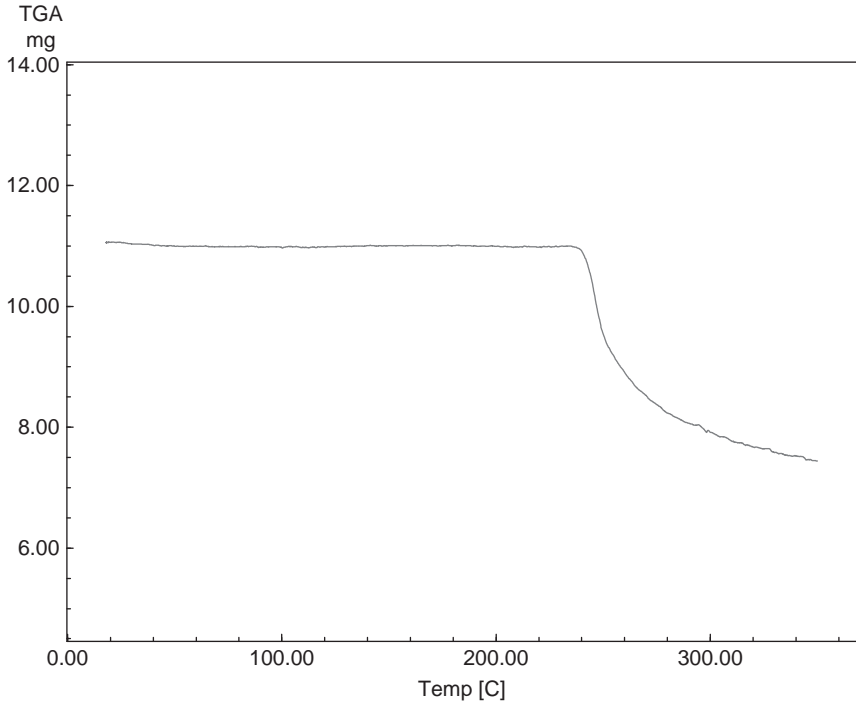
FIGURE 7.4   TG Thermogram of paclitaxel.

4.4. Partition coefficients

The partition coefficient of paclitaxel in PBS (pH 7.4) and 1-octanol has been determined and the log D has been reported to be 3.62 [112].

4.5. Spectroscopy

4.5.1. UV spectroscopy [109]
The UV absorption spectra of paclitaxel in mobile phase (acetonitrile: methanol:0.1 M ammonium acetate (48.5:16.5:35%, v/v/v) and methanol were recorded at a concentration 5 µg/ml, using a Shimadzu UV–vis Spectrophotometer Model (Pharm Spec UV-1700). The resulting spectra are shown in Fig. 7.5 (paclitaxel in mobile phase) and Fig. 7.6 (paclitaxel in methanol). The absorption maximum was noted at 227 nm in both these conditions.

4.5.2. Infrared spectroscopy
The infrared absorption spectra of amorphous paclitaxel, anhydrous paclitaxel, and the dihydrate have been reported by Lee *et al.* 2001 [113], and are shown in Fig. 7.7. Anhydrous paclitaxel and the dihydrate show two

TABLE 7.2   Solubility of paclitaxel [46]

Solvent	Solubility (mg/ml)
Methylene Chloride	>19
Acetonitrile	>22
n-Heptane	<<1
Ethanol	~39
Isopropanol	~12
75% Isopropanol/water	~0.2
75% Propylene glycol	<1.4
30% Polyvinylpyrolidone in water	<0.3
75% PEG 400*	31
65% PEG 400	3.8
55% PEG 400	0.9
50% PEG 400	0.2
45% PEG 400	0.14
35% PEG 400	0.03
Soybean oil	0.3
Triacetin	75

PEG 400* = polyethylene glycol 400.

TABLE 7.3   Reported pharmaceutics approaches to enhance paclitaxel solubility in formulations [46]

Approach	Examples
pH adjustment/salt formation	Hydrochloride, citrate, lactate, megumine, sodium, potassium
Cosolvent	Ethanol, dimethylsulfoxide, polyethylene glycol, propylene glycol
Complexation	Cyclodextrins, povidone
Oil–water emulsions	10–20% Soyabean oil
Micellar solubilization	Cremphor EL, polysorbate 80

carbonyl absorptions near $1720\,cm^{-1}$. However, the amorphous form showed only one carbonyl absorption in this region. Other characteristic patterns were also noted near 3000, 1650, and $1522\,cm^{-1}$.

4.5.3. Nuclear magnetic resonance spectrometry

4.5.3.1. ^{1}H-NMR spectrum   Proton nuclear magnetic resonance spectra of paclitaxel were obtained using a Bruker AVANCE DMX50 spectrometer. Samples used in liquid state NMR studies were 12.2 mg paclitaxel in
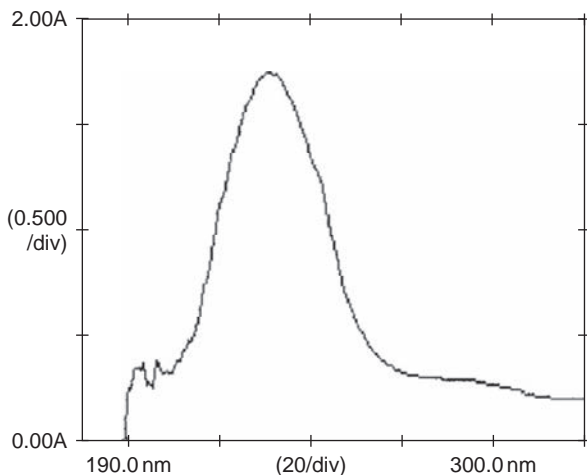
FIGURE 7.5   UV spectrum of paclitaxel in mobile phase.
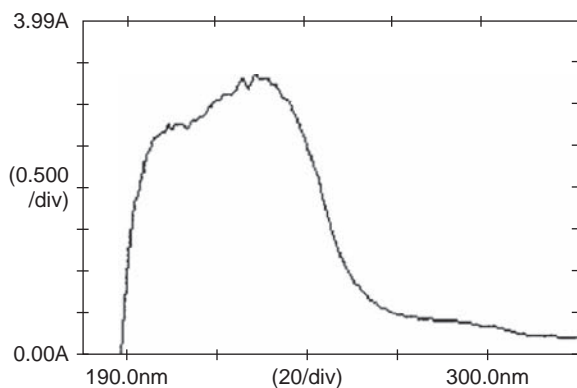
FIGURE 7.6   UV spectrum of paclitaxel in methanol.

0.6 ml $CDCl_3$ and 60 mg paclitaxel in 0.6 ml of $CDCl_3$. Chemical shifts were determined and are referenced to tetramethylsilane (TMS) for ^{1}H and to solvent peak for ^{13}C which are shown in Fig. 7.8 [114]. Figure 7.8 demonstrate the effect of paclitaxel concentration on the NMR at 298 K. Decreasing the concentration from 100 to 20.3 mg/ml has shifted only three OH protons which include C_2–OH, C_1–OH, and C_7–OH. This finding was in accordance with the study done by Mastropaolo *et al.* 1995 [115], which have shown that these three protons form intermolecular hydrogen bonding.

Voelker *et al.* 1991 [116] has shown that determination of ^{13}C T_1 relaxation is helpful in understanding the internal dynamics of this
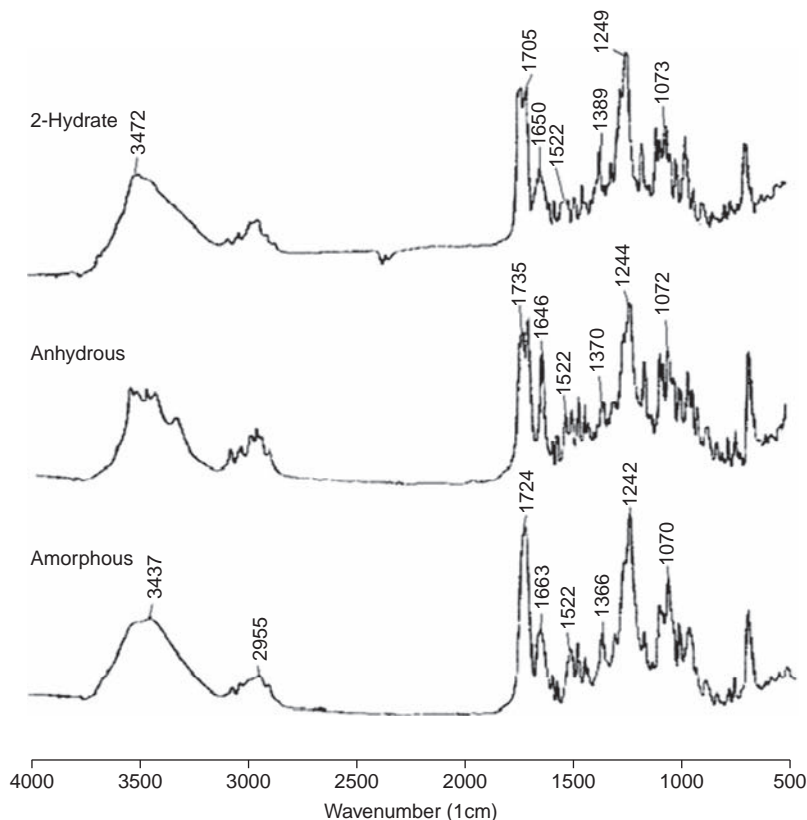
FIGURE 7.7   Infrared absorption spectra of paclitaxel.

molecule. Inversion recovery experiments were used to determine the spin lattice (T_1) relaxation time of different ^{13}C nuclei of a molecule. In this study, an inversion experiment was carried out at 125 MHz and Bruker–Xwinnmur built-in macro program was used for calculation. The chemical shifts and spin lattice relaxation time were summarized in Table 7.4 [114].

4.5.3.2. ^{13}C-NMR spectrum   A comparison has been shown in Fig. 7.9 between the solution phase and solid state NMR spectra of paclitaxel. The chemical shift assignments of the solid state ^{13}C-NMR spectra were made on the basis of solution NMR data. The analyzed data were shown in Table 7.5 [114]. Double peak patterns seen in solid state NMR represent the rigid crystalline structure of paclitaxel.
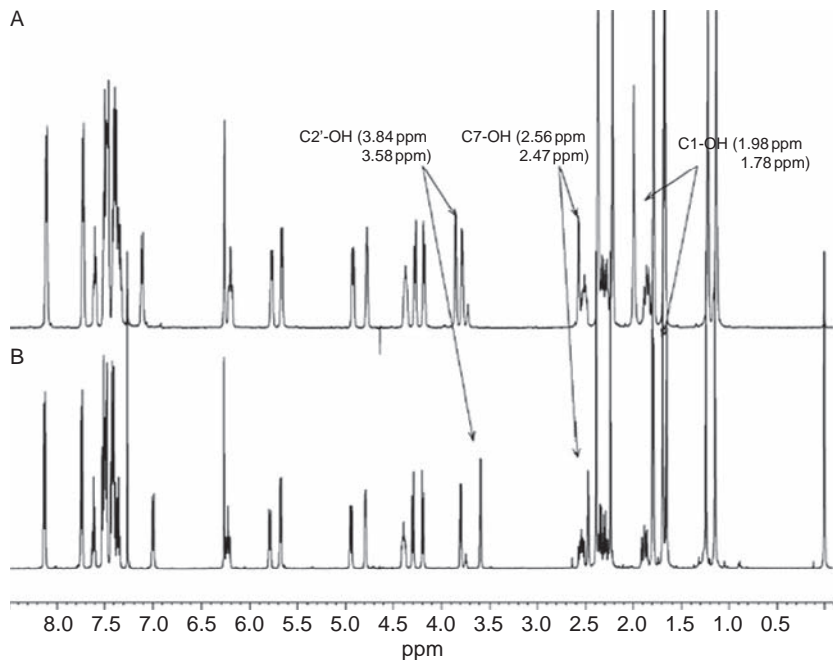
FIGURE 7.8 ^{1}H-NMR spectrum of paclitaxel [114]

A Chemagnetics CMX300 NMR spectrometer with a commercial double bearing 5.0 mm MAS probe was used for high power proton decoupling ^{13}C CP/MAS NMR spectra. NMR spectrums were recorded at 75 MHz. ^{79}Br resonance of KBr was used for setting the magic angle. Zicornia pencil rotors packed with the sample were spun at 10 kHz at the magic angle. For thermal equilibrium, a relaxation time of 2 s was used and for adequate signal to noise ratio 2048 or 10,240 acquisitions were utilized. Cross polarization was used for the ^{13}C spectra recording. ^{13}C-labeled glycine standard was used to set the Hartmann-Hahn match condition for the experiment.

4.5.4. Mass spectroscopy

A mass spectrum of paclitaxel is reported, which used a method based on selected reaction monitoring in a liquid chromatography tandem mass spectrometry method (Sciex API II tandem quadrupole mass spectrometer [117].

The substructures of paclitaxel characteristic of specific protonated ions are shown in Fig. 7.10A, and its mass spectrum is shown in Fig. 7.10B.

TABLE 7.4 ^{13}C and ^{1}H Chemical shifts and ^{13}C T1 measurements of paclitaxel [114]

Carbons	60 mg Paclitaxel in CDCl$_3$		
	^{13}C (ppm)	^{13}C T1 (ms)	^{1}H (ppm)
C-9	203.57	1.387	
C-28	170.33	1.467	
C-30	171.18	1.59	
C-I′	172.63	1.506	
C-5′	166.87	1.63	
C-II	133.07	1.284	
C-12	141.88	1.067	
C-21	167.14	1.954	
C-22	129.1	1.56	
C-23, 27	130.13	0.293	8.11
C-24, 26	128.66	0.313	7.49
C-25	133.64	0.351	7.6
C-32	133.58	0.284	
C-33, 37	127.02	0.835	7.46
C-34, 36	128.92	0.709	7.37
C-35	128.25	0.352	7.33
C-38	137.94	1.543	
C-39, 43	126.98	0.74	7.73
C-40, 42	128.6	0.757	7.4
C-41	131.88	0.371	7.47
C–I	78.88	3.002	
C-2	74.89	0.306	5.66
C-3	45.61	3.109	3.78
C-4	81.04	0.366	
C-5	84.33		4.92
C-6	35.62	0.315	2.51,1.85
C–I	72.06	3.451	4.38
C-8	58.47	0.362	
C–IO	75.51	0.389	6.27
C-13	72.15		6.2
C-14	35.58	3.756	2.32, 2.27
C-15	43.09	1.412	
C-17	26.76	0.2	1.22
C-16	21.75″	1.049	1.12
C-18	14.75	0.639	1.67
C-19	9.52	0.201	1.78
C-20	76.42	1.629	4.28, 4.18
C-29	22.53	1.474	2.36

(*continued*)

TABLE 7.4 (*continued*)

Carbons	60 mg Paclitaxel in CDCl₃		
	^{13}C (ppm)	^{13}C T1 (ms)	^{1}H (ppm)
C-31	20.8	0.378	2.21
C-2′	73.16	0.355	4.77
C-3′	55.06		5.76
C2–OH			3.84
C–OH			1.98
C7–0H			2.56
N–H			7.11

5. METHOD OF ANALYSIS

5.1. Compendial methods of analysis [117]

The United States Pharmacopoeia defines a number of test methods that define the USP grade of paclitaxel.

5.1.1. Test 1. (for materials labeled as isolated from natural sources)

Diluent: Prepare as directed in the assay.
Solution A: Acetonitrile is degassed and filtered.
Solution B: Water is degassed and filtered.
Chromatographic condition: The chromatographic separation was achieved on a column 150×4.6 mm, 3 μm, with a flow rate of 1.2 ml/min with UV detection at 227 nm. The column temperature is maintained at 30 °C. The chromatographic conditions are programmed as follows.

Time (Min)	Solution A (%)	Solution B (%)	Elution
0–35	35	65	Isocratic
35–60	35–80	65–20	Linear gradient
60–70	80–35	20–65	Linear gradient
70–80	35	65	isocratic

5.1.2. Test 2. (for material labeled as produced by a semisynthetic process)

Diluent: acetonitrile.
Solution A: Mixture of water and acetonitrile (3:2) is filtered and degassed.
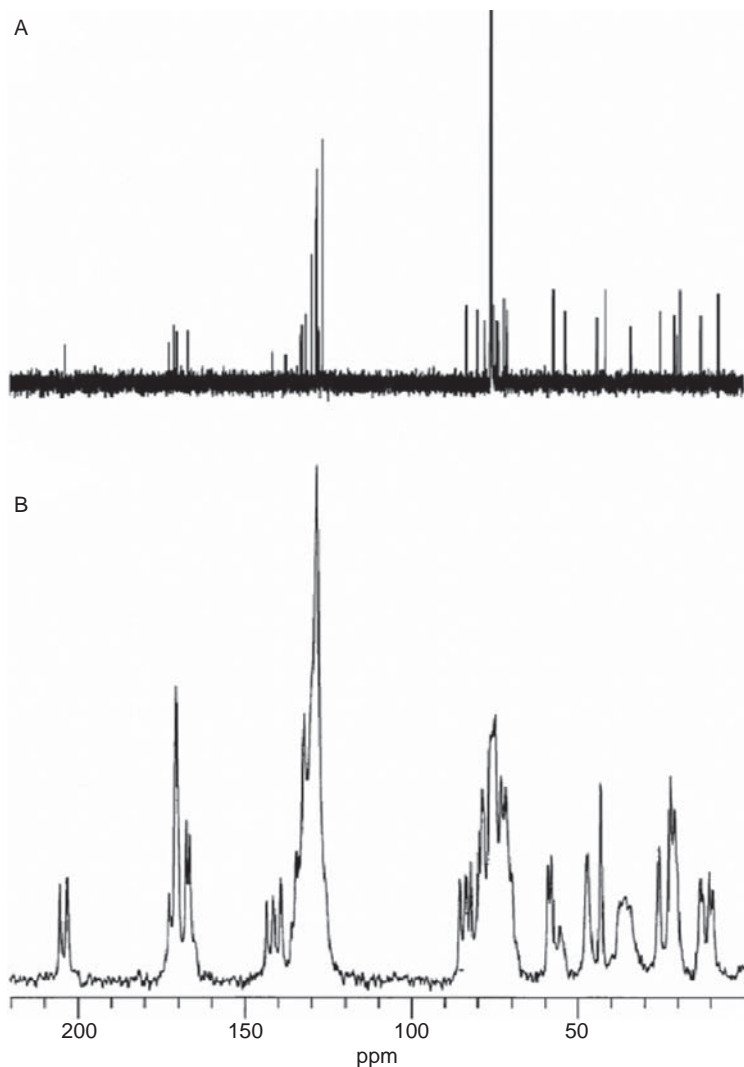
FIGURE 7.9 ^{13}C-NMR spectrum of paclitaxel, (A) paclitaxel in CDCl$_3$ solution, and (B) solid state paclitaxel [114].

Solution B: Acetonitrile is degassed and filtered.

Chromatographic condition: The chromatographic separation was achieved on a column 150 × 4.6 mm, 3 μm, with a flow rate of 1.2 ml/ min with UV detection at 227 nm. The column temperature is maintained at 35 °C. The chromatographic conditions are programmed as follows.

TABLE 7.5   ^{13}C-NMR spectrum of paclitaxel. Comparison of solution and solid state NMR spectra [114]

Carbons	Solution NMR paclitaxel 13C (ppm)	^{13}C Solid-state CPIMAS NMR Paclitaxel		
		[13]C (ppm)	T1 (s)	T1pH (ms)
C-9	203.57	205.7	35.6	14.4
		203.5	35.6	14.4
C-I′	172.63	172.8	79	14.5
C-30	171.18	170.8	79	14.5
C-21	167.14			
C-5′	166.87	166.9	42	13.9
		165.2	42	13.9
C-12	141.88	143.8	87.3	11.4
		141.9	87.3	11.8
C-38	137.94	139.5	60.5	11.5
		136.1	55	
C-25	133.64	134.8	38.8	
C-II	133.07	133.5	34.8	
C-41	131.88	132.5	51.5	14.1
C-24, 26	128.66	128.6	39.7	14.6
C-5	84.33	85.8	88.7	15.3
		84	70.2	15.3
C-4	81.04	82.7	79.2	15.2
		80.2	76.3	
C–I	78.88	79.1	48.9	14.9
C-20	76.42	76.8	57.4	
C–IO	75.51	75.9	50.6	15.4
		75.2	49.7	15.4
C-2′	73.16	73.6	55.1	15.3
C-13	72.15	72.1	39.4	15.5
C-7	72.06	69.2	40.3	
C-8	58.47	59.3	41.5	13.8
		58.3	35.6	138
C-3′	55.06	55.8	43.7	16.1
	′′			
C-3	45.61	47.6	84	15.9
C-15	43.09	43.5	11.5	138
C-6	35.62	37.6	82.5	18.8
C-14	35.58	36.2	38.4	18.7
		35	36.4	18.7

(continued)

TABLE 7.5 (*continued*)

| | | ^{13}C Solid-state CPIMAS NMR | | |
| | | Paclitaxel | | |
Carbons	Solution NMR paclitaxel 13C (ppm)	^{13}C (ppm)	T1 (s)	T1pH (ms)
C-17	26.76	26	I I.7	13.8
C-29	22.53	22.7	11.6	13.8
C-16	21.75	21.2	7.54	13.8
C-18	14.75	13.7	15.2	12.4
		12.9	20.9	12.7

Time (Min)	Solution A (%)	Solution B (%)	Elution
0–20	100	0	Isocratic
20–60	100–10	0–90	Linear gradient
60–62	10–100	90–0	Linear gradient
62–70	100	0	isocratic

5.1.3. Test 3. (for organic volatile impurities)

Diluent—Mixture of methanol and acetic acid (200:1) is used as diluent.
Chromatographic system: The chromatographic separation was achieved
  on a column 250 × 4.6 mm, 5 µm, with a flow rate of 1.5 ml/min with
  UV detection at 227 nm.

5.2. High performance liquid chromatography (HPLC)

Several LC methods have been used for separation and quantitation of
paclitaxel in various pharmaceutical dosage forms, as well as in biological
samples. The majority of the LC methods employ reversed phase HPLC
systems. Chromatographic conditions of some of the reported methods
are summarized in Table 7.6.

6. STABILITY

6.1. Stability in solution

Paclitaxel is reported to be stable over 24 h at a concentration of 0.3–
1.2 mg/ml [130, 131]. Waugh *et al.* [132] have determined the stability of
paclitaxel in infusion solutions and dilutions in 0.9% saline and dextrose
5% solutions at various concentrations of paclitaxel (0.3, 0.6, 0.9, and
1.2 mg/ml). Paclitaxel solutions were stored in PVC infusion bags,
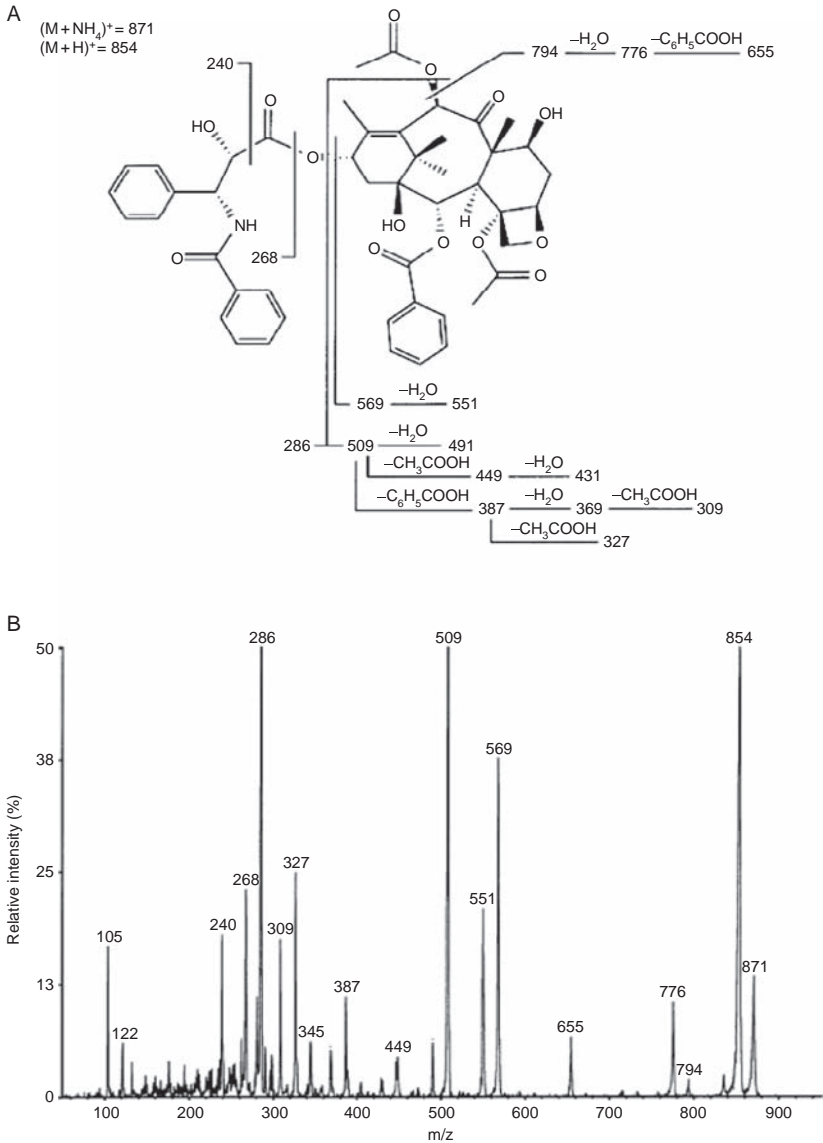
FIGURE 7.10   (A) Structure of paclitaxel showing substructures characteristic of specific protonated ions (B) Mass spectrum of paclitaxel [117].

polyolefin plastic containers, and glass bottles. These solutions were filtered through a 0.22 μm filter, and maintained at ambient temperature. No loss of potency was noticed in any of the solutions.

TABLE 7.6 Reported HPLC methods for analysis of paclitaxel

Column	Mobile phase (v/v)	Flow rate (ml/min)	Wave length (nm)	Retention time (min)	References
C-18 column (4.6 × 150 mm, 3 μm)	Potassium phosphate buffer, 20 mM (pH 3.0): acetonitrile (55:45)	1	227	11.5	[118]
C18 (250 × 4 mm, 5 μm)	Gradient system was applied to a quantitation of paclitaxel consisting of acetonitrile–deionized water	1.0	227	18.0	[119]
C 18 (50 × 2.1 mm)	Acetronitrile:water:acetic acid (50;50:0.1)	0.2	227	2.9	[120]
ODS C18, (100 × 2 mm, 5 μm)	Methanol: water (70:30) in 0.1% formic acid.	0.2	*	7	[121]
C18 (150 × 4.6 mm, 5 μm)	Acetonitrile:methanol: ammonium acetate buffer (10 mM, pH 5.0) (48.5:16.5:35)	0.8	227	8.5	[122]
C18 (150 × 4.6 mm, 3 μm)	Acetonitrile:0.1% phosphoric acid (55:45) in deionized water.	1.3	200–400	3.4	[123]
ODS-80A C18 (150 × 4.6 mm, 3 μm)	Water–methanol–tetrahydrofuran–ammonium hydroxide (37.5:60:2.5:0.1).	1.0	230	7.5	[124]
C18 (250 × 4.6 mm, 5 μm)	Acetonitrile:methanol:water (48:11:41).	1.5	227	6.4	[125]

C18 (8 × 100 mm, 10 μm)	Sodium phosphate buffer, 1 mM (pH 5):acetonitrile (55.5:45.5)	4.5	227	5.26	[126]
C 8 (150 × 4.6 mm,5 μm)	Acetonitrile:methanol: ammonium acetate buffer, 0.2 mM pH 5 (4:1:5)	1.0	227	10.1	[127]
C8 (75 × 3.9 mm, 4 μm) C 18 (250 × 4.6 mm, 5 μm)	(37.5% acetonitrile in distilled water 49% acetonitrile in distilled water)	1	229	17.5	[128]
60 A phenyl column (150 × 4.6 mm, 5 μm)	Methanol:acetonitrile:50 mm ammonium acetate. (20:32:48). pH 4.2 with acetic acid.	1.0	230	15.0	[129]

* = Mass spectrometric detection using electro spray positive mode electron ionization.

6.2. Stability in formulations

HPLC analysis of the paclitaxel solution formulations at different time points over a period of 24 h showed no change in the concentration of paclitaxel, indicating that paclitaxel is stable in these formulations. Solutions were found to be hazy, which was attributed to the presence of surfactant in the formulation [131, 132].

6.3. Incompatibilities with other drugs

Trissel *et al.* [133] has reported the visual and turbidimetric compatibility of paclitaxel with other drugs. The results of this work are shown in Table 7.7.

7. PHARMACOKINETICS AND METABOLISM

7.1. Animal studies

To determine the pharmacokinetics of paclitaxel in different formulations, inbred adult male swiss mice were used. The route of administration for all formulations was either intravenous or subcutaneous. Pharmacokinetic parameters were calculated by a compartment model independent method using PCNONLIN [134].

7.2. Patient studies

Eisenhauer *et al.* [135] have reported the pharmacokinetics of paclitaxel in phase 1 trials at a dose of 175 mg/m^2, and the results of this study are summarized in Table 7.8.

Paclitaxel pharmacokinetics have also been evaluated in phase 1 trials using reverse phase HPLC. Paclitaxel doses ranging from 15–275 mg/m^2 were infused for 1, 6, and 24 h, and the data are shown in Tables 7.9 and 7.10.

7.3. Toxicity

Paclitaxel has exhibited many toxic effects, which may arise from the drug itself or from the diluting vehicle used in the formulation. These toxic effects, as reported by Stephan *et al.* [139] include Type 1 anaphylactic reaction such as dyspnea with bronchospasm, urticaria and hypotension, neutropenia, sensory peripheral neuropathy (even seen in non-Cremophor EL delivery systems) and other minor toxicities like alopecia, myopathy, fatigue, and pulmonary lipid embolism. One study found the severe adverse effects of paclitaxel as adjuvant therapy for early breast cancer therapy as shown in Fig. 7.11. This study reported the clinically

TABLE 7.7 Visual and turbidimetric compatibility of PTX (1.2 mg/ml) with other drugs [133]

Drug	Concentration (mg/ml)
Acyclovir sodium	7
Amikacin sulfate	5
Aminophylline	2.5
Ampicillin sodium/sulbactam sodium	20/10[a]
Bleomycin sulfate	1 unit/ml
Butorphanol tartrate	0.04
Calcium chloride	20
Carboplatin	5
Ceforanide	20
Cefotetan disodium	20
Ceftazidime	40
Ceftriaxone sodium	20
Cimetidine hydrochloride	12
Cisplatin	1[b]
Cyclophosphamide	10
Cytarabine	50[b]
Dacarbazin	4
Dexamethasone sodium phosphate	1
Diphenhydramine hydrochloride	2
Doxorubicin hydrochloride	2[b]
Droperidol	0.4
Etoposide	0.4
Famotidine	2
Floxuridine	3
Fluconazole	2[b]
Fluorouracil	16
Furosemide	3
Ganciclovir sodium	20
Gentamicin sulfate	5
Haloperidol lactate	0.2
Heparin sodium	100 units/ml
Hydrocortisone sodium phosphate	1
Hydrocortisone sodium succinate	1
Hydromorphone hydrochloride	0.5
Ifosfamide	25
Lorazepam	0.1
Magnesium sulfate	100
Mannitol	15%[b]
Meperidine hydrochloride	4
Mesna	10
Methotrexate sodium	15

TABLE 7.7   (*continued*)

Drug	Concentration (mg/ml)
Metoclopramide hydrochloride	5[a]
Morphine sulfate	1
Nalbuphine hydrochloride	10[b]
Ondansetron hydrochloride	0.5
Pentostatin	0.4[a]
Potassium chloride	0.1 mEq/ml
Prochlorperazine edisylate	0.5
Railitidine hydrochloride	2
Sodium bicarbonate	1 mEq/ml
Vancomycin hydrochloride	10
Vinblastine sulfate	0.12[a]
Vincristine sulfate	0.05
Zidovudine	4
Drugs of uncertain visual and turbidimetric compatibility	
Amphotericin B	0.6
Chlorpromazine hydrochloride	2
Hydroxyzine hydrochloride	4
Methylprednisolone sodium succinate	5
Mitoxantrone hydrochloride	0.5

Paclitaxel and all test drugs were dissolved in D5W injection USP, unless otherwise noted.
[a] In NaCl 0.9% injection, USP.
[b] Undiluted solution.

TABLE 7.8   Mean pharmacokinetic parameters of paclitaxel in humans (175 mg/m^2, 3-h infusion) [135]

Parameter	Paclitaxel
$t_{1/2\alpha}$ (min)	16
$t'_{1/2\beta}$ (min)	140
$t_{1/2\gamma}$ (h)	18.75
CL (l/h/m^2)	12.69
C_{max} (μmol/l)	4.27
AUC (μmol/l h)	16081
V_{ss} (l/m^2)	99.25
Protein binding (%)[a]	>95
48-h urinary excretion	<10
48-h fecal excretion	=70

AUC = area under the plasma concentration-time curve
CL = total body clearance
C$_{max}$ = peak plasma concentration
t$_{1/2\alpha}$ and t$_{1/2\beta}$ = distribution phase half-lives
t$_{1/2\gamma}$ = terminal plasma half-life
V$_{ss}$ = volume of distribution at steady-state.
[a] = Major plasma proteins involved are an acid glycoprotein (AAG:albumin) and lipoproteins.

TABLE 7.9 Comparative evaluation of *in vivo* pharmacokinetic profile of paclitaxel

Route	I.V.[a]					S.C.[b]	
Formulation	CrEL-Paclitaxel	Pro drug	Paclitaxel liposome	Paclitaxel liposome[d]	Micelle	Paclitaxel liposome	Liposome gel
Dose (mg/kg)	10	10	10	5	10	10	20
C_{max} (ng/ml)	9292	7366	9954	6623	5930	1095	1334
$t_{1/2}$ (h)	2.4	2.1	3.4	5.1	6.2	18.0	15.0
AUCo-inf (ng h)/ml	9286	6568	11138	11670	15225	11454	18373
AUMCo-inf (ng h^2)/ml	25012	18322	34787	57858	111794	110380	356862
MRT (h)	2.69	2.79	3.12	4.96	7.34	9.64	19.42
V_{ss} (l/kg)	2.90	4.25	2.80	2.12	4.82	8.41	21.14
CLT (l/h/kg)	1.07	1.52	0.89	0.43	0.65	0.87	0.54
V_z (l/kg)	3.71	4.61	4.40	3.16	5.87	22.67	11.78

[a] 196 μl was administered by tail I.V. route.
[b] 200 μl was injected in neck region.
[c] All formulation were tested within 48 h of preparation.
[d] due to viscosity of formulation only 5 mg/kg was administered.

TABLE 7.10 Pharmacokinetics of PTX in humans [136]

References	Dose/duration of infusion (schedule)	$t_{1/2\beta}$ (h)	Cl (l/h/m^2)	V_d (l/m^2)	C_p (μmol/l)
[136]	15–40 mg/m^2/1 and 6 h (daily * 5, q28d)	1.4	53	81^a	0.06–0.37
[24]	175–275 mg/ m^2/6 h (single dose, q21d)	8.3	8.1	59	2.0–10.1
[137]	175–275 mg/ m^2/6 h (single dose, q21d)	4.3	14	49	1.7–8.5
[24]	200–275 mg/ m^2/24 h (single dose, q21d)	3.2	22	119	5.0–1.3
[138, 177]	15–265 mg/m^2/ 1 and 6 h (single dose q21d)	6.4	15	67	1.3–13.0

C_p = peak plasma concentration; Cl = systemic clearance; $t_{1/2\beta}$ = harmonic beta half-life of elimination; V_d = volume of distribution at steady-state.^{a} Beta V_d.

important, severe adverse effects with paclitaxel (T) as adjuvant therapy for early breast cancer. The toxic effect of paclitaxel in the group receiving a 3 h infusion of T (175 mg/m^2) every 3 weeks for four cycles following similarly cycled AC (Doxorubicin 60,75, or 90 mg/m^2 and cyclophosphamide 600 mg/m^2) [AC-T] with four cycles of the AC regimen alone are depicted in Fig. 7.11. Eisenhauer *et al.* 1998 [135] have reported the toxicity of taxoids in recommended dosages which is tabulated in Table 7.11.

7.4. Preclinical activity

Paclitaxel preclinical activity has been studied, as shown in Tables 7.12 and 7.13 [141].

7.5. Clinical trials

Various clinical trials have been carried out to evaluate the activity of paclitaxel, and the results of these studies are summarized in Tables 7.14–7.17.
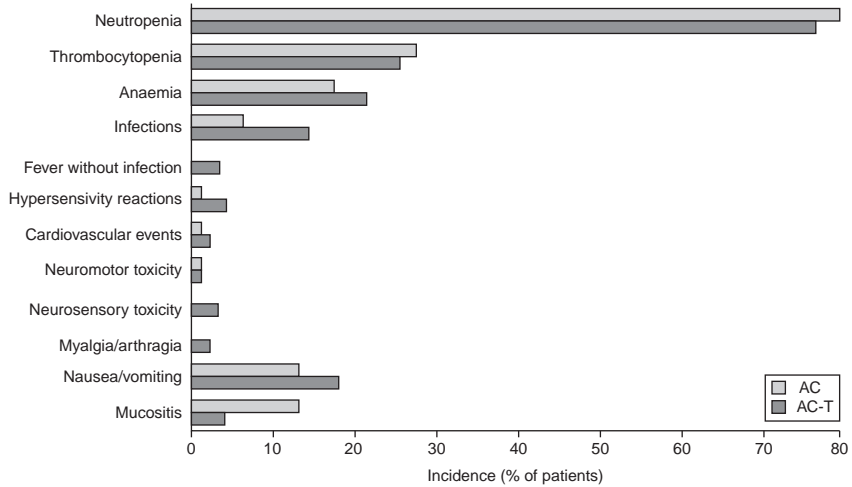
FIGURE 7.11   Toxic effect of paclitaxel [140]

TABLE 7.11   Toxicity of taxoids in recommended dosages [135]

Adverse effect	3 h	24 h
Neutropenia	+	++
HSR	+	+
Hair loss	++	++
Mucositis	−	+
Cardiac arrhythmia	+	−
Arthralgia/myalgia	+	−
Neurosensory	+[a]	+/−
Cumulative edema	−	+
Skin/nail	−	+

HSR = hypersensitivity reactions; − = absent; +/− = mild; + = moderate; ++ = severe.
[a] Dose-related and also more prominent when paclitaxel is given over 3 h.

7.6. Drug interactions

Paclitaxel is metabolized by hepatic cytochrome P-450 enzymes, particularly isoenzymes 3A and 2C. When administered with other drugs, altered metabolism is expected, which depends upon the target molecule, schedule, and sequence of administration. Some of the interactions [175, 176, 178] include decrease in the clearance of paclitaxel when paclitaxel was administered after cisplatin. Myelosuppression is more severe when paclitaxel precedes cyclophosphamide. With carboplatin there is no

TABLE 7.12   Preclinical activity of paclitaxel

Tumor	Optimal dose (mg/kg)	Schedule	ILS (%)
B16 melanoma	4.4	daily* 9	131
B16 melanoma	10	daily* 9	141
P388 leukemia	6	every 3 h, day 1	78
P388 leukemia	6	daily* 1	0
P388 leukemia	6	daily* 9	44
P388 leukemia	9	daily, days 1, 5, 9	44

ILS = increased life span.

TABLE 7.13   Phase I trial of paclitaxel [136]

Reference	Schedule	Recommended phase II (mg/m²/d)	Toxicities
[136]	1-h infusion daily × 5	30	Neutropenia, HSR, TCP, mucositis, nausea, vomiting, Alopecia
[141]	1-h infusion daily × 5	30	neutropenia, diarrhea, alopecia
[142]	3-h infusion day 1	NA	HSR, neutropenia, TCP, nausea, alopecia
[25]	6-h infusion day 1	250	Neuropathy, neutropenia, HSR, nausea, vomiting, alopecia, mucositis
[143]	6-h infusion day 1	212,170c	Neutropenia, HSR, neuropathy, myalgias mucositis
[137]	6-h infusion day 1	225	Neutropenia, HSR, mucositis, myalgias, alopecia
[25]	24-h infusion day 1	250	neuropathy, neutropenia, HSR
[144]	24-h infusion day 1	135–170	neutropenia, nausea, vomiting, alopecia

TABLE 7.14 Single agent trial of paclitaxel in breast cancer [135]

Reference	Prior chemotherapy for metastases (no. of prior regimens)	Dose (mg/m^2)	Schedule (h)	CR/PR	No. of evaluable pts	Response rate (%)
[145]	0–1	250	24	3/11	25	56
[146]	0	250 + G-CSF	24	3/13	26	62
[147]	0	135	24	2/4	19	32
[148]	0	225	3	0/13	25	52
[149]	0–1 (all pts)	175–225	3	7/12	50	38
	0	175–225	3	11	24	46
	1 (anthracycline)	175–225	3	8	26	31
[150]	0; ≥22 (all pts)	175/250	3	1/12	49	26
	0	250	3	1/7	25	32
	≥2 (anthracycline)	175	3	0/5	24	21
[151]	0–2 (all pts)	175	3	2/12	33	42
	0	175	3	1/5	11	55
	1–2 (anthracycline)	175	3	1/7	22	36
[152]	0–1	135	3	5/46	227	22
(randomized)	0–1	175	3	12/53	223	29
[153]	0–1	175	3	N/A		29
(randomized)	0–1	175	24	N/A		32
[150]	≥1 (anthracycline)	200–250 + G-CSF	24	2/36	76	33
[154]	1–2 (short taxoid)	120–140	96	0/7	26	27
[155]	≥2	135–175	24	4/36	172	23
[156]	≥1 (doxorubicin or mitoxantrone)	140	96	0/16	33	48

CR = complete response; G-CSF = granulocyte-colony-stimulating factor; N/A = not available; PR = partial response; pts = patients.

TABLE 7.15 Single agent trial of paclitaxel in pretreated ovarian cancer [135]

References	Dose (mg/m^2)	Schedule (h)	CR/PR	No. of evaluable patients	Response rate (%)
[157]	110–250	24	1/11	40	37
[158]	180–250	24	1/5	30	20
[159]	170	24	8/8	43	37
[44]	135/175	3/24	6/60	382	17 (all pts)
	135	3/24	2/27	195	15
	175	3/24	4/33	187	20
	135/175	3	3/26	182	16
	135/175	24	3/34	200	19
[160]	250	24	6/19	100	25
[161]	135/175	3	2/20	140	16

CR = complete response; PR = partial response.

TABLE 7.16 Single agent trial of paclitaxel in non-small-cell and small-cell lung cancer [135]

References	Prior chemotherapy	Dose (mg/m^2)	Schedule (h)	CR/PR	No. of evaluable patients	Response rate (%)
Non-small-cell lung cancer						
[162]	No	250	24	0/5	24	21
[163]	No	200	24	1/5	25	24
[164]	No	225	3	0/8	37	22
[165]	No	210	3	23	60	38
[166]	No	175	3	0/5	51	10
[167]	Yes	175	24	0/1	35	3
[168]	Yes	200–250	24	0/2	14	14
Small-cell lung cancer						
[169]	No	250	24	0/11	32	34
[170]	No	250 + G-CSF	24	0/15	37	41
[171]	Yes	175	3	0/5	14	36

CR = complete response; G-CSF = granulocyte-colony-stimulating factor; PR = partial response; pts = patients.

TABLE 7.17 Single agent trial of paclitaxel in squamous cell carcinoma of the head and neck [135]

References	Prior chemotherapy for recurrence	Dose (mg/m^2)	Schedule (h)	CR/PR	No. of evaluable pts	Response rate (%)
[172]	0	250 + G-CSF	24	2/10	28	43
[173]	0	250 + G-CSF	24	2/4	23	26
[174]	0–1	175	3	0/4	20	20

CR = complete response; PR = partial response; pts = patients.

change in the pharmacokinetics of both the drugs, but thrombocytopenia decreases. Doxorubicin and epirubicin should be administered 24 h before paclitaxel. Because of enhanced toxicity, anthracyline dose with paclitaxel has been limited to 360 mg/m^2. Paclitaxel is administrated 24 h after administration of doxorubicin and epirubicin.

ACKNOWLEDGMENT

REFERENCES

[1] M. C. Wani, H. L. Taylor, M. E. Wall, P. Coggon, and A. T. McPhail *J. Am. Chem. Soc.*, 1971, **93**, 2325–2327.

[2] M. E. Wall *Med. Res. Rev.*, 1998, **18**, 299–314.

[3] M. E. Wall, and M. C. Wani *J. Ethnopharmaco.*, 1996, **51**, 239–253.

[4] M. E. Wall, and M. C. Wani *Cancer Res.*, 1995, **55**, 753–760.

[5] Paclitaxel In *Wikipedia, The Free Encyclopedia*. Retrieved 19:28, April 16, (2007), from http://en.wikipedia.org/w/index.php?title=Paclitaxel&oldid=121197808.

[6] R. A. Holton *U.S. Patent No.* **5015744** 1991.

[7] R. A. Holton, *U.S. Patent No.* **5175315** 1992.

[8] R. A. Holton, *U.S. Patent No.* **5254703** 1993.

[9] P. Sherline, and K. Schiavone *Science*, 1877, **198**, 1038–1040.

[10] D. L. Gard, and M. W. Kirschner *J. Cell BioI.*, 1985, **100**, 764–774.

[11] D. B. Murphy, K. A. Johnson, and G. G. Borisy *J. Mol. BioI.*, 1977, **117**, 33–52.

[12] J. Parness, and S. B. Horwitz *J. Cell BioI.*, 1981, **91**, 479–487.

[13] P. B. Schiff, and S. B. Horwitz *Biochemistry*, 1981, **20**, 3247–3252.

[14] S. B. Horwitz *Trends Pharmacol. Sci.*, 1992, **13**, 134–136.

[15] E. K. Rowinsky, and R. C. Donehower *N. Engl. J. Med.*, 1995, **131**, 1004–1014.

[16] E. K. Rowinsky *Paclitaxelin Cancer Treatment* (eds. W. P. McGuire and E. K. Rowinsky), Marcel Dekker, Inc., New York, 1995, pp. 91–120.

[17] T. Cresteil, B. Monsarrat, P. Alvinerie, J. M. Treluyer, I. Vieira, and M. Wright *Cancer Res.*, 1994, **54**, 386–392.

[18] B. Monsarrat, P. Alvinerie, M. Wright, J. Dubois, F. Gueritte-Voegelein, D. Guenard, R. C. Donehower, and E. K. Rowinsky *J. Natl. Cancer Inst. Monogr.*, 1993, **15**, 39–46.

[19] E. Mutch, A. K. Daly, J. B. Leathart, P. G. Blain, and F. M. Williams *Arch. Toxicol.*, 2003, **77**, 313–320.

[20] E. K. Rowinsky, E. A. Eisenhauer, V. Chaudhry, S. G. Arbuck, and R. C. Donehower *Semin. Oncol.*, 1993, **20**, 1–15.

[21] E. K. Rowinsky, V. Chaudhry, A. A. Forastiere, S. E. Sartorius, D. S. Ettinger, L. B. Grochow, B. G. Lubejko, D. R. Cornblath, and R. C. Donehower *J. Clin. Oncol.*, 1993, **11**, 2010–2020.

[22] E. K. Rowinsky, M. R. Gilbert, W. P. McGuire, D. A. Noe, L. B. Grochow, A. A. Forastiere, D. S. Ettinger, B. G. Lubejko, B. Clark, and S. E. Sartorius *J. Clin. Oncol.*, 1991, **9**, 1692–1703.

[23] M. T. Huizing, A. C. Keung, H. Rosing, V. van der Kuij, W. W. Huinink, I. M. Mandjes, A. C. Dubbelman, H. M. Pinedo, and J. H. Beijnen *J. Clin. Oncol.*, 1993, **11**, 2127–2135.

[24] P. H. Wiernik, E. L. Schwartz, A. Einzig, J. J. Strauman, R. B. Lipton, and J. P. Dutcher *J. Clin. Oncol.*, 1987, **5**, 1232–1239.

[25] P. H. Wiernik, E. L. Schwartz, J. J. Strauman, J. P. Dutcher, R. B. Lipton, and E. Paietta *Cancer Res.*, 1987, **47**, 2486–2493.

[26] R. L. Juliano, and V. Ling *Biochim. Biophys. ACTA*, 1976, **455**, 152–162.

[27] F. Thiebaut *Proc. Natl. Acad. Sci.*, 1987, **84**, 7735–7738.

[28] G. L. Scheffer *Cancer Res.*, 2000, **60**, 2589–2593.

[29] A. Haimeur *Curr.Drug. Metab.*, 2004, **5**, 21–53.

[30] F. Cabral, I. Abraham, and M. M. Gottesman *Proc. Natl. Acad. Sci. USA*, 1981, **78**, 4388–4391.

[31] M. J. Schibler, and F. Cabral *J. Cell Biol.*, 1986, **102**, 1552–1531.

[32] K. Kamath, L. Wilson, F. Cabral, and M. A. Jordan *J. Biol. Chem.*, 2005, **280**, 12902–12907.

[33] S. M. Hahn, J. E. Liebmann, and B. R. Goldspiel *Proc. Am. Assoc. Cancer Res.*, 1992, **33**, 2634.

[34] W. R. Waud, S. M. Schmid, and O. Plowman *Second NCI Workshop on Taxol and Taxus*, Alexandria, VA, 1992.

[35] T. Taniki, N. Prajda, and Y. Hata *Proc. Am. Assoc. Cancer Res.*, 1993, **34**, 1769.

[36] D. G. Streeter, and J. P. Miller *Biochem. Biophys. Res. Comm.*, 1981, **103**, 1409–1412.

[37] I. Okamoto, E. Moriyama, S. Fujii, H. Kishi, M. E. C. Kiyofuji, F. Imamura, T. Mori, and M. Matsumoto *Jpn. J. Clin. Oncol.*, 2005, **35**, 188–194.

[38] T. C. Chou, G. M. Otter, and F. M. Sirotnak *Proc. Am. Assoc. Cancer Res.*, 1993, **34**, 1783.

[39] S. M. Schmid, B. D. Garrett, R. T. Coffield, and S. D. Harrison *Proc. Am. Assoc. Cancer Res.*, 1992, **33**, 2646.

[40] A. Eniu, F. M. Palmieri, and E. A. Perez *Oncologist*, 2005, **10**, 665–685.

[41] A. K. Singla, A. Garg, and D. Aggarwal *Int. J. Pharm.*, 2002, **235**, 179–192.

[42] H. Gelderblom, J. Verweij, K. Nooter, and A. Sparreboom *Eur. J. Cancer*, 2001, **37**, 1590–1598.

[43] G. Liu, E. Franssen, M. I. Fitch, and E. Warner *J. Clin. Oncol.*, 1997, **15**, 110–115.

[44] E. A. Eisenhauer, W. W. Huinink, K. D. Swenerton, L. Gianni, J. Myles, M. E. vander Burg, I. Kerr, J. B. Vermorken, K. Buser, and N. Colombo *J. Clin. Oncol.*, 1994, **2**, 2654–2666.

[45] R. B. Weiss, R. C. Donehower, P. H. Wiernik, T. Ohnuma, R. J. Gralla, D. L. Trump, J. R. Baker, D. A. Van Echo, D. D. Von Hoff, and J. B. Leyland *J. Clin. Oncol.*, 1990, **8**, 1263–1268.

[46] J. D. Adams, K. P. Flora, B. R. Goldspiel, J. W. Wilson, S. G. Arbuck, and R. Finley *J. Natl. Cancer Inst. Monogr.*, 1993, **15**, 141–147.

[47] G. J. Lesser, S. A. Grossman, S. Eller, and E. K. Rowinsky *Cancer Chemother. Pharmacol.*, 1995, **37**, 173–178.

[48] A. J. Windebank, M. D. Blexrud, and P. C. de Groen *J. Pharmacol. Exp. Ther.*, 1994, **268**, 1051–1056.

[49] D. S. Chervinsky, M. L. Brecher, and M. J. Hoelcle *Anticancer Res.*, 1993, **3**, 93–96.

[50] E. Friche, P. S. Jensen, M. Sehested, E. J. Demant, and N. N. Nissen *Cancer Commun.*, 1990, **2**, 297–303.

[51] G. J. Schuurhuis, H. J. Broxterman, H. M. Pinedo, T. H. van Heijningen, C. K. vanKalken, J. B. Vermorken, E. C. Spoelstra, and J. Lankelma *Br. J. Cancer*, 1990, **62**, 591–594.

[52] D. M. Woodcock, S. Jefferson, M. E. Linsenmeyer, P. J. Crowther, G. M. Chojnowski, and B. Williams *Cancer Res.*, 1990, **50**, 4199–4203.

[53] M. Stephan, A. Sparreboom, S. M. Steinberg, H. Gelderblom, C. Unger, D. Behringer, and K. Mross *Clin. Cancer Res.*, 2005, **11**, 4843–4850.

[54] B. Idson, and J. L. Semisolids in *The Theory and Practice of Industrial Pharmacy* (eds. L. Lachman, H. Lieberman and J. Kanig), **7**, Lea & Febiger, Philadelphia, USA, 1976, pp. 215–244.

[55] C. I. Winternitz, J. K. Jackson, A. M. Oktaba, and H. M. Burt *Pharm.*, 1996, **13**, 368–375.

[56] S. K. Dordunoo, A. M. Oktaba, W. L. Hunter, W. Min, T. Cruz, and H. M. Burt *J. Cont. Rel.*, 1997, **44**, 87–94.

[57] A. R. Scialli, T. Waterhouse, J. M. Desesso, A. Rahman, and G. C. Goeringer *Teratology*, 1997, **56**, 305–310.

[58] A. Sharma, R. M. Straubinger, I. Ojima, and R. J. Bernacki *J. Pharm. Sci.*, 1995, **84**, 1400–1404.

[59] S. S. Feng, G. F. Huang, and L. Mu *Ann. Acad. Med. Singapore*, 2000, **29**, 633–639.

[60] S. Feng, and G. Huang *J. Cont. Rel.*, 2001, **71**, 53–69.

[61] R. Greg, Y. Minamitake, M. Peracchia, V. Trubetskoy, V. Torchilin, and R. Langer *Science*, 1994, **263**, 1600–1603.

[62] T. Niwa, H. Takeuchi, T. Hino, N. Kunou, and Y. Kawashima *J. Cont. Rel.*, 1993, **25**, 89–98.

[63] W. R. Perkins, I. Ahmad, X. Li, D. J. Hirsh, G. R. Masters, C. J. Fecko, J. Lee, S. Ali, J. Nguyen, J. Schupsky, C. Herbert, A. S. Janoff, *et al. Int J Pharm.*, 2000, **200**, 27–39.

[64] D. Sharma, T. P. Chelvi, J. Kaur, K. Chakravorty, T. K. De, A. Maitra, and R. Ralhan *Oncol. Res.*, 1996, **8**, 281–286.

[65] B. Damascelli, G. Cantu, F. Mattavelli, P. Tamplenizza, P. Bidoli, E. Leo, F. Dosio, A. M. Cerrotta, L. Di, L. F. Frigerio, F. Garbagnati, R. Lanocita, *et al. Cancer*, 2001, **92**, 2592–2602.

[66] S. Alcaro, C. A. Ventura, D. Paolino, D. Battaglia, F. Ortuso, L. Cattel, G. Puglisi, and M. Fresta *Bioorg. Med. Chem. Lett.*, 2002, **12**, 1637–1641.

[67] U. S. Sharma, S. V. Balasubramanian, and R. M. Straubinger *J. Pharm. Sci.*, 1995, **84**, 1223–1230.

[68] B. D. Tarr, T. G. Sambandan, and S. H. Yalkowsky *Pharm. Res.*, 1987, **4**, 162–165.

[69] J. S. Urn *J. Surg.*, 1997, **173**, 403–406.

[70] Y. M. Wang, H. Sato, I. Adachi, and I. Horikoshi *Chem. Pharm. Bull. (Tokyo)*, 1996, **44**, 1935–1940.

[71] G. S. Das, G. H. Rao, R. F. Wilson, and T. Chandy *J. Biomed. Mater. Res.*, 2001, **55**, 96–103.

[72] H. Sato, Y. M. Wang, and H. Adachii *Bio. Pharm. Bull.*, 1996, **19**, 1596–1605.

[73] A. Bragdon, A. L. Bertone, J. Hardy, E. J. Simmons, and S. E. Weisbrode *J. Invest. Surg.*, 2001, **14**, 169–182.

[74] H. M. Burt, J. K. Jackson, S. K. Bains, R. T. Liggins, A. M. Oktaba, A. L. Arsenault, and W. L. Hunter *Cancer Lett.*, 1995, **88**, 73–79.

[75] M. A. Attawia, M. D. Borden, K. M. Herbert, D. S. Katti, F. Asrari, K. E. Uhrich, and C. T. Laurencin *J. Cont. Rel.*, 2001, **71**, 193–202.

[76] M. Ceruti, P. Crosasso, P. Brusa, S. Arpicco, F. Dosio, and L. Cattel *J Control Release*, 2000, **63**, 141–53.

[77] S. Ali, I. Ahmad, A. Peters, G. Masters, S. Minchey, A. Janoff, and E. Mayhew *Anticancer Drugs*, 2001, **12**, 117–128.

[78] G. M. Dubowchik, K. Mosure, J. O. Knipe, and R. A. Firestone *Bioorg. Med. Chem. Lett.*, 1998, **8**, 3347–3352.

[79] V. Luo, M. R. Ziebell, and G. D. Prestwich *Biomacromol.*, 2000, **1**, 208–218.

[80] P. D. Senter, H. Marquardt, B. A. Thomas, B. D. Hammock, I. S. Frank, and H. P. Svensson *Cancer Res.*, 1996, **56**, 1471–1474.

[81] T. Takahashi, H. Tsukamoto, and H. Yamada *Bioorg. Med. Chem.*, 1998, **8**, 113–8116.

[82] V. M. Vrudhula, J. F. MacMaster, Z. Li, D. E. Kerr, and P. D. Senter *Bioorg. Med. Chem. Lett.*, 2002, **12**, 3591–3594.

[83] V. M. Vrudhula, D. E. Kerr, N. O. Siemers, G. M. Dubowchik, and P. D. Senter *Bioorg. Med. Chem. Lett.*, 2003, **13**, 539–542.

[84] F. Dosio, S. Arpicco, P. Brusa, B. Stella, and L. Cattel *J. Cont. Rel.*, 2001, **76**, 107–117.

[85] V. Guillemard, and H. U. Saragovi *Cancer Res.*, 2001, **61**, 694–699.

[86] S. Ke, L. Milas, C. Charnsangavej, S. Wallace, and C. Li *J. Cont. Rel.*, 2001, **74**, 237–242.

[87] J. W. Lee, J. Y. Lu, P. S. Low, and P. L. Fuchs *Bioorg. Med. Chem.*, 2002, **10**, 2397–2414.

[88] H. Ohtsu, Y. Nakanishi, K. F. Bastow, F. Y. Lee, and K. H. Lee *Bioorg. Med. Chem.*, 2003, **11**, 1851–1857.

[89] I. Ojima, X. Geng, X. Wu, C. Qu, C. P. Borella, H. Xie, S. D. Wilhelm, A. Leece, L. M. Bartle, and V. S. Goldmacher *J. Med. Chem.*, 2002, **45**, 5620–5623.

[90] O. Shi, H. K. Wang, K. F. Bastow, Y. Tachibana, K. Chen, F. Y. Lee, and K. H. Lee *Bioorg. Med. Chern.*, 2001, **9**, 2999–3004.

[91] S. Jauhari, and A. K. Dash *AAPS Pharm. Sci. Tech.*, 2006, **7,** article 53.

[92] MicromedexHealthcare Seires: Retrieved from Martindale on April 19, 2007 at http:// www.thomsonhc.com/hcs/librarian/ND_PR/Main/SBK/5/PFPUI/ Li1apgD1PG8oS2/ND_PG/PRIH/CS/097559/ND_T/HCS/ND_P/Main/ DUPLICATIONSHIELDSYNC/C25450/ND_B/HCS/PFActionId/hcs.drugs. TradeGenericDrugList.Search?SearchTerm=MARTINDALE-DOC-EN2453-y&ContentSetId=55&DisplayTerm=Paclitaxel.

[93] S. Budavari (Ed.), *Merck Index*, 13th ed., Merck and Co., Inc., Rahway, NJ, 2001, p. 1251.

[94] G. K. McEvoy (Ed.), *AHFS drug information*, The American Society of Health-System Pharmacists, Maryland, 2003, p. 1099.

[95] P. Ramesh *Int. J. Pharm.*, 1998, **172**, 1–15.

[96] K. Whiterup, S. A. Look, M. W. Stasko, T. J. Ghiorzi, G. M. Muschik, and G. M. Cragg *J. Nat. Prod.*, 1990, **53**, 1249–1255.

[97] K. Rao, J. B. Hanuman, C. Alvarez, M. Stoy, and R. Baxley *Pharm. Res.*, 1995, **12**, 1003–1010.

[98] E. Blume *J. Natl. Cancer Inst.*, 1989, **81**, 1122–1123.

[99] K. C. Nicolaou, C. F. Clauborne, P. G. Nanternest, E. A. Couladouros, and E. J. Sorensen *J. Am. Chem. Soc.*, 1994, **116**, 1591–1592.

[100] C. Lucatelli, F. Viton, Y. Gimbert, and A. E. Greene *J. Org. Chem.*, 2002, **67**, 9468–9470.

[101] A. Strerle, G. Strobel, and D. Stierle *Science*, 1993, **260**, 214–215.

[102] Y. Yukimune, H. Tabata, Y. Higashi, and Y. Hara *Nat. Biotechnol.*, , **14**, 1129–1132.

[103] D. Ellis, E. L. Zeldin, M. Brodhagen, W. A. Russin, and B. H. McCown *J. Nat. Prod.*, 1996, **59**, 246–250.

[104] W. Ma, G. L. Park, G. A. Gomez, M. H. Nieder, and C. Shackleton *J. Nat. Prod.*, 1994, **57**, 116–122.

[105] R. A. Holton, H. B. Kim, C. Somoza, F. Liang, R. J. Biediger, P. D. Boatman, M. Shindo, C. C. Smith, S. Kim, H. Nadizadeh, Y. Suzuki, C. Tao, *et al. J. Am. Chem. Soc.*, 1994, **116**, 1599–1600.

[106] R. A. Holton, C. Somoza, H. B. Kim, F. Liang, R. J. Biediger, P. D. Boatman, M. Shindo, C. C. Smith, S. Kim, H. Nadizadeh, Y. Suzuki, C. Tao, *et al. J. Am. Chem. Soc.*, 1994, **116**, 1597–1598.

[107] K. Nicolaou, C. Riemer, M. A. Kerr, D. Rideout, and W. Wrasidlo *Nature*, 1993, **364**, 464–466.

[108] S. J. Danishefsky, J. J. Masters, W. B. Young, J. T. Link, L. B. Snyder, T. V. Magee, D. K. Jung, R. C. A. Issacs, W. G. Bornmann, C. A. Alaimo, C. A. Coburn, and M. J. D. Grandi *J. Am. Chem. Soc.*, 1996, **118**, 2843–2859.

[109] S. Jauhari *A mucoadhesive in situ gel delivery system for paclitaxel*, MS thesis, Pharmacy Sciences, Creighton University, Omaha, NE, USA.

[110] C. S. Swindell, and N. E. Krauss *J. Med. Chem.*, 1991, **34**, 1177–1184.

[111] R. T. Liggins, W. L. Hunter, and H. M. Burt *J. Pharm. Sci.*, 1997, **86**, 1458–1463.

[112] http://www.cerep.fr/Cerep/Users/pages/Downloads/Documents/Marketing/ Pharmacology%20&%20ADME/Application%20notes/PartitionCoefficient.pdf.

[113] J. H. Lee, U. S. Gi, J. H. Kim, Y. Kim, S. H. Kim, H. Oh, and B. Min *Bull. Korean Chem. Soc.*, 2001, **22**, 925–928.

[114] J. Z. Chen, V. S. Ranade, and X. Q. Xie *Int. J. Pharm.*, 2005, **305**, 129–144.

[115] D. Mastropaolo, A. Camerman, Y. Luo, G. D. Brayer, and N. Camerman *Proc. Natl. Acad. Sci. USA*, 1995, **92**, 6920–6924.

[116] R. Voelker in *Solid state NMR of Polymers* (Ed. L. J. Mathias), Plenum press, New York, 1991, pp. 234–244.

[117] E. H. Kerns, S. E. Hill, D. J. Detlefsen, K. J. Volk, B. H. Long, J. Carboni, and M. S. Lee *Rapid Commun. Mass Spectrom.*, 1998, **12**, 620–624.

[118] *US Pharmacopeia National Formulary, USP*, 2006, **29**, 1624–1626.

[119] A. Andersen, D. J. Warren, P. F. Brunsvig, S. Aamdal, G. B. Kristensen, and H. Olsen *BMC Clin. Pharmacol.*, 2006, **6**, 2.

[120] S. C. Kim, J. Yu, J. W. Lee, E. S. Park, and S. C. Chi *J. Pharm. Biomed. Anal.*, 2005, **39**, 170–176.

[121] M. S. Alexander, M. M. Kiser, T. Culley, J. R. Kern, L. W. Dolan, J. D. McChesney, J. Zygmunt, and S. J. Bannister *J. Chromatogr. B. Analyt. Technol. Biomed. Life Sci.*, 2003, **785**, 253–261.

[122] R. A. Parise, R. K. Ramanathan, W. C. Zamboni, and M. J. Egorin *J. Chromatogr. B. Analyt. Technol. Biomed. Life Sci.*, 2003, **783**, 231–236.

[123] L. Z. Wang, P. C. Ho, H. S. Lee, H. K. Vaddi, Y. W. Chan, and C. S. Yung *J. Pharm. Biomed. Anal.*, , **31**, 283–289.

[124] S. H. Lee, S. D. Yoo, and K. H. Lee *J. Chromatogr. B. Analyt. Technol. Biomed. Life Sci. Appl.*, 1999, **724**, 357–363.

[125] A. Sparreboom, P. de Bruijn, K. Nooter, W. J. Loos, G. Stoter, and J. Verweij *J. Chromatogr. B. Analyt. Technol. Biomed. Life Sci. Appl.*, 1998, **705**, 159–167.

[126] M. Andreeva, P. D. Niedmann, L. Binder, V. W. Armstrong, H. Meden, M. Binder, and M. Oellerich *Ther. Drug Monit.*, 1997, **19**, 327–332.

[127] A. El-Yazigi, and A. Yusuf *Ther. Drug Monit.*, 1995, **17**, 511–515.

[128] M. T. Huizing, H. Rosing, F. Koopman, A. C. Keung, H. M. Pinedo, and J. H. Beijnen *J. Chromatogr. B. Biomed. Appl.*, 1995, **664**, 373–382.

[129] D. Song, and J. L. Au *J. Chromatogr. B. Biomed. Appl.*, 1995, **663**, 337–344.

[130] K. C. Chan, A. B. Alvarado, M. T. McGuire, G. M. Muschik, H. J. Issaq, and K. M. Snader *J. Chromatogr. B. Biomed. Appl.*, 1994, **657**, 301–306.

[131] Bristol-Myers Squibb Company Package inserts, *Taxol for injection concentrate*, Bristol-Myers Squibb Company, New Jersey, Princeton, 1992.

[132] W. N. Waugh, L. A. Trissel, and V. J. Stella *Am. J. Hosp. Pharm.*, 1993, **51**, 2804–2810.

[133] L. A. Trissel, and B. B. Bready *Am. Hosp. Pharm.*, 1992, **49**, 1716–1719.

[134] A. B. Dhanikula, D. R. Singh, and R. Panchagnula *Curr. Drug Del.*, 2005, **2**, 35–44.

[135] E. A. Eisenhauer, and J. B. Vermorken *Drugs*, 1998, **55**, 5–30.

[136] J. M. Koeller, and R. T. Dorr Pharmaceutical issues of Paclitaxel, *Annals of Pharmacotherapy*, 1994, **28**(Suppl. 5–34) (1994).

[137] J. L. Grem, K. D. Tutsch, K. J. Simon, D. B. Alberti, J. K. Willson, and D. C. Tormey *Cancer Treat. Rep.*, 1987, **71**, 1179–1184.

[138] T. Brown, K. Havlin, G. Weiss, J. Cagnola, J. Koeller, and J. Kuhn *J. Clin. Oncol.*, 1991, **9**, 1261–267.

[139] S. Mielke, A. Sparreboom, and K. Mross *Eur. J. Cancer*, 2006, **42**, 24–30.

[140] S. Dene, and P. L. Greg *Drugs*, 2004, **64**, 1839–1847.

[141] H. A. Burris 3rd *Ann. Pharmacother.*, , **28**(5 Suppl), S7–S10.

[142] S. S. Legha, D. M. Tenney, and I. R. Krakoff *J. Clin. Oncol.*, 1986, **4**, 762–766.

[143] M. G. Kris, J. P. O'Connell, R. J. Gralla, M. S. Wertheim, R. M. Parente, and P. B. Schiff *Cancer Treat. Rep.*, 1986, **70**, 605–607.

[144] R. C. Donehower, E. K. Rowinsky, L. B. Grochow, S. M. Longnecker, and D. S. Ettinger *Cancer Treat. Rep.*, 1987, **71**, 1171–1177.

[145] T. Ohnuma, A. S. Zimet, and V. A. Coffey *Proc. Am. Assoc. Cancer Res.*, 1985, **26**, 167.

[146] F. A. Holmes, R. S. Walters, and R. L. Theriault *J. Natl. Cancer Inst.*, 1991, **83**, 1797–805.

[147] B. S. Reichman, A. D. Seidman, and J. P. A. Crown *J. Clin. Oncol.*, 1993, **11**, 1943–1951.

[148] S. M. Swain, S. F. Honig, and M. C. Tefft *Invest. New Drugs*, 1995, **13**, 217–222.

[149] N. G. Davidson, T. J. Perren, and Y. T. S. Chao *Proc. 6th Int. Congress Anti-Cancer Treat.*, 1995, **5**, 119.

[150] L. Gianni, E. Munzone, and G. Capri *J. Natl. Cancer Inst.*, 1995, **87**, 1169–1175.

[151] A. D. Seidman, A. Tiersten, and C. Hudis *J. Clin. Oncol.*, 1995, **13**, 2575–2581.

[152] G. Fountzilas, A. Athanassiades, and T. Giannakakis *Eur. J. Cancer*, 1996, **32A**, 47–51.

[153] J. M. Nabholtz, K. Gelmon, and M. Bontenbal *J. Clin. Oncol.*, 1996, **14**, 1858–1867.

[154] T. Peretz, A. Sulkes, and P. Chollet *Eur. J. Cancer*, 1995, **31A**, S75.

[155] A. D. Seidman, D. Hochhauser, and M. Gollub *J. Clin. Oncol.*, , **14**, 1877–1884.

[156] J. S. Abrams, D. A. Vena, and J. Baltz *J. Clin. Oncol.*, 1995, **13**, 2056–2065.

[157] W. H. Wilson, S. L. Berg, and G. Bryant *J. Clin. Oncol.*, 1994, **12**, 1621–1629.

[158] W. P. McGuire, E. K. Rowinsky, and N. B. Rosenshein *Ann. Int. Med.*, 1989, **111**, 273–279.

[159] A. I. Einzig, P. H. Wiernik, and J. I. Sasloff *J. Clin. Oncol.*, 1992, **10**, 1748–1753.

[160] I. T. Thigpen, J. A. Blessing, and H. Ball *J. Clin. Oncol.*, 1994, **12**, 1748–1753.

[161] V. L. Seewaldt, B. E. Greer, and J. M. Cain *Am. J. Obstet. Gynecol.*, 1994, **170**, 1666–1670.

[162] M. E. Gore, V. Levy, and G. Rustin *Br. J. Cancer*, 1995, **72**, 1016–1019.

[163] A. Y. Chang, K. Kim, and J. Glick *J. Natl. Cancer Inst.*, 1993, **85**, 388–394.

[164] W. K. Murphy, F. V. Fossella, and R. J. Winn *J. Natl. Cancer Inst.*, 1993, **85**, 384–388.

[165] U. Gatzmeier, M. Heckmayr, and R. Neuhauss *Lung Cancer*, 1995, **12**, 101–106.

[166] I. Sekine, Y. Nishiwaki, and K. Watanabe *Clin. Cancer Res.*, 1996, **2**, 941–945.

[167] M. J. Milward, J. F. Bishop, and M. Friedlander *J. Clin. Oncol.*, , **14**, 142–148.

[168] W. K. Murph, R. J. Winn, and M. Huber *Proc. Am. Soc. Clin. Oncol.*, 1994, **13**, 363.

[169] J. Ruckdeschel, Jr., H. Wagne, and C. Williams *Proc. Am. Soc. Clin. Oncol.*, 1994, **13**, 357.

[170] D. S. Ettinger, D. M. Finkelstein, and R. P. Sarma *J. Clin. Oncol.*, 1995, **13**, 1430–1435.

[171] R. J. Kirschling, S. H. Jung, and J. R. Jett *Proc. Am. Soc. Clin. Oncol.*, 1994, **13**, 326.

[172] E. F. Smit, C. Kloosterziel, and H. J. M. Groen *Proc. Am. Soc. Clin. Oncol.*, 1996, **15**, 394.

[173] A. A. Forastiere *Ann. Oncol.*, 1995, **5**, S51–S54.

[174] D. Thornton, K. Singh, and B. Putz *Proc. Am. Soc. Clin. Oncol.*, 1994, **13**, 288.

[175] A. F. Baker *Pharmacotherapy*, 1997, **17**, 126S–132S.

[176] A. F. Baker, and R. T. Dorr *Cancer Treat. Rev.*, 2001, **27**, 221–233.

[177] S. M. Longnecker, R. C. Donehower, A. E. Cates, T. L. Chen, R. B. Brundratt, and L. B. Grochow *Cancer Treat. Rep.*, 1987, **71**, 53–7159.

[178] V. Gebbia, A. Testa, and G. Cannata *Eur. J. Cancer*, 1996, **32A**, 901–902.

Cumulative Index

Bold numerals refer to volume numbers.